UNIVERSIDAD COMPLUTENSE DE MADRID
FACULTAD DE CIENCIAS QUÍMICAS



TESIS DOCTORAL

Efecto neuroprotector de moléculas orgánicas y nanopartículas de selenio en la enfermedad de Alzheimer

Neuroprotective effect of organic molecules and selenium naoparticles on Alzheimer's disease

MEMORIA PARA OPTAR AL GRADO DE DOCTOR

PRESENTADA POR

David Vicente Zurdo

Directoras

Yolanda Madrid Albarrán
María Eugenia de León González
Noelia Rosales Conrado

Madrid

© David Vicente Zurdo, 2023

UNIVERSIDAD COMPLUTENSE DE MADRID

FACULTAD DE CIENCIAS QUÍMICAS



TESIS DOCTORAL

EFECTO NEUROPROTECTOR DE MOLÉCULAS ORGÁNICAS Y NANOPARTÍCULAS DE SELENIO EN LA ENFERMEDAD DE ALZHEIMER

NEUROPROTECTIVE EFFECT OF ORGANIC MOLECULES AND SELENIUM NANOPARTICLES ON ALZHEIMER'S DISEASE

MEMORIA PARA OPTAR AL GRADO DE DOCTOR

PRESENTADA POR

David Vicente Zurdo

DIRECTORAS

Yolanda Madrid Albarrán

María Eugenia de León González

Noelia Rosales Conrado

UNIVERSIDAD COMPLUTENSE DE MADRID

FACULTAD DE CIENCIAS QUÍMICAS

Doctorado en Química Avanzada



TESIS DOCTORAL

EFECTO NEUROPROTECTOR DE MOLÉCULAS ORGÁNICAS Y NANOPARTÍCULAS DE SELENIO EN LA ENFERMEDAD DE ALZHEIMER

NEUROPROTECTIVE EFFECT OF ORGANIC MOLECULES AND SELENIUM NANOPARTICLES ON ALZHEIMER'S DISEASE

David Vicente Zurdo

DIRECTORAS

Yolanda Madrid Albarrán

María Eugenia de León González

Noelia Rosales Conrado

El trabajo desarrollado durante esta Tesis Doctoral se ha realizado en el marco de los Proyectos de Investigación financiados por el Ministerio de Economía, Industria y Competitividad (CTQ2014-54801-C2-1-R, CTQ2017-83569-C2-1-R), el Ministerio de Ciencia e Innovación (PID2020-114714RB-I00), la Comunidad Autónoma de Madrid y los fondos europeos de los programas FEDER y FSE (S2013/ABI-3028 (AVANSECAL-CM) y S2018/BAA-4393 (AVANSECAL-II-CM)), y la Universidad Complutense de Madrid y el Banco Santander (PR26/16-16B).

Se agradece la financiación recibida a través de los contratos de Investigador Predoctoral de la Unión Europea y la Comunidad de Madrid (PEJD-2018-PRE/BMD-8300), de Personal Investigador Predoctoral en Formación de la Universidad Complutense de Madrid y el Banco Santander (CT42/18-CT43/18) y de Formación de Profesorado Universitario del Ministerio de Ciencia, Innovación y Universidades (FPU18/00573) para desarrollar el trabajo de investigación presentado.

La verdadera ciencia enseña,
por encima de todo,
a dudar y a ser ignorante.

Miguel de Unamuno

El desarrollo de una Tesis Doctoral supone un arduo camino, lleno de retos y adversidades, a las que hay que hacer frente de la mejor forma posible. Sin embargo, a veces conviene levantar la mirada del suelo y disfrutar de las vistas, ya que es una experiencia única y gratificante, tanto científica como personalmente. Gracias a esta etapa que está finalizando puedo decir, con orgullo y en el mejor de los sentidos, que no soy la misma persona que la comenzó.

A lo largo de toda esta Tesis Doctoral, he tenido la enorme suerte de poder trabajar bajo la dirección de grandes científicas como la Dra. Noelia Rosales Conrado, la Dra. María Eugenia de León González y la Dra. Yolanda Madrid Albarrán. Sin ellas, sencillamente, esta investigación no hubiese sido posible. Han sido las mejores compañeras de viaje que podría haber tenido, ya que con su amplia experiencia han sabido guiarme, enseñarme y apoyarme en los momentos de mayor dificultad. Como dijo Isaac Newton "*si he logrado ver más lejos, ha sido porque he subido a hombros de gigantes*". Infinitas gracias por haberme dado la oportunidad de trabajar con vosotras.

Agradecer también el enorme trabajo realizado por las alumnas de TFG y TFM que han contribuido a esta línea de investigación: Laura, Sara y Sandra. Espero que hayáis tenido una experiencia tan grata como la mía al haber trabajado codo con codo, y quizás en el futuro nos volvamos a encontrar.

Mediante la colaboración con los grupos de investigación de las Facultades de Farmacia y Veterinaria he tenido la suerte de haber trabajado en un equipo multidisciplinar y conocer a verdaderos profesionales en su campo, como el Dr. Juan Francisco González Matilla y el Dr. Javier del Pino. Además, esto me ha permitido haber conocido a Cris, una bellísima persona llena de vitalidad y de energía, con la que disfruté de una gran complicidad en nuestra etapa inicial de Tesis. Encargada de sintetizar las moléculas que, según ella, "*me tenían que durar pa' toda la vida*". Gracias por todo el esfuerzo realizado, Cris, porque hasta el último momento no me di cuenta de que cada miligramo de compuesto, sintetizado y purificado, costaba sudor y lágrimas obtener.

Como consequência da pandemia, as estadias pré-doutorais no estrangeiro foram complicadas. É por isso que gostaria de agradecer de todo o coração a amabilidade da Dra. Sílvia Chaves e da Dra. Amélia Santos por me receberem no seu laboratório num momento tão difícil como o que sofreu devido à COVID-19. Amélia, nunca esquecerei os quatro meses de síntese de compostos no teu laboratório de química orgânica, pois para um químico analítico como eu, cada dia se assemelhava a uma odisseia. De vós aprendi a constância no

trabalho, a perseverança e a desfrutar de cada pequena vitória, porque isso nos aproximava do objectivo final. Sílvia, muito obrigado por partilhar comigo toda a tua sabedoria e conhecimentos de Química Física e Analítica, e pelo excelente trabalho de supervisão que fizeste durante a minha estadia no teu laboratório. Espero ter estado à altura da situação e espero que nos encontremos de novo.

A pesar del confinamiento sufrido en Lisboa debido a la COVID-19, eso no impidió que conociese a una de las personas que ya se ha convertido en amigo para toda la vida. David, con raíces pacense y bilbotar de nacimiento, e raízes lusas de própria vontade. Lo primero que me sorprendió de ti fue tu amor por aquello que hacías, uno de los mayores expertos de Oteiza a nivel mundial, y cómo eras capaz de transmitírselo a los demás, poniendo en práctica aquella frase de Pessoa: "*coloque tudo o que você é no mínimo que você faz*". Sigue por ese camino, *desafiando al oleaje sin timón ni timonel*, porque de verdad que harás cosas grandes, y seguro que lo mejor está aún por descubrir. A pesar de que no pudimos pasar tanto tiempo juntos como me hubiese gustado, ya que me sumergí en el trabajo y *qué pequeña es la luz de los faros de quien sueña con la libertad*, al final lo hicimos lo mejor que pudimos. Como dijo Sabina, "*al lugar donde has sido feliz no debieras tratar de volver*", pero yo volvería a aquella Lisboa contigo.

Tampoco puedo olvidarme de todos los compañeros del grupo de investigación de Trazas, Especiación y Proteómica que han pasado por el Maldi. Bea, gracias por tu inestimable ayuda en mis primeros pasos por el laboratorio, y por toda la paciencia que tuviste y sigues teniendo conmigo, ya que eres un claro ejemplo de esfuerzo y constancia en la investigación. Gus, desde el primer día me has dado tu apoyo en todo lo que he necesitado, y después de los análisis de los líquenes me di cuenta de lo fácil que es trabajar contigo. Emma, gracias a los proyectos de innovación educativa que hemos realizado, ha quedado constancia de lo enormemente trabajadora y gran investigadora que eres, y seguro que llegarás muy lejos. También dar las gracias a compañeras de trabajo con las que compartí menos tiempo, ya que estaban en su etapa final: Mari, Sandra, Gema… Y a Marina, en cuya estancia en nuestro laboratorio tuve la suerte de colaborar con ella.

Por supuesto no podían faltar los que, a día de hoy, siguen siendo compañeros de despacho. Gracias a Paloma, Elena y Tamara por los buenos momentos que hemos pasado estos años, todas las risas y todos los cafés que, sin lugar a dudas, han hecho el día a día mucho más ameno. Miguel, aunque has sido el último en llegar, y no hemos podido pasar tanto tiempo juntos, ya eres uno más del equipo.

También agradecer a los *senior* del grupo de investigación por ofrecerme su ayuda cuando la he necesitado. Teresa, gracias por el apoyo que me diste como tutora de mi TFM, ya que siempre es de agradecer contar con cuatro manos charras en lugar de solo con dos, y por el increíble trabajo que haces gestionando la titánica labor de las facturas. Jon, estás siempre al pie del cañón, y no dudas nunca en ofrecerte cuando hay algún marrón que solucionar, muchísimas gracias por ello. Por supuesto, también agradecer al resto de miembros del grupo de investigación de Trazas, Especiación y Proteómica: Rian, Estefanía, Lola, Milagros y Juanjo. Gracias también a todos los compañeros de QBA, Guille, Andrés y Héctor, por la inestimable ayuda en el laboratorio de cultivo celular, al Dr. José Luis Luque y a la Dra. María Luz Mena.

Gracias, Iván, por ser el mejor compañero de trabajo que podía haber tenido. Desde que llegaste te has convertido en un imprescindible, tanto dentro como fuera de la facultad, y en un gran amigo para toda la vida. Alex, qué decirte que ya no sepas, ¡además de que tienes unos ojos azules preciosos! Desde que llegué a la facultad ya estabas por aquí, y aunque a veces apareces y desapareces como un fantasma, con el paso de los años nos hemos cogido cariño. Rodri, muchas gracias por amenizarnos los días a todos con tus *quotes*, desde luego que eres alguien inolvidable.

También dar las gracias a todos aquellos alumnos con los que he tenido la suerte de poder coincidir. Marta: panadera, azafata o química, todo lo que haces se te da de lujo. Llegó el momento, estaba deseando poder decirte esto desde hace mucho tiempo… ¡Ya soy doctor! Ana, hemos compartido mucho tiempo tanto dentro como fuera de la facultad, incluso esas tres semanas intentando sobrevivir en Londres, y aún seguimos quedando de vez en cuando para ponernos al día de nuestras vidas. Y cómo olvidarme del mejor alumno que he tenido jamás, Ricky, y de su compañero inseparable, Alex, cuya curiosidad científica no conoce límites. Fuisteis de las primeras personas que tuvieron la mala suerte de tenerme como profesor, y yo fui terriblemente afortunado de teneros a vosotros como alumnos. No sé quién aprendió más de quién, solo sé, y es lo que verdaderamente importa, que fue una experiencia inolvidablemente divertida.

Infinitas gracias al inmenso grupo de los autodenominados Quimitrones, que me acogieron con los brazos abiertos y con los que las comidas y los cafés se hacían interminables, permitiendo una agradable desconexión de vez en cuando. Rober, aprendimos mucho juntos y te convertiste en un inseparable, gracias por todo. Diana, aunque cada vez nos veamos menos por las circunstancias personales de cada uno, sigues siendo una gran

amiga con la que se puede contar. Isa, aunque seas "de otro milenio", gracias por todas las risas que nos hemos echado y… ¡que sepas que tus padres me caen genial! Mirichunga, gracias por haber estado siempre ahí aportando un granito de cordura y sensatez, espero que todo te vaya genial y protégete del agua. Juls, con el paso de los años te has convertido en una gran amiga, perfecta para ir de camping a tierras gallegas y lusas, siempre equipada con crema solar y muchas risas contagiosas. Eres un tercio de las personas necesarias para emprender aventuras de no retorno en la montaña. Cuando no sabes si vas a poder volver a la civilización, echar la vista atrás y verte (aunque sea con el pelo congelado a veinte grados bajo cero, luchando contra el viento huracanado que intenta levantarte) es una bocanada de aire fresco que te da energías para llegar a la cima. Antonio, el salmantino, y Dani, el leonés, a pesar de vuestros orígenes informáticos os habéis hecho hueco en este grupo tan poco selecto. Sois unos compañeros de viaje perfectos allí donde se presente la oportunidad, y estoy deseando saber cuál será el próximo destino.

Por supuesto dar las gracias a aquellos amigos de Salamanca con los que aún tengo la gran suerte de poder mantener el contacto y quedar con ellos cada vez que visito la ciudad. Ricar, el mejor compañero de judo que podría haber tenido, y con el que me he llevado algún que otro susto cuando el *tatami* no estaba de nuestra parte. Tus habilidades como *tori* solo se ven eclipsadas por tu gran capacidad de ejercer como *uke*. Espero que algún día podamos volver a entrenar juntos cuando vuelvas de Asturias. Santi, el último adalid en Salamanca, ya sabes que eres la pieza esencial del grupo, indispensable para que todo siga funcionando. Tu sentido del humor, aunque a veces demasiado ácido, hace que las veladas se esfumen más rápido que una *Guiness* cuya espuma ha terminado de reposar. Sara, ya casi ni me acuerdo de nuestros orígenes en el pueblo, cuando paradójicamente nos caíamos mal sin apenas conocernos. Por suerte, hace años que eso cambió, y te has convertido en una gran amiga. Venimos de la misma ciudad, del mismo pueblo, y ambos hemos acabado luchando por hacernos un pequeño hueco en Madrid. A pesar del calor, las prisas y las jornadas interminables, espero que consigas encontrar la felicidad en esta ciudad que tiene muchas otras cosas que ofrecer. Estrella, la mejor prima que podría haber tenido, y con la que he compartido tantas cosas que ya he perdido la cuenta… por suerte tu memoria es mejor que la mía. Echo de menos cuando ambos vivíamos en la misma ciudad y hacíamos multitud de planes, nos poníamos al día de lo que nos había pasado aquella semana, y nos dábamos consejos más o menos infructuosos. Que el calor de Sevilla no pueda contigo, porque aún tenemos pendiente alguna quedada más. Javi, has tenido la suerte de acabar en Segovia, a medio camino entre Madrid y Salamanca. Muchas gracias por ser como eres, siempre

manteniendo la calma. A pesar de decir que estabas cansado de oír mis historias cuando buscaba consejo, la verdad es que nunca has dejado que me las guardase para mí solo. La vida sigue, y cada vez somos menos en Salamanca, pero lo importante es que aún seguimos manteniendo la esencia de nuestro grupo, otrora *Desperdicios humanos* o *Cacahüetes*, y nos vemos para *pinchear* o celebrar la nochevieja.

No podían faltar aquellas dos personas con las que di mis primeros pasos en el mundo universitario. Jesús, nuestro filósofo zamorano, más concretamente de Gema del Vino, pueblo que perteneció al antiguo reino de León. Qué hubiese sido de nosotros sin tus sabias palabras y tu cultura sin igual. Fuiste mi primer referente cinéfilo, aunque siento decirte que posteriormente te superaron. Muchas gracias, a ti y a tus maravillosos padres, por abrirme las puertas de tu casa cada verano. Siempre recordaré aquella grandiosa demostración de cómo subirse a un remolque en plena espantada: debe ser que la sangre de Viriato corre por tus venas. Sandra, mi compañera abulense de laboratorio, hemos compartido tantas cosas que difícilmente podría rememorarlas todas. Todo lo que te pudiese escribir en estas líneas se iba a quedar corto, pero estoy seguro de que eso ya lo sabes. Eres una gran amiga, y espero que lo sigas siendo mucho tiempo más.

Gracias, Argentino, por haber perseverado en *hacerme la gamba*, porque si no hubiera sido por ese goteo constante de planes que me proponías, ambos sabemos que nada hubiese transcurrido de la misma forma. Para mi abuela, eres su tercer nieto; para mi madre, su tercer hijo; por lo que resulta innegable que, para mí, eres mi segundo hermano. Jamás tendré palabras para agradecerte todo lo que me has dado, y si ahora soy una persona diferente a cuando empecé la Tesis, es en parte gracias a ti. Espero poner en práctica todos los vocablos argentinos que me has enseñado cuando hagamos aquel viaje por la Argentina y lleguemos a Tierra del Fuego. Viajar con vos es sinónimo de volver con historias que contar, ya sea Luxemburgo, Milán, o Granada. No pasa un día sin que nos demos los buenos días y las buenas noches, porque, aunque no tengamos nada que contarnos, sabemos que siempre hay alguien al otro lado del charco dispuesto a escucharnos. No te he incluido dentro de los tercios con los que emprender aventuras temerarias, porque representas la mismísima esencia de la aventura. La primera persona con la que atravesé el Risco de los Claveles, sin saber si seríamos capaces de volver por donde habíamos venido. Aquella con la que me di cuenta de que una piedra en el camino es algo deseable, cuando la alternativa es pisar sobre metros de nieve implacable. No dejes que te digan que no vas bien equipado a la montaña, porque lo que más se necesita allá arriba, vos lo llevás equipado de serie. Chango, te quiero mucho, porque eres *one in a million*. Muchas gracias por todo, y seguro que en el futuro conseguimos

estar más cerca, y emprender nuevas aventuras allá donde acabemos. *Y, por si no nos vemos luego: buenos días, buenas tardes y buenas noches.*

Las siguientes dos dedicatorias sé que son las que más me va a costar escribir, no solo por la intensidad de nuestra amistad, si no por la inmensidad de historia que hay detrás. Barqui y Diego, amigos insustituibles desde que empezó mi viaje en Madrid. Cada uno tenemos nuestras peculiaridades, que hacen de nuestras quedadas algo único. El año que pasamos juntos en aquel Colegio Mayor fue el mejor de nuestras vidas, con aquella lucha constante por la supervivencia, los cónclaves interminables donde revisábamos una y otra vez nuestros planes, los domingos de churros con chocolate, nuestras divagaciones y, sobre todo, nuestras grandes aventuras.

Barqui, el talaverano que terminó de introducirme en la pasión cinéfila, el hombre de las mil y una carreras que, por limitación autoimpuesta de caracteres, no voy a proceder a enumerar. Aquél a cuyo antepasado le arrebataron su apellido, a modo de castigo familiar atemporal, en una cruel muestra del poder de la realeza contra el fuego de la rebelión. Fuiste el mejor compañero de habitación que pude haber tenido: nuestros métodos organizativos, totalmente opuestos; nuestra adaptación mutua, como el mecanismo de un reloj suizo. Probablemente no haya habido ningún tema del que no hayamos debatido hasta horas intempestivas, y más probable es aún que sepamos más del otro que lo que él mismo pueda llegar a percibir. Muchas gracias a tu madre, Marina, que tanto me ha ayudado a lo largo de estos años, bien sea invitándome a pasar los veranos en Prado del Arca u orientándome profesionalmente. Una vez me dijo tu madre que, en Madrid, yo era como un hermano mayor para ti, y aunque en ese momento no le faltaba razón, ha pasado tanto tiempo que ya dudo de esa afirmación. Poco queda ya del antiguo Barqui, aquel joven con el pelo largo y aspecto descuidado que un día cogió su mochila y una garrafa vacía (llena de agua, como es lógico, pesaba demasiado), y se fue una semana a dormir con los lobos al Bosque Negro. Sin embargo, esa clase de aventuras que la mayoría denominarían imprudentes, y con razón, han contribuido a forjar una persona de la que estar orgulloso. Serás un gran médico, dios no lo quiera cirujano, y llegará un momento en el que ya no "lo des todo en clase" porque poseerás un vasto conocimiento sobre absolutamente todo.

Diego… Sé que ninguna de las palabras que te escriba te hará darte cuenta de todo lo que vales, pero el amor que has demostrado por la Física es algo que solo se ve una vez cada siglo. Aún recuerdo cuando, en aquellas esperas pre-cena en *los sofases*, tenías la libreta preparada para mostrarme lo que habías aprendido en la escuela. Llamabas así a la

universidad porque decías que, considerando su origen griego *scholē* (ocio/tiempo libre), el aprendizaje de algo que te enamora debe considerarse una forma de entretenimiento. Contigo me encantaba poner en cuestión, en una aplicación pura de mayéutica, toda clase de hipótesis y ecuaciones sobre el universo, como aquel ya famoso *cono de luz*. Sé que solo lo hacías por consolidar tus conocimientos (*tema 1, tema 1, tema 1*…), pero lo que nunca te dije era que yo lo hacía por forjar un vínculo contigo. Espero, de verdad, que retomes tu camino en la física, porque estás destinado a hacer cosas grandes. Gracias por generar esa locura contagiosa a tu alrededor, al percibir gatos magentas debido a tus alucinaciones y alteraciones de la realidad. Has sido mi compañero inseparable en este tiempo en Madrid, de piso en piso, y sobre todo de montaña en montaña. Porque efectivamente, eres el último tercio de personas imprescindibles para que una aventura sea digna de convertirse en memorable. No es solo porque fuiste scout, ni porque "encuentres" senderos que en lugar de sacarnos hagan que nos adentremos más en el bosque, sino porque tantos años en *el pozo* te han vuelto resistente a todo tipo de adversidades. He de decir, sin temor a equivocarme, que contigo he tenido las carcajadas más sonoras, y las más abundantes lágrimas de felicidad. Voy a omitir, sin embargo, que probablemente fueron al sobrevivir a alguna de tus brillantes ideas scout que nos adentraban *hacia rutas salvajes*.

Esther, no hay nada que pueda decirte que no sepas ya. Muchas gracias por toda tu comprensión y apoyo durante estos años, desde luego que te has convertido en alguien fundamental para mí. Ha sido un último año *relampagueantemente* frenético, pero sin duda el mejor de todos. Está claro que este mundo necesita más personas como tú, llevando felicidad y alegría con cada paso que das, pero eso mismo es lo que te hace única. Gracias por querer compartirlo conmigo.

Por supuesto agradecer a toda la familia Vicente, tan extensa que es imposible enumerar a todos sus componentes. Gracias por todo el apoyo recibido, por los ánimos que me habéis dado y por haber estado siempre a mi lado. Aunque estemos distribuidos por toda la geografía española, aún seguimos encontrando momentos para reunirnos, hacer barbacoas, cumpleaños y cafés. Gracias a todos y cada uno de vosotros, porque sin vuestro constante apoyo no estaría tampoco aquí.

Finalmente, mis más efusivas gracias las reservo para la familia más cercana, por haberme apoyado día a día y haber hecho posible que continuase investigando. Papá y mamá, sin vuestra generosidad no hubiese llegado hasta el final, gracias por enseñarme la constancia en los estudios y lo importante que es tener una buena educación. También por haberos

sacrificado tanto por mí, no solo en mi etapa en Salamanca si no también en Madrid, por ello os estaré eternamente agradecido. Gracias a mi hermano, Dani, con el que he tenido la suerte de haber crecido y desarrollado un vínculo de complicidad único. Aunque ya no vivamos juntos, sabes que me tienes aquí para todo lo que necesites. Carol, muchas gracias por haber estado también a mi lado en esta travesía. Espero que consigas tu objetivo de ser maestra, porque seguro que serás una excelente. Por supuesto gracias también a mi tía Eli, que nunca ha dudado en ofrecerme valiosos consejos, y apoyarme durante mi estancia en Madrid. A sus padres: Titi, que siempre estuvo ahí con una memoria prodigiosa; y Boni, que falleció con la enfermedad de Alzheimer; ambos grandes personas. Gracias a mi tío Mero, una persona amable allá donde las haya, siempre con una sonrisa y rememorando historias de su juventud. Abuela, eres un claro ejemplo de superación, demostrando con fortaleza ser una auténtica luchadora contra el cáncer. Muchas gracias por todo el cariño que me das, y estoy muy contento por haber tenido una abuela como tú.

Sin duda esta sección de agradecimientos es extremadamente extensa. No obstante, es inevitable, ya que estoy en deuda con todas las personas que aquí han sido mencionadas, y así debe constar. Y, no pudiendo ser de otra forma, el final de la misma lo reservo para una persona que fue muy especial para mí. Todos tenemos a alguien que nos ha marcado a lo largo de nuestra vida, y sin la que el rumbo que hemos emprendido hubiese sido sumamente diferente. Muchas gracias, abuelo, por haber despertado en mí toda esa curiosidad acerca de todo lo que nos rodea, por plantearme siempre acertijos y adivinanzas que retaban mi mente, por ser mi primera pareja de tute y mi último oponente de ajedrez. Aún recuerdo aquellos fines de semana cuando era un niño en los que, mientras tú te devanabas los sesos completando crucigramas en las últimas páginas de algún periódico, yo resolvía sudokus a tu lado. Desde luego que mi pasión por la lectura se vio alentada al tener un abuelo escritor de varios libros. Fuiste un referente a seguir, ya que pese a tus humildes orígenes como pastor *chinato*, oriundo de Malpartida de Plasencia, en las dehesas extremeñas, no dejaste nunca de intentar aprender. Mientras los demás niños tenían el privilegio de poder estudiar en la escuela, no perdías ocasión de mirar a través de la ventana cómo los maestros impartían sus lecciones, impregnándote de ladrillos de conocimiento con los cuales tú podías construir edificios. Tuve la suerte de poder compartir mucho tiempo contigo hasta que, lamentablemente y por azares de la vida, sufriste aquel accidente que bien me podría haber sucedido a mí. Como dijo Plutarco, "*el cerebro no es una vasija que se deba llenar, si no una chispa por encender*". Tú fuiste aquella chispa, por ello ojalá estuvieses aquí para ver todo lo que hemos conseguido. Espero que, allá donde estés, también lleguen los periódicos con crucigramas.

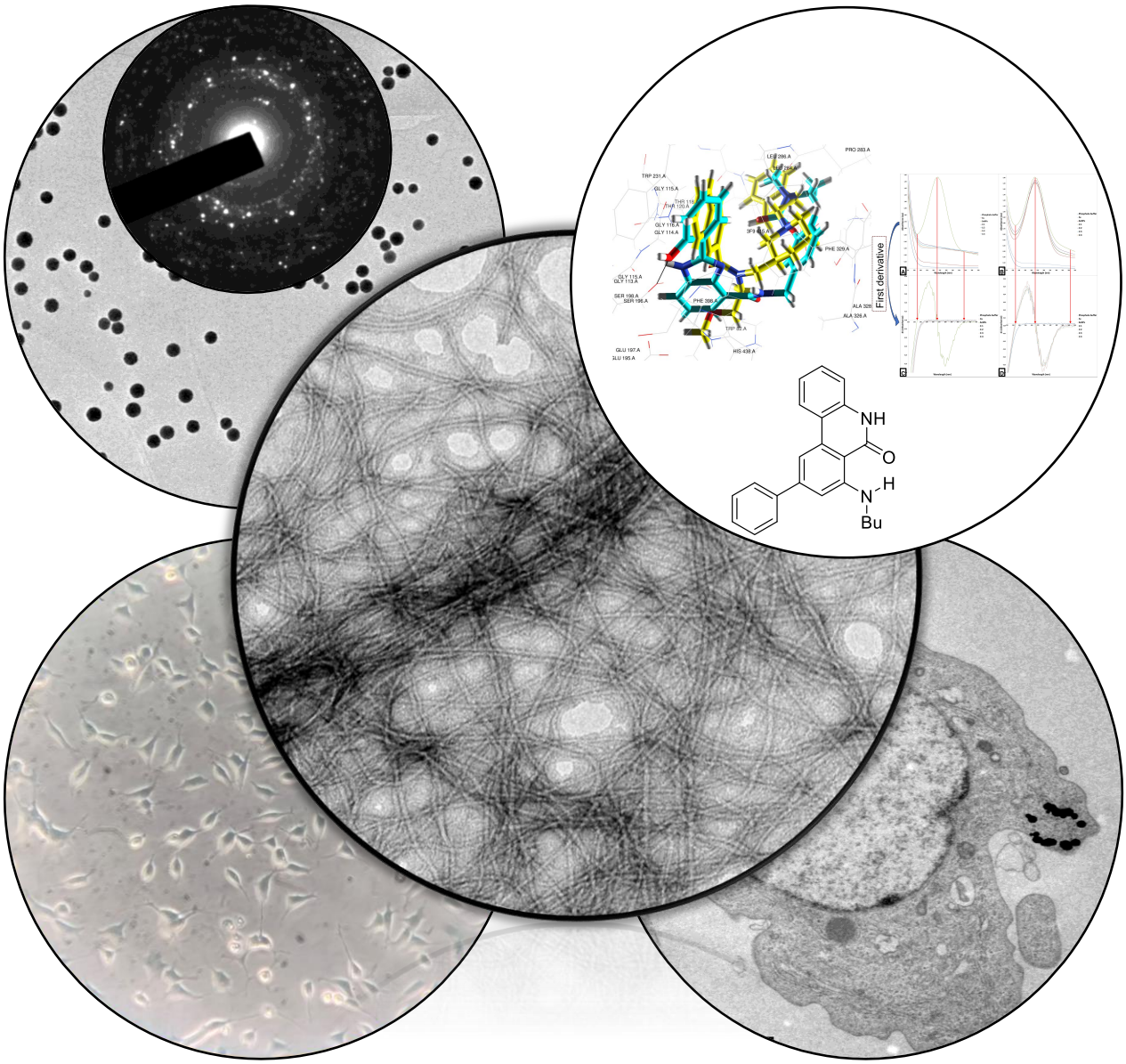
A mi abuelo

Cuando recordar no pueda,
¿dónde mi recuerdo irá?
Una cosa es el recuerdo
y otra cosa recordar.

Antonio Machado

EFECTO NEUROPROTECTOR DE MOLÉCULAS ORGÁNICAS Y NANOPARTÍCULAS DE SELENIO EN LA ENFERMEDAD DE ALZHEIMER

NEUROPROTECTIVE EFFECT OF ORGANIC MOLECULES AND SELENIUM NANOPARTICLES ON ALZHEIMER'S DISEASE



DAVID VICENTE ZURDO

DIRECTORAS:
YOLANDA MADRID ALBARRÁN MARÍA
EUGENIA DE LEÓN GONZÁLEZ NOELIA
ROSALES CONRADO

ÍNDICE

ÍNDICE

I. GLOSARIO DE TÉRMINOS 29

II. RESUMEN 37

III. SUMMARY 45

IV. INTRODUCCIÓN 53

1. ENFERMEDADES NEURODEGENERATIVAS 53
2. ENFERMEDAD DE ALZHEIMER 55
   2.1. Principales hipótesis involucradas en el desarrollo de la enfermedad de Alzheimer 58
   2.2. Proteína beta-amiloide (Aβ) 61
   2.3. Efecto de los metales y de los aminoácidos en la enfermedad de Alzheimer 65
3. MOLÉCULAS ORGÁNICAS COMO POSIBLES FÁRMACOS EN LA ENFERMEDAD DE ALZHEIMER 79
4. IMPORTANCIA DEL SELENIO EN LA ENFERMEDAD DE ALZHEIMER 87
   4.1. Especies de selenio 89
   4.2. Nanopartículas de selenio como posibles agentes neuroprotectores 93
5. TÉCNICAS Y MÉTODOS (BIO)ANALÍTICOS PARA LA CARACTERIZACIÓN Y LA EVALUACIÓN DE LA CAPACIDAD NEUROPROTECTORA DE MOLÉCULAS ORGÁNICAS Y DE ESPECIES DE SELENIO 95
   5.1. Técnicas analíticas para los estudios de inducción e inhibición de la agregación de la proteína $A\beta_{42}$, inhibición enzimática y capacidad antioxidante 95
      5.1.1. Caracterización de nanopartículas de selenio como agente inhibidor de la agregación de la proteína $A\beta_{42}$ 96
      5.1.2. Estudio de las interacciones con metales y aminoácidos 97
      5.1.3. Determinación de la inhibición enzimática 98
      5.1.4. Evaluación de la capacidad antioxidante 99
   5.2. Técnicas bioinformáticas para la síntesis inteligente de fármacos 100
      5.2.1. Diseño y modelización computacional 100
      5.2.2. Predicción de propiedades farmacocinéticas 101
   5.3. Técnicas bioanalíticas para el estudio *in vitro* del efecto de metales, moléculas orgánicas y nanopartículas de selenio en líneas celulares de fenotipo neuronal 103
      5.3.1. Evaluación de la viabilidad celular 103
      5.3.2. ICP-MS como herramienta para el estudio de la acumulación de metales y nanopartículas en células individuales 104
      5.3.3. Microscopía electrónica de transmisión para evaluar la localización intracelular de nanopartículas en cultivos celulares 106
      5.3.4. Reducción de la toxicidad de la proteína $A\beta_{42}$ y de metales en líneas celulares neuronales 106
      5.3.5. Reducción del estrés oxidativo en células 107
      5.3.6. Contenido proteínico total y expresión génica de proteínas de choque térmico y proteosomas en células 108
      5.3.7. Contenido de la proteína $A\beta_{42}$ en células 108
      5.3.8. Análisis de la actividad de las caspasas en apoptosis celular 108
   5.4. Técnicas quimiométricas para la evaluación de propiedades neuroprotectoras 108

V. REFERENCIAS....113

VI. OBJETIVOS....157

VII. OBJECTIVES....163

VIII. PARTE EXPERIMENTAL....169

1. SÍNTESIS DE MOLÉCULAS ORGÁNICAS Y EVALUACIÓN DE SUS PROPIEDADES FISICOQUÍMICAS Y BIOLÓGICAS EN LA ENFERMEDAD DE ALZHEIMER....169

Artículo 1: Acción neuroprotectora de derivados multi-diana de la 7-aminofenantridin-6(5H)-ona frente a la muerte celular inducida por metales y el estrés oxidativo empleando la línea celular SN56 175

Artículo 2: Mecanismos neuroprotectores de derivados multi-diana de la 7-aminofenantridin-6(5H)-ona frente a la generación y agregación de proteínas amiloides inducida por metales 199

Artículo 3: Nuevos derivados de la rivastigmina como compuestos multi-diana prometedores para el tratamiento potencial de la enfermedad de Alzheimer....219

2. EVALUACIÓN DE LAS PROPIEDADES FISICOQUÍMICAS Y BIOLÓGICAS DE NANOPARTÍCULAS DE SELENIO EN LA ENFERMEDAD DE ALZHEIMER....253

Artículo 4: Capacidad de las especies de selenio para inhibir la agregación Aβ inducida por metales involucrados en el desarrollo de la enfermedad de Alzheimer....259

Artículo 5: Actividad neuroprotectora de las nanopartículas de selenio frente al efecto de enantiómeros de aminoácidos en la enfermedad de Alzheimer....275

Artículo 6: Acumulación de nanopartículas de selenio y otras especies de selenio en líneas celulares de neuroblastoma relacionadas con la enfermedad de Alzheimer mediante TEM y single cell-ICP-MS 291

IX. DISCUSIÓN INTEGRADORA....333

X. CONCLUSIONES....367

XI. CONCLUSIONS....375

XII. ANEXO-PRODUCCIÓN CIENTÍFICA....383

A.1. ARTÍCULOS CIENTÍFICOS INCLUIDOS EN LA TESIS DOCTORAL....383

A.2. OTROS ARTÍCULOS CIENTÍFICOS....383

A.3. COMUNICACIONES A CONGRESOS....384

A.4. ESTANCIAS DE INVESTIGACIÓN Y COLABORACIONES....386

A.5. OTROS MÉRITOS....387

A.6. COMPETENCIAS LINGÜÍSTICAS....387

I.GLOSARIO DE TÉRMINOS

I. GLOSARIO DE TÉRMINOS

AcD	Dominio ácido Acidic domain
ACh	Acetilcolina Acetylcholine
AChE	Acetilcolinesterasa Acetylcholinesterase
AChEi	Inhibidor de la acetilcolinesterasa Inhibitor of acetylcholinesterase
AD	Enfermedad de Alzheimer Alzheimer's disease
ADMET	Absorción, distribución, metabolismo, excreción y toxicidad Absorption, distribution, metabolism, excretion and toxicity
ADMETsar	Relación estructura-actividad ADMET ADMET structure−activity relationship
AICD	Dominio intracelular del APP APP intracelular domain
ANOVA	Análisis de la varianza Analysis of variance
APOE	Apolipoproteína E Apolipoprotein E
APP	Proteína precursora amiloide Amyloid precursor protein
AS	Sitio de unión aniónico Anionic substrate binding site
Aβ	Proteína beta-amiloide Amyloid beta-protein
$A\beta_{40}$	Proteína beta-amiloide fragmento 1-40 Amyloid beta-protein fragment 1-40
$A\beta_{42}$	Proteína beta-amiloide fragmento 1-42 Amyloid beta-protein fragment 1-42
AβOs	Oligómeros de la proteína beta-amiloide Beta-amyloid protein oligomers
BACE1	Enzima β-secretasa de la APP β- site – APP – cleaving enzyme
BBB	Barrera hematoencefálica Blood brain barrier
BCh	Butirilcolina Butyrylcholine
BChE	Butirilcolinesterasa Butyrylcholinesterase
BChEi	Inhibidor de la butirilcolinesterasa Inhibitor of butyrylcholinesterase
BIM	Hidroxifenilbenzimidazol Hydroxyphenylbenzimidazole

Caco-2	Células de adenocarcinoma colorrectal humano Human colorectal carcinoma cell
CAS	Sitio catalítico aniónico Catalitic anionic site
CGA	Ácido clorogénico Chlorogenic acid
CGA@ChSeNPs	Nanopartículas de selenio estabilizadas con quitosano y ácido clorogénico Selenium nanoparticles stabilized with chitosan and chlorogenic acid
Ch-SeNPs	Nanopartículas de selenio estabilizadas con quitosano Selenium nanoparticles stabilized with chitosan
cLC-DAD	Cromatografía de líquidos capilar con detector de diodos Capillary liquid chromatography with diode array detection
CNS	Sistema nervioso central Central nervous system
CuBD	Dominio de unión del cobre Copper binding domain
d1(UV-Vis)	Primera derivada de la espectroscopía ultravioleta-visible First derivative of ultraviolet-visible spectroscopy
DASPO	D-Aspartato oxidasa D-aspartate oxidase
DCF	2',7'-diclorofluoresceína 2',7'-dichlorofluorescein
DCFH-DA	Diacetato de 2',7'-dihidrodiclorofluoresceina 2',7'-dichlorodihydrofluorescein diacetate
DLS	Dispersión dinámica de luz Dynamic light scattering
DMHP	1,2-dimetil-3-hidroxi-4-piridona 1,2-dimethyl-3-hydroxy-4-pyridinone
DNP	Donepezilo Donepezil
DOE	Diseño de experimentos Design of experiments
DPPH	2,2-difenil-1-picrilhidrazilo 2,2-diphenyl-1-picrylhydrazyl
DS	Síndrome de Down Down syndrome
DTNB	Ácido 5,5-ditio-bis-(2-nitrobenzoico) 5,5'-dithiobis-(2-nitrobenzoic) acid
ED	Difracción electrónica Electron diffraction
EDXS	Espectroscopía de energía dispersiva de rayos-X Energy-dispersive X-ray spectroscopy
EOAD	Enfermedad de Alzheimer de inicio temprano Early- onset Alzheimer's disease
ES	Subsitio esteárico Esteratic subsite

ESI-MS	Ionización por electroespray con detección de espectrometría de masas Electrospray ionization with mass spectrometry detection
FAD	Enfermedad de Alzheimer familiar Familial Alzheimer's disease
GFLD	Dominio del factor de crecimiento Growth factor-like domain
GPx	Glutatión peroxidasas Glutathione peroxidases
GPx1	Glutatión peroxidasa 1 Glutathione peroxidase 1
GPx4	Glutatión peroxidasa 4 Glutathione peroxidase 4
HD	Enfermedad de Huntington Huntington's disease
HFIP	1,1,1,3,3,3-hexafluoro-2-propanol 1,1,1,3,3,3-hexafluoro-2-propanol
HOMO	Orbital molecular ocupado más alto Highest occupied molecular orbital
HSA	Albúmina de suero humano Human serum albumin
HSP70	Proteína de choque térmico 70 Heat shock protein 70
Hup	Huperzina Huperzine
IC_{50}	Concentración media inhibitoria Half maximal inhibitory concentration
ICP-MS	Plasma acoplado inductivamente con analizador de espectrometría de masas Inductively coupled plasma with mass spectrometer analyzer
JMR	Región yuxtamembrana Juxtamembrane region
KBD	Enfermedad de Kashin-Beck Kashin-Beck disease
KD	Enfermedad de Keshan Keshan disease
Keap1	Proteína 1 asociada a ECH tipo Kelch Kelch-like ECH-associated protein 1
KPI	Inhibidor de proteasa tipo Kunitz Kunitz-type protease inhibitor
LC_{50}	Concentración letal para el 50% de la población Lethal concentration for 50% cell population
LOAD	Enfermedad de Alzheimer de inicio tardío Late-onset Alzheimer's disease
LSD	Diferencia menos significativa Least significant difference
LUMO	Orbital molecular vacío más bajo Lowest unoccupied molecular orbital

m/z	Relación masa-carga Mass-to-charge ratio
MBD	Dominio de unión metálica Metal-binding domain
MDA	Malondialdehido Malondialdehyde
MDCK	Células de riñón canino de Madin-Darby Madin–Darby canine kidney cell
MeSeCys	Selenometilselenocisteína Selenomethylselenocysteine
MMPs	Metaloproteasas de matriz Matrix metalloproteases
MsrB1	Metionina sulfóxido reductasa Methionine sulfoxide reductase
MT	Metiltioninio Methylthioninium
MTT	Bromuro de 3-(4,5- dimetiltiazol-2-ilo)-2,5-difeniltetrazol 3-[4,5-dimethylthiazol-2-yl]-2,5 diphenyl tetrazolium bromide
Neuro-2a	Células de neuroblastoma de ratón Mouse neuroblastoma cells
NFTs	Ovillos neurofibrilares Neurofibrillary tangles
NMDA	N-metil-D-aspartato N-methyl-D-aspartate
Nrf2	Factor nuclear eritroide 2 Nuclear factor erythroid 2-related factor 2
OPA	Orto-ftalaldehído O-phthaldialdehyde
P19S	Proteosoma 19S Proteasome 19S
P20S	Proteosoma 20S Proteasome 20S
P26S	Proteosoma 26S Proteasome 26S
PAS	Sitio periférico de unión aniónico Peripheral anionic binding site
PCA	Análisis de componentes principales Principal component analysis
PD	Enfermedad de Parkinson Parkinson's disease
PDB	Banco de datos de proteínas Protein Data Bank
PI	Yoduro de propidio Propidium iodide
PLC	Placas de capa preparativa Preparative layer plates

PSA	Área de superficie polar de Van der Waals de átomos de oxígeno y nitrógeno Van der Waals surface area of polar nitrogen and oxygen atoms
RIV	Rivastigmina Rivastigmine
RMN	Resonancia magnética nuclear Nuclear magnetic resonance
ROS	Especies reactivas de oxígeno Reactive oxygen species
RSM	Metodología de superficie de respuesta Response surface methodology
SAD	Enfermedad de Alzheimer esporádica Sporadic Alzheimer's disease
SC-ICP-MS	Detección individual de células mediante plasma acoplado inductivamente con analizador de espectrometría de masas Single cell inductively coupled plasma with mass spectrometer analyser
SeCys	Selenocisteína Selenocysteine
SeMet	Selenometionina Selenomethionine
SeNPs	Nanopartículas de selenio Selenium nanoparticles
SH-SY5Y	Células de neuroblastoma humano Human neuroblastoma cells
SI	Índice de selectividad AChE/BChE Selectivity index AChE/BChE
SN56	Células de prosencéfalo basal murino Basal forebrain murine cells
SOD	Superóxido dismutasa Superoxide dismutase
TAC	Tacrina Tacrine
TBA	Ácido tiobarbitúrico Tiobarbituric acid
TBARS	Sustancias reactivas del ácido tiobarbitúrico Thiobarbituric acid reactive substances
TEM	Microscopía electrónica de transmisión Transmission electron microscopy
ThT	Tioflavina T Thioflavin T
TLC	Cromatografía en capa fina Thin layer chromatography
TNB	Ácido 5-tio-2-nitrobenzoico 5-thio-2-nitrobenzoic acid
UV-Vis	Ultravioleta-visible Ultraviolet-visible
ZP	Potencial zeta Zeta potential

II.RESUMEN

II. RESUMEN

Las **enfermedades neurodegenerativas** se caracterizan por un progresivo deterioro en los aspectos cognitivos, como la memoria, el lenguaje, el comportamiento y la capacidad ejecutiva, siendo el envejecimiento el principal factor de riesgo. Suponen un gran reto para la sociedad, ya que son el primer motivo de discapacidad y la segunda causa de muerte a nivel global. Actualmente, afectan a más de 50 millones de personas en todo el mundo, con solo el 25% de los pacientes diagnosticados oficialmente, y estando previsto que alcancen los 152 millones de afectados para el año 2050. Por el momento no hay tratamientos efectivos para estos desórdenes neurológicos, con el consiguiente elevado coste socioeconómico que ello conlleva. Las cuatro enfermedades neurodegenerativas más frecuentes son la **enfermedad de Alzheimer** (**AD**), la enfermedad de Parkinson (PD), la esclerosis lateral amiotrófica (ALS) y la enfermedad de Huntington (HD). De entre ellas, la AD es la más prevalente, representando un 80% del total de los casos de demencia.

La AD se caracteriza por el deterioro progresivo de la memoria y la disfunción cognitiva, debido a la pérdida masiva de neuronas del hipocampo, lo que conlleva cambios de personalidad, dificultades en el habla y la deglución, y desencadena fallos en el sistema respiratorio o circulatorio. Se manifiesta histológicamente por la deposición extracelular de placas de la **proteína beta-amiloide** (**$A\beta_{42}$**) y la formación intracelular de ovillos neurofibrilares de la proteína tau (p-tau) en las neuronas.

A pesar de que se desconoce el origen de la AD, existen varias hipótesis sobre cómo se desencadena dicha enfermedad, siendo la "**hipótesis de la cascada amiloide**" la que reúne, actualmente, un mayor consenso. Esta hipótesis considera que la **agregación de la proteína $A\beta_{42}$** es el suceso primario que desencadena los eventos correspondientes a la cascada amiloide, conduciendo a la pérdida masiva de neuronas. Las **placas amiloides extracelulares** afectan a las sinapsis interneuronales, reducen la respiración mitocondrial neuronal, favorecen la hiperfosforilación intercelular de la p-tau afectando al metabolismo neuronal y a los microtúbulos, provocan neuroinflamación y, finalmente, desencadenan la muerte neuronal. Al mismo tiempo, la agregación de la proteína $A\beta_{42}$ se explica a través de la "**hipótesis del ion metálico**", estando por tanto en total sinergia con la "**hipótesis de la cascada amiloide**". De esta forma, la dishomeostasis en las concentraciones de **biometales** y **metales tóxicos** en el cerebro favorece la agregación de la proteína $A\beta_{42}$, debido a su interacción con dicha proteína y al estrés oxidativo que producen. Por otro lado, el **desequilibrio enantiomérico de ciertos aminoácidos** también influye en la

agregación amiloide, debido a las propiedades neurotóxicas que poseen los D-aminoácidos, favoreciendo la deposición de la proteína $A\beta_{42}$ en placas amiloides.

Por todo ello, y debido a la **naturaleza multifactorial** de la enfermedad, las estrategias actuales para combatirla se centran en la búsqueda de **compuestos multi-diana**. En este sentido, las **moléculas orgánicas**, y la síntesis de híbridos entre ellas, ofrecen una amplia variedad de propiedades neuroprotectoras, entre las que destacan la inhibición de la agregación de la proteína $A\beta_{42}$, la quelación de metales, la capacidad antioxidante y la inhibición de las enzimas acetilcolinesterasa (AChE) y butirilcolinesterasa (BChE). Otro elemento clave es el **selenio**, debido a sus múltiples beneficios para la salud. En concreto, las **nanopartículas de selenio** (**SeNPs**) pueden ser funcionalizadas con diversos compuestos, aportando propiedades únicas contra la AD.

En este sentido, la presente Tesis Doctoral titulada "**Efecto neuroprotector de moléculas orgánicas y nanopartículas de selenio en la enfermedad de Alzheimer. Neuroprotective effect of organic molecules and selenium nanoparticles on Alzheimer's disease**" ha tenido como objetivo principal la evaluación de las propiedades neuroprotectoras de cinco moléculas orgánicas **derivadas de la 7-aminofenantridin-6-ona (APH)**, de siete moléculas orgánicas híbridas entre la rivastigmina y el hidroxifenilbenzimidazol (**RIV-BIM**) y de **nanopartículas de selenio estabilizadas con quitosano** (**Ch-SeNPs**). Como propiedades neuroprotectoras se han evaluado la capacidad de quelación metálica, la reducción del estrés oxidativo, la inhibición de la agregación de la proteína $A\beta_{42}$ y la inhibición de las enzimas AChE y BChE. Con respecto a las técnicas utilizadas para evaluar la neuroprotección cabe destacar la espectroscopía UV-Vis y su primera derivada (d^1(UV-Vis)), la espectroscopía de fluorescencia, la microscopía electrónica de transmisión (TEM), ensayos *in vitro* con líneas celulares de fenotipo neuronal (Neuro-2a, SH-SY5Y y SN56) empleando espectroscopía UV-Vis y citometría de flujo, el uso de single cell-ICP-MS (SC-ICP-MS), la modelización computacional y herramientas de predicción *in silico*.

Las cinco moléculas **APH** fueron estudiadas en términos de **quelación metálica** frente a **biometales** (Fe(II), Cu(II) y Zn(II)) y **metales tóxicos** (Hg(II), Cd(II) y Al(III)) involucrados en la AD, empleando para ello la espectroscopía de absorción UV-Vis, d^1(UV-Vis) y análisis computacionales *in silico* de los orbitales HOMO y LUMO. Dichas moléculas interaccionaron con Fe(II) y Cu(II), y en algunos casos también con Hg(II), siendo posible determinar la relación de concentración metal:APH óptima de la

interacción. Mediante ensayos *in vitro* con la línea celular SN56, las moléculas evaluadas demostraron **reducir la citotoxicidad, el estrés oxidativo y la peroxidación lipídica inducidos por los metales.** Mediante TEM, se evaluó la capacidad de las moléculas APH de **inhibir la agregación de la proteína Aβ$_{42}$**, inducida por biometales y metales tóxicos. Las moléculas APH no solo demostraron una **alta capacidad anti-amiloidogénica**, inhibiendo directamente la agregación amiloide, si no que aumentaron la expresión de **proteínas de choque térmico** (**HSP70**) y **proteosomas** (**P20S**), encargadas de la degradación de la proteína Aβ$_{42}$. Estas moléculas APH también **disminuyeron** *in vitro* la **citotoxicidad** y la **actividad apoptótica** inducidas por la Aβ$_{42}$. Mediante métodos *in silico*, se predijeron las **propiedades farmacocinéticas** y las propiedades de absorción, distribución, metabolismo, excreción y toxicidad (**ADMET**), siendo todas ellas aceptables. Por ello, las moléculas APH se podrían considerar como potenciales candidatos a fármacos en la AD.

Las siete moléculas **híbridas RIV-BIM** se sintetizaron, purificaron y caracterizaron con éxito, empleando cromatografía en capa fina (TLC), resonancia magnética nuclear (RMN) de ^{1}H y ^{13}C, ionización por electroespray con detección de espectrometría de masas (ESI-MS) (+/-) y medidas del punto de fusión. Mediante herramientas de modelización computacional *in silico* y técnicas como la espectroscopía UV-Vis, se ha demostrado la **inhibición de las enzimas AChE y BChE** por parte de los híbridos RIV-BIM aumentando, por tanto, los niveles de neurotransmisores tan importantes como la **acetilcolina** (**ACh**) y **butirilcolina** (**BCh**), y retrasando los síntomas de la AD. Mediante TEM y espectroscopía de fluorescencia, se estudió la **inhibición de la agregación de la proteína Aβ$_{42}$**, propia e inducida por el Cu(II), siendo algunos de estos híbridos altamente anti-amiloidogénicos al inhibir la acumulación de dicha proteína. Mediante el ensayo *in vitro* del MTT empleando la línea celular SH-SY5Y, se observó la capacidad de algunos híbridos para **reducir la citotoxicidad de la proteína Aβ$_{42}$** y **reducir el estrés oxidativo** generado por el Fe(II). Por último, la predicción *in silico* de las **propiedades farmacocinéticas** de las moléculas RIV-BIM ha demostrado la idoneidad de dichos híbridos como fármacos potenciales para ser administrados por vía oral. Estos resultados han evidenciado las ventajas de la **hibridación** para contrarrestar la naturaleza multifactorial de la AD.

Finalmente, se evaluaron las propiedades neuroprotectoras de las **Ch-SeNPs** frente a **biometales** y **enantiómeros de aminoácidos**. Con este fin, se sintetizaron las Ch-SeNPs y se caracterizaron mediante TEM, espectroscopía de energía dispersiva de rayos-X (EDXS), difracción electrónica (ED) y dispersión dinámica de luz (DLS). Posteriormente,

se evaluaron las propiedades de **quelación metálica** de diversas especies de selenio frente a biometales, incluidas las Ch-SeNPs, mediante UV-Vis y d^1(UV-Vis). Se determinó la **capacidad antioxidante** de las especies de selenio mediante espectroscopía UV-Vis empleando el método DPPH, y manifestando las Ch-SeNPs una elevada capacidad antioxidante en comparación al resto de especies de selenio estudiadas. Además, se evaluó la capacidad antioxidante de ciertos **enantiómeros de aminoácidos** involucrados en la AD mediante los métodos DPPH y TBARS, no mostrando ninguno de ellos un efecto significativo en la reducción del estrés oxidativo. La **agregación de la proteína Aβ_{42}** bajo el efecto de **biometales**, **especies de selenio** y **enantiómeros de aminoácidos** se estudió mediante TEM. Así, se puso de manifiesto el papel que ejercen los biometales aumentando la agregación amiloide, en consonancia con la "**hipótesis del ion metálico**". El entorno quiral también afectó a la agregación de la proteína Aβ_{42}, siendo inducida **enantioméricamente** por determinados aminoácidos, principalmente D-enantiómeros. Sin embargo, las Ch-SeNPs lograron **inhibir la agregación** inducida por los biometales y, posteriormente, **desagregar las fibras de la proteína Aβ_{42}**. Además, debido al quitosano que estabiliza las Ch-SeNPs y les confiere **propiedades quirales**, fueron capaces de **inhibir la agregación enantioméricamente inducida por los aminoácidos amiloidogénicos**. Por ello, se estudió la interacción de las Ch-SeNPs con los enantiómeros de aminoácidos involucrados en la AD mediante espectroscopía UV-Vis y espectroscopía de fluorescencia, previa derivatización de los enantiómeros con orto-ftalaldehído (OPA). Esta **interacción** resultó ser **enantioselectiva**, interaccionando predominantemente las Ch-SeNPs con el enantiómero D de los aminoácidos, siendo esta forma la no presente de forma natural en el organismo humano. Mediante ensayos *in vitro* empleando el método del MTT, se determinó la **citotoxicidad** de las Ch-SeNPs frente a **líneas celulares de fenotipo neuronal**, demostrando que el efecto neuroprotector ejercido por las nanopartículas es eficaz a concentraciones siete veces menores a la concentración letal para el 50% de la población (LC_{50}). Empleando TEM, se observó la presencia de las Ch-SeNPs en lugares clave de las células SH-SY5Y, destacando su **adhesión a la membrana extracelular**, las **mitocondrias**, el interior del **núcleo** y el nucleolo. De tal forma que las Ch-SeNPs podrían inhibir y/o reducir la agregación extracelular de la proteína Aβ_{42}, y disminuir el nivel de ROS que producen la oxidación del ADN mitocondrial, haciendo frente a la progresión de la AD. Finalmente, mediante SC-ICP-MS se cuantificó la **masa de selenio acumulada** por **célula individual**, al exponer las líneas celulares SH-SY5Y y Neuro-2a a tres niveles de concentración de las especies de

selenio, siendo las Ch-SeNPs las **más fácilmente asimiladas** por las células y presentando una elevada variabilidad en la población estudiada.

Como resumen de la presente Tesis Doctoral, se puede destacar la necesidad de emplear una amplia variedad de **métodos y técnicas multidisciplinares** para la evaluación de las **propiedades neuroprotectoras** de posibles fármacos contra la **AD**, y el uso de herramientas quimiométricas para la correcta interpretación, análisis y comparación de resultados. De entre las diversas propiedades neuroprotectoras presentadas por los compuestos evaluados en esta Tesis Doctoral, se pueden destacar la **quelación de biometales y metales tóxicos** y la **reducción** de la **citotoxicidad** y del **estrés oxidativo** generados por los mismos, interviniendo de esta forma en la "**hipótesis del ion metálico**". Otro aspecto fundamental en la evaluación de potenciales fármacos es la capacidad de **inhibir la agregación de la proteína $A\beta_{42}$ inducida por biometales, metales tóxicos y enantiómeros de aminoácidos**, de forma directa o indirecta, y de **reducir la citotoxicidad** *in vitro* de dicha proteína, frenando la cascada amiloide y evitando la neurodegeneración. Algunos de los compuestos evaluados, según los resultados obtenidos mediante los ensayos de **inhibición de la AChE y BChE**, podrían aumentar los niveles de neurotransmisores como la **ACh** y la **BCh**, retrasando la neurodegeneración. Las predicciones *in silico* de las **propiedades farmacocinéticas** de las moléculas orgánicas confirman su uso potencial como fármacos frente a la AD. Así, considerando los resultados obtenidos en esta Tesis Doctoral, los compuestos más prometedores en la AD serían la molécula **APH4**, sobresaliendo en la mayoría de las propiedades neuroprotectoras objeto de estudio; las moléculas híbridas RIV-BIM pertenecientes a la serie 5 (**5a**, **5b** y **5d**), que poseen elevadas propiedades anti-amiloidogénicas frente a la agregación de la proteína $A\beta_{42}$ y de reducción *in vitro* del estrés oxidativo; y las **Ch-SeNPs**, que muestran una elevada capacidad de inhibición de la agregación de la proteína $A\beta_{42}$ y de desagregación de sus fibras, así como una considerable interacción enantioselectiva con los principales aminoácidos involucrados en la AD y la interacción *in vitro* con células de neuroblastoma.

III.SUMMARY

III. SUMMARY

Neurodegenerative diseases are characterised by a progressive impairment in cognitive aspects such as memory, language, behaviour, and executive capacity, with ageing being the main risk factor. They represent a major challenge for society since they are the leading cause of disability and the second leading cause of death globally. Currently, they affect more than 50 million people worldwide, with only 25% of patients officially diagnosed, and projected to reach 152 million by 2050. Now, there are no effective treatments for these neurological disorders, with the resulting high socio-economic costs. The four most widespread neurodegenerative diseases are **Alzheimer's disease** (**AD**), Parkinson's disease (PD), amyotrophic lateral sclerosis (ALS) and Huntington's disease (HD). Among these, AD is the most prevalent, representing 80% of the total number of dementia cases.

AD is characterised by a progressive memory impairment and cognitive dysfunction, due to massive loss of hippocampal neurons, leading to personality changes, speech and swallowing difficulties, triggering respiratory or circulatory system failures. It is histologically manifested by extracellular deposition of **beta-amyloid** (**$A\beta_{42}$**) **protein** plaques and intracellular formation of neurofibrillary tangles of tau protein (p-tau) in neurons.

Although the origin of AD remains unclear, there are several hypotheses concerning how the disease is triggered, being the "**amyloid cascade hypothesis**" the most widely accepted one at the present time. This hypothesis considers the **aggregation of the $A\beta_{42}$ protein** to be the primary event that triggers the amyloid cascade, leading to the massive loss of neurons. **Extracellular amyloid plaques** affect interneuronal synapses, reduce neuronal mitochondrial respiration, promote intercellular hyperphosphorylation of p-tau affecting neuronal metabolism and microtubules, cause neuroinflammation, and finally trigger neuronal death. At the same time, the aggregation of the $A\beta_{42}$ protein is explained through the "**metal ion hypothesis**", thus being in full synergy with the "**amyloid cascade hypothesis**". Hence, the dishomeostasis of the concentrations of **biometals** and **toxic metals** in the brain favours the aggregation of the $A\beta_{42}$ protein, due to their interaction with such protein and the oxidative stress they produce. On the other hand, the **enantiomeric imbalance of certain amino acids** also influences amyloid aggregation, due to the neurotoxic properties of D-amino acids, favouring the deposition of $A\beta_{42}$ protein in amyloid plaques.

On this basis, and due to the **multifactorial nature** of the disease, current strategies to mitigate AD focused on the development of **multi-target compounds** are being developed. In this regard, **organic molecules**, and particularly, the synthesis of hybrids between them, exhibit a wide variety of neuroprotective properties, including inhibition of $A\beta_{42}$ protein aggregation, metal chelation, antioxidant capacity and inhibition of acetylcholinesterase (AChE) and butyrylcholinesterase (BChE) enzymes. Another key element is **selenium**, which has multiple health benefits. Specifically, **selenium nanoparticles** (**SeNPs**) can be functionalised with various compounds, providing unique properties against AD.

For all these reasons, the present Doctoral Thesis entitled "**Efecto neuroprotector de moléculas orgánicas y nanopartículas de selenio en la enfermedad de Alzheimer. Neuroprotective effect of organic molecules and selenium nanoparticles on Alzheimer's disease**" is focused on the evaluation of the neuroprotective properties of five organic molecules **derived from 7-aminophenanthrenanthridin-6-one** (**APH**), seven hybrid organic molecules between rivastigmine and hydroxyphenylbenzimidazole (**RIV-BIM**) and **selenium nanoparticles stabilised with chitosan** (**Ch-SeNPs**). Neuroprotective properties evaluated include metal chelation, reduction of oxidative stress, inhibition of $A\beta_{42}$ protein aggregation and inhibition of AChE and BChE enzymes. With regard to the techniques used to assess neuroprotection, it is worth mentioning UV-Vis spectroscopy and its first derivative (d^1(UV-Vis)), fluorescence spectroscopy, transmission electron microscopy (TEM), *in vitro* assays with neuronal phenotype cell lines (Neuro-2a, SH-SY5Y and SN56) employing UV-Vis spectroscopy and flow cytometry, single cell-ICP-MS (SC-ICP-MS), computational modelling and *in silico* prediction tools.

The five target **APH** molecules were studied in terms of **metal chelation** towards **biometals** (Fe(II), Cu(II) and Zn(II)) and **toxic metals** (Hg(II), Cd(II) and Al(III)) involved in AD and by using UV-Vis, d^1(UV-Vis) absorption spectroscopy and in silico computational analysis of the HOMO and LUMO orbitals. These molecules interacted with Fe(II) and Cu(II), and in some cases also with Hg(II), being possible to estimate the optimum APH:metal interaction relationship. By using *in vitro* assays with SN56 cell line, the molecules under evaluation also demonstrated a **reduction in cytotoxicity, oxidative stress and lipid peroxidation induced by metals**. The ability of APH molecules to inhibit $A\beta_{42}$ protein aggregation induced by biometals and toxic metals was evaluated by TEM. APH molecules not only demonstrated a **high anti-amyloidogenic capacity**, directly inhibiting amyloid aggregation, but also increased the expression of **heat shock**

proteins (**HSP70**) **and proteosomes** (**P20S**), responsible for the degradation of the $A\beta_{42}$ protein. These APH molecules also **reduced** *in vitro* **cytotoxicity** and **apoptotic activity** induced by $A\beta_{42}$ over SN56 cell line. Through *in silico* methods, **pharmacokinetic properties** and absorption, distribution, metabolism, excretion and toxicity (**ADMET**) properties were predicted with all of them being acceptable. Taking this into account, APH molecules could be considered as potential drug candidates on AD.

On the other hand, the seven **RIV-BIM hybrid** molecules were successfully synthesised, purified and characterised using thin layer chromatography (TLC), ^{1}H and ^{13}C nuclear magnetic resonance (NMR), electrospray ionisation with mass spectrometry detection (ESI-MS) (+/-) and melting point measurements. Using *in silico* computational modelling tools and techniques such as UV-Vis spectroscopy, the **inhibition of AChE and BChE enzymes** by RIV-BIM hybrids has been demonstrated, thereby increasing the levels of important neurotransmitters such as **acetylcholine** (**ACh**) and **butyrylcholine** (**BCh**) and consequently delaying AD symptoms. By means of TEM and fluorescence spectroscopy, the **inhibition** of self- and Cu(II)-induced **$A\beta_{42}$ protein aggregation** was studied, with some of these hybrids being highly anti-amyloidogenic since they inhibit the accumulation of this protein. By *in vitro* MTT assay in SH-SY5Y cell line, the ability of some hybrids to **reduce the cytotoxicity of $A\beta_{42}$ protein** and **reduce oxidative stress** generated by Fe(II) was detected. Finally, *in silico* prediction of the **pharmacokinetic properties** of RIV-BIM molecules demonstrated the suitability of these hybrids as potential drugs for oral administration. These results proved the advantages of **hybridisation** to counteract the multifactorial nature of AD.

Finally, the neuroprotective properties of **Ch-SeNPs** against **biometals** and **amino acid enantiomers** were evaluated. To this end, Ch-SeNPs were synthesised and characterised by TEM, energy dispersive X-ray spectroscopy (EDXS), electron diffraction (ED) and dynamic light scattering (DLS). Subsequently, the **metal chelating** properties of various selenium species against biometals, including Ch-SeNPs, were evaluated by UV-Vis and d^{1}(UV-Vis). The **antioxidant capacity** of the selenium species was determined by UV-Vis spectroscopy using the MTT method, revealing the high antioxidant capacity of Ch-SeNPs compared to the rest of selenium species evaluated. The antioxidant capacity of certain **enantiomers of amino acids** involved in AD was also investigated by DPPH and TBARS methods, neither of them showing a significant effect on the reduction of oxidative stress. The **aggregation of $A\beta_{42}$ protein** under the effect of **biometals**, **selenium species** and **amino acid enantiomers** was studied by TEM. Thus, the role of biometals in

enhancing amyloid aggregation was revealed, which is consistent with the "**metal ion hypothesis**". Additionally, the chiral environment also affected $A\beta_{42}$ protein aggregation, being **enantiomerically induced** by certain amino acids, mainly D-enantiomers. However, the Ch-SeNPs were able to **inhibit** the biometal-induced **aggregation**, and afterwards **disaggregate the $A\beta_{42}$ protein fibrils**. Moreover, due to the chitosan stabilising the Ch-SeNPs, which provides nanoparticles with **chiral properties**, Ch-SeNPs were able to **inhibit the enantiomerically induced aggregation by amyloidogenic amino acids**. The interaction of Ch-SeNPs with amino acid enantiomers involved in AD was studied by UV-Vis and fluorescence spectroscopy, after derivatization of the enantiomers with ortho-phthalaldehyde (OPA). This **interaction** proved to be **enantioselective**, interacting predominantly with the D-enantiomer of the amino acids, which is not naturally present in the human body. *In vitro* assays using the MTT method determined the **cytotoxicity** of Ch-SeNPs against **neuronal phenotype cell lines**, demonstrating that the neuroprotective effect exerted by the nanoparticles is effective at concentrations seven times lower than the lethal concentration for 50% of the population (LC_{50}). Using TEM, the presence of Ch-SeNPs was observed in important regions of SH-SY5Y cells, highlighting their **adhesion to the extracellular membrane**, the **mitochondria**, the interior of the **nucleus** and the nucleolus. Consequently, Ch-SeNPs could inhibit and/or reduce the extracellular aggregation of the $A\beta_{42}$ protein, and decrease the level of ROS that produce mitochondrial DNA oxidation, thus counteracting AD progression. Finally, by means of SC-ICP-MS, **selenium mass accumulated** per **individual cell** was quantified in SH-SY5Y and Neuro-2a cell lines exposed to three concentration levels of selenium species, with Ch-SeNPs being the **most easily assimilated** by the cells and also presenting a high variability in the studied population.

In summary, this Doctoral Thesis has highlighted the importance of using a wide variety of **multidisciplinary methods and techniques** for the evaluation of the **neuroprotective properties** of possible drugs against **AD**, as well as the use of chemometric tools for correct data interpretation, analysis and comparison. Among the diverse neuroprotective properties presented by the compounds evaluated in this Doctoral Thesis, it is worth mentioning the **chelation of biometals and toxic metals** and the **reduction of cytotoxicity** and **oxidative stress** generated by them, thus intervening in the **"metal ion hypothesis"**. Another key aspect in the evaluation of potential drugs is the ability to **inhibit $A\beta_{42}$ protein aggregation induced by biometals, toxic metals and amino acid enantiomers**, directly or indirectly, and to **reduce** the *in vitro* **cytotoxicity** of

this protein, thus halting the amyloid cascade and preventing neurodegeneration. Some of the evaluated compound, based on the obtained results in **AChE and BChE inhibition**, might increase the levels of neurotransmitters such as **ACh** and **BCh**, delaying neurodegeneration. *In silico* predictions of the **pharmacokinetic properties** of organic molecules confirm their potential use as AD drugs. Thus, considering the results obtained in this Doctoral Thesis, the most promising compounds were: **APH4** molecule, excelling in most of the neuroprotective properties under study; RIV-BIM hybrid molecules belonging to the series 5 (**5a**, **5b** and **5d**), possessing high anti-amyloidogenic properties against $A\beta_{42}$ protein aggregation and *in vitro* reduction of oxidative stress; and **Ch-SeNPs**, which show a high inhibition ability of $A\beta_{42}$ protein aggregation and disaggregation of its fibrils, as well as a considerable enantioselective interaction with amino acids involved in AD and *in vitro* interaction with neuroblastoma cells.

IV.INTRODUCCIÓN

IV. INTRODUCCIÓN

1. Enfermedades neurodegenerativas

El término "demencia", del latín "*demens*" (sin mente), proviene etimológicamente del prefijo "*de*" (fuera/no) y la raíz "*mens*" (mente), y engloba el conjunto de **enfermedades neurodegenerativas**. A pesar de que el deterioro cognitivo relacionado con la edad es una dolencia bien conocida desde la antigüedad, no fue hasta principios del siglo XVIII cuando adquirió un significado clínico (Cipriani et al., 2011).

Las enfermedades neurodegenerativas se caracterizan por un deterioro progresivo en varios aspectos cognitivos, como la memoria, el lenguaje, la capacidad ejecutiva, la visión espacial, la personalidad y el comportamiento (Weller & Budson, 2018). Son la primera causa de discapacidad en el mundo, y la segunda causa de muerte a nivel global (Feigin et al., 2017). El envejecimiento es el principal factor de riesgo a la hora de padecer dichas enfermedades (Y. Hou et al., 2019).

Actualmente afectan a más de 50 millones de personas en todo el mundo, diagnosticándose un caso nuevo cada 3 segundos, y se espera que esta cifra alcance los 152 millones para el año 2050 (Crous-Bou et al., 2017; Patterson, 2018). Sin embargo, se estima que el 75% de las personas que padecen demencia no están oficialmente diagnosticadas (Alzheimer's Disease International, 2021). Por el momento no hay tratamientos efectivos para estos desórdenes neurológicos, que conllevan grandes costes socioeconómicos (Y. Hou et al., 2019). Existen diversas enfermedades neurodegenerativas, entre las que destacan la enfermedad de Alzheimer (**AD**), la enfermedad de Parkinson (**PD**), la esclerosis lateral amiotrófica (**ALS**) y la enfermedad de Huntington (**HD**) (**Tabla 1**).

Tabla 1. Principales enfermedades neurodegenerativas.

Enfermedad	Prevalencia	Principales síntomas	Factores de riesgo	Características neuropatológicas	Referencias
Enfermedad de Alzheimer (**AD**)	40 millones de personas	Dificultad para recordar, deterioro comunicativo, cambios de personalidad, confusión y desorientación	Ambientales (95%-99%) y genéticos (1%-5%). Edad avanzada y género femenino	Deposición extracelular de placas de Aβ, formación intracelular de ovillos neurofibrilares de p-tau y neuroinflamación	Alzheimer' s Disease International, 2021 Alzheimer' s Association, 2020 Crous-Bou et al., 2017
Enfermedad de Parkinson (**PD**)	6.1 millones de personas 2-3% de la población (> 65 años)	Temblor en reposo, bradicinesia, deterioro cognitivo, disfunción autonómica y trastornos del sueño	Ambientales (90%) y genéticos (10%). Edad avanzada y género masculino	Agregados intracelulares de la α-sinucleína en los cuerpos de Lewy (LB), pérdida neuronal en la sustancia negra pars compacta (SNc) del cerebro, deficiencia dopaminérgica y neuroinflamación	Ray Dorsey et al., 2018 Poewe et al., 2017 Cacabelos, 2017 Nazario et al., 2017 Moisan et al., 2016 Tysnes & Storstein, 2017
Esclerosis lateral amiotrófica (**ALS**)	5 individuos por cada 100000 personas	Defectos motores, atrofia y espasmos	Ambientales y genéticos. Mutaciones en 50 genes diferentes (SOD1, etc…)	Degeneración progresiva de las neuronas motoras del cerebro y de la médula espinal	Taylor et al., 2016
Enfermedad de Huntington (**HD**)	5-10 individuos por cada 100000 personas en la población caucásica	Motores (movimientos coreiformes con alteraciones de la marcha, bradicinesia, rigidez), cognitivos y de comportamiento	Hereditario. Naturaleza autosómica dominante del gen de la huntingtina (HTT)	Reducción del núcleo estriado y adelgazamiento de la corteza cerebral. Alteración funcional y muerte de neuronas estriatales	Saudou & Humbert, 2016 McColgan & Tabrizi, 2018 Ross & Tabrizi, 2011

Dentro de estas enfermedades, la **AD** es la más común, afectando a una de cada diez personas mayores de 65 años, y siendo más prevalente conforme aumenta la edad (Y. Hou et al., 2019). Se caracteriza por el progresivo deterioro de la memoria y el aumento de la disfunción cognitiva, debido a la pérdida masiva de neuronas corticales y del hipocampo. Se manifiesta histológicamente por la deposición extracelular de placas de la proteína beta-amiloide (Aβ), la formación intracelular de ovillos neurofibrilares de la proteína tau (p-tau) y la neuroinflamación (Crous-Bou et al., 2017; Keren-Shaul et al., 2017). La AD representa un 80% del total de los casos de demencia, coexistiendo a menudo con otras enfermedades neurodegenerativas y denominándose "demencia mixta" (Crous-Bou et al., 2017).

2. Enfermedad de Alzheimer

La enfermedad de Alzheimer (**AD**) debe su nombre al primer descubridor de los síntomas de dicha demencia: Alois Alzheimer (1864-1915), psiquiatra y neurólogo alemán (ALZHEIMER, 1907). La primera persona en ser diagnosticada con la AD fue Auguste Deter (1850-1906). Auguste fue una mujer escolarizada, capaz de leer, escribir y realizar pruebas matemáticas desde una temprana edad. Más adelante, al alcanzar los 51 años, empezó a mostrar un declive gradual a lo largo de 8 meses. Los síntomas incluían cambios en su personalidad, celos hacia su marido, pérdida progresiva de memoria, alucinaciones y delirios persecutorios. Debido a todo lo expuesto, fue ingresada en un manicomio de Frankfurt, donde la famosa paciente conoció al hombre que daría nombre a su enfermedad: Alois Alzheimer. Su deterioro fue inexorable: mientras que al principio mostraba desorientación espaciotemporal y confusión, a la larga comenzó a mantener conversaciones ininteligibles, creció su apatía y pasaba la mayor parte del tiempo en la cama. En 1906, a sus 55 años, Auguste Deter falleció (Cipriani et al., 2011).

Alois Alzheimer realizó la autopsia neuropatológica del cerebro de Auguste, observando una pérdida masiva de neuronas y la presencia de lo que ahora sabemos que son placas de la proteína beta-amiloide ($A\beta_{1-42}$, también denominada $A\beta_{42}$ para mayor simplicidad) y ovillos neurofibrilares (NFTs) de la proteína tau (p-tau). Para visualizar los cambios neuropatológicos intracelulares empleó una modificación del método de impregnación de Bielschowsky (Bielschowsky, 1902). Fue en 1907 cuando Alois, ya jefe del Laboratorio Anatómico de la Clínica Real Psiquiátrica de la Universidad de Múnich, publicó sus resultados bajo el título "*Über eine eigenartige Erkrankung der Hirnrinde*" (Una grave enfermedad característica de la corteza cerebral), describiendo a la AD como "una

enfermedad rara" (ALZHEIMER, 1907). Tres años más tarde, Emil Kraepelin fue el primero en utilizar el término "Enfermedad de Alzheimer" en honor a Alois Alzheimer para describir dicha enfermedad (Kraepelin, 1910). Lo que por aquel entonces se pensaba que era una enfermedad rara es, hoy en día, la enfermedad neurodegenerativa más común (Y. Hou et al., 2019), ya que la AD constituye un 80% del total de los casos diagnosticados de demencia en todo el mundo, afectando a más de 40 millones de personas (Alzheimer's Disease International, 2021; Weller & Budson, 2018).

El principal factor de riesgo de la AD es el envejecimiento, debido a que los síntomas suelen comenzar a manifestarse a partir de los 60 años (Agrawal & Jha, 2020). En estadíos tempranos de esta enfermedad se observa apatía, depresión y dificultad para recordar conversaciones recientes, nombres o sucesos. En fases más avanzadas es frecuente observar un deterioro comunicativo, cambios de personalidad, confusión y desorientación. Finalmente, el paciente tiene grandes dificultades para hablar, tragar e incluso caminar (Alzheimer's Association, 2020). La principal causa de muerte de personas diagnosticadas con AD es un fallo en el sistema respiratorio, representando más del 50% de los fallecimientos y, en segundo lugar, un fallo del sistema circulatorio, con un 25% (**Figura 1**) (Brunnström & Englund, 2009).

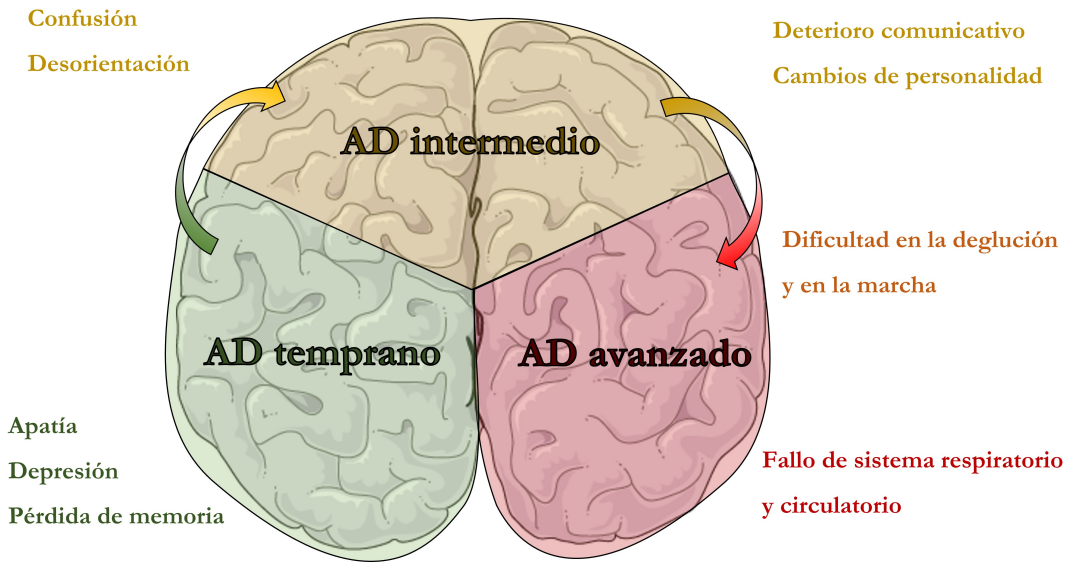


Figura 1. Síntomas observados en pacientes diagnosticados con AD.

No obstante, la AD comienza mucho antes de que los primeros síntomas sean observables. El origen de la AD puede ser esporádico (SAD), en el cual la causa exacta de la aparición es desconocida, o familiar (FAD), representando este último tan solo entre el 1% y el 5% del total (Bekris et al., 2010; J. Wang et al., 2017). Mientras que el FAD suele afectar a personas menores de 65 años, denominándose enfermedad de Alzheimer de inicio temprano (EOAD), el SAD afecta principalmente a personas mayores, conociéndose como enfermedad de Alzheimer de inicio tardío (LOAD) (Isabel Castanho & Katie Lunnon, 2019).

La aparición del SAD está relacionada tanto con factores genéticos como ambientales (Bondi et al., 2017). Dentro de los factores genéticos, el más relevante es el gen que codifica la apolipoproteína E (APOE), proteína responsable de transportar grasas como el colesterol a través del torrente sanguíneo (Long & Holtzman, 2019). El gen APOE tiene tres alelos: e2, e3 y e4. Cada progenitor le transfiere una de estas tres variantes a su descendencia, siendo la e3 la más común, seguida por la e4 y finalmente la e2. Las seis posibles combinaciones son, de la más frecuente a la menos frecuente, las siguientes: e3/e3, e3/e4, e3/e2, e2/e4, e4/e4 y e2/e2 (Rajan et al., 2017). Mientras que la variante e4 aumenta considerablemente el riesgo de padecer AD, la e2 lo disminuye (Y. T. Lin et al., 2018). Los individuos que portan las copias e3/e4 tienen una probabilidad tres veces mayor de desarrollar AD en comparación a individuos con e3/e3, mientras que portar dos copias e4 aumenta el riesgo entre ocho y doce veces (Michaelson, 2014).

La aparición del FAD se debe a mutaciones autosómicas dominantes en el gen que codifica la proteína precursora amiloide (APP) o a los genes PSEN1 y PSEN2, que codifican las proteínas presenilina-1 y presenilina-2 respectivamente. Dichas presenilinas forman parte de la enzima γ-secretasa, responsable de la hidrólisis de la APP. Estos tres genes están involucrados en la generación y eliminación de las placas de $A\beta_{42}$ (Baranello et al., 2015). La probabilidad de desarrollar AD para los individuos que porten las mutaciones en los genes APP o PSEN1 es de un 100%, mientras que en el gen PSEN2 es de un 95%, comenzando normalmente a los 30 años (Goldman et al., 2011). Por tanto, tener progenitores diagnosticados con AD aumenta la probabilidad de desarrollar dicha enfermedad (Alzheimer's Association, 2018).

Además, las personas diagnosticadas con síndrome de Down (DS) tienen mayores probabilidades de desarrollar AD. Esto se debe a la posesión de una copia extra del cromosoma 21, en el que se encuentra el gen que codifica la APP, por lo que aumenta la

cantidad de moléculas $A\beta_{42}$ en el cerebro. La probabilidad para las personas con DS de sufrir AD es de más del 50% a los 40 años, y casi del 80% a los 60 años, en comparación con personas sin DS (Lott & Head, 2019).

A pesar de que los principales factores de riesgo, como la edad, la genética y la herencia familiar, no se puedan modificar, hay otros factores que sí se pueden alterar. Realizar actividad física, dejar de fumar, mantener la mente activa mediante el aprendizaje continuo, realizar actividades sociales y seguir una dieta saludable pueden reducir el riesgo de padecer demencia en un 40% (Livingston et al., 2020).

2.1. Principales hipótesis involucradas en el desarrollo de la enfermedad de Alzheimer

La hipótesis más antigua acerca de cómo se desencadena la AD es la "**hipótesis colinérgica**", propuesta en 1976 (Davies & Maloney, 1976). En dicha hipótesis se consideran ciertas alteraciones que impiden el normal funcionamiento de las neuronas colinérgicas, como son la adquisición de colina, el empeoramiento en la liberación de acetilcolina (ACh) y los déficits en el transporte a través de los axones (**Figura 2**) (Sanabria-Castro et al., 2017; Tang et al., 2017).

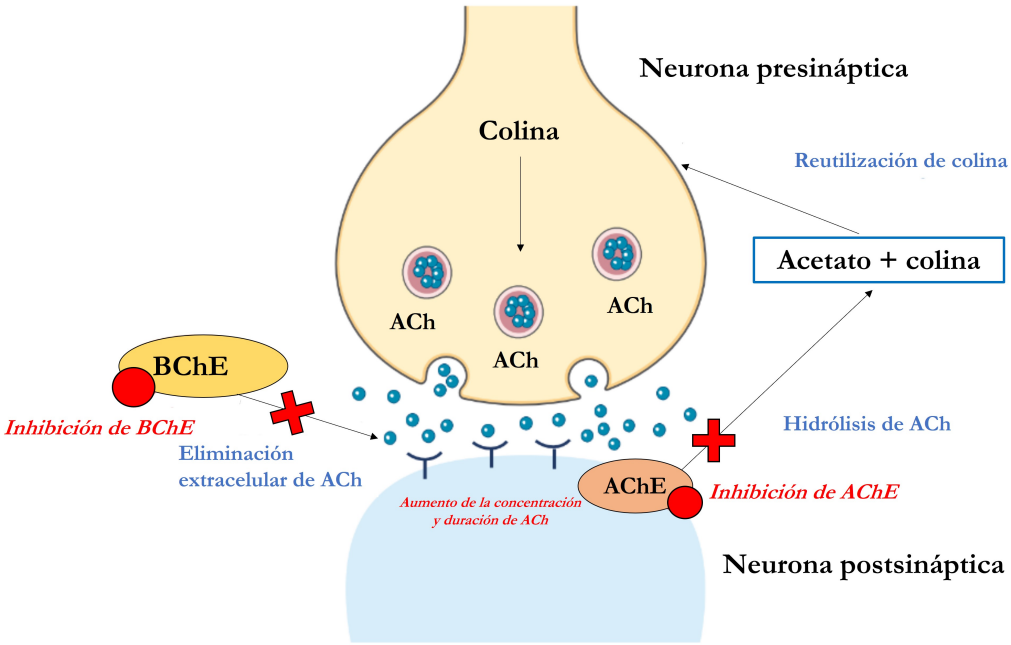


Figura 2. Hipótesis colinérgica y su papel en el desarrollo de la AD. Adaptación de (Min et al., 2022).

A través de estudios *post mortem* de cerebros de pacientes diagnosticados con AD y pacientes control, se ha observado que la actividad de la enzima colinacetiltransferasa, encargada de la síntesis del neurotransmisor ACh, es menor en la amígdala, el hipocampo y el córtex. Por este motivo, la ACh está en menor concentración en las sinapsis de pacientes diagnosticados con AD, presentando un fallo del sistema colinérgico (Ferreira-Vieira et al., 2016). Para solventar este déficit de ACh, algunas de las estrategias actuales se basan en la inhibición de la enzima acetilcolinesterasa (AChE). Mediante el uso de inhibidores de la acetilcolinesterasa (AChEi), se consigue evitar la degradación de la ACh y preservar la integridad del sistema colinérgico lo máximo posible (Deardorff et al., 2015). No obstante, el efecto de estos AChEi es limitado y, a pesar de que mejoran la calidad de vida de personas diagnosticadas con AD, no frenan el avance de la enfermedad.

La "**hipótesis de la cascada amiloide**", propuesta en 1991 (Hardy & Allsop, 1991), es la explicación que reúne un mayor consenso acerca de cómo se desencadena la AD (P. P. Liu et al., 2019). En dicha hipótesis, **la agregación de la proteína beta-amiloide ($A\beta_{42}$)** es la responsable del daño y la muerte neuronal, que provoca el desarrollo de la AD. Dicha hipótesis está en total simbiosis con la "**hipótesis del ión metálico**", tal y como se explicará más adelante.

Según esta hipótesis, la enfermedad comienza con un desequilibrio entre la formación y la eliminación de la proteína $A\beta_{42}$ debido a una proteólisis errónea de la proteína precursora amiloide (APP), por lo que se produce su acumulación en el exterior de las neuronas y neuritas, formando placas amiloides extracelulares. Esto produce una pérdida de las comunicaciones interneuronales, afectando a las sinapsis (Karran & de Strooper, 2016). Además, esta agregación de la $A\beta_{42}$ reduce la respiración mitocondrial en neuronas y astrocitos (Angelova & Abramov, 2018).

La proteína tau, presente en elevadas concentraciones en las neuronas, contribuye a la estabilización de los microtúbulos (Bacchella et al., 2020). Sin embargo, el suceso primario de la agregación de la $A\beta_{42}$ provoca la formación de ovillos neurofibrilares de la proteína tau (NTFs), debido a su hiperfosforilación, en el interior de las neuronas. La acumulación intracelular de los NFTs impide el paso de los nutrientes y moléculas esenciales al interior de las células, dificultando su normal funcionamiento y desencadenando la muerte neuronal (Congdon & Sigurdsson, 2018).

Además, la neuroinflamación también ha demostrado ser clave en el desarrollo de la AD. En pacientes diagnosticados con AD, hay una concentración hasta 5 veces más

elevada de microglías alrededor de las placas amiloides y neuronas con NFTs intracelulares. La proteína $A\beta_{42}$ se une a dichas células gliales y las destruye, liberando factores que inducen inflamación, provocando una respuesta inmune y aumentando la hiperfosforilación de la p-tau (Lučiūnaitė et al., 2020; Michaud et al., 2013; Sy et al., 2011). Otro factor que favorece el desarrollo de la AD es el estrés oxidativo producido en el interior del cerebro (Angelova & Abramov, 2018; Nasrabady et al., 2018). El conjunto de estos eventos provoca la inevitable neurodegeneración y el diagnóstico clínico de la AD (**Figura 3**) (Alzheimer's Association, 2018; C. A. Lane et al., 2018).

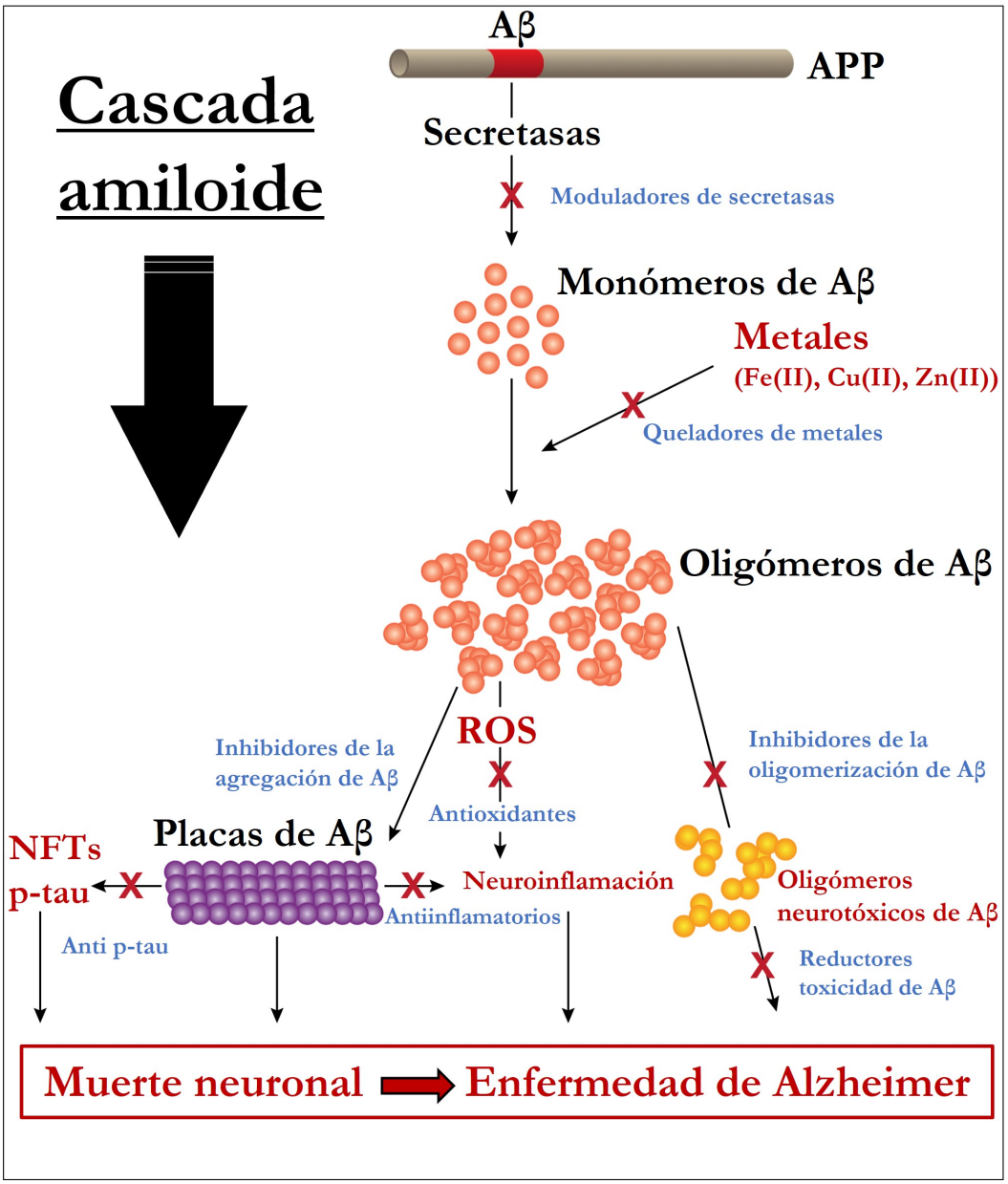


Figura 3. Hipótesis de la cascada amiloide y su papel en el desarrollo de la AD. Adaptación de (Vijaya Kumar & Moir, 2017).

2.2. Proteína beta-amiloide (Aβ)

La generación de **$A\beta_{42}$** se produce por la proteólisis anómala de la APP, una metaloproteína transmembrana expresada especialmente en las sinapsis neuronales (**Figura 4**). Existen tres isoformas de la APP, variando en el número de aminoácidos: APP770, APP751 y APP695, siendo esta última la más abundante en el cerebro y la que se expresa principalmente en las neuronas (Guerreiro et al., 2012).

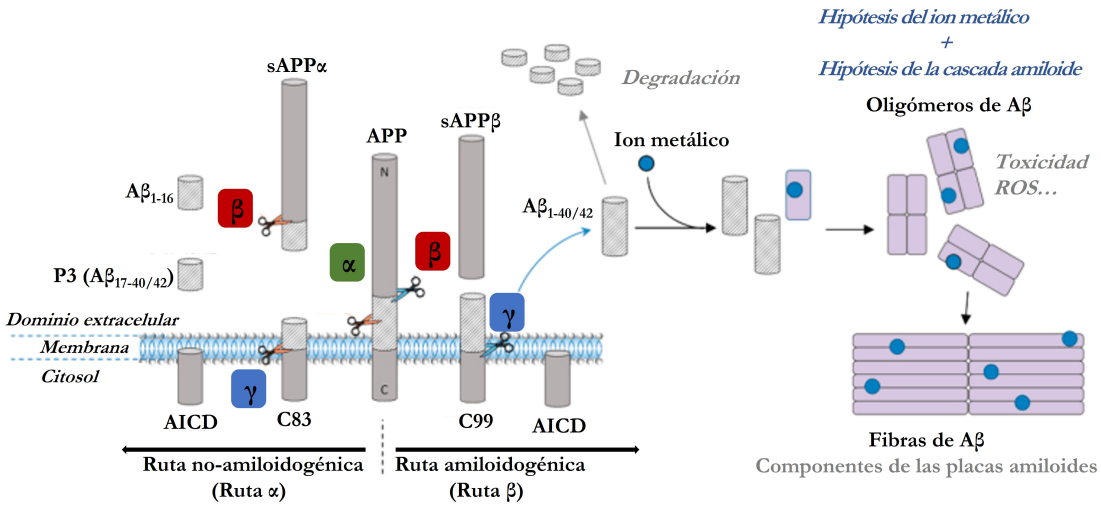


Figura 4. Rutas no-amiloidogénica (α) y amiloidogénica (β) del procesamiento de la APP, en sinergia con la hipótesis del ion metálico y la hipótesis de la cascada amiloide. Adaptación de (Cheignon et al., 2018).

La APP770 consta de varias regiones: el dominio N-terminal del factor de crecimiento (GFLD) (residuos 18-123), el dominio de unión del cobre (CuBD) (residuos 124-189) que junto con el GFLD forman la región E1, un dominio ácido no estructurado (AcD) (residuos 190-289), un dominio inhibidor de proteasa tipo Kunitz (KPI) (residuos 290-364), el dominio E2 (residuos 365-575) responsable del crecimiento celular y la extensión de las neuritas, y la región yuxtamembrana (JMR) (residuos 576-699) (Roisman et al., 2019; Wild et al., 2017).

En condiciones normales la APP se hidroliza por la vía no-amiloidogénica, también llamada vía α, siendo cortada por la α-secretasa, generando los fragmentos carboxílico

terminal C83 y amino terminal sAPPα y, posteriormente, el fragmento C83 es hidrolizado por la γ-secretasa, una aspartil proteasa, dando lugar al péptido P3 en el dominio extracelular y al dominio intracelular del APP (AICD), que se transloca al núcleo donde regula la inducción de genes apoptóticos (**Figura 4**). Ninguno de estos fragmentos provoca el desarrollo de la AD (P. P. Liu et al., 2019).

Sin embargo, una pequeña cantidad de APP puede seguir la vía amiloidogénica, también llamada vía β, provocando la anteriormente mencionada cascada amiloide. En ella, la primera hidrólisis de la proteína se debe a la acción de la enzima β-secretasa de la APP (BACE1), una aspartil proteasa cuyos niveles están relacionados con el estrés oxidativo y la edad (Tamagno et al., 2012). Esta hidrólisis genera un pequeño fragmento amino terminal (sAPPβ) y un fragmento carboxílico más grande (C99). Posteriormente actúa la γ-secretasa, un complejo heteromérico de 4 subunidades que contiene las PSEN1 y PSEN2. Dicha secretasa hidroliza el fragmento C99, generando el AICD en el citosol y la proteína beta-amiloide (Aβ) con una longitud variada de entre 38 y 43 aminoácidos en el dominio extracelular (**Figura 4**) (Cheignon et al., 2018; G. F. Chen et al., 2017; Sanabria-Castro et al., 2017), representando la aloforma de 40 aminoácidos ($A\beta_{40}$) un 90% del total de Aβ generadas (Younkin, 1995). Sin embargo, de las proteínas Aβ generadas, la que contiene 42 aminoácidos ($A\beta_{42}$) es la más patogénica y amiloidogénica debido a sus características hidrófobas de los residuos C-terminales alanina e isoleucina, siendo por tanto más propensa a la agregación (X. Q. Chen & Mobley, 2019).

Es esta proteína $A\beta_{42}$ la que, debido a su baja solubilidad, se secreta y se agrega acumulándose en el exterior de las neuronas en placas amiloides (Agrawal & Jha, 2020). Normalmente, las proteínas que adquieren un plegamiento incorrecto o una elevada agregación son degradadas por el sistema inmune del propio organismo. Sin embargo, algunas proteínas, propensas a la agregación de oligómeros ricos en láminas beta, son resistentes a todas las vías proteolíticas, formando por tanto placas extracelulares (Ciechanover & Kwon, 2015). Así, las estrategias más recientes para solventar la formación de placas amiloides consisten en la búsqueda de inhibidores de la agregación de la proteína $A\beta_{42}$.

El monómero $A\beta_{42}$ fue descubierto por primera vez en 1984, a partir de placas amiloides (Glenner & Wong, 1984). Los 42 aminoácidos que lo componen son los siguientes: Asp-Ala-Glu-Phe-Arg-His-Asp-Ser-Gly-Tyr-Glu-Val-His-His-Gln-Lys-Leu-Val-Phe-Phe-Ala-Glu-Asp-Val-Gly-Ser-Asn-Lys-Gly-Ala-Ile-Ile-Gly-Leu-Met-Val-Gly-

Gly-Val-Val-Ile-Ala. Su código es "UniProt" P05067, su masa molecular 4514.10 g · mol^{-1} y su punto isoeléctrico teórico 5.31. Este monómero rico en láminas beta se agrega progresivamente en sucesivas estructuras oligomerizándose, desde pequeños dímeros, y fibrilándose, hasta largas fibras insolubles. Los principales estados de agregación por los que transita son: oligómeros, protofibras y fibras amiloides, todos ellos neurotóxicos (**Figura 5**) (Stine et al., 2003; Thibaudeau et al., 2018; Zou et al., 2019).

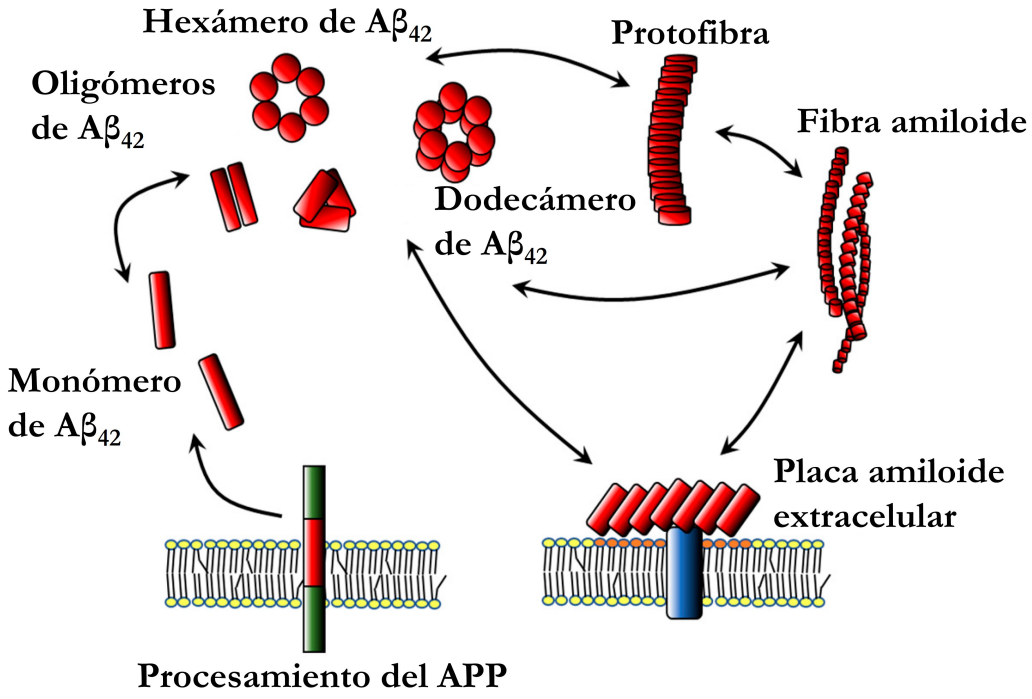


Figura 5. Monómero $A\beta_{42}$ y sus principales estados de agregación. Adaptación de (Rudajev & Novotny, 2020).

Los oligómeros de la proteína beta-amiloide (AβOs) son productos metaestables intermedios que poseen efectos patógenos, como inhibir el transporte axonal, deteriorar las sinapsis, provocar estrés oxidativo, aumentar la hiperfosforilación de la proteína tau, alterar la homeostasis del calcio, provocar la muerte selectiva de ciertas neuronas, y afectar a la microglía y a los astrocitos (Cline et al., 2018). Para que se produzca la oligomerización se necesita la aproximación de dos o más monómeros, bien con una nucleación primaria en ausencia de una fibra, o una secundaria en presencia de esta (Michaels et al., 2020). Los hexámeros, con una altura de 0.75 nm, y los dodecámeros, con una altura de 1.5 nm, se

convierten rápidamente en los oligómeros dominantes. Posteriormente, los dodecámeros empiezan la formación de estructuras protofibrilares, consistentes en una capa que se extiende varios cientos de nanómetros en longitud con una altura de 0.75 nm, siendo estos dodecámeros los núcleos de fibrilación para el resto de los monómeros (**Figura 5**) (Economou et al., 2016).

Sin embargo, la mayoría de estos oligómeros se disocian rápidamente en sus precursores monoméricos de nuevo, existiendo solo una pequeña fracción de ellos que son capaces de agregarse para formar protofibras, debido a la cinética relativamente lenta inherente a este paso (Michaels et al., 2020). No obstante, esta cinética de conversión de oligómeros en protofibras se ve favorecida cuando la concentración de monómeros de $A\beta_{42}$ es elevada (Michaels et al., 2020).

La elongación de las protofibras, debido a la deposición de oligómeros en su superficie, se produce en el eje perpendicular a estos (Gremer et al., 2017). Las protofibras están formadas por el apilamiento sucesivo de dos moléculas de $A\beta_{42}$ planas unidas por los residuos Asp_1-Lys_{28}' y Lys_{28}-Asp_1', cada una con tres giros en su estructura coincidiendo con los residuos de Gly, formando una doble herradura cada una de ellas. Ambas están unidas por enlaces de hidrógeno, con una distancia de 4.7 Å, al par de moléculas $A\beta_{42}$ inferior y superior de la protofibra (Eisenberg & Sawaya, 2017). Las protofibras son normalmente más cortas y curvadas que las fibras amiloides, teniendo una anchura de 2-3 nm aproximadamente. Dichas fibras están compuestas por varias protofibras, generalmente cinco o seis, enrolladas longitudinalmente hasta alcanzar una anchura de 6-8 nm (Ritter et al., 2005; Serpell, 2000). Estas fibras ricas en láminas beta se agregan extracelularmente alrededor de las neuronas y las neuritas del hipocampo, siendo los principales componentes de las placas seniles, provocando los eventos anteriormente mencionados en la "hipótesis de la cascada amiloide" (Cheignon et al., 2018).

La agregación de la proteína $A\beta_{42}$ se puede deber a múltiples factores. Por ejemplo, se ha demostrado que cuanto mayor es la concentración de la proteína, el tiempo de incubación y la temperatura (37 °C *vs* 4 °C), y menores son el pH y la fuerza iónica, se obtiene una mayor agregación de fibras amiloides con respecto a la cantidad de oligómeros de $A\beta_{42}$ (Stine et al., 2003). La AChE también ha demostrado aumentar el proceso de fibrilación de la $A\beta_{42}$ (Inestrosa et al., 1996).

2.3. Efecto de los metales y de los aminoácidos en la enfermedad de Alzheimer

Los **metales** se encuentran presentes en el medioambiente debido principalmente a las actividades antropogénicas. Por ese motivo, los seres humanos están sometidos a una exposición crónica de metales esenciales (**biometales**) como el hierro, el cobre o el zinc, y a **metales tóxicos**, como el mercurio, el cadmio o el aluminio, alterando la homeostasis en el organismo (Huat et al., 2019). Los metales esenciales, o biometales, como el hierro, el cobre y el zinc, tienen una concentración óptima en la cual son beneficiosos para el cuerpo humano. Sin embargo, si hay un déficit o un exceso de estos, pueden originar problemas para la salud (Huat et al., 2019). Por el contrario, para los metales tóxicos como el mercurio, el cadmio o el aluminio, sus efectos tóxicos se observan a niveles muy bajos de concentración ($\mu g \cdot kg^{-1}$) (Huat et al., 2019).

La hipótesis que mejor explica la agregación de las fibras de $A\beta_{42}$ para formar placas seniles es la llamada "**hipótesis del ion metálico**". Según dicha hipótesis, la dishomeostasis en las concentraciones de biometales esenciales como Fe, Cu y Zn favorece la agregación de la proteína $A\beta_{42}$, desencadenando los eventos descritos en la "hipótesis de la cascada amiloide", entrando dichas hipótesis en una inevitable sinergia (**Figura 6**) (P. P. Liu et al., 2019; Chen et al., 2023).

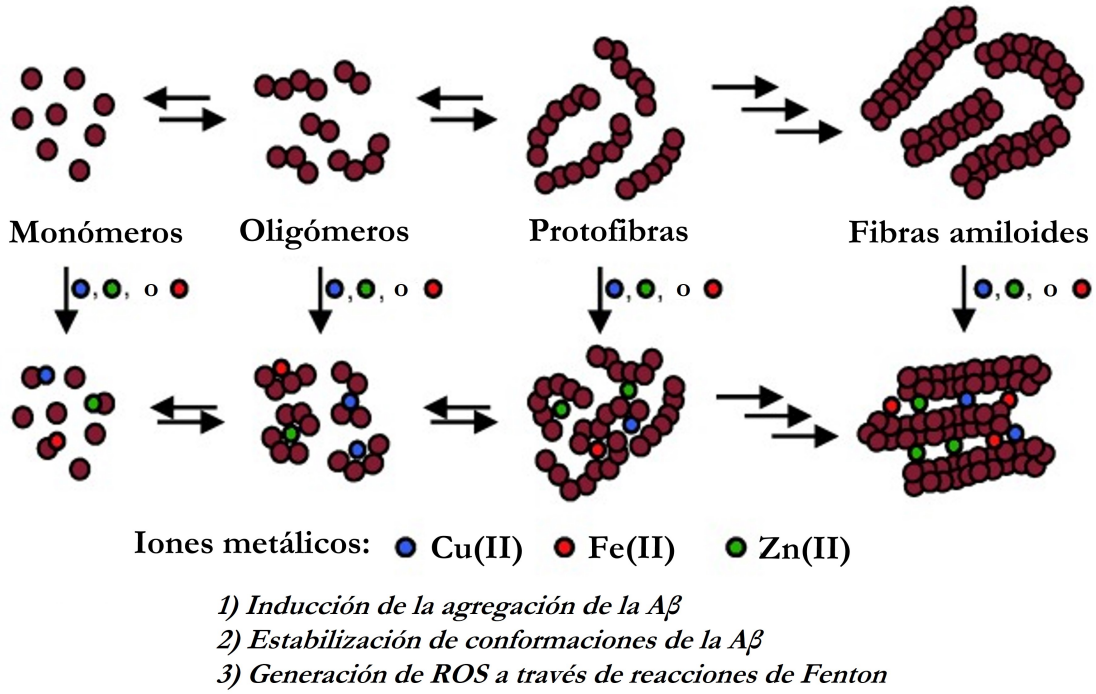


Figura 6. Hipótesis del ion metálico y su papel en el desarrollo de la AD. Adaptación de (Derrick & Lim, 2015).

Dentro del sistema nervioso central (CNS), algunos biometales actúan como cofactores para la actividad enzimática, la función mitocondrial y la función neuronal, por lo que la alteración en la homeostasis de estos biometales puede conducir a desarrollar ciertas enfermedades (**Tabla 2**) (Que et al., 2008). Mediante estudios *post mortem* de cerebros de pacientes diagnosticados con AD, se ha observado que las placas seniles compuestas principalmente de fibras amiloides, también contienen metales como hierro, cobre y zinc que han colaborado en su agregación (James et al., 2017; Kozlowski et al., 2012; Lovell et al., 1998; Nasrabady et al., 2018). En pacientes sanos, los biometales se mantienen regulados y en bajas concentraciones. Sin embargo, las concentraciones de cobre en cerebros de pacientes con AD son 5.7 veces mayores que en cerebros sanos, de igual forma que el hierro y el zinc, 2.8 y 3.1 veces respectivamente (Y. Liu et al., 2019).

Tabla 2. Efectos de biometales y metales tóxicos en el desarrollo de la AD.

Catión	Categoría	APP	$A\beta_{42}$	Estrés oxidativo	p-tau	Referencias
Fe(II)	Esencial (biometal)	Incrementa la expresión de la APP y favorece la vía β	Mayor generación de $A\beta_{42}$ Aumento de la agregación de la $A\beta_{42}$ Disminución de la expresión de HSP70 y P20S	Generación de ROS	Relación entre la homeostasis del hierro y la p-tau	D. J. R. Lane et al., 2018 James et al., 2017 Masaldan et al., 2019
Cu(II)	Esencial (biometal)	Regulación de la sinaptogénesis mediante la unión a la APP	Aumento de la agregación de la $A\beta_{42}$ Disminución de la expresión de HSP70 y P20S	Generación de ROS	Aumento de la hiperfosforilación de la p-tau	Baumkötter et al., 2014 Tang et al., 2017 Young et al., 2018 di Natale et al., 2018
Zn(II)	Esencial (biometal)	Unión a la APP	Aumento de la agregación de la $A\beta_{42}$	-	Aumento de la hiperfosforilación de la p-tau	Wild et al., 2017 Khmeleva et al., 2016 Huang et al., 2014
Hg(II)	Tóxico	Incrementa la expresión de la APP	Mayor generación de $A\beta_{42}$ Aumento de la agregación de la $A\beta_{42}$ Disminución de la expresión de HSP70 y P20S	Generación de ROS	Aumento de la hiperfosforilación de la p-tau	Y. Li et al., 2017 Cicero et al., 2017 Andrade et al., 2017 Cariccio et al., 2019
Cd(II)	Tóxico	Favorece la vía β de la APP	Aumento de la agregación de la $A\beta_{42}$	Generación de ROS	Incremento de p-tau y de su hiperfosforilación	Ashok et al., 2015 Wallin et al., 2017 Branca et al., 2019 del Pino et al., 2016
Al(III)	Tóxico	-	Aumento de la agregación de la $A\beta_{42}$ Disminución de la expresión de HSP70 y P20S	Generación de ROS	-	Hussien et al., 2018

El **hierro** es el metal de transición más abundante en la tierra y en el cuerpo humano, existiendo en estado de oxidación +2, Fe(II), y +3, Fe(III), siendo esencial para la vida (Masaldan et al., 2019). Está involucrado en la catálisis de procesos metabólicos imprescindibles para la vida, en la respiración mitocondrial, en la síntesis y reparación del ADN y en la señalización celular. En el interior del CNS tiene un papel fundamental en la mielinización de la médula espinal y la materia blanca, y con respecto a la síntesis, empaquetamiento, adquisición y degradación de moléculas neurotransmisoras (Bonfio et al., 2017; Torti et al., 2018).

El cerebro es el órgano donde se produce un mayor incremento en la concentración de hierro conforme avanza la edad (Masaldan et al., 2019). La acumulación descontrolada del hierro en el cerebro está asociada a diversas enfermedades neurodegenerativas, como la AD, el PD y la ALS, debido al estrés oxidativo producido por las especies reactivas de oxígeno (ROS) y a la asociación de proteínas como la α-sinucleína, p-tau y APP con la homeostasis del hierro (Angelova & Abramov, 2018; Masaldan et al., 2019; Pirpamer et al., 2016). Por estos motivos, la elevada concentración de hierro en el cerebro se considera una característica patológica de la AD (D. J. R. Lane et al., 2018).

Los astrocitos se encargan de mitigar la toxicidad del hierro y de su transporte desde las células endoteliales cerebrales, que mantienen la integridad de la barrera hematoencefálica (BBB), hasta las neuronas (Masaldan et al., 2019). El mayor contenido de hierro en el cerebro, aumentando con la edad y la progresión de la AD, se encuentra en los oligodendrocitos, un tipo de célula glial presente exclusivamente en el CNS, por lo que son las células más vulnerables al estrés oxidativo ya que contienen grandes cantidades de ferritina, encargada del almacenamiento de hierro, y transferrina, encargada de su movilización (Nasrabady et al., 2018).

Este hierro contenido en los oligodendrocitos se libera con la edad, afectando mecanismos clave en el desarrollo de la AD (Bartzokis et al., 2007). En primer lugar, el hierro aumenta la expresión de la APP, proteína precursora de la $A\beta_{42}$, mediante un incremento en su traslación (D. J. R. Lane et al., 2018). Además, la APP oxida el Fe(II) a Fe(III), lo inserta en la transferrina e interacciona con la ferroportina, transportadora de hierro a través de la sangre (Duce et al., 2010). En segundo lugar, el hierro favorece la vía amiloidogénica (vía β) de la APP. Esto se debe a la unión de la ferritina, principal proteína transportadora de hierro, con la PSEN2, componente de la γ-secretasa encargada de hidrolizar la APP, aumentando su actividad y generando un mayor contenido de proteína

$A\beta_{42}$ (Peters et al., 2018; Rogers et al., 2008). Además, el Fe(II) interacciona con la $A\beta_{42}$, favoreciendo su oligomerización y posterior agregación y aumentando su neurotoxicidad (Bartzokis et al., 2007; Boopathi & Kolandaivel, 2016; James et al., 2017). La interacción entre el hierro y la $A\beta_{42}$ es mucho más fuerte que la del resto de proteínas involucradas en su almacenaje y transporte. Por ejemplo, es casi 10 veces más fuerte que la de la transferrina, por lo que la $A\beta_{42}$ compite con ellas acumulando hierro y alterando su homeostasis (D. Jiang et al., 2009).

Además, el hierro actúa como agente pro-oxidante mediante la reacción de Fenton, generando ROS (*reacción 1*) (D. J. R. Lane et al., 2018).

$$Fe^{2+} + H_2O_2 \rightarrow Fe^{3+} + HO^{\bullet} + HO^{-} \qquad (\textit{reacción 1})$$

El factor de transcripción antioxidante, llamado factor nuclear eritroide 2 (Nrf2), que actúa como factor de protección frente a diversos virus como el SARS-CoV2, también regula cientos de genes que ayudan a proteger frente al estrés oxidativo (Cuadrado et al., 2020; Olagnier et al., 2020). El Nrf2 se encuentra en el citosol unido a la proteína 1 asociada a ECH tipo Kelch (Keap1), que es su regulador negativo, inhibiendo su actividad. Sin embargo, en condiciones de estrés oxidativo, la Keap1 se disocia del Nrf2 translocándolo al interior del núcleo, donde interacciona con genes antioxidantes provocando su activación transcripcional (Abdalkader et al., 2018). Se ha demostrado que el factor Nrf2 protege frente a la ferroptosis, un tipo de muerte celular provocada por la acumulación de hierro, ayudando por tanto a retrasar la AD (Stockwell et al., 2017).

El **cobre** existe en el organismo como Cu(I), estado reducido, y Cu(II), estado oxidado, estando en su mayoría unido a cuproenzimas y siendo esencial para una gran variedad de procesos bioquímicos. Sin embargo, una pequeña parte de este cobre se encuentra libre, denominándose cobre lábil (Huat et al., 2019). Es un cofactor esencial de varias enzimas involucradas en el transporte de electrones, actividad antioxidante, modificaciones de proteínas, y síntesis de neurotransmisores (T. Chen et al., 2020). La alteración de la homeostasis del cobre agrava el desarrollo de la AD (Sensi et al., 2018).

La unión del cobre a la APP regula el proceso de sinaptogénesis, es decir, la formación de conexiones entre neuronas del CNS (Baumkötter et al., 2014). El cobre se puede unir a

la APP por los residuos His_{108}-His_{110} de la región GFLD y, con una geometría piramidal, por los residuos His_{147}-His_{151}-Tyr_{168} del dominio CuBD, todos ellos dentro del dominio E1 de la APP. Además, también se puede unir a los residuos His_{313}-His_{382}-His_{432}-His_{436} del dominio E2 de la APP (August et al., 2019; Wild et al., 2017). La unión del cobre a la $A\beta_{42}$ se produce en el dominio de unión metálica (MBD) (residuos 1-16). En concreto, el Cu(II) se une a los residuos Asp_1-Ala_2-His_6-His_{13}/His_{14} y Asp_1-Ala_2-His_6/His_{13}/His_{14}, mientras que el Cu(I) se da principalmente entre los residuos His_{13}-His_{14} y en menor proporción entre His_6-His_{13} e His_6-His_{14} (Atrián-Blasco et al., 2017; Karr et al., 2005). El residuo Tyr_{10} también ha demostrado ser capaz de unirse al cobre (Simunkova et al., 2019). Debido a estas uniones, el cobre estabiliza las cadenas de la proteína $A\beta_{42}$ a través de los residuos de His, favoreciendo su conformación en lámina β (Tang et al., 2017). Una vez que el Cu(II) se une a la $A\beta_{42}$, se reduce a Cu(I) debido al efecto del residuo Met_{35}, y favorece la agregación en fibras amiloides que a su vez generan ROS, provocando un aumento del estrés oxidativo en el interior del cerebro (Mayes et al., 2014; Simunkova et al., 2019; Young et al., 2018). La producción de ROS por parte del cobre se lleva a cabo mediante la reacción de Fenton, de igual forma que para el hierro (*reacción 2*).

$$Cu^{+} + H_2O_2 \rightarrow Cu^{2+} + HO^{\bullet} + HO^{-} \qquad (\textit{reacción 2})$$

Esta excesiva generación de ROS se puede controlar con enzimas como la superóxido dismutasa (SOD), la catalasa y la glutatión peroxidasa (GPx) que catalizan las reacciones para eliminar dichos radicales (Simunkova et al., 2019).

La unión del cobre a la $A\beta_{42}$ aumenta la activación de la microglía, liberando factores que aumentan la neuroinflamación (F. Yu et al., 2015). Experimentos *in vivo* han demostrado sobre modelos animales de AD, que la ingesta de agua con cobre en cantidades traza da lugar a una acumulación de $A\beta_{42}$ formando placas seniles en el hipocampo y en el lóbulo temporal, reduciendo su capacidad de aprendizaje (Sparks & Schreurs, 2003). Al incrementarse la concentración de cobre en el interior de las placas amiloides, disminuye su concentración en otras regiones del cerebro, lo que reduce la actividad de enzimas esenciales como la SOD1, aumentando la neurotoxicidad en la AD (Young et al., 2018).

La proteína tau se une a la tubulina a través de un dominio con cuatro péptidos repetidos, donde los más relevantes son el primero (R_1) y el tercero (R_3). Dichos péptidos

son importantes sitios de unión para el cobre: mientras que el péptido R1 tiene un residuo de His por el cual el Cu(I) siente una afinidad moderada, el R3 tiene un tándem de His-His siendo un importante sitio de unión tanto para el Cu(I) como para el Cu(II), generando un elevado estrés oxidativo (Bacchella et al., 2020; Sendzik et al., 2017). Esta unión del cobre a la p-tau favorece su hiperfosforilación en neuronas del hipocampo (di Natale et al., 2018).

Por otro lado, el cerebro es el órgano que contiene una mayor cantidad de **zinc** en todo el organismo humano (Huat et al., 2019). Aproximadamente un 90% del zinc presente en el cerebro está unido a proteínas, mientras que el 10% restante se encuentra en las vesículas presinápticas que han sido liberadas debido a la actividad neuronal (August et al., 2019). El zinc, al igual que el cobre, es un cofactor de varias enzimas con actividades indispensables para el organismo, entre las que se incluyen la síntesis de neurotransmisores (T. Chen et al., 2020). Al contrario que el hierro y el cobre, el zinc no participa en la generación de estrés oxidativo que agrava la AD (Cheignon et al., 2018; Simunkova et al., 2019).

El zinc tiene cien veces menos afinidad por la APP que el cobre, uniéndose a los dominios CuBD dentro de la E1 (Cys_{186}-Cys_{187}) y al dominio E2 (His_{382}-His_{432}-His_{436} al igual que el cobre, y His_{430}-His_{433}-His_{450}-His_{452}), sin tener ninguna posición de unión en el dominio GFLD de la E1 (August et al., 2019; Wild et al., 2017). Se une al dominio MBD de la proteína $A\beta_{42}$ a través de los residuos Asp_1-His_6-His_{13}-His_{14} y con menos afinidad a ciertos residuos entre Asp_{23} y Lys_{28} (Atrián-Blasco et al., 2017; Kawahara et al., 2017; Rezaei-Ghaleh et al., 2011). Al unirse al MBD, provoca una rápida agregación de la $A\beta_{42}$ (Khmeleva et al., 2016). El zinc también se une a la proteína tau, aumentando su agregación y fosforilación, lo que incrementa su toxicidad (Huang et al., 2014).

Las metaloproteasas de matriz (MMPs), que contienen zinc para su normal funcionamiento, son un conjunto de 23 proteasas encargadas de degradar cualquier componente de la matriz extracelular (Cabral-Pacheco et al., 2020; K. Li et al., 2020). Todas las células del CNS son capaces de expresarlas (Rivera et al., 2019). En condiciones normales, los niveles de MMPs se mantienen bajos. Sin embargo, en situaciones patológicas, se produce una sobreexpresión de las MMPs, lo que conduce a ciertas enfermedades como el cáncer o la AD (Kumar et al., 2018; K. Li et al., 2020).

En concreto, las MMP-2 y MMP-9 se han encontrado sobreexpresadas en neuronas del hipocampo de pacientes de AD *post mortem* (Rivera et al., 2019). Estas MMP-2 y MMP-9 afectan a la neurogénesis, por lo que tienen especial importancia en la AD (Cabral-Pacheco et al., 2020). Aunque en principio las MMP-2 y MMP-9 podrían degradar la

proteína $A\beta_{42}$ en ciertas situaciones, y por tanto ralentizar la progresión de la AD, sus características neurotóxicas dependen del tipo de células que las expresan (Rivera et al., 2019). Entre estas características neurotóxicas se encuentran su habilidad para modular la neuroinflamación y la impermeabilidad de la BBB, agravando la AD (Rivera et al., 2019). Por ejemplo, la MMP-9 expresada por la microglía aumenta la acumulación de $A\beta_{42}$, contribuyendo al AD esporádico (Rivera et al., 2019). Actualmente, se buscan inhibidores para mantener un equilibrio en la expresión de dichas MMPs (Chopra et al., 2019).

Por su parte, el **mercurio** es uno de los metales pesados más tóxicos presentes en el medioambiente. Su ingestión se produce principalmente a través de la dieta, especialmente pescados en una posición elevada de la cadena trófica, debido a la biomagnificación y bioacumulación del mercurio (Akhbarizadeh et al., 2018).

Este mercurio impide el desarrollo cerebral y produce alteraciones cognitivas y motoras (Chin-Chan et al., 2015). Está involucrado en múltiples enfermedades neurodegenerativas, como la AD, el PD y la ALS (Cariccio et al., 2019; Cicero et al., 2017). Los niveles de mercurio en la sangre, suero y plasma de pacientes con AD son superiores a los presentes en pacientes control, lo cual pone de manifiesto su papel en dicha enfermedad (Xu et al., 2018).

La citotoxicidad del mercurio se debe, entre otros factores, a su elevada generación de estrés oxidativo mediante la producción de ROS (Andrade et al., 2017). La elevada presencia de mercurio provoca una mayor generación de APP y $A\beta_{42}$ (Y. Li et al., 2017). Este papel oxidante del mercurio aumenta la generación de $A\beta_{42}$ mientras reduce su eliminación, lo cual conduce a una elevada agregación amiloide (Cicero et al., 2017). Al provocar la agregación en placas amiloides, favorece la hiperfosforilación de la p-tau en ovillos neurofibrilares (Cariccio et al., 2019; Kim et al., 2018). Además, degenera los microtúbulos y altera la integridad estructural de las membranas de las neuritas y de las neuronas (Yegambaram et al., 2015).

El **aluminio** es uno de los elementos más abundantes en la corteza terrestre, representando un 8% del total de esta. Se introduce en el organismo, principalmente, a través de la vía oral, mediante la ingestión de comida, agua o fármacos. Sin embargo, tan solo el 0.1% del Al(III) ingerido es absorbido por el tracto gastrointestinal (Drüeke, 2002). Este aluminio puede conducir a pérdida neuronal y déficits de memoria, además de generar estrés oxidativo mediante la producción de ROS (Hussien et al., 2018). Por este motivo, el aluminio está relacionado con la progresión de la AD (Mirza et al., 2017). Los niveles de

aluminio encontrados en la sangre, suero y plasma son mayores en pacientes diagnosticados con AD (Xu et al., 2018). Este elemento tiene tendencia a unirse a aminoácidos específicos de las proteínas e inducir cambios en su estructura. En concreto, se une a la $A\beta_{42}$ favoreciendo su oligomerización (Kawahara et al., 2017).

El **cadmio** no tiene ninguna función fisiológica en el cuerpo humano, y está considerado como un potente agente carcinogénico (Bakulski et al., 2020). Es un metal pesado muy soluble en agua, lo cual facilita su movilidad desde el suelo hasta las plantas y su biomagnificación a través la cadena trófica (Huat et al., 2019). La principal vía por la que entra en el organismo es el tabaco o la ingesta de comida, y su vida media en el interior del cuerpo humano es de 25 años debido a su baja tasa de excreción, entrando en las neuronas a través de los canales del calcio (Branca, Morucci, & Pacini, 2018). Puede penetrar la BBB, provocando cambios de comportamiento y disfunción neuronal (Unsal et al., 2020).

La presencia de Cd(II) está relacionada con algunas enfermedades neurodegenerativas como la AD, el PD, el HD y la ALS (Cabral Pinto et al., 2018; Cicero et al., 2017). Sus niveles en ciertas regiones del cerebro, como el hipocampo, son significativamente más elevadas en pacientes con AD (Bakulski et al., 2020). Sus principales características citotóxicas son debidas a la generación indirecta de ROS, alteraciones en procesos dependientes de zinc y calcio y modificaciones de los sistemas de reparación celular (Branca et al., 2019; Branca, Morucci, Maresca, et al., 2018). Se ha demostrado que el cadmio induce indirectamente estrés oxidativo y apoptosis en neuronas y astrocitos, aumentando la neuroinflamación y provocando la muerte neuronal, afectando a las funciones cognitivas (Y. Li et al., 2017; Phuagkhaopong et al., 2017). Además, inhibe la neurogénesis en el hipocampo y el bulbo olfatorio (Bakulski et al., 2020).

El cadmio es capaz de activar la vía amiloidogénica de la APP (vía β), aumentando la actividad de la BACE y de las presenilinas encargadas de su hidrólisis, debido a su efecto sobre el estrés oxidativo y la neuroinflamación (Ashok et al., 2015). Interacciona con la $A\beta_{42}$ favoreciendo su agregación y deposición en placas amiloides (Notarachille et al., 2014; Wallin et al., 2017). También afecta al sistema colinérgico, aumentando la expresión de la AChE, disminuyendo por tanto la cantidad del neurotransmisor ACh y empeorando las conexiones sinápticas del hipocampo, conllevando déficits de memoria (del Pino et al., 2014; Green & Planchart, 2018).

El cadmio se une a la tercera repetición del dominio de unión a microtúbulos de la p-tau (R_3), siendo dicha unión un dímero R_3 con un átomo de Cd en el medio, haciendo que

pierda su estructura desordenada y formando una estructura de hélice-α, promoviendo su agregación (L. F. Jiang et al., 2007). Además, aumenta la cantidad total de p-tau y favorece su hiperfosforilación (del Pino et al., 2016).

Las proteínas de choque térmico, especialmente la 70 (HSP70), son chaperonas que junto con el proteosoma 26S (P26S) se encargan de degradar las proteínas tóxicas, oxidadas y plegadas incorrectamente, como la $A\beta_{42}$ (J. Cao et al., 2019; Lackie et al., 2017). El P26S está formado por el proteosoma 19S (P19S) y 20S (P20S), siendo este último su núcleo catalítico. Al prevenir la acumulación y agregación de la proteína $A\beta_{42}$, pueden evitar el daño y la muerte neuronal (Campanella et al., 2018; Gorantla & Chinnathambi, 2018). Sin embargo, ciertos metales como el hierro, el cobre, el mercurio y el aluminio pueden alterar la expresión de la HSP70 y P20S, provocando la acumulación de dichas proteínas amiloides y el consecuente deterioro cognitivo (Asthana et al., 2014; Chernyak & Merinova, 2017; Dunham et al., 2017; Verma et al., 2020).

Además del efecto neurotóxico de dichos metales, el **desequilibrio enantiomérico de ciertos aminoácidos** también influye en el desarrollo de la AD (**Figura 7**). Los aminoácidos tienen un papel esencial dentro del organismo. Sin embargo, cualquier cambio en su concentración o isomerización puede desencadenar la progresión de varias enfermedades, como la AD (**Tabla 3**) (Bastings et al., 2019; Piubelli et al., 2021). La agregación de la $A\beta_{42}$ es estereoselectiva, ya que está compuesta por estructuras de hélices α y láminas β, por lo que cualquier cambio en el entorno quiral puede modificar la agregación de sus fibras amiloides (N. Gao et al., 2019; K. Hou et al., 2020; Malishev et al., 2018).

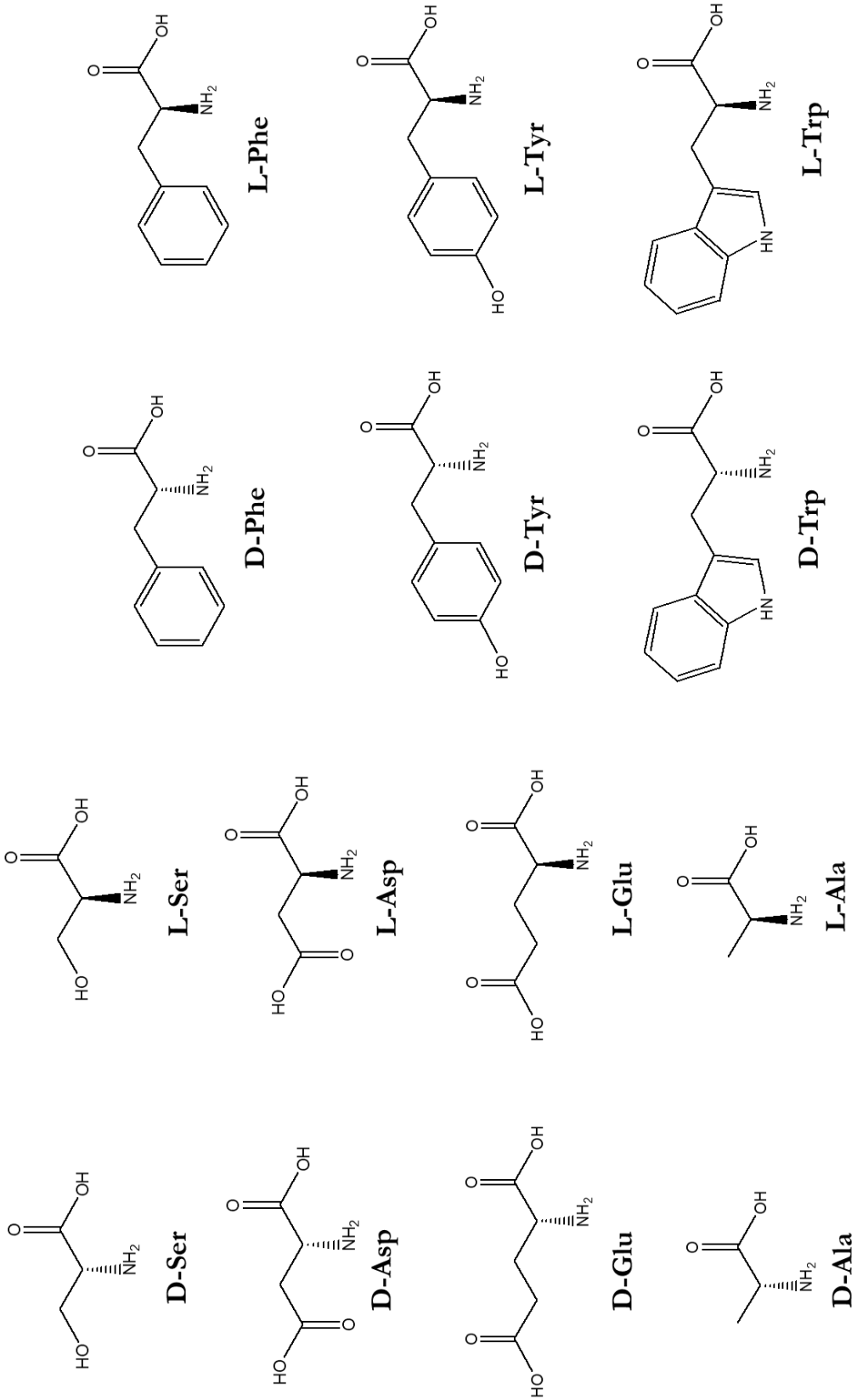


Figura 7. Enantiómeros de aminoácidos involucrados en la AD.

Tabla 3. Efectos de algunos enantiómeros de aminoácidos en el desarrollo de la AD.

Aminoácido	Racemización	Enantiómero	Neurotoxicidad	Esencialidad	Referencias
Ser	Intrínseca	D	Aumenta la agregación de la proteína $A\beta_{42}$. Antagonista del receptor NMDA	-	Du et al., 2020 Jirásková-Vaníčková et al., 2011
		L	-	Mantiene la homeostasis redox. Involucrado en procesos de neurotransmisión y señalización neuronal	Nelson et al., 2017 Fujii et al., 2018
Asp	Intrínseca	D	Favorece la formación de fibras de $A\beta_{42}$ y aumenta su agregación. Provoca deterioro de la memoria espacial y el aprendizaje. Disminuye la plasticidad sináptica y las funciones cognitivas, provocando la muerte neuronal. Antagonista del receptor NMDA	Involucrado en el desarrollo neuronal en la etapa embrionaria y perinatal	Readel et al., 2021 Rabattoni et al., 2021 Nuzzo et al., 2019 Genchi, 2017 Molla et al., 2020
		L	-	Involucrado en procesos de neurotransmision y señalización neuronal	Fujii et al., 2018
Phe	Extrínseca	D	Aumenta la agregación de la proteína $A\beta_{42}$	-	Azriel & Gazit, 2001
		L	-	Biomarcador negativo de la AD	Takayama et al., 2015

Los L-aminoácidos son la forma enantiomérica habitual en el cuerpo humano. Sin embargo, cuando estos aminoácidos que forman parte de las proteínas sufren un cambio estructural, como su racemización a D-aminoácidos, alteran las características y funciones de dichas proteínas, desencadenando la progresión de enfermedades como la AD (Bastings et al., 2019). Cuando se sustituye un L-aminoácido por un D-aminoácido en una proteína, cambia su orientación, lo que a su vez modifica su interacción con otras proteínas (Morvan & Mikšík, 2021). A medida que aumenta la edad, los D-aminoácidos se acumulan en diversas estructuras y tejidos, como la piel, ojos, huesos y cerebro (Sun et al., 2017). Las concentraciones de ciertos D-aminoácidos en el cerebro varían en función del estadío en el que se encuentren los pacientes de AD (Samakashvili et al., 2011).

La generación de D-Ser y D-Asp, al contrario que el resto de los aminoácidos, se produce de forma intrínseca en el organismo debido a la acción de la serina y aspartato racemasa sobre la L-Ser y L-Asp, ambas involucradas en procesos de neurotransmisión y señalización neuronal (Fujii et al., 2018; Genchi, 2017). Esta racemización de los L-aminoácidos a D-aminoácidos está relacionada con un aumento de la citotoxicidad y de inmunogenicidad (Abdulbagi et al., 2021). Además, el procesamiento de los alimentos favorece la racemización dando lugar a enantiómeros D, entrando a formar parte de los tejidos a través de la dieta (Bastings et al., 2019). Algunos alimentos, como las frutas, los vegetales, y la leche, contienen D-Ala, D-Asp, D-Glu y D-Ser (Abdulbagi et al., 2021). Debido a que varios D-aminoácidos tienen un sabor más dulce que sus enantiómeros L, son más usados en la industria alimentaria (Chattopadhyay et al., 2014).

Además, los neuropéptidos que contienen D-aminoácidos poseen una mayor actividad biológica que aquellos que contienen exclusivamente L-aminoácidos. Por ejemplo, la dermorfina, un hexapéptido que posee el enantiómero D-Ala en la segunda posición, tiene un efecto analgésico superior a la morfina y un efecto opioide que se pierde cuando la Ala se encuentra en la forma L (Keppel Hesselink & Schatman, 2018). La ω-agatoxina IV, una neurotoxina proveniente de la araña venenosa *Agelenopsis aperta*, contiene en su secuencia de 48 aminoácidos un residuo D-Ser en la posición Ser_{46}, lo que le facilita bloquear exclusivamente los canales del calcio tipo P en las membranas neuronales, sin afectar a los de tipo T, L y N (Kuwada et al., 1994).

Por otro lado, la presencia de D-aminoácidos en las proteínas favorece su acumulación, ya que las enzimas encargadas de degradarlas solo reconocen péptidos y proteínas compuestos exclusivamente por L-aminoácidos (Ha et al., 2017). La presencia de

enantiómeros D en la $A\beta_{42}$ es superior en las personas que padecen AD (Du et al., 2020). Esta racemización en la proteína $A\beta_{42}$, concretamente en sus residuos de Ser y Asp, favorece su deposición en placas amiloides (Readel et al., 2021). Algunos D-aminoácidos como la D-Ala, D-Ser, D-Asp y D-Glu favorecen el desarrollo de la AD, ya que se encuentran en elevadas concentraciones en los cerebros de pacientes con AD. Además, afectan a la actividad del receptor N-metil-D-aspartato (NMDA), involucrado en la adquisición de memoria y el aprendizaje, promoviendo la aparición de enfermedades neurodegenerativas (Genchi, 2017; Nuzzo et al., 2019; Wu et al., 2004). Otros aminoácidos, como la Phe, también tienen un papel fundamental en la agregación fibrilar amiloide (Azriel & Gazit, 2001). En concreto, la L-Phe se considera biomarcador de la AD, ya que un nivel bajo de este enantiómero en el cerebro es indicativo de dicha enfermedad (Takayama et al., 2015).

En el interior del cerebro, el D-Asp se localiza en las vesículas sinápticas del axón terminal de las neuronas, ejerciendo un papel neurotransmisor (Abdulbagi et al., 2021). Está involucrado en el desarrollo neuronal, morfología cerebral y el comportamiento humano (Rabattoni et al., 2021). En condiciones normales, sus niveles son más elevados en la etapa embrionaria y perinatal, y van disminuyendo posteriormente, debido a la progresiva expresión de la enzima D-Aspartato oxidasa (DASPO) que lo cataboliza (Molla et al., 2020). Sin embargo, con el tiempo la L-Asp se transforma en D-Asp de forma natural, en un proceso dependiente de la edad (Fujii et al., 2017; Readel et al., 2021). Estos residuos de D-Asp tienen tendencia a acumularse en proteínas asociadas con enfermedades relacionadas con la edad, como la AD. Por este motivo se puede considerar un biomarcador de dicha enfermedad (Ha et al., 2017).

El D-Asp provoca un deterioro de la memoria espacial, el aprendizaje y la capacidad de recordar eventos (Rabattoni et al., 2021). La exposición a concentraciones elevadas de D-Asp disminuye la plasticidad sináptica y las funciones cognitivas, a la vez que favorece la muerte celular en regiones del cerebro tales como el hipocampo, el córtex prefrontal y la sustancia negra (Nuzzo et al., 2019). También produce otros efectos neurotóxicos como la activación de la caspasa-3 y la apoptosis neuronal (Kiriyama & Nochi, 2016). El D-Asp juega un papel importante en la AD, ya que modifica la estructura de ciertas proteínas como la $A\beta_{42}$ (Fujii et al., 2018). La presencia de residuos de D-Asp en la $A\beta_{42}$ contribuye a la neurodegeneración (Du et al., 2020). Los residuos Asp_1, Asp_7 y Asp_{23} tienden a racemizarse a D-Asp, dificultando la eliminación de la $A\beta_{42}$ y favoreciendo su incorrecto plegamiento (Du et al., 2020; Fujii et al., 2016). En concreto, la racemización del Asp_{23} acelera la

formación de fibras y favorece la agregación en placas amiloides de la $A\beta_{42}$ (Tomiyama et al., 1994)

Los astrocitos son los únicos encargados de producir L-Ser en el cerebro. Este enantiómero favorece la liberación de la ApoE, involucrado en el FAD, en las células de la microglía (Mori et al., 2004). La L-Ser tiene también otras funciones fisiológicas, como mantener la homeostasis redox (Nelson et al., 2017). La D-Ser se encuentra en el cerebro en mayores concentraciones que el D-Asp y la D-Ala (Abdulbagi et al., 2021). Principalmente está ubicado en el córtex cerebral, el hipocampo, y el cuerpo estriado (Kiriyama & Nochi, 2016). Su producción proviene principalmente por la acción de la serina racemasa, transformando la L-Ser en D-Ser (Jirásková-Vaníčková et al., 2011).

Los niveles de D-Ser en sangre y en fluido cerebroespinal son superiores en pacientes con AD. Estas altas concentraciones de D-Ser provocan un empeoramiento en la memoria, concretamente en la dificultad para encontrar las palabras correctas, pérdida de la orientación y falta de comprensión (C. H. Lin et al., 2019). También aumenta la degeneración de las neuronas motoras (Kiriyama & Nochi, 2016). Entre un 5% y un 10% de la Ser, ubicada en los residuos Ser_8 y Ser_{26} en la $A\beta_{42}$, existe como D-Ser, evitando la degradación de dicha proteína (Du et al., 2020). La $A\beta_{42}$ con un residuo D-Ser en la posición Ser_{26} provoca un elevado daño a las neuronas y favorece la neurodegeneración (Abdulbagi et al., 2021). Además, la D-Ser actúa como antagonista al receptor NMDA en el CNS, que está relacionado con enfermedades neurodegenerativas como la AD, el PD, la ALS, y el HD (Jirásková-Vaníčková et al., 2011).

3. Moléculas orgánicas como posibles fármacos en la enfermedad de Alzheimer

La **Tabla 4** recoge una serie de **moléculas orgánicas** con efecto neuroprotector que han sido estudiadas durante los últimos 30 años como fármacos potenciales en la AD. Sin embargo, hasta el año 2021, solo cinco de ellas habían sido aprobadas por la agencia de Administración de Alimentos y Medicamentos de Estados Unidos (FDA) para el tratamiento de la AD: la tacrina (TAC) (1993), el donepezilo (DNP) (1996), la rivastigmina (RIV) (1998), la galantamina (2001) y la memantina (2003) (**Figura 8**). Mientras que las cuatro primeras son inhibidores de la colinesterasa, aumentando por tanto la cantidad de colina en el CNS, la última de las moléculas es un antagonista del receptor N-metil-D-aspartato (NMDA) (Cumming et al., 2014).

Tabla 4. Características de las principales moléculas orgánicas neuroprotectoras.

Molécula orgánica	Características neuroprotectoras	Referencias
TAC	AChEi y BChEi	Fernández-Bachiller et al., 2010
DNP	AChEi y anti-Aβ	Luisa et al., 2007 Ignasik et al., 2012
RIV	AChEi y BChEi	Ogura et al., 2000
Galantamina	AChEi	Cumming et al., 2014
Memantina	Antagonista NMDA	Cumming et al., 2014
Fisostigmina	AChEi	Coelho Filho & Birks, 2001
Fenserina	AChEi y anti-Aβ	Klein, 2007
Tolserina	AChEi y BChEi	Q. S. Yu et al., 2010
Eserolina	AChEi y BChEi	Zhan et al., 2010
BIM	Anti-Aβ, antioxidante y quelante de metales	Hiremathad et al., 2018 Chaves et al., 2018 Maru & Shah, 2012
Fenantridina	Antioxidante y antiinflamatorio	Yam-Canul et al., 2008 Weltin et al., 1995
Hup	AChEi	Mak et al., 2021
Cardanol	AChEi, BChEi, antioxidante y anti-Aβ	de Andrade Ramos et al., 2021
Olivetol	AChEi, BChEi, antioxidante y quelante de metales	Taslimi & Gulçin, 2018
Éster fenetílico	Anti-Aβ, antioxidante, antiinflamatorio	Morroni et al., 2018
Ácido vanílico	Antioxidante, antiinflamatorio y anti-Aβ	Singh et al., 2015 Ul Amin et al., 2017
Sesquiterpenoides	Antioxidante	Lee et al., 2018
Curcumina	Antioxidante, antiinflamatorio, anti-Aβ, y quelante de metales	M. Chen et al., 2018
Hidroxamato	Quelante de metales e inhibidor de MMP	Vandenbroucke & Libert, 2014
Teprenona	Aumenta HSP70 y anti-Aβ	Shichinohe et al., 2004
Carbenoxolona	Aumenta HSP70 y anti-Aβ	Nagayama et al., 2001
MT	Anti p-tau	Panza et al., 2016
Geldanamicina	Aumenta HSP70 y anti p-tau	Petrucelli et al., 2004
Híbridos de las moléculas anteriores	AChEi, BChEi, anti-Aβ, antioxidante y quelante de metales	Simunkova et al., 2019

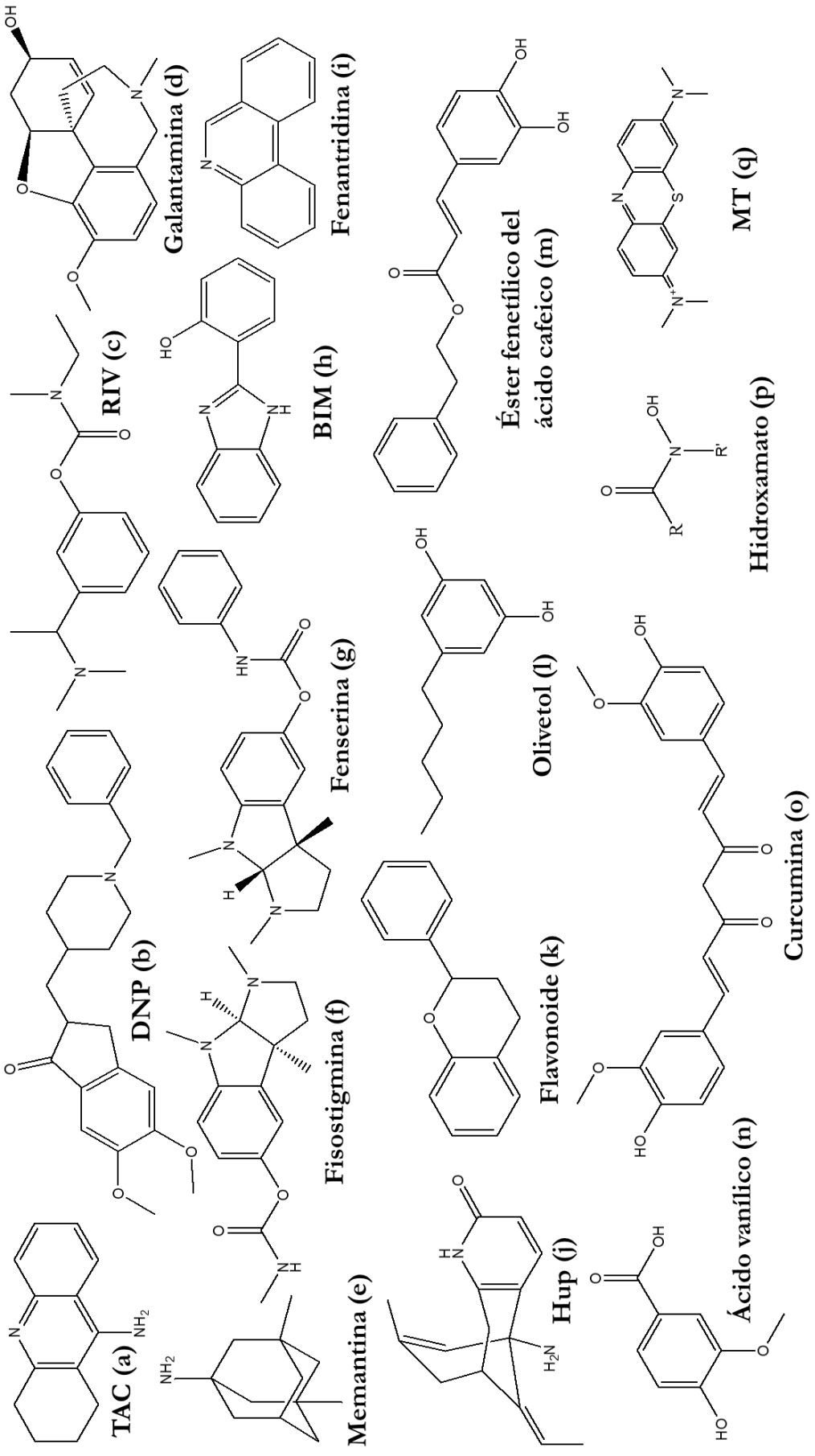


Figura 8. Estructuras de las principales moléculas orgánicas con propiedades neuroprotectoras.

La eficacia de dichos fármacos es, en muchos casos, limitada debido a la presencia de efectos secundarios y su incapacidad para detener por completo el avance de la AD. Sin embargo, en junio de 2021, la FDA otorgó la aprobación acelerada para el uso clínico del anticuerpo monoclonal Aducanumab, un fármaco que ha demostrado reducir la agregación amiloide debido a su afinidad por los aminoácidos 3-7 de la $A\beta_{42}$, siendo la primera molécula que consigue alterar la progresión de la enfermedad y no simplemente retrasarla (Karran & de Strooper, 2022). Actualmente se buscan moléculas con un potencial multi-diana, capaces de hacer frente al aspecto multifactorial de la AD: inhibidores de la agregación de la proteína $A\beta_{42}$, quelantes de metales, antioxidantes e inhibidores de la colinesterasa (Sharma, 2019).

Los inhibidores de la acetilcolinesterasa (AChEis) pueden mitigar el deterioro cognitivo en la AD disminuyendo la degradación de la ACh debida a la acción de la AChE. El sitio activo de la AChE consiste en una cavidad hidrofóbica, formada por el subsitio esteárico (ES) y el sitio de unión aniónico (AS) (Berg et al., 2011). En concreto, el AS se une a la amina cuaternaria de la ACh cargada positivamente, mientras que el ES posee una tríada catalítica, cuyos residuos son Ser_{200}, Glu_{327} e His_{440} (Tripathi & Srivastava, 2008). Entre dichos residuos, el Ser_{200} es el encargado de la hidrólisis de la ACh. El residuo Trp_{84} es el aminoácido aromático más importante en la interacción entre la AChE y la ACh, disminuyendo dicha interacción cuando este residuo es sustituido (Tougu, 2005). El sitio periférico del AS (PAS) tiene la capacidad de unirse a los péptidos de $A\beta_{42}$, favoreciendo su fibrilogénesis (Ignasik et al., 2012).

La tacrina, TAC, (**Figura 8.a**) inhibe tanto la AChE, mediante su interacción con los residuos Phe_{330} y Trp_{84} del AS de la AChE, y la butirilcolinesterasa (BChE), la enzima encargada de degradar el neurotransmisor butirilcolina (BCh) (Fernández-Bachiller et al., 2010). El DNP (**Figura 8.b**) inhibe el sitio activo de la AChE sin interaccionar con su tríada catalítica. Por el contrario, la región carbamato de la RIV (**Figura 8.c**) inhibe la ES de la AChE con más afinidad que la región acetato de la ACh (Luisa et al., 2007).

Estos inhibidores se han utilizado desde que la TAC fue aprobada por la FDA en 1993. Sin embargo, la TAC presenta varios efectos secundarios relacionados, principalmente, con la toxicidad hepática. Por ese motivo, se desarrollaron otras moléculas que también actúan como AChEi y que son más utilizadas actualmente debido a sus menores efectos secundarios y mayor selectividad, como el DNP, la RIV y la galantamina (**Figura 8.d**) (P. P. Liu et al., 2019). Mientras que el DNP y la galantamina son inhibidores altamente

selectivos de la AChE, la RIV es un inhibidor reversible tanto de la AChE como de la BChE (Ogura et al., 2000). La RIV y el DNP mejoran la capacidad cognitiva y el comportamiento de forma similar en pacientes con AD moderado. Sin embargo, la RIV presenta mayores beneficios que el DNP con respecto al funcionamiento en general y las actividades del día a día (Bullock et al., 2005). Por otra parte, la galantamina ofrece mayores mejoras en las capacidades cognitivas que el DNP (Wilcock et al., 2003). El DNP es capaz de unirse al PAS de la AChE, inhibiendo de esta forma la agregación de la $A\beta_{42}$ inducida por la AChE (Ignasik et al., 2012). En general, los derivados del DNP son eficaces deteniendo los eventos de la cascada amiloide en la AD (Mezeiova et al., 2019).

Entre los fármacos que no han sido aprobados para su uso contra la AD, se encuentra la fisostigmina (**Figura 8.f**), también llamada eserina. Esta molécula orgánica es capaz de atravesar la barrera hematoencefálica (BBB) e inhibir la AChE. Sin embargo, se degrada fácilmente y produce numerosos efectos secundarios, entre los que se incluyen diarrea, y una excesiva salivación y sudoración. Por este motivo, se ha descartado como fármaco para el tratamiento de la AD (Coelho Filho & Birks, 2001).

Además de los fármacos mencionados anteriormente, actualmente se están desarrollando nuevas moléculas orgánicas que puedan inhibir la AChE y BChE y posean propiedades adicionales. Entre ellas se encuentran la fenserina, la tolserina y la eserolina. La fenserina (**Figura 8.g**) actúa como inhibidor de la AChE mientras que paralelamente es capaz de disminuir la producción de APP, mejorando la memoria y el aprendizaje, con una toxicidad inferior a la TAC y la fisostigmina. Por lo tanto, la fenserina tiene propiedades AChEi y anti-Aβ (Klein, 2007). La tolserina tiene una estructura similar a la fenserina, siendo más inhibidora que esta última, y 200 veces más selectiva para la AChE que para la BChE (Q. S. Yu et al., 2010). La eserolina, un metabolito de la fisostigmina, es más efectiva inhibiendo selectivamente la AChE en comparación a la BChE (Zhan et al., 2010).

Otra molécula de especial relevancia es el hidroxifenilbenzimidazol (BIM) (**Figura 8.h**). Los derivados del BIM son capaces de inhibir la agregación amiloide causada por la proteína $A\beta_{42}$ (Hiremathad et al., 2018; Rodríguez-Rodríguez et al., 2009). Además, posee capacidad antioxidante, por lo que es capaz de reducir los niveles de ROS en el cerebro (Chaves et al., 2018). Los derivados del BIM interaccionan con los metales involucrados en la AD, formando complejos y evitando sus efectos tóxicos (Maru & Shah, 2012; Rodríguez-Rodríguez et al., 2009).

Las moléculas orgánicas derivadas de la fenantridina (**Figura 8.i**), han demostrado propiedades antioxidantes y reducción de la nefrotoxicidad (Yam-Canul et al., 2008). Estos derivados también aumentan la expresión del Nrf2, lo que aumenta su protección frente a los ROS (D. zhi Chen et al., 2019). Además, debido a la inhibición de la actividad de la polimerasa poli-(ADP-ribosa), poseen propiedades antiinflamatorias (Weltin et al., 1995).

Por otro lado, existen moléculas orgánicas de origen natural o procedentes de fuentes naturales que también poseen inhibición frente a la AChE. Entre ellos se encuentran la huperzina (Hup), los flavonoides y el cardanol. La Hup (**Figura 8.j**) interacciona con los residuos Trp_{84} y Phe_{330} de la AChE, existiendo dos homólogos: Hup-A y Hup-B. La Hup-A inhibe fuertemente la AChE, más eficazmente que la RIV, la galantamina y la TAC, siendo más selectiva para esta que para la BChE. Además, los híbridos entre la TAC y la Hup-A han mostrado resultados prometedores como AChEis (Camps et al., 2000; Mak et al., 2021). Los flavonoides (**Figura 8.k**), caracterizados por ser altamente antioxidantes (Gómez-Mejía et al., 2021), muestran además inhibición de la AChE (Ayaz et al., 2019). El cardanol, extraído de las cáscaras del anacardo, posee actividad AChEi, de inhibición de la BChE (BChEi), antioxidante y anti-Aβ (de Andrade Ramos et al., 2021).

El olivetol (**Figura 8.l**) es producido por algunos insectos, se encuentra presente en varias especies de líquenes y es uno de los precursores del tetrahidrocannabinol. Además, es un buen inhibidor de la AChE y de la BChE. Tiene una alta capacidad antioxidante mediante la cual reduce el Cu(II) a Cu(I) y el Fe(III) a Fe(II), siendo además capaz de quelar el Fe(II) e inhibir sus efectos tóxicos (Taslimi & Gulçin, 2018).

El éster fenetílico del ácido cafeico (**Figura 8.m**), un polifenol abundante en la miel, disminuye la apoptosis y neuroinflamación inducida por los AβOs, y protege los procesos cognitivos mejorando el aprendizaje y la memoria. Además, induce la activación de la vía Nrf2, uno de los mejores reguladores del estrés oxidativo y de la respuesta antioxidante del organismo (Morroni et al., 2018).

El ácido vanílico (**Figura 8.n**), usado como agente aromatizante, tiene múltiples propiedades beneficiosas retrasando el avance de la AD. Entre ellas se encuentran su protección frente a la neuroinflamación y su capacidad antioxidante, disminuyendo la presencia de ROS e inhibiendo la peroxidación lipídica, protegiendo la memoria y el aprendizaje (Singh et al., 2015). Además, reduce la toxicidad de la $Aβ_{42}$, inhibe su agregación y disminuye la expresión de la BACE1, enzima encargada de procesar la APP. También induce la vía Nrf2, activando una respuesta antioxidante (Ul Amin et al., 2017).

Los sesquiterpenoides presentes en el tusilago, una planta medicinal, protegen frente al efecto citotóxico provocado por el estrés oxidativo y la neurodegeneración en ratones. Esta protección antioxidante viene dada por la activación natural de la vía Nrf2, siendo considerada una prometedora aproximación terapéutica para la AD (Lee et al., 2018).

La curcumina (**Figura 8.o**), un colorante natural, aporta diversas propiedades neuroprotectoras en varias enfermedades neurodegenerativas, como en la AD. Entre ellas cabe destacar sus características de inhibición de la agregación Aβ, capacidad antioxidante, actividad antiinflamatoria y quelación del hierro. Todo ello favorece el mantenimiento estructural y funcional de los vasos cerebrales, mitocondrias, y sinapsis neuronales, disminuyendo por tanto el riesgo de padecer AD (M. Chen et al., 2018).

Actualmente, y debido a la naturaleza multifactorial de la AD, se están desarrollando compuestos híbridos entre moléculas orgánicas neuroprotectoras. Esta aproximación proporciona una gran ventaja en la lucha contra la AD, ya que se pueden obtener moléculas que combinen una amplia gama de características neuroprotectoras. Dichas características incluyen la inhibición de AChE y BChE, la inhibición de la agregación $A\beta_{42}$, la complejación metálica y el poder antioxidante (Simunkova et al., 2019; Chaves et al., 2021).

Entre estos híbridos se encuentran los provenientes del DNP con la AP2238, que actúan como AChEi y reductores de la toxicidad de la Aβ (Rizzo et al., 2010). Los híbridos DNP-TAC son capaces de interaccionar por múltiples sitios con la AChE y la BChE, siendo por tanto mejores inhibidores que sus moléculas precursoras, y además inhiben la agregación de la Aβ (Camps et al., 2008). La hibridación entre el DNP y el BIM da lugar a moléculas que combinan inhibición de la AChE con la inhibición de la $A\beta_{42}$, capacidad antioxidante y quelación de metales (Piemontese et al., 2018). Los híbridos entre la Hup y el DNP están entre los mejores inhibidores de la AChE, inhibiendo además la agregación de la $A\beta_{40}$ (Munoz-Torrero & Camps, 2006). El híbrido entre la TAC y el ácido ferúlico muestra una mayor inhibición de la AChE que la TAC, inhibe la BChE, y además tiene una alta capacidad para reducir la toxicidad derivada de la Aβ e inhibir su agregación, aumentando las habilidades cognitivas (Pi et al., 2012). Los híbridos de la TAC con la 8-hidroxiquinolina son mejores AChEi y BChEi que la TAC y, además, forman complejos con metales redox, como el Fe y el Cu, reduciendo por tanto los niveles de Aβ. Adicionalmente tienen excelentes habilidades antioxidantes, poseen baja toxicidad y son capaces de penetrar la BBB con relativa facilidad (Fernández-Bachiller et al., 2010). Los

híbridos entre la 4-benzilpiperidina/piperazina y el 3,4-dimetoxibenzil son inhibidores de la AChE, BChE y de la agregación de la $A\beta_{40}$ y $A\beta_{42}$ (Özturan Özer et al., 2013).

Con respecto a la inhibición de las metaloproteasas de matriz (MMPs), se han desarrollado múltiples moléculas capaces de reducir su actividad metaloproteasa. Los primeros inhibidores estaban basados en la estructura del colágeno con un grupo hidroxamato (**Figura 8.p**). Este grupo hidroxamato es el responsable de quelar, con una geometría muy estable, el Zn^{2+} de la enzima, de tal forma que impide la realización de su proceso catalítico (Vandenbroucke & Libert, 2014). Entre dichos inhibidores de MMPs basados en el hidroxamato se encuentran el marimastat, ilomastat y el batimastat. El marimastat fue el primero en entrar en fase clínica, siendo capaz de inhibir las MMP-2, MMP-2, MMP-7 y MMP-9 (Acharya et al., 2004). Sin embargo, estos primeros candidatos tenían numerosos efectos secundarios, por lo que se han descartado (Fingleton, 2006). Así, la nueva generación de inhibidores de las MMPs consiste en moléculas con un grupo arilo sustituido, sulfonamida y el hidroxamato. Los más conocidos son MMI-166, un inhibidor selectivo de las MMP-2, MMP-9 y MMP-14, y MMI-270. Las moléculas PD-166793, ABT-770 y prinomastat son buenos inhibidores de la MMP-1, mientras que el cipemastat es inhibidor de las MMP-1, MMP-3 y MMP-9 (Cabral-Pacheco et al., 2020). Además, también hay nuevas moléculas que no están basadas en el hidroxamato capaces de inhibir las MMPs, incluyendo grupos como carboxilatos, sulfhidrilos, derivados del ácido fosfórico e hidantoinas. Ejemplos de dichos inhibidores son el rebimastat, tanomastat, Ro 28-2653, doxiciclina y minociclina (Vandenbroucke & Libert, 2014).

Además, existen diversas moléculas orgánicas que son capaces de aumentar la expresión de proteínas de choque térmico como la HSP70, encargadas de eliminar proteínas mal plegadas como la $A\beta_{42}$. Entre ellas se encuentran la teprenona, cuya acción protege a las neuronas de la isquemia (Shichinohe et al., 2004). La carbenoxolona, usada para el tratamiento de úlceras, también aumenta la expresión de la HSP70 (Nagayama et al., 2001). Otros fármacos como la aspirina, el blimoclomol o el arimoclomol también aumentan la síntesis de la HSP70, protegiendo al organismo del plegamiento incorrecto de las proteínas (Sõti et al., 2005).

Con respecto a la inhibición de la hiperfosforilación de la p-tau, la molécula más prometedora es el metiltioninio (MT) (**Figura 8.q**), que existe en equilibrio entre su forma reducida, leuco-metiltioninio, y oxidada, MT^{+}. Activa las tau-fosfatasas e inhibe las tau-quinasas, por lo que reduce la agregación de la p-tau (Panza et al., 2016). La geldanamicina

aumenta la expresión de la HSP70, disminuyendo los niveles de p-tau y su hiperfosforilación, degradando por tanto sus especies anómalas (Petrucelli et al., 2004).

4. Importancia del selenio en la enfermedad de Alzheimer

El carácter esencial o tóxico del **selenio** ha sido objeto de controversia desde su descubrimiento hace más de 200 años. A principios del siglo XX, el selenito se consideró tóxico para los animales (Levine, 1915). Sin embargo, a mediados de siglo, se observó un efecto beneficioso del selenio a la hora de prevenir la necrosis causada por la deficiencia de la vitamina E (Schwarz & Foltz, 1957). Este efecto protector se esclareció más adelante, cuando se demostró el papel del selenio en la enzima glutatión peroxidasa 4 (GPx4) y su función frente a la peroxidación lipídica, debido a la presencia del selenio como el aminoácido selenocisteína (SeCys) (Ursini et al., 1985). Esta dualidad entre elemento esencial y tóxico se debe principalmente a dos variables: su concentración y su especie química (Nogueira et al., 2021). La toxicidad y esencialidad del selenio se suele describir con una gráfica con forma de U, en la que las concentraciones beneficiosas del selenio se encuentran en la zona intermedia (**Figura 9**) (W.-H. Cheng & Lei, 2017). El selenio es beneficioso a bajas concentraciones, siendo tóxico cuando la exposición es mayor (Hawrylak-Nowak et al., 2015). Así pues, el intervalo en el que el selenio pasa de ser esencial a ser tóxico es muy estrecho (H. El-Ramady et al., 2016).

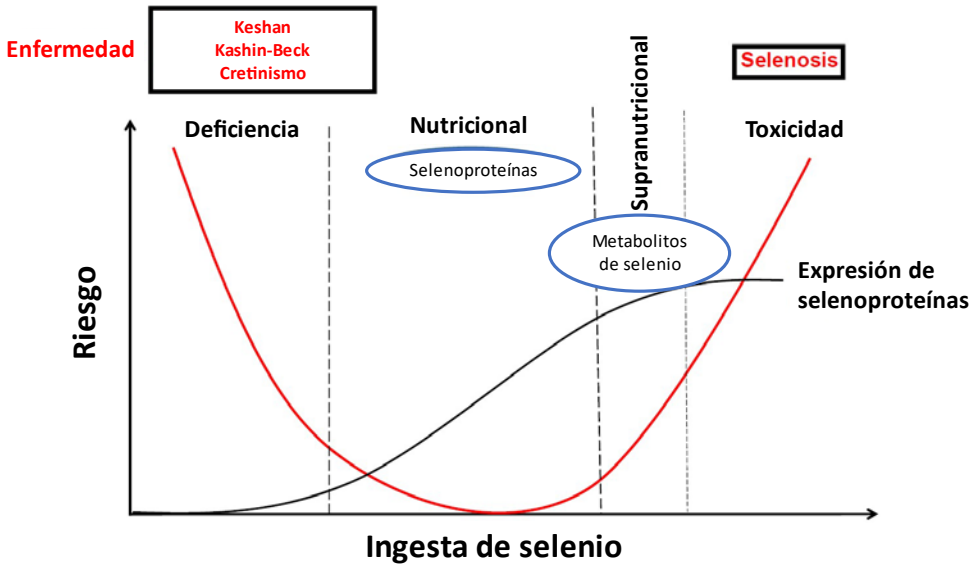


Figura 9. Esencialidad y toxicidad del selenio en función de su ingesta. Adaptación de (W.-H. Cheng & Lei, 2017).

Se considera que entre un 7% y un 15% de la población mundial tiene deficiencia de selenio, por lo que su adquisición adquiere una importancia relevante (L. C. Tan et al., 2016). Los límites de consumo diario mínimo y máximo recomendados de este micronutriente se encuentran entre 30 y 400 μg · día^{-1} (Dinh et al., 2018). El selenio es adquirido por el organismo principalmente a través de los alimentos (Emmanuelle et al., 2012). Entre dichos alimentos destacan especialmente los productos cárnicos y el pescado (dos Santos et al., 2017). Sin embargo, otro tipo de alimentos como los cereales, las verduras, las frutas y el agua de consumo también poseen cantidades considerables de este micronutriente (J. S. Dias, 2012; H. R. El-Ramady et al., 2015; Lemire et al., 2010; Qin et al., 2013).

Los organismos acuáticos, principalmente los pescados, tienen la mayor cantidad de selenoproteínas de entre todos los seres vivos, incluyendo los mamíferos (Lobanov et al., 2009). Por tanto, los pescados, como el salmón o el pez espada, son una gran fuente de selenio, especialmente en forma de selenometionina (SeMet) (Sele et al., 2018). Además, el selenio puede estar presente en los pescados en menor medida en forma de selenocisteína (SeCys) y de selenometilselenocistina (MeSeCys) (Bryszewska & Måge, 2015). Debido a la gran variedad de las propiedades del selenio en función de su especie química, se hace necesaria su especiación en alimentos y en muestras biológicas (Jagtap et al., 2016).

Cuando el organismo posee niveles bajos de selenio, padeciendo por tanto una deficiencia de este, se originan varias enfermedades entre las que se pueden destacar la enfermedad de Keshan (KD), la enfermedad de Kashin-Beck (KBD) y el cretinismo. La KD es una cardiomiopatía endémica, cuyo origen tuvo lugar en el año 1935 en el condado de Keshan en la provincia de Heilongjiang, China (Zhou et al., 2018), mientras que la KBD es una afectación osteoarticular degenerativa endémica detectada en ciertas áreas del Tibet, y el cretinismo una deficiencia congénita autosómica recesiva de la glándula tiroides.

La ingesta moderada de selenio orgánico aporta múltiples beneficios para el organismo. El consumo de levadura enriquecida con selenio mejora la memoria espacial y el aprendizaje, aumenta la actividad neuronal, ayuda a la preservación sináptica, y reduce los niveles de la p-tau y su hiperfosforilación, siendo un candidato prometedor contra el avance de la AD (Z. H. Zhang et al., 2017). También se ha demostrado que el selenio es capaz de aportar beneficios contra otro tipo de enfermedades, como el cáncer y la tiroides (Soriano-Garcia, 2012). Sus características antioxidantes vienen en gran medida por su presencia en diversas enzimas, como las GPx (Sors et al., 2009). El selenio posee, además, una elevada

facilidad para quelar biometales cuyo estrés oxidativo favorece el desarrollo de la AD, como el Cu y el Fe, y biometales implicados en las metaloproteasas de matriz (MMP), como el Zn (Rahmanto & Davies, 2012). Además, es capaz de quelar metales tóxicos, como el Hg, el Cd y el Al, y de reducir su toxicidad mediante la formación de complejos inertes (Ismael et al., 2019; Nuttall & Allen, 1984; Peak, 2006; Rahman et al., 2019; Zwolak, 2020).

Con respecto al consumo supranutricional de selenio, se ha demostrado que elevadas dosis de determinadas especies de selenio pueden provocar problemas para la salud, tal y como se hablará en la siguiente sección. Entre los cuales se pueden encontrar, por ejemplo, el aumento del riesgo de padecer la EOAD y la sobreexpresión de selenoenzimas cuyos niveles anormales causan resistencia a la insulina, como la glutatión peroxidasa 1 (GPx1) y la metionina sulfóxido reductasa (MsrB1) (Adani et al., 2020; Labunskyy et al., 2011).

4.1. Especies de selenio

Sin embargo, las propiedades del selenio dependen de la forma química en la que se encuentre presente (**Tabla 5**). Estas formas químicas, también llamadas especies, se diferencian en el estado de oxidación del selenio, su composición isotópica, o su estructura química (Feldmann et al., 2014). Dicha estructura puede variar en función de los ligandos unidos al selenio o si dicho selenio se encuentra en forma de **nanopartículas** (**Figura 10**) (H. W. Tan et al., 2019). La principal división entre especies no nanoparticuladas de selenio, se realiza entre el llamado selenio inorgánico y el selenio orgánico. La especiación entre ambas formas del selenio es crucial a la hora de determinar la neurotoxicidad en enfermedades degenerativas (Vinceti et al., 2019).

Tabla 5. Propiedades de las diferentes especies del selenio.

Especie de Se	Propiedades	Referencias
Se(IV)	Provoca estrés oxidativo, muerte celular y daño mitocondrial Daño en el ADN	Romero et al., 2019 Letavayová et al., 2006
Se(VI)	Provoca estrés oxidativo, muerte celular y daño mitocondrial Aumenta riesgo de padecer AD	Romero et al., 2019 Vinceti et al., 2017
SeMet	Forma parte de proteínas que contienen selenio Antioxidante y reparadora del ADN Quelante de metales Reduce neurotoxicidad de metales Reparadora del CNS	Letavayová et al., 2006 Seo et al., 2002 Battin et al., 2011 Whanger, 2001 Zheng et al., 2017
SeCys	Forma parte de selenoproteínas Antioxidante Anticarcinogénica Quelante de metales	Zoidis et al., 2018 Khurana et al., 2019 Hatfield et al., 2014 Battin et al., 2011
MeSeCys	Forma parte de proteínas que contienen selenio Anticarcinogénica	Letavayová et al., 2006 M. Chen et al., 2019
Nanopartículas	Anti-Aβ Quimiopreventivas, anticarcinogénicas y antimicrobianas	Wang et al., 2017 Wadhwani et al., 2016

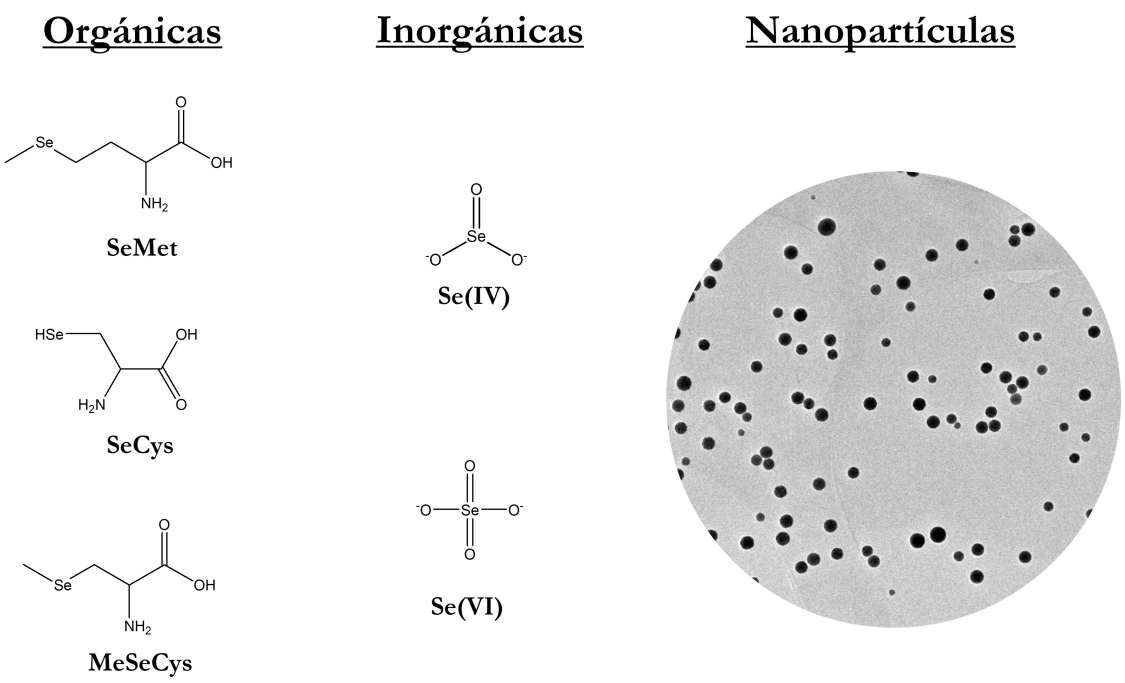


Figura 10. Estructura química de las principales especies del selenio.

Las principales especies inorgánicas del selenio son el selenito, Se(IV), y el selenato, Se(VI), (**Figura 10**) mucho más tóxicas que las especies orgánicas (Vinceti et al., 2018). En ambientes secos, el Se(IV) es la especie predominante, mientras que en ambientes oxidantes el Se(VI) es mayoritario (Y. Li et al., 2020). Ambas formas de selenio inorgánico producen estrés oxidativo, muerte celular y daño mitocondrial (**Tabla 5**) (Romero et al., 2019). En términos generales, se considera el Se(VI) más tóxico que el Se(IV), aunque sus mecanismos de citotoxicidad no están del todo definidos (Tian et al., 2017). La sustitución del S de las proteínas por Se puede destruir la función molecular de dichas proteínas, lo que convierte al selenio inorgánico en tóxico para el organismo. La presencia de altos niveles de Se(VI) en el líquido cerebroespinal aumenta el riesgo de desarrollar AD (Vinceti et al., 2017). El Se(IV) ha demostrado inducir daños en el ADN, especialmente en las bases nitrogenadas y en las cadenas, provocando rupturas (Letavayová et al., 2006). Este daño se debe a su reducción a Se(0) a través de ciclos bioquímicos, provocando estrés oxidativo (Khurana et al., 2019).

Por otra parte, las principales especies orgánicas del selenio son la selenometionina (SeMet), la selenocisteína (SeCys) y la selenometilselenocisteína (MeSeCys) (**Figura 10**) (Hariharan & Dharmaraj, 2020). La SeCys y la SeMet poseen una estructura similar a la

cisteína y a la metionina, excepto por la sustitución del átomo de azufre por un átomo de selenio (Zoidis et al., 2018). El selenio se incorpora de forma específica a las proteínas como SeCys, siendo consideradas selenoproteínas, y de forma no-específica como SeMet, ocupando el lugar de la metionina y siendo consideradas proteínas que contienen selenio (Letavayová et al., 2006).

La SeCys, considerada como el aminoácido número 21, está codificada por el codón UGA. Mediante una incorporación co-traduccional, esta SeCys se incorpora a la cadena polipeptídica de las proteínas, siendo consideradas a partir de ese momento selenoproteínas (Zoidis et al., 2018). La SeCys está presente en la parte más importante del centro activo de la zona enzimática de las selenoproteínas, mediando la actividad oxidorreductasa y el equilibrio redox fisiológico (Khurana et al., 2019). Puesto que forma parte de las selenoproteínas, ejerce un papel fundamental en diversas actividades como la reducción de las tiorredoxinas, hormonas tiroideas, y en el papel anticarcinogénico del sistema inmune, entre otros (**Tabla 5**) (Hatfield et al., 2014). Inhibe el daño oxidativo provocado al ADN mediante la quelación del Cu (Battin et al., 2006) con estequiometrías 1:1 y 1:2 (Cu:SeCys) (Battin et al., 2011). Además, es capaz de interaccionar con proteínas que contienen complejos de Zn-S, como las metalotioneínas, modificando la liberación del zinc y su homeostasis (Blessing et al., 2004).

La SeMet ha demostrado ser capaz de reparar el ADN mediante un mecanismo redox (Seo et al., 2002). Este mecanismo consiste en la quelación de metales redox activos, como el cobre y el hierro (Battin et al., 2006), con estequiometrías desde 1:1 hasta 1:3 (metal:SeMet) (Battin et al., 2011). Además, es la especie de selenio que llega con más facilidad al cerebro, ejerciendo un efecto neuroprotector frente a la toxicidad de ciertos metales como el cadmio, el mercurio, el vanadio y el plomo (Whanger, 2001). Ha demostrado una gran efectividad promoviendo la proliferación de células madre neuronales y su diferenciación en neuronas maduras, reparando por tanto el CNS (**Tabla 5**) (Zheng et al., 2017).

La MeSeCys es la especie de selenio que más beneficios anticarcinogénicos aporta (M. Chen et al., 2019). Es capaz de inducir la apoptosis, detener el crecimiento y bloquear vías de señalización en líneas celulares tumorales (**Tabla 5**) (Unni et al., 2005).

4.2. Nanopartículas de selenio como posibles agentes neuroprotectores

Las **nanopartículas** son partículas cuyas tres dimensiones tienen una longitud menor de 100 nm. Este tamaño particular les confiere características y propiedades únicas (Shchipunov, 2012). Pueden ser utilizadas para el tratamiento de diversas enfermedades, como la AD o el PD, ya que en función de su forma, composición, tamaño y funcionalización de la superficie poseen diversas propiedades, entre las que se incluyen la inhibición de la agregación Aβ y la reducción de su toxicidad (Radic et al., 2015; B. Wang et al., 2017; C. Wang et al., 2013). En concreto, las nanopartículas de selenio (SeNPs) poseen propiedades fisicoquímicas muy variadas, ya que pueden ser quimiopreventivas, anticarcinogénicas y antimicrobianas (**Figura 11**) (Wadhwani et al., 2016). Su papel en el tratamiento de la AD es prometedor, ya que debido a su tamaño son capaces de penetrar la BBB (Gupta et al., 2019). Como se ha mencionado anteriormente, el intervalo en el que el selenio pasa de ser esencial a tóxico es muy estrecho, por lo que las SeNPs al poseer una baja toxicidad son candidatos idóneos para tratar enfermedades como la artritis, la diabetes o el cáncer (Khurana et al., 2019).

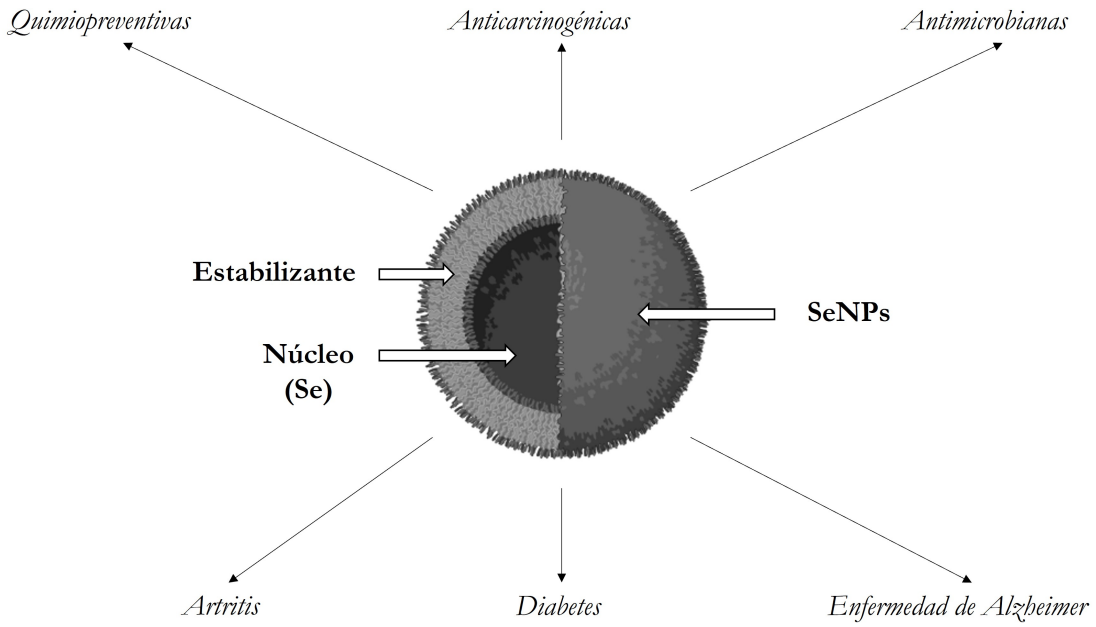


Figura 11. Estructura de las nanopartículas de selenio y principales aplicaciones.

La superficie de las SeNPs, una vez sintetizadas por procedimientos químicos y/o biogénicos, puede funcionalizarse con una plétora de ligandos que las estabilizan y les

aportan características adicionales. Esta amplia gama de propiedades beneficiosas que se les pueden aportar a las SeNPs constituye una nueva vía para el tratamiento sinérgico de una multitud de enfermedades (Sims et al., 2017). Entre dichas moléculas cabe destacar el quitosano, el polisacárido alcalino natural más biocompatible y biodegradable, que además posee baja toxicidad (S. Yu et al., 2019). Su uso médico está aprobado para el transporte de fármacos a través de varias rutas de administración (Mohammed et al., 2017). El quitosano protege a las nanopartículas de la degradación enzimática, además de favorecer la biodisponibilidad, la liberación controlada, el transporte desde la cavidad nasal hasta el cerebro y la permeabilidad de la BBB (S. Yu et al., 2019). Debido a su superficie mucoadhesiva, las nanopartículas de selenio estabilizadas con quitosano (Ch-SeNPs) se pueden adherir a las membranas mucosas y liberarse progresivamente (Mohammed et al., 2017). Otra propiedad del quitosano es su quiralidad, siendo especialmente útil para el tratamiento de la AD cuando intervienen distintos enantiómeros de aminoácidos (Jafari et al., 2018; Z. Li et al., 2017). Otro ejemplo de SeNPs con capacidad quiral son aquellas estabilizadas con D-penicilamina, siendo capaces de inhibir la agregación Aβ causada por el Zn(II) (Sun et al., 2017).

Además, las SeNPs se pueden recubrir con multitud de compuestos con el objetivo de reducir su toxicidad e incluso de reducir la agregación de la Aβ. Esta inhibición de la formación de fibras de Aβ se puede llevar a cabo mediante la disrupción, por parte de las SeNPs, de las interacciones hidrofóbicas y electrostáticas en la nucleación amiloide (L. Yang et al., 2017). El sulfato de condroitina es otra molécula usada en el recubrimiento de las SeNPs que inhibe la agregación y la citotoxicidad de la Aβ (F. Gao et al., 2020). Los polifenoles han demostrado propiedades muy beneficiosas para el organismo, como su alta capacidad antioxidante, antiinflamatoria, anticancerígena, antibactericida, antimicrobiana y antiviral (Shahidi & Ambigaipalan, 2015). Ciertos polifenoles tienen además propiedades neuroprotectoras, por lo que su uso en el recubrimiento de las SeNPs podría ayudar en la lucha contra la AD (J. Zhang et al., 2014). En concreto, el polifenol hesperidina mejora la memoria y el aprendizaje, además de ser antioxidante, antiinflamatoria y neurogénica (Naewla et al., 2019). El resveratrol es antioxidante, antitumoral, aumenta la plasticidad neuronal y la neurogénesis del hipocampo y las habilidades cognitivas (G. P. Dias et al., 2016). El ácido clorogénico (CGA) es un estimulante del CNS, además de ser cardioprotector, antiinflamatorio, y antioxidante (Naveed et al., 2018).

5. Técnicas y métodos (bio)analíticos para la caracterización y la evaluación de la capacidad neuroprotectora de moléculas orgánicas y de especies de selenio

La evaluación de la actividad neuroprotectora de moléculas potencialmente eficaces en el tratamiento de la AD requiere el uso de una gran variedad de técnicas y metodologías. Dichas técnicas son muy diversas, partiendo desde la escala más fundamental de las interacciones moleculares y su estudio espectroscópico, transitando por el análisis y cuantificación de la agregación de proteínas, y culminando con experimentos *in vitro* con líneas celulares e *in vivo*.

5.1. Técnicas analíticas para los estudios de inducción e inhibición de la agregación de la proteína $A\beta_{42}$, inhibición enzimática y capacidad antioxidante

La parte más extensa de esta tesis se ha basado en la evaluación de diversos agentes que inducen (metales y enantiómeros de aminoácidos) o inhiben (moléculas orgánicas y Ch-SeNPs) la agregación amiloide de la proteína $A\beta_{42}$.

La proteína **$A\beta_{42}$** es la piedra angular de las actuales estrategias en el desarrollo de fármacos para el tratamiento de la AD, ya que su agregación es la iniciadora en la "hipótesis de la cascada amiloide", principal responsable del desarrollo de la AD. Como se ha mencionado anteriormente, los eventos provocados por la agregación de la $A\beta_{42}$ en placas amiloides extracelulares incluyen el deterioro de las sinapsis interneuronales, disminución de la respiración mitocondrial en neuronas y astrocitos, estrés oxidativo, neuroinflamación y la formación de ovillos intracelulares debidos a la hiperfosforilación de la p-tau con la consecuente interrupción del metabolismo celular en las neuronas (Karran & de Strooper, 2016).

La agregación de la proteína $A\beta_{42}$ y la consecuente neurodegeneración puede deberse a varios motivos, entre los cuales destacan el efecto de biometales, metales tóxicos y enantiómeros de aminoácidos. Con el objeto de neutralizar el efecto neurotóxico de metales y aminoácidos, se hace necesaria la búsqueda de inhibidores de la agregación amiloide provocada por la proteína $A\beta_{42}$. Para obtener las fibras amiloides se deben incubar los monómeros de $A\beta_{42}$, pretratados con un disruptor de láminas beta como el 1,1,1,3,3,3-hexafluoro-2-propanol (HFIP), durante un determinado tiempo a 37 °C, en presencia y ausencia de compuestos que favorezcan o inhiban su agregación (Zhang-Haagen et al.,

2016). Existen diversos parámetros a tener en cuenta para evaluar las fibras amiloides, como su morfología, determinada por su anchura y longitud, y la cantidad de agregación.

Para evaluar la morfología de la agregación de la proteína $A\beta_{42}$ se puede hacer uso de técnicas de microscopía, como la **microscopía electrónica de transmisión** (**TEM**) (Nilsson, 2004). Para observar correctamente dichas fibras es necesario emplear métodos de tinción negativa, como el uso de acetato de uranilo. Además, el voltaje utilizado por el microscopio no debe ser demasiado elevado para evitar la degradación de la materia orgánica. Con las micrografías obtenidas se pueden obtener datos de agregación de la proteína $A\beta_{42}$ bajo diferentes condiciones, y estimar la longitud y anchura de las fibras utilizando programas como ImageJ (Moreno, 2007).

No obstante, para determinar y cuantificar exactamente el porcentaje de inhibición de agregación amiloide, debido al uso de moléculas neuroprotectoras, el método más preciso consiste en la utilización de la **tioflavina T (ThT)** y la **fluorescencia molecular**. La ThT se intercala entre fibras de $A\beta_{42}$ agregadas, cambiando su estructura y por tanto su longitud de excitación, de 415 nm en su forma libre a 450 nm en unión con la proteína, con una emisión a 490 nm. Este aumento en la intensidad de la ThT a 490 nm, debido a la agregación de la $A\beta_{42}$, se puede determinar mediante espectroscopía de fluorescencia (M. Yu et al., 2019).

5.1.1. Caracterización de nanopartículas de selenio como agente inhibidor de la agregación de la proteína $A\beta_{42}$

Como se ha mencionado en apartados anteriores, las nanopartículas de selenio pueden ser una herramienta útil para la lucha contra la AD, siendo imprescindible su correcta caracterización mediante diversas técnicas (Khurana et al., 2019).

Existe una gran variedad de técnicas para la caracterización de nanomateriales. En la presente Tesis Doctoral se han aplicado la espectroscopía ultravioleta-visible (UV-Vis), la microscopía electrónica de transmisión (TEM) y la dispersión dinámica de luz (DLS), proporcionando esta última el radio hidrodinámico y la medida del potencial Z (ZP).

La banda que presentan las nanopartículas en la espectroscopía UV-Vis se relaciona con su morfología, tamaño y dispersión. Por tanto, es una herramienta analítica útil y sencilla a la hora de evaluar los resultados obtenidos en la síntesis de las nanopartículas y su estabilidad frente a la agregación durante su almacenamiento (Rolim et al., 2019). La

TEM constituye la técnica de referencia para la caracterización de nanopartículas, ya que permite obtener información sobre el diámetro, morfología, agregación y dispersión de tamaños a partir de las micrografías. Generalmente, los análisis mediante TEM van acompañados de análisis de espectroscopía de energía dispersiva de rayos-X (EDXS), que proporciona información sobre la composición de las nanopartículas (Hayat et al., 2011). El análisis por TEM permite estimar el tamaño "core" de las nanopartículas. Sin embargo, cuando estas se encuentran en dispersión, es preferible determinar el tamaño hidrodinámico, que abarcaría el núcleo del metal/metaloide de la nanopartícula además de todo lo que le rodea (estabilizante, solvente, proteínas, etc).

Otro parámetro de gran interés para caracterizar nanopartículas es el potencial zeta (ZP), definido como el potencial con el cuál se mueven las partículas coloidales bajo un campo eléctrico. El ZP ofrece información acerca de la estabilidad de las nanopartículas frente a la aglomeración, considerándose altamente inestables ($|ZP| < 10$ mV), relativamente estables (10 mV $< |ZP| < 20$ mV), moderadamente estables (20 mV $< |ZP| < 30$ mV) y altamente estables ($|ZP| > 30$ mV). La determinación del diámetro hidrodinámico y la determinación del ZP se realiza mediante la técnica de dispersión dinámica de luz (DLS) (Bhattacharjee, 2016).

5.1.2. Estudio de las interacciones con metales y aminoácidos

A lo largo de esta introducción se ha hecho especial énfasis en los efectos neurotóxicos de determinados biometales (Fe(II), Cu(II) y Zn(II)), metales tóxicos (Hg(II), Cd(II) y Al(III)) y enantiómeros de aminoácidos (D-Ser, D-Asp, D-Phe, D-Ala y D-Glu). Sin embargo, para hacer frente a estos efectos perjudiciales, que agravan la AD, una de las principales vías es el desarrollo de moléculas que puedan interaccionar con dichos metales y aminoácidos y que contrarresten, por tanto, su efecto. Para estudiar la interacción entre estas moléculas de interés se pueden emplear técnicas espectroscópicas como la espectroscopía UV-Vis y la espectroscopía de fluorescencia.

La espectroscopía UV-Vis permite determinar la formación de complejos mediante la observación en las bandas de absorción, ya que están irremediablemente ligadas a la estructura de las moléculas. De esta forma, cualquier cambio en la absorción en el intervalo UV-Vis de una molécula puede implicar la formación de un complejo con los metales o aminoácidos de interés (Battin et al., 2011). Para lograr una mayor eficacia en el análisis de

las medidas de absorbancia se pueden llevar a cabo tratamientos matemáticos de los espectros registrados, como la primera derivada del espectro de absorción. La espectroscopía derivada permite acentuar las diferencias espectrales, resolver superposiciones de bandas, minimizar el efecto de moléculas que no sean de interés y reducir el ruido de fondo (Georgieva et al., 2018). Adicionalmente, se pueden usar estas técnicas para elucidar la relación de concentración metal:molécula óptima de los posibles complejos formados, mediante la búsqueda de la banda de absorción que presente un mayor cambio en su intensidad.

No obstante, la sensibilidad de la espectroscopía UV-Vis no alcanza, en ocasiones, los niveles requeridos. En estos casos se pueden usar otras técnicas como la espectroscopía de fluorescencia, mucho más sensible y selectiva, aunque limitada a ciertos compuestos. Para emplear dicha técnica, el primer requisito básico que deben cumplir las moléculas objeto de estudio es poseer fluorescencia o ser susceptibles de ser derivatizadas para producir derivados fluorescentes. En el caso de los enantiómeros de aminoácidos que no poseen fluorescencia y necesitan, por tanto, una derivatización previa, uno de los reactivos más utilizados es el orto-ftalaldehído (OPA) (Rubio-Barroso et al., 2006). Mediante la fijación de una longitud de excitación y haciendo un barrido del espectro de emisión, o viceversa, se puede obtener un espectro de fluorescencia de la molécula en presencia y ausencia del agente quelante. Comparando ambos espectros se puede determinar la existencia o no de la interacción entre ambos y estudiar de la relación de concentración óptima de los posibles complejos formados.

5.1.3. Determinación de la inhibición enzimática

Según la "hipótesis colinérgica" anteriormente mencionada, el déficit de neurotransmisores como la ACh y la BCh impide el correcto funcionamiento de las sinapsis entre las neuronas del hipocampo. Este fallo del sistema colinérgico produce un empeoramiento en la calidad de vida de las personas afectadas con AD. Las estrategias actuales para solventar dicho problema se basan en la búsqueda de inhibidores de la AChE (AChEi) y la BChE (BChEi). Estos inhibidores, al contrarrestar el efecto de las colinesterasas, aumentan las cantidades disponibles de ACh y BCh en el cerebro, protegiéndolas de su degradación enzimática. Estas moléculas neuroprotectoras pueden presentar diferentes afinidades a la hora de inhibir la AChE y la BChE, cuantificando esta especificidad mediante el llamado índice de selectividad AChE/BChE (SI).

Para determinar la capacidad de inhibición enzimática de posibles moléculas neuroprotectoras se hace imprescindible el uso de métodos analíticos que permitan un adecuado seguimiento en el tiempo de la actividad de la AChE y BChE sobre la ACh y BCh, respectivamente. Una de las estrategias más ampliamente utilizadas, con diversas variantes, es el método de Ellman (Quintanova et al., 2015).

El fundamento del método Ellman consiste en la reacción de la ACh (o BCh) con la AChE (o BChE) para generar colina, que a su vez degrada el ácido incoloro 5,5-ditio-bis-(2-nitrobenzoico) (DTNB) transformándolo en el ácido de color amarillo 5-tio-2-nitrobenzoico (TNB). La cinética de la reacción se monitoriza midiendo la absorbancia del producto TNB a 405 nm frente al tiempo utilizando un espectrofotómetro UV-Vis. Paralelamente, se mide la generación de TNB en presencia de la molécula inhibidora de la AChE o BChE, obteniendo una disminución en la cinética de la reacción frente a la obtenida en la reacción control. Representando la inhibición enzimática frente al tiempo se puede calcular el valor de IC_{50} para las moléculas objeto de estudio, siendo mejores índices AChEi/BChEi cuanto menor sea este valor.

5.1.4. Evaluación de la capacidad antioxidante

El estrés oxidativo provocado en el cerebro ha demostrado tener un papel relevante en el progreso de la AD. Por ello, la búsqueda de moléculas con capacidad antioxidante es una de las múltiples estrategias para el desarrollo de fármacos con potencial neuroprotector. Existen varios métodos para determinar la capacidad antioxidante de las moléculas, entre los que cabe destacar el método del radical libre 2,2-difenil-1-picrilhidrazilo (DPPH$^{\bullet}$) y el método de las sustancias reactivas del ácido tiobarbitúrico (TBARS). Ambos métodos utilizan la espectroscopía UV-Vis para la determinación de la capacidad antioxidante.

El método del radical libre DPPH$^{\bullet}$ se basa en su reducción a DPPH-H mediante la acción antioxidante de los compuestos neuroprotectores. El radical DPPH$^{\bullet}$ es estable en oscuridad y de color violeta, presentando un máximo de absorción a 515 nm. En presencia de concentraciones crecientes de una molécula antioxidante, el DPPH$^{\bullet}$ se va reduciendo mediante una cesión de protones por parte de dicha molécula, pasando por un violeta menos intenso hasta alcanzar un color amarillo, indicativo de la presencia de la especie DPPH-H. Este proceso de reducción requiere de la fijación del tiempo estacionario, es decir, el periodo de tiempo necesario para que se desarrolle la actividad antioxidante de la

molécula neuroprotectora. La efectividad en esta inhibición de la absorbancia medida a 515 nm es la que determina la capacidad antioxidante de la molécula. El resultado de dicho método se expresa como concentración media inhibitoria (IC_{50}), en la cual la intensidad de la banda de absorbancia se reduce a la mitad, siendo más antioxidante cuanto menor sea su valor de concentración (Gulcin, 2020).

Otro método, con una aproximación más realista ya que se desarrolla *in vitro* en una matriz biológica, es el del TBARS. En este método, el malondialdehido (MDA), un producto de peroxidación lipídica, reacciona con el ácido tiobarbitúrico (TBA), en presencia de calor y medio ácido, con una estequiometría 1:2 produciendo el complejo de color rosa MDA-TBA_2 que absorbe a 532 nm. Para lograr la oxidación, se emplea un ion metálico, como por ejemplo una mezcla de Fe con ascorbato. En presencia de moléculas antioxidantes, se reduce la formación del complejo rosa, por lo que mediante espectroscopía UV-Vis se observa una disminución de su banda de absorción, siendo menos intensa a medida que aumenta la capacidad antioxidante de la molécula. De la misma forma que para el método del $DPPH^{\bullet}$, se obtiene un valor de IC_{50} que permite cuantificar el poder antioxidante de la molécula neuroprotectora (Gulcin, 2020).

5.2. Técnicas bioinformáticas para la síntesis inteligente de fármacos

5.2.1. Diseño y modelización computacional

El diseño y modelización computacional de las moléculas orgánicas, con potencial aplicación en el desarrollo de fármacos, es una herramienta indispensable. Mediante este diseño utilizando técnicas computacionales se pueden construir moléculas que teóricamente sean capaces de inhibir enzimas relevantes en la AD, como la AChE y la BChE, para su posterior síntesis en el laboratorio (Acuna et al., 2020).

Para llevar a cabo esta simulación se deben obtener las estructuras cristalográficas de rayos-X de complejos modelo enzima-inhibidor del banco de datos de proteínas (PDB), de inhibidores que previamente hayan demostrado interacción con dichas enzimas (Berman et al., 2000). Utilizando el programa Maestro de Schrödinger se pueden tratar las estructuras obtenidas del PDB, eliminando el inhibidor original del centro activo de la enzima, y construir las estructuras de las moléculas orgánicas deseadas (Demirayak et al., 2019). Estas estructuras se deben optimizar para encontrar la de menor energía mediante una búsqueda conformacional aleatoria utilizando un programa como Ghemical (Kayshev et al., 2019).

Posteriormente, se realiza un *docking* de la estructura optimizada de la molécula orgánica en la cavidad enzimática, para lo que se puede usar el programa GOLD, previa comprobación de sus parámetros mediante un *re-docking* del inhibidor original (Islam et al., 2021). Para visualizar y analizar las interacciones entre los potenciales fármacos y los sitios activos de las cavidades enzimáticas, se pueden usar programas como Chimera (Pettersen et al., 2004).

Mediante estudios computacionales también se puede predecir la quelación de metales involucrados en la AD por parte de moléculas orgánicas. Una de las estrategias es la utilización de la teoría de orbitales moleculares frontera, que consiste en la transferencia de electrones desde el orbital molecular ocupado más alto (HOMO) hasta el orbital molecular vacío más bajo (LUMO) para formar nuevos enlaces. Debido a que el HOMO es el encargado de donar electrones, mientras que el LUMO se encarga de aceptarlos, cuanto mayor es la distancia entre ambos orbitales, mayor es la polarizabilidad y normalmente su reactividad (Kumer et al., 2019).

5.2.2. Predicción de propiedades farmacocinéticas

El proceso de desarrollo de fármacos es, generalmente, prolongado en el tiempo, consistiendo además de múltiples etapas. Las propiedades de dichos fármacos están ligadas inexorablemente a su estructura, por lo que conocerla en detalle con anterioridad resulta de utilidad para comenzar las primeras etapas de experimentación (Meanwell, 2016).

Para desarrollar una molécula, que pueda ser útil para el tratamiento de alguna enfermedad, conviene seguir el llamado "diseño racional de fármacos". Este diseño consiste en un estudio previo a la síntesis orgánica, en el cual se pueden predecir *in silico* algunas propiedades indispensables que deben tener las nuevas moléculas orgánicas para poder ser administradas como fármacos (Lipinski, 2000). Esto se debe a que el fármaco debe alcanzar su objetivo con la suficiente concentración en su forma bioactiva y perdurar el tiempo necesario para ejercer su papel neuroprotector (Daina et al., 2017).

Las características farmacocinéticas más deseables se encuentran definidas por la regla de Lipinski. Esta regla empírica enuncia que la absorción y la permeabilidad son más elevadas cuando hay cinco o menos donadores de enlaces por puentes de hidrógeno (aquellos átomos de nitrógeno y oxígeno con un átomo de hidrógeno), diez o menos aceptores de enlaces por puentes de hidrógeno (aquellos átomos de nitrógeno, oxígeno y flúor), la masa molecular menor de 500 $g \cdot mol^{-1}$, y un coeficiente de partición octanol-agua log P menor de 5. Es decir, cuanto más pequeña y lipofílica sea la molécula orgánica,

mayores probabilidades tendrá de cumplir los requisitos para ser un posible fármaco. Debido a que todos estos límites son múltiplos de 5, a esta regla se la conoce como "regla de 5 de Lipinski" (Lipinski et al., 2012). La regla se fundamenta, principalmente, en el hecho de que el 90% de los fármacos de vía oral cumplen al menos tres de estos cuatro requisitos (Matsson et al., 2016). Debido a que la ruta oral es la más empleada en la administración de fármacos, al contrario que las vías de inyección e inhalación, es importante predecir la absorción oral de las moléculas orgánicas (L. Lin & Wong, 2017).

Entre las propiedades farmacocinéticas más relevantes se encuentran la absorción gastrointestinal, principal factor de la biodisponibilidad, y la permeabilidad de la BBB. Estas dos características son esenciales en el descubrimiento de nuevos fármacos (Daina & Zoete, 2016). Para predecir la absorción gastrointestinal se suelen utilizar modelos celulares de adenocarcinoma colorrectal humano (Caco-2) (Artursson et al., 1996) y de riñón canino de Madin-Darby (MDCK) (Irvine et al., 1999). Las células MDCK tienen bajos niveles de expresión de transportadores de fármacos, al contrario que las Caco-2, por lo que se suelen utilizar para evaluar la permeabilidad pasiva a través del epitelio intestinal (Matsson et al., 2016). Otra propiedad farmacocinética relevante en la absorción intestinal es el área de superficie polar de Van der Waals de átomos de oxígeno y nitrógeno (PSA), ya que valores menores de 140 $Å^2$ indican una alta absorción del fármaco en el organismo (Palm et al., 1997).

La albúmina de suero humano (HSA) es la proteína más importante y abundante en el plasma, representando un 55% del total del contenido proteico (Lambrinidis et al., 2015). Su función principal es el transporte de ácidos grasos, aunque también está involucrada en el mantenimiento de la presión arterial osmótica y la distribución de fluidos entre compartimentos (Mendez et al., 2005). La interacción de las moléculas orgánicas con las proteínas del plasma, principalmente con la HSA, puede dar lugar a efectos tóxicos, baja penetración de la BBB y una pérdida de eficacia del fármaco (Lambrinidis et al., 2015; Vallianatou et al., 2013). Para desarrollar un posible fármaco eficaz en el tratamiento de la AD, es indispensable que llegue al CNS a través de la BBB, por lo que la permeabilidad frente a la BBB adquiere un papel muy relevante (Ali et al., 2017).

El desequilibrio en las propiedades absorción, distribución, metabolismo, excreción y toxicidad (ADMET) son una causa muy común para la retirada de potenciales fármacos en las últimas etapas de ensayos de medicamentos (X. Yang et al., 2019). Por ello, es importante determinar dichas propiedades al inicio del proceso de desarrollo de fármacos (Y. Wang et al., 2015). Las propiedades ADMET se pueden calcular con la base de datos

"relación estructura-actividad" (ADMETsar) que posee más de 96 000 compuestos con 45 tipos de propiedades asociadas (F. Cheng et al., 2012). Otra herramienta útil para calcular dichas propiedades es SwissADME, creada por el Instituto Suizo de Bioinformática (Daina et al., 2017). Además, existen programas como QikProp de Schrödinger que permiten predecir algunas de las anteriormente mencionadas propiedades farmacocinéticas (Hall et al., 2013).

5.3. Técnicas bioanalíticas para el estudio *in vitro* del efecto de metales, moléculas orgánicas y nanopartículas de selenio en líneas celulares de fenotipo neuronal

Para determinar si una molécula es un candidato a fármaco en el tratamiento de enfermedades neurodegenerativas, como la AD, no solo es necesario determinar sus propiedades neuroprotectoras, si no también sus efectos sobre líneas celulares neuronales. En los últimos años, se ha potenciado el uso de cultivos celulares, en concreto de líneas de fenotipo neuronal, para el estudio de la neurotoxicidad de los metales involucrados en la AD. Entre dichas líneas celulares cabe destacar las del prosencéfalo basal murino (SN56), las de neuroblastoma de ratón (Neuro-2a) y las de neuroblastoma humano (SH-SY5Y). Para llevar a cabo estos estudios se deben subcultivar las células en condiciones específicas, dependientes de las características de cada línea (del Pino et al., 2014). Cada una de ellas posee una forma de subcultivo y unas velocidades de crecimiento diferentes que hay que tener en cuenta a la hora de trabajar con ellas (del Pino et al., 2016; Knez et al., 2018; Laulagnier et al., 2018)

Los ensayos *in vitro* permiten una aproximación más realista a la hora de determinar la citotoxicidad de los considerados biometales, como el Fe(II), Cu(II) y Zn(II), y de los metales tóxicos, como el Hg(II), Cd(II) y Al(III). Dichos metales pueden inducir diferentes daños en las células, desde inhibición del crecimiento hasta estrés oxidativo (Stockwell et al., 2017). Por otra parte, se pueden evaluar la citotoxicidad de los compuestos, la reducción de la toxicidad de la proteína beta-amiloide y el estrés oxidativo, entre otros.

5.3.1. Evaluación de la viabilidad celular

La citotoxicidad de las moléculas neuroprotectoras se determina en función de la viabilidad celular, durante un periodo de 24-72 h, sobre la línea objeto de estudio. Existen varios métodos para evaluar este parámetro, entre los que destacan el ensayo colorimétrico

del bromuro de 3-(4,5- dimetiltiazol-2-ilo)-2,5-difeniltetrazol (MTT) y la citometría de flujo. El ensayo del MTT se basa en la reducción de su sal de tetrazolio soluble en agua, de color amarillo, en cristales de formazano insolubles, de color violeta, por parte de las deshidrogenasas de las células viables durante una incubación de 4 h con dicho compuesto. Posteriormente, los cristales de formazano se disuelven en DMSO, se mide la absorbancia a 570 nm y se compara la intensidad con respecto a una muestra sin tratar (Ezhilarasan et al., 2019).

El ensayo del MTT es un método rápido para determinar la citotoxicidad. No obstante, existen otros métodos más complejos, como la citometría de flujo, que aportan un resultado más fiable. Para la cuantificación de la viabilidad celular mediante citometría de flujo es necesario el uso de fluorocromos, como el yoduro de propidio (PI). Debido a la hidrofobicidad y alta masa molecular del PI, solo penetra en células cuya membrana esté rota, uniéndose a los ácidos nucleicos mediante la intercalación en sus bases. La fluorescencia que presenta el PI en su unión a células no viables tiene una longitud de onda de excitación de 535 nm y de emisión de 615 nm, poseyendo por tanto fluorescencia roja. De esta forma, utilizando un citómetro de flujo se pueden distinguir las células muertas, correspondientes a una fluorescencia alta de PI, de las células vivas, con baja fluorescencia de PI (Sathiya Kamatchi et al., 2020).

5.3.2. ICP-MS como herramienta para el estudio de la acumulación de metales y nanopartículas en células individuales

La técnica del plasma acoplado inductivamente por radio frecuencia con analizador de espectrometría de masas (ICP-MS) es ampliamente utilizada en la determinación de concentraciones muy bajas, llamadas trazas, de una gran mayoría de elementos químicos. Entre sus ventajas cabe destacar su alta sensibilidad, selectividad, precisión, amplio intervalo lineal y determinación multielemental e isotópica (Squadrone et al., 2020).

La técnica de ICP-MS se ha empleado frecuentemente para estudios cuantitativos de asimilación y acumulación de nanopartículas metálicas/metaloides y elementos traza en poblaciones de células. El procedimiento seguido de forma general es la exposición de los cultivos a las nanopartículas o elementos traza durante un tiempo determinado, tras el que se procede a la medida del contenido metálico total en el pellet celular, previa digestión ácida. De esta manera, se determina la concentración de nanopartículas o elementos trazas

(en masa total del metal o metaloide) que una población celular puede acumular con respecto al número o masa de células en un tiempo determinado. Sin embargo, este tipo de análisis no tiene en cuenta la variabilidad que puede existir entre células individuales en cuanto a la asimilación de los analitos. El creciente interés que han suscitado los análisis a nivel de células individuales ha originado de forma paralela un incremento en el número de estudios que desarrollan nuevas metodologías o introducen mejoras en las ya existentes. Entre ellas, la detección de células individuales mediante single cell-ICP-MS (SC-ICP-MS) se ha posicionado como una de las técnicas emergentes más prometedoras para el análisis cuantitativo de elementos traza y nanopartículas en células individuales de diferentes organismos vivos. La técnica presenta ventajas tales como la elevada sensibilidad, sencillez, mínima preparación de la muestra e información de la heterogeneidad celular dentro de una misma población (Gomez-Gomez et al., 2020).

Uno de los aspectos más importantes a la hora de la optimización es el sistema de transporte, con el fin de asegurar que las células llegan intactas al sistema de atomización. Además, los cultivos celulares deben introducirse en el plasma lo suficientemente diluidos para que cada evento corresponda a una única célula, y se permita por tanto establecer de forma precisa la acumulación por célula individual (Corte Rodríguez et al., 2017). En SC-ICP-MS la intensidad de los eventos proporciona información sobre la masa del analito acumulada en una célula individual, y el número de eventos está relacionado con el número de células que han acumulado el analito en cuestión. En este tipo de análisis, también se monitorizan otros elementos constitutivos de las células como magnesio, fósforo y manganeso, que sirven como marcadores de las poblaciones celulares y que, comparados con los datos de la citometría de flujo, permitan establecer la eficiencia de nebulización.

Mediante esta técnica se puede obtener un perfil completo sobre el porcentaje de células que acumulan concentraciones específicas de los elementos expuestos, y no solo la media de bioacumulación que se obtendría con un análisis por ICP-MS. Por ello, se está aplicando con éxito para evaluar la acumulación de metales, metaloides y nanopartículas en poblaciones celulares y bacterianas (Y. Cao et al., 2020). En la presente Tesis Doctoral esta técnica se ha aplicado en los estudios de acumulación de metales y especies de selenio, incluidas nanopartículas, en líneas celulares de fenotipo neuronal, como las Neuro-2a y las SH-SY5Y.

5.3.3. Microscopía electrónica de transmisión para evaluar la localización intracelular de nanopartículas en cultivos celulares

Para evaluar el efecto de las Ch-SeNPs en las líneas celulares de fenotipo neuronal es indispensable determinar si son capaces de atravesar la membrana celular y, por tanto, presentan localización intracelular, o si por el contrario se encuentran adheridas a la parte externa de la misma. Para este análisis tan laborioso se requiere el uso, una vez más, de la TEM.

Mediante un proceso de exposición a las Ch-SeNPs durante 48 h por parte de las células, se procede a su fijación con paraformaldehído y glutaraldehído a pH fisiológico durante 4 h a 4 °C. A continuación, se realiza la post-fijación con tetróxido de osmio durante a 1 h a temperatura ambiente en oscuridad, mediante la tinción del contenido lipídico celular de color negro, sirviendo de agente de contraste. Posteriormente, se lleva a cabo una deshidratación progresiva con acetona y una infiltración gradual en resina. Se realizan bloques de la muestra y se polimeriza en estufa a 70 °C durante 48 h. Finalmente, se corta la muestra con un microtomo y se visualizan las células en el TEM, observando la presencia o ausencia de las Ch-SeNPs en el interior de las células de fenotipo neuronal. De esta forma, se puede determinar el efecto que producen las nanopartículas en los mecanismos celulares (Roy et al., 2021).

5.3.4. Reducción de la toxicidad de la proteína $A\beta_{42}$ y de metales en líneas celulares neuronales

Debido a la toxicidad inherente de la proteína $A\beta_{42}$ y de los metales involucrados en la AD, se pueden evaluar otros parámetros neuroprotectores, como la reducción de dicha toxicidad por parte de potenciales moléculas neuroprotectoras que posean baja citotoxicidad. Para ello, se exponen las líneas celulares objeto de estudio al monómero $A\beta_{42}$ o a los metales durante 24 h, en ausencia y presencia del compuesto neuroprotector, y se evalúa la viabilidad celular mediante el método MTT anteriormente descrito. Aquellos compuestos más neuroprotectores evitarán la muerte celular producida tanto por la proteína $A\beta_{42}$ como por dichos metales (Alghazwi et al., 2019).

5.3.5. Reducción del estrés oxidativo en células

El estrés oxidativo provocado en la AD es otro de los parámetros susceptibles de ser estudiado *in vitro*. Existen diversos métodos con los cuales se puede evaluar el estrés oxidativo. Uno de los más usados es la exposición de las células, previamente tratadas con las moléculas neuroprotectoras, a sustancias oxidantes como el H_2O_2 o el Fe con ácido L-ascórbico, con su posterior medida con el ensayo del MTT. No obstante, para una mayor fiabilidad de los resultados, se puede recurrir a la técnica de citometría de flujo. Para ello, se debe usar el fluorocromo diacetato de 2',7'-dihidrodiclorofluoresceina (DCFH-DA), que mediante la presencia de ROS celulares lo transforman en 2',7'-diclorofluoresceína (DCF). El DCF posee unas longitudes de onda de excitación y de emisión de 485 nm y 530 nm, respectivamente, lo que le otorga una fluorescencia de color verde. La intensidad de la fluorescencia medida por citometría de flujo da una idea de la presencia de ROS en las células, ya que la intensidad del DCF es mayor en aquellas con mayor estrés oxidativo (Liao et al., 2019).

Por otra lado, es bien conocido el efecto sobre el estrés oxidativo de ciertos metales, como el Fe(II) y el Cd(II), en concreto en la peroxidación lipídica. Para determinar esta peroxidación se emplea como biomarcador el MDA, producto de la degradación del ácido araquidónico. En este método se cuantifica la producción intracelular de MDA después de haber expuesto las células durante 24 h a los metales objeto de estudio o al H_2O_2. Existen kits comerciales de cuantificación de peroxidación lipídica que permiten determinar la concentración de MDA, midiendo posteriormente la absorbancia a 532 nm mediante espectroscopía UV-Vis (Qiu et al., 2019).

La vía Nrf2, uno de los principales mecanismos de protección frente a ROS que posee el organismo, también puede ser alterada por las moléculas neuroprotectoras. Esta vía se puede inducir mediante la reducción de la expresión de la proteína Keap1, liberando la proteína Nrf2 que es translocada al núcleo donde regula la actividad de enzimas antioxidantes como la GPx y la catalasa. Así, una baja concentración de la proteína Keap1, y una alta concentración de las proteínas Nrf2, GPx y catalasa, son indicativos de una elevada capacidad antioxidante de las moléculas neuroprotectoras. Para determinar la expresión proteica de la Keap1, Nrf2, GPx y la catalasa se pueden emplear test comerciales ELISA o western blot (Fu et al., 2018).

5.3.6. Contenido proteínico total y expresión génica de proteínas de choque térmico y proteosomas en células

Las proteínas de choque térmico, como la HSP70, junto con el P20S son piezas fundamentales en la reparación de proteínas que poseen un plegamiento incorrecto, como es el caso de la $A\beta_{42}$ o la p-tau hiperfosforilada en la AD. Los compuestos neuroprotectores pueden inducir su expresión, resolviendo de esa forma los problemas de la agregación amiloide de raíz. Para ello se puede determinar el contenido total de proteínas mediante un kit BCA y el de las proteínas HSP70 y P20S mediante kits ELISA (Rothammer et al., 2019).

5.3.7. Contenido de la proteína $A\beta_{42}$ en células

El contenido de proteína $A\beta_{42}$ en células se puede determinar mediante un kit ELISA. Para ello, se ponen en contacto las células con el anticuerpo de detección y con el cromógeno estabilizador. Posteriormente, se mide la absorbancia a 450 nm y se cuantifica el contenido total de la proteína $A\beta_{42}$ (Hulstaert et al., 1999).

5.3.8. Análisis de la actividad de las caspasas en apoptosis celular

Las caspasas son indicadores de la apoptosis celular, por lo que su cuantificación permite identificar el efecto apoptótico de las potenciales moléculas neuroprotectoras. Existen diversos kits de luminiscencia que permiten cuantificar tanto la caspasa 3 como la caspasa 7 mediante su medida en un espectrofotómetro UV-Vis (Xie et al., 2006).

5.4. Técnicas quimiométricas para la evaluación de propiedades neuroprotectoras

Debido a la complejidad inherente de la determinación de las propiedades neuroprotectoras y a la gran multitud y variedad de datos obtenidos para cada compuesto, se hace indispensable el uso de técnicas que permitan su interpretación. Las herramientas quimiométricas proporcionan la posibilidad de evaluar, de una forma sencilla, el potencial neuroprotector de las moléculas orgánicas y nanopartículas de selenio en base a propiedades determinadas experimentalmente. La quimiometría es la disciplina que se basa en la aplicación de métodos matemáticos y estadísticos sobre datos químicos con el objeto de aportar la máxima información (Sultanbawa et al., 2021). Las técnicas quimiométricas

empleadas en esta tesis se pueden dividir en tres bloques: análisis de la varianza (ANOVA), análisis de componentes principales (PCA) y diseño de experimentos (DOE) y metodología de superficie de respuesta (RSM).

El **ANOVA** permite conocer si los efectos de variables independientes (por ejemplo, la presencia de metales o moléculas orgánicas) sobre una variable dependiente cuantitativa (por ejemplo, la anchura de las fibras de proteína $A\beta_{42}$, la determinación *in vitro* del contenido total y toxicidad de la $A\beta_{42}$, la expresión de las proteínas HSP70 y P20S, expresión de la Keap1, Nrf2, Gpx y catalasa, la actividad de las caspasas, la peroxidación lipídica o la viabilidad celular) son o no significativos. En el caso de la existencia de diferencias significativas entre medias, se pueden aplicar varios métodos para conocer dónde radican dichas diferencias. Uno de estos métodos es el de la diferencia menos significativa (LSD) de Fisher, que permite la división en grupos homogéneos de aquellas variables independientes que produzcan un efecto similar sobre la variable dependiente cuantitativa (Pilikidou et al., 2021). De esta forma, se puede agrupar a las moléculas neuroprotectoras en función de su potencial para disminuir la anchura, y por tanto la toxicidad, de la proteína $A\beta_{42}$, entre otras propiedades ya mencionadas.

El **PCA** es un método descriptivo, por lo que no distingue entre variables dependientes e independientes. Su utilidad radica en la síntesis de la información, mediante una reducción en el número de dimensiones necesarias, llamadas componentes, para explicar diferencias entre conjuntos elevados de datos, y su correspondiente ponderación en función del porcentaje de varianza explicada por cada una de ellas. De esta forma, el componente 1 es el que mayor porcentaje de varianza explica, seguido por el componente 2, y así sucesivamente. Estos componentes se obtienen mediante una combinación lineal de las variables iniciales, no correlacionadas entre sí, determinadas experimentalmente. Dicha reducción de componentes tiene como objetivo explicar la mayor cantidad de variabilidad entre los datos con la mínima pérdida posible de información (Arco et al., 2021). Mediante el PCA se puede obtener una representación gráfica que permita visualizar, por ejemplo, las moléculas orgánicas que más contribuyen a determinados aspectos neuroprotectores como la inhibición enzimática, la agregación de la proteína $A\beta_{42}$, y diversas propiedades farmacocinéticas.

El **diseño de experimentos** (**DOE**) es una herramienta quimiométrica que permite una obtener unos valores óptimos para cada uno de los factores (por ejemplo, concentración de Ch-SeNPs y enantiómeros de aminoácidos) involucrados en el problema

analítico a resolver (por ejemplo, la determinación estequiométrica de la posible interacción). Dichos factores deben estar normalizados, entre -1 y +1, y las posibles combinaciones vienen dadas por el diseño, de tal forma que el número de experimentos necesario sea mínimo. El diseño factorial completo, por ejemplo, necesita la realización de 2^k o 3^k experimentos, siendo el exponente (k) el número de factores objeto de la optimización y la base (2 o 3) el número de niveles de variabilidad de los factores (-1 para el valor más bajo, 0 para el valor intermedio y +1 para el valor más alto). En ocasiones en las que el número de experimentos es demasiado elevado y se pretende reducirlos, se puede recurrir al diseño factorial fraccionado, 2^{k-p} o 3^{k-p} (Y. Liu et al., 2021). Con el objeto de interpretar matemáticamente los efectos de los factores que afectan al problema analítico a resolver, se puede hacer uso de la **metodología de superficie de respuesta** (**RSM**). Mediante su visualización en forma de gráfico, se puede minimizar o maximizar la respuesta estudiada, y encontrar de esta forma las condiciones requeridas para los estudios analíticos. Por tanto, se consigue una optimización de los factores objeto de estudio, y en el caso concreto de las interacciones entre Ch-SeNPs y enantiómeros de aminoácidos involucrados en la AD, se puede elucidar si el comportamiento de los enantiómeros es diferente y, en el caso de existir interacción, la posible relación estequiométrica del complejo formado.

Mediante este conjunto de métodos se puede analizar y evaluar el potencial neuroprotector de las moléculas orgánicas y de las nanopartículas de selenio de una forma más completa debido a la cantidad de información proporcionada por las técnicas quimiométricas utilizadas.

V.REFERENCIAS

V. REFERENCIAS

Abdalkader, M., Lampinen, R., Kanninen, K. M., Malm, T. M., & Liddell, J. R. (2018). Targeting Nrf2 to suppress ferroptosis and mitochondrial dysfunction in neurodegeneration. *Frontiers in Neuroscience*, *12*, 1–10. https://doi.org/10.3389/fnins.2018.00466

Abdulbagi, M., Wang, L., Siddig, O., Di, B., & Li, B. (2021). D-amino acids and d-amino acid-containing peptides: Potential disease biomarkers and therapeutic targets? *Biomolecules*, *11*(11). https://doi.org/10.3390/biom11111716

Acharya, M. R., Venitz, J., Figg, W. D., & Sparreboom, A. (2004). Chemically modified tetracyclines as inhibitors of matrix metalloproteinases. *Drug Resistance Updates*, *7*(3), 195–208. https://doi.org/10.1016/j.drup.2004.04.002

Acuna, V. v., Hopper, R. M., & Yoder, R. J. (2020). Computer-Aided Drug Design for the Organic Chemistry Laboratory Using Accessible Molecular Modeling Tools. *Journal of Chemical Education*, *97*(3), 760–763. https://doi.org/10.1021/acs.jchemed.9b00592

Adani, G., Filippini, T., Garuti, C., Malavolti, M., Vinceti, G., Zamboni, G., Tondelli, M., Galli, C., Costa, M., Vinceti, M., & Chiari, A. (2020). Environmental risk factors for early-onset alzheimer's dementia and frontotemporal dementia: A case-control study in northern italy. *International Journal of Environmental Research and Public Health*, *17*(21), 1–18. https://doi.org/10.3390/ijerph17217941

Agrawal, I., & Jha, S. (2020). Mitochondrial Dysfunction and Alzheimer's Disease: Role of Microglia. *Frontiers in Aging Neuroscience*, *12*, 1–8. https://doi.org/10.3389/fnagi.2020.00252

Akhbarizadeh, R., Moore, F., & Keshavarzi, B. (2018). Investigating a probable relationship between microplastics and potentially toxic elements in fish muscles from northeast of Persian Gulf. *Environmental Pollution*, *232*, 154–163. https://doi.org/10.1016/j.envpol.2017.09.028

Alghazwi, M., Smid, S., Musgrave, I., & Zhang, W. (2019). In vitro studies of the neuroprotective activities of astaxanthin and fucoxanthin against amyloid beta (Aβ 1-42) toxicity and aggregation. *Neurochemistry International*, *124*, 215–224. https://doi.org/10.1016/j.neuint.2019.01.010

Ali, M., Muhammad, S., Shah, M. R., Khan, A., Rashid, U., Farooq, U., Ullah, F., Sadiq, A., Ayaz, M., Ali, M., Ahmad, M., & Latif, A. (2017). Neurologically potent molecules from

Crataegus oxyacantha; isolation, anticholinesterase inhibition, and molecular docking. *Frontiers in Pharmacology*, *8*, 1–11. https://doi.org/10.3389/fphar.2017.00327

ALZHEIMER, A. (1907). Uber eine eigenartige Erkrankung der Hirnrinde. *Zentralbl. Nervenh. Psych.*, *18*, 177–179. http://ci.nii.ac.jp/naid/10008335947/en/

Alzheimer's Association. (2018). 2018 Alzheimer's disease facts and figures. *Alzheimer's and Dementia*, *14*(3), 367–429. https://doi.org/10.1016/j.jalz.2018.02.001

Alzheimer's Association. (2020). 2020 Alzheimer's disease facts and figures. *Alzheimer's and Dementia*, *16*(3), 391–460. https://doi.org/10.1002/alz.12068

Alzheimer's Disease International. (2021). *World Alzheimer Report 2021*. https://www.alzint.org/resource/world-alzheimer-report-2021/

Andrade, V. M., Aschner, M., & Marreilha dos Santos, A. P. (2017). Neurotoxicity of Metal Mixtures. *Advances in Neurobiology*, *18*, 227–265. https://doi.org/10.1007/978-3-319-60189-2_12

Angelova, P. R., & Abramov, A. Y. (2018). Role of mitochondrial ROS in the brain: from physiology to neurodegeneration. *FEBS Letters*, *592*(5), 692–702. https://doi.org/10.1002/1873-3468.12964

Arco, J. E., Ramírez, J., Górriz, J. M., & Ruz, M. (2021). Data fusion based on Searchlight analysis for the prediction of Alzheimer's disease. *Expert Systems with Applications*, *185*, 115549. https://doi.org/10.1016/j.eswa.2021.115549

Artursson, P., Palm, K., & Luthman, K. (1996). Caco-2 monolayers in experimental and theoretical predictions of drug transport. *Advanced Drug Delivery Reviews*, *22*, 67–84. https://doi.org/10.1016/S0169-409X(96)00415-2

Ashok, A., Rai, N. K., Tripathi, S., & Bandyopadhyay, S. (2015). Exposure to As-, Cd-, and Pb-mixture induces Aβ, amyloidogenic APP processing and cognitive impairments via oxidative stress-dependent neuroinflammation in young rats. *Toxicological Sciences*, *143*(1), 64–80. https://doi.org/10.1093/toxsci/kfu208

Asthana, A., Bollapalli, M., Tangirala, R., Bakthisaran, R., & Mohan Rao, C. (2014). Hsp27 suppresses the Cu2+-induced amyloidogenicity, redox activity, and cytotoxicity of α-synuclein by metal ion stripping. *Free Radical Biology and Medicine*, *72*, 176–190. https://doi.org/10.1016/j.freeradbiomed.2014.04.012

Atrián-Blasco, E., Santoro, A., Pountney, D. L., Meloni, G., Hureau, C., & Faller, P. (2017). Chemistry of mammalian metallothioneins and their interaction with amyloidogenic peptides and proteins. *Chemical Society Reviews*, *46*(24), 7683–7693. https://doi.org/10.1039/c7cs00448f

August, A., Schmidt, N., Klingler, J., Baumkötter, F., Lechner, M., Klement, J., Eggert, S., Vargas, C., Wild, K., Keller, S., & Kins, S. (2019). Copper and zinc ions govern the trans-directed dimerization of APP family members in multiple ways. *Journal of Neurochemistry*, *151*(5), 626–641. https://doi.org/10.1111/jnc.14716

Ayaz, M., Sadiq, A., Junaid, M., Ullah, F., Ovais, M., Ullah, I., Ahmed, J., & Shahid, M. (2019). Flavonoids as prospective neuroprotectants and their therapeutic propensity in aging associated neurological disorders. *Frontiers in Aging Neuroscience*, *11*(155), 1–21. https://doi.org/10.3389/fnagi.2019.00155

Azriel, R., & Gazit, E. (2001). Analysis of the minimal amyloid-forming fragment of the islet amyloid polypeptide. An experimental support for the key role of the phenylalanine residue in amyloid formation. *Journal of Biological Chemistry*, *276*, 34156–34161. https://doi.org/10.1074/jbc.M102883200

Bacchella, C., Gentili, S., Bellotti, D., Quartieri, E., Draghi, S., Baratto, M. C., Remelli, M., Valensin, D., Monzani, E., Nicolis, S., Casella, L., Tegoni, M., & Dell'Acqua, S. (2020). Binding and Reactivity of Copper to R1 and R3 Fragments of tau Protein. *Inorganic Chemistry*, *59*(1), 274–286. https://doi.org/10.1021/acs.inorgchem.9b02266

Bakulski, K. M., Seo, Y. A., Hickman, R. C., Brandt, D., Vadari, H. S., Hu, H., & Park, S. K. (2020). Heavy Metals Exposure and Alzheimer's Disease and Related Dementias. *Journal of Alzheimer's Disease*, *76*(4), 1215–1242. https://doi.org/10.3233/JAD-200282

Baranello, R., Bharani, K., Padmaraju, V., Chopra, N., Lahiri, D., Greig, N., Pappolla, M., & Sambamurti, K. (2015). Amyloid-Beta Protein Clearance and Degradation (ABCD) Pathways and their Role in Alzheimer's Disease. *Current Alzheimer Research*, *12*(1), 32–46. https://doi.org/10.2174/1567205012666141218140953

Bartzokis, G., Lu, P. H., & Mintz, J. (2007). Human brain myelination and amyloid beta deposition in Alzheimer's disease. *Alzheimer's and Dementia*, *3*(2), 122–125. https://doi.org/10.1016/j.jalz.2007.01.019

Bastings, J. J. A. J., van Eijk, H. M., Damink, S. W. O., & Rensen, S. S. (2019). D-amino acids in health and disease: A focus on cancer. *Nutrients*, *11*, 2205–2222. https://doi.org/10.3390/nu11092205

Battin, E. E., Perron, N. R., & Brumaghim, J. L. (2006). The central role of metal coordination in selenium antioxidant activity. *Inorganic Chemistry*, *45*(2), 499–501. https://doi.org/10.1021/ic051594f

Battin, E. E., Zimmerman, M. T., Ramoutar, R. R., Quarles, C. E., & Brumaghim, J. L. (2011). Preventing metal-mediated oxidative DNA damage with selenium compounds. *Metallomics*, *3*(5), 503–512. https://doi.org/10.1039/c0mt00063a

Baumkötter, F., Schmidt, N., Vargas, C., Schilling, S., Weber, R., Wagner, K., Fiedler, S., Klug, W., Radzimanowski, J., Nickolaus, S., Keller, S., Eggert, S., Wild, K., & Kins, S. (2014). Amyloid precursor protein dimerization and synaptogenic function depend on copper binding to the growth factor-like domain. *Journal of Neuroscience*, *34*(33), 11159–11172. https://doi.org/10.1523/JNEUROSCI.0180-14.2014

Bekris, L. M., Yu, C. E., Bird, T. D., & Tsuang, D. W. (2010). Genetics of Alzheimer disease. *Journal of Geriatric Psychiatry and Neurology*, *23*(4), 213–227. https://doi.org/10.1177/0891988710383571

Berg, L., da Andersson, C. D., Artursson, E., Hörnberg, A., Tunemalm, A. K., Linusson, A., & Ekström, F. (2011). Targeting acetylcholinesterase: Identification of chemical leads by high throughput screening, structure determination and molecular modeling. *PLoS ONE*, *6*(11), 26039. https://doi.org/10.1371/journal.pone.0026039

Berman, H. M., Westbrook, J., Feng, Z., Gilliland, G., Bhat, T. N., Weissig, H., Shindyalov, I. N., & Bourne, P. E. (2000). The Protein Data Bank. *Nucleic Acids Research*, *28*(1), 235–242. https://doi.org/https://doi.org/10.1093/nar/28.1.235

Bhattacharjee, S. (2016). DLS and zeta potential - What they are and what they are not? *Journal of Controlled Release*, *235*, 337–351. https://doi.org/10.1016/j.jconrel.2016.06.017

Bielschowsky, M. (1902). Die Silberimprägnation der Achsencylinder. *Neurologisches Zentralblatt*, *21*, 579–584.

Blessing, H., Kraus, S., Heindl, P., Bal, W., & Hartwig, A. (2004). Interaction of selenium compounds with zinc finger proteins involved in DNA repair. *European Journal of Biochemistry*, *271*(15), 3190–3199. https://doi.org/10.1111/j.1432-1033.2004.04251.x

Bondi, M. W., Edmonds, E. C., & Salmon, D. P. (2017). Alzheimer's disease: Past, present, and future. *Journal of the International Neuropsychological Society*, *23*(9–10), 818–831. https://doi.org/10.1017/S135561771700100X

Bonfio, C., Valer, L., Scintilla, S., Shah, S., Evans, D. J., Jin, L., Szostak, J. W., Sasselov, D. D., Sutherland, J. D., & Mansy, S. S. (2017). UV-light-driven prebiotic synthesis of iron-sulfur clusters. *Nature Chemistry*, *9*(12), 1229–1234. https://doi.org/10.1038/nchem.2817

Boopathi, S., & Kolandaivel, P. (2016). Fe2+ binding on amyloid β-peptide promotes aggregation. *Proteins: Structure, Function and Bioinformatics*, *84*(9), 1257–1274. https://doi.org/10.1002/prot.25075

Branca, J. J. V., Maresca, M., Morucci, G., Mello, T., Becatti, M., Pazzagli, L., Colzi, I., Gonnelli, C., Carrino, D., Paternostro, F., Nicoletti, C., Ghelardini, C., Gulisano, M., Mannelli, L. D. C., & Pacini, A. (2019). Effects of cadmium on ZO-1 tight junction integrity of the blood brain barrier. *International Journal of Molecular Sciences*, *20*(23), 6010. https://doi.org/10.3390/ijms20236010

Branca, J. J. V., Morucci, G., Maresca, M., Tenci, B., Cascella, R., Paternostro, F., Ghelardini, C., Gulisano, M., di Cesare Mannelli, L., & Pacini, A. (2018). Selenium and zinc: Two key players against cadmium-induced neuronal toxicity. *Toxicology in Vitro*, *48*, 159–169. https://doi.org/10.1016/j.tiv.2018.01.007

Branca, J. J. V., Morucci, G., & Pacini, A. (2018). Cadmium-induced neurotoxicity: Still much ado. *Neural Regeneration Research*, *13*(11), 1879–1882. https://doi.org/10.4103/1673-5374.239434

Brunnström, H. R., & Englund, E. M. (2009). Cause of death in patients with dementia disorders. *European Journal of Neurology*, *16*(4), 488–492. https://doi.org/10.1111/j.1468-1331.2008.02503.x

Bryszewska, M. A., & Måge, A. (2015). Determination of selenium and its compounds in marine organisms. *Journal of Trace Elements in Medicine and Biology*, *29*, 91–98. https://doi.org/10.1016/j.jtemb.2014.10.004

Bullock, R., Touchon, J., Bergman, H., Gambina, G., He, Y., Rapatz, G., Nagel, J., & Lane, R. (2005). Rivastigmine and donepezil treatment in moderate to moderately-severe Alzheimer's disease over a 2-year period. *Current Medical Research and Opinion*, *21*(8), 1317–1327. https://doi.org/10.1185/030079905X56565

Cabral Pinto, M. M. S., Marinho-Reis, A. P., Almeida, A., Ordens, C. M., Silva, M. M. V. G., Freitas, S., Simões, M. R., Moreira, P. I., Dinis, P. A., Diniz, M. L., Ferreira da Silva, E. A., & Condesso de Melo, M. T. (2018). Human predisposition to cognitive impairment and its relation with environmental exposure to potentially toxic elements. *Environmental Geochemistry and Health*, *40*(5), 1767–1784. https://doi.org/10.1007/s10653-017-9928-3

Cabral-Pacheco, G. A., Garza-Veloz, I., Rosa, C. C. D. la, Ramirez-Acuña, J. M., Perez-Romero, B. A., Guerrero-Rodriguez, J. F., Martinez-Avila, N., & Martinez-Fierro, M. L. (2020). The roles of matrix metalloproteinases and their inhibitors in human diseases. *International Journal of Molecular Sciences*, *21*(24), 1–53. https://doi.org/10.3390/ijms21249739

Cacabelos, R. (2017). Parkinson's disease: From pathogenesis to pharmacogenomics. *International Journal of Molecular Sciences*, *18*(3), 551. https://doi.org/10.3390/ijms18030551

Campanella, C., Pace, A., Bavisotto, C. C., Marzullo, P., Gammazza, A. M., Buscemi, S., & Piccionello, A. P. (2018). Heat shock proteins in Alzheimer's disease: Role and targeting. *International Journal of Molecular Sciences*, *19*(9), 2603. https://doi.org/10.3390/ijms19092603

Camps, P., el Achab, R., Morral, J., Munoz-Torrero, D., Badia, A., Eladi Banos, J., Vivas, N. M., Barril, X., Orozco, M., & Javier Luque, F. (2000). New tacrine-huperzine A hybrids (huprines): Highly potent tight-binding acetylcholinesterase inhibitors of interest for the treatment of Alzheimer's Disease. *Journal of Medicinal Chemistry*, *43*(24), 4657–4666. https://doi.org/10.1021/jm000980y

Camps, P., Formosa, X., Galdeano, C., Gómez, T., Muñoz-Torrero, D., Scarpellini, M., Viayna, E., Badia, A., Clos, M. V., Camins, A., Pallàs, M., Bartolini, M., Mancini, F., Andrisano, V., Estelrich, J., Lizondo, M., Bidon-Chanal, A., & Luque, F. J. (2008). Novel donepezil-based inhibitors of acetyl- and butyrylcholinesterase and acetylcholinesterase-induced β-amyloid aggregation. *Journal of Medicinal Chemistry*, *51*(12), 3588–3598. https://doi.org/10.1021/jm8001313

Cao, J., Zhong, M. B., Toro, C. A., Zhang, L., & Cai, D. (2019). Endo-lysosomal pathway and ubiquitin-proteasome system dysfunction in Alzheimer's disease pathogenesis. *Neuroscience Letters*, *703*, 68–78. https://doi.org/10.1016/j.neulet.2019.03.016

Cao, Y., Feng, J., Tang, L., Yu, C., Mo, G., & Deng, B. (2020). A highly efficient introduction system for single cell- ICP-MS and its application to detection of copper in single human red blood cells. *Talanta*, *206*, 120174. https://doi.org/10.1016/j.talanta.2019.120174

Cariccio, V. L., Samà, A., Bramanti, P., & Mazzon, E. (2019). Mercury Involvement in Neuronal Damage and in Neurodegenerative Diseases. *Biological Trace Element Research*, *187*(2), 341–356. https://doi.org/10.1007/s12011-018-1380-4

Chattopadhyay, S., Raychaudhuri, U., & Chakraborty, R. (2014). Artificial sweeteners - A review. *Journal of Food Science and Technology*, *51*(4), 611–621. https://doi.org/10.1007/s13197-011-0571-1

Chaves, S., Hiremathad, A., Tomás, D., Keri, R. S., Piemontese, L., & Santos, M.A. (2018). Exploring the chelating capacity of 2-hydroxyphenyl-benzimidazole based hybrids with multi-target ability as anti-Alzheimer's agents. *New Journal of Chemistry*, *42*(20), 16503–16515. https://doi.org/10.1039/c8nj00117k

Chaves, S., Várnagy, K., & Santos, M.A. (2021). Recent multi-target approaches on the development of anti-Alzheimer's agents integrating metal chelation activity. *Current Medicinal Chemistry*, *28*(35), 7247-7277. https://doi.org/10.2174/0929867328666210218183032

Cheignon, C., Tomas, M., Bonnefont-Rousselot, D., Faller, P., Hureau, C., & Collin, F. (2018). Oxidative stress and the amyloid beta peptide in Alzheimer's disease. *Redox Biology*, *14*, 450–464. https://doi.org/10.1016/j.redox.2017.10.014

Chen, D. zhi, Yang, B. juan, He, X. li, Fan, S. rui, Cai, J. yun, Jing, C. xu, Zhang, H., Zhang, Y., Li, L., & Hao, X. jiang. (2019). Design, synthesis and structure-activity relationship optimization of phenanthridine derivatives as new Wnt/β-catenin signalling pathway agonists. *Bioorganic Chemistry*, *84*, 285–294. https://doi.org/10.1016/j.bioorg.2018.11.020

Chen, G. F., Xu, T. H., Yan, Y., Zhou, Y. R., Jiang, Y., Melcher, K., & Xu, H. E. (2017). Amyloid beta: Structure, biology and structure-based therapeutic development. *Acta Pharmacologica Sinica*, *38*(9), 1205–1235. https://doi.org/10.1038/aps.2017.28

Chen, L.-L., Fan, Y.-G., Zhao, L.-X., Zhang, Q., & Wang, Z.-Y. (2023). The metal ion hypothesis of Alzheimer's disease and the anti-neuroinflammatory effect of metal chelators. *Bioorganic Chemistry*, *131*, 106301. https://doi.org/10.1016/j.bioorg.2022.106301

Chen, M., Du, Z. Y., Zheng, X., Li, D. L., Zhou, R. P., & Zhang, K. (2018). Use of curcumin in diagnosis, prevention, and treatment of Alzheimer's disease. *Neural Regeneration Research*, *13*(4), 742–752. https://doi.org/10.4103/1673-5374.230303

Chen, M., Zeng, L., Luo, X., Zubair Mehboob, M., & Lang, M. (2019). Identification and functional characterization of a novel selenocysteine methyltransferase BjSMT from

Brassica juncea L. *J Exp Bot*, *70*(21), 6401–6416. https://doi.org/10.1093/jxb/erz390/5556905

Chen, T., Yang, Y., Zhu, S., Lu, Y., Zhu, L., Wang, Y., & Wang, X. (2020). Inhibition of Aβ aggregates in Alzheimer's disease by epigallocatechin and epicatechin-3-gallate from green tea. *Bioorganic Chemistry*, *105*, 104382. https://doi.org/10.1016/j.bioorg.2020.104382

Chen, X. Q., & Mobley, W. C. (2019). Alzheimer disease pathogenesis: Insights from molecular and cellular biology studies of oligomeric Aβ and tau species. *Frontiers in Neuroscience*, *13*, 1–21. https://doi.org/10.3389/fnins.2019.00659

Cheng, F., Li, W., Zhou, Y., Shen, J., Wu, Z., Liu, G., Lee, P. W., & Tang, Y. (2012). AdmetSAR: A comprehensive source and free tool for assessment of chemical ADMET properties. *Journal of Chemical Information and Modeling*, *52*(11), 3099–3105. https://doi.org/10.1021/ci300367a

Cheng, W.-H., & Lei, X. G. (2017). Selenium: Basic Nutritional Aspects. In *Molecular, Genetic, and Nutritional Aspects of Major and Trace Minerals* (pp. 449–461). Elsevier Inc. https://doi.org/10.1016/B978-0-12-802168-2.00037-3

Chernyak, Y. I., & Merinova, A. P. (2017). HSP70 (HSPA1) polymorphisms in former workers with chronic mercury vapor exposure. *International Journal of Occupational Medicine and Environmental Health*, *30*(1), 77–85. https://doi.org/10.13075/ijomeh.1896.00732

Chin-Chan, M., Navarro-Yepes, J., & Quintanilla-Vega, B. (2015). Environmental pollutants as risk factors for neurodegenerative disorders: Alzheimer and Parkinson diseases. *Frontiers in Cellular Neuroscience*, *9*(124), 1–23. https://doi.org/10.3389/fncel.2015.00124

Chopra, S., Overall, C. M., & Dufour, A. (2019). Matrix metalloproteinases in the CNS: interferons get nervous. *Cellular and Molecular Life Sciences*, *76*(16), 3083–3095. https://doi.org/10.1007/s00018-019-03171-9

Cicero, C. E., Mostile, G., Vasta, R., Rapisarda, V., Signorelli, S. S., Ferrante, M., Zappia, M., & Nicoletti, A. (2017). Metals and neurodegenerative diseases. A systematic review. *Environmental Research*, *159*, 82–94. https://doi.org/10.1016/j.envres.2017.07.048

Ciechanover, A., & Kwon, Y. T. ae. (2015). Degradation of misfolded proteins in neurodegenerative diseases: therapeutic targets and strategies. *Experimental & Molecular Medicine*, *47*, 147. https://doi.org/10.1038/emm.2014.117

Cipriani, G., Dolciotti, C., Picchi, L., & Bonuccelli, U. (2011). Alzheimer and his disease: A brief history. *Neurological Sciences*, *32*(2), 275–279. https://doi.org/10.1007/s10072-010-0454-7

Cline, E. N., Bicca, M. A., Viola, K. L., & Klein, W. L. (2018). The Amyloid-β Oligomer Hypothesis: Beginning of the Third Decade. *Journal of Alzheimer's Disease*, *64*(s1), S567–S610. https://doi.org/10.3233/JAD-179941

Coelho Filho, J. M. J. M. C., & Birks, J. (2001). Physostigmine for dementia due to Alzheimer's disease. *Cochrane Database of Systematic Reviews*, *2010*(1), 1–60. https://doi.org/10.1002/14651858.CD001499

Congdon, E. E., & Sigurdsson, E. M. (2018). Tau-targeting therapies for Alzheimer disease. *Nature Reviews Neurology*, *14*(7), 399–415. https://doi.org/10.1038/s41582-018-0013-z

Corte Rodríguez, M., Álvarez-Fernández García, R., Blanco, E., Bettmer, J., & Montes-Bayón, M. (2017). Quantitative Evaluation of Cisplatin Uptake in Sensitive and Resistant Individual Cells by Single-Cell ICP-MS (SC-ICP-MS). *Analytical Chemistry*, *89*(21), 11491–11497. https://doi.org/10.1021/acs.analchem.7b02746

Crous-Bou, M., Minguillón, C., Gramunt, N., & Molinuevo, J. L. (2017). Alzheimer's disease prevention: From risk factors to early intervention. *Alzheimer's Research and Therapy*, *9*(1), 71. https://doi.org/10.1186/s13195-017-0297-z

Cuadrado, A., Pajares, M., Benito, C., Jiménez-Villegas, J., Escoll, M., Fernández-Ginés, R., Garcia Yagüe, A. J., Lastra, D., Manda, G., Rojo, A. I., & Dinkova-Kostova, A. T. (2020). Can Activation of NRF2 Be a Strategy against COVID-19? *Trends in Pharmacological Sciences*, *41*(9), 598–610. https://doi.org/10.1016/j.tips.2020.07.003

Cumming, J. L., Morstorf, T., & Zhong, K. (2014). Alzheimer's disease drug-development pipeline few candidates, frequent failures. *Alzheimer's Research & Therapy*, *6*(1), 37–44. http://alzres.com/content/6/4/37

Daina, A., Michielin, O., & Zoete, V. (2017). SwissADME: A free web tool to evaluate pharmacokinetics, drug-likeness and medicinal chemistry friendliness of small molecules. *Scientific Reports*, *7*(42717), 1–13. https://doi.org/10.1038/srep42717

Daina, A., & Zoete, V. (2016). A BOILED-Egg To Predict Gastrointestinal Absorption and Brain Penetration of Small Molecules. *ChemMedChem*, *11*, 1117–1121. https://doi.org/10.1002/cmdc.201600182

Davies, P., & Maloney, A. J. (1976). Selective loss of central cholinergic neurons in Alzheimer's disease. *The Lancet*, *2*, 1403. https://doi.org/10.1016/s0140-6736(76)91936-x

de Andrade Ramos, G., Souza de Oliveira, A., Bartolini, M., Naldi, M., Liparulo, I., Bergamini, C., Uliassi, E., Wu, L., Fraser, P. E., Abreu, M., Kiametis, A. S., Gargano, R., Silveira, E. R., Brand, G. D., Prchal, L., Soukup, O., Korábečný, J., Bolognesi, M. L., & Soares Romeiro, L. A. (2021). Discovery of sustainable drugs for Alzheimer's disease: cardanol-derived cholinesterase inhibitors with antioxidant and anti-amyloid properties. *RSC Medicinal Chemistry*, *12*(7), 1154–1163. https://doi.org/10.1039/D1MD00046B

Deardorff, W. J., Feen, E., & Grossberg, G. T. (2015). The Use of Cholinesterase Inhibitors Across All Stages of Alzheimer's Disease. *Drugs and Aging*, *32*(7), 537–547. https://doi.org/10.1007/s40266-015-0273-x

del Pino, J., Zeballos, G., Anadon, M. J., Capo, M. A., Díaz, M. J., García, J., & Frejo, M. T. (2014). Higher sensitivity to cadmium induced cell death of basal forebrain cholinergic neurons: A cholinesterase dependent mechanism. *Toxicology*, *325*, 151–159. https://doi.org/10.1016/j.tox.2014.09.004

del Pino, J., Zeballos, G., Anadón, M. J., Moyano, P., Díaz, M. J., García, J. M., & Frejo, M. T. (2016). Cadmium-induced cell death of basal forebrain cholinergic neurons mediated by muscarinic M1 receptor blockade, increase in GSK-3β enzyme, β-amyloid and tau protein levels. *Archives of Toxicology*, *90*(5), 1081–1092. https://doi.org/10.1007/s00204-015-1540-7

Demirayak, Ş., Şahin, Z., Ertaş, M., Bülbül, E. F., Bender, C., Biltekin, S. N., Berk, B., Sağlık, B. N., Levent, S., & Yurttaş, L. (2019). Novel thiazole-piperazine derivatives as potential cholinesterase inhibitors. *Journal of Heterocyclic Chemistry*, *56*(12), 3370–3386. https://doi.org/10.1002/jhet.3734

Derrick, J. S., & Lim, M. H. (2015). Tools of the Trade:I nvestigations into Design Strategies of Small Molecules to Target Components in Alzheimer's Disease. *ChemBioChem*, *16*, 887–898. https://doi.org/10.1002/cbic.201402718

di Natale, G., Bellia, F., Sciacca, M. F. M., Campagna, T., & Pappalardo, G. (2018). Tau-peptide fragments and their copper(II) complexes: Effects on Amyloid-β aggregation. *Inorganica Chimica Acta*, *472*, 82–92. https://doi.org/10.1016/j.ica.2017.09.061

Dias, G. P., Cocks, G., do Nascimento Bevilaqua, M. C., Nardi, A. E., & Thuret, S. (2016). Resveratrol: A Potential Hippocampal Plasticity Enhancer. *Oxidative Medicine and Cellular Longevity*, *2016*, 1–14. https://doi.org/10.1155/2016/9651236

Dias, J. S. (2012). Nutritional Quality and Health Benefits of Vegetables: A Review. *Food and Nutrition Sciences*, *3*(10), 1354–1374. https://doi.org/10.4236/fns.2012.310179

Dinh, Q. T., Cui, Z., Huang, J., Tran, T. A. T., Wang, D., Yang, W., Zhou, F., Wang, M., Yu, D., & Liang, D. (2018). Selenium distribution in the Chinese environment and its relationship with human health: A review. *Environment International*, *112*, 294–309. https://doi.org/10.1016/j.envint.2017.12.035

dos Santos, M., da Silva, F. M. R., & Muccillo-Baisch, A. L. (2017). Selenium content of Brazilian foods: A review of the literature values. *Journal of Food Composition and Analysis*, *58*, 10–15. https://doi.org/10.1016/j.jfca.2017.01.001

Drüeke, T. B. (2002). Intestinal absorption of aluminium in renal failure. *Nephrology Dialysis Transplantation*, *17*(SUPPL. 2), 13–16. https://doi.org/10.1093/ndt/17.suppl_2.13

Du, S., Readel, E. R., Wey, M., & Armstrong, D. W. (2020). Complete identification of all 20 relevant epimeric peptides in β-amyloid: A new HPLC-MS based analytical strategy for Alzheimer's research. *Chemical Communications*, *56*(10), 1537–1540. https://doi.org/10.1039/c9cc09080k

Duce, J. A., Tsatsanis, A., Cater, M. A., James, S. A., Robb, E., Wikhe, K., Leong, S. L., Perez, K., Johanssen, T., Greenough, M. A., Cho, H. H., Galatis, D., Moir, R. D., Masters, C. L., McLean, C., Tanzi, R. E., Cappai, R., Barnham, K. J., Ciccotosto, G. D., … Bush, A. I. (2010). Iron-Export Ferroxidase Activity of β-Amyloid Precursor Protein is Inhibited by Zinc in Alzheimer's Disease. *Cell*, *142*(6), 857–867. https://doi.org/10.1016/j.cell.2010.08.014

Dunham, J., Bauer, J., Campbell, G. R., Mahad, D. J., van Driel, N., van der Pol, S. M. A., 't Hart, B. A., Lassmann, H., Laman, J. D., van Horssen, J., & Kap, Y. S. (2017). Oxidative injury and iron redistribution are pathological hallmarks of marmoset experimental autoimmune encephalomyelitis. *Journal of Neuropathology and Experimental Neurology*, *76*(6), 467–478. https://doi.org/10.1093/jnen/nlx034

Economou, N. J., Giammona, M. J., Do, T. D., Zheng, X., Teplow, D. B., Buratto, S. K., & Bowers, M. T. (2016). Amyloid β-Protein Assembly and Alzheimer's Disease: Dodecamers

of Aβ42, but Not of Aβ40, Seed Fibril Formation. *Journal of the American Chemical Society*, *138*(6), 1772–1775. https://doi.org/10.1021/jacs.5b11913

Eisenberg, D. S., & Sawaya, M. R. (2017). Structural studies of amyloid proteins at the molecular level. *Annual Review of Biochemistry*, *86*, 69–95. https://doi.org/10.1146/annurev-biochem-061516-045104

El-Ramady, H., Abdalla, N., Taha, H. S., Alshaal, T., El-Henawy, A., Faizy, S. E. D. A., Shams, M. S., Youssef, S. M., Shalaby, T., Bayoumi, Y., Elhawat, N., Shehata, S., Sztrik, A., Prokisch, J., Fári, M., Domokos-Szabolcsy, É., Pilon-Smits, E. A., Selmar, D., Haneklaus, S., & Schnug, E. (2016). Selenium and nano-selenium in plant nutrition. *Environmental Chemistry Letters*, *14*(1), 123–147. https://doi.org/10.1007/s10311-015-0535-1

El-Ramady, H. R., Domokos-Szabolcsy, É., Shalaby, T. A., Prokisch, J., & Fári, M. (2015). Selenium in Agriculture: Water, Air, Soil, Plants, Food, Animals and Nanoselenium. In *D. Robert (Eds.), CO2 Sequestration, Biofuels and Depollution, Springer International Publishing, Cham* (pp. 153–232). https://doi.org/10.1007/978-3-319-11906-9_5

Emmanuelle, B., Virginie, M., Fabienne, S., Isabelle, I., Martine, P. G., Bernard, L., & Sylvie, R. (2012). Selenium exposure in subjects living in areas with high selenium concentrated drinking water: Results of a French integrated exposure assessment survey. *Environment International*, *40*(1), 155–161. https://doi.org/10.1016/j.envint.2011.07.007

Ezhilarasan, D., Apoorva, V. S., & Ashok Vardhan, N. (2019). Syzygium cumini extract induced reactive oxygen species-mediated apoptosis in human oral squamous carcinoma cells. *Journal of Oral Pathology and Medicine*, *48*(2), 115–121. https://doi.org/10.1111/jop.12806

Feigin, V. L., Krishnamurthi, R. v., Theadom, A. M., Abajobir, A. A., Mishra, S. R., Ahmed, M. B., Abate, K. H., Mengistie, M. A., Wakayo, T., Abd-Allah, F., Abdulle, A. M., Abera, S. F., Mohammed, K. E., Abyu, G. Y., Asgedom, S. W., Atey, T. M., Betsu, B. D., Mezgebe, H. B., Tuem, K. B., … Zaki, M. E. (2017). Global, regional, and national burden of neurological disorders during 1990–2015: a systematic analysis for the Global Burden of Disease Study 2015. *The Lancet Neurology*, *16*(11), 877–897. https://doi.org/10.1016/S1474-4422(17)30299-5

Feldmann, J., Elgazali, A., Ezzeldin, M. F., Gajdosechova, Z., Krupp, E., Aborode, F., Lawan, M. M., Raab, A., Petursdottir, A. H., & Amayo, K. (2014). Microwave-Assisted Sample Preparation for Element Speciation. In *Microwave-Assisted Sample Preparation for Trace Element*

Determination (pp. 281–312). Elsevier B.V. https://doi.org/10.1016/B978-0-444-59420-4.00010-6

Fernández-Bachiller, M. I., Pérez, C., González-Muñoz, G. C., Conde, S., López, M. G., Villarroya, M., García, A. G., & Rodríguez-Franco, M. I. (2010). Novel tacrine-8-hydroxyquinoline hybrids as multifunctional agents for the treatment of Alzheimers disease, with neuroprotective, cholinergic, antioxidant, and copper-complexing properties. *Journal of Medicinal Chemistry*, *53*(13), 4927–4937. https://doi.org/10.1021/jm100329q

Ferreira-Vieira, T. H., Guimaraes, I. M., Silva, F. R., & Ribeiro, F. M. (2016). Alzheimer's disease: Targeting the cholinergic system. *Current Neuropharmacology*, *14*(1), 101–115. https://doi.org/10.2174/1570159x13666150716165726

Fingleton, B. (2006). Matrix metalloproteinases: Roles in cancer and metastasis. *Frontiers in Bioscience*, *11*, 479–491. https://doi.org/10.2741/1811

Fu, J., Sun, H., Zhang, Y., Xu, W., Wang, C., Fang, Y., & Zhao, J. (2018). Neuroprotective Effects of Luteolin Against Spinal Cord Ischemia-Reperfusion Injury by Attenuation of Oxidative Stress, Inflammation, and Apoptosis. *Journal of Medicinal Food*, *21*(1), 13–20. https://doi.org/10.1089/jmf.2017.4021

Fujii, N., Fujii, N., Takata, T., & Sakaue, H. (2017). The Importance of the Idea of "Parachirality" in Life Science. In *Advances in Asymmetric Autocatalysis and Related Topics* (pp. 119–131). Elsevier. https://doi.org/10.1016/B978-0-12-812824-4.00006-X

Fujii, N., Takata, T., Fujii, N., Aki, K., & Sakaue, H. (2016). D-amino acid residues in proteins related to aging and age-related diseases and a new analysis of the isomers in proteins. In *D-Amino Acids: Physiology, Metabolism, and Application* (pp. 241–254). Springer Japan. https://doi.org/10.1007/978-4-431-56077-7_15

Fujii, N., Takata, T., Fujii, N., Aki, K., & Sakaue, H. (2018). D-Amino acids in protein: The mirror of life as a molecular index of aging. *Biochimica et Biophysica Acta - Proteins and Proteomics*, *1866*, 840–847. https://doi.org/10.1016/j.bbapap.2018.03.001

Gao, F., Zhao, J., Liu, P., Ji, D., Zhang, L., Zhang, M., Li, Y., & Xiao, Y. (2020). Preparation and in vitro evaluation of multi-target-directed selenium-chondroitin sulfate nanoparticles in protecting against the Alzheimer's disease. *International Journal of Biological Macromolecules*, *142*, 265–276. https://doi.org/10.1016/j.ijbiomac.2019.09.098

Gao, N., Du, Z., Guan, Y., Dong, K., Ren, J., & Qu, X. (2019). Chirality-Selected Chemical Modulation of Amyloid Aggregation. *Journal of the American Chemical Society*, *141*, 6915–6921. https://doi.org/10.1021/jacs.8b12537

Genchi, G. (2017). An overview on d-amino acids. *Amino Acids*, *49*, 1521–1533. https://doi.org/10.1007/s00726-017-2459-5

Georgieva, S., Todorov, P., Bezfamilnyi, A., & Georgiev, A. (2018). Coordination behavior of 3-amino-5,5'-dimethylhydantoin towards Ni(II) and Zn(II) ions: Synthesis, spectral characterization and DFT calculations. *Journal of Molecular Structure*, *1166*, 377–387. https://doi.org/10.1016/j.molstruc.2018.04.064

Glenner, G. G., & Wong, C. W. (1984). Alzheimer's disease: Initial report of the purification and characterization of a novel cerebrovascular amyloid protein. *Biochemical and Biophysical Research Communications*, *120*(3), 885–890. https://doi.org/10.1016/S0006-291X(84)80190-4

Goldman, J. S., Hahn, S. E., Catania, J. W., Larusse-Eckert, S., Butson, M. B., Rumbaugh, M., Strecker, M. N., Roberts, J. S., Burke, W., Mayeux, R., & Bird, T. (2011). Genetic counseling and testing for Alzheimer disease: Joint practice guidelines of the American College of Medical Genetics and the National Society of Genetic Counselors. *Genetics in Medicine*, *13*(6), 597–605. https://doi.org/10.1097/GIM.0b013e31821d69b8

Gomez-Gomez, B., Corte-Rodríguez, M., Perez-Corona, M. T., Bettmer, J., Montes-Bayón, M., & Madrid, Y. (2020). Combined single cell and single particle ICP-TQ-MS analysis to quantitatively evaluate the uptake and biotransformation of tellurium nanoparticles in bacteria. *Analytica Chimica Acta*, *1128*, 116–128. https://doi.org/10.1016/j.aca.2020.06.058

Gómez-Mejía, E., Mikkelsen, L. H., Rosales-Conrado, N., León-González, M. E., & Madrid, Y. (2021). A combined approach based on matrix solid-phase dispersion extraction assisted by titanium dioxide nanoparticles and liquid chromatography to determine polyphenols from grape residues. *Journal of Chromatography A*, *1644*, 462128–462139. https://doi.org/10.1016/j.chroma.2021.462128

Gorantla, N. V., & Chinnathambi, S. (2018). Tau Protein Squired by Molecular Chaperones During Alzheimer's Disease. *Journal of Molecular Neuroscience*, *66*(3), 356–368. https://doi.org/10.1007/s12031-018-1174-3

Green, A. J., & Planchart, A. (2018). The neurological toxicity of heavy metals: A fish perspective. *Comparative Biochemistry and Physiology Part - C: Toxicology and Pharmacology*, *208*, 12–19. https://doi.org/10.1016/j.cbpc.2017.11.008

Gremer, L., Schölzel, D., Schenk, C., Reinartz, E., Labahn, J., Ravelli, R. B. G., Tusche, M., Lopez-Iglesias, C., Hoyer, W., Heise, H., Willbold, D., & Schröder, G. F. (2017). Fibril structure of amyloid-β(1–42) by cryo–electron microscopy. *Science*, *358*(6359), 116–119. https://doi.org/10.1126/science.aao2825

Guerreiro, R. J., Gustafson, D. R., & Hardy, J. (2012). The genetic architecture of Alzheimer's disease: Beyond APP, PSENS and APOE. *Neurobiology of Aging*, *33*(3), 437–456. https://doi.org/10.1016/j.neurobiolaging.2010.03.025

Gulcin, İ. (2020). Antioxidants and antioxidant methods: an updated overview. *Archives of Toxicology*, *94*(3), 651–715. https://doi.org/10.1007/s00204-020-02689-3

Gupta, J., Fatima, M. T., Islam, Z., Khan, R. H., Uversky, V. N., & Salahuddin, P. (2019). Nanoparticle formulations in the diagnosis and therapy of Alzheimer's disease. *International Journal of Biological Macromolecules*, *130*, 515–526. https://doi.org/10.1016/j.ijbiomac.2019.02.156

Ha, S., Kim, I., Takata, T., Kinouchi, T., Isoyama, M., Suzuki, M., & Fujii, N. (2017). Identification of D-amino acid-containing peptides in human serum. *PLoS ONE*, *12*, e0189972. https://doi.org/10.1371/journal.pone.0189972

Hall, M. L., Jorgensen, W. L., & Whitehead, L. (2013). Automated ligand-and structure-based protocol for in silico prediction of human serum albumin binding. *Journal of Chemical Information and Modeling*, *53*(4), 907–922. https://doi.org/10.1021/ci3006098

Hardy, J., & Allsop, D. (1991). Amyloid deposition as the central event in the aetiology of Alzheimer's disease. *Trends in Pharmacological Sciences*, *12*, 383–388. https://doi.org/10.1016/0165-6147(91)90609-V

Hariharan, S., & Dharmaraj, S. (2020). Selenium and selenoproteins: it's role in regulation of inflammation. *Inflammopharmacology*, *28*(3), 667–695. https://doi.org/10.1007/s10787-020-00690-x

Hatfield, D. L., Tsuji, P. A., Carlson, B. A., & Gladyshev, V. N. (2014). Selenium and selenocysteine: Roles in cancer, health, and development. *Trends in Biochemical Sciences*, *39*(3), 112–120. https://doi.org/10.1016/j.tibs.2013.12.007

Hawrylak-Nowak, B., Matraszek, R., & Pogorzelec, M. (2015). The dual effects of two inorganic selenium forms on the growth, selected physiological parameters and macronutrients accumulation in cucumber plants. *Acta Physiologiae Plantarum*, *37*(41), 1–13. https://doi.org/10.1007/s11738-015-1788-9

Hayat, K., Gondal, M. A., Khaled, M. M., Ahmed, S., & Shemsi, A. M. (2011). Nano ZnO synthesis by modified sol gel method and its application in heterogeneous photocatalytic removal of phenol from water. *Applied Catalysis A: General*, *393*(1–2), 122–129. https://doi.org/10.1016/j.apcata.2010.11.032

Hiremathad, A., Keri, R. S., Esteves, A. R., Cardoso, S. M., Chaves, S., & Santos, M. A. (2018). Novel Tacrine-Hydroxyphenylbenzimidazole hybrids as potential multitarget drug candidates for Alzheimer's disease. *European Journal of Medicinal Chemistry*, *148*, 255–267. https://doi.org/10.1016/j.ejmech.2018.02.023

Hou, K., Zhao, J., Wang, H., Li, B., Li, K., Shi, X., Wan, K., Ai, J., Lv, J., Wang, D., Huang, Q., Wang, H., Cao, Q., Liu, S., & Tang, Z. (2020). Chiral gold nanoparticles enantioselectively rescue memory deficits in a mouse model of Alzheimer's disease. *Nature Communications*, *11*(1), 1–11. https://doi.org/10.1038/s41467-020-18525-2

Hou, Y., Dan, X., Babbar, M., Wei, Y., Hasselbalch, S. G., Croteau, D. L., & Bohr, V. A. (2019). Ageing as a risk factor for neurodegenerative disease. *Nature Reviews Neurology*, *15*(10), 565–581. https://doi.org/10.1038/s41582-019-0244-7

Huang, Y., Wu, Z., Cao, Y., Lang, M., Lu, B., & Zhou, B. (2014). Zinc binding directly regulates tau toxicity independent of tau hyperphosphorylation. *Cell Reports*, *8*(3), 831–842. https://doi.org/10.1016/j.celrep.2014.06.047

Huat, T. J., Camats-Perna, J., Newcombe, E. A., Valmas, N., Kitazawa, M., & Medeiros, R. (2019). Metal Toxicity Links to Alzheimer's Disease and Neuroinflammation. *Journal of Molecular Biology*, *431*(9), 1843–1868. https://doi.org/10.1016/j.jmb.2019.01.018

Hulstaert, F., Blennow, K., Ivanoiu, A., Schoonderwaldt, H. C., Riemenschneider, M., de Deyn, P. P., Bancher, C., Cras, P., Wiltfang, J., Mehta, P. D., Iqbal, K., Pottel, H., Vanmechelen, E., & Vanderstichele, H. (1999). Improved discrimination of AD patients using-amyloid (1-42) and tau levels in CSF. *Neurology*, *52*(8), 1555–1562.

Hussien, H. M., Abd-Elmegied, A., Ghareeb, D. A., Hafez, H. S., Ahmed, H. E. A., & El-moneam, N. A. (2018). Neuroprotective effect of berberine against environmental heavy

metals-induced neurotoxicity and Alzheimer's-like disease in rats. *Food and Chemical Toxicology*, *111*, 432–444. https://doi.org/10.1016/j.fct.2017.11.025

Ignasik, M., Bajda, M., Guzior, N., Prinz, M., Holzgrabe, U., & Malawska, B. (2012). Design, synthesis and evaluation of novel 2-(Aminoalkyl)-isoindoline-1,3- dione derivatives as dual-binding site acetylcholinesterase inhibitors. *Archiv Der Pharmazie*, *345*(7), 509–516. https://doi.org/10.1002/ardp.201100423

Inestrosa, N. C., Alvarez, A., Pérez, C. A., Moreno, R. D., Vicente, M., Linker, C., Casanueva, O. I., Soto, C., & Garrido, J. (1996). Acetylcholinesterase accelerates assembly of amyloid-β-peptides into Alzheimer's fibrils: Possible role of the peripheral site of the enzyme. *Neuron*, *16*(4), 881–891. https://doi.org/10.1016/S0896-6273(00)80108-7

Irvine, J. D., Takahashi, L., Lockhart, K., Cheong, J., Tolan, J. W., Selick, H. E., & Grove, J. R. (1999). MDCK (Madin-Darby canine kidney) cells: A tool for membrane permeability screening. *Journal of Pharmaceutical Sciences*, *88*(1), 28–33. https://doi.org/10.1021/js9803205

Isabel Castanho, & Katie Lunnon. (2019). Chapter 8 - Epigenetic processes in Alzheimer's disease. In *Chromatin Signaling and Neurological Disorders* (Vol. 7, pp. 153–180). https://doi.org/https://doi.org/10.1016/B978-0-12-813796-3.00008-0

Islam, R., Parves, M. R., Paul, A. S., Uddin, N., Rahman, M. S., Mamun, A. al, Hossain, M. N., Ali, M. A., & Halim, M. A. (2021). A molecular modeling approach to identify effective antiviral phytochemicals against the main protease of SARS-CoV-2. *Journal of Biomolecular Structure and Dynamics*, *39*(9), 3213–3224. https://doi.org/10.1080/07391102.2020.1761883

Ismael, M. A., Elyamine, A. M., Moussa, M. G., Cai, M., Zhao, X., & Hu, C. (2019). Cadmium in plants: uptake, toxicity, and its interactions with selenium fertilizers. *Metallomics*, *11*(2), 255–277. https://doi.org/10.1039/c8mt00247a

Jafari, M., Tashkhourian, J., & Absalan, G. (2018). Chiral recognition of tryptophan enantiomers using chitosan-capped silver nanoparticles: Scanometry and spectrophotometry approaches. *Talanta*, *178*, 870–878. https://doi.org/10.1016/j.talanta.2017.10.005

Jagtap, R., Maher, W., Krikowa, F., Ellwood, M. J., & Foster, S. (2016). Measurement of selenomethionine and selenocysteine in fish tissues using HPLC-ICP-MS. *Microchemical Journal*, *128*, 248–257. https://doi.org/10.1016/j.microc.2016.04.021

James, S. A., Churches, Q. I., de Jonge, M. D., Birchall, I. E., Streltsov, V., McColl, G., Adlard, P. A., & Hare, D. J. (2017). Iron, Copper, and Zinc Concentration in Aβ Plaques in the

APP/PS1 Mouse Model of Alzheimer's Disease Correlates with Metal Levels in the Surrounding Neuropil. *ACS Chemical Neuroscience*, *8*(3), 629–637. https://doi.org/10.1021/acschemneuro.6b00362

Jiang, D., Li, X., Williams, R., Patel, S., Men, L., Wang, Y., & Zhou, F. (2009). Ternary complexes of iron, amyloid-β, and nitrilotriacetic acid: Binding affinities, redox properties, and relevance to iron-induced oxidative stress in Alzheimer's disease. *Biochemistry*, *48*(33), 7939–7947. https://doi.org/10.1021/bi900907a

Jiang, L. F., Yao, T. M., Zhu, Z. L., Wang, C., & Ji, L. N. (2007). Impacts of Cd(II) on the conformation and self-aggregation of Alzheimer's tau fragment corresponding to the third repeat of microtubule-binding domain. *Biochimica et Biophysica Acta - Proteins and Proteomics*, *1774*(11), 1414–1421. https://doi.org/10.1016/j.bbapap.2007.08.014

Jirásková-Vaníčková, J., Ettrich, R., Vorlová, B., Hoffman, H. E., Lepšík, M., Jansa, P., & Konvalinka, J. (2011). Inhibition of Human Serine Racemase, an Emerging Target for Medicinal Chemistry. *Current Drug Targets*, *12*(7), 1037–1055. https://doi.org/10.2174/138945011795677755

Karr, J. W., Akintoye, H., Kaupp, L. J., & Szalai, V. A. (2005). N-terminal deletions modify the Cu2+ binding site in amyloid-β. *Biochemistry*, *44*(14), 5478–5487. https://doi.org/10.1021/bi047611e

Karran, E., & de Strooper, B. (2016). The amyloid cascade hypothesis: are we poised for success or failure? *Journal of Neurochemistry*, *139*, 237–252. https://doi.org/10.1111/jnc.13632

Karran, E., & de Strooper, B. (2022). The amyloid hypothesis in Alzheimer disease: new insights from new therapeutics. *Nature Reviews Drug Discovery*, *21*(4), 306-318. https://doi.org/10.1038/s41573-022-00391-w

Kawahara, M., Kato-Negishi, M., & Tanaka, K. (2017). Cross talk between neurometals and amyloidogenic proteins at the synapse and the pathogenesis of neurodegenerative diseases. *Metallomics*, *9*(6), 619–633. https://doi.org/10.1039/c7mt00046d

Kayshev, V. G., Blinov, A. V., Serov, A. V., Gvozdenko, A. A., Kravtsov, A. A., Blinova, A. A., & Khramtsov, A. G. (2019). Quantum-chemical simulation of the interaction between the Zn2+ ions with C-terminal sites of kappa-casein. *Journal of Hygienic Engineering and Design*, *29*, 119–124.

Keppel Hesselink, J. M., & Schatman, M. E. (2018). Rediscovery of old drugs: The forgotten case of dermorphin for postoperative pain and palliation. *Journal of Pain Research*, *11*, 2991–2995. https://doi.org/10.2147/JPR.S186082

Keren-Shaul, H., Spinrad, A., Weiner, A., Matcovitch-Natan, O., Dvir-Szternfeld, R., Ulland, T. K., David, E., Baruch, K., Lara-Astaiso, D., Toth, B., Itzkovitz, S., Colonna, M., Schwartz, M., & Amit, I. (2017). A Unique Microglia Type Associated with Restricting Development of Alzheimer's Disease. *Cell*, *169*(7), 1276–1290. https://doi.org/10.1016/j.cell.2017.05.018

Khmeleva, S. A., Radko, S. P., Kozin, S. A., Kiseleva, Y. Y., Mezentsev, Y. v., Mitkevich, V. A., Kurbatov, L. K., Ivanov, A. S., & Makarov, A. A. (2016). Zinc-Mediated Binding of Nucleic Acids to Amyloid-β Aggregates: Role of Histidine Residues. *Journal of Alzheimer's Disease*, *54*(2), 809–819. https://doi.org/10.3233/JAD-160415

Khurana, A., Tekula, S., Saifi, M. A., Venkatesh, P., & Godugu, C. (2019). Therapeutic applications of selenium nanoparticles. *Biomedicine and Pharmacotherapy*, *111*, 802–812. https://doi.org/10.1016/j.biopha.2018.12.146

Kim, A. C., Lim, S., & Kim, Y. K. (2018). Metal ion effects on Aβ and tau aggregation. *International Journal of Molecular Sciences*, *19*(128), 1–15. https://doi.org/10.3390/ijms19010128

Kiriyama, Y., & Nochi, H. (2016). D-Amino Acids in the Nervous and Endocrine Systems. *Scientifica*, *2016*, 1–9. https://doi.org/10.1155/2016/6494621

Klein, J. (2007). Phenserine. *Expert Opinion on Investigational Drugs*, *16*(7), 1087–1097. https://doi.org/10.1517/13543784.16.7.1087

Knez, D., Coquelle, N., Pišlar, A., Žakelj, S., Jukič, M., Sova, M., Mravljak, J., Nachon, F., Brazzolotto, X., Kos, J., Colletier, J. P., & Gobec, S. (2018). Multi-target-directed ligands for treating Alzheimer's disease: Butyrylcholinesterase inhibitors displaying antioxidant and neuroprotective activities. *European Journal of Medicinal Chemistry*, *156*, 598–617. https://doi.org/10.1016/j.ejmech.2018.07.033

Kozlowski, H., Luczkowski, M., Remelli, M., & Valensin, D. (2012). Copper, zinc and iron in neurodegenerative diseases (Alzheimer's, Parkinson's and prion diseases). *Coordination Chemistry Reviews*, *256*(19–20), 2129–2141. https://doi.org/10.1016/j.ccr.2012.03.013

Kraepelin, E. (1910). Das senile und präsenile Irresein. *Psychiatrie: Ein Lehrbuch Fur Studierende Und Alzte*, *533*, 593–632.

Kumar, D., Gupta, S. K., Ganeshpurkar, A., Gutti, G., Krishnamurthy, S., Modi, G., & Singh, S. K. (2018). Development of Piperazinediones as dual inhibitor for treatment of Alzheimer's disease. *European Journal of Medicinal Chemistry*, *150*, 87–101. https://doi.org/10.1016/j.ejmech.2018.02.078

Kumer, A., Sarker, N. M., & Paul, S. (2019). The simulating study of HOMO, LUMO, thermo physical and quantitative structure of activity relationship (QSAR) of some anticancer active ionic liquids. *Eurasian Journal of Environmental Research EJERE*, *3*(1), 1–10.

Kuwada, M., Teramoto, T., Kumagaye, K. Y., Nakajima, K., Watanabe, T., Kawai, T., Kawakami, Y., Niidome, T., Sawada, K., Nishizawa, Y., & Katayama, K. (1994). ω-Agatoxin-TK containing D-serine at position 46, but not synthetic ω- [L-Ser46]agatoxin-TK, exerts blockade of P-type calcium channels in cerebellar Purkinje neurons. *Molecular Pharmacology*, *46*(4), 587–593.

Labunskyy, V. M., Lee, B. C., Handy, D. E., Loscalzo, J., Hatfield, D. L., & Gladyshev, V. N. (2011). Both maximal expression of selenoproteins and selenoprotein deficiency can promote development of type 2 diabetes-like phenotype in mice. *Antioxidants and Redox Signaling*, *14*(12), 2327–2336. https://doi.org/10.1089/ars.2010.3526

Lackie, R. E., Maciejewski, A., Ostapchenko, V. G., Marques-Lopes, J., Choy, W. Y., Duennwald, M. L., Prado, V. F., & Prado, M. A. M. (2017). The Hsp70/Hsp90 chaperone machinery in neurodegenerative diseases. *Frontiers in Neuroscience*, *11*, 1–24. https://doi.org/10.3389/fnins.2017.00254

Lambrinidis, G., Vallianatou, T., & Tsantili-Kakoulidou, A. (2015). In vitro, in silico and integrated strategies for the estimation of plasma protein binding. A review. *Advanced Drug Delivery Reviews*, *86*, 27–45. https://doi.org/10.1016/j.addr.2015.03.011

Lane, C. A., Hardy, J., & Schott, J. M. (2018). Alzheimer's disease. *European Journal of Neurology*, *25*(1), 59–70. https://doi.org/10.1111/ene.13439

Lane, D. J. R., Ayton, S., & Bush, A. I. (2018). Iron and Alzheimer's Disease: An Update on Emerging Mechanisms. *Journal of Alzheimer's Disease*, *64*(s1), S379–S395. https://doi.org/10.3233/JAD-179944

Laulagnier, K., Javalet, C., Hemming, F. J., Chivet, M., Lachenal, G., Blot, B., Chatellard, C., & Sadoul, R. (2018). Amyloid precursor protein products concentrate in a subset of exosomes specifically endocytosed by neurons. *Cellular and Molecular Life Sciences*, *75*(4), 757–773. https://doi.org/10.1007/s00018-017-2664-0

Lee, J., Song, K., Huh, E., Oh, M. S., & Kim, Y. S. (2018). Neuroprotection against 6-OHDA toxicity in PC12 cells and mice through the Nrf2 pathway by a sesquiterpenoid from Tussilago farfara. *Redox Biology*, *18*, 6–15. https://doi.org/10.1016/j.redox.2018.05.015

Lemire, M., Fillion, M., Barbosa, F., Guimarães, J. R. D., & Mergler, D. (2010). Elevated levels of selenium in the typical diet of Amazonian riverside populations. *Science of the Total Environment*, *408*(19), 4076–4084. https://doi.org/10.1016/j.scitotenv.2010.05.022

Letavayová, L., Vlčková, V., & Brozmanová, J. (2006). Selenium: From cancer prevention to DNA damage. *Toxicology*, *227*(1–2), 1–14. https://doi.org/10.1016/j.tox.2006.07.017

Levine, V. E. (1915). BIOCHEMICAL STUDIES OF SELENIUM. *ANNALS N. Y. Acm. SOL*, *XXVI*, 385–394. https://doi.org/https://doi.org/10.1111/j.1749-6632.1915.tb55179.x

Li, K., Tay, F. R., & Yiu, C. K. Y. (2020). The past, present and future perspectives of matrix metalloproteinase inhibitors. *Pharmacology and Therapeutics*, *207*, 107465. https://doi.org/10.1016/j.pharmthera.2019.107465

Li, Y., Jiao, Q., Xu, H., Du, X., Shi, L., Jia, F., & Jiang, H. (2017). Biometal dyshomeostasis and toxic metal accumulations in the development of alzheimer's disease. *Frontiers in Molecular Neuroscience*, *10*(339), 1–19. https://doi.org/10.3389/fnmol.2017.00339

Li, Y., Zhu, N., Liang, X., Zheng, L., Zhang, C., Li, Y. F., Zhang, Z., Gao, Y., & Zhao, J. (2020). A comparative study on the accumulation, translocation and transformation of selenite, selenate, and SeNPs in a hydroponic-plant system. *Ecotoxicology and Environmental Safety*, *189*, 109955. https://doi.org/10.1016/j.ecoenv.2019.109955

Li, Z., Mo, Z., Guo, R., Meng, S., Wang, R., Gao, H., & Niu, X. (2017). Electrochemical enantiorecognition of tryptophan enantiomers based on a multi-walled carbon nanotube-hydroxyethyl chitosan composite film. *Analytical Methods*, *9*(35), 5149–5155. https://doi.org/10.1039/c7ay01775h

Liao, S., Zhang, Y., Pan, X., Zhu, F., Jiang, C., Liu, Q., Cheng, Z., Dai, G., Wu, G., Wang, L., & Chen, L. (2019). Antibacterial activity and mechanism of silver nanoparticles against

multidrug-resistant pseudomonas aeruginosa. *International Journal of Nanomedicine*, *14*, 1469–1487. https://doi.org/10.2147/IJN.S191340

Lin, C. H., Yang, H. T., & Lane, H. Y. (2019). D-glutamate, D-serine, and D-alanine differ in their roles in cognitive decline in patients with Alzheimer's disease or mild cognitive impairment. *Pharmacology Biochemistry and Behavior*, *185*, 172760. https://doi.org/10.1016/j.pbb.2019.172760

Lin, L., & Wong, H. (2017). Predicting oral drug absorption: Mini review on physiologically-based pharmacokinetic models. *Pharmaceutics*, *9*(41), 1–14. https://doi.org/10.3390/pharmaceutics9040041

Lin, Y. T., Seo, J., Gao, F., Feldman, H. M., Wen, H. L., Penney, J., Cam, H. P., Gjoneska, E., Raja, W. K., Cheng, J., Rueda, R., Kritskiy, O., Abdurrob, F., Peng, Z., Milo, B., Yu, C. J., Elmsaouri, S., Dey, D., Ko, T., … Tsai, L. H. (2018). APOE4 Causes Widespread Molecular and Cellular Alterations Associated with Alzheimer's Disease Phenotypes in Human iPSC-Derived Brain Cell Types. *Neuron*, *98*(6), 1141-1154.e7. https://doi.org/10.1016/j.neuron.2018.05.008

Lipinski, C. A. (2000). Drug-like properties and the causes of poor solubility and poor permeability. *Journal of Pharmacological and Toxicological Methods*, *44*, 235–249. https://doi.org/https://doi.org/10.1016/S1056-8719(00)00107-6

Lipinski, C. A., Lombardo, F., Dominy, B. W., & Feeney, P. J. (2012). Experimental and computational approaches to estimate solubility and permeability in drug discovery and development settings. *Advanced Drug Delivery Reviews*, *64*(SUPPL.), 4–17. https://doi.org/10.1016/j.addr.2012.09.019

Liu, P. P., Xie, Y., Meng, X. Y., & Kang, J. S. (2019). History and progress of hypotheses and clinical trials for alzheimer's disease. *Signal Transduction and Targeted Therapy*, *4*(1). https://doi.org/10.1038/s41392-019-0063-8

Liu, Y., Liu, Q., Yin, G., & Luo, X. (2021). Research on the operational modal prediction of dry gas seal system based on response surface method. *Journal of Physics: Conference Series*, *2101*(1), 012040. https://doi.org/10.1088/1742-6596/2101/1/012040

Liu, Y., Nguyen, M., Robert, A., & Meunier, B. (2019). Metal Ions in Alzheimer's Disease: A Key Role or Not? *Accounts of Chemical Research*, *52*(7), 2026–2035. https://doi.org/10.1021/acs.accounts.9b00248

Livingston, G., Huntley, J., Sommerlad, A., Ames, D., Ballard, C., Banerjee, S., Brayne, C., Burns, A., Cohen-Mansfield, J., Cooper, C., Costafreda, S. G., Dias, A., Fox, N., Gitlin, L. N., Howard, R., Kales, H. C., Kivimäki, M., Larson, E. B., Ogunniyi, A., … Mukadam, N. (2020). Dementia prevention, intervention, and care: 2020 report of the Lancet Commission. *The Lancet*, *396*(10248), 413–446. https://doi.org/10.1016/S0140-6736(20)30367-6

Lobanov, A. v., Hatfield, D. L., & Gladyshev, V. N. (2009). Eukaryotic selenoproteins and selenoproteomes. *Biochimica et Biophysica Acta - General Subjects*, *1790*(11), 1424–1428. https://doi.org/10.1016/j.bbagen.2009.05.014

Long, J., & Holtzman, D. (2019). Alzheimer Disease: An Update on Pathobiology and Treatment Strategies. *Cell*, *179*(2), 312–339. https://doi.org/10.1016/j.cell.2019.09.001

Lott, I. T., & Head, E. (2019). Dementia in Down syndrome: unique insights for Alzheimer disease research. *Nature Reviews Neurology*, *15*(3), 135–147. https://doi.org/10.1038/s41582-018-0132-6

Lovell, M. A., Robertson, J. D., Teesdale, W. J., Campbell, J. L., & Markesbery, W. R. (1998). Copper, iron and zinc in Alzheimer's disease senile plaques. *Journal of the Neurological Sciences*, *158*, 47–52. https://doi.org/10.1177/1066896907302118

Lučiūnaitė, A., McManus, R. M., Jankunec, M., Rácz, I., Dansokho, C., Dalgėdienė, I., Schwartz, S., Brosseron, F., & Heneka, M. T. (2020). Soluble Aβ oligomers and protofibrils induce NLRP3 inflammasome activation in microglia. *Journal of Neurochemistry*, *155*(6), 650–661. https://doi.org/10.1111/jnc.14945

Luisa, M., Mariannatrevisiol, O., Aguglia, E., & Onor, M. L. (2007). Rivastigmine in the treatment of Alzheimer's disease: an update. *Clinical Interventions in Aging*, *2*(1), 17–32. https://doi.org/10.2147/ciia.2007.2.1.17

Mak, S., Li, W., Fu, H., Luo, J., Cui, W., Hu, S., Pang, Y., Carlier, P. R., Tsim, K. W., Pi, R., & Han, Y. (2021). Promising tacrine/huperzine A-based dimeric acetylcholinesterase inhibitors for neurodegenerative disorders: From relieving symptoms to modifying diseases through multitarget. *Journal of Neurochemistry*, *158*(6), 1381–1393. https://doi.org/10.1111/jnc.15379

Malishev, R., Arad, E., Bhunia, S. K., Shaham-Niv, S., Kolusheva, S., Gazit, E., & Jelinek, R. (2018). Chiral modulation of amyloid beta fibrillation and cytotoxicity by enantiomeric

carbon dots. *Chemical Communications*, *54*(56), 7762–7765. https://doi.org/10.1039/C8CC03235A

Maru, M., & Shah, M. K. (2012). Transition metal complexes of 2-(substituted-1H-pyrazole-4-yl)-1H-benzo[d]imidazoles: Synthesis and characterization. *Journal of Chemical and Pharmaceutical Research*, *4*(3), 1638–1643.

Masaldan, S., Bush, A. I., Devos, D., Rolland, A. S., & Moreau, C. (2019). Striking while the iron is hot: Iron metabolism and ferroptosis in neurodegeneration. *Free Radical Biology and Medicine*, *133*, 221–233. https://doi.org/10.1016/j.freeradbiomed.2018.09.033

Matsson, P., Doak, B. C., Over, B., & Kihlberg, J. (2016). Cell permeability beyond the rule of 5. *Advanced Drug Delivery Reviews*, *101*, 42–61. https://doi.org/10.1016/j.addr.2016.03.013

Mayes, J., Tinker-Mill, C., Kolosov, O., Zhang, H., Tabner, B. J., & Allsop, D. (2014). β-Amyloid fibrils in alzheimer disease are not inert when bound to copper ions but can degrade hydrogen peroxide and generate reactive oxygen species. *Journal of Biological Chemistry*, *289*(17), 12052–12062. https://doi.org/10.1074/jbc.M113.525212

McColgan, P., & Tabrizi, S. J. (2018). Huntington's disease: a clinical review. *European Journal of Neurology*, *25*(1), 24–34. https://doi.org/10.1111/ene.13413

Meanwell, N. A. (2016). Improving Drug Design: An Update on Recent Applications of Efficiency Metrics, Strategies for Replacing Problematic Elements, and Compounds in Nontraditional Drug Space. *Chemical Research in Toxicology*, *29*(4), 564–616. https://doi.org/10.1021/acs.chemrestox.6b00043

Mendez, C. M., McClain, C. J., & Marsano, L. S. (2005). Albumin therapy in clinical practice. *Nutrition in Clinical Practice*, *20*(3), 314–320. https://doi.org/10.1177/0115426505020003314

Mezeiova, E., Chalupova, K., Nepovimova, E., Gorecki, L., Prchal, L., Malinak, D., Kuca, K., Soukup, O., & Korabecny, J. (2019). Donepezil Derivatives Targeting Amyloid-β Cascade in Alzheimer's Disease. *Current Alzheimer Research*, *16*(9), 772–800. https://doi.org/10.2174/1567205016666190228122956

Michaels, T. C. T., Šarić, A., Curk, S., Bernfur, K., Arosio, P., Meisl, G., Dear, A. J., Cohen, S. I. A., Dobson, C. M., Vendruscolo, M., Linse, S., & Knowles, T. P. J. (2020). Dynamics of oligomer populations formed during the aggregation of Alzheimer's Aβ42 peptide. *Nature Chemistry*, *12*(5), 445–451. https://doi.org/10.1038/s41557-020-0452-1

Michaelson, D. M. (2014). APOE ε4: The most prevalent yet understudied risk factor for Alzheimer's disease. *Alzheimer's and Dementia*, *10*(6), 861–868. https://doi.org/10.1016/j.jalz.2014.06.015

Michaud, M., Balardy, L., Moulis, G., Gaudin, C., Peyrot, C., Vellas, B., Cesari, M., & Nourhashemi, F. (2013). Proinflammatory cytokines, aging, and age-related diseases. *Journal of the American Medical Directors Association*, *14*(12), 877–882. https://doi.org/10.1016/j.jamda.2013.05.009

Min, S. L. S., Liew, S. Y., Chear, N. J. Y., Goh, B. H., Tan, W. N., & Khaw, K. Y. (2022). Plant Terpenoids as the Promising Source of Cholinesterase Inhibitors for Anti-AD Therapy. *Biology*, *11*(307), 1–16. https://doi.org/10.3390/biology11020307

Mirza, A., King, A., Troakes, C., & Exley, C. (2017). Aluminium in brain tissue in familial Alzheimer's disease. *Journal of Trace Elements in Medicine and Biology*, *40*, 30–36. https://doi.org/10.1016/j.jtemb.2016.12.001

Mohammed, M. A., Syeda, J. T. M., Wasan, K. M., & Wasan, E. K. (2017). An overview of chitosan nanoparticles and its application in non-parenteral drug delivery. *Pharmaceutics*, *9*, 53. https://doi.org/10.3390/pharmaceutics9040053

Moisan, F., Kab, S., Mohamed, F., Canonico, M., le Guern, M., Quintin, C., Carcaillon, L., Nicolau, J., Duport, N., Singh-Manoux, A., Boussac-Zarebska, M., & Elbaz, A. (2016). Parkinson disease male-to-female ratios increase with age: French nationwide study and meta-analysis. *Journal of Neurology, Neurosurgery and Psychiatry*, *87*(9), 952–957. https://doi.org/10.1136/jnnp-2015-312283

Molla, G., Chaves-Sanjuan, A., Savinelli, A., Nardini, M., & Pollegioni, L. (2020). Structure and kinetic properties of human d-aspartate oxidase, the enzyme-controlling d-aspartate levels in brain. *FASEB Journal*, *34*(1), 1182–1197. https://doi.org/10.1096/fj.201901703R

Moreno, N. (2007). Image Processing with ImageJ. *Biophotonics International*, *11*(7), 249–258. https://doi.org/10.1201/9781420005615.ax4

Mori, K., Yokoyama, A., Yang, L., Yang, L., Maeda, N., Mitsuda, N., & Tanaka, J. (2004). L-Serine-mediated release of apolipoprotein E and lipids from microglial cells. *Experimental Neurology*, *185*(2), 220–231. https://doi.org/10.1016/j.expneurol.2003.10.010

Morroni, F., Sita, G., Graziosi, A., Turrini, E., Fimognari, C., Tarozzi, A., & Hrelia, P. (2018). Neuroprotective effect of caffeic acid phenethyl ester in a mouse model of alzheimer's

disease involves Nrf2/HO-1 pathway. *Aging and Disease*, *9*(4), 605–622. https://doi.org/10.14336/AD.2017.0903

Morvan, M., & Mikšík, I. (2021). Recent advances in chiral analysis of proteins and peptides. *Separations*, *8*(8), 1–29. https://doi.org/10.3390/separations8080112

Munoz-Torrero, D., & Camps, P. (2006). Dimeric and Hybrid Anti-Alzheimer Drug Candidates. *Current Medicinal Chemistry*, *13*(4), 399–422. https://doi.org/10.2174/092986706775527974

Naewla, S., Sirichoat, A., Pannangrong, W., Chaisawang, P., Wigmore, P., & Welbat, J. U. (2019). Hesperidin alleviates methotrexate-induced memory deficits via hippocampal neurogenesis in adult rats. *Nutrients*, *11*(4), 936. https://doi.org/10.3390/NU11040936

Nagayama, S.-I., Jono, H., Suzaki, H., Sakai, K., Tsuruya, E., Yamatsu, I., Isohama, Y., Miyata, T., & Kai, H. (2001). Carbenoxolone, a new inducer of heat shock protein 70. *Life Sciences*, *69*, 2867–2873.

Nasrabady, S. E., Rizvi, B., Goldman, J. E., & Brickman, A. M. (2018). White matter changes in Alzheimer's disease: a focus on myelin and oligodendrocytes. *Acta Neuropathologica Communications*, *6*(1), 22. https://doi.org/10.1186/s40478-018-0515-3

Naveed, M., Hejazi, V., Abbas, M., Kamboh, A. A., Khan, G. J., Shumzaid, M., Ahmad, F., Babazadeh, D., FangFang, X., Modarresi-Ghazani, F., WenHua, L., & XiaoHui, Z. (2018). Chlorogenic acid (CGA): A pharmacological review and call for further research. *Biomedicine and Pharmacotherapy*, *97*, 67–74. https://doi.org/10.1016/j.biopha.2017.10.064

Nazario, L. R., da Silva, R. S., & Bonan, C. D. (2017). Targeting adenosine signaling in Parkinson's disease: From pharmacological to non-pharmacological approaches. *Frontiers in Neuroscience*, *11*(658), 1–12. https://doi.org/10.3389/fnins.2017.00658

Nelson, D. L., Applegate, G. A., Beio, M. L., Graham, D. L., & Berkowitz, D. B. (2017). Human serine racemase structure/activity relationship studies provide mechanistic insight and point to position 84 as a hot spot for β-elimination function. *Journal of Biological Chemistry*, *292*(34), 13986–14002. https://doi.org/10.1074/jbc.M117.777904

Nilsson, M. R. (2004). Techniques to study amyloid fibril formation in vitro. *Methods*, *34*(1), 151–160. https://doi.org/10.1016/j.ymeth.2004.03.012

Nogueira, C. W., Barbosa, N. v., & Rocha, J. B. T. (2021). Toxicology and pharmacology of synthetic organoselenium compounds: an update. *Archives of Toxicology*, *95*(4), 1179–1226. https://doi.org/10.1007/s00204-021-03003-5

Notarachille, G., Arnesano, F., Calò, V., & Meleleo, D. (2014). Heavy metals toxicity: Effect of cadmium ions on amyloid beta protein 1-42. Possible implications for Alzheimer's disease. *BioMetals*, *27*(2), 371–388. https://doi.org/10.1007/s10534-014-9719-6

Nuttall, K. L., & Allen, F. S. (1984). Selenium Detoxification of Heavy Metals: a Possible Mechanism for the Blood Plasma. *Inorganica Chimica Acta*, *92*, 187–189.

Nuzzo, T., Feligioni, M., Cristino, L., Pagano, I., Marcelli, S., Iannuzzi, F., Imperatore, R., D'Angelo, L., Petrella, C., Carella, M., Pollegioni, L., Sacchi, S., Punzo, D., de Girolamo, P., Errico, F., Canu, N., & Usiello, A. (2019). Free D-aspartate triggers NMDA receptor-dependent cell death in primary cortical neurons and perturbs JNK activation, Tau phosphorylation, and protein SUMOylation in the cerebral cortex of mice lacking D-aspartate oxidase activity. *Experimental Neurology*, *317*, 51–65. https://doi.org/10.1016/j.expneurol.2019.02.014

Ogura, H., Kosasa, T., Kuriya, Y., & Yamanishi, Y. (2000). Comparison of inhibitory activities of donepezil and other cholinesterase inhibitors on acetylcholinesterase and butylcholinesterase in vitro. *Methods and Findings in Experimental and Clinical Pharmacology*, *22*(8), 609. https://doi.org/10.1358/mf.2000.22.8.701373

Olagnier, D., Farahani, E., Thyrsted, J., Blay-Cadanet, J., Herengt, A., Idorn, M., Hait, A., Hernaez, B., Knudsen, A., Iversen, M. B., Schilling, M., Jørgensen, S. E., Thomsen, M., Reinert, L. S., Lappe, M., Hoang, H. D., Gilchrist, V. H., Hansen, A. L., Ottosen, R., … Holm, C. K. (2020). SARS-CoV2-mediated suppression of NRF2-signaling reveals potent antiviral and anti-inflammatory activity of 4-octyl-itaconate and dimethyl fumarate. *Nature Communications*, *11*(1), 1–12. https://doi.org/10.1038/s41467-020-18764-3

Özturan Özer, E., Unsal Tan, O., Ozadali, K., Küçükkilinç, T., Balkan, A., & Uçar, G. (2013). Synthesis, molecular modeling and evaluation of novel N'-2-(4- benzylpiperidin-/piperazin-1-yl)acylhydrazone derivatives as dual inhibitors for cholinesterases and Aβ aggregation. *Bioorganic and Medicinal Chemistry Letters*, *23*(2), 440–443. https://doi.org/10.1016/j.bmcl.2012.11.064

Palm, K., Stenberg, P., Luthman, K., & Artursson, P. (1997). Polar molecular surface properties predict the intestinal absorption of drugs in humans. *Pharmaceutical Research*, *14*(5), 568–571.

Panza, F., Solfrizzi, V., Seripa, D., Imbimbo, B. P., Lozupone, M., Santamato, A., Zecca, C., Barulli, M. R., Bellomo, A., Pilotto, A., Daniele, A., Greco, A., & Logroscino, G. (2016). Tau-Centric Targets and Drugs in Clinical Development for the Treatment of Alzheimer's Disease. *BioMed Research International*, *2016*(3245935), 1–15. https://doi.org/10.1155/2016/3245935

Patterson, C. (2018). *World Alzheimer Report 2018 - The state of the art of dementia research: New frontiers. Alzheimer Research International.* https://www.alz.co.uk/research/world-report - 2018

Peak, D. (2006). Adsorption mechanisms of selenium oxyanions at the aluminum oxide/water interface. *Journal of Colloid and Interface Science*, *303*(2), 337–345. https://doi.org/10.1016/j.jcis.2006.08.014

Peters, D. G., Pollack, A. N., Cheng, K. C., Sun, D., Saido, T., Haaf, M. P., Yang, Q. X., Connor, J. R., & Meadowcroft, M. D. (2018). Dietary lipophilic iron alters amyloidogenesis and microglial morphology in Alzheimer's disease knock-in APP mice. *Metallomics*, *10*(3), 426–443. https://doi.org/10.1039/c8mt00004b

Petrucelli, L., Dickson, D., Kehoe, K., Taylor, J., Snyder, H., Grover, A., de Lucia, M., McGowan, E., Lewis, J., Prihar, G., Kim, J., Dillmann, W. H., Browne, S. E., Hall, A., Voellmy, R., Tsuboi, Y., Dawson, T. M., Wolozin, B., Hardy, J., & Hutton, M. (2004). CHIP and Hsp70 regulate tau ubiquitination, degradation and aggregation. *Human Molecular Genetics*, *13*(7), 703–714. https://doi.org/10.1093/hmg/ddh083

Pettersen, E. F., Goddard, T. D., Huang, C. C., Couch, G. S., Greenblatt, D. M., Meng, E. C., & Ferrin, T. E. (2004). UCSF Chimera - A visualization system for exploratory research and analysis. *Journal of Computational Chemistry*, *25*(13), 1605–1612. https://doi.org/10.1002/jcc.20084

Phuagkhaopong, S., Ospondpant, D., Kasemsuk, T., Sibmooh, N., Soodvilai, S., Power, C., & Vivithanaporn, P. (2017). Cadmium-induced IL-6 and IL-8 expression and release from astrocytes are mediated by MAPK and NF-κB pathways. *NeuroToxicology*, *60*, 82–91. https://doi.org/10.1016/j.neuro.2017.03.001

Pi, R., Mao, X., Chao, X., Cheng, Z., Liu, M., Duan, X., Ye, M., Chen, X., Mei, Z., Liu, P., Li, W., & Han, Y. (2012). Tacrine-6-ferulic acid, a novel multifunctional dimer, inhibits amyloid-β-mediated Alzheimer's disease-associated pathogenesis in vitro and in vivo. *PLoS ONE*, *7*(2), 1–8. https://doi.org/10.1371/journal.pone.0031921

Piemontese, L., Tomás, D., Hiremathad, A., Capriati, V., Candeias, E., Cardoso, S. M., Chaves, S., & Santos, M. A. (2018). Donepezil structure-based hybrids as potential multifunctional anti-Alzheimer's drug candidates. *Journal of Enzyme Inhibition and Medicinal Chemistry*, *33*(1), 1212–1224. https://doi.org/10.1080/14756366.2018.1491564

Pilikidou, M., Palyvou, F., Papadopoulou, S. K., Tsiouda, T., Tsekitsidi, E., Arvaniti, K., Miziou, A., Tsingerlioti, Z., Apostolidis, G., Ntiloudis, R., Boniou, K., Tsioudas, A. A., Cheva, A., Petridis, D., & Zarogoulidis, P. (2021). Lung cancer, treatment and nutritional status. *Molecular and Clinical Oncology*, *15*(6). https://doi.org/10.3892/MCO.2021.2410

Pirpamer, L., Hofer, E., Gesierich, B., de Guio, F., Freudenberger, P., Seiler, S., Duering, M., Jouvent, E., Duchesnay, E., Dichgans, M., Ropele, S., & Schmidt, R. (2016). Determinants of iron accumulation in the normal aging brain. *Neurobiology of Aging*, *43*, 149–155. https://doi.org/10.1016/j.neurobiolaging.2016.04.002

Piubelli, L., Murtas, G., Rabattoni, V., & Pollegioni, L. (2021). The Role of D-Amino Acids in Alzheimer's Disease. *Journal of Alzheimer's Disease*, *80*, 475–492. https://doi.org/10.3233/JAD-201217

Poewe, W., Seppi, K., Tanner, C. M., Halliday, G. M., Brundin, P., Volkmann, J., Schrag, A. E., & Lang, A. E. (2017). Parkinson disease. *Nature Reviews Disease Primers*, *3*, 1–21. https://doi.org/10.1038/nrdp.2017.13

Qin, H. bo, Zhu, J. ming, Liang, L., Wang, M. shi, & Su, H. (2013). The bioavailability of selenium and risk assessment for human selenium poisoning in high-Se areas, China. *Environment International*, *52*, 66–74. https://doi.org/10.1016/j.envint.2012.12.003

Qiu, Y. N., Wang, G. H., Zhou, F., Hao, J. J., Tian, L., Guan, L. F., Geng, X. K., Ding, Y. C., Wu, H. W., & Zhang, K. Z. (2019). PM2.5 induces liver fibrosis via triggering ROS-mediated mitophagy. *Ecotoxicology and Environmental Safety*, *167*, 178–187. https://doi.org/10.1016/j.ecoenv.2018.08.050

Que, E. L., Domaille, D. W., & Chang, C. J. (2008). Metals in neurobiology: Probing their chemistry and biology with molecular imaging. *Chemical Reviews*, *108*(5), 1517–1549. https://doi.org/10.1021/cr800447y

Quintanova, C., Keri, R. S., Marques, S. M., G-Fernandes, M., Cardoso, S. M., Luísa Serralheiro, M., & Amélia Santos, M. (2015). Design, synthesis and bioevaluation of tacrine hybrids

with cinnamate and cinnamylidene acetate derivatives as potential anti-Alzheimer drugs. *MedChemComm*, *6*(11), 1969–1977. https://doi.org/10.1039/c5md00236b

Rabattoni, V., Pollegioni, L., Tedeschi, G., Maffioli, E., & Sacchi, S. (2021). Cellular studies of the two main isoforms of human d-aspartate oxidase. *FEBS Journal*, *288*(16), 4939–4954. https://doi.org/10.1111/febs.15797

Radic, S., Davis, T. P., Ke, P. C., & Ding, F. (2015). Contrasting effects of nanoparticle-protein attraction on amyloid aggregation. *RSC Advances*, *5*(127), 105489–105498. https://doi.org/10.1039/c5ra20182a

Rahman, M. M., Hossain, K. F. B., Banik, S., Sikder, M. T., Akter, M., Bondad, S. E. C., Rahaman, M. S., Hosokawa, T., Saito, T., & Kurasaki, M. (2019). Selenium and zinc protections against metal-(loids)-induced toxicity and disease manifestations: A review. *Ecotoxicology and Environmental Safety*, *168*, 146–163. https://doi.org/10.1016/j.ecoenv.2018.10.054

Rahmanto, A. S., & Davies, M. J. (2012). Selenium-containing amino acids as direct and indirect antioxidants. *IUBMB Life*, *64*(11), 863–871. https://doi.org/10.1002/iub.1084

Rajan, K. B., Barnes, L. L., Wilson, R. S., McAninch, E. A., Weuve, J., Sighoko, D., & Evans, D. A. (2017). Racial Differences in the Association Between Apolipoprotein E Risk Alleles and Overall and Total Cardiovascular Mortality Over 18 Years. *Journal of the American Geriatrics Society*, *65*(11), 2425–2430. https://doi.org/10.1111/jgs.15059

Ray Dorsey, E., Elbaz, A., Nichols, E., Abd-Allah, F., Abdelalim, A., Adsuar, J. C., Ansha, M. G., Brayne, C., Choi, J. Y. J., Collado-Mateo, D., Dahodwala, N., Do, H. P., Edessa, D., Endres, M., Fereshtehnejad, S. M., Foreman, K. J., Gankpe, F. G., Gupta, R., Hankey, G. J., … Murray, C. J. L. (2018). Global, regional, and national burden of Parkinson's disease, 1990–2016: a systematic analysis for the Global Burden of Disease Study 2016. *The Lancet Neurology*, *17*(11), 939–953. https://doi.org/10.1016/S1474-4422(18)30295-3

Readel, E. R., Wey, M., & Armstrong, D. W. (2021). Rapid and selective separation of amyloid beta from its stereoisomeric point mutations implicated in neurodegenerative Alzheimer's disease. *Analytica Chimica Acta*, *1163*, 338506. https://doi.org/10.1016/j.aca.2021.338506

Rezaei-Ghaleh, N., Giller, K., Becker, S., & Zweckstetter, M. (2011). Effect of zinc binding on β-amyloid structure and dynamics: Implications for Aβ aggregation. *Biophysical Journal*, *101*(5), 1202–1211. https://doi.org/10.1016/j.bpj.2011.06.062

Ritter, C., Adrian, M., Riek-loher, D., Bohrmann, B., Do, H., Schubert, D., & Riek, R. (2005). 3D structure of Alzheimer's amyloid-B (1 – 42) fibrils. *Proceedings of the National Academy of Sciences of the United States of America*, *102*(48), 17342–17347.

Rivera, S., García-González, L., Khrestchatisky, M., & Baranger, K. (2019). Metalloproteinases and their tissue inhibitors in Alzheimer's disease and other neurodegenerative disorders. *Cellular and Molecular Life Sciences*, *76*(16), 3167–3191. https://doi.org/10.1007/s00018-019-03178-2

Rizzo, S., Bartolini, M., Ceccarini, L., Piazzi, L., Gobbi, S., Cavalli, A., Recanatini, M., Andrisano, V., & Rampa, A. (2010). Targeting Alzheimer's disease: Novel indanone hybrids bearing a pharmacophoric fragment of AP2238. *Bioorganic and Medicinal Chemistry*, *18*(5), 1749–1760. https://doi.org/10.1016/j.bmc.2010.01.071

Rodríguez-Rodríguez, C., de Groot, N. S., Rimola, A., Álvarez-Larena, Á., Lloveras, V., Vidal-Gancedo, J., Ventura, S., Vendrell, J., Sodupe, M., & González-Duarte, P. (2009). Design, selection, and characterization of thioflavin-based intercalation compounds with metal chelating properties for application in alzheimer's disease. *Journal of the American Chemical Society*, *131*(4), 1436–1451. https://doi.org/10.1021/ja806062g

Rogers, J., Bush, A., Cho, H., Smith, D., Thomson, A., Lahiri, D. K., Leedman, P., Huang, X., & Cahill, C. C. (2008). Iron and the translation of the amyloid precursor protein (APP) and ferritin mRNAs: riboregulation against neural oxidative damage in Alzheimer's disease. *Biochem Soc Trans*, *36*(6), 1282–1287. https://doi.org/10.1042/BST0361282.Iron

Roisman, L. C., Han, S., Chuei, M. J., Connor, A. R., & Cappai, R. (2019). The crystal structure of amyloid precursor–like protein 2 E2 domain completes the amyloid precursor protein family. *FASEB Journal*, *33*(4), 5076–5081. https://doi.org/10.1096/fj.201802315R

Rolim, W. R., Pelegrino, M. T., de Araújo Lima, B., Ferraz, L. S., Costa, F. N., Bernardes, J. S., Rodigues, T., Brocchi, M., & Seabra, A. B. (2019). Green tea extract mediated biogenic synthesis of silver nanoparticles: Characterization, cytotoxicity evaluation and antibacterial activity. *Applied Surface Science*, *463*, 66–74. https://doi.org/10.1016/j.apsusc.2018.08.203

Romero, I., de Francisco, P., Gutiérrez, J. C., & Martín-González, A. (2019). Selenium cytotoxicity in Tetrahymena thermophila: New clues about its biological effects and cellular resistance mechanisms. *Science of the Total Environment*, *671*, 850–865. https://doi.org/10.1016/j.scitotenv.2019.03.115

Ross, C. A., & Tabrizi, S. J. (2011). Huntington's disease: From molecular pathogenesis to clinical treatment. *The Lancet Neurology*, *10*(1), 83–98. https://doi.org/10.1016/S1474-4422(10)70245-3

Rothammer, A., Sage, E. K., Werner, C., Combs, S. E., & Multhoff, G. (2019). Increased heat shock protein 70 (Hsp70) serum levels and low NK cell counts after radiotherapy - Potential markers for predicting breast cancer recurrence? *Radiation Oncology*, *14*(78), 1–9. https://doi.org/10.1186/s13014-019-1286-0

Roy, A., Das, B., Sengupta, M., & Mohanta, B. (2021). Cellular uptake of spherical and triangular shaped gold nanoparticles synthesised using Eupatorium odoratum leaf extract. *Advances in Natural Sciences: Nanoscience and Nanotechnology*, *12*(3), 1–7. https://doi.org/10.1088/2043-6262/ac00a4

Rubio-Barroso, S., Santos-Delgado, M. J., Martín-Olivar, C., & Polo-Díez, L. M. (2006). Indirect chiral HPLC determination and fluorimetric detection of D-amino acids in milk and oyster samples. *Journal of Dairy Science*, *89*(1), 82–89. https://doi.org/10.3168/jds.S0022-0302(06)72071-9

Rudajev, V., & Novotny, J. (2020). The role of lipid environment in ganglioside gm1-induced amyloid β aggregation. *Membranes*, *10*(9), 1–22. https://doi.org/10.3390/membranes10090226

Samakashvili, S., Ibáñez, C., Simó, C., Gil-Bea, F. J., Winblad, B., Cedazo-Mínguez, A., & Cifuentes, A. (2011). Analysis of chiral amino acids in cerebrospinal fluid samples linked to different stages of Alzheimer disease. *Electrophoresis*, *32*(19), 2757–2764. https://doi.org/10.1002/elps.201100139

Sanabria-Castro, A., Alvarado-Echeverría, I., & Monge-Bonilla, C. (2017). Molecular pathogenesis of alzheimer's disease: An update. *Annals of Neurosciences*, *24*(1), 46–54. https://doi.org/10.1159/000464422

Sathiya Kamatchi, T., Mohamed Subarkhan, M. K., Ramesh, R., Wang, H., & Malecki, J. G. (2020). Investigation into antiproliferative activity and apoptosis mechanism of new arene Ru(ii) carbazole-based hydrazone complexes. *Dalton Transactions*, *49*(32), 11385–11395. https://doi.org/10.1039/d0dt01476a

Saudou, F., & Humbert, S. (2016). The Biology of Huntingtin. *Neuron*, *89*(5), 910–926. https://doi.org/10.1016/j.neuron.2016.02.003

Schwarz, K., & Foltz, C. M. (1957). SELENIUM AS AN INTEGRAL PART OF FACTOR 3 AGAINST DIETARY NECROTIC LIVER DEGENERATION. *J. Am. Chem. Soc*, *79*(12), 3292–3293. https://doi.org/https://doi.org/10.1021/ja01569a087

Sele, V., Ørnsrud, R., Sloth, J. J., Berntssen, M. H. G., & Amlund, H. (2018). Selenium and selenium species in feeds and muscle tissue of Atlantic salmon. *Journal of Trace Elements in Medicine and Biology*, *47*, 124–133. https://doi.org/10.1016/j.jtemb.2018.02.005

Sendzik, M., Pushie, M. J., Stefaniak, E., & Haas, K. L. (2017). Structure and Affinity of Cu(I) Bound to Human Serum Albumin. *Inorganic Chemistry*, *56*(24), 15057–15065. https://doi.org/10.1021/acs.inorgchem.7b02397

Sensi, S. L., Granzotto, A., Siotto, M., & Squitti, R. (2018). Copper and Zinc Dysregulation in Alzheimer's Disease. *Trends in Pharmacological Sciences*, *39*(12), 1049–1063. https://doi.org/10.1016/j.tips.2018.10.001

Seo, Y. R., Kelley, M. R., & Smith, M. L. (2002). Selenomethionine regulation of p53 by a ref1-dependent redox mechanism. *Proc Natl Acad Sci U S A*, *99*, 14548–14553. www.pnas.orgcgidoi10.1073pnas.212319799

Serpell, L. C. (2000). Alzheimer's amyloid fibrils: structure and assembly. *Biochimica et Biophysica Acta*, *1502*, 16–30. https://doi.org/10.1016/s0925-4439(00)00029-6

Shahidi, F., & Ambigaipalan, P. (2015). Phenolics and polyphenolics in foods, beverages and spices: Antioxidant activity and health effects - A review. *Journal of Functional Foods*, *18*, 820–897. https://doi.org/10.1016/j.jff.2015.06.018

Sharma, K. (2019). Cholinesterase inhibitors as Alzheimer's therapeutics (Review). *Molecular Medicine Reports*, *20*(2), 1479–1487. https://doi.org/10.3892/mmr.2019.10374

Shchipunov, Y. (2012). Bionanocomposites: Green sustainable materials for the near future. *Pure and Applied Chemistry*, *84*(12), 2579–2607. https://doi.org/10.1351/PAC-CON-12-05-04

Shichinohe, H., Kuroda, S., Yasuda, H., Ishikawa, T., Iwai, M., Horiuchi, M., & Iwasaki, Y. (2004). Neuroprotective effects of the free radical scavenger Edaravone (MCI-186) in mice permanent focal brain ischemia. *Brain Research*, *1029*(2), 200–206. https://doi.org/10.1016/j.brainres.2004.09.055

Sims, C. M., Hanna, S. K., Heller, D. A., Horoszko, C. P., Johnson, M. E., Montoro Bustos, A. R., Reipa, V., Riley, K. R., & Nelson, B. C. (2017). Redox-active nanomaterials for

nanomedicine applications. *Nanoscale*, *9*(40), 15226–15251. https://doi.org/10.1039/c7nr05429g

Simunkova, M., Alwasel, S. H., Alhazza, I. M., Jomova, K., Kollar, V., Rusko, M., & Valko, M. (2019). Management of oxidative stress and other pathologies in Alzheimer's disease. *Archives of Toxicology*, *93*(9), 2491–2513. https://doi.org/10.1007/s00204-019-02538-y

Singh, J. C. H., Kakalij, R. M., Kshirsagar, R. P., Kumar, B. H., Komakula, S. S. B., & Diwan, P. V. (2015). Cognitive effects of vanillic acid against streptozotocin-induced neurodegeneration in mice. *Pharmaceutical Biology*, *53*(5), 630–636. https://doi.org/10.3109/13880209.2014.935866

Soriano-Garcia, M. (2012). Organoselenium Compounds as Potential Therapeutic and Chemopreventive Agents: A Review. *Current Medicinal Chemistry*, *11*(12), 1657–1669. https://doi.org/10.2174/0929867043365053

Sors, T. G., Martin, C. P., & Salt, D. E. (2009). Characterization of selenocysteine methyltransferases from Astragalus species with contrasting selenium accumulation capacity. *Plant Journal*, *59*(1), 110–122. https://doi.org/10.1111/j.1365-313X.2009.03855.x

Sõti, C., Nagy, E., Giricz, Z., Vígh, L., Csermely, P., & Ferdinandy, P. (2005). Heat shock proteins as emerging therapeutic targets. *British Journal of Pharmacology*, *146*(6), 769–780. https://doi.org/10.1038/sj.bjp.0706396

Sparks, D. L., & Schreurs, B. G. (2003). Trace amounts of copper in water induce β-amyloid plaques and learning deficits in a rabbit model of Alzheimer's disease. *Proc Natl Acad Sci U S A*, *100*(19), 11065–11069. https://doi.org/10.1073/pnas.1832769100

Squadrone, S., Brizio, P., Stella, C., Mantia, M., Pederiva, S., Giordanengo, G., Pistone, G., & Abete, M. C. (2020). Distribution and bioaccumulation of trace elements and lanthanides in apples from Northwestern Italy. *Journal of Trace Elements in Medicine and Biology*, *62*, 126646. https://doi.org/10.1016/j.jtemb.2020.126646

Stine, W. B., Dahlgren, K. N., Krafft, G. A., & LaDu, M. J. (2003). In vitro characterization of conditions for amyloid-β peptide oligomerization and fibrillogenesis. *Journal of Biological Chemistry*, *278*(13), 11612–11622. https://doi.org/10.1074/jbc.M210207200

Stockwell, B. R., Friedmann Angeli, J. P., Bayir, H., Bush, A. I., Conrad, M., Dixon, S. J., Fulda, S., Gascón, S., Hatzios, S. K., Kagan, V. E., Noel, K., Jiang, X., Linkermann, A., Murphy, M. E., Overholtzer, M., Oyagi, A., Pagnussat, G. C., Park, J., Ran, Q., … Zhang, D. D.

(2017). Ferroptosis: A Regulated Cell Death Nexus Linking Metabolism, Redox Biology, and Disease. *Cell*, *171*(2), 273–285. https://doi.org/10.1016/j.cell.2017.09.021

Sultanbawa, Y., Smyth, H. E., Truong, K., Chapman, J., & Cozzolino, D. (2021). Insights on the role of chemometrics and vibrational spectroscopy in fruit metabolite analysis. *Food Chemistry: Molecular Sciences*, *3*, 100033. https://doi.org/10.1016/j.fochms.2021.100033

Sun, D., Zhang, W., Yu, Q., Chen, X., Xu, M., Zhou, Y., & Liu, J. (2017). Chiral penicillamine-modified selenium nanoparticles enantioselectively inhibit metal-induced amyloid β aggregation for treating Alzheimer's disease. *Journal of Colloid and Interface Science*, *505*, 1001–1010. https://doi.org/10.1016/j.jcis.2017.06.083

Sy, M., Kitazawa, M., Medeiros, R., Whitman, L., Cheng, D., Lane, T. E., & LaFerla, F. M. (2011). Inflammation induced by infection potentiates tau pathological features in transgenic mice. *American Journal of Pathology*, *178*(6), 2811–2822. https://doi.org/10.1016/j.ajpath.2011.02.012

Takayama, T., Mochizuki, T., Todoroki, K., Min, J. Z., Mizuno, H., Inoue, K., Akatsu, H., Noge, I., & Toyo'oka, T. (2015). A novel approach for LC-MS/MS-based chiral metabolomics fingerprinting and chiral metabolomics extraction using a pair of enantiomers of chiral derivatization reagents. *Analytica Chimica Acta*, *898*, 73–84. https://doi.org/10.1016/j.aca.2015.10.010

Tamagno, E., Guglielmotto, M., Monteleone, D., & Tabaton, M. (2012). Amyloid-β production: Major link between oxidative stress and BACE1. *Neurotoxicity Research*, *22*(3), 208–219. https://doi.org/10.1007/s12640-011-9283-6

Tan, H. W., Mo, H. Y., Lau, A. T. Y., & Xu, Y. M. (2019). Selenium species: Current status and potentials in cancer prevention and therapy. *International Journal of Molecular Sciences*, *20*(75), 1–26. https://doi.org/10.3390/ijms20010075

Tan, L. C., Nancharaiah, Y. v., van Hullebusch, E. D., & Lens, P. N. L. (2016). Selenium: environmental significance, pollution, and biological treatment technologies. *Biotechnology Advances*, *34*(5), 886–907. https://doi.org/10.1016/j.biotechadv.2016.05.005

Tang, M., Taghibiglou, C., & Liu, J. (2017). The Mechanisms of Action of Curcumin in Alzheimer's Disease. *Journal of Alzheimer's Disease*, *58*(4), 1003–1016. https://doi.org/10.3233/JAD-170188

Taslimi, P., & Gulçin, İ. (2018). Antioxidant and anticholinergic properties of olivetol. *Journal of Food Biochemistry*, *42*(3), 1–12. https://doi.org/10.1111/jfbc.12516

Taylor, J. P., Brown, R. H., & Cleveland, D. W. (2016). Decoding ALS: From genes to mechanism. *Nature*, *539*(7628), 197–206. https://doi.org/10.1038/nature20413

Thibaudeau, T. A., Anderson, R. T., & Smith, D. M. (2018). A common mechanism of proteasome impairment by neurodegenerative disease-associated oligomers. *Nature Communications*, *9*, 1097. https://doi.org/10.1038/s41467-018-03509-0

Tian, M., Hui, M., Thannhauser, T. W., Pan, S., & Li, L. (2017). Selenium-induced toxicity is counteracted by sulfur in broccoli (Brassica oleracea L. var. italica). *Frontiers in Plant Science*, *8*(1425), 1–13. https://doi.org/10.3389/fpls.2017.01425

Tomiyama, T., Asano, S., Furiya, Y., Shirasawa, T., Endo, N., & Mori, H. (1994). Racemization of Asp23 Residue Affects the Aggregation Properties of Alzheimer Amyloid p Protein Analogues. *J. Biol. Chem*, *269*(14), 10205–10208.

Torti, S. v, Manz, D. H., Paul, B. T., Blanchette-Farra, N., & Torti, F. M. (2018). Iron and Cancer. *Annual Review of Nutrition*, *38*, 97–125. https://doi.org/10.1146/annurev-nutr-082117

Tougu, V. (2005). Acetylcholinesterase: Mechanism of Catalysis and Inhibition. *Current Medicinal Chemistry-Central Nervous System Agents*, *1*(2), 155–170. https://doi.org/10.2174/1568015013358536

Tripathi, A., & Srivastava, U. C. (2008). ACETYLCHOLINESTERASE: A VERSATILE ENZYME OF NERVOUS SYSTEM. *Annals of Neurosciences*, *15*, 106–111. https://doi.org/10.5214/95

Tysnes, O. B., & Storstein, A. (2017). Epidemiology of Parkinson's disease. *Journal of Neural Transmission*, *124*(8), 901–905. https://doi.org/10.1007/s00702-017-1686-y

Ul Amin, F., Shah, S. A., & Kim, M. O. (2017). Vanillic acid attenuates Aβ1-42-induced oxidative stress and cognitive impairment in mice. *Scientific Reports*, *7*(40853), 1–15. https://doi.org/10.1038/srep40753

Unni, E., Koul, D., Yung, W. K. A., & Sinha, R. (2005). Se-methylselenocysteine inhibits phosphatidylinositol 3-kinase activity of mouse mammary epithelial tumor cells in vitro. *Breast Cancer Research*, *7*(5), 699–707. https://doi.org/10.1186/bcr1276

Unsal, V., Dalkiran, T., Çiçek, M., & Kölükçü, E. (2020). The role of natural antioxidants against reactive oxygen species produced by cadmium toxicity: A review. *Advanced Pharmaceutical Bulletin*, *10*(2), 184–202. https://doi.org/10.34172/apb.2020.023

Ursini, F., Maiorino, M., & Gregolin, C. (1985). The selenoenzyme phospholipid hydroperoxide glutathione peroxidase. *BBA - General Subjects*, *839*(1), 62–70. https://doi.org/10.1016/0304-4165(85)90182-5

Vallianatou, T., Lambrinidis, G., & Tsantili-Kakoulidou, A. (2013). In silico prediction of human serum albumin binding for drug leads. *Expert Opinion on Drug Discovery*, *8*(5), 583–595. https://doi.org/10.1517/17460441.2013.777424

Vandenbroucke, R. E., & Libert, C. (2014). Is there new hope for therapeutic matrix metalloproteinase inhibition? *Nature Reviews Drug Discovery*, *13*(12), 904–927. https://doi.org/10.1038/nrd4390

Verma, S., Sharma, S., Ranawat, P., & Nehru, B. (2020). Modulatory Effects of Ginkgo biloba Against Amyloid Aggregation Through Induction of Heat Shock Proteins in Aluminium Induced Neurotoxicity. *Neurochemical Research*, *45*(2), 465–490. https://doi.org/10.1007/s11064-019-02940-z

Vijaya Kumar, D., & Moir, R. (2017). The Emerging Role of Innate Immunity in Alzheimer's Disease. *Neuropsychopharmacology*, *42*(1), 362–363. https://doi.org/https://doi.org/10.1038/npp.2016.226

Vinceti, M., Chiari, A., Eichmüller, M., Rothman, K. J., Filippini, T., Malagoli, C., Weuve, J., Tondelli, M., Zamboni, G., Nichelli, P. F., & Michalke, B. (2017). A selenium species in cerebrospinal fluid predicts conversion to Alzheimer's dementia in persons with mild cognitive impairment. *Alzheimer's Research and Therapy*, *9*(1), 1–11. https://doi.org/10.1186/s13195-017-0323-1

Vinceti, M., Filippini, T., Malagoli, C., Violi, F., Mandrioli, J., Consonni, D., Rothman, K. J., & Wise, L. A. (2019). Amyotrophic lateral sclerosis incidence following exposure to inorganic selenium in drinking water: A long-term follow-up. *Environmental Research*, *179*, 108742. https://doi.org/10.1016/j.envres.2019.108742

Vinceti, M., Filippini, T., & Wise, L. A. (2018). Environmental Selenium and Human Health: an Update. *Current Environmental Health Reports*, *5*(4), 464–485. https://doi.org/10.1007/s40572-018-0213-0

Wadhwani, S. A., Shedbalkar, U. U., Singh, R., & Chopade, B. A. (2016). Biogenic selenium nanoparticles: current status and future prospects. *Applied Microbiology and Biotechnology*, *100*(6), 2555–2566. https://doi.org/10.1007/s00253-016-7300-7

Wallin, C., Sholts, S. B., Österlund, N., Luo, J., Jarvet, J., Roos, P. M., Ilag, L., Gräslund, A., & Wärmländer, S. K. T. S. (2017). Alzheimer's disease and cigarette smoke components: Effects of nicotine, PAHs, and Cd(II), Cr(III), Pb(II), Pb(IV) ions on amyloid-β peptide aggregation. *Scientific Reports*, *7*(1), 1–15. https://doi.org/10.1038/s41598-017-13759-5

Wang, B., Pilkington, E. H., Sun, Y., Davis, T. P. T., Ke, P. C., & Ding, F. (2017). Modulating protein amyloid aggregation with nanomaterials. *Environmental Science: Nano*, *4*(9), 1772–1783. https://doi.org/10.1039/c7en00436b

Wang, C., Zhang, M., Mao, X., Yu, Y., Wang, C. X., & Yang, Y. L. (2013). Nanomaterials for reducing amyloid cytotoxicity. *Advanced Materials*, *25*(28), 3780–3801. https://doi.org/10.1002/adma.201301210

Wang, J., Gu, B. J., Masters, C. L., & Wang, Y. J. (2017). A systemic view of Alzheimer disease - Insights from amyloid-β metabolism beyond the brain. *Nature Reviews Neurology*, *13*(10), 612–623. https://doi.org/10.1038/nrneurol.2017.111

Wang, Y., Xing, J., Xu, Y., Zhou, N., Peng, J., Xiong, Z., Liu, X., Luo, X., Luo, C., Chen, K., Zheng, M., & Jiang, H. (2015). In silico ADME/T modelling for rational drug design. *Quarterly Reviews of Biophysics*, *48*(4), 488–515. https://doi.org/10.1017/S0033583515000190

Weller, J., & Budson, A. (2018). Current understanding of Alzheimer's disease diagnosis and treatment. *F1000Research*, *7*, 1–9. https://doi.org/10.12688/f1000research.14506.1

Weltin, D., Picard, V., Aupeix, K., Varin, M., Oth, D., Marchal, J., Dufour, P., & Bischoff, P. (1995). Immunosuppressive activities of 6(5h)-phenanthridinone, a new poly(adp-ribose)polymerase inhibitor. *International Journal of Immunopharmacology*, *17*(4), 265–271. https://doi.org/10.1016/0192-0561(95)00007-O

Whanger, P. D. (2001). Selenium and the brain: A review. *Nutritional Neuroscience*, *4*(2), 81–97. https://doi.org/10.1080/1028415X.2001.11747353

Wilcock, G., Howe, I., Coles, H., Lilienfeld, S., Truyen, L., Zhu, Y., & Bullock, R. (2003). A Long-Term Comparison of Galantamine and Donepezil in the Treatment of Alzheimer's

Disease. *Drugs Aging*, *20*(10), 777–789. https://doi.org/10.2165/00002512-200320100-00006

Wild, K., August, A., Pietrzik, C. U., & Kins, S. (2017). Structure and synaptic function of metal binding to the amyloid precursor protein and its proteolytic fragments. *Frontiers in Molecular Neuroscience*, *10*. https://doi.org/10.3389/fnmol.2017.00021

Wu, S.-Z., Bodles, A. M., Porter, M. M., Griffin, S. T., Basile, A. S., & Barger, S. W. (2004). Induction of serine racemase expression and D-serine release from microglia by amyloid β-peptide. *Journal of Neuroinflammation*, *1*, 1–11. https://doi.org/https://doi.org/10.1186/1742-2094-1-2

Xie, Z., Dong, Y., Maeda, U., Alfille, P., Culley, D. J., Crosby, G., & Tanzi, R. E. (2006). The Common Inhalation Anesthetic Isoflurane Induces Apoptosis and Increases Amyloid Protein Levels. *Anesthesiology*, *104*, 988–994.

Xu, L., Zhang, W., Liu, X., Zhang, C., Wang, P., & Zhao, X. (2018). Circulatory Levels of Toxic Metals (Aluminum, Cadmium, Mercury, Lead) in Patients with Alzheimer's Disease: A Quantitative Meta-Analysis and Systematic Review. *Journal of Alzheimer's Disease*, *62*(1), 361–372. https://doi.org/10.3233/JAD-170811

Yam-Canul, P., Chirino, Y. I., Sánchez-González, D. J., Martínez-Martínez, C. M., Cruz, C., & Pedraza-Chaverri, J. (2008). PJ34, a poly adenosine diphosphate-ribose polymerase inhibitor, attenuates chromate-induced nephrotoxicity. *Basic and Clinical Pharmacology and Toxicology*, *102*(5), 483–488. https://doi.org/10.1111/j.1742-7843.2008.00224.x

Yang, L., Sun, J., Xie, W., Liu, Y., & Liu, J. (2017). Dual-functional selenium nanoparticles bind to and inhibit amyloid β fiber formation in Alzheimer's disease. *Journal of Materials Chemistry B*, *5*(30), 5954–5967. https://doi.org/10.1039/c6tb02952c

Yang, X., Wang, Y., Byrne, R., Schneider, G., & Yang, S. (2019). Concepts of Artificial Intelligence for Computer-Assisted Drug Discovery. *Chemical Reviews*, *119*(18), 10520–10594. https://doi.org/10.1021/acs.chemrev.8b00728

Yegambaram, M., Manivannan, B., Beach, T. G., & Halden, R. U. (2015). Role of Environmental Contaminants in the Etiology of Alzheimer's Disease: A Review. *Current Alzheimer Research*, *12*, 116–146. http://www.worldlifeexpectancy.com/cause-of-death/alzheimers-dementia/by-country/.

Young, T. R., Pukala, T. L., Cappai, R., Wedd, A. G., & Xiao, Z. (2018). The Human Amyloid Precursor Protein Binds Copper Ions Dominated by a Picomolar-Affinity Site in the Helix-Rich E2 Domain. *Biochemistry*, *57*(28), 4165–4176. https://doi.org/10.1021/acs.biochem.8b00572

Younkin, S. G. (1995). Evidence that Aβ42 is the real culprit in Alzheimer's disease. *Annals of Neurology*, *37*(3), 287–288. https://doi.org/10.1002/ana.410370303

Yu, F., Gong, P., Hu, Z., Qiu, Y., Cui, Y., Gao, X., Chen, H., & Li, J. (2015). Cu(II) enhances the effect of Alzheimer's amyloid-β peptide on microglial activation. *Journal of Neuroinflammation*, *12*(1). https://doi.org/10.1186/s12974-015-0343-3

Yu, M., Chen, X., Liu, J., Ma, Q., Zhuo, Z., Chen, H., Zhou, L., Yang, S., Zheng, L., Ning, C., Xu, J., Gao, T., & Hou, S. T. (2019). Gallic acid disruption of Aβ1–42 aggregation rescues cognitive decline of APP/PS1 double transgenic mouse. *Neurobiology of Disease*, *124*, 67–80. https://doi.org/10.1016/j.nbd.2018.11.009

Yu, Q. S., Holloway, H. W., Luo, W., Lahiri, D. K., Brossi, A., & Greig, N. H. (2010). Long-acting anticholinesterases for myasthenia gravis: Synthesis and activities of quaternary phenylcarbamates of neostigmine, pyridostigmine and physostigmine. *Bioorganic and Medicinal Chemistry*, *18*(13), 4687–4693. https://doi.org/10.1016/j.bmc.2010.05.022

Yu, S., Xu, X., Feng, J., Liu, M., & Hu, K. (2019). Chitosan and chitosan coating nanoparticles for the treatment of brain disease. *International Journal of Pharmaceutics*, *560*, 282–293. https://doi.org/10.1016/j.ijpharm.2019.02.012

Zhan, Z. J., Bian, H. L., Wang, J. W., & Shan, W. G. (2010). Synthesis of physostigmine analogues and evaluation of their anticholinesterase activities. *Bioorganic and Medicinal Chemistry Letters*, *20*(5), 1532–1534. https://doi.org/10.1016/j.bmcl.2010.01.097

Zhang, J., Zhou, X., Yu, Q., Yang, L., Sun, D., Zhou, Y., & Liu, J. (2014). Epigallocatechin-3-gallate (EGCG)-stabilized selenium nanoparticles coated with Tet-1 peptide to reduce amyloid-β aggregation and cytotoxicity. *ACS Applied Materials and Interfaces*, *6*(11), 8475–8487. https://doi.org/10.1021/am501341u

Zhang, Z. H., Wen, L., Wu, Q. Y., Chen, C., Zheng, R., Liu, Q., Ni, J. Z., & Song, G. L. (2017). Long-Term Dietary Supplementation with Selenium-Enriched Yeast Improves Cognitive Impairment, Reverses Synaptic Deficits, and Mitigates Tau Pathology in a Triple

Transgenic Mouse Model of Alzheimer's Disease. *Journal of Agricultural and Food Chemistry*, *65*(24), 4970–4979. https://doi.org/10.1021/acs.jafc.7b01465

Zhang-Haagen, B., Biehl, R., Nagel-Steger, L., Radulescu, A., Richter, D., & Willbold, D. (2016). Monomeric Amyloid beta peptide in hexafluoroisopropanol detected by small angle neutron scattering. *PLoS ONE*, *11*(2), 1–12. https://doi.org/10.1371/journal.pone.0150267

Zheng, R., Zhang, Z. H., Chen, C., Chen, Y., Jia, S. Z., Liu, Q., Ni, J. Z., & Song, G. L. (2017). Selenomethionine promoted hippocampal neurogenesis via the PI3K-Akt-GSK3β-Wnt pathway in a mouse model of Alzheimer's disease. *Biochemical and Biophysical Research Communications*, *485*(1), 6–15. https://doi.org/10.1016/j.bbrc.2017.01.069

Zhou, H., Wang, T., Li, Q., & Li, D. (2018). Prevention of Keshan Disease by Selenium Supplementation: a Systematic Review and Meta-analysis. *Biological Trace Element Research*, *186*(1), 98–105. https://doi.org/10.1007/s12011-018-1302-5

Zoidis, E., Seremelis, I., Kontopoulos, N., & Danezis, G. P. (2018). Selenium-dependent antioxidant enzymes: Actions and properties of selenoproteins. *Antioxidants*, *7*, 66. https://doi.org/10.3390/antiox7050066

Zou, Y., Qian, Z., Chen, Y., Qian, H., Wei, G., & Zhang, Q. (2019). Norepinephrine Inhibits Alzheimer's Amyloid-β Peptide Aggregation and Destabilizes Amyloid-β Protofibrils: A Molecular Dynamics Simulation Study. *ACS Chemical Neuroscience*, *10*, 1585–1594. https://doi.org/10.1021/acschemneuro.8b00537

Zwolak, I. (2020). The Role of Selenium in Arsenic and Cadmium Toxicity: an Updated Review of Scientific Literature. *Biological Trace Element Research*, *193*, 44–63. https://doi.org/10.1007/s12011-019-01691

VI.OBJETIVOS

VI. OBJETIVOS

La presente Tesis Doctoral tiene como objetivo principal la **evaluación de moléculas orgánicas** (derivados de la **7-aminofenantridin-6-ona** (**APH**) e **híbridos** entre la **rivastigmina** (**RIV**) y el **hidroxifenilbenzimidazol** (**BIM**)) y de **nanopartículas de selenio** para **prevenir, tratar y/o mitigar los efectos de la enfermedad de Alzheimer** (**AD**), empleando técnicas (bio)analíticas. Para ello, se ha establecido como hipótesis de partida la "hipótesis de la cascada amiloide", que reúne un mayor consenso acerca del desarrollo de la AD y que está en completa sinergia con la "hipótesis del ion metálico". Así, en esta Tesis Doctoral se han estudiado los efectos que permiten contrarrestar el efecto perjudicial de determinados **biometales, metales tóxicos y enantiómeros de aminoácidos** como son la quelación metálica, la reducción del estrés oxidativo, la inhibición de la agregación de la proteína beta-amiloide (Aβ) y la inhibición de las enzimas acetilcolinesterasa (AChE) y butirilcolinesterasa (BChE). Además, se han evaluado *in vitro* con líneas celulares de fenotipo neuronal (Neuro-2a, SH-SY5Y y SN56) parámetros bioquímicos de las **moléculas orgánicas y nanopartículas de selenio**, con objeto de determinar su idoneidad como potenciales fármacos en la AD.

Para la consecución de este objetivo principal, se han planteado los siguientes objetivos específicos:

1. Evaluación de las **propiedades fisicoquímicas y biológicas** de cinco moléculas orgánicas pertenecientes a la familia de **derivados de la 7-aminofenantridin-6-ona (APH)**. Para ello, se han considerado los siguientes aspectos:

    1.1. Estudio de su capacidad de **quelación metálica** frente a biometales (Fe(II), Cu(II) y Zn(II)) y metales tóxicos (Hg(II), Cd(II) y Al(III)) involucrados en la AD, mediante espectroscopía de absorción UV-Vis y su primera derivada (d^1(UV-Vis)), así como el análisis computacional de los orbitales HOMO y LUMO.

    1.2. Estudio de la capacidad de las moléculas APH **de inhibir la agregación**, propia e inducida por biometales y metales tóxicos, de la **proteína Aβ** mediante microscopía electrónica de transmisión (TEM).

    1.3. Determinación ***in vitro***, empleando la línea celular SN56, de la capacidad de las moléculas APH para **reducir la citotoxicidad inducida por los metales** involucrados en la AD mediante el ensayo del MTT. Incluye la evaluación de las **propiedades antioxidantes** con respecto a la vía Nrf2 y la peroxidación lipídica

inducida por dichos metales, así como el estudio del efecto de las moléculas APH en la disminución de **proteínas de choque térmico** (**HSP70**) y **proteosomas** (**P20S**) y el aumento de la **concentración de la proteína Aβ,** inducido por biometales y metales tóxicos. Adicionalmente, se evaluará el efecto de las moléculas APH sobre la posible **disminución de la citotoxicidad** y **actividad apoptótica provocada por la proteína Aβ** mediante el método del MTT.

1.4. Evaluación del potencial uso de las moléculas APH como fármacos en la AD mediante la **predicción *in silico*** de sus propiedades de absorción, distribución, metabolismo, excreción y toxicidad (**ADMET**) y sus **propiedades farmacocinéticas**.

2. **Síntesis** de siete **híbridos** orgánicos entre la **rivastigmina (RIV)** y el **hidroxifenilbenzimidazol (BIM)** y **evaluación** de sus **propiedades fisicoquímicas y biológicas** frente a la AD**.** La consecución de este objetivo específico implicará los siguientes estudios:

2.1. **Síntesis** y purificación de siete híbridos RIV-BIM y su caracterización mediante cromatografía en capa fina (TLC) utilizando el factor de retención (RF), resonancia magnética nuclear (RMN) de ^{1}H y ^{13}C, ionización por electroespray con detección de espectrometría de masas (ESI-MS) (+/-) y medidas del punto de fusión.

2.2. Predicción, mediante herramientas de **modelización computacional *in silico***, de la interacción de los híbridos RIV-BIM con las enzimas AChE y BChE. Incluye la determinación experimental de la **inhibición** de dichas enzimas por parte de las moléculas RIV-BIM, mediante espectroscopía UV-Vis empleando el método de Ellman.

2.3. Evaluación, mediante TEM y espectroscopía de fluorescencia, de la **inhibición de la agregación**, propia e inducida por Cu(II), **de la proteína Aβ** por parte de los híbridos RIV-BIM.

2.4. Determinación de la **capacidad antioxidante** de los híbridos RIV-BIM mediante el método del DPPH empleando espectroscopía UV-Vis.

2.5. Evaluación ***in vitro*** de la **reducción de la citotoxicidad inducida por la proteína Aβ** y la **capacidad antioxidante** frente al Fe(II), mediante el método espectrofotométrico del MTT.

2.6. **Predicción *in silico*** de las **propiedades farmacocinéticas** de los híbridos RIV-BIM para determinar su idoneidad como potenciales fármacos en la AD.

3. **Síntesis de nanopartículas de selenio (SeNPs)** y evaluación de sus **propiedades fisicoquímicas y biológicas** frente a biometales y enantiómeros de aminoácidos. Para ello, se han llevado a cabo los siguientes ensayos:

   3.1. S**íntesis** de **SeNPs** estabilizadas con quitosano (Ch-SeNPs) y quitosano y ácido clorogénico (CGA@ChSeNPs). **Caracterización** mediante TEM, espectroscopía de energía dispersiva de rayos-X (EDXS), difracción electrónica (ED) y dispersión dinámica de luz (DLS).

   3.2. Evaluación, mediante UV-Vis y d^1(UV-Vis), de la **quelación metálica** por parte de las SeNPs y otras especies de selenio orgánicas (SeMet, MeSeCys y $(SeCys)_2$) e inorgánicas (Se(IV) y Se(VI)) con respecto a biometales involucrados en la AD.

   3.3. Determinación de la **capacidad antioxidante** de las especies de selenio y de enantiómeros de aminoácidos, mediante los métodos del DPPH y del TBARS, utilizando espectroscopía UV-Vis.

   3.4. Determinación de la **inhibición de la agregación de la proteína Aβ**, propia e inducida por biometales, por parte de las especies de selenio mediante TEM. Evaluación del efecto de **enantiómeros** de ciertos **aminoácidos** (Phe, Ala, Glu, Asp, Trp, Tyr y Ser) y selenoaminoácidos (SeMet) en la **agregación de la proteína Aβ**. Estudio del efecto producido por las Ch-SeNPs, debido a su recubrimiento quiral, sobre la posible agregación de la proteína Aβ, inducida enantioméricamente por los aminoácidos, mediante TEM.

   3.5. Evaluación de la posible **interacción enantioselectiva** entre las **Ch-SeNPs** y los **aminoácidos**, mediante espectroscopía UV-Vis y de fluorescencia.

   3.6. Determinación ***in vitro***, empleando las líneas celulares SH-SY5Y y Neuro-2a, de la **citotoxicidad** de las **especies de selenio** mediante los métodos de MTT y citometría de flujo. Evaluación de la **internalización de las Ch-SeNPs** por parte de las células mediante TEM, y cuantificación de la **acumulación de las especies de selenio** en células individuales mediante single cell-ICP-MS (SC-ICP-MS).

Además, en esta Tesis Doctoral se han **evaluado estadísticamente** todos los resultados obtenidos mediante el uso de **herramientas quimiométricas** para su adecuado análisis, interpretación y comparación. Así, se utilizarán el análisis de la varianza (ANOVA), el diseño de experimentos (DOE), la metodología de superficie de respuesta (RSM) y el análisis de componentes principales (PCA).

VII.OBJECTIVES

VII. OBJECTIVES

The main objective of this Doctoral Thesis is the **evaluation** of **organic molecules** (**7-aminophenanthrenanthridin-6-one** (**APH**) **derivatives and hybrids** between **rivastigmine** (**RIV**) and **hydroxyphenylbenzimidazole** (**BIM**)) and **selenium nanoparticles to prevent, treat and/or mitigate the effects of Alzheimer's disease** (**AD**), using (bio)analytical techniques. For this purpose, the "amyloid cascade hypothesis", which is the most widely accepted hypothesis for the development of AD and is in complete synergy with the "metal ion hypothesis", will be taken in consideration. Therefore, in this Doctoral Thesis, parameters to counteract the detrimental effect of certain **biometals, toxic metals and amino acid enantiomers**, such as metal chelation, reduction of oxidative stress, inhibition of beta-amyloid (Aβ) protein aggregation and inhibition of acetylcholinesterase (AChE) and butyrylcholinesterase (BChE) enzymes, will be evaluated. Additionally, certain biochemical parameters of the **organic molecules and selenium nanoparticles** will be evaluated *in vitro* with neuronal phenotype cell lines (Neuro-2a, SH-SY5Y and SN56) to determine their suitability as potential drugs against AD.

To achieve this main objective, the following specific objectives have been proposed:

1. Evaluation of **physico-chemical and biological properties** of five organic molecules belonging to the family of **7-aminophenanthrenanthridin-6-one (APH) derivatives**. To this end, the following aspects have been considered:

    1.1. To study their **metal chelating** capacity towards biometals (Fe(II), Cu(II) and Zn(II)) and toxic metals (Hg(II), Cd(II) and Al(III)) involved in AD, by UV-Vis absorption spectroscopy and its first derivative (d^1(UV-Vis)), as well as the computational analysis of the HOMO and LUMO orbitals.

    1.2. To study the ability of APH molecules to **inhibit** self- and metal-induced **aggregation of the Aβ** protein by transmission electron microscopy (TEM).

    1.3. To determine the ***in vitro*** ability of these APH molecules to **reduce the cytotoxicity**, in SN56 cell line, **induced by the metals** involved in AD, by means of the MTT assay. Including the evaluation of the **antioxidant properties** with respect to the Nrf2 pathway and the lipid peroxidation, induced by these metals. The effect of APH molecules on the decrease of heat shock proteins (HSP70) and proteosomes (P20S), and the increase of Aβ protein concentration induced by

biometals and toxic metals will also be studied. In addition, the effect of APH molecules on the possible **reduction of cytotoxicity** and **apoptotic activity caused by the Aβ protein** will be evaluated using the MTT method.

1.4. Evaluation of the potential use of APH molecules as drugs on AD by ***in silico*** **prediction** of their absorption, distribution, metabolism, excretion and toxicity (**ADMET**) and **pharmacokinetic properties**.

2. **Synthesis** of seven organic **hybrids** between **rivastigmine** (**RIV**) and **hydroxyphenylbenzimidazole** (**BIM**) and evaluation of their **physico-chemical and biological properties** against AD. To this end, the following studies will be involved:

2.1. **Synthesis** and purification of seven RIV-BIM hybrids, and their characterisation by thin layer chromatography (TLC) thorough retention factor (RF), ^{1}H and ^{13}C nuclear magnetic resonance (NMR), electrospray ionisation with mass spectrometry detection (ESI-MS) (+/-) and melting point measurements.

2.2. Prediction, using ***in silico*** **computational modelling tools**, of the interaction of RIV-BIM hybrids with AChE and BChE enzymes. Include the experimental determination of the **inhibition** of these enzymes by RIV-BIM molecules by UV-Vis spectroscopy using Ellman's method.

2.3. Evaluation, by TEM and fluorescence spectroscopy, of the **inhibition** of self- and Cu(II)-induced **aggregation of Aβ protein** by RIV-BIM hybrids.

2.4. Determination of the **antioxidant capacity** of RIV-BIM hybrids by the DPPH method using UV-Vis spectroscopy.

2.5. ***In vitro*** evaluation of the **reduction of Aβ-induced cytotoxicity**, and **antioxidant capacity** against Fe(II), by the spectrophotometric MTT method.

2.6. ***In silico*** **prediction** of the **pharmacokinetic properties** of RIV-BIM hybrids to determine their suitability as potential AD drugs.

3. **Synthesis of selenium nanoparticles (SeNPs)** and evaluation of their **physico-chemical and biological properties** against biometals, toxic metals and amino acid enantiomers. To this end, the following studies have been performed:

3.1. **Synthesis** of **SeNPs** stabilised with chitosan (Ch-SeNPs) and both chitosan and chlorogenic acid (CGA@ChSeNPs). **Characterisation** by TEM, energy dispersive X-ray spectroscopy (EDXS), electron diffraction (ED) and dynamic light scattering (DLS).

3.2. Evaluation, by UV-Vis and d^1(UV-Vis), of **metal chelation** by SeNPs and other organic (SeMet, MeSeCys and $(SeCys)_2$) and inorganic (Se(IV) and Se(VI)) selenium species regarding biometals involved in AD.

3.3. Determination of the **antioxidant capacity** of selenium species and amino acid enantiomers, by the DPPH and TBARS method, using UV-Vis spectroscopy.

3.4. Determination of the **inhibition of self- and biometal-induced protein Aβ aggregation** by selenium species by TEM. Evaluation of the effect of amino acid enantiomers (Phe, Ala, Glu, Asp, Trp, Tyr and Ser) and seleno-amino acids (SeMet) on Aβ aggregation. Study of the effect produced by Ch-SeNPs, through their chiral coating, with respect to the possible enantiomerically-induced Aβ aggregation caused by amino acids.

3.5. Evaluation of the possible **enantioselective interaction** between **Ch-SeNPs** and **amino acids** by UV-Vis and fluorescence spectroscopy.

3.6. ***In vitro*** determination, using SH-SY5Y and Neuro-2a cell lines, of the **cytotoxicity** of **selenium species** by MTT and flow cytometry methods. Evaluation of the **internalisation of Ch-SeNPs** by cells using TEM, and quantification of the **accumulation of selenium species** in individual cells using single cell-ICP-MS (SC-ICP-MS).

Moreover, in this Doctoral Thesis all the obtained results have been **statistically evaluated** by using **chemometric tools** for their proper analysis, interpretation and comparison. Thus, analysis of variance (ANOVA), design of experiments (DOE), response surface methodology (RSM) and principal component analysis (PCA) have been employed.

VIII.PARTE EXPERIMENTAL

VIII. PARTE EXPERIMENTAL

1. SÍNTESIS DE MOLÉCULAS ORGÁNICAS Y EVALUACIÓN DE SUS PROPIEDADES FISICOQUÍMICAS Y BIOLÓGICAS EN LA ENFERMEDAD DE ALZHEIMER

Las propiedades de las moléculas orgánicas son muy variadas debido a su diversidad estructural y versatilidad de sus respectivas síntesis. Es por ello por lo que su estudio para su uso potencial como moléculas neuroprotectoras contra la AD resulta de gran interés. Hasta el año 2021, solo cinco moléculas orgánicas habían sido aprobadas por la FDA como fármacos para el tratamiento de la AD: tacrina (TAC), donepezilo (DNP), rivastigmina (RIV), galantamina y memantina, actuando fundamentalmente sobre el sistema colinérgico. Sin embargo, ninguno de ellos ha conseguido detener el avance de la AD, por lo que se han seguido estudiando nuevas moléculas, o compuestos derivados de las anteriores, para alcanzar dicho fin. Entre los fármacos más prometedores se encuentra Aducanumab, aprobado de forma acelerada por la FDA en junio de 2021, siendo pionero en la reducción de la agregación amiloide, a falta de más evidencias clínicas que demuestren sus beneficios.

Las propiedades que debe tener una molécula orgánica para ser considerada potencialmente eficaz en la lucha contra la AD son muy variadas. Las estrategias actuales se basan, principalmente, en la detención o ralentización de la "**hipótesis de la cascada amiloide**". Para ello, las moléculas orgánicas deben ser capaces de **inhibir la agregación de la proteína Aβ** para evitar la cascada de eventos que conduce, en último término, al desarrollo de la AD.

Otra característica deseable para un potencial fármaco es la interacción con ciertos biometales o metales tóxicos, que mediante la "**hipótesis del ion metálico**", en sinergia con la "**hipótesis de la cascada amiloide**", producen la agregación amiloide y la formación de placas seniles en el exterior de las neuronas, desencadenando una inevitable neurodegeneración. Mediante la **quelación de metales** que han demostrado afinidad por residuos del fragmento 1-42 de la proteína Aβ, como el Cu(II) o el Zn(II), o la neutralización del **estrés oxidativo** generado por el Fe(II) y el Cu(II), se pueden mitigar sus efectos neurotóxicos y, por ende, ralentizar o paliar el desarrollo de la AD.

Sin embargo, para que un potencial fármaco pueda ejercer su efecto neuroprotector es necesario que posea una baja o nula toxicidad a concentraciones en las que su neuroprotección es observable y eficaz. Para ello, la aplicación de métodos de

determinación de la **citotoxicidad** de dichas moléculas sobre líneas celulares relacionadas con la AD adquiere especial relevancia.

Por todo lo expuesto, en el primer trabajo (**Artículo 1**), titulado "**Neuroprotective Action of Multi-target 7-Aminophenanthridin-6(5H)-one Derivatives against Metal-Induced Cell Death and Oxidative Stress in SN56 Cells**" (*ACS Chemical Neuroscience 12 (2021) 3358-3372*), se explora el uso de nuevas moléculas orgánicas pertenecientes a una familia de derivados de la 7-aminofenantridin-6-ona para contrarrestar el **efecto citotóxico** y el **estrés oxidativo** generado por ciertos metales en la AD.

Para ello, las cinco moléculas más prometedoras en relación a su baja citotoxicidad y actividad antioxidante, denominadas **APH1**, **APH2**, **APH3**, **APH4** y **APH5**, se estudiaron en términos de **quelación** metálica frente a **Fe(II)**, **Cu(II)**, **Zn(II)**, **Hg(II)**, **Cd(II)** y **Al(III)** a diferentes relaciones de concentración metal:APH, utilizando como técnica de medida la espectroscopía de absorción UV-Vis y su primera derivada (d^1(UV-Vis)). Todos los compuestos ensayados interaccionaron con alguno de los metales, siendo posible determinar, en algunos casos, la relación de concentración metal:APH óptima del complejo formado entre las moléculas y los metales evaluados. Para justificar de forma teórica la quelación metálica observada experimentalmente, se realizaron análisis computacionales de los orbitales **HOMO** y **LUMO** de las moléculas orgánicas, que permitieron predecir la interacción de los compuestos APH1-5 con el Fe(II) y el Cu(II). Asimismo, y para evaluar su potencial uso como fármacos en la AD, se realizó la predicción computacional de las propiedades **farmacocinéticas** y de absorción, distribución, metabolismo, excreción y toxicidad (ADMET), mediante ADMETsar y Swiss ADME, obteniéndose valores óptimos para todas las moléculas evaluadas.

La disminución del **efecto citotóxico de los metales** producido por la presencia de las moléculas APH, se evaluó mediante experimentos *in vitro* empleando la línea celular SN56 y el ensayo MTT. En primer lugar, se realizó la selección de un intervalo de concentración no tóxico para las moléculas APH mediante su estudio a diferentes concentraciones. En segundo lugar, empleando este intervalo seguro de concentraciones, se evaluó la reducción de la citotoxicidad inducida por Fe(II), Cu(II), Zn(II), Hg(II), Cd(II) y Al(III) sobre las células SN56 pretratadas con las moléculas APH1-5. Todas ellas ejercieron un papel protector frente a la citotoxicidad provocada por los biometales y metales tóxicos a las concentraciones estudiadas. Finalmente, se evaluaron las **propiedades antioxidantes de las moléculas APH1-5**, concluyendo que son capaces de inducir la vía

Nrf2 que produce la sobreexpresión de enzimas antioxidantes como las GPx y la catalasa, mediante la disminución de la expresión génica de la Keap1, protegiendo, por tanto, del estrés oxidativo generado por los metales en la AD. Además, se evaluó su protección frente a la **peroxidación lipídica** inducida por los metales mediante la determinación del malondialdehido (MDA).

Para estudiar otros posibles mecanismos neuroprotectores de los derivados de la 7-aminofenantridin-6-ona, en el segundo trabajo (**Artículo 2**) titulado "**Neuroprotective mechanisms of multi-target 7-aminophenanthridin-6(5H)-one derivatives against metal-induced amyloid proteins generation and aggregation**" (*Food and Chemical Toxicology 167 (2022) 113264*) se evaluó su efecto con respecto a la generación y agregación de **proteínas amiloides** inducidas por metales en la AD.

En primer lugar, se estudió la **agregación del fragmento 1-42 de la proteína beta-amiloide ($A\beta_{42}$)**, principal responsable de la cascada amiloide, mediante el uso de TEM con tinción previa de acetato de uranilo 2% (p/v). Para ello, se incubó el monómero $A\beta_{42}$ en presencia de las moléculas orgánicas neuroprotectoras a 37 ºC durante 48 h, con el objetivo de no observar un cambio significativo en la agregación. Posteriormente, se evaluó el aumento de la agregación amiloide por parte de biometales como el Fe(II), Cu(II) y Zn(II) y metales tóxicos como Hg(II), Cd(II) y Al(III). Finalmente, se evaluó la capacidad de inhibición de las moléculas orgánicas neuroprotectoras de la agregación inducida por los metales, obteniendo resultados satisfactorios en la mayoría de los casos. Además de evaluar la agregación mediante TEM, se midió la anchura de las fibras de la proteína $A\beta_{42}$ bajo el efecto de los metales y de las moléculas APH utilizando el programa ImageJ. Para determinar la existencia de diferencias significativas entre muestras se utilizó ANOVA y, en caso afirmativo, el test LSD de Fisher al nivel de confianza del 95% permitió detectar las muestras diferentes estadísticamente.

Posteriormente, mediante ensayos *in vitro* con la línea celular SN56, se determinó el efecto de las moléculas APH sobre el contenido de las proteínas **HSP70** y **P20S**, encargadas de la degradación de proteínas tóxicas con un plegamiento incorrecto, como la $A\beta_{42}$, ayudando por tanto a reducir la agregación amiloide en el cerebro. Para ello, se estudió el efecto neurotóxico que tenía la incubación durante 24 h con ciertos metales como el Fe(II) y el Cd(II) sobre la disminución del nivel de las proteínas HSP70 y P20S y el aumento de la concentración de la proteína $A\beta_{42}$. A continuación, mediante el pretratamiento con los compuestos APH1-5 durante 24 h, se evaluó la reversión de dicha disminución (HSP70

y P20S) o el aumento ($A\beta_{42}$) inducido por los metales. Adicionalmente, se estudió el efecto de las moléculas APH sobre la **reducción de la citotoxicidad de la proteína $A\beta_{42}$** co-incubada durante 24 h en células SN56, mediante el método MTT. A su vez, se monitorizó la actividad de las caspasas 3 y 7 para evaluar la **actividad apoptótica** de las células cuando se sometieron durante 24 h a la proteína $A\beta_{42}$, y para estudiar su reducción mediante el pretratamiento con las moléculas orgánicas.

Como se ha comentado en la introducción de esta Tesis, una de las líneas de investigación en el tratamiento de la enfermedad de Alzheimer es la búsqueda de nuevos fármacos con actividad neuroprotectora basados en híbridos entre la RIV y el BIM. En este sentido, en el (**Artículo 3**) titulado "**Novel rivastigmine derivatives as promising multi-target compounds for potential treatment of Alzheimer's disease**" (*Biomedicines 10 (2022) 1510*) se realizó la síntesis, purificación y caracterización de siete moléculas orgánicas (**RIV-BIM**), denominadas **4a**, **4b**, **4c**, **4d**, **5a**, **5b** y **5d**, y la posterior evaluación de sus propiedades fisicoquímicas y biológicas. La principal ventaja de la hibridación entre la **RIV** (inhibidor de la acetilcolinestarasa (AChEi) y butirilcolinestarasa (BChEi)) y el **BIM** (inhibidor de agregación de la proteína $A\beta_{42}$, antioxidante y quelante de metales) sería la obtención de moléculas orgánicas que combinen dichas propiedades neuroprotectoras.

En primer lugar, se realizó la síntesis de las 7 moléculas mediante cuatro pasos de reacción, haciendo un total de 28 síntesis. Dichas síntesis tuvieron una duración de entre 6 y 20 h y se realizaron a presiones en el intervalo 1-4 bar, bajo atmósfera de hidrógeno o nitrógeno, y temperaturas comprendidas entre 0 y 100 ºC. Finalizada la síntesis, se realizó una purificación por cromatografía en columna, recristalización o placas de capa preparativa (PLC). Finalmente, las moléculas intermedias y finales se caracterizaron mediante cromatografía en capa fina (TLC), resonancia magnética nuclear (RMN) de ^{1}H, e ionización por electroespray con detección de espectrometría de masas (ESI-MS) (+/-) y, además, las moléculas orgánicas finales se caracterizaron mediante ^{13}C RMN, factor de retención y punto de fusión.

Posteriormente, mediante **herramientas de modelización computacional *in silico***, se estudió la interacción entre las moléculas orgánicas RIV-BIM y las enzimas AChE y BChE para predecir la posible inhibición enzimática, aumentando los niveles de los neurotransmisores ACh y BCh. Para ello, se diseñaron las estructuras moleculares de los compuestos mediante el programa Maestro v. 9.3 y se encontró la conformación estructural con mínima energía mediante una búsqueda conformacional aleatoria con el programa

Ghemical v. 3.0.0 para cada una de ellas. Utilizando las estructuras cristalográficas de las enzimas obtenidas del PDB, se realizó un acoplamiento de los híbridos en las cavidades enzimáticas mediante cien pasos de algoritmos genéticos con la función ASP del programa GOLD v. 5.2. y se construyeron las figuras de la hipotética interacción entre ambos con el programa Chimera. Mediante la observación de la zona comprendida entre 0.0 y 5.0 Å de distancia del híbrido RIV-BIM, se pudo comprobar si cada una de estas moléculas era capaz de interaccionar con los aminoácidos presentes en la parte activa de la cavidad enzimática de la AChE o BChE, siendo por tanto un inhibidor de dichas enzimas y aumentando los niveles de los neurotransmisores ACh y BCh.

El estudio de la **inhibición de las AChE y BChE** se llevó a cabo mediante una adaptación del método de Ellman, monitorizando la cinética de reacción durante 5 min midiendo la absorbancia con un espectrofotómetro UV-Vis a 405 nm. En función del IC_{50} presentado por cada molécula, se determinó la capacidad de inhibición enzimática para cada una de las dos enzimas, expresándose mediante el índice de selectividad (SI) en relación a la afinidad por dichas enzimas.

La **agregación de la proteína $A\beta_{42}$**, natural e inducida por el Cu(II), se estudió empleando dos técnicas diferentes: espectroscopía de fluorescencia para cuantificar la inhibición y TEM para observar la morfología de las fibras. En el primer caso, se realizó la incubación del monómero $A\beta_{42}$ a 37 ºC durante 24 h, en presencia y ausencia de Cu(II) y/o de los híbridos RIV-BIM y moléculas de referencia como la TAC y la curcumina. Posteriormente, se añadió tioflavina (ThT) para su intercalación entre fibras amiloides, y se fijó una longitud de excitación de 446 nm, midiéndose la emisión de fluorescencia a 485 nm. Mediante la intensidad de la $A\beta_{42}$ sola e incubada en diferentes condiciones se determinó el porcentaje de agregación amiloide. Para la medida de la agregación por TEM, se incubó el monómero $A\beta_{42}$ a 37 ºC durante 48 h en presencia y ausencia de Cu(II) y/o de los híbridos RIV-BIM. Finalmente, las muestras se tiñeron negativamente utilizando acetato de uranilo 2% (p/v) y se visualizaron mediante TEM. De esta forma, se pudo evaluar la agregación inducida por el Cu(II) y la correspondiente inhibición de dicha agregación por parte de los híbridos RIV-BIM. La anchura de las fibras amiloides se midió usando el programa ImageJ para evaluar el efecto del Cu(II) y de las moléculas orgánicas en la morfología de dichas fibras.

La determinación de la capacidad antioxidante de las moléculas híbridas se llevó a cabo mediante el método del DPPH, midiendo la absorbancia a 517 nm de dicha sustancia en

presencia de las moléculas y de la 1,2-dimetil-3-hidroxi-4-piridona (DMHP) como sustancia control. Mediante la determinación del IC_{50} se evaluó la capacidad antioxidante de todas las moléculas orgánicas.

Además, se realizaron experimentos *in vitro*, utilizando la línea celular SH-SY5Y y el método MTT. En primer lugar, se evaluó la citotoxicidad de los híbridos RIV-BIM y se eligió una concentración no tóxica de cada molécula para esta línea celular. Posteriormente, se estudió la reducción de la citotoxicidad de la $A\beta_{42}$ cuando dichas células fueron pretratadas con los híbridos durante 1 h y co-tratadas con los híbridos y el monómero $A\beta_{42}$ durante 24 h adicionales. Para evaluar la capacidad antioxidante *in vitro*, las células se pretrataron con los híbridos durante 1 h y, posteriormente, se co-trataron con los híbridos y una mezcla de hierro/ascorbato. Se midió la intensidad de la absorbancia de los cristales de formazano formados mediante espectroscopía UV-Vis a 570 nm para determinar disminución de la viabilidad celular provocada por la proteína $A\beta_{42}$ o los ROS generados por el estrés oxidativo del hierro.

Finalmente se predijeron *in silico* las propiedades farmacocinéticas de los híbridos para confirmar su idoneidad como potenciales fármacos en la AD. Para ello, se construyeron las estructuras moleculares con el programa Maestro v. 9.3 y se minimizó su energía. Mediante el programa QikProp v. 2.5 se predijeron parámetros relevantes como el área de superficie polar de Van der Waals de átomos de oxígeno y nitrógeno (PSA), el coeficiente de partición octanol/agua (k_{ow}), la interacción con la albúmina humana (HSA), la permeabilidad de la barrera hematoencefálica (BBB), la actividad frente al sistema nervioso central (CNS), la permeabilidad celular frente a las células de adenocarcinoma colorrectal humano (Caco-2) y las células de riñón canino de Madin-Darby (MDCK), la absorción oral y las violaciones de la regla de Lipinski.

Para la interpretación de los resultados, debido a la gran cantidad y complejidad de los datos obtenidos, se realizó un análisis estadístico empleando análisis de componentes principales (PCA), lo que permitió clasificar a los híbridos RIV-BIM en función de las propiedades neuroprotectoras presentadas por los mismos.

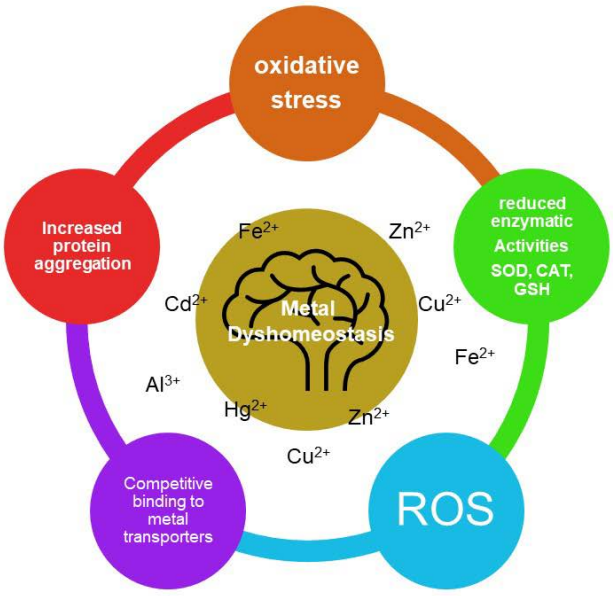
Artículo 1: Acción neuroprotectora de derivados multi-diana de la 7-aminofenantridin-6(5H)-ona frente a la muerte celular inducida por metales y el estrés oxidativo empleando la línea celular SN56

Neuroprotective Action of Multi-target 7-Aminophenanthridin-6(5H)-one Derivatives against Metal-Induced Cell Death and Oxidative Stress in SN56 Cells

Paula Moyano,‖ David Vicente-Zurdo,‖ Cristina Blázquez-Barbadillo, J. Carlos Menéndez, Juan F. González, Noelia Rosales-Conrado, Javier del Pino

‖Autores con igual contribución

ACS Chemical Neuroscience 12 (2021) 3358-3372 (*Impact factor: 5.780*)



ACS Chemical Neuroscience

pubs.acs.org/chemneuro

Research Article

Neuroprotective Action of Multitarget 7-Aminophenanthridin-6(5*H*)-one Derivatives against Metal-Induced Cell Death and Oxidative Stress in SN56 Cells

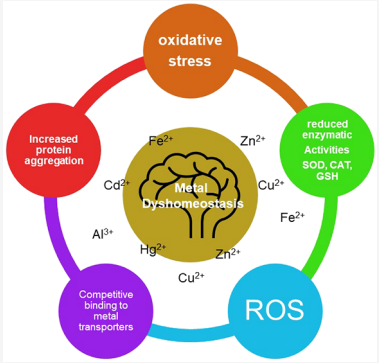
Paula Moyano,[‖] David Vicente-Zurdo,[‖] Cristina Blázquez-Barbadillo, J. Carlos Menéndez, Juan F. González,* Noelia Rosales-Conrado,* and Javier del Pino*

Cite This: *ACS Chem. Neurosci.* 2021, 12, 3358−3372

Read Online

ACCESS | Metrics & More | Article Recommendations | Supporting Information

ABSTRACT: Neurodegenerative diseases have been associated with brain metal accumulation, which produces oxidative stress (OS), matrix metalloproteinases (MMPs) induction, and neuronal cell death. Several metals have been reported to downregulate both the nuclear factor erythroid 2-related factor 2 (Nrf2) pathway and the antioxidant enzymes regulated by it, mediating OS induction and neurodegeneration. Among a recently discovered family of multitarget 7-amino-phenanthridin-6-one derivatives (**APH**) the most promising compounds were tested against metal-induced cell death and OS in SN56 cells. These compounds, designed to have chelating activity, are known to inhibit some MMPs and to present antioxidant and neuroprotective effects against hydrogen peroxide treatment to SN56 neuronal cells. However, the mechanisms that mediate this protective effect are not fully understood. The obtained results show that compounds **APH1**, **APH2**, **APH3**, **APH4**, and **APH5** were only able to chelate iron and copper ions among all metals studied and that **APH3**, **APH4**, and **APH5** were also able to chelate mercury ion. However, none of them was able to chelate zinc, cadmium, and aluminum, thus exhibiting selective chelating activity that can be partly responsible for their neuroprotective action. Otherwise, our results indicate that their antioxidant effect is mediated through induction of the Nrf2 pathway that leads to overexpression of antioxidant enzymes. Finally, these compounds exhibited neuroprotective effects, reversing partially or completely the cytotoxic effects induced by the metals studied depending on the compound used. **APH4** was the most effective and safe compound.



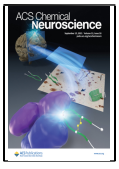
KEYWORDS: *Metal cytotoxicity, neuroprotection, chelating activity, antioxidants, phenanthridones*

INTRODUCTION

Several neurodegenerative disorders including Alzheimer's disease (AD), Parkinson's disease (PD), Huntington's disease (HD), and amyotrophic lateral sclerosis (ALS), among others, are undergoing a worrying increase in incidence worldwide. Although the ultimate causes of these diseases remain unknown, the possible involvement of environmental factors in their development has been suggested.[1−3] The rise in human industrial activity has exponentially increased the population's exposure to heavy metals and their body accumulation, leading to toxic effects.[1−4] Brain accumulation of heavy metals, such as aluminum (Al), cadmium (Cd), and mercury (Hg) due to overexposure, or essential metals, including iron (Fe), copper (Cu) and zinc (Zn) due to pathological circumstances, has been correlated with the development of neurodegenerative diseases.[1−8] Accumulation of metals in the brain was related with the induction of oxidative stress generation.[1,2] Oxidative stress, which results from the mismatch between reactive oxygen species (ROS), reactive nitrogen species (RNS), and antioxidant defense can cause oxidative damage to cell structures and cell death.[1,2] The central nervous system (CNS) is the most metabolically active organ, resulting in a high production of superoxide radical anion (O_2^-), hydroxyl radical (OH•), and hydrogen peroxide (H_2O_2), thus being particularly susceptible to oxidative stress and ROS damage.[1,2] Furthermore, ROS generation was reported to mediate the brain accumulation of oxidized, misfolded, and aggregated proteins such as tau-phosphorylated (p-tau), α-synuclein (α-syn), and Aβ peptides. After their accumulation, they induce neurofibrillary tangles, amyloid plaques, and Lewy bodies, the main hallmarks of AD and PD, neuroinflammation, mitochondrial dysfunction, and finally neuronal cell death.[1,2]

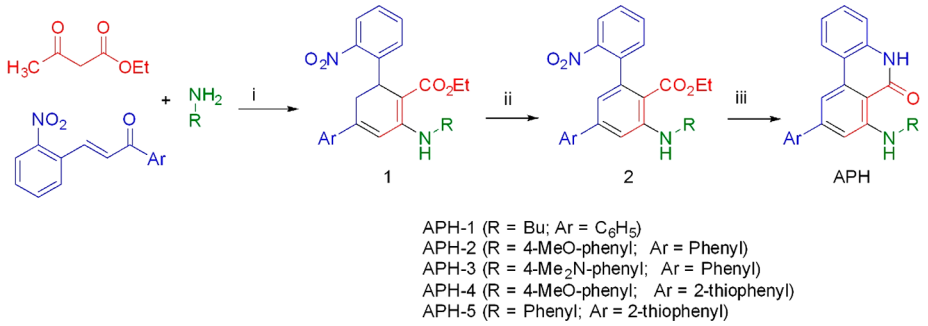
Calcium and zinc regulate the activity of matrix metalloproteinases (MMPs), which control a variety of physiological processes. Under pathological conditions, MMPs overexpres-

Received: May 21, 2021
Accepted: August 19, 2021
Published: August 30, 2021



ACS Publications © 2021 American Chemical Society

Scheme 1. Synthesis of the Target Compounds APH[a]



[a]Reagents and conditions: (i) EtOH, CAN (5%) reflux, 16 h; (ii) DDQ (1.5 equiv), toluene, 2 h at room temperature; (iii) EtOH, Pd/C (10%), H_2 1 atm, 2 h at room temperature.

sion or abnormal expression has been related with the induction of brain damage and with neurodegenerative disease, including AD, PD, HD, and ALS.[9] Otherwise, heavy metals were also related to the induction of MMPs, which could lead to cytotoxicity.[10] The main MMPs present in the brain are MMP-2/3/9/14, which play a key role in the neuroinflammatory processes and brain damage.[11,12] Besides, MMPs dysfunction was related with the production of Aβ, p-tau, α-synuclein, and other abnormal proteins related with neurodegenerative diseases, especially MMP-9.[9,13−15] Therefore, MMP inhibitors were tested to improve symptoms of different neurodegenerative diseases and to reduce the toxicity associated with metals.[16]

In this context, the control of metal accumulation in the CNS and its pathological effects is an important target in the development of new therapeutic agents against neurodegeneration and neurodegenerative disorders. In this sense, we have previously reported the discovery of new multitarget phenanthridin-6(5*H*)-one derivatives (APH) that are able to inhibit MMP enzymes, reduce oxidative stress, and protect against ROS.[17] Although these compounds were designed to present chelating activity, computational studies indicated binding to a distal region at the S1′ site, with no involvement of the catalytic zinc ion.[16] Thus, it is necessary to confirm experimentally the role of the Zn^{2+} ion in MMPs inhibition by these compounds.

Furthermore, the neuroprotective effects shown for these compounds against oxidative stress and cell death induced by metals could be mediated through a direct ROS scavenger activity. The induction of cellular antioxidant enzymes, which reduce ROS, may also be involved, since they show neuroprotective and antioxidant action against hydrogen peroxide in SN56 cells.[17] Nuclear factor erythroid 2-related factor 2 (Nrf2) is a key factor in the transcription regulation of antioxidant cytoprotective enzymes such as superoxide dismutase 1, catalase, glutathione peroxidase, NAD(P)H quinone oxidoreductase 1, and heme oxygenase-1, among others.[18−20] Dysfunction of the Nrf2 pathway has been identified, in different neurodegenerative diseases, as a factor of oxidative stress generation.[21−23] Besides, many metals were reported to alter the regulation of the Nrf2 pathway, leading to oxidative stress and cell death induction.[24−27] Nrf2 levels are regulated by kelch-like ECH-associated protein 1 (Keap1), which under normal conditions binds to Nrf2 in the cytoplasm, promoting its degradation. However, under oxidative stress, Keap1 is inactivated and releases Nrf2, which is transported to the nucleus, inducing the expression of downstream pathway antioxidant enzymes.[19,20] Another mechanism to avoid the oxidative stress, and other harmful actions of metals, is to sequester them with chelator compounds. Thus, as these compounds were designed to present chelating activity, they could also protect against metals toxicity through this mechanism.

In the context of the treatment of neurodegenerative diseases, it is crucial to find new multitarget drugs that reduce the neurotoxic effects of metals that may avoid the onset and progression of these diseases. In this sense, the use of molecules designed to possess antioxidant action and as metal ionophores to sequester, redistribute, and remove metals in the CNS is an attractive therapy to reduce the neurotoxic effect of metals in the brain. To reach this aim, we studied the chelating activity, the action on Nrf2 pathway, and the neuroprotective action against heavy and essential metals of a small library of 7-amino-phenanthridin-6-one derivatives that had been previously characterized as MMP inhibitors and found to exert the most neuroprotection against oxidative stress.

RESULTS AND DISCUSSION

Chemistry. The target compounds **APH1−APH5** were synthesized as shown in Scheme 1 by our previously reported method.[17] Thus, 4,6-diaryl-5,6-dihydroanthranylate derivatives **1** were obtained by a CAN-catalyzed multicomponent reaction between *ortho*-nitrochalcone, ethyl acetoacetate, and the suitable primary amines. This was followed by oxidative dehydrogenation of the central ring in the presence of 2,3-dichloro-5,6-dicyano-1,4-benzoquinone (DDQ) and reductive cyclization to give the target compounds **APH1−APH5** in good overall yield.

Metal-Chelating Properties of Compounds APH1−APH5. N and O electron-donor atoms and carbonyl group assembled to a cyclic system are considered suitable for efficient interactions with metal cations. These binding moieties are present in some biological relevant compounds such as the tetracycline,[28] 3-hydroxy flavonoids,[29] and anthranilic acid,[30] all of which have chelating properties. Thus, we designed the **APH** compounds as bidentate ligands to interact with the metal anions guest via a potential metal-binding site formed by the lactam group and the exocyclic nitrogen atom, hypothesizing that the substituents R on the nitrogen atom at C-7 position could modulate the affinity of the nitrogen atom for metals (Figure 1). For the current study, we selected compounds **APH1−APH5** from our library, due to their higher activity on the selected targets (i.e., MMPs

https://doi.org/10.1021/acschemneuro.1c00333
ACS Chem. Neurosci. 2021, 12, 3358−3372

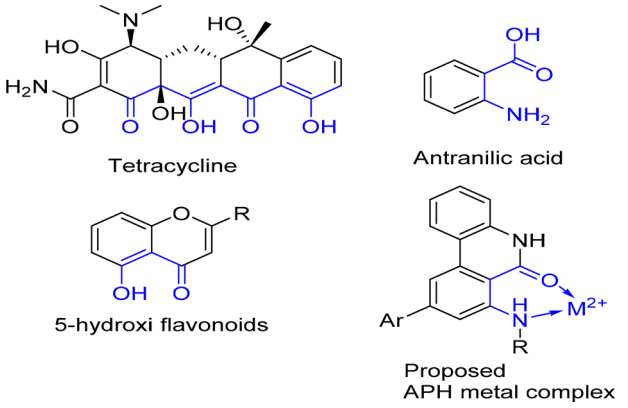


Figure 1. Hypothesized **APH**−metal interaction and some therapeutically useful chelating biomolecules.

inhibition and antioxidant activity), according to our previous studies.[17]

The ability of the **APH1**−**APH5** to bind Fe^{2+}, Cu^{2+}, Zn^{2+}, Hg^{2+}, Cd^{2+}, and Al^{3+} was studied by ultraviolet−visible (UV−vis) spectroscopy. This is one of the most widely used techniques to study chelation and to elucidate the stoichiometry of the formed metal complexes.[31−34] To this end, the UV−vis spectra of the compounds alone and in the presence of one of the evaluated metals were compared. Blank solutions composed of dimethyl sulfoxide (DMSO) 100 mM phosphate buffer at pH 7.30 showed high absorption values between 190 and 240 nm, and consequently only absorbances from 240 to 480 nm were considered.

When $FeCl_2$ or $CuCl_2$ were added to individual solutions containing **APH1**−**APH5**, and when $HgCl_2$ was added to solutions containing **APH3**, **APH4**, or **APH5**, new optical bands did not appear, and, therefore, the wavelengths corresponding to the maximum absorption bands of the Fe^{2+}/compound, Cu^{2+}/compound, or Hg^{2+}/compound solutions were similar to those of the compounds alone. By contrast, the analysis of solutions at different Fe^{2+}/compound, Cu^{2+}/compound, and Hg^{2+}/compound molar ratios evidenced important differences regarding the intensity of the absorption bands. The observed changes suggest an interaction between the tested compounds and Fe^{2+}, Cu^{2+}, and Hg^{2+} and, consequently, the formation of iron, copper, and mercury complexes, respectively. However, when the same experiments were performed with $ZnCl_2$, $CdCl_2$, or $AlCl_3$ and solutions containing **APH1**−**APH5**, and when $HgCl_2$ was added to solutions containing **APH1** or **APH2**, no differences between spectra of the different Zn^{2+}/compound, Cd^{2+}/compound, Al^{3+}/compound, and Hg^{2+}/compound molar ratios and the compounds alone were observed. This absence of spectral changes suggests the lack of interaction between the tested compounds and Zn^{2+}, Cd^{2+}, Al^{3+}, and Hg^{2+}.

Due to the high spectral similarity between the compounds and their Fe^{2+}, Cu^{2+}, Hg^{2+}, Zn^{2+}, Cd^{2+}, or Al^{3+} complexes, derivative spectroscopy was applied in order to enhance differences among spectra, to resolve overlapping bands, to reduce the effects of other absorbing compounds, and to eliminate the background. Once UV−vis spectra were registered, mathematical methods were used to generate the first-order derivative spectra. Our analysis shows excellent results in enhancing differences among spectra, increasing the resolution of the overlapped bands, reducing the effects of other absorbing compounds, and eliminating the background. In fact, as the first derivative spectrum passes through zero at

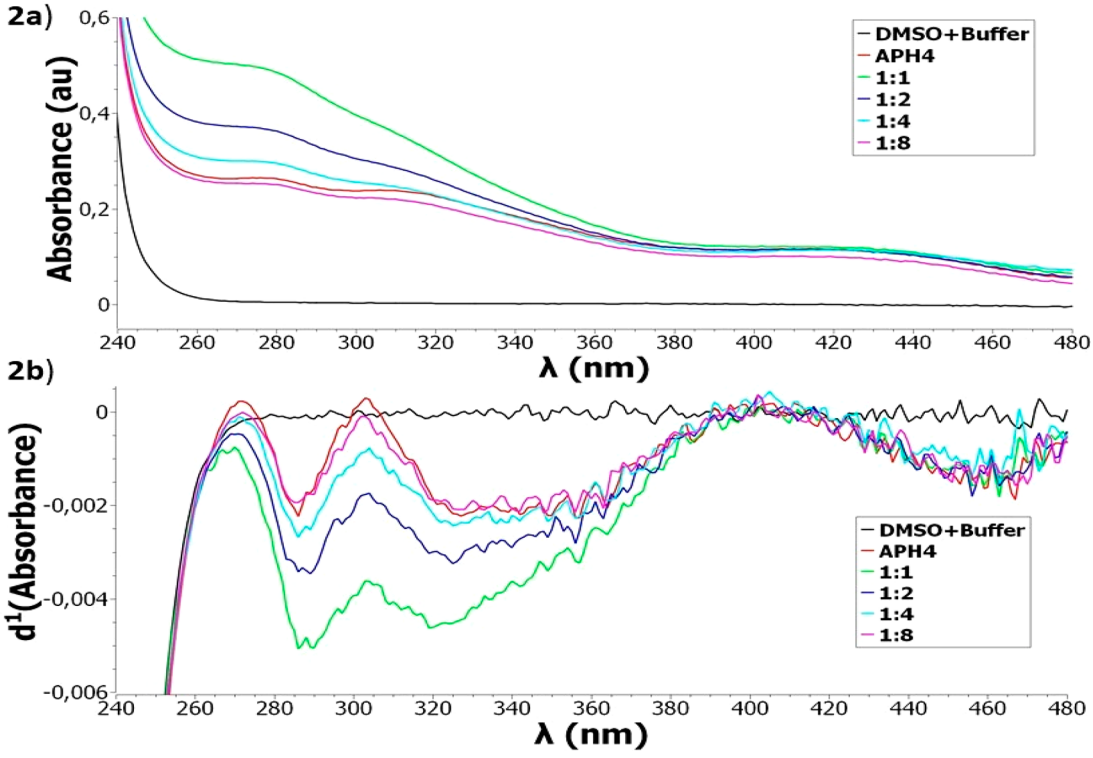


Figure 2. UV−vis spectra (a) and first-order derivative absorption spectra (b) of **APH4** alone and in the presence of $FeCl_2$ in buffer (100 mM phosphate, pH= 7.30) at room temperature. [**APH4**] = 50 μM and [Fe^{2+}] = 50, 25, 12.5, and 6.25 μM, corresponding to stoichiometries 1:1, 1:2, 1:4 and 1:8, respectively.

https://doi.org/10.1021/acschemneuro.1c00333
ACS Chem. Neurosci. 2021, 12, 3358−3372

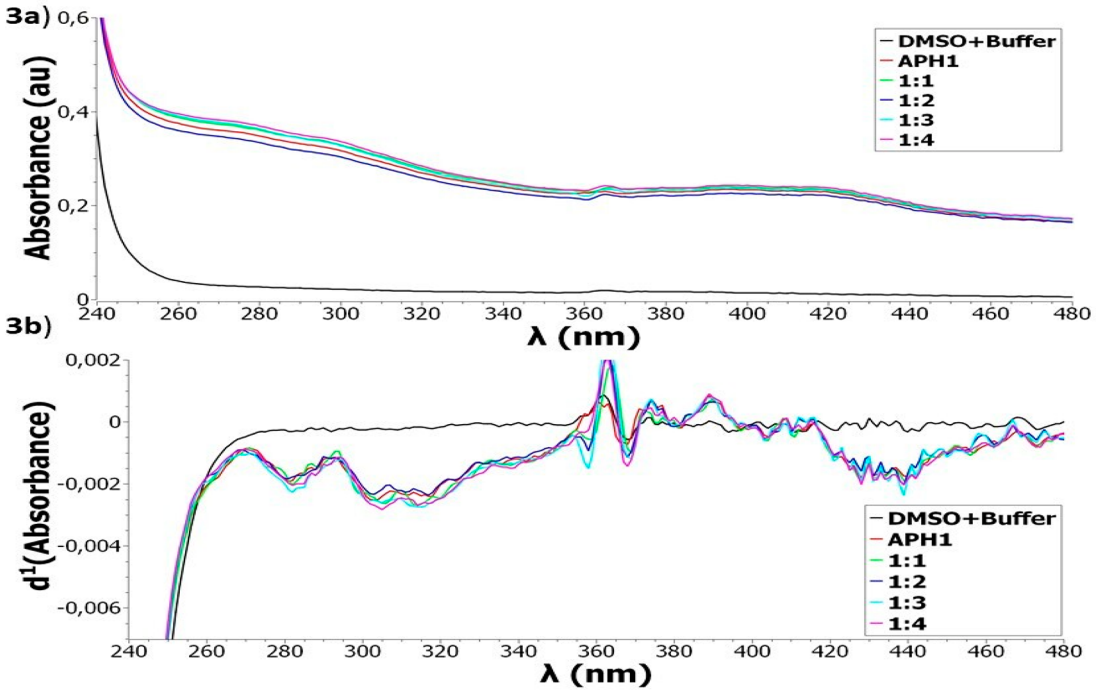


Figure 3. UV−vis spectra (a) and first-order derivative absorption spectra (b) of **APH1** alone and in the presence of $CdCl_2$ in buffer (100 mM phosphate, pH= 7.30) at room temperature. [**APH1**] = 50 μM and [Cd^{2+}] = 50, 25, 16.7, and 12.5 μM corresponding to stoichiometries 1:1, 1:2, 1:3 and 1:4, respectively.

the same wavelength as λ_{max} of the absorbance band, the spectral differences are highlighted. Thus, the analysis of derivative spectra allowed to confirm, through a resolution enhancement effect, that **APH1**−**APH5** were able to interact with Fe^{2+} and Cu^{2+}. Moreover, it was verified that **APH3**, **APH4**, and **APH5** were also able to interact with Hg^{2+} and, thus, to form iron, copper or mercury complexes. Otherwise, no changes were appreciated in Hg^{2+}-**APH1** and Hg^{2+}-**APH2** and neither in Zn^{2+}, Cd^{2+}, or $Al^{3+}$with **APH1**−**APH5** from derivative spectra.

The stoichiometry of the chelated iron, copper, and mercury compounds were estimated by means of the derivative spectra collected under two different conditions: (i) maintaining constant the metal ion concentration (50 μM) and varying the compound concentration and (ii) maintaining constant the compound concentration (50 μM) and varying the metal concentration. The results showed that the five compounds evaluated presented a similar behavior regarding Fe^{2+} and Cu^{2+} chelation. Figure 2a,b shows the UV−vis spectra registered for Fe^{2+}-**APH4**, as an example of metal-compound interaction. Figure 2a evidenced differences between absorbance spectra of the compound alone and in the presence of $FeCl_2$. Nevertheless, differences among the spectra corresponding to different stoichiometries are not properly appreciated. However, as depicted in Figure 2b, first-order derivative absorption spectra revealed some differences depending on the evaluated stoichiometry. The maximum absorption band at 280 nm (Figure 2a) appeared in all stoichiometries, being associated with the negative band at 290 nm as reflected in the derivative spectra (Figure 2b). This band may correspond to the absorption of the iron complex as it increases, as metal concentration reaches its maximum in Figure 2a. Otherwise, a ligand absorption band was observed at 300 nm, which overlaps with the optical band of the Fe^{2+} complex. This effect is shown in Figure 2b, where the derivative spectra of the compound alone passed through 0 at 300 nm wavelength, in contrast with the different stoichiometries. By analysis of the first-order derivative spectra (Figure 2b), the stoichiometry of the Fe^{2+}-**APH4** complex is consistent with a 1:1 Fe^{2+}/compound molar ratio. However, complexes of different stoichiometry could be simultaneously formed.

Similar observations were made for Fe^{2+} and Cu^{2+} with **APH1**−**APH5** and for Hg^{2+} with **APH4** and **APH5**. The spectra revealed bands that could be associated with the iron complexes at wavelengths of 280 nm (Fe^{2+}-**APH1**), 270 and 305 nm (Fe^{2+}-**APH2**), 280 nm (Fe^{2+}-**APH3**), and 270 nm (Fe^{2+}-**APH5**), while the copper complexes showed bands at 275 and 300 nm (Cu^{2+}-**APH1**), 265 nm (Cu^{2+}-**APH2**), 260 nm (Cu^{2+}-**APH3**), 265 nm (Cu^{2+}-**APH4**), and 270 nm (Cu^{2+}-**APH5**). Moreover, with the mercury complexes bands appeared at 295 and 300 nm (Hg^{2+}-**APH4**) and 300 and 305 nm (Hg^{2+}-**APH5**). Once again the 1:1 metal/compound molar ratio seems to be the main common stoichiometry for the formed complexes. However, for Hg^{2+}-**APH3**, showing an absorption band at 305 nm, the stoichiometry remains unclear.

Figure 3a,b shows the Cd^{2+}-**APH1** spectra, as an example of an noninteracting metal-compound. There were no differences between compound bands (**APH1**) and metal-compound bands at different molar ratios (1:1−1:4) in the UV−vis spectra (Figure 3a). These differences were not appreciated in the first derivative spectra (Figure 3b). Similar observations were deduced for Zn^{2+}, Cd^{2+} and Al^{3+} with **APH1**-**APH5** and for Hg^{2+} with **APH1** and **APH2**. The rest of UV−vis and first-order derivative absorption spectra data for **APH** compounds and the metals studies are shown in Figures S3−S7 in the Supporting Information.

In our previous work, we showed that **APHs** are able to inhibit MMP enzymes and computational studies suggested that this inhibitory activity is not mediated by the chelation of Zn^{2+} ion at the catalytic site, as is the case for many other

https://doi.org/10.1021/acschemneuro.1c00333
ACS Chem. Neurosci. 2021, 12, 3358−3372

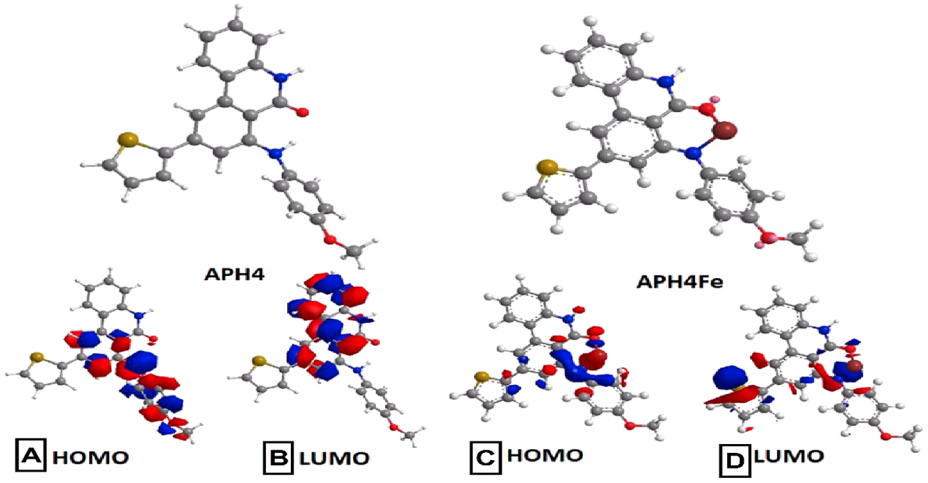


Figure 4. Optimized molecular structure of the **APH4** and **APH4-Fe** complex (upper) and their corresponding HOMOs (A and C) and LUMOs (B and D). Color scheme: Carbon is gray, hydrogen is white, nitrogen is blue, oxygen is red, and iron is brown. HOMOs and LUMOs are shown in red and blue.

Table 1. Predicted Physicochemical Properties of APH Compounds

property	APH1	APH2	APH3	APH4	APH5	favorable value
			Drug-likeness			
molecular weight (g/mol)	342.44	392.46	405.50	398.49	368.46	≤500
log *P*	5.56[a]; 5.03[b]	6.10[a]; 5.16[b]	6.16[a]; 5.18[b]	6.19[a]; 5.21[b]	6.15[a]; 5.31[b]	≤5
no. rotatable bonds	5	4	4	4	3	≤7
no. H-bond acceptors	2	3	3	2	3	≤10
no. H-bond donors	2	2	2	2	2	≤5

[a]Prediction with ADMETsar version 2. [b]Prediction with Swiss ADME.

MMP inhibitors.[17] Our present results show that **APH** compounds tested were not able to chelate Zn^{2+} ion, confirming the computational results. Further analysis should be performed to determine the mode of action behind MMPs inhibition by **APHs**.

Highest Occupied Molecular Orbital and Lowest Unoccupied Molecular Orbital analysis. The obtained results also show that all five **APH** compounds are able to bind to Fe^{2+} and Cu^{2+}, while they are unable to bind to bigger cations such as Cd^{2+}, Al^{3+}, and Hg^{2+}. The Hg^{2+} binding capacity of **APH3**−**APH5** is probably due to coordination with the nitrogen atom of dimethylamino group for **APH3** and with the thiophen sulfur of **APH4** and **APH5**. Furthermore, Zn^{2+} and Cd^{2+} ions usually form five-membered complexes with bidentate species, while Fe^{2+} and Cu^{2+} preferentially lead to the formation of six-membered metallocycles, consistent with the observed results.

To corroborate our experimental results of the chelating capacity of **APH** compounds and to relate these results with the compound structures, we studied highest occupied molecular orbital (HOMO) and lowest unoccupied molecular orbital (LUMO) orbital energies and energy gaps for the **APH** compounds and for the corresponding **APH-Fe** complexes (Table S1). Iron was chosen since, together with copper, it was chelated by all APH compounds. Our results for compounds **APH1**−**APH5** show that the proposed metal binding site was accessible (without impediment from the substituent of the exocyclic nitrogen in the most stable conformation calculated) for the five compounds (Figure S1). It was also observed that the HOMO orbital is mainly extended on the alkyl or the π system at the C-7 position. Particularly, for **APH3**, the charge density is concentrated on the dimethylamino group. Finally, the HOMO−LUMO energy gap (7.049, 7.799, 4.494, 5.982, and 6.643 eV for **APH1**−**APH5**, respectively), calculated at Merck molecular force field 94 (MMFF94) level, is compatible with complex formation.

The HOMO and LUMO levels for the **APH** compounds complexed with iron showed a reduction of gap energy of 0.917, 0.712, 3.922, 0.145, 0.299 eV for **APH1-Fe** to **APH5-Fe** complexes, respectively (Table S1), indicating a high stability for the complexes. The highest reduction of gap energy was observed in **AHP4-Fe**, showing that this compound is the most stable (Table S1) and therefore that **AHP4** has the highest chelating activity, a prediction that correlates well with the fact that this compound presented the best neuroprotective activity as shown below. Taking **APH4** as an example, it is apparent that the exocyclic nitrogen gives a higher contribution to the HOMO levels of **APH4** than to the HOMO levels of the **APH4-Fe** complex (Figure 4a,c), which indicates that the nitrogen atom depletes charge from the Fe^{2+} ions. Additionally, the presence of an aromatic amine at C-7 seems to stabilize the iron complex in comparison to the alkyl amine (see **APH1-Fe** and **APH2-Fe** in Table S1), and the amine group on the aromatic ring seems to destabilize the complex compared to the methoxy group (see **APH3-Fe** in Table S1). Finally, the presence of a thiophene at the C-9 position appears to lead to a smaller gap than the presence of a benzene ring (compare **APH4-Fe** and **APH2-Fe** in Table S1).

Therefore, although the number of compounds studied is somewhat limited to conclude a structure-complex formation ability relationship, it could be confirmed that their ability to interact with Fe^{2+} and Cu^{2+} does not depend on the

https://doi.org/10.1021/acschemneuro.1c00333
ACS Chem. Neurosci. 2021, 12, 3358−3372

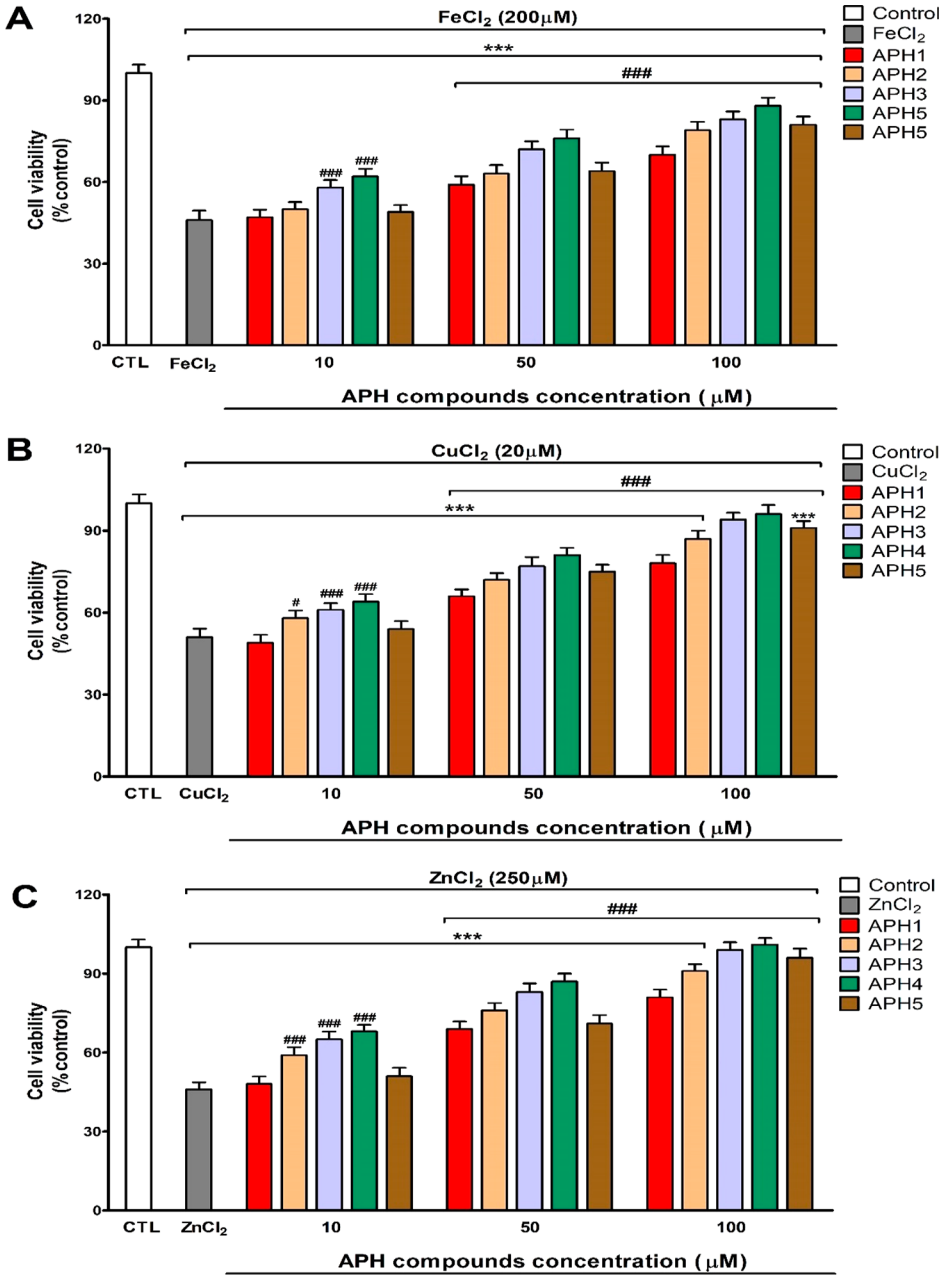


Figure 5. Cell viability effects after $FeCl_2$ (A) for $CuCl_2$ (B) and $ZnCl_2$ (C) treatment with or without selected **APH** compounds (10−100 μM) pretreatment. Data represent the mean ± SEM of three independent experiments in triplicate. ***$p \leq 0.001$ compared to control; $^{\#}p \leq 0.05$ and $^{\#\#\#}p \leq 0.001$ compared to metal treatment.

substituent of 7-amino phenanthridi-6-one skeleton. The computational analysis also revealed that phenyl moieties on the exocyclic nitrogen by the iron complex stabilizes the HOMO charge. Thus, the chelating cavity is suitable for small metal cations.

Computational Prediction of Physicochemical and Absorption, Distribution, Metabolism, Excretion, and Toxicological Properties of APH Compounds. According to the ADMETsar version 2.0 and swissADME software analysis, as shown in Table 1, the **APH** compounds satisfied all the values required except for the lipophilicity values,[35] which are slightly above the Lipinski limit.

Based on the results shown in Table S2, it can be assumed that **APH** compounds have favorable intestinal absorption and Caco2 cell permeability. The CNS distribution properties of our molecules was estimated through the calculation of the brain distribution parameter, which can evaluate the ability of small molecules to cross the blood−brain barrier (BBB) and be distributed into the brain. The predictions of the two methods used were fully consistent for **APH1**, where both predicted a good BBB penetration ability. For **APH2**, **APH3**, **APH4** and **APH5**, ADMETsar version 2.0 showed good BBB penetration data, but swissADME gave borderline negative results. The metabolic properties of these compounds were estimated according to the predicted inhibitory capacity of cytochrome P450 isoforms Cyp1a2, Cyp2c19, Cyp2c9, and Cyp2d6. As an additional piece of information connected to the prediction of pharmacokinetic properties, glycoprotein substrate capacity was assessed, but again the results from the two softwares were not homogeneous. To summarize, it was found that, although

https://doi.org/10.1021/acschemneuro.1c00333
ACS Chem. Neurosci. 2021, 12, 3358−3372

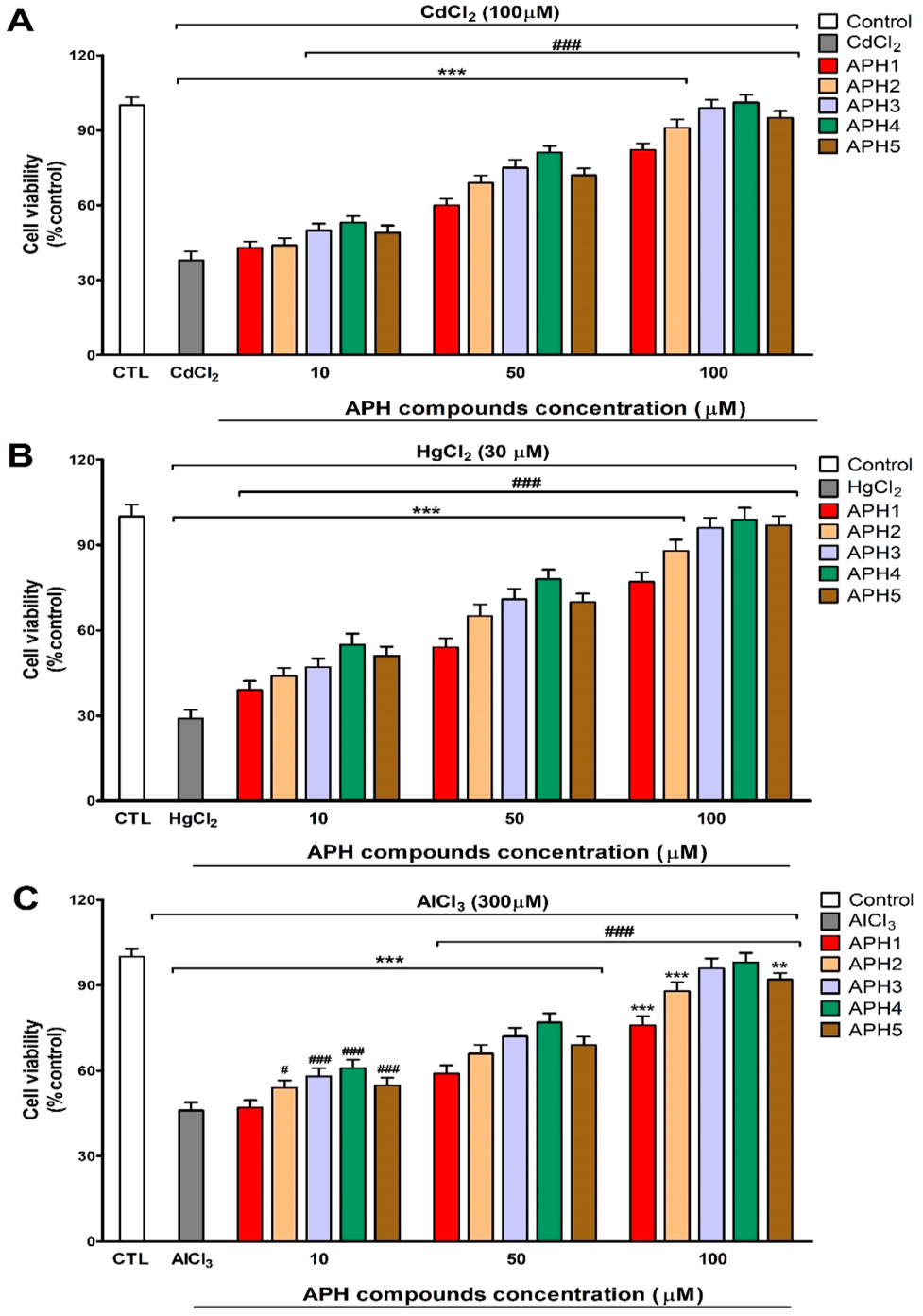


Figure 6. Cell viability effects after $CdCl_2$ (A) for $HgCl_2$ (B) and $AlCl_3$ (C) treatment with or without selected **APH** compounds (10−100 μM) pretreatment. Data represent the mean ± SEM of three independent experiments in triplicate. $^{**}p \leq 0.01$ and $^{***}p \leq 0.001$ compared to control; $p \leq 0.05$ and $^{\#\#\#}p \leq 0.001$ compared to metal treatment.

the lipophilicity scores may need to be further optimized, the predicted absorption, distribution, metabolism, excretion, and toxicological (ADMET) properties of the **APH** compounds characterize them as a suitable starting point to develop a leader compound. All the predicted characteristics of **APHs** in passing the BBB, permeability to Caco-2 cells, interaction of the compound with the cytochrome P450 isoenzymes and P-glycoproteins are shown in Table S2.

Neuroprotective Activity of Compounds APH1−APH5 against Metal-Induced Cell Viability Reduction. **APH1-APH5** were selected because they were, out of all the **APH** compounds tested, the ones with less cytotoxic effects, also presenting the most potent antioxidant and neuroprotective effect against ROS isults.[17] Thus, the treatment of SN56 cells with **APH1−APH5** at different concentrations (1, 10, 50, 100, 150, and 200 μM) only started to reduce cell viability at 200 μM (Figure S2). Thus, the range of 10−100 μM concentrations was selected, as it has shown no cytotoxicity, to tests **APHs** neuroprotective effects.

Treatment of neurons with the heavy (cadmium, mercury, and aluminum) and essential (iron, copper, and zinc) metals' produced a reduction of cell viability. This effect was avoided

https://doi.org/10.1021/acschemneuro.1c00333
ACS Chem. Neurosci. 2021, 12, 3358−3372

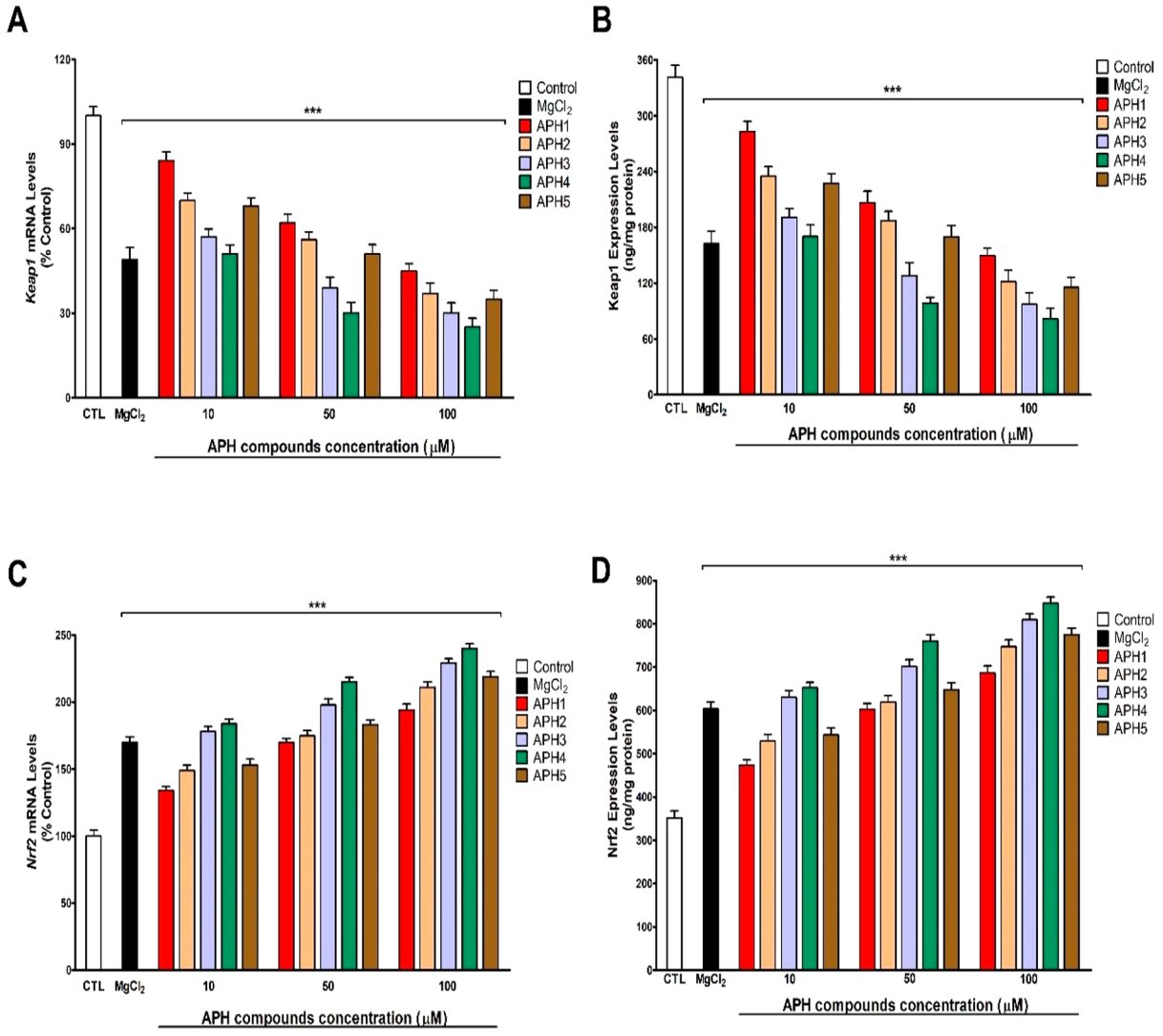


Figure 7. Obtained results from *Keap1* (A) and *Nrf2* (C) gene expression and Keap1 (C) and Nrf2 (D) protein expression after 24 h treatment. *Keap1* and *Nrf2* gene and protein expressions are compared with controls [cells treated with vehicle were the negative control]. Each bar represents mean ± SEM of three separate experiments from cells of different cultures, each one performed in triplicate and presented as percent untreated control for gene expression and in ng/mg protein form protein expression. ***$p < 0.001$ significantly different from controls.

completely or partially when cells were pretreated with **APH1−APH5** in a concentration-dependent way (Figures 3 and 4). The heavy and essential metals studied were reported to induce neuronal cell death,[1−8] supporting our results.

The protection against essential metals started from 10 μM after pretreatment with **AHP2**, **APH3**, or **APH4**. For $FeCl_2$, pretreatment with **APH2** started the protection from 50 μM as well as after the pretreatment with **APH1** or **AHP2** in cells treated with essential metals (Figure 5a−c). Besides, in cells treated with heavy metals, the **APH1−APH5** pretreatment started to protect, from 10 μM, against the cell viability reduction observed after heavy metals treatment alone. For $CdCl_2$, pretreatment with **APH1** and **APH2** and for $AlCl_3$, pretreatment with **APH1** started cell death reversion from 50 μM (Figure 5a−c). Pretreatment with compounds **APH3** and **APH4**, at the concentration of 100 μM, protected completely against the cytotoxic effects induced by all metals studied except for $FeCl_2$ (Figures 5 and 6). Besides, pretreatment with compound **APH5**, at the concentration of 100 μM, only protected completely against the cytotoxic effects induced by $ZnCl_2$, $CdCl_2$, and $HgCl_2$ (Figures 5 and 6).

The differences observed in the concentrations from which these compounds start to show protection against the metal-induced cytotoxic effects can be ascribed to the different potency in their different protective mechanisms. These differences may also be produced because each APH compound may induce different mechanisms that mediate the neuroprotection observed. In this sense, our chelating studies suggest that Zn^{2+}, Cd^{2+}, and Al^{3+} ions are not chelated by any of the **APH** compounds studied and that Hg^{2+} is only chelated by **APH3**, **APH4**, and **APH5** compounds. This fact indicates that the neuroprotection observed against zinc, cadmium, and aluminum by all these compounds or against mercury by compounds **APH1** and **APH2** is not mediated by their chelating activity and other mechanisms are involved. Besides, the protection observed against iron, and probably copper, at the lowest compound concentrations should be limited, especially for iron. The chelating activity at the higher concentrations used of these metals only blocked a very limited part of the metal pool, suggesting other mechanisms are involved. In this sense, we previously described that these compounds are MMP inhibitors and present antioxidant

https://doi.org/10.1021/acschemneuro.1c00333
ACS Chem. Neurosci. 2021, 12, 3358−3372

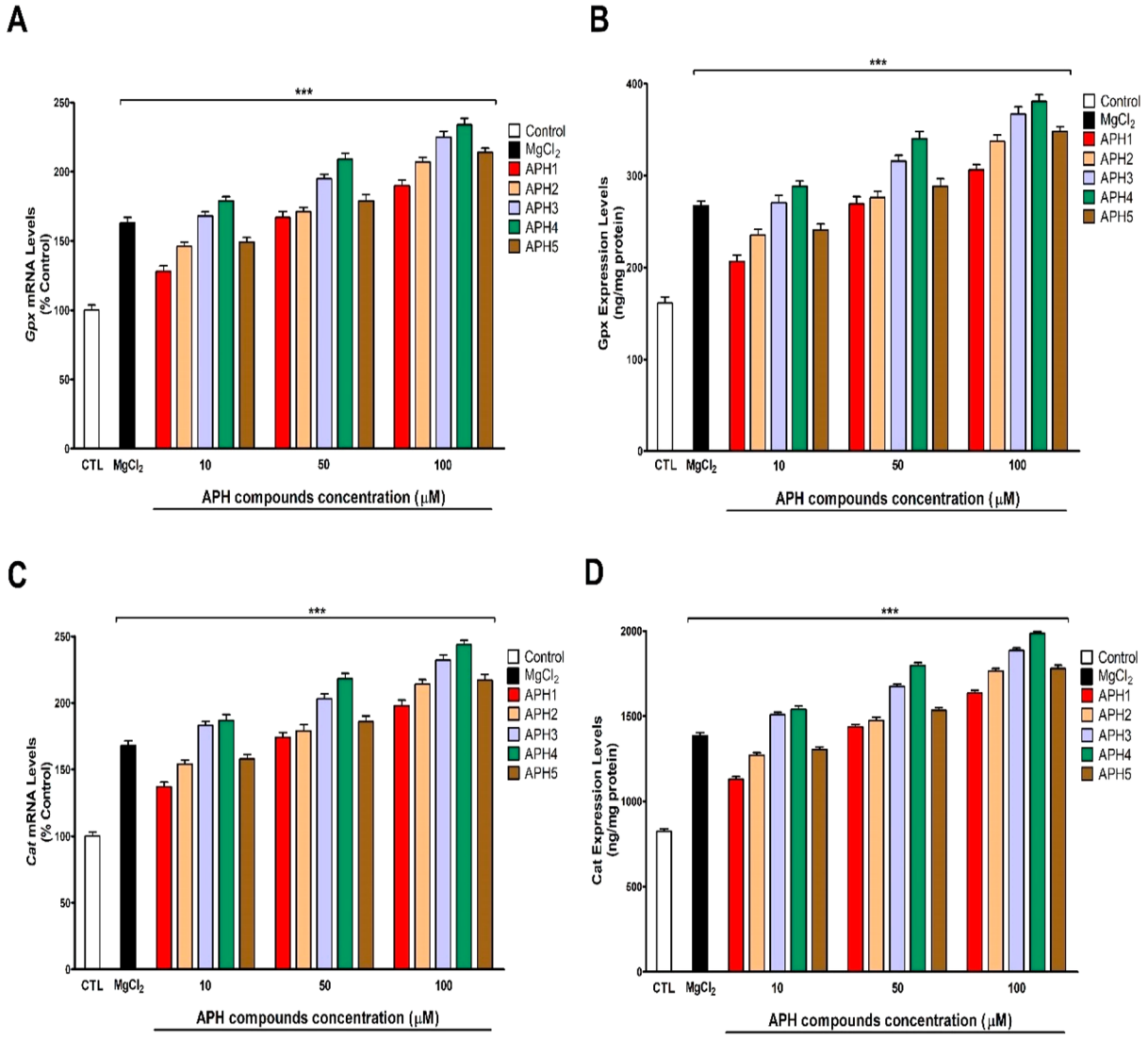


Figure 8. Obtained results from *Gpx* (A) and *Cat* (B) gene expression and Gpx (C) and Cat (D) protein expression after 24 h treatment. *Gpx* and *Cat* gene and protein expressions are compared with controls [cells treated with vehicle were the negative control]. Each bar represents mean ± SEM of three separate experiments from cells of different cultures, each one performed in triplicate and presented as percent untreated control for gene expression and in ng/mg protein for protein expression. ***$p < 0.001$ significantly different from controls.

activity,[17] which could participate in these neuroprotective effects. The greater neuroprotective action observed after pretreatment with all metals studied was mediated by compound **APH4**. This effect is correlated with our previous results on MMPs inhibition and antioxidant effect[17] that support that these mechanisms are probably involved in the neuroprotective effects of these compounds.

NRF2 Pathway Induction by Compounds APH1−APH5. The treatment of SN56 cells with compounds **APH1−APH5** induced a concentration-dependent decrease in the gene and protein expression of Keap1 (Figure 7a,b). A correlated concentration-dependent increase in the gene and proteins expression of Nrf2 factor (Figure 7c,d) was observed. Besides, the gene and protein expression of Gpx and Cat enzymes was increased, in a concentration-dependent way, after the treatment with compounds **APH1−APH5** (Figures 8a−c). Thus, **APH** compounds induce Nrf2 pathway.

Keap1 protein regulate Nrf2 proteins levels, inducing its degradation under no stress situations, through proteasome degradation. However, after stress situations, like ROS generation, its affinity for Nrf2 protein is reduced, increasing Nrf2 levels. Nrf2 is then translocated to the nucleus where it acts as the master regulator of the expression of different antioxidant enzymes such as Gpx and Cat among others.[18−20,36,37] *Keap1* downregulation was reported to induce Nrf2 protein overexpression and the enzymes regulated by it.[38,39] Besides, *Keap1* and *Nrf2* gene expression was reported to be regulated by different factors like microRNAs (miRNAs) or different transcription factors.[38,40] Nrf2 protein levels were shown to be altered by mechanisms independent of Keap1 protein action.[36] In this sense, we showed that compounds **APH1−APH5** induced the Nrf2 pathway by different mechanisms. On one hand, they induce the Nrf2 pathway by an independent mechanism of Keap1 regulation of Nrf2 proteins degradation, since these compounds act to upregulate the *Nrf2* gene expression. On the other hand, compounds **APH1−APH5** regulate the Nrf2 pathway by a mechanism dependent on keap1, since they downregulated *Keap1* gene expression, contributing to the overexpression of Nrf2 protein and of the Gpx and Cat antioxidant enzymes regulated by it.

https://doi.org/10.1021/acschemneuro.1c00333
ACS Chem. Neurosci. 2021, 12, 3358−3372

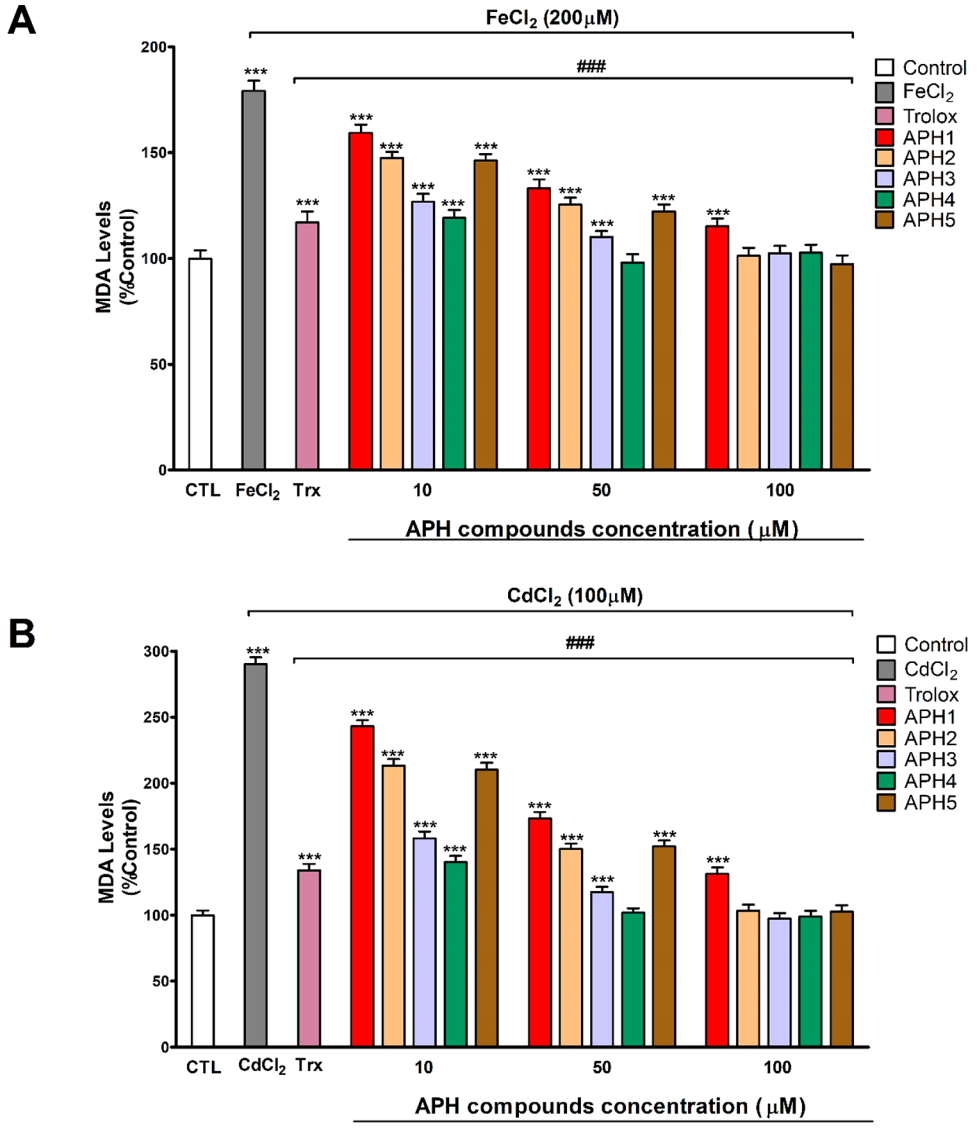


Figure 9. Neuroprotective action of selected **APH** compounds against lipid peroxidation induced by $FeCl_2$ and $CdCl_2$ metals in SN56 cells was measured by MDA assay. (A) MDA content after $FeCl_2$ treatment with or without **APH** compounds. (B) MDA content after $CdCl_2$ treatment with or without **APH** compounds. Values are given as mean ± SEM of three separate experiments from cells of different cultures, each one performed in triplicate and presented as percent untreated control. $^{***}p \leq 0.001$ compared to control; $^{###}p \leq 0.001$ compared to metal treatment.

Further studies are needed to determine the mechanism through which **APH** compounds mediate the *Keap1* and *Nrf2* gene expression alteration.

We previously described that **APH** compounds present antioxidant activity against ROS-induced lipid peroxidation.[17] In the present study, we show that this action is mediated through the induction of Nrf2 pathway, but we cannot discard other mechanisms are involved. Besides, the greater effect on Keap1, Nrf2, Gpx, and Cat expression was mediated by compound **APH4** (Figures 7 and 8), which is correlated with the higher antioxidant effect observed for this compound,[17] supporting our results.

Antioxidant Activity of Compounds APH1−APH5 against Metal-Induced Lipid Peroxidation. The heavy ($CdCl_2$) and essential ($FeCl_2$) metals generation of malondialdehyde (MDA) was determined as a marker of oxidative stress damage induced by metals. MDA, a product of the ROS-promoted degradation of arachidonic acid, is the best-known lipid peroxidation marker. Obtained results show that both metals induced lipid peroxidation at the concentrations used (Figure 9a,b). Concentrations used were selected because they were the ones that produce cell damage (data no shown). Several *in vitro* studies reported that $FeCl_2$ and $CdCl_2$ induced, at these concentrations, oxidative stress and cell death,[8,41,42] supporting our results.

Treatment of SN56 cells with **APH** compounds alone did not produce any effect on MDA levels (data not shown). Pretreatment with the antioxidant trolox at 100 μM concentration prevented partially the lipid peroxidation induced by cadmium and iron (Figure 9a,b). Pretreatment with compounds **APH1**, **AHP2**, **APH3**, **APH4**, or **APH5**, prior to heavy or essential metal treatment, averted lipid peroxidation in a concentration-dependent way, starting from the 10 μM concentration (Figure 9a,b). This protection was complete after pretreatment with **APH4** compound at 50 μM concentration in both metals (Figure 9a,b). Finally, pretreatment with compounds **APH2**, **APH3**, or **APH5**, at 100 μM concentration, the same one used for trolox, protected

https://doi.org/10.1021/acschemneuro.1c00333
ACS Chem. Neurosci. 2021, 12, 3358−3372

completely against the lipid peroxidation induced by both metals (Figure 9a,b). Thus, compounds **APH2**−**APH5** are more potent than trolox. These data support the antioxidant effect of these compounds not only after H_2O_2 insults as previously shown[17] but also against all insults induced by ROS generated after metals exposure.

Otherwise, the compound **APH4** was not able to protect completely against the cell damage induced by any metal at the concentration of 50 μM (Figures 5 and 6). However, it was able to avoid completely the oxidative stress induced by $FeCl_2$ and $CdCl_2$ (Figure 9a,b). Besides, the compounds **APH3**, **APH4**, and **APH5**, at the concentration of 100 μM, were not able to completely protect against the cell damage induced by $FeCl_2$ (Figure 5a), but they prevented completely the oxidative stress induced by this metal (Figure 9a). These facts indicate that, besides the oxidative stress, additional mechanisms should be involved in the cytotoxicity of these metals. It also suggests that, in addition to the antioxidant effect of these compounds, they mediate their neuroprotective effect by other mechanisms, probably different than MMPs inhibition or the chelating activity depending of the metal. These metals were reported to induce the accumulation and aggregation of amyloid proteins leading to cell death.[1−3] Moreover, these metals were related with the alteration of Wnt/β-catenin pathway and glutamatergic system and the induction of neuroinflammation, producing neurodegeneration.[1−3,43,44] Studies to elucidate the neuroprotective mechanisms of **APH** compounds, besides of those commented already, have not been previously performed. However, the parent compound 6(5H)-phenanthridinone was described to present poly(ADP-ribose)polymerase (PARP) inhibitor activity.[45] PARP was involved in inflammation induction. Its inhibition produces anti-inflammatory effects,[46] and it was also observed that its inhibition increases the NRF2 nuclear and cytosolic levels in rat retinal cells injured by chronic hypoxia/reoxygenation process.[47] Thus, **AHP1**−**APH5** compounds could mediate their antioxidant effects as well as other neuroprotective mechanisms through PARP inhibition. Besides, phenanthridin-6(5H)-one derivatives were also shown to act as Wnt/β-catenin signaling pathway agonists.[48] Additionally, Wnt/β-catenin signaling pathway activation was reported to possibly induce the NFR2 expression through GSK-3β inhibition.[49] Therefore, **APH** compounds could also block these cytotoxic actions through these mechanisms, contributing together with the antioxidant, chelating, and MMPs inhibition activities to the neuroprotective effects observed against the neurotoxic action of these metals. Further studies are required to determine the rest of the neuroprotective mechanisms of these multitarget compounds that could be used in the treatment of different neurodegenerative diseases.

CONCLUSIONS

To summarize, all compounds **APH1**−**APH5** were able to chelate iron and copper ions. Moreover, **APH3**, **APH4**, and **APH5** were also able to chelate mercury ions. Nevertheless, none of the **APH** compounds was able to chelate zinc, cadmium, and aluminum. The cytotoxic effects induced by all studied metals were prevented completely or partially depending on the compound used, with the most promising compound **APH4**. However, it is necessary to corroborate the neuroprotection action *in vivo* and against other toxic stimuli to confirm **APH4** compound as the best **APH** therapeutic tool.

Otherwise, the antioxidant effect of the evaluated compounds is mediated through induction of the Nrf2 pathway that leads to overexpression of antioxidant enzymes. Further studies are required to survey the rest of the possible mechanisms involved in the neuroprotective effect of these compounds.

Consequently, the relevance of our results lies in finding the chelating, antioxidant, and neuroprotective properties of new multitarget 7-aminophenanthridin-6(5*H*)-one derivatives that could help improve the treatment management of different neurodegenerative diseases.

METHODS

General Experimental Information. All reagents were purchased from Sigma-Aldrich and Fluka (Madrid, Spain), and solvents from SDS (Madrid, Spain) were of commercial quality and were used as received. Reactions were monitored by thin-layer chromatography, 0.20 mm silica gel 60 F254 plates (Merck, Madrid, Spain) with fluorescent indicator (SDS CCM221254), and then visualized with an ultraviolet (UV) lamp. Separations by flash chromatography were performed on silica gel (SDS 60 ACC 15 40−63 μm). Infrared spectra were recorded on a PerkinElmer Paragon 1000 FT-IR spectrophotometer (PerkinElmer, Madrid, Spain). NMR spectra were obtained on a Bruker Avance 250 spectrometer working at 250 MHz for ^{1}H and 63 MHz for ^{13}C and operated via the standard Bruker software (Nuclear Magnetic Resonance, Centre for Research Assistance, Complutense University, Madrid, Spain). Chemical shifts are reported in parts per millions relative to tetramethylsilane, and spin multiplicities are given as s (singlet), d (doublet), t (triplet), q (quartet), or m (multiplet).

General Synthesis Procedure for the Target APH Compounds. *Synthesis of 1.* A solution of ethyl acetoacetate (3 mmol, 1 equiv) and the suitable primary amine (3−3.9 mmol, 1−1.3 equiv) in ethanol (5 mL) was added to cerium(IV) ammonium nitrate (5 mol) and was stirred for 30 min at room temperature. Then, appropriate *ortho*-nitrochalcone (2.4−3.6 mmol, 0.8−1.2 equiv) was added to the stirred solution, and the mixture was heated to 80 °C overnight. The reaction mixture was dissolved in ethyl acetate (30 mL) and washed consecutively with water and brine, and the organic layer was dried with anhydrous Na_2SO_4. The solvent was removed under reduced pressure, and the solid was purified by flash column chromatography on silica gel, eluting with a petroleum ether and ethyl acetate mixture (9:1, v/v). Compounds **1** were reported in the literature, and their characterization data were identical to those previously described.[17]

Synthesis of 2. A solution of appropriate dihydroantranilate **1** (1.5 mmol) and DDQ (1.5 equiv) in 10 mL of toluene was stirred (10 mL) for 2 h at room temperature. Then, the reaction mixture was extracted with ethyl acetate (30 mL × 3), and the combined organic phase was washed with 30 mL water and 30 mL brine solution. The residue was concentrated under vacuum, and the crude was purified by flash chromatography on silica gel with a petroleum ether and ethyl acetate gradient (from 9/1 to 8/2). Compounds **2** were reported in the literature, and their characterization data were identical to those previously described.[17]

*Synthesis of **APH**.* A solution of appropriate *meta*-terphenyl compound **2** (1 mmol) was dissolved in ethanol (25 mL), and 10% palladium on carbon (Pd/C) (0.1 mmol, 10 mol %) was added. The suspension was stirred at room temperature for 14 h under hydrogen atmosphere, the catalyst was removed by filtration over Celite and washed with dichloromethane, and the solvent evaporated. The crude was purified by column chromatography on silica gel, eluting with a petroleum ether-ethyl acetate gradient (from 8:2 to 1:1). Compounds **APH** were reported in the literature, and their characterization data were identical to those previously described.[17]

*7-(Butylamino)-9-phenylphenanthridin-6(5H)-one (**APH1**).* ^{1}H NMR (250 MHz, DMSO-d_6) δ 9.46 (t, J = 4.9 Hz, 1H), 8.42 (d, J = 7.9 Hz, 1H), 7.86 (d, J = 6.9 Hz, 2H), 7.74 (s, 1H), 7.57−7.40 (m, 4H), 7.31 (d, J = 7.1 Hz, 1H), 7.21 (t, J = 7.5 Hz, 1H), 6.88 (s, 1H),

https://doi.org/10.1021/acschemneuro.1c00333
ACS Chem. Neurosci. 2021, 12, 3358−3372

3.31−3.24 (m, 2H), 1.75−1.61 (m, 2H), 1.56−1.38 (m, 2H), 0.96 (t, J = 7.3 Hz, 3H).

*7-((4-Methoxyphenyl)amino)-9-phenylphenanthridin-6(5H)-one (**APH2**).* ^{1}H NMR (250 MHz, $CDCl_3$) δ 10.93 (s, 1H), 9.20 (s, 1H), 8.27 (d, J = 7.8 Hz, 1H), 7.73 (d, J = 1.3 Hz, 1H), 7.63 (dd, J = 8.1, 1.5 Hz, 2H), 7.52−7.40 (m, 4H), 7.33−7.27 (m, 3H), 7.26 (d, J = 1.4 Hz, 1H), 7.18 (d, J = 7.9 Hz, 1H), 6.99 (d, J = 8.9 Hz, 2H), 3.88 (s, 3H).

*7-((4-Dimethylaminophenyl)amino)-9-phenylphenanthridin-6(5H)-one (**APH3**).* ^{1}H NMR (250 MHz, DMSO-d_6) δ 8.46 (d, J = 8.1 Hz, 1H), 7.84 (s, 1H), 7.68 (d, J = 6.9 Hz, 2H), 7.59−7.42 (m, 5H), 7.42−7.32 (m, 2H), 7.29−7.17 (m, 3H), 7.11 (s, 1H), 6.80 (d, J = 8.9 Hz, 2H), 2.91 (s, 5H).

*7-((4-Methoxyphenyl)amino)-9-(thiophen-2-yl)phenanthridin-6(5H)-one (**APH4**).* ^{1}H NMR (250 MHz, DMSO-d_6) δ 11.62 (s, 1H), 11.19 (s, 1H), 8.46 (d, J = 7.9 Hz, 1H), 7.94 (s, J = 1.0 Hz, 1H), 7.74 (dd, J = 3.7, 1.0 Hz, 1H), 7.62 (dd, J = 5.0, 1.0 Hz, 1H), 7.50 (t, J = 8.1 Hz, 1H), 7.38−7.23 (m, 4H), 7.21−7.14 (m, 2H), 7.02 (d, J = 8.9 Hz, 2H), 3.79 (s, 3H).

*7-(Phenylamino)-9-(thiophen-2-yl)phenanthridin-6(5H)-one (**APH5**).* ^{1}H NMR (250 MHz, DMSO-d_6) δ 11.35 (d, J = 9.0 Hz, 2H), 8.64 (d, J = 8.1 Hz, 1H), 8.12 (d, J = 1.6 Hz, 1H), 7.84 (dd, J = 3.7, 1.2 Hz, 1H), 7.77 (d, J = 8.3 Hz, 1H), 7.72−7.63 (m, 2H), 7.52−7.45 (m, 2H), 7.45−7.37 (m, 3H), 7.29−7.08 (m, 2H).

Metal-Chelating Study. The chelating studies were performed with a diode array HP8543 UV−vis spectrophotometer (Agilent Technologies), by using a 1.0 cm quartz cuvette and the HP Chemstation software. The absorption spectra were collected at room temperature. Absorbance measurements of the tested compounds alone or in the presence of $FeCl_2$, $CuCl_2$, $HgCl_2$, $ZnCl_2$, $CdCl_2$, or $AlCl_3$ were carried out in 100 mM phosphate buffer solution at pH 7.30 and registered within the 200−600 nm range. In all cases, blank solutions were properly analyzed.

Stock solutions of Fe^{2+}, Cu^{2+}, Hg^{2+}, Zn^{2+}, Cd^{2+}, and Al^{3+} (2.5 mM, final concentration) were prepared in Milli-Q water. The metal solutions were stirred until complete dissolution by using an ultrasound probe (Vibracell Sonics), equipped with a 2 mm diameter titanium microtip, at 60% power width during 2 min. Evaluated compounds were dissolved in an aqueous mixture of DMSO 100 mM phosphate buffer pH = 7.30 at ratios 1:2 v/v (0.50 mM, final concentration) and 1:14 v/v (0.10 mM, final concentration) by employing an ultrasonic bath for 10 min. Working solutions of compounds alone and compound-metal complexes were daily prepared by dilution of stock solutions in buffer as required.

Chelation was detected as a consequence of the changes observed in the absorption spectra after 30 min of incubation. With the aim of estimating the stoichiometry of the compound-metal complexes, a fixed amount of **APH1**, **AHP2**, **APH3**, **APH4**, or **APH5** compounds (50 μM) was mixed with increasing amounts of metal ion (6.25−50 μM). Similarly, a fixed amount of metal (50 μM) was mixed with increasing amounts of **APH1**, **AHP2**, **APH3**, **APH4**, or **APH5** compounds to achieve compound concentrations from 50 to 200 μM. UV−vis spectra were carefully examined in order to evaluate absorption differences and to estimate the ratio metal/compound in the formed complexes. Derivative spectroscopy was also applied to resolve stoichiometry studies.

HOMO and LUMO Analysis. The ability of a molecule to form complexes can be examined by the molecular orbital frontier approach. This approach is based on the premise that electrons are transferred from the HOMO orbital to the LUMO orbital in the formation of new bonds between the atoms. Thus, HOMO orbital indicates the ability to donate electrons, the LUMO orbitals show the ability to accept electrons of a molecule, and the greater the energy gap is between these HOMO/LUMO orbitals, the higher the molecule polarizability is, which is usually translated into a higher chemical reactivity.[50]

Molecular modeling was performed with ChemBio3D software (version 14.0 ultra), and HOMO and LUMO levels were researched using molecular mechanics (MM2) and MMFF94 force field analysis. For the optimized structure, HOMO−LUMO energies were analyzed.

Physicochemical and Prediction of ADMET Properties Analysis. In silico assessment of relevant drug-likeness properties and a series of ADMET properties was carried out using ADMETsar version 2.0 (http://lmmd.ecust.edu.cn/admetsar2) and SwissADME; S (http://www.swissadme.ch/) software.[51,52] We calculated the most significant physicochemical properties required for absorption into the central nervous system such as the molecular weight and octanol−water partition coefficient (log P), as other parameters in association with Lipinski's rule of five and the suitability of a drug molecule for oral administration such as H-bond acceptors and H-bond donors.[53]

Culture of SN56 Cells. The protection induced by **APH** compounds against metals toxic effects was evaluated using a cholinergic murine neuroblastoma cell line (SN56 cells) derived from the basal forebrain septum. Basal forebrain contains the majority of CNS cholinergic neurons,[54] which innervate the hippocampus and frontal cortex, regulating learning and memory process.[55,56] Their selective degeneration, as observed in AD and other neurodegenerative diseases, induced cognitive dysfunction.[57,58] We chose this cells line since the essential and heavy metals brain accumulation was related with memory and learning alterations,[1−3] with some of them reported to induce a more pronounced damage in basal forebrain cholinergic neurons,[8,59] so it is a sensitive model to study their toxic effects. Dulbecco's modified Eagle's medium (DMEM) supplemented with 10% fetal bovine serum, penicillin/streptomycin, 2 mM L-glutamine (Sigma, Madrid, Spain), and 1 mM sodium pyruvate was used to maintain cells at 37 °C and 5% CO_2. This medium was changed every 48 h.[60] Cells were differentiated via culture for 3 days with 1 mM dibutyryl-cAMP and 1 μM retinoic acid.[61,62] Following cells differentiation, there were no differences in cells regarding the periods of treatment. All cells used in these studies showed to be mycoplasma-free using the Look Out Mycoplasma PCR Detection Kit (Sigma, Madrid, Spain).

Cells were seeded in 6-well plates at a density of 10^6 cells/well. To determine **APH** compounds neuroprotective effects against $FeCl_2$ (200 μM), $CuCl_2$ (20 μM), $ZnCl_2$ (250 μM), $CdCl_2$ (100 μM), $HgCl_2$ (30 μM), and $AlCl_3$ (300 μM) cytotoxic effects, cells were treated with the **APH1**, **AHP2**, **APH3**, **APH4**, or **APH5** compounds in concentrations between 10 and 100 μM and with trolox at 100 μM concentration. Besides, to determine the antioxidant mechanisms of **APH1**, **AHP2**, **APH3**, **APH4**, and **APH5** compounds, cells were treated for 24 h with them in concentrations between 10 and 100 μM. At least three replicate wells/treatment were used. A vehicle group was employed in parallel for each experiment as a control.

APH1−APH5 compounds were selected because they were the **APH** compounds with less cytotoxic effects and because they presented the most potent antioxidant and neuroprotective effect against ROS stimulus.[17] The range of 10−100 μM concentrations was chosen because it is a range of concentrations without cytotoxicity in which it is more probable that their neuroprotective effects are developed. The concentrations of metals used were selected because they were observed to induce cell death (data not shown). The metals used were selected because they were reported to induce neurodegeneration and were mainly associated with neurodegenerative disese.[1−3]

Cytotoxic and Neuroprotective Effect on SN56 Cells. The 3-(4,5-dimethylthiazol-2-yl)-2,5-diphenyltetrazolium bromide (MTT) assay, which is based on the cleavage of the yellow tetrazolium salt MTT to purple formazan crystals by mitochondrial dehydrogenase, was used to evaluate SN56 cells viability. The cytotoxic effects of metals on SN56 cells were determined after incubation for 24 h with $FeCl_2$ (200 μM), $CuCl_2$ (20 μM), $ZnCl_2$ (250 μM), $CdCl_2$ (100 μM), $HgCl_2$ (30 μM), and $AlCl_3$ (300 μM). The metal concentrations used were previously tested and observed to induce cell death (data not shown). The neuroprotective effects of compounds **APH1**, **AHP2**, **APH3**, **APH4**, and **APH5** against these metals were evaluated after incubation for 24 h with $FeCl_2$ (200 μM), $CuCl_2$ (20 μM), $ZnCl_2$ (250 μM), $CdCl_2$ (100 μM), $HgCl_2$ (30 μM), and $AlCl_3$ (300 μM) of SN56 cells pretreated with compounds **4** at various concentrations (10−100 μM) for 2 h.

https://doi.org/10.1021/acschemneuro.1c00333
ACS Chem. Neurosci. 2021, 12, 3358−3372

At the end of the assays, cells were incubated with 100 μL of yellow MTT solution (final concentration 0.5 mg/mL) for 4 h. After 4 h at 37 °C, the medium was removed, and 150 μL DMSO was used to dissolve the formazan reaction product. The formation of solubilized formazan product was measured spectrophotometrically at 570 nm (Fluoroskan Ascent FL Microplate Fluorometer and Luminometer, Thermo Fisher Scientific, Madrid, Spain). Control cells were taken as 100% viability.

Real-Time PCR Analysis. The Trizol reagent method (Invitrogen, Madrid, Spain) was used to extract total RNA. A Nanodrop 2000 (Thermo Fisher Scientific, Madrid, Spain) spectrophotometer and an Experion Lab Chip (Bio-Rad, Madrid, Spain) gel were used to determine the final RNA concentration and assess the quality of total RNA samples, respectively. We synthesized the first strand cDNA using a PCR array first strand-synthesis kit (C-02; Super Array Bioscience, Madrid, Spain) with 1000 ng of cRNA, following the manufacturer's instructions, with an added genomic DNA elimination step and external RNA controls. Following reverse transcription, QPCR was performed using prevalidated primer sets (SuperArray Bioscience) for mRNAs encoding *Keap1* (PPM34919B), *Nrf2* (PPM24614A), *Cat* (PPM04394C), *Gpx* (PPM04345E), and *Actb* (PPM02945B). *Actb* was used as an internal control for normalization. A CFX96 was used to run reactions with real-time SYBR green PCR master mix PA-012 (SuperArray Bioscience). The thermocycler parameters were established as 95 °C for 10 min, followed by 40 cycles of 95 °C for 15 s and 72 °C for 30 s. We used the Ct (cycle threshold) method to calculate relative changes in gene expression. The expression data are presented as actual change multiples.[63]

Protein Expression Analysis. Treated cells were washed with cold PBS, scraped, and harvested. Then, harvested cells were lysed using radioimmunoprecipitation assay (RIPA) reagent (Thermo Fisher, Madrid, Spain) with a protease repressors mixture (Thermo Fisher, Madrid, Spain), following the manufacturer's protocol. Finally, cell lysates were centrifuged at 10,000*g* during 10 min at 4 °C, and the supernatant was collected. Total protein levels were assayed with a bicinchoninic acid (BCA) assay kit (catalog number 23225; ThermoFisher, Madrid, Spain), according to manufacturer's guideline.

Keap1, Nrf2, Gpx, and Cat protein expression was determined employing commercial ELISA tests in cell lysate supernatant (catalog numbers MBS7212746, MBS776676, MBS732750, and MBS728474, respectively; MyBiosource, CA, USA) in accordance with producer's protocols. The protein concentrations of each target gene were normalized with the total protein levels measured by BCA kit, to prevent possible interferences with the real value of the targets' protein concentrations measured due to the induction of cell death. Protein levels were expressed in ng/mg protein.

Protective Effects on Cell Lipid Peroxidation. MDA concentration was determined as an indicator of lipid peroxidation products induced by free radicals. Intracellular MDA production was quantified after 24 h exposure to $FeCl_2$ (200 μM) or $CdCl_2$ (100 μM) with or without **APH1**, **AHP2**, **APH3**, **APH4**, or **APH5** compounds (10−100 μM), using a Lipid Peroxidation MDA Assay Kit (Abcam, Cambridge, UK), following the manufacturer's protocol. Briefly, following treatment, we collected 1×10^6 cells and homogenized them on ice in MDA lysis buffer (300 μL) with 3 μL BHT (100×). Then, the mix was centrifuged for 10 min at 13,000*g* to remove insoluble material. Sample (200 μL) or standard (200 μL of MDA) was mixed with 600 μL of thiobarbituric acid solution, incubated at 95 °C for 50 min, and cooled to room temperature in an ice bath for 10 min. We loaded all samples and standards (200 μL) (duplicate) into a clear 96-well plate, and a microplate reader (Fluoroskan Ascent FL Microplate Fluorometer and Luminometer, Thermo Fisher Scientific, Madrid, Spain) was used to record the absorbance at 532 nm. Concentration of MDA, determined as nmol/mg protein, is presented as percent untreated control.

Statistical Analysis. At least three replicates for each experimental condition were performed, and the presented results were representative of these replicates. Data are presented as means ± standard error of the mean. Comparisons between experimental and control groups were performed by two-ways ANOVA analyses (concentration vs treatment) or one-way ANOVA analyses (analysis of different 7-aminophenanthridin compounds concentrations) followed by the Tukey posthoc test. Statistical difference was accepted when $p \leq 0.05$. Statistical analysis of data was carried out using GraphPad Prism 5.01 software.

■ ASSOCIATED CONTENT

Supporting Information

The Supporting Information is available free of charge at https://pubs.acs.org/doi/10.1021/acschemneuro.1c00333.

Figures showing optimized molecular structure of **APH1−APH3** and **APH5**, their iron complex and their corresponding HOMOs and LUMOs; cell viability effects after **APH1−APH5** treatment; and **APH1−APH5** UV−vis spectra and first-order derivative absorption spectra, alone and in the presence of metals. Tables with results of HOMO/LUMO gap energy analysis and ADMET prediction of APH compounds (PDF)

■ AUTHOR INFORMATION

Corresponding Authors

Juan F. González − *Unidad de Química Orgánica y Farmacéutica, Departamento de Química en Ciencias Farmacéuticas, Facultad de Farmacia, Universidad Complutense, 28040 Madrid, Spain*; Email: jfgonzal@ucm.es

Noelia Rosales-Conrado − *Departamento de Química Analítica, Facultad de Ciencias Químicas, Universidad Complutense, 28040 Madrid, Spain*; Email: nrosales@ucm.es

Javier del Pino − *Departamento de Farmacología y Toxicología, Facultad de Veterinaria, Universidad Complutense, 28040 Madrid, Spain*; orcid.org/0000-0001-6937-7701; Email: jdelpino@pdi.ucm.es

Authors

Paula Moyano − *Departamento de Farmacología y Toxicología, Facultad de Veterinaria, Universidad Complutense, 28040 Madrid, Spain*

David Vicente-Zurdo − *Departamento de Química Analítica, Facultad de Ciencias Químicas, Universidad Complutense, 28040 Madrid, Spain*

Cristina Blázquez-Barbadillo − *Unidad de Química Orgánica y Farmacéutica, Departamento de Química en Ciencias Farmacéuticas, Facultad de Farmacia, Universidad Complutense, 28040 Madrid, Spain*

J. Carlos Menéndez − *Unidad de Química Orgánica y Farmacéutica, Departamento de Química en Ciencias Farmacéuticas, Facultad de Farmacia, Universidad Complutense, 28040 Madrid, Spain*; orcid.org/0000-0002-0560-8416

Complete contact information is available at: https://pubs.acs.org/10.1021/acschemneuro.1c00333

Author Contributions

‖These authors contributed equally.

Funding

This research was supported by the following grants: CTQ2015-68380-R and RTI2018-097662-B-I00 (from MICINN) to J.C.M. and PR26/16-16B (from UCM) to J.F.G., J.P., and N.R.C.

Notes

The authors declare no competing financial interest.

■ ACKNOWLEDGMENTS

We gratefully acknowledge MINECO, MICINN, and UCM for financial support of this research.

■ ABBREVIATIONS

AD, Alzheimer's disease; ADMET, absorption, distribution, metabolism, excretion, and toxicological properties; ALS, amyotrophic lateral sclerosis; ANOVA, analysis of variance; APH, 7-amino-phenanthridin-6-one derivatives; BBB, blood−brain barrier; BHT, butylated hydroxytoluene; CNS, central nervous system; DDQ, 2,3-dichloro-5,6-dicyano-1,4-benzoquinone; DMEM, Dulbecco's modified Eagle's medium; DMSO, dimethyl sulfoxide; HD, Huntington's disease; HOMO, Highest occupied molecular orbital; KEAP1, Kelch-like ECH-associated protein 1; LUMO, Lowest unoccupied molecular orbital; MDA, malondialdehyde; MMP, matrix metalloproteinase; MMFF94, Merck molecular force field 94; MM2, molecular mechanics force field; MTT, 3-(4,5-dimethylthiazol-2-yl)-2,5-diphenyltetrazolium; NRF2, nuclear factor erythroid 2-related factor 2; PARP-1, poly(ADP-ribose) polymerase-1; PD, Parkinson's disease; p-tau, tau-phosphorylated; ROS, reactive oxygen species; UV−vis, ultraviolet−visible spectroscopy

■ REFERENCES

(1) Cannon, J. R.; Greenamyre, J. T. The role of environmental exposures in neurodegeneration and neurodegenerative diseases. *Toxicol. Sci.* **2011**, *124* (2), 225.
(2) Chin-Chan, M.; Navarro-Yepes, J.; Quintanilla-Vega, B. Environmental pollutants as risk factors for neurodegenerative disorders: Alzheimer and Parkinson diseases. *Front. Cell. Neurosci.* **2015**, *9*, 124.
(3) Mir, R. H.; Sawhney, G.; Pottoo, F. H.; Mohi-Ud-Din, R.; Madishetti, S.; Jachak, S. M.; Ahmed, Z.; Masoodi, M. H. Role of environmental pollutants in Alzheimer's disease: a review. *Environ. Sci. Pollut. Res.* **2020**, *27* (36), 44724.
(4) Chen, P.; Miah, M. R.; Aschner, M. Metals and Neurodegeneration. *F1000Research* **2016**, *5*, 366.
(5) Gozzelino, R.; Arosio, P. Iron Homeostasis in Health and Disease. *Int. J. Mol. Sci.* **2016**, *17* (1), 130.
(6) Zheng, W.; Monnot, A. D. Regulation of brain iron and copper homeostasis by brain barrier systems: implication in neurodegenerative diseases. *Pharmacol. Ther.* **2012**, *133* (2), 177.
(7) Choi, S.; Hong, D. K.; Choi, B. Y.; Suh, S. W. Zinc in the Brain: Friend or Foe? *Int. J. Mol. Sci.* **2020**, *21* (23), 8941.
(8) Moyano, P.; De Frias, M.; Lobo, M.; Anadon, M. J.; Sola, E.; Pelayo, A.; Díaz, M. J.; Frejo, M. T.; Del Pino, J. Cadmium induced ROS alters M1 and M3 receptors, leading to SN56 cholinergic neuronal loss, through AChE variants disruption. *Toxicology* **2018**, *394*, 54.
(9) Brkic, M.; Balusu, S.; Libert, C.; Vandenbroucke, R. E. Friends or foes: matrix metalloproteinases and their multifaceted roles in neurodegenerative diseases. *Mediators Inflammation* **2015**, *2015*, 620581.
(10) Dagouassat, M.; Lanone, S.; Boczkowski, J. Interaction of matrix metalloproteinases with pulmonary pollutants. *Eur. Respir. J.* **2012**, *39* (4), 1021.
(11) Rosenberg, G. A. Matrix metalloproteinases and their multiple roles in neurodegenerative diseases. *Lancet Neurol.* **2009**, *8* (2), 205.
(12) Rosenberg, G. A. Metalloproteinases and neurodegenerative diseases: pathophysiological and therapeutic perspectives. *Metalloproteinases. Med.* **2015**, *2015* (2), 39.
(13) Bjerke, M.; Zetterberg, H.; Edman, Å.; Blennow, K.; Wallin, A.; Andreasson, U. Cerebrospinal fluid matrix metalloproteinases and tissue inhibitor of metalloproteinases in combination with subcortical and cortical biomarkers in vascular dementia and Alzheimer's disease. *J. Alzheimer's Dis.* **2011**, *27* (3), 665.
(14) Asahina, M.; Yoshiyama, Y.; Hattori, T. Expression of matrix metalloproteinase-9 and urinary-type plasminogen activator in Alzheimer's disease brain. *Clin. Neuropathol.* **2001**, *20* (2), 60.
(15) Su, X.; Maguire-Zeiss, K. A.; Giuliano, R.; Prifti, L.; Venkatesh, K.; Federoff, H. J. Synuclein activates microglia in a model of Parkinson's disease. *Neurobiol. Aging* **2008**, *29* (11), 1690.
(16) Vandenbroucke, R. E.; Libert, C. Is there new hope for therapeutic matrix metalloproteinase inhibition? *Nat. Rev. Drug Discovery* **2014**, *13* (12), 904.
(17) Rocchi, D.; Blázquez-Barbadillo, C.; Agamennone, M.; Laghezza, A.; Tortorella, P.; Vicente-Zurdo, D.; Rosales-Conrado, N.; Moyano, P.; Pino, J. D.; González, J. F.; Menéndez, J. C. Discovery of 7-aminophenanthridin-6-one as a new scaffold for matrix metalloproteinase inhibitors with multitarget neuroprotective activity. *Eur. J. Med. Chem.* **2021**, *210*, 113061.
(18) Li, N.; Alam, J.; Venkatesan, M. I.; Eiguren-Fernandez, A.; Schmitz, D.; Di Stefano, E.; Slaughter, N.; Killeen, E.; Wang, X.; Huang, A.; Wang, M.; Miguel, A. H.; Cho, A.; Sioutas, C.; Nel, A. E. Nrf2 is a key transcription factor that regulates antioxidant defense in macrophages and epithelial cells: protecting against the proinflammatory and oxidizing effects of diesel exhaust chemicals. *J. Immunol.* **2004**, *173* (5), 3467.
(19) Luo, D. D.; Chen, J. F.; Liu, J. J.; Xie, J. H.; Zhang, Z. B.; Gu, J. Y.; Zhuo, J. Y.; Huang, S.; Su, Z. R.; Sun, Z. H. Tetrahydrocurcumin and octahydrocurcumin, the primary and final hydrogenated metabolites of curcumin, possess superior hepatic-protective effect against acetaminophen-induced liver injury: role of CYP2E1 and Keap1-Nrf2 pathway. *Food Chem. Toxicol.* **2019**, *123*, 349.
(20) Li, S.; Tan, H.-Y.; Wang, N.; Zhang, Z.-J.; Lao, L.; Wong, C.-W.; Feng, Y. The role of oxidative stress and antioxidants in liver diseases. *Int. J. Mol. Sci.* **2015**, *16*, 26087.
(21) Osama, A.; Zhang, J.; Yao, J.; Yao, X.; Fang, J. Nrf2: a dark horse in Alzheimer's disease treatment. *Ageing Res. Rev.* **2020**, *64*, 101206.
(22) Khan, H.; Tundis, R.; Ullah, H.; Aschner, M.; Belwal, T.; Mirzaei, H.; Akkol, E. K. Flavonoids targeting NRF2 in neurodegenerative disorders. *Food Chem. Toxicol.* **2020**, *146*, 111817.
(23) Li, Q.; Xing, S.; Chen, Y.; Liao, Q.; Li, Q.; Liu, Y.; He, S.; Feng, F.; Chen, Y.; Zhang, J.; Liu, W.; Guo, Q.; Sun, Y.; Sun, H. Reasonably activating Nrf2: A long-term, effective and controllable strategy for neurodegenerative diseases. *Eur. J. Med. Chem.* **2020**, *185*, 111862.
(24) Suzuki, T.; Hidaka, T.; Kumagai, Y.; Yamamoto, M. Environmental pollutants and the immune response. *Nat. Immunol.* **2020**, *21* (12), 1486.
(25) Iqubal, A.; Ahmed, M.; Ahmad, S.; Sahoo, C. R.; Iqubal, M. K.; Haque, S. E. Environmental neurotoxic pollutants: review. *Environ. Sci. Pollut. Res.* **2020**, *27* (33), 41175.
(26) Zheng, F.; Gonçalves, F. M.; Abiko, Y.; Li, H.; Kumagai, Y.; Aschner, M. Redox toxicology of environmental chemicals causing oxidative stress. *Redox Biol.* **2020**, *34*, 101475.
(27) Akbari, G. Role of Zinc Supplementation on Ischemia/Reperfusion Injury in Various Organs. *Biol. Trace Elem. Res.* **2020**, *196* (1), 1.
(28) Guerra, W.; Silva-Caldeira, P. P.; Terenzi, H.; Pereira-Maia, E. C. Impact of metal coordination on the antibiotic and non-antibiotic activities of tetracycline-based drugs. *Coord. Chem. Rev.* **2016**, *327*−*328*, 188.
(29) Říha, M.; Karlíčková, J.; Filipský, T.; Macáková, K.; Rocha, L.; Bovicelli, P.; Silvestri, I. P.; Saso, L.; Jahodář, L.; Hrdina, R.; Mladěnka, P. In vitro evaluation of copper-chelating properties of flavonoids. *RSC Adv.* **2014**, *4*, 32628.
(30) Zheng, J. W.; Ma, L. Metal complexes of anthranilic acid derivatives: A new class of non-competitive α-glucosidase inhibitors. *Chin. Chem. Lett.* **2016**, *27* (5), 627.

https://doi.org/10.1021/acschemneuro.1c00333
ACS Chem. Neurosci. 2021, 12, 3358−3372

(31) Wang, Z.; Wang, Y.; Li, W.; Mao, F.; Sun, Y.; Huang, L.; Li, X. Design, Synthesis, and Evaluation of Multitarget-Directed Selenium-Containing Clioquinol Derivatives for the Treatment of Alzheimer's Disease. *ACS Chem. Neurosci.* **2014**, *5*, 952.
(32) Carmona-Vargas, C. C.; Aristizábal, S. L.; Belalcázar, M. I.; D'Vries, R. F.; Chaur, M. N. Determination of the binding constants of propeller-like metal complexes of picolinaldehyde-2-pyridylhydrazone. *Inorg. Chim. Acta* **2019**, *487*, 275.
(33) Kılınçarslan, R.; Erdem, E.; Kocaokutgen, H. Synthesis and spectral characterization of some new azo dyes and their metal complexes. *Transition Met. Chem.* **2007**, *32*, 102.
(34) Georgieva, S.; Todorov, P.; Bezfamilnyi, A.; Georgiev, A. Coordination behaviour of 3-amino-5,5′-dimethylhydantoin towards Ni(II) and Zn(II) ions: Synthesis, spectral characterization and DFT calculations. *J. Mol. Struct.* **2018**, *1166*, 377.
(35) Leeson, P. D.; Young, R. J. Molecular Property Design: Does Everyone Get It? *ACS Med. Chem. Lett.* **2015**, *6* (7), 722.
(36) Nguyen, T.; Yang, C. S.; Pickett, C. B. The pathways and molecular mechanisms regulating Nrf2 activation in response to chemical stress. *Free Radical Biol. Med.* **2004**, *37*, 433.
(37) Gong, P.; Cederbaum, A. I. Nrf2 is increased by CYP2E1 in rodent liver and HepG2 cells and protects against oxidative stress caused by CYP2E1. *Hepatology* **2006**, *43* (1), 144.
(38) Kabaria, S.; Choi, D. C.; Chaudhuri, A. D.; Jain, M. R.; Li, H.; Junn, E. MicroRNA-7 activates Nrf2 pathway by targeting Keap1 expression. *Free Radical Biol. Med.* **2015**, *89*, 548.
(39) Sparaneo, A.; Fabrizio, F. P.; La Torre, A.; Graziano, P.; Di Maio, M.; Fontana, A.; Bisceglia, M.; Rossi, A.; Pizzolitto, S.; De Maglio, G.; Tancredi, A.; Grimaldi, F.; Balsamo, T.; Centra, F.; Manzorra, M. C.; Trombetta, D.; Pantalone, A.; Bonfitto, A.; Maiello, E.; Fazio, V. M.; Muscarella, L. A. Effects of KEAP1 Silencing on the Regulation of NRF2 Activity in Neuroendocrine Lung Tumors. *Int. J. Mol. Sci.* **2019**, *20* (10), 2531.
(40) Padmavathi, G.; Ramkumar, K. M. MicroRNA mediated regulation of the major redox homeostasis switch, Nrf2, and its impact on oxidative stress-induced ischemic/reperfusion injury. *Arch. Biochem. Biophys.* **2021**, *698*, 108725.
(41) Bautista, E.; Vergara, P.; Segovia, J. Iron-induced oxidative stress activates AKT and ERK1/2 and decreases Dyrk1B and PRMT1 in neuroblastoma SH-SY5Y cells. *J. Trace Elem. Med. Biol.* **2016**, *34*, 62.
(42) Bruce-Keller, A. J.; Li, Y. J.; Lovell, M. A.; Kraemer, P. J.; Gary, D. S.; Brown, R. R.; Markesbery, W. R.; Mattson, M. P. 4-Hydroxynonenal, a product of lipid peroxidation, damages cholinergic neurons and impairs visuospatial memory in rats. *J. Neuropathol. Exp. Neurol.* **1998**, *57* (3), 257.
(43) Huat, T. J.; Camats-Perna, J.; Newcombe, E. A.; Valmas, N.; Kitazawa, M.; Medeiros, R. Metal Toxicity Links to Alzheimer's Disease and Neuroinflammation. *J. Mol. Biol.* **2019**, *431* (9), 1843.
(44) Lee, K.; Cao, J.; Lee, C.; Hsiao, T.; Yeh, C.; Huynh, T.; Han, Y.; Li, X.; Chuang, K.; Tian, L.; Ho, K.; Chuang, H. Inhibition of the WNT/β-catenin pathway by fine particulate matter in haze: Roles of metals and polycyclic aromatic hydrocarbons. *Atmos. Environ.* **2015**, *109*, 118.
(45) Weltin, D.; Picard, V.; Aupeix, K.; Varin, M.; Oth, D.; Marchal, J.; Dufour, P.; Bischoff, P. Immunosuppressive activities of 6(5H)-phenanthridinone, a new poly(ADP-ribose)polymerase inhibitor. *Int. J. Immunopharmacol.* **1995**, *17* (4), 265.
(46) Haddad, M.; Rhinn, H.; Bloquel, C.; Coqueran, B.; Szabó, C.; Plotkine, M.; Scherman, D.; Margaill, I. Anti-inflammatory effects of PJ34, a poly(ADP-ribose) polymerase inhibitor, in transient focal cerebral ischemia in mice. *Br. J. Pharmacol.* **2006**, *149*, 23.
(47) Kovacs, K.; Vaczy, A.; Fekete, K.; Kovari, P.; Atlasz, T.; Reglodi, D.; Gabriel, R.; Gallyas, F.; Sumegi, B. PARP Inhibitor Protects Against Chronic Hypoxia/Reoxygenation-Induced Retinal Injury by Regulation of MAPKs, HIF1α, Nrf2, and NFκB. *Invest. Ophthalmol. Visual Sci.* **2019**, *60* (5), 1478.
(48) Chen, D. Z.; Yang, B. J.; He, X. L.; Fan, S. R.; Cai, J. Y.; Jing, C. X.; Zhang, H.; Zhang, Y.; Li, L.; Hao, X. J. Design, synthesis and structure-activity relationship optimization of phenanthridine derivatives as new Wnt/beta-catenin signalling pathway agonists. *Bioorg. Chem.* **2019**, *84*, 285.
(49) Moyano, P.; García, J. M.; García, J.; Pelayo, A.; Muñoz-Calero, P.; Frejo, M. T.; Anadon, M. J.; Naval, M. V.; Flores, A.; Mirat, V. A.; Del Pino, J. Chlorpyrifos induces cell proliferation in MCF-7 and MDA-MB-231 cells, through cholinergic and Wnt/β-catenin signaling disruption, AChE-R upregulation and oxidative stress generation after single and repeated treatment. *Food Chem. Toxicol.* **2021**, *152*, 112241.
(50) Kumer, A.; Sarker, N.; Paul, S. The simulating study of HOMO, LUMO, thermo physical and quantitative structure of activity relationship (QSAR) of some anticancer active ionic liquids. *Eurasian. J. Environ. Res.* **2019**, *3* (1), 1.
(51) Yang, H.; Lou, C.; Sun, L.; Li, J.; Cai, Y.; Wang, Z.; Li, W.; Liu, G.; Tang, Y. admetSAR 2.0: web-service for prediction and optimization of chemical ADMET properties. *Bioinformatics* **2019**, *35* (6), 1067.
(52) Cheng, F.; Li, W.; Zhou, Y.; Shen, J.; Wu, Z.; Liu, G.; Lee, P. W.; Tang, Y. admetSAR: a comprehensive source and free tool for assessment of chemical ADMET properties. *J. Chem. Inf. Model.* **2012**, *52* (11), 3099.
(53) Lipinski, C. A. Lead- and drug-like compounds: the rule-of-five revolution. *Drug Discovery Today: Technol.* **2004**, *1* (4), 337.
(54) Voytko, M. L. Cognitive functions of the basal forebrain cholinergic system in monkeys: memory or attention? *Behav. Brain Res.* **1996**, *75* (1−2), 13.
(55) Everitt, B. J.; Robbins, T. W. Central cholinergic systems and cognition. *Annu. Rev. Psychol.* **1997**, *48*, 649.
(56) Ward, N. L.; Hagg, T. BDNF is needed for postnatal maturation of basal forebrain and neostriatum cholinergic neurons in vivo. *Exp. Neurol.* **2000**, *162* (2), 297.
(57) Scheiderer, C. L.; McCutchen, E.; Thacker, E. E.; Kolasa, K.; Ward, M. K.; Parsons, D.; Harrell, L. E.; Dobrunz, L. E.; McMahon, L. L. Sympathetic sprouting drives hippocampal cholinergic reinnervation that prevents loss of a muscarinic receptor-dependent long-term depression at CA3-CA1 synapses. *J. Neurosci.* **2006**, *26* (14), 3745.
(58) Bierer, L. M.; Haroutunian, V.; Gabriel, S.; Knott, P. J.; Carlin, L. S.; Purohit, D. P.; Perl, D. P.; Schmeidler, J.; Kanof, P.; Davis, K. L. Neurochemical correlates of dementia severity in Alzheimer's disease: relative importance of the cholinergic deficits. *J. Neurochem.* **1995**, *64* (2), 749.
(59) Moyano, P.; García, J. M.; Anadon, M. J.; Lobo, M.; García, J.; Frejo, M. T.; Sola, E.; Pelayo, A.; Pino, J. D. Manganese induced ROS and AChE variants alteration leads to SN56 basal forebrain cholinergic neuronal loss after acute and long-term treatment. *Food Chem. Toxicol.* **2019**, *125*, 583.
(60) Hudgens, E. D.; Ji, L.; Carpenter, C. D.; Petersen, S. L. The GAD2 promoter is a transcriptional target of estrogen receptor (ER) alpha and ER beta: a unifying hypothesis to explain diverse effects of estradiol. *J. Neurosci.* **2009**, *29*, 8790.
(61) Bielarczyk, H.; Jankowska, A.; Madziar, B.; Matecki, A.; Michno, A.; Szutowicz, A. Differential toxicity of nitric oxide, aluminum, and amyloid-β-peptide in SN56 cholinergic cells from mouse septum. *Neurochem. Int.* **2003**, *42*, 323.
(62) Szutowicz, A.; Bielarczyk, H.; Gul, S.; Ronowska, A.; Pawełczyk, T.; Jankowska-Kulawy, A. Phenotype-dependent susceptibility of cholinergic neuroblastoma cells to neurotoxic inputs. *Metab. Brain Dis.* **2006**, *21*, 143.
(63) Livak, K. J.; Schmittgen, T. D. Analysis of relative gene expression data using real time quantitative PCR and the 2(-Delta DeltaC(T)) method. *Methods* **2001**, *25*, 402.

https://doi.org/10.1021/acschemneuro.1c00333
ACS Chem. Neurosci. 2021, 12, 3358−3372

Supporting Information

Neuroprotective action of multitarget 7-aminophenanthridin-6(*5H*)-one derivatives against metal-induced cell death and oxidative stress in SN56 cells.

Paula Moyano,[1,‡] David Vicente-Zurdo,[2,‡] Cristina Blázquez-Barbadillo,[3] J. Carlos Menéndez,[3] Juan F. González,[3*] Noelia Rosales-Conrado,[2*] and Javier del Pino[1,*]

[1]Departamento de Farmacología y Toxicología, Facultad de Veterinaria, Universidad Complutense, 28040 Madrid, Spain.

[2]Departamento de Química Analítica, Facultad de Ciencias Químicas, Universidad Complutense, 28040 Madrid, Spain.

[3]Unidad de Química Orgánica y Farmacéutica, Departamento de Química en Ciencias Farmacéuticas, Facultad de Farmacia, Universidad Complutense, 28040 Madrid, Spain.

[‡]Authors with equal contribution

Running Title: Neuroprotective action of 7-aminophenanthridin-6(*5H*)-one derivatives against metals.

***Corresponding authors**:

J. Del Pino jdelpino@pdi.ucm.es
N. Rosales-Conrado nrosales@ucm.es
J.F. González jfgonzal@ucm.es

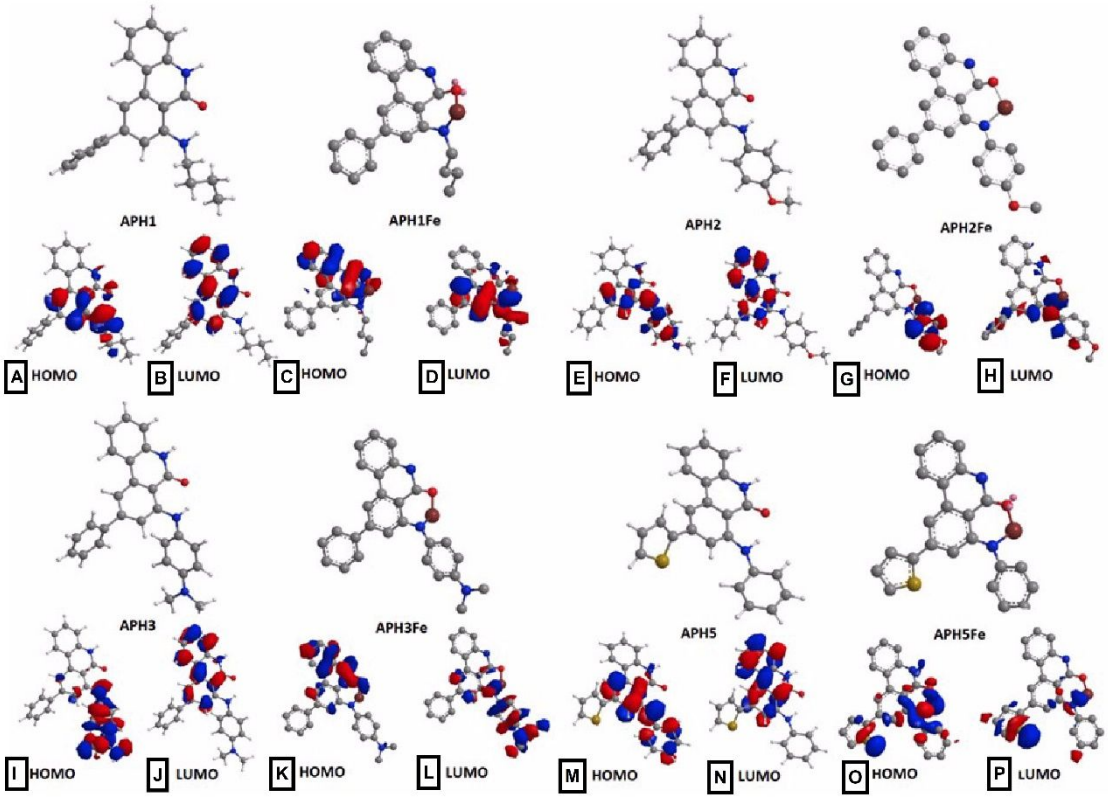


Figure S1. Optimized molecular structure of the **APH1**, **APH2**, **APH3** and **APH5** compounds, their iron complex (upper) and their corresponding HOMOs (A, C, E, G, I, K, M and O) and LUMOs (B, D, F, H, J, L, N and P). Color scheme: carbons is gray, hydrogen is white, nitrogen is blue, oxygen is red, sulphur is yellow, and iron is brown. HOMOs and LUMOs are shown in red and blue.

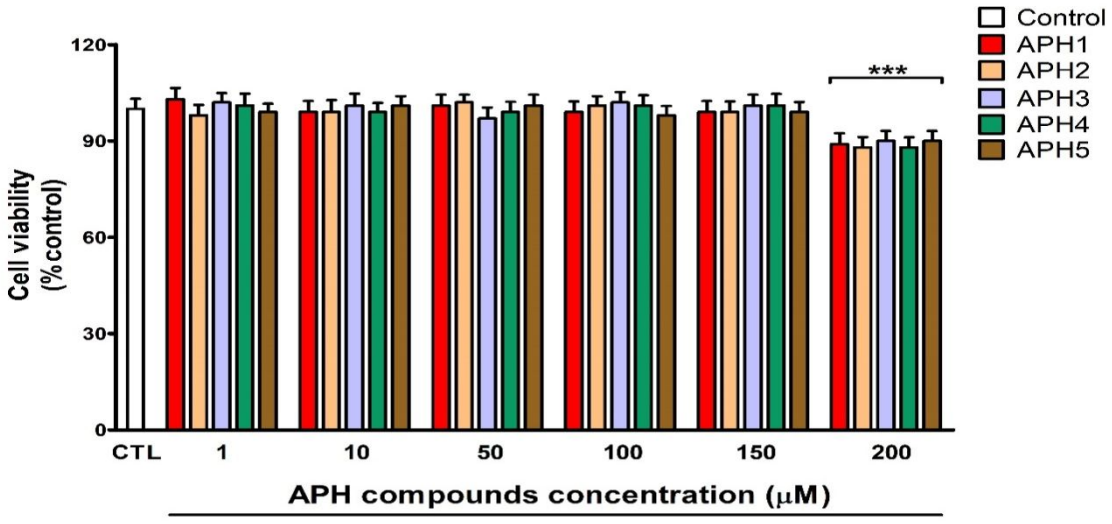


Figure S2. Cell viability effects after APH compounds (10-100 μM) treatment. Data represents the mean ± SEM of three independent experiments in triplicate. $^{***}p \leq 0.001$ compared to control.

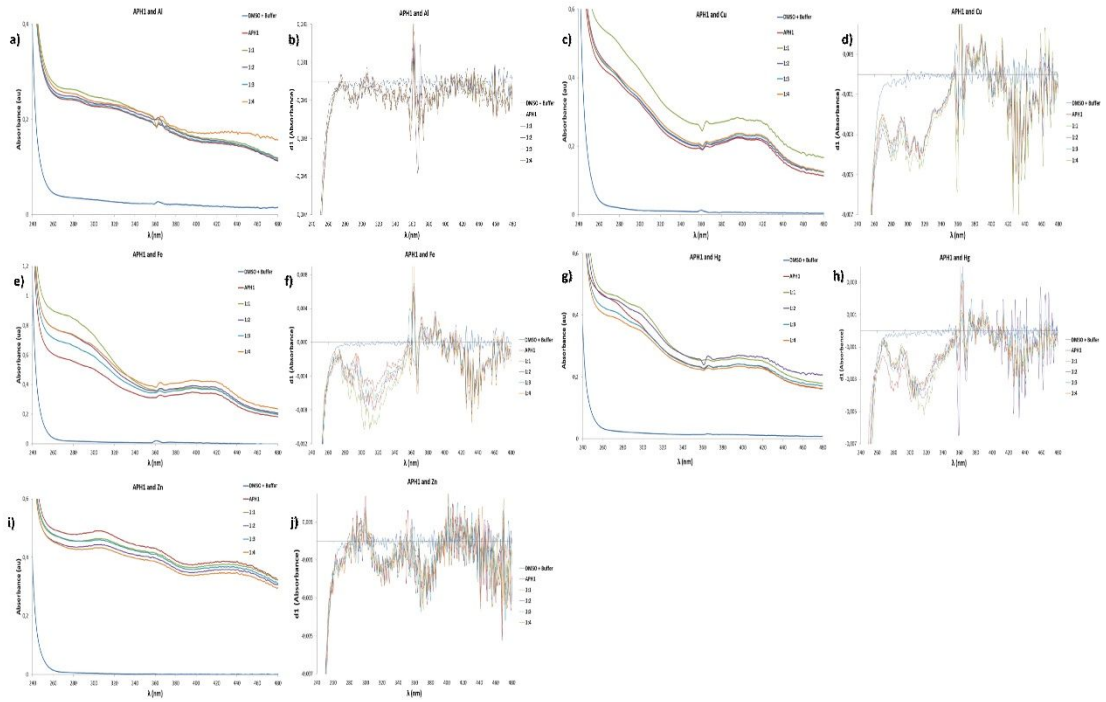


Figure S3. UV-Vis spectra (a, c, e, g and i) and first-order derivative absorption spectra (b, d, f, h and j) of **APH1** alone and in the presence of metals in buffer (100 mM phosphate, pH= 7.30) at room temperature. [**APH1**] = 50 μM and [Metal] = 50, 25, 12.5 and 6.25 μM corresponding to stoichiometries 1:1, 1:2, 1:4 and 1:8, respectively.

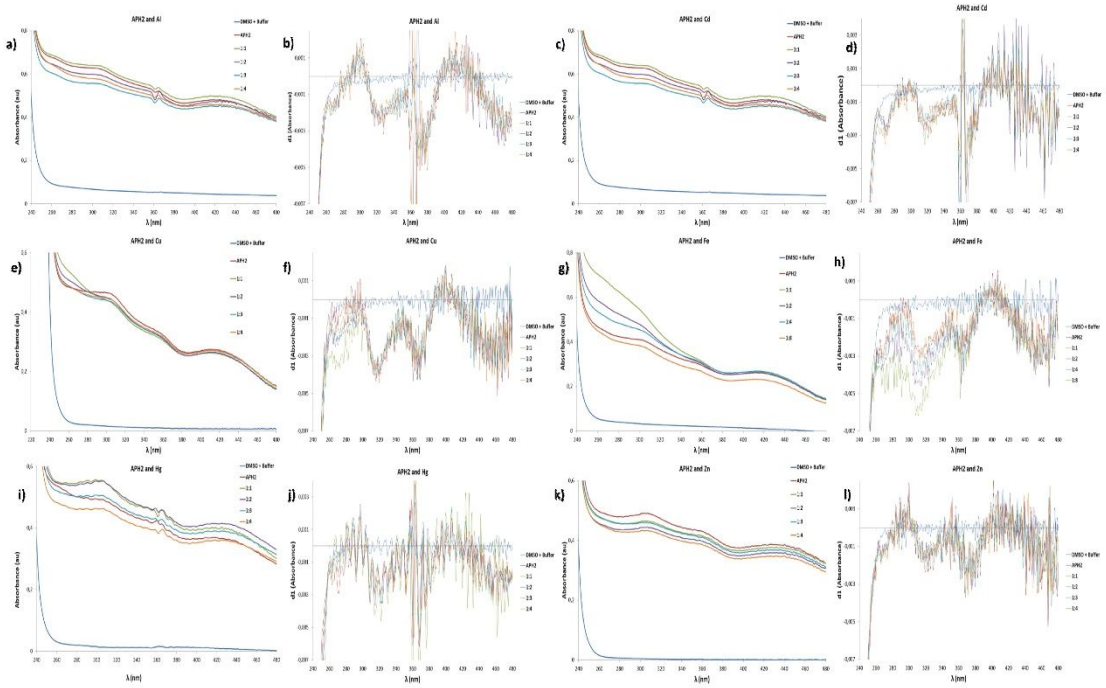


Figure S4. UV-Vis spectra (a, c, e, g, i and k) and first-order derivative absorption spectra (b, d, f, h, j and l) of **APH2** alone and in the presence of metals in buffer (100 mM phosphate, pH= 7.30) at room temperature. [**APH2**] = 50 μM and [Metal] = 50, 25, 12.5 and 6.25 μM corresponding to stoichiometries 1:1, 1:2, 1:4 and 1:8, respectively.

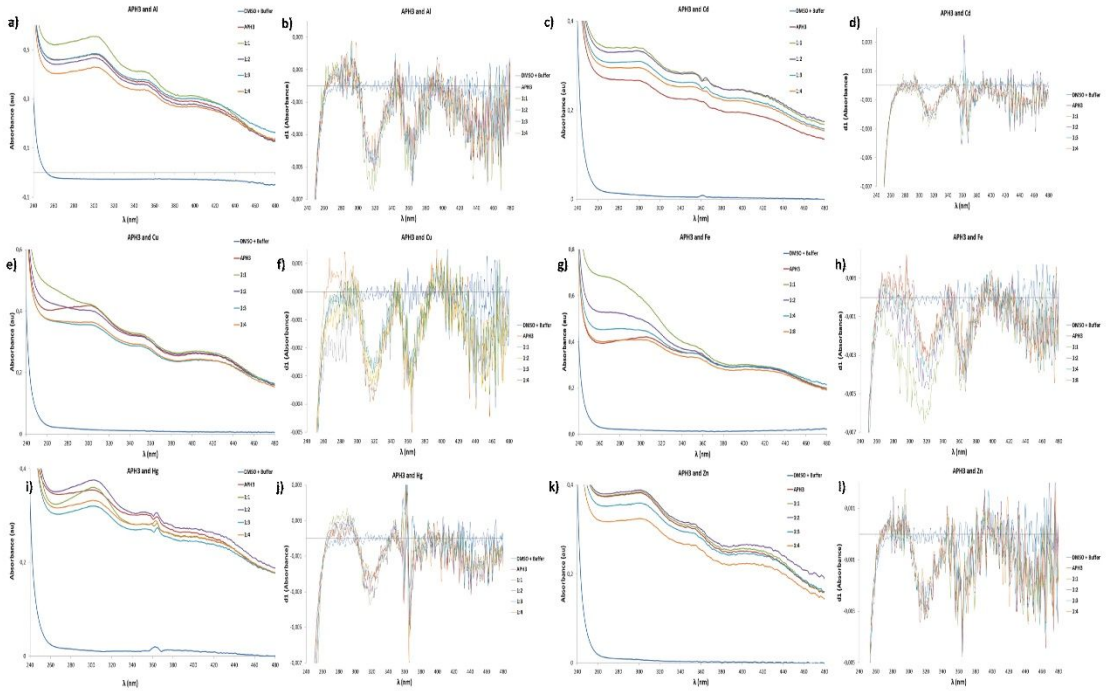


Figure S5. Figure S4. UV-Vis spectra (a, c, e, g, i and k) and first-order derivative absorption spectra (b, d, f, h, j and l) of **APH3** alone and in the presence of metals in buffer (100 mM phosphate, pH= 7.30) at room temperature. [**APH3**] = 50 µM and [Metal] = 50, 25, 12.5 and 6.25 µM corresponding to stoichiometries 1:1, 1:2, 1:4 and 1:8, respectively.

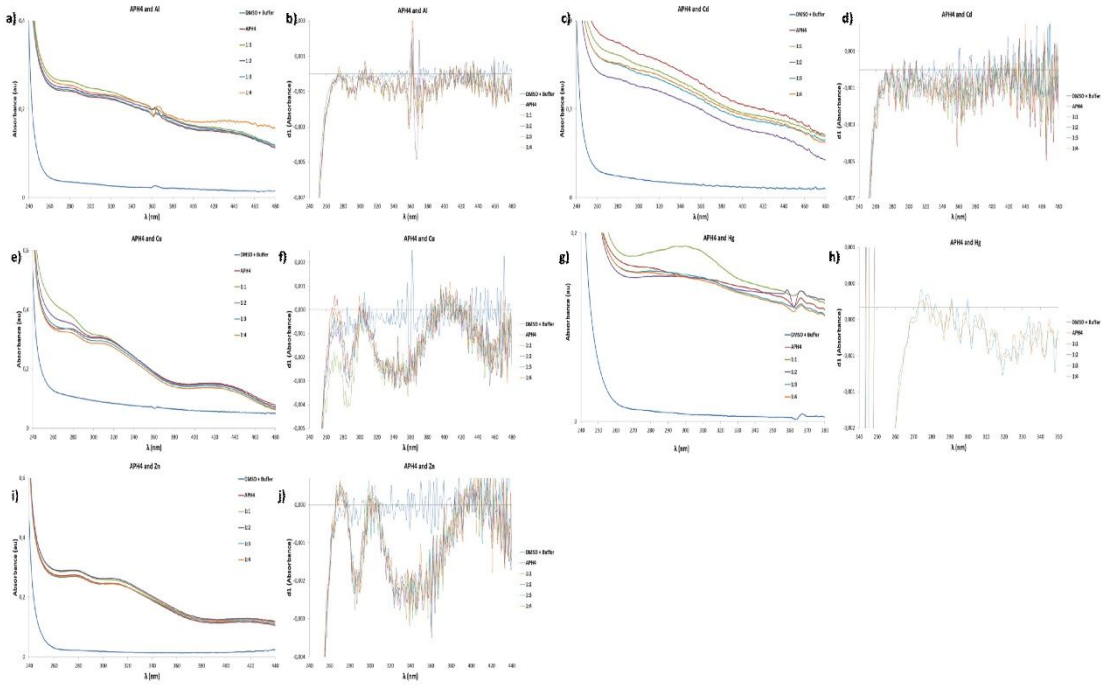


Figure S6. UV-Vis spectra (a, c, e, g and i) and first-order derivative absorption spectra (b, d, f, h and j) of **APH4** alone and in the presence of metals in buffer (100 mM phosphate, pH= 7.30) at room temperature. [**APH4**] = 50 µM and [Metal] = 50, 25, 12.5 and 6.25 µM corresponding to stoichiometries 1:1, 1:2, 1:4 and 1:8, respectively.

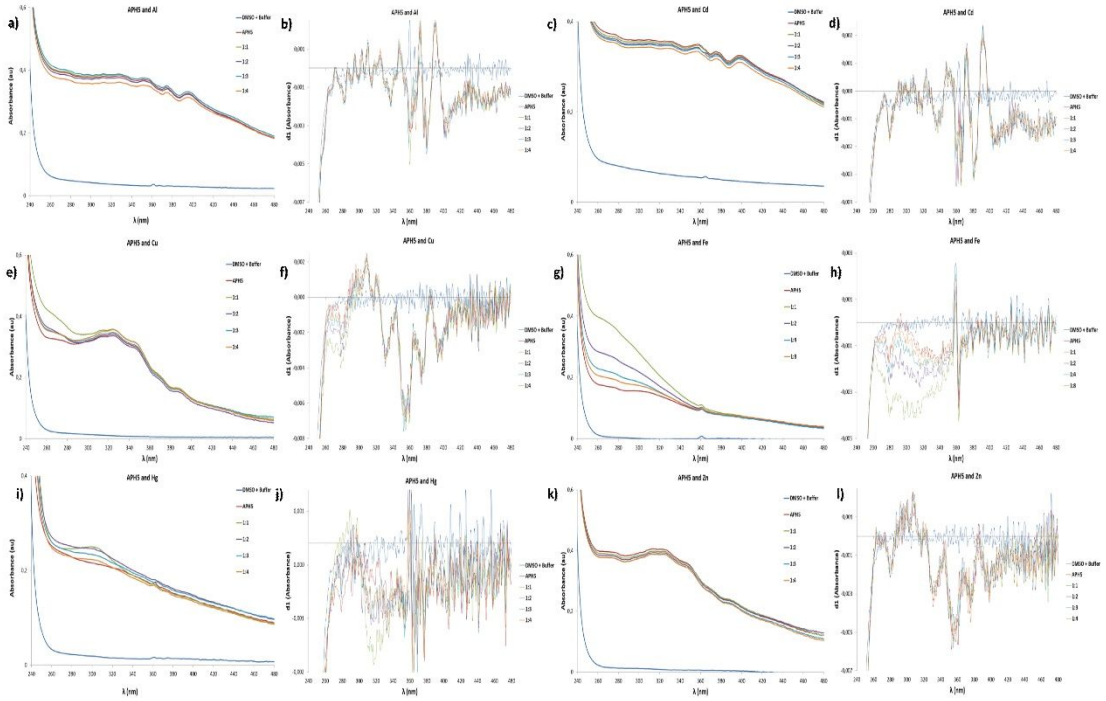


Figure S7. UV-Vis spectra (a, c, e, g, i and k) and first-order derivative absorption spectra (b, d, f, h, j and l) of **APH5** alone and in the presence of metals in buffer (100 mM phosphate, pH= 7.30) at room temperature. [**APH5**] = 50 μM and [Metal] = 50, 25, 12.5 and 6.25 μM corresponding to stoichiometries 1:1, 1:2, 1:4 and 1:8, respectively.

Table S1. HOMO/LUMO gap energy analysis.

Compounds	LUMO (eV)	HOMO (eV)	Gap (eV)
APH1	-3.386	-10.435	7.049
APH2	-3.361	-11.160	7.799
APH3	-3.543	-8.037	4.494
APH4	-3.456	-9.438	5.982
APH5	-3.652	-10.295	6.643
APH1Fe	-10.205	-11.122	0.917
APH2Fe	-9.051	-9.763	0.712
APH3Fe	-7.018	-10.940	3.922
APH4Fe	-7.450	-7.595	0.145
APH5Fe	-7.419	-7.718	0.299

Table S2. ADMET prediction of APH compounds.

	APH1	APH2	APH3	APH4	APH5
Caco-2 permeability Value/Probability	Yes, (0.66)[a]	Yes, (0.71)[a]	Yes, (0.71)[a]	Yes, (0.66)[a]	Yes, (0.67)[a]
GI absorption Value/Probability	Yes, (0.98)[a]; High[b]	Yes, (0.98)[a]; High[b]	Yes, (0.98)[a]; High[b]	Yes, (0.97)[a]; High[b]	Yes, (0.96)[a]; High[b]
BBB permeant Value/Probability	Yes, (0.99)[a]; Yes[b]	Yes, (0.98)[a]; No[b]	Yes, (0.99)[a]; No[b]	Yes, (0.98)[a]; No[b]	Yes, (0.99)[a]; No[b]
CYP1A2 inhibitor Value/Probability	Yes, (0.82)[a]; Yes[b]	Yes, (0.79)[a]; Yes[b]	Yes, (0.79)[a]; Yes[b]	Yes, (0.82)[a]; Yes[b]	Yes, (0.82)[a]; Yes[b]
CYP2C19 inhibitor Value/Probability	No, (0.53)[a]; Yes[b]	Yes, (0.84)[a]; Yes[b]	No, (0.81)[a]; Yes[b]	Yes, (0.93)[a]; Yes[b]	Yes, (0.53)[a]; Yes[b]
CYP2C9 inhibitor Value/Probability	No, (0.59)[a]; No[b]	Yes, (0.84)[a]; No[b]	No, (0.80)[a]; No[b]	Yes, (0.93)[a]; Yes[b]	Yes, (0.53)[a]; No[b]
CYP2D6 substrate Value/Probability	No, (0.67)[a]; Yes[b]	No, (0.82)[a]; No[b]	No, (0.84)[a]; No[b]	No, (0.83)[a]; Yes[b]	No, (0.80)[a]; No[b]
P glycoprotein substrate Value/Probability	No, (0.70)[a]; Yes[b]	No, (0.83)[a]; Yes[b]	No, (0.76)[a]; Yes[b]	No, (0.58)[a]; Yes[b]	No, (0.88)[a]; Yes[b]

[a]Prediction with ADMETsar version 2 (Probability). [b]Prediction with Swiss ADME.

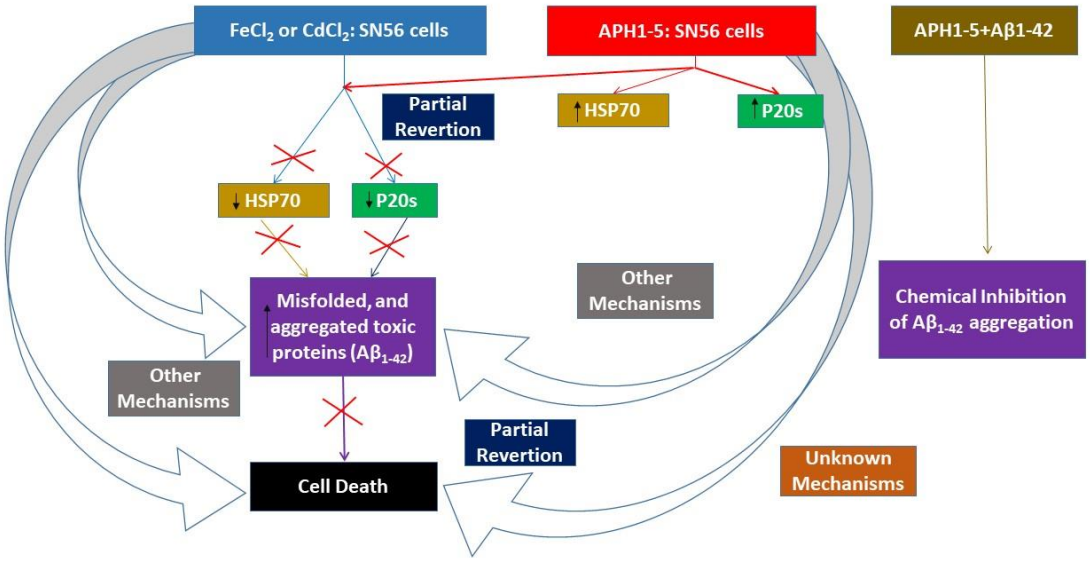
Artículo 2: <u>Mecanismos neuroprotectores de derivados multi-diana de la 7-aminofenantridin-6(5H)-ona frente a la generación y agregación de proteínas amiloides inducida por metales</u>

Neuroprotective mechanisms of multi-target 7-aminophenanthridin-6(5H)-one derivatives against metal-induced amyloid proteins generation and aggregation

Paula Moyano,‖ <u>David Vicente-Zurdo,‖</u> Cristina Blázquez-Barbadillo, J. Carlos Menéndez, Juan F. González, Noelia Rosales-Conrado, Javier del Pino

‖Autores con igual contribución

Food and Chemical Toxicology 167 (2022) 113264 (*Impact factor: 5.572*)



Food and Chemical Toxicology 167 (2022) 113264

Contents lists available at ScienceDirect

Food and Chemical Toxicology

journal homepage: www.elsevier.com/locate/foodchemtox

Neuroprotective mechanisms of multitarget 7-aminophenanthridin-6(5H)-one derivatives against metal-induced amyloid proteins generation and aggregation

Paula Moyano [a,1], David Vicente-Zurdo [b,1], Cristina Blázquez-Barbadillo [c], J. Carlos Menéndez [c], Juan F. González [c,***], Noelia Rosales-Conrado [b,**], Javier del Pino [a,*]

[a] Departamento de Farmacología y Toxicología, Facultad de Veterinaria, Universidad Complutense, 28040, Madrid, Spain
[b] Departamento de Química Analítica, Facultad de Ciencias Químicas, Universidad Complutense, 28040, Madrid, Spain
[c] Unidad de Química Orgánica y Farmacéutica, Departamento de Química en Ciencias Farmacéuticas, Facultad de Farmacia, Universidad Complutense, 28040, Madrid, Spain

ARTICLE INFO

Handling Editor: Dr. Jose Luis Domingo

Keywords:
Phenanthridones
SN56 basal forebrain cholinergic neurons
Metal neurotoxicity
HSP70
Proteasome 20S
Amyloid proteins

ABSTRACT

Brain's metals accumulation is associated with toxic proteins, like amyloid-proteins (Aβ), formation, accumulation, and aggregation, leading to neurodegeneration. Metals downregulate the correct folding, disaggregation, or degradation mechanisms of toxic proteins, as heat shock proteins (HSPs) and proteasome. The 7-amino-phenanthridin-6(5H)-one derivatives (**APH**) showed neuroprotective effects against metal-induced cell death through their antioxidant effect, independently of their chelating activity. However, additional neuroprotective mechanisms seem to be involved. We tested the most promising **APH** compounds (**APH1-5**, 10–100 μM) chemical ability to prevent metal-induced Aβ proteins aggregation; the **APH1-5** effect on HSP70 and proteasome 20S (P20S) expression, the metals effect on Aβ formation and the involvement of HSP70 and P20S in the process, and the **APH1-5** neuroprotective effects against Aβ proteins (1 μM) and metals in SN56 cells. Our results show that **APH1-5** compounds chemically avoid metal-induced Aβ proteins aggregation and induce HSP70 and P20S expression. Additionally, iron and cadmium induced Aβ proteins formation through downregulation of HSP70 and P20S. Finally, **APH1-5** compounds protected against Aβ proteins-induced neuronal cell death, reversing partially or completely this effect. These data may help to provide a new therapeutic approach against the neurotoxic effect induced by metals and other environmental pollutants, especially when mediated by toxic proteins.

1. Introduction

Neurodegenerative diseases are the second global cause of death, and their incidence and prevalence have risen continually and drastically, being expected to continue increasing in the coming years (GBD 2016 Neurology Collaborators, 2019). The neurodegenerative disease causes are not well known, but it is believed that they are a combination of a genetic predisposition and environmental factors (Cannon and Greenamyre, 2011; Chin-Chan et al., 2015; Mir et al., 2020; Strafella et al., 2018). Parallel to the increase in the number of patients with neurodegenerative diseases, there has been an increase in the environmental pollutant levels that could explain this increment. Environmental pollutants exposure reproduces the main neurodegenerative disease hallmarks in animals and *in vitro* studies, supporting their plausible involvement in these diseases (Acevedo et al., 2019; Chen et al., 2016; Chin-Chan et al., 2015; Crichton et al., 2008; White et al., 2015).

* Corresponding author. Pharmacology and Toxicology Department, Veterinary School, Complutense University of Madrid, Avda. Puerta de Hierro s/n, 28040, Madrid, Spain.
** Corresponding author. Analytical Chemistry Department, Chemistry Sciences School, Complutense University of Madrid, Avda. Puerta de Hierro s/n, 28040, Madrid, Spain.
*** Corresponding author. Chemistry in Pharmaceutical Sciences, Department Pharmacy School Complutense University of Madrid, Avda. Puerta de Hierro s/n, 28040, Madrid, Spain.
E-mail addresses: jfgonzal@ucm.es (J.F. González), nrosales@ucm.es (N. Rosales-Conrado), jdelpino@pdi.ucm.es (J. Pino).
[1] Authors with equal contribution.

https://doi.org/10.1016/j.fct.2022.113264
Received 26 March 2022; Received in revised form 28 May 2022; Accepted 24 June 2022
Available online 30 June 2022
0278-6915/© 2022 The Authors. Published by Elsevier Ltd. This is an open access article under the CC BY-NC-ND license (http://creativecommons.org/licenses/by-nc-nd/4.0/).

Abbreviations

Aβ	Amyloid beta proteins
ACTB	beta-actin
AD	Alzheimer's disease
ANOVA	Analysis of variance
APH	7-amino-phenanthridin-6(5H)-one derivatives
APP	amyloid-precursor-protein
AR	androgen receptor
BF	basal forebrain
BFCN	BF cholinergic neurons
BSA	bovine serum albumin
ChAT	acetylcholine transferase
DMEM	Dulbecco's Modified Eagle's Medium
DMSO	dimethyl sulfoxide
ER	estrogen receptor
FBS	fetal bovine serum
GR	glucocorticoid receptor
hERG	human ether-a-go-go related gene
HSP	heat shock protein
MMP	Matrix metalloproteinase
MTT	3-[4,5-dimethylthiazol-2-yl]-2,5-diphenyl-tetrazolium bromide
NRF2	nuclear factor erythroid 2-related factor 2
NRF1	nuclear respiratory factor 1
OS	oxidative stress
PBS	phosphate-buffered saline
PPAR	peroxisome proliferator-activated receptor
P26S	proteasome 26S
P20S	proteasome 20S
P19S	proteasome 19S
ROS	reactive oxygen species
RHSP70	recombinant HSP70 protein
RP20S	recombinant P20S protein
SEM	standard error of the mean
TEM	transmission electron microscope
THR	thyroid receptor

Heavy metals exposure has increased due to their widespread use for many industrial applications, being a cause of concern since they are highly toxic environmental pollutants and could accumulate in the body for years, producing toxic effects (Cannon and Greenamyre, 2011; Chen et al., 2016; Chin-Chan et al., 2015; Mir et al., 2020). In this regard, brain accumulation of different heavy metals, especially aluminum (Al), mercury (Hg), and cadmium (Cd), was associated with the development of neurodegenerative diseases (Chen et al., 2016; Chin-Chan et al., 2015; Moyano et al., 2018). Additionally, essential metal brain dyshomeostasis, especially, iron (Fe), copper (Cu) and zinc (Zn) was also associated with the development of neurodegenerative diseases (Acevedo et al., 2019; Choi et al., 2020; Crichton et al., 2008; Gozzelino and Arosio, 2016; White et al., 2015; Zheng and Monnot, 2012).

The most relevant neurodegenerative diseases are considered proteinopathies since the normal structure and conformation of specific proteins is altered, or the aggregation of specific toxic proteins is produced, leading to neurodegeneration and neuronal loss (Campanella et al., 2018; Bovolenta et al., 2017; Erkkinen et al., 2018; Katsnelson et al., 2016). In this context, certain metals have been described to induce the cellular formation, accumulation, and deposit of toxic misfolded proteins, which trigger neurodegeneration (Acevedo et al., 2019; Chen et al., 2016; Crichton et al., 2008; Dales and Desplat-Jégo, 2020; Wright and Baccarelli, 2007). Alzheimer's disease (AD) is the most prevalent neurodegenerative disease (Grothe et al., 2016), being characteristic the formation, accumulation, and aggregation of amyloid beta (Aβ) proteins, among other toxic proteins that induce selective neurodegeneration and basal forebrain (BF) cholinergic neuronal loss (Kwakowsky et al., 2016). Heat shock proteins (HSP) and proteasome 26S (P26S), formed by proteasomes 19S (P19S) and 20S (P20S, the catalytic core) mediate the degradation of misfolded, oxidized and aggregated toxic proteins such as Aβ, together with other mechanisms (Cao et al., 2019; Esser et al., 2004; Leak, 2014; Maiti et al., 2014). HSP70 was reported to prevent the accumulation and aggregation of toxic proteins like Aβ, avoiding neuronal damage and loss (Gorantla and Chinnathambi, 2018; Campanella et al., 2018; Wilhelmus et al., 2006). HSPs and P20S expression or activity were reported to be altered after metals exposure, producing neuronal damage and loss (Asthana et al., 2014; Chen et al., 2018; Chernyak and Merinova 2017; Dunham et al., 2017; Figueiredo et al., 2016; Gerspacher et al., 2009; Kumar et al., 2018; Moyano et al., 2020; Verma et al., 2020). Thus, a therapeutic approach to treat the neurodegeneration induced by the toxic proteins could be the discovery of new therapeutic agents that mediate the induction of HSP and P20S expression.

We recently described the multitarget profile of phenanthridin-6(5H)-one derivatives (**APH**), with matrix metalloproteinases (MMPs) inhibition and antioxidant properties (Rocchi et al., 2021). Additional studies showed that the safest and most active compounds for these effects were **APH1-5** (Fig. 1), which present metal-selective chelating activity, chelating Fe, Cu and Hg, but not Al, Cd and Zn. We found that APHs are able to protect neurons, completely or partially, against oxidative stress, through the induction of nuclear factor erythroid 2-related factor 2 (NRF2) pathway, and against the reduction of SN56 neuronal viability induced by all these metals, suggesting that **APH1-5** compounds display additional neuroprotection mechanisms (Moyano et al., 2021). NRF2 regulates the expression of HSPs and P26S components, which, under stress situations, are induced through upregulation of NRF2 (Chapple et al., 2012; Kim et al., 2017; Ramos et al., 2018). Therefore, we hypothesized that **APH1-5** compounds could also mediate their neuroprotective action through reduction of the levels of toxic proteins, such as Aβ proteins, by the induction of HSP70 and proteasome P20S expression.

Furthermore, another approach to AD treatment is the search for $A\beta_{1-42}$ aggregation inhibitors. Numerous planar non-polar aromatic small molecules such as naphthalene sulfonates, congo-red, thioflavin and curcumin have been identified as inhibitors of Aβ aggregation acting by intercalation agents between the β-sheets, through π-stacking interactions (Biancalana and Koide, 2010; Maezawa et al., 2008). In this sense, we also hypothesized that the phenanthridone core of the APH compounds could prevent Aβ aggregation, due to their planarity and the presence of aromatic rings, which could be intercalated between the β-sheets of the Aβ proteins.

To test these hypotheses we pre-treated wild type or βAPP, HSP70 and/or P20S silenced SN56 cholinergic neurons from basal forebrain, the main brain cholinergic region where selective damage on cholinergic neurons is observed in AD (Do Carmo et al., 2021), as a model of basal forebrain cholinergic neurons (BFCN) *in vitro*, with or without **APH1-5** compounds (10–100 μM), and then treated with or without $FeCl_2$ (200 μM) or $CdCl_2$ (100 μM), as models of essential and heavy metals that are chelated and not chelated by **APH1-5** compounds, respectively (Moyano et al., 2021), and with or without rHSP70 (30 μM) and/or rP20S(25 μM). We also examined their protective effects against β-amyloid-induced neurodegeneration.

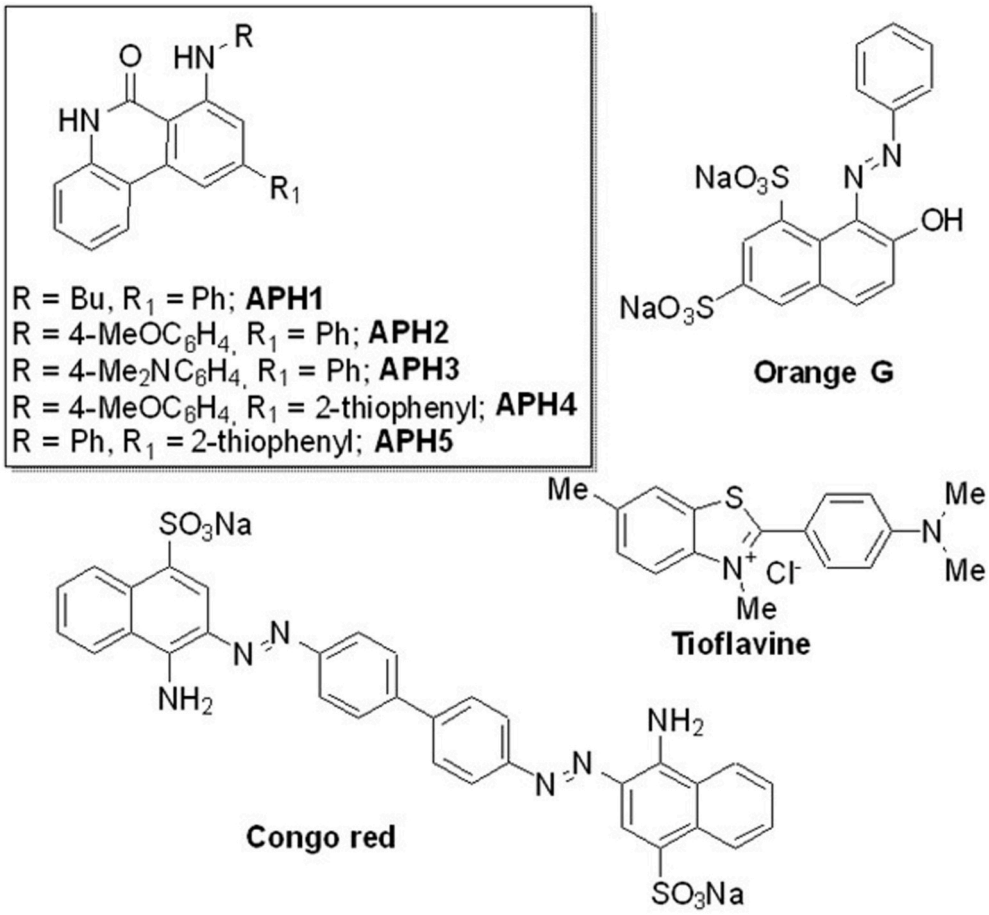


Fig. 1. Chemical structures of **APH** compounds and known inhibitors of Aβ aggregation.

2. Materials and methods

2.1. Chemicals and standards

All reagents and solvents used were of analytical grade. Methanol, dimethyl sulfoxide (DMSO) and hydrochloric acid were provided by Scharlab (Barcelona, Spain). Milli-Q water (Millipore, Madrid, Spain) was employed for all the experiments. $FeCl_2$, $CuCl_2$, $ZnCl_2$, $CdCl_2$, $HgCl_2$ and $AlCl_3$ were purchased from Merck (Madrid, Spain). The **AHP1-5** compounds were synthesized by our group following the protocol previously described (Rocchi et al., 2021; Moyano et al., 2021). Poly-L-lysine, dibutyryl-cAMP, retinoic acid, 3-[4,5-dimethylthiazol-2-yl]-2,5-diphenyl-tetrazolium bromide (MTT), amyloid β protein fragment 1–42 ($A\beta_{1\text{-}42}$, A9810) and 1,1,1,3,3,3-hexafluoro-2-propanol used to pre-treat $A\beta_{1\text{-}42}$ proteins were purchased from Sigma-Aldrich (Madrid, Spain).

2.2. $A\beta_{1\text{-}42}$ aggregation assays

The $A\beta_{1\text{-}42}$ pre-treatment was performed as described by Vicente-Zurdo et al. (2020), using a SpeedVac Concentrator Plus (Eppendorf, Madrid, Spain) and a WX vortex mixer (VELP Scientifica, Usmate, Italy). For incubation assays, pre-treated $A\beta_{1\text{-}42}$ monomer was thawed at room temperature for 10 min. Then, DMSO was added to the monomer to obtain a 5 mM solution, which was sonicated for 10 min. After sonication, 10 mM HCl solution was added to obtain a 200 μM $A\beta_{1\text{-}42}$ working solution. Stock metals solutions of 200 μM (Fe(II), Cu(II), Zn (II), Cd(II), Hg(II), and Al(III)) and organic compounds (**APH1**, **APH2**, **APH3**, **APH4** and **APH5**) under assay were prepared daily. Working solutions of $A\beta_{1\text{-}42}$ + metal (50 μM + 50 μM) and $A\beta_{1\text{-}42}$ + metal + **APH** compounds (50 μM + 50 μM + 50 μM) were prepared by diluting the stock solutions in 10 mM HCl. We chose the 50 μM concentration for metals, **APH1-5** compounds, and $A\beta_{1\text{-}42}$ proteins, to evaluate metal- and/or APH-$A\beta_{1\text{-}42}$ interactions since it was the most appropriate $A\beta_{1\text{-}42}$ concentration for Aβ fibrils aggregation TEM analysis (Vicente-Zurdo et al., 2020), and because it is a safe and neuroprotective **APH1-5** concentration (Rocchi et al., 2021; Moyano et al., 2021). Finally, it was also chosen because the main common stoichiometry for the formed complexes between **APH** compounds and tested metals (Fe, Cu, Zn, Hg, Cd and Al) was 1:1 metal/compound molar ratio (Moyano et al., 2021).

To test the inhibition of the metal-induced $A\beta_{1\text{-}42}$ aggregation for each **APH** compound, working solutions were incubated for 48 h at 37 °C, using a Thermo Scientific MaxQ 4000 incubator from Fisher Scientific (Madrid, Spain). Using a negative staining with uranyl acetate 2% (w/v) over the copper grid for 5 min, samples were analyzed employing a transmission electron microscope (TEM) (JEM-1400 Plus, JEOL, Tokyo, Japan) at 100 kV. Measurements of $A\beta_{1\text{-}42}$ fibrils width were performed using the ImageJ software (n = 20). To evaluate the inhibition of the amyloid β aggregation and the reduction in the fibril width by **APH1-5** compounds, samples of $A\beta_{1\text{-}42}$ alone, $A\beta_{1\text{-}42}$ + **APH** compounds, $A\beta_{1\text{-}42}$ + metals, and $A\beta_{1\text{-}42}$ + **APH** compounds + metals were compared. The metals used were chosen as they have been described to produce neurodegenerative effects and were suggested to be involved with neurodegenerative diseases (Cannon and Greenamyre, 2011; Chin-Chan et al., 2015; Mir et al., 2020).

2.3. Culture of SN56 cells

The cholinergic murine neuroblastoma SN56 cell line, which is derived from BF septal neurons (Hammond et al., 1990), was used to

evaluate $A\beta_{1\text{-}42}$, $FeCl_2$ and $CdCl_2$ toxic effects on this specific type of neurons and the **APH1-5** compounds neuroprotective mechanisms against these effects. The cells were kept at 37 °C and 5% CO_2 in a Dulbecco's Modified Eagle's Medium (DMEM) that was supplemented with 2 mM L-glutamine, penicillin/streptomycin, and 10% fetal bovine serum (FBS) obtained from Sigma (Madrid, Spain), and 1 mM sodium pyruvate, that was used as maintenance medium. Every 48 h the medium was changed (Hudgens et al., 2009). A 3-4-fold increase of ChAT activity and acetylcholine level in the cells were generated to morphologically mature cells by culturing them for 3 days with 1 mM dibutyryl-cAMP and 1 μM retinoic acid as previously described (Bielarczyk et al., 2003; Szutowicz et al., 2006). Differentiation renders the cells more sensitive to neurotoxic compounds that affect cholinergic pathways (Bielarczyk et al., 2003; Szutowicz et al., 2006). Cells were checked for absence of mycoplasma infection with the Look Out Mycoplasma PCR Detection Kit (Sigma, Madrid, Spain).

Cells were seeded in 6-well plates at a density of 10^6 cells/well. Wild type or βAPP, HSP70 and/or P20S silenced cells pre-treated or not with **APH1-5** compounds, at various concentrations (10–100 μM) for 2 h, were treated for 24 h with $FeCl_2$ (200 μM), $CdCl_2$ (100 μM), or $A\beta_{1\text{-}42}$ (1 μM) with or without rP20S (25 μM) and with or without rHSP70 (30 μM). At least 3 replicate wells/treatment were used. A vehicle group was employed in parallel for each experiment as a control.

The **APH1-5** compounds selected from the **APH** library were the ones with less cytotoxic effects and the ones that presented the most potent antioxidant and neuroprotective effect against ROS stimulus and metals (Fe, Cd, Al, Zn, Cu, Hg) toxic effects in SN56 cells (Rocchi et al., 2021; Moyano et al., 2021). The concentrations chosen (10 μM–100 μM) did not manifest cytotoxic effects, but presented the neuroprotective effect indicated in SN56 cells. We selected 50 μM concentration, the minimum concentration to induce neuroprotective effects for all **APH** compounds in SN56 cells following single pre-treatment against metal-induced toxic effects (Moyano et al., 2021) to elucidate the possible effect of **APH1-5** compounds on $A\beta_{1\text{-}42}$ protein levels and the mechanisms of neuroprotection against $A\beta_{1\text{-}42}$ proteins- and metals-induced cytotoxicity. We selected the lowest concentrations of rHSP70 (30 μM) and rP20S (25 μM) that induce the maximum reversion on the metal-induced $A\beta_{1\text{-}42}$ protein levels increase. Finally, the metals' concentrations employed were chosen since they produce cell death (data not shown). $A\beta_{1\text{-}42}$ proteins were used since they were described to be the most cytotoxic amyloid proteins (Klein et al., 1999).

APH4, the most neuroprotective **APH1-5** compound against metal-induced cytotoxicity (Moyano et al., 2021), was chosen to determine the involvement of HSP70 and P20S induction in the neuroprotective action of **APH1-5** compounds against caspases 3/7 activation, $A\beta_{1\text{-}42}$ protein levels increase and cell death.

2.4. Real-time PCR analysis

Total RNA was extracted through the Trizol reagent method (Invitrogen, Madrid, Spain). Final RNA concentration and quality of total RNA samples were determined and assessed, respectively, with a spectrophotometer Nanodrop 2000 (Thermo Fisher Scientific, Madrid, Spain) and with an Experion Lab Chip (Bio-Rad, Madrid, Spain) gel. An amount of 1000 ng of cRNA were used to synthesize, with a PCR array first strand-synthesis kit (C-02; Super Array Bioscience, Madrid, Spain), first-strand cDNA following the manufacturer's instructions, with added external RNA controls and genomic DNA elimination step. Following reverse transcription, prevalidated primer sets (SuperArray Bioscience) for mRNAs encoding HSP701A (catalog number PPM04801F), P20S (catalog number PPM30970A), β-amyloid-precursor-protein (βAPP; catalog number PPM37085A), and ACTB (PPM02945B), were used to perform QPCR. Internal control for normalization used was ACTB. Real-Time SYBR Green PCR master mix PA-012 (SuperArray Bioscience) was used for reactions running on a CFX96. The parameters set on the thermocycler were 95 °C for 10 min, followed by 40 cycles of 95 °C for 15 s and 72 °C for 30 s. Relative changes in gene expression were calculated using the Ct (cycle threshold) method. The expression data are presented as actual change multiples (Livak and Schmittgen, 2001).

2.5. Protein determination

Fresh protease inhibitors cocktail (ThermoFisher Scientific, Madrid, Spain) was added to RIPA buffer (Thermo Scientific, Madrid, Spain) at the end of the treatments, to collect, by scrapping, and lyse SN56 cells that had been previously washed with pre-chilled PBS. Cell lysate supernatant was collected after 10,000×*g* centrifugation at 4 °C for 10 min. Protein concentration was assayed using a BCA kit (Thermo Fisher Scientific, Madrid, Spain) and normalized.

HSP701A and P20S protein levels were measured by ELISA kits (MBS760601, and MBS8805890, respectively; MyBioSource, CA, USA), following the producer's guidelines. A negative control was used to check that there were no interferences between **APH1-5** or metals and kits' reagents. Protein concentrations of each target gene were normalized with the total protein concentration determined by BCA kit, to avoid deviation of the real value proteins content due to the induction of cell death. Protein content was determined as ng/mg of protein.

2.6. Beta-amyloid levels analysis

To remove cell debris, media from control and treated cultures (from 6 well plates per sample) was centrifuged at 4 °C for 120 min at 3000×*g* after being collected. Cultures were incubated on ice for 5 min after scrapping in 100 μL cold homogenizing buffer (50 mM Tris, pH 7.6, 1 mM EDTA, 150 mM NaCl, 1% Triton X-100, phosphatase, and protease inhibitors; Sigma, Madrid, Spain) following washing with phosphate-buffered saline (PBS; Sigma, Madrid, Spain). Supernatant obtained from centrifugation at 14,000×*g* for 10 min at 4 °C of lysates was saved for analysis. Determination of $A\beta_{1\text{-}42}$ (catalog number KMB3441) was performed by analysis of media and cell lysates using Invitrogen's ELISA tests (Madrid, Spain), following the manufacturer's protocols. Standards and samples (100 μL/well) were added to a 96-well plate. Content of wells was removed following 2 h of incubation, then they were washed and a detection antibody (100 μL) was added and incubated for another 1 h. Horseradish-peroxidase-labeled anti-detection antibody (100 μL) was added following a second removal and washing of wells and incubated for 30 min. Reaction was finished by adding the stop solution following last plate content was discarding and washing that was followed by incubation at room temperature in dark for 20–30 min after addition of stabilized chromogen (100 μL). The absorbance was recorded at 450 nm with a Fluoroskan FL microplate reader (Thermo Fisher, Madrid, Spain). Resulted peptides concentrations (pg/mL) were normalized with the total protein concentration (μg/mL), resulting in pg/μg units.

2.7. Measurement of cell viability (MTT assay)

Cell viability was determined following 24 h single $A\beta_{1\text{-}42}$ protein, $FeCl_2$ or $CdCl_2$ treatment of SN56 cells, by MTT assay. The assay is based on the cleavage of the yellow tetrazolium MTT salt to purple formazan crystals by mitochondrial dehydrogenase. Cells were incubated in yellow MTT solution at a final concentration of 0.5 mg/mL for 4 h after treatment with $A\beta_{1\text{-}42}$ protein. Following incubation at 37 °C, the resulted formazan product obtained after medium removal was dissolved in 250 μL DMSO. The formation of solubilized formazan product was measured spectrophotometrically at 570 nm (Fluoroskan Ascent FL Microplate Fluorometer and Luminometer, ThermoFisher Scientific, Madrid, Spain). Control cells treated with vehicle were taken as 100% viability.

2.8. Caspase activity analysis

Induction of apoptosis was detected following $A\beta_{1\text{-}42}$ protein treatment of SN56 cells by Caspase-Glo 3/7 luminescence assay kits (Promega, Madrid, Spain), according to the manufacturer's protocol. In brief, at the end of treatment, culture cells were scraped and collected in a microfuge tube in the dark after being washed with phosphate-buffered saline (PBS). Luminescence resulting from incubation in white-walled 96-well plates, at room temperature in the dark for 1 h, of equal volumes of reagent and cell lysis buffer was read in a PerkinElmer LS50B plate-reading spectrometer (PerkinElmer, Madrid, Spain). The luminescence of each sample was measured. The experiments were performed in triplicate.

2.8. Genes knock out.

The silencing of βAPP was performed to determine the involvement of Aβ proteins level increase in the metal-induced cell death. siRNA sets, homologous to mouse βAPP, HSP701A and P20S, were predesigned using the HiPerformance Design Algorithm (Novartis AG, Basel, Switzerland) and purchased from Qiagen (catalog number GS11820, GS193740 and, GS26440 respectively; Barcelona, Spain). βAPP, HSP701A, and P20S siRNAs were transfected into cells, in 6 wellsplates, using HiPerfect Transfection reagent (Qiagen, Barcelona, Spain), according to producer's guidelines. Briefly, 150 ng siRNA diluted in 100 μL culture medium without serum were mixed with 12 μL HiPerfect Transfection reagent per well to form the transfection complex. Cells were incubated with transfection complex under their normal growth conditions. Silencing quality control was performed using the Qiagen's negative control (Barcelona, Spain). Following two days of siRNA introduction into the cells, both efficacy and effectiveness of gene silencing was evaluated through gene and protein expression analysis. Cell viability, following silencing, was analyzed by MTT and Caspases 3/7 assays.

2.9. ADMET properties analysis

In silico assessment of absorption, distribution, metabolism, excretion and toxicity (ADMET) properties predictions of APH compounds was carried out using ADMETsar version 2.0 (http://lmmd. ecust.edu. cn/admetsar2/) software (Cheng et al., 2012; Yang et al., 2019).

2.10. Statistical analysis

In order to evaluate the chemical interaction between the selected **APH** compounds and/or metals with $A\beta_{1\text{-}42}$ proteins, we performed $A\beta_{1\text{-}42}$ fibril width measurements, expressed as mean ± standard deviation (n = 20), and analyzed them through one-way analysis of variance (ANOVA) followed by the Fisher LSD test (95% confidence level). For the *in vitro* studies, at least three replicates for each experimental condition were performed, and the presented results were representative of these replicates. Data are expressed as mean ± standard error of the mean (SEM; n = 9). Comparisons between experimental and control groups were performed by two-ways ANOVA analyses (gene manipulation vs treatment) or one-way ANOVA analyses (analysis of different **APH1-5** compounds concentrations) followed by the Tukey post-hoc test. Statistical differences were accepted when $p \leq 0.05$. Statistical analysis of data was carried out using both GraphPad 5.01 (*in vitro* studies; San Diego, USA) and Statgraphics 19 (chemical interactions; Rockville, USA) softwares.

3. Results

3.1. $A\beta_{1\text{-}42}$ aggregation analysis

$A\beta_{1\text{-}42}$ monomer was incubated during 48 h at 37 °C with different metals salts (Fe^{2+}, Cu^{2+}, Zn^{2+}, Cd^{2+}, Hg^{2+} and Al^{3+}) and tested compounds (**APH1-5**) (Fig. 2 and Supplementary Fig. S1 and S2). We first studied the effect of the **APH1-5** compounds on Aβ aggregation in absence of selected metals, and we observed that in the presence of **APH1-5** compounds, $A\beta_{1\text{-}42}$ fibrils remained disaggregated (**APH2**, as an example in Fig. 1D) than $A\beta_{1\text{-}42}$ alone (Fig. 2A). These results showed that **APH1-5** compounds did not induce $A\beta_{1\text{-}42}$ fibril aggregation. Then, selected metal salts were co-incubated with $A\beta_{1\text{-}42}$ to determine their ability to aggregate amyloid proteins. All tested metal salts induced the aggregation of $A\beta_{1\text{-}42}$ fibrils (Fe- and Hg-induced amyloid aggregation are shown as examples in Fig. 2B and C, respectively). To examine the **APH1-5** compounds inhibition ability on the metal-induced amyloid β

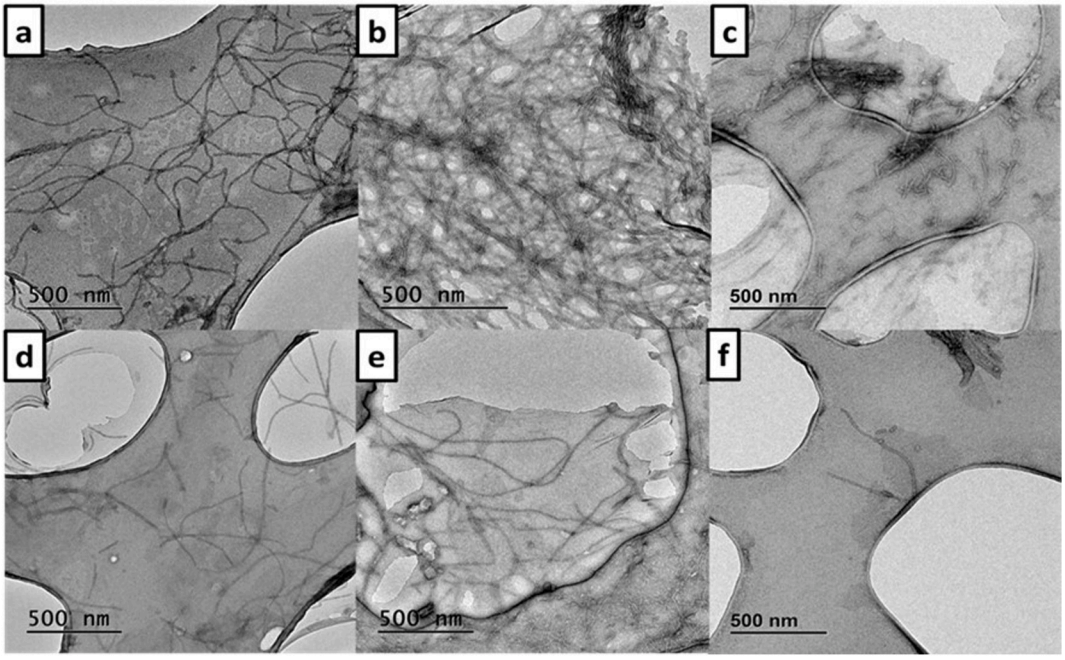


Fig. 2. TEM images of $A\beta_{1\text{-}42}$ aggregation assays under the presence of several metals (50 μM) and APH2, APH3 and APH5 compounds (50 μM): a) $A\beta_{1\text{-}42}$ alone; b) $A\beta_{1\text{-}42}$ + Fe^{2+}; c) $A\beta_{1\text{-}42}$ + Hg^{2+}; d) $A\beta_{1\text{-}42}$ + APH2; e) $A\beta_{1\text{-}42}$ + Fe^{2+} + APH3; f) $A\beta_{1\text{-}42}$ + Hg^{2+} + APH5.

aggregation, they were co-incubated with $A\beta_{1\text{-}42}$ and the selected metal salts. Compounds **APH1-5** were able to inhibit Fe-, Cu-, Zn-, Cd-, Al-, and Hg-induced aggregation, except for **APH1** and **APH4**, which were unable to inhibit it for Zn and Fe, respectively (Fe + **APH3** and Hg + **APH5** as an inhibition example of Fe- and Hg-induced aggregation in Fig. 2E and F, respectively).

TEM analysis also revealed the effects of the **APH1-5** compounds, metals, and **APH1-5** + metals on $A\beta_{1\text{-}42}$ fibrils width (Table 1). The results show that $A\beta_{1\text{-}42}$ fibrils width under the sole presence of **APH1-5** compounds was significantly reduced, but all metals significantly increased the $A\beta_{1\text{-}42}$ fibrils width (Table 1). Especially relevant was the Zn- and Hg-induced $A\beta_{1\text{-}42}$ fibril width increase from 5.4 nm to 13 and 16 nm, respectively (Table 1). All **APH1-5** compounds were able to significantly reduce the metal-induced $A\beta_{1\text{-}42}$ fibrils width increase to original size or even lower (Table 1). The most effective compound in the $A\beta_{1\text{-}42}$ fibrils width reduction due to the Fe-induced aggregation was **APH3**, followed by **APH1**, **APH5** and **APH2** compounds, being the latter similar to **APH4** compound (Table 1). For Cu-induced aggregation, **APH1** and **APH4** compounds presented the highest width reduction; the latter presented a similar reduction to **APH5** compound, which was statistically equal to **APH2** and **APH3** compounds (Table 1). Zn-induced $A\beta_{1\text{-}42}$ fibrils width increase was significantly reduced in presence of all **APH1-5** compounds. **APH2**, **APH3** and **APH4** showed similar behaviour, producing the highest fibril width reduction (Table 1). The reduction in fibril width produced by **APH3** and **APH4** in the presence of Cd was similar, and the effect of **APH4** was analogous to **APH5**; these compounds exhibited the highest reduction effect, followed by **APH2** and then, by **APH1** compounds (Table 1). All **APH1-5** compounds produced an important fibril narrowing of the Hg-induced $A\beta_{1\text{-}42}$ fibrils width increase. Among them, **APH1**, **APH2** and **APH3** compounds showed the most significant reduction, being the behaviour of the latter statistically similar to **APH5**, which was also equal to **APH4** (Table 1). Finally, Al-induced fibril width increase was reduced by all **APH1-5** compounds, being the most important reduction derived from **APH2** and **APH5** compounds, followed by both **APH1** and **APH4**, and finally by **APH3** (Table 1). Consequently, all tested compounds were able to reduce the width of the tested metal-induced fibrils at the 95% confidence level, although the results obtained also show that **APH1-5** compounds acted differently depending on the specific metal co-incubated with $A\beta_{1\text{-}42}$ (Table 1).

Table 1
$A\beta_{1\text{-}42}$ fibrils width (nm) measured from TEM images, corresponding to the incubation of $A\beta_{1\text{-}42}$ with different metals (50 μM) and APH1-5 compounds (50 μM).

Incubation	Without metal (nm)	Fe (nm)	Cu (nm)	Zn (nm)	Cd (nm)	Hg (nm)	Al (nm)
Aβ	5.4 ± 0.7[a]	6.6 ± 0.9[a]	7 ± 1[a]	13 ± 1[a]	6.7 ± 0.7[a]	16 ± 2[a]	8.9 ± 0.8[a]
Aβ + APH1	5 ± 1 [b]	4.2 ± 0.3[c]	3.7 ± 0.4[d]	6 ± 1 [b]	5.3 ± 0.5 [b]	3.8 ± 0.5[d]	4.7 ± 0.7[c]
Aβ + APH2	4.6 ± 0.8 [b]	4.5 ± 0.8[b.c]	4.6 ± 0.6 [b]	4.7 ± 0.5[c]	4.6 ± 0.6[c]	3.6 ± 0.5[d]	4 ± 1[d]
Aβ + APH3	4.3 ± 0.7 [b]	3.4 ± 0.4[d]	4.5 ± 0.5 [b]	4.8 ± 0.4[c]	3.7 ± 0.6[e]	4.1 ± 0.6[c.d]	7.0 ± 0.8 [b]
Aβ + APH4	4.2 ± 0.7 [b]	4.9 ± 0.6 [b]	3.9 ± 0.4[c.d]	4.7 ± 0.9[c]	4.1 ± 0.6[de]	5 ± 1 [b]	4.6 ± 0.7[c]
Aβ + APH5	4.5 ± 0.9 [b]	4.2 ± 0.8[c]	4.3 ± 0.8[b.c]	6 ± 1 [b]	4.2 ± 0.5[d]	4.7 ± 0.8[b.c]	3.5 ± 0.5[d]

Data are expressed as mean ± standard deviation (n = 20). Mean values in the same column with a common letter indicate no significant differences at *p*-values > 0.05, according to ANOVA and Fisher LSD test.

3.2. Analysis of HSP70, and P20S gene expression and proteins content

The protein content of HSP70 (Fig. 3A and B) and P20S (Fig. 3D and E) was reduced, after 24 h $FeCl_2$ (200 μM) and $CdCl_2$ (100 μM) treatment. Pre-treatment with **APH1-5** compounds reverted, in a concentration-dependent way, partially (**APH1** and **APH2** for both metals and proteins) and completely (**APH3** and **APH4** for both metals and proteins, but **APH5** only reversed Cd effect on HSP70 protein) the reduction of HSP70 and P20S expression. This reversion in HSP70 expression started for **APH3-5** compounds at 10 μM concentration, and in P20S expression it started for **APH1-5** compounds at 50 μM concentration, for both metals. These data were similar to those obtained after gene expression analysis (data not shown). Individual and concurrent HSP70 and P20S knockdown induced a pronounced decrease in HSP70 and P20S gene expression (data not shown). HSP70 and P20S knockdown induced a pronounced decrease in HSP70 and P20S protein content (Supplementary Fig. S3). Treatment with **APH4** of HSP70 and P20S knockdown SN56 cells increased the HSP70 and P20S proteins content with respect to control (Supplementary Fig. S3). SN56 cells treatment with **APH1-5** compounds increased HSP70 (Fig. 3C) and P20S protein (Fig. 3F) content.

3.3. Analysis of $A\beta_{1\text{-}42}$ proteins content

The $A\beta_{1\text{-}42}$ protein content (Fig. 4A and B) was increased, after 24 h $FeCl_2$ (200 μM) and $CdCl_2$ (100 μM) treatment. Pre-treatment with **APH1-5** compounds reverted, in a concentration-dependent way, partially (**APH1** and **APH2** for both metals) and completely (**APH3**, **APH4** and **APH5** for both metals) the increase of $A\beta_{1\text{-}42}$ proteins content. This reversion started for compounds **APH3-5** at 10 μM concentration with $CdCl_2$, but for compound **APH5** the neuroprotective effect started at 50 μM concentration for $FeCl_2$. Individual (βAPP, HSP70 or P20S) and concurrent (HSP70 and P20S) gene knockdown did not alter the $A\beta_{1\text{-}42}$ proteins content in SN56 cells (Fig. 4C). Additionally, we found that co-treatment with recombinant P20S (25 μM) and HSP70 (30 μM) proteins or pre-treatment with **APH1-5** compounds did not alter the $A\beta_{1\text{-}42}$ proteins content in SN56 cells (Fig. 4D). Pre-treatment with **APH4** compound of HSP70 or P20S silenced SN56 cells reverted partially the increase of $A\beta_{1\text{-}42}$ proteins content induced by both metals, but this reversion was lower than that observed after **APH4** pre-treatment of wild type cells (Fig. 4C). Pre-treatment with **APH4** compound of concomitant HSP70 and P20S silenced SN56 cells induced a lower reversion on the increase of $A\beta_{1\text{-}42}$ proteins content induced by both metals than that observed after individual silencing (Fig. 4C). Co-treatment with rP20S or rHSP70 of SN56 cells reverted partially the increase of $A\beta_{1\text{-}42}$ proteins content (Fig. 4D) for both metals. The concomitant co-treatment with rP20S and rHSP70 of SN56 cells reverted partially the increase of $A\beta_{1\text{-}42}$ proteins content (Fig. 4D) for both metals.

3.4. Analysis of $CdCl_2$, $FeCl_2$, and $A\beta_{1\text{-}42}$ effect on MTT and caspases 3/7 assays

MTT test was performed to determine cell viability effects following 24 h single $CdCl_2$, $FeCl_2$, or $A\beta_{1\text{-}42}$ proteins (1 μM) treatment with or without pre-treatment with **APH1-5** compounds of wild type or βAPP, HSP70 and/or P20S silenced SN56 cells. After 24 h treatment with $A\beta_{1\text{-}42}$ proteins a decrease in cell viability was observed (Fig. 5A). Pre-treatment with **APH1-5** compounds reverted, in a concentration-dependent way, partially (**APH1**, **APH2** and **APH5**) and completely (**APH3** and **APH4**) the reduction of cell viability induced after $A\beta_{1\text{-}42}$ proteins treatment alone. This reversion started at 10 μM concentration for **AHP2-5**, but **APH1** compound started its neuroprotective effect at 50 μM concentration (Fig. 5A). Individual (βAPP, HSP70 or P20S) or

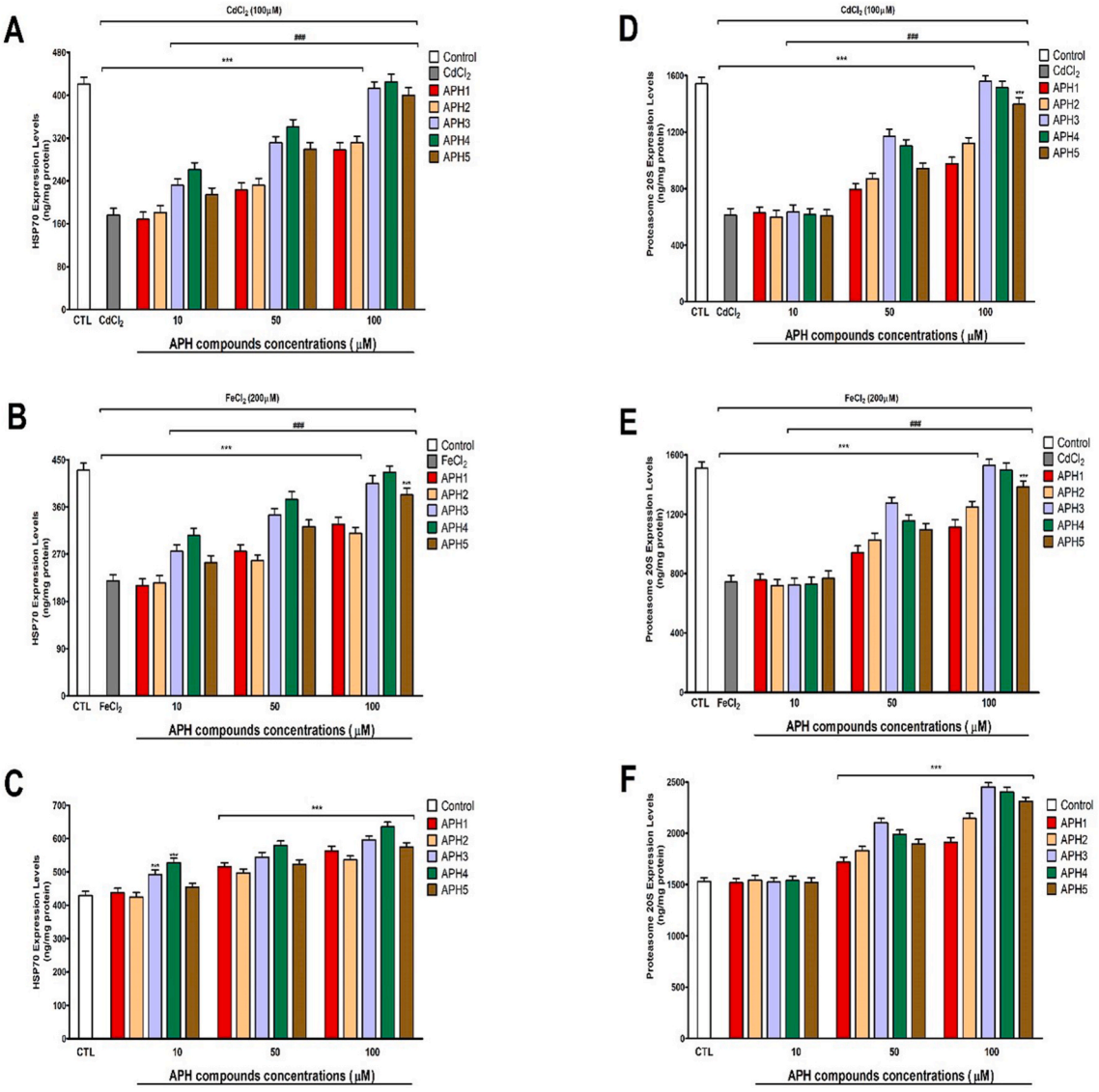


Fig. 3. $CdCl_2$ (100 μM), $FeCl_2$ (200 μM) and/or APH1-5 (10–100 μM) effects on HSP70 (A, B and C) and on P20S (D, E and F) proteins content in SN56 cell homogenates. Data represents the mean ± SEM of three separate experiments from cells of different cultures, each one performed in triplicate. ***$p \leq 0.001$ compared to control. $^{###}p \leq 0.001$ compared to metal treatment.

concomitant (HSP70 and P20S) genes knockdown had no effect on cell viability (Fig. 5C). Knockdown of βAPP, or pre-treatment with **APH4** compound of HSP70 or P20S silenced SN56 cells treated with $CdCl_2$ or $FeCl_2$, reverted partially the reduction of cell viability observed after single metal treatment alone (Fig. 5C). This reversion was lower than that induced after pre-treatment with **APH4** compound of wild type cell for both metals (Fig. 5C). Pre-treatment with **APH4** compound of concomitant HSP70 and P20S silenced SN56 cells, treated with CdCl2 or FeCl2, induced a lower reversion of the cell viability reduction induced by both metals than that observed after individual silencing (Fig. 5C). No significant differences were found between vehicle-treated and control cells data.

Caspases 3/7 activation test was performed as a marker of apoptosis induction. Caspases 3/7 were activated in SN56 cells after $A\beta_{1\text{-}42}$ proteins (Fig. 5B), $CdCl_2$ (Fig. D) or $FeCl_2$ (Fig. 5D) treatment for 24 h. Pre-treatment with **APH1-5** compounds reverted, in a concentration-dependent way, partially (**APH1**, **APH2** and **APH5**) and completely (**APH3** and **APH4**) the caspases activation induced after $A\beta_{1\text{-}42}$ proteins treatment alone. This reversion started for **AHP2-5** compounds at 10 μM concentration, but **APH1** compound started its neuroprotective effect at 50 μM concentration (Fig. 5B). Individual (βAPP, HSP70 or P20S) or concomitant (HSP70 and P20S) gene knockdown had no effect on caspases 3/7 activation (Fig. 5D). Knockdown of βAPP, or pre-treatment with **APH4** compound of HSP70 or P20S silenced SN56 cells treated with $CdCl_2$ or $FeCl_2$, reverted partially the caspases activation observed after single metal treatment alone (Fig. 5D). This reversion was lower than that induced after pre-treatment with **APH4** compound of wild type cell for both metals (Fig. 5D). Pre-treatment with **APH4** compound of concomitant HSP70 and P20S silenced SN56 cells, treated with $CdCl_2$ or $FeCl_2$, induced a lower reversion of the caspases activation induced by both metals than that observed after individual silencing (Fig. 5D). These data show apoptotic cell death induction by $CdCl_2$, $FeCl_2$, and $A\beta_{1\text{-}42}$ proteins and corroborate the MTT results.

3.5. *ADMET predicted properties analysis*

ADMETsar analysis shows that the physicochemical drug-likeness, as a result of the calculated values of molecular weight, alogP, number of atoms, number of rings, H-bond acceptors, and H-bond donors, was positive in all cases. **APH1-5** compounds show a positive predilected

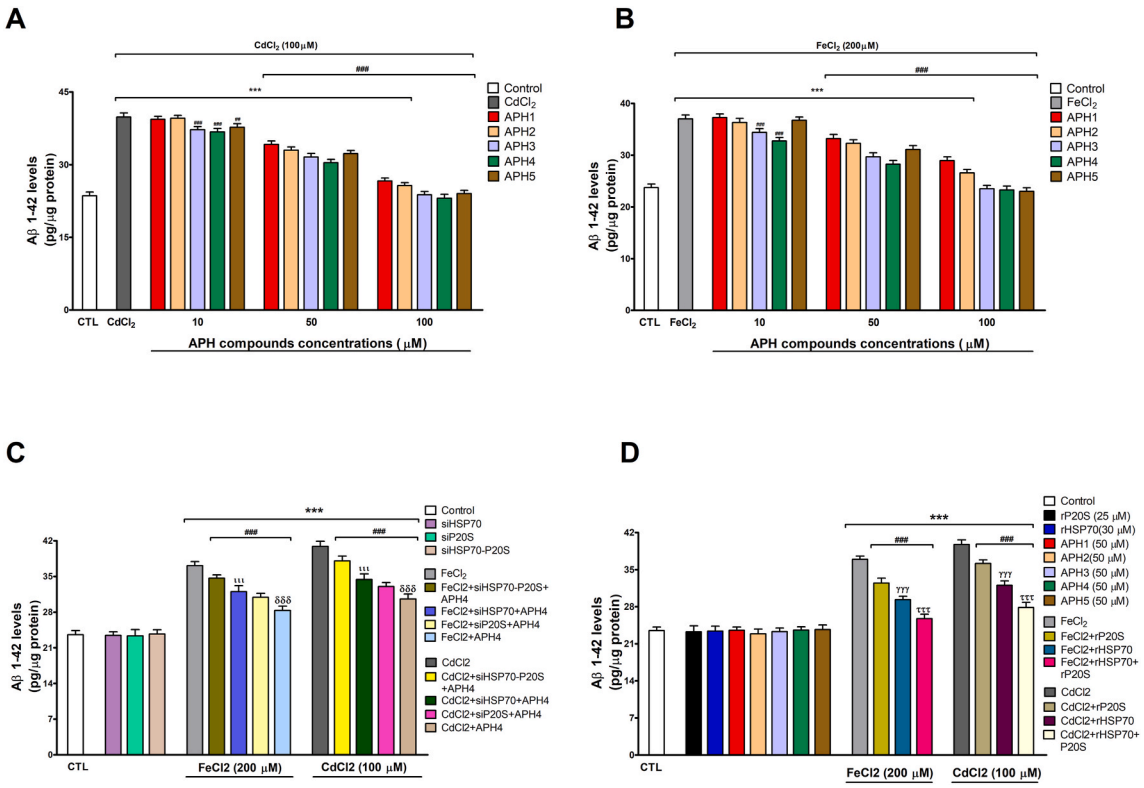


Fig. 4. (A) $CdCl_2$ (100 μM) + APH1-5 (10–100 μM) or (B) $FeCl_2$ (200 μM) + APH1-5 (10–100 μM) effects on $A\beta_{1\text{-}42}$ proteins content. (C) siHSP70, siP20S, siHSP70-P20S, CdCl2 (100 μM) or FeCl2 (200 μM) + APH4 (50 μM), $CdCl_2$ (100 μM) or FeCl2 (200 μM) + siHSP70 and/or siP20S + APH4 (50 μM) effect on $A\beta_{1\text{-}42}$ proteins content in SN56 cell homogenates. (D) APH1-5 (10–100 μM), rHSP70 (30 μM), rP20S (25 μM), $CdCl_2$ (100 μM) + rHSP70 (30 μM) and/or rP20S (25 μM), and $FeCl_2$ (200 μM) + rHSP70 (30 μM) and/or rP20S (25 μM) effect on $A\beta_{1\text{-}42}$ proteins content in SN56 cell homogenates. Data represents the mean ± SEM of three separate experiments from cells of different cultures, each one performed in triplicate. $^{***}p \leq 0.001$ compared to control. $^{\#\#\#}p \leq 0.001$ compared to metal treatment. $^{\gamma\gamma\gamma}p \leq 0.001$ compared to rP20S treatment. $^{\tau\tau\tau}p \leq 0.001$ compared to rHSP70 treatment. $^{\iota\iota\iota}p \leq 0.001$ compared to APH4 and metal treatment. $^{\delta\delta\delta}p \leq 0.001$ compared to P20S silenced cells treated with APH4 and metal.

result to be a substrate of CYP3A4, but not to be a substrate of CYP2C9 and CYP2D6 enzymes. The inhibitory promiscuity results were favorable for the binding to different CYP enzymes (3A4, 2C9, 2C19, 2D6, 1A2). ADMETsar analysis on **APH** compounds possible binding to estrogen receptor (ER), androgen receptor (AR), thyroid receptor (THR), glucocorticoid receptor (GR), peroxisome proliferator-activated receptor (PPAR) gamma and aromatase, or human ether-a-go-go related gene (hERG) potassium channel inhibition showed predictive positive results. Finally, **APH** compounds show predictive positive hepatoxicity and were classified as category III for acute oral toxicity. These results are shown in Table S1(Supporting Information).

4. Discussion

Our results show that **APH1-5** compounds co-incubation with $A\beta_{1\text{-}42}$ fibrils prevented $A\beta_{1\text{-}42}$ fibrils aggregation. The existence of π-stacking interactions between aromatic residues in the Aβ monomer, such as phenylalanines (Phe4, Phe19 and Phe20) and tryptophan (Tyr10), has been proposed to mediate the Aβ self-assembly process and lead to the formation of Aβ fibrils (Landau et al., 2011). Naphthalene sulfonates, congo red, thioflavin and curcumin, which are planar, non-polar aromatic small molecules, are known to interfere with aromatic interactions, inhibiting Aβ aggregation (Biancalana and Koide, 2010; Maezawa et al., 2008). Thus, the sp^3-low nature of **APH1-5** compounds may help them interact alongside the Aβ sheets, preventing in this way the assembly of more complex aggregates. Moreover, **APH1-5** compounds co-incubation with $A\beta_{1\text{-}42}$ fibrils shows, for the first time, that the metal-induced $A\beta_{1\text{-}42}$ chemical aggregation was inhibited by **APH1-5** compounds co-incubation with the metals tested except for **APH1** and **APH4** compounds, which were unable to inhibit Zn- and Fe-induced chemical aggregation, respectively. Additionally, **APH1-5** compounds were able to reduce the metal-induced fibrils width, although they acted differently depending on the specific metal co-incubated with $A\beta_{1\text{-}42}$, so it can be concluded that **APH** compounds containing phenanthridin-6(5*H*)-one core, prevent the aggregation generated by the metals tested. Otherwise, **APH1-5** compounds were reported to chelate Fe and Cu, and **APH3-5** compounds to chelate Hg, but none of them was able to chelate Al, Zn and Cd (Moyano et al., 2021). Therefore, the ability of the **APH1-5** compounds to inhibit the metal-induced $A\beta_{1\text{-}42}$ chemical aggregation seems to be mediated by a direct interaction with $A\beta_{1\text{-}42}$ fibrils, independently of their chelating activity, and may probably be due to an intercalation effect between the β-sheet through π-stacking interactions with the polypeptide $A\beta_{1\text{-}42}$, preventing the formation of $A\beta_{1\text{-}42}$ aggregates.

Otherwise, our results show that, after single treatment with $FeCl_2$ or $CdCl_2$ of SN56 cells, a reduction in the HSP70 and P20S expression was observed. Previous studies showed that $FeCl_2$ and $CdCl_2$ alter the expression of HSP70 and the expression and activity of P20S proteins (Amici et al., 2002; Correa-Vela et al., 2020; Djebali et al., 2008; Kanthasamy et al., 2012; Moyano et al., 2018; Sanders et al., 2015), supporting our results. Additionally, we show for the first time that **AHP1-5** compounds are inducers of HSP70 and P20S expression, which is probably extensive to all family of APH compounds. Besides, pre-treatment with **APH1-5** compounds reversed, in a concentration-dependent way, completely or partially, depending on the concentration and the **APH1-5** compound, the reduction observed in the HSP70 and P20S expression after $FeCl_2$ and $CdCl_2$ treatment alone. NRF2 pathway has been reported to regulate the expression of HSPs and

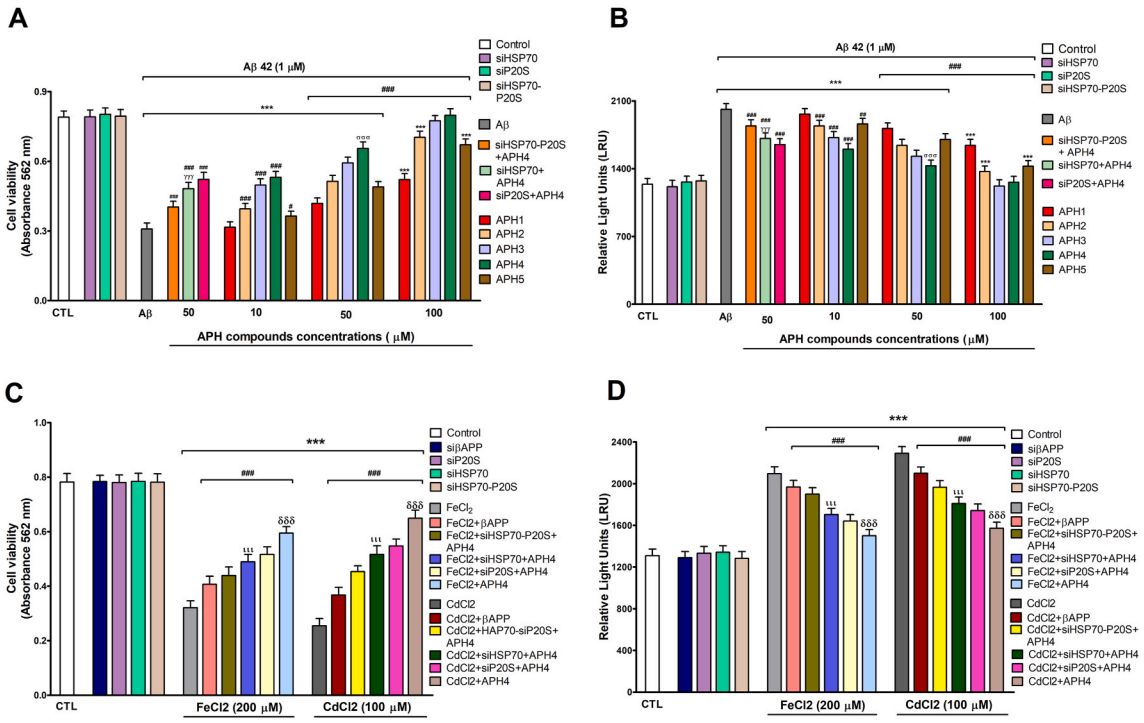


Fig. 5. (A, C) Cell viability and (B, D) caspases 3/7 activity effects after $A\beta_{1\text{-}42}$ proteins or metal ($FeCl_2$ or $CdCl_2$) treatment of wild type, or single (βAPP, HSP70 or P20S)/concomitant (HSP70 and P20S) silenced SN56 cells pre-treated with or without APH4 (50 μM) or APH1**-5** compounds (10–100 μM). Data represents the mean ± SEM of three independent experiments in triplicate. ***$p \leq 0.001$ compared to control. $^{\#}p \leq 0.05$, $^{\#\#}p \leq 0.01$, and $^{\#\#\#}p \leq 0.001$ compared to $A\beta_{1\text{-}42}$ treatment. $^{\text{ttt}}p \leq 0.001$ compared to APH4 and metal treatment. $^{\delta\delta\delta}p \leq 0.001$ compared to P20S silenced cells treated with APH4 and metal.

proteasome P20S (Chapple et al., 2012; Kim et al., 2017; Ramos et al., 2018), and therefore the previously described induction of NRF2 pathway by **APH1-5** compounds (Moyano et al., 2021) could mediate the effect observed on HSP70 and P20S proteins expression. However, NRF2 pathway was induced by **APH1-5** compounds starting at 10 μM concentration (Moyano et al., 2021), but these compounds were only able to start P20S upregulation at 50 μM concentration, while **APH3** and **APH4** started the HSP70 upregulation at 10 μM concentration. These results suggest that NRF2 pathway could contribute to the effects observed on both proteins expression from 50 μM concentration for **APH1-5** compounds, and from 10 μM concentration for **APH3** and **APH4** for HSP70 upregulation, but other mechanisms seem to be involved. In this sense, HSP70 expression is regulated by heat shock factor 1 (HSF1) (Zhu et al., 2015), which could be also being induced by **APH1-5** compounds. P20S expression is regulated also by the nuclear respiratory factor 1 (NRF-1) (Ben-Nissan and Sharon, 2014), which could also be modified by **APH1-5** compounds. Further studies are needed to confirm the NRF2 pathway involvement in these effects and the complete mechanisms that mediate these effects.

Our results also show that single treatment with $FeCl_2$ or $CdCl_2$ of SN56 cells, induced an increase in the levels of $A\beta_{1\text{-}42}$ proteins. Previous studies showed that $FeCl_2$ and $CdCl_2$ rise the levels of these proteins (Choi et al., 2021; Moyano et al., 2018), supporting our results. Additionally, we show, for the first time, that pre-treatment with **APH1-5** compounds reversed, in a concentration-dependent way, partially (**APH1** and **APH2**) or completely (**APH3, APH4** and **APH5**), the increase in the Aβ proteins levels observed after $FeCl_2$ and $CdCl_2$ treatment alone. **APH3** and **APH4** started to revert the increase of Aβ proteins levels at 10 μM concentrations for both metals; and **APH5** starts to mediate this protection from 10 μM concentration only for $FeCl_2$. **APH3** and **APH4** were the only compounds able to reverse completely these effects after pre-treatment at 100 μM concentrations for both metals, and **APH5** only reversed completely this effect at the same concentration for $CdCl_2$. In addition, co-treatment with recombinant HSP70 and/or P20S proteins and the tested metals reverted partially the increase in the Aβ proteins levels observed after $FeCl_2$ and $CdCl_2$ treatment alone, showing that both mechanisms, decreased by these metals, are involved in the rise of the Aβ proteins levels observed after these metals' treatment alone. Besides, pre-treatment with **APH4** compound of single or concomitant HSP70 and/or P20S SN56 silenced cells, which were treated with $FeCl_2$ or $CdCl_2$, induced a lower reversion in the rise of the Aβ proteins levels observed after pre-treatment with **APH4** compound of wild type SN56 cells treated with $FeCl_2$ and $CdCl_2$ alone. This shows that both mechanisms, induced by **APH1-5** compounds, mediate the **APH1-5** reduction of the Aβ proteins levels increase observed after the treatment with these metals. HSP70 and P20S proteins were described to regulate two different pathway of toxic proteins elimination (Campanella et al., 2018; Cao et al., 2019; Lackie et al., 2017; Schmidt et al., 2021), supporting our results. Thus, both mechanisms seem to contribute to the effect observed.

However, other mechanisms seem to be involved since pre-treatment with **APH4** compound of single or concomitant HSP70 and/or P20S silenced cells treated with these metals produced a lower reduction of Aβ proteins levels than **APH4** pre-treatment of wild type cells. In this sense, pre-treatment with **APH3**, **APH4** and **APH5** compounds protected completely against the increase in the Aβ proteins levels observed after $FeCl_2$ and $CdCl_2$ treatment alone, but the HSP70 and P20S downregulation was only completely reverted after pre-treatment with **APH3** and **APH4** for both metals, while **APH5** only reverted completely the HSP70 downregulation for $FeCl_2$. Besides, this hypothesis is also supported by the fact that none of the **APH1-5** compounds starts to reverse P20S downregulation at 10 μM concentrations for both metals, although they start to reverse the rise of Aβ proteins levels from this concentration; and that co-treatment with recombinant HSP70 and P20S proteins did not reverse completely the increase in the Aβ proteins levels observed. All this suggests that the only mechanism to start its protective action against Aβ proteins levels increase at 10 μM concentration was HSP70 for **APH3** and **APH4** compounds, but other mechanisms are

involved in this protective effect of **APH1-5** compounds against Aβ proteins accumulation. In this sense, MMPs dysfunction was associated with the production of Aβ proteins (Asahina et al., 2001; Bjerke et al., 2011; Brkic et al., 2015). Several metals were also reported to mediate the MMPs induction (Dagouassat et al., 2012). **APH** compounds have MMP inhibitor activity (Rocchi et al., 2021), and thus they could mediate the reduction of Aβ proteins levels observed through this mechanism. Moreover, we previously showed that **APH** compounds reverse the oxidative stress (OS) induced by both metals through the induction of NRF2 pathway (Moyano et al., 2021). OS was described to induce the brain accumulation of Aβ peptides among other toxic proteins (Cannon and Greenamyre, 2011; Chin-Chan et al., 2015). Furthermore, metals were also reported to mediate the brain accumulation of Aβ peptides and other toxic proteins through other mechanisms such as acetylcholinesterase variants or Cathepsin D expression alteration among others (Bluhm et al., 2021; Del Pino et al., 2016). Thus, **APH** compounds could also mediate their neuroprotective effect through all these mechanisms, and we cannot discard that the processing enzymes of βAPP to the amyloidogenic peptides could also be involved.

Finally, pre-treatment with **APH1-5** compounds reversed, in a concentration-dependent way, partially (**APH1**, **APH2** and **APH5**) or completely (**APH3** and **APH4**), the cell death observed after $A\beta_{1\text{-}42}$ proteins treatment alone. **APH2**, **APH3**, **APH4** and **APH5** started to revert the cell death observed at 10 μM concentrations. Besides, pre-treatment with **APH4** compound of single or concomitant HSP70 and/or P20S silenced cells treated with $A\beta_{1\text{-}42}$ proteins induced a lower reversion of the cell death observed after pre-treatment with **APH4** compound of wild type cells treated with $A\beta_{1\text{-}42}$ proteins alone. This suggests that both mechanisms mediate the **APH1-5** neuroprotective action against the cell death observed after $A\beta_{1\text{-}42}$ proteins treatment alone. $FeCl_2$ or $CdCl_2$ treatment of βAPP silenced SN56 cells reverted partially the cell death induced after single treatment with these metals, showing that the rise of Aβ proteins levels induced by these metals mediates, in part, the cell death observed. Pre-treatment with **APH4** compound of single or concomitant HSP70 and/or P20S silenced cells treated with $FeCl_2$ or $CdCl_2$ induced a lower reversion of the cell death observed after pre-treatment with **APH4** compound of wild type cells treated with $FeCl_2$ or $CdCl_2$ alone. This suggests that both mechanisms mediate the **APH1-5** neuroprotective action against the cell death observed after $FeCl_2$ and $CdCl_2$ treatment alone through the reduction of $A\beta_{1\text{-}42}$ proteins levels. Additionally, we previously showed that $FeCl_2$ and $CdCl_2$ treatment of SN56 cells induced cell death that was reverted completely by pre-treatment with **APH3**, **APH4** and **APH5** for $CdCl_2$ and partially for $FeCl_2$ (Moyano et al., 2021). **APH3**, **APH4** and **APH5** started their neuroprotective effect at 10 μM concentrations for $CdCl_2$ and only **APH3** and **APH4** started this neuroprotective effect from the same concentration for $FeCl_2$ (Moyano et al., 2021). Moreover, **APH3** and **APH4** reversed completely HSP70 and P20S proteins down-regulation after pre-treatment at 100 μM concentrations for both metals, and **APH5** only for $CdCl_2$. Besides, only **APH3** and **APH4** started their protective effect on HSP70 expression at 10 μM concentration for both metals, but **APH1-5** compounds were only able to start their protective effect on P20S expression at 50 μM concentrations for both metals. These results support that the neuroprotective effect of the **APH1-5** compounds against metal cytotoxicity is mediated by the reduction of metal-induced Aβ protein accumulation. However, since βAPP silencing was unable to revert completely the cell death induced by both metals and **APH5** compound was unable to revert completely the Aβ induced cytotoxicity, but it was able to start the reversion of Cd-induced cell death from 10 μM concentration and revert it completely at 100 μM concentration (Moyano et al., 2021), it appears that, apart from $A\beta_{1\text{-}42}$ reduction, other neuroprotective mechanisms collaborate to mediate the reversion of cadmium-induced cell death. In this sense, we showed that these **APH1-5** compounds present antioxidant, chelating and MMP inhibitory activities (Rocchi et al., 2021; Moyano et al., 2021), which could also contribute to this effect. Furthermore, according to our results and our previous studies indicated above, the neuroprotective effect of HSP70 upregulation (and probably P20S) seems to not only mediate the reduction of $A\beta_{1\text{-}42}$ proteins, but also of other toxic proteins production that contribute to the metal-induced cell death.

In our previous study we showed, after computational studies with ADMETsar version 2.0 and swissADME software, that the **APH1-5** compounds have positive-predicted Caco-2 cell permeability, intestinal absorption, and blood brain barrier (BBB) penetration ability (Moyano et al., 2021). Moreover, these compounds presented a favorable molecular weight (≤500 g/mol) and octanol-water partition coefficients (log P) or not P glycoprotein interaction (BBB excretion marker) in ADMETsar analysis, suggesting good capacity of oral absorption, supported by our present physicochemical drug-likeness analysis, and brain distribution (Moyano et al., 2021). We also analyzed the predicted metabolic activity, suggesting a cytochrome P450 isoforms CYP1A2, CYP2C19, CYP2C9, and CYP2D6 inhibitory capacity depending on the **APH1-5** compounds (Moyano et al., 2021). We now show that **APH1-5** compounds may be substrate for CYP3A4, but not of CYP2C9, and CYP2D6 enzymes. In the present study we show that **APH** compounds present predicted binding to ER, AR, THR, GR, and PPAR gamma, and aromatase. Further studies are necessary to confirm the binding abilities of **APH** compounds to these receptors, and if so the agonistic/antagonistic effects, the potency and their possible involvement in toxicological/pharmacological actions. The toxicity predicted results for all **APH** compounds show relevance for hepatotoxicity and cardiotoxicity, as shown by the positive predictive inhibition of hERG potassium channel, except for **APH5** in cardiotoxicity effect. Additional studies should be developed to confirm these results *in vitro* and *in vivo*, and if so, the concentrations at which these compounds could reach these organs at therapeutic doses and the potency on these effects. Finally, we show that **APH1-5** compounds have low oral acute toxicity prediction and could be categorized in a level III, according to the median lethal dose (LD_{50}) for oral administration. These low predicted toxicity effects were supported by our cell viability studies that do not show any reduction of SN56 cell viability at the effective concentrations tested (Rocchi et al., 2021). Thus, these compounds seem to present low toxicity and favorable properties to be absorbed and distributed to the brain, to produce their neuroprotective effect, and represent the starting point to develop a leader compound. Further studies should be developed to confirm these properties, the absence of toxicity, and determine the necessity of their optimization for these properties.

Summarizing all described above, **APH1-5** compounds exhibit affinity for $A\beta_{1\text{-}42}$ proteins, which prevents their aggregation. In addition, these compounds reduce partially and completely the accumulation of Aβ proteins induced by $FeCl_2$ and $CdCl_2$ in SN56 cells through HSP70 and P20S upregulation. Finally, **APH1-5** compounds mediate their neuroprotective effect against $FeCl_2$ and $CdCl_2$ through reduction of Aβ proteins levels. Additional studies are required to elucidate all the mechanisms involved in the neuroprotective effects of **APH1-5** compounds, the mechanisms through which they interact with $A\beta_{1\text{-}42}$ fibrils, inhibiting their aggregation, and to confirm that the induction of HSP70 and P20S expression is mediated by the upregulation of NRF2 pathway, and the rest of mechanisms involved. Moreover, further experiments should be performed to prove their suggested low toxicity and ability to be absorbed and distributed to the brain. Our results are relevant since they inform of the mechanisms that mediate neuroprotective effect of **APH1-5** compounds that could help to prevent not only the neurotoxic effect of metals, but also other environmental pollutants that mediate their neurotoxic effects through the alteration of the mechanisms that regulate **APH** compounds.

CRediT authorship contribution statement

Paula Moyano: Methodology, Investigation, Writing – original draft, Writing – review & editing. **David Vicente-Zurdo:** Methodology,

Investigation, Writing – original draft, Writing – review & editing. **Cristina Blázquez-Barbadillo:** Investigation, Writing – original draft, Writing – review & editing. **J. Carlos Menéndez:** Conceptualization, Methodology, Project administration, Supervision, Writing – review & editing. **Juan F. González:** Conceptualization, Methodology, Project administration, Supervision, Writing – review & editing. **Noelia Rosales-Conrado:** Conceptualization, Methodology, Project administration, Supervision, Writing – review & editing. **Javier del Pino:** Conceptualization, Methodology, Project administration, Supervision, Writing – review & editing.

Declaration of competing interest

The authors declare that they have no known competing financial interests or personal relationships that could have appeared to influence the work reported in this paper.

Acknowledgments

This work was supported by the Spanish Ministry of Science and Innovation (RTI2018-097662-B-I00, PID2020-114714RB-I00), the Community of Madrid and European Union from FSE and FEDER programs (S2018/BAA-4393, AVANSECAL-II-CM) and Complutense University (PR26/16-16B). David Vicente-Zurdo acknowledges the Spanish Ministry of Science, Innovation and Universities for a pre-doctoral grant (FPU18/00573).

Appendix A. Supplementary data

Supplementary data to this article can be found online at https://doi.org/10.1016/j.fct.2022.113264.

References

Acevedo, K., Masaldan, S., Opazo, C.M., Bush, A.I., 2019. Redox active metals in neurodegenerative diseases. J. Biol. Inorg. Chem. 24 (8), 1141–1157.
Amici, M., Forti, K., Nobili, C., Lupidi, G., Angeletti, M., Fioretti, E., Eleuteri, A.M., 2002. Effect of neurotoxic metal ions on the proteolytic activities of the 20S proteasome from bovine brain. J. Biol. Inorg. Chem. 7 (7–8), 750–756.
Asahina, M., Yoshiyama, Y., Hattori, T., 2001. Expression of matrix metalloproteinase-9 and urinary-type plasminogen activator in Alzheimer's disease brain. Clin. Neuropathol. 20 (2), 60.
Asthana, A., Bollapalli, M., Tangirala, R., Bakthisaran, R., Mohan Rao, Ch, 2014. Hsp27 suppresses the Cu(2+)-induced amyloidogenicity, redox activity, and cytotoxicity of α-synuclein by metal ion stripping. Free Radic. Biol. Med. 72, 176–190.
Ben-Nissan, G., Sharon, M., 2014. Regulating the 20S proteasome ubiquitin-independent degradation pathway. Biomolecules 4 (3), 862–884.
Biancalana, M., Koide, S., 2010. Molecular mechanism of Thioflavin-T binding to amyloid fibrils. Biochim. Biophys. Acta 1804 (7), 1405–1412.
Bielarczyk, H., Jankowska, A., Madziar, B., Matecki, A., Michno, A., Szutowicz, A., 2003. Differential toxicity of nitric oxide, aluminum, and amyloid-β-peptide in SN56 cholinergic cells from mouse septum. Neurochem. Int. 42, 323–331.
Bjerke, M., Zetterberg, H., Å, Edman, Blennow, K., Wallin, A., Andreasson, U., 2011. Cerebrospinal fluid matrix metalloproteinases and tissue inhibitor of metalloproteinases in combination with subcortical and cortical biomarkers in vascular dementia and Alzheimer's disease. J. Alzheimers Dis. 27 (3), 665.
Bluhm, A., Schrempel, S., von Hörsten, S., Schulze, A., Roßner, S., 2021. Proteolytic α-synuclein cleavage in health and disease. Int. J. Mol. Sci. 22 (11), 5450.
Bovolenta, T.M., De Azevedo Silva, S.M.C., Arb Saba, R., Borges, V., Ferraz, H.B., Felicio, A.C., 2017. Systematic review and critical analysis of cost studies associated with Parkinson's disease. Park Dis. 2017, 1–11.
Brkic, M., Balusu, S., Libert, C., Vandenbroucke, R.E., 2015. Friends or foes: matrix metalloproteinases and their multifaceted roles in neurodegenerative diseases. Mediat. Inflamm. 2015, 620581.
Campanella, C., Pace, A., Caruso Bavisotto, C., Marzullo, P., Marino Gammazza, A., Buscemi, S., Palumbo Piccionello, A., 2018. Heat shock proteins in Alzheimer's disease: role and targeting. Int. J. Mol. 19 (9), 2603.
Cannon, J.R., Greenamyre, J.T., 2011. The role of environmental exposures in neurodegeneration and neurodegenerative diseases. Toxicol. Sci. 124 (2), 225.
Cao, J., Zhong, M.B., Toro, C.A., Zhang, L., Cai, D., 2019. Endo-lysosomal pathway and ubiquitin-proteasome system dysfunction in Alzheimer's disease pathogenesis. Neurosci. Lett. 703, 68–78.
Chapple, S.J., Siow, R.C., Mann, G.E., 2012. Crosstalk between Nrf2 and the proteasome: therapeutic potential of Nrf2 inducers in vascular disease and aging. Int. J. Biochem. Cell Biol. 44 (8), 1315–1320.
Chen, P., Miah, M.R., Aschner, M., 2016. In: Metals and Neurodegeneration. F1000Res, vol. 5, p. F1000. Faculty Rev-366.
Chen, X., Wu, J., Yang, Q., Zhang, X., Zhang, P., Liao, S., He, Z., Wang, X., Zhao, C., Liu, J., 2018. Cadmium pyrithione suppresses tumor growth in vitro and in vivo through inhibition of proteasomal deubiquitinase. Biometals 31 (1), 29–43.
Cheng, F., Li, W., Zhou, Y., Shen, J., Wu, Z., Liu, G., Lee, P.W., Tang, Y., 2012. AdmetSAR: a comprehensive source and free tool for assessment of chemical ADMET properties. J. Chem. Inf. Model. 52 (11), 3099–3105, 2012 Nov 26.
Chin-Chan, M., Navarro-Yepes, J., Quintanilla-Vega, B., 2015. Environmental pollutants as risk factors for neurodegenerative disorders: Alzheimer and Parkinson diseases. Front. Cell. Neurosci. 9, 124.
Choi, S., Hong, D.K., Choi, B.Y., Suh, S.W., 2020. Zinc in the brain: friend or foe? Int. J. Mol. Sci. 21 (23), 8941.
Choi, D.H., Kwon, K.C., Hwang, D.J., Koo, J.H., Um, H.S., Song, H.S., Kim, J.S., Jang, Y., Cho, J.Y., 2021. Treadmill exercise Alleviates brain iron dyshomeostasis Accelerating neuronal amyloid-beta production, neuronal cell death, and cognitive impairment in transgenic mice model of Alzheimer's disease. Mol. Neurobiol. 58 (7), 3208–3223.
Correa-Vela, M., Lupo, V., Montpeyó, M., Sancho, P., Marcé-Grau, A., Hernández-Vara, J., Darling, A., Jenkins, A., Fernández-Rodríguez, S., Tello, C., Ramírez-Jiménez, L., Pérez, B., Sánchez-Montáñez, Á., Macaya, A., Sobrido, M.J., Martinez-Vicente, M., Pérez-Dueñas, B., Espinós, C., 2020. Impaired proteasome activity and neurodegeneration with brain iron accumulation in FBXO7 defect. Ann. Clin. Transl. Neurol. 7 (8), 1436–1442.
Crichton, R.R., Dexter, D.T., Ward, R.J., 2008. Metal based neurodegenerative diseases-From molecular mechanisms to therapeutic strategies. Coord. Chem. Rev. 252, 1189–1199.
Dagouassat, M., Lanone, S., Boczkowski, J., 2012. Interaction of matrix metalloproteinases with pulmonary pollutants. Eur. Respir. J. 39 (4), 1021.
Dales, J.P., Desplat-Jégo, S., 2020. Metal imbalance in neurodegenerative diseases with a specific concern to the brain of multiple sclerosis patients. Int. J. Mol. Sci. 21 (23), 9105.
Del Pino, J., Zeballos, G., Anadon, M.J., Díaz, M.J., Moyano, P., Díaz, G.G., García, J., Lobo, M., Frejo, M.T., 2016. Muscarinic M1 receptor partially modulates higher sensitivity to cadmium-induced cell death in primary basal forebrain cholinergic neurons: a cholinesterase variants dependent mechanism. Toxicology 361–362, 1–11.
Djebali, W., Gallusci, P., Polge, C., Boulila, L., Galtier, N., Raymond, P., Chaibi, W., Brouquisse, R., 2008. Modifications in endopeptidase and 20S proteasome expression and activities in cadmium treated tomato (Solanum Lycopersicum L.) plants. Planta 227 (3), 625–639.
Do Carmo, S., Kannel, B., Cuello, A.C., 2021. The nerve growth factor metabolic pathway dysregulation as cause of Alzheimer's cholinergic atrophy. Cells 11 (1), 16.
Dunham, J., Bauer, J., Campbell, G.R., Mahad, D.J., van Driel, N., van der Pol, S.M.A., t Hart, B.A., Lassmann, H., Laman, J.D., van Horssen, J., Kap, Y.S., 2017. Oxidative injury and iron redistribution are pathological hallmarks of marmoset experimental Autoimmune encephalomyelitis. J. Neuropathol. Exp. Neurol. 76 (6), 467–478.
Erkkinen, M.G., Kim, M.O., Geschwind, M.D., 2018. Clinical Neurology and epidemiology of the major neurodegenerative diseases. Cold Spring Harbor Perspect. Biol. 10, a033118.
Esser, C., Alberti, S., Höhfeld, J., 2004. Cooperation of molecular chaperones with the ubiquitin/proteasome system. Biochim. Biophys. Acta 1695 (1–3), 171–188.
Figueiredo, L.S., de Freitas, B.S., Garcia, V.A., Dargél, V.A., Köbe, L.M., Kist, L.W., Bogo, M.R., Schröder, N., 2016. Iron loading selectively increases hippocampal levels of ubiquitinated proteins and impairs hippocampus-dependent memory. Mol. Neurobiol. 53 (9), 6228–6239.
GBD 2016 Neurology Collaborators, 2019. Global, regional, and national burden of neurological disorders, 1990-2016: a systematic analysis for the Global Burden of Disease Study 2016. Lancet Neurol. 18 (5), 459–480.
Gerspacher, C., Scheuber, U., Schiera, G., Proia, P., Gygax, D., Di Liegro, I., 2009. The effect of cadmium on brain cells in culture. Int. J. Mol. Med. 24 (3), 311–318.
Gorantla, N.V., Chinnathambi, S., 2018. Tau protein squired by molecular chaperones during Alzheimer's disease. J. Mol. Neurosci. 66 (3), 356–368.
Gozzelino, R., Arosio, P., 2016. Iron homeostasis in health and disease. Int. J. Mol. Sci. 17 (1), 130.
Grothe, M.J., Heinsen, H., Amaro Jr., E., Grinberg, L.T., Teipel, S.J., 2016. Cognitive correlates of basal forebrain atrophy and associated cortical hypometabolism in mild cognitive impairment. Cerebr. Cortex 26 (6), 2411–2426.
Hammond, D.N., Lee, H.J., Tonsgard, J.H., Wainer, B.H., 1990. Development and characterization of clonal cell lines derived from septal cholinergic neurons. Brain Res. 512, 190–200.
Hudgens, E.D., Ji, L., Carpenter, C.D., Petersen, S.L., 2009. The gad2 promoter is a transcriptional target of estrogen receptor (ER)alpha and ER beta: a unifying hypothesis to explain diverse effects of estradiol. J. Neurosci. 29 (27), 8790–8797.
Kanthasamy, A.G., Choi, C., Jin, H., Harischandra, D.S., Anantharam, V., Kanthasamy, A., 2012. Effect of divalent metals on the neuronal proteasomal system, prion protein ubiquitination and aggregation. Toxicol. Lett. 214 (3), 288–295.
Katsnelson, A., De Strooper, B., Zoghbi, H.Y., 2016. Neurodegeneration: from cellular concepts to clinical applications. Sci. Transl. Med. 8 (364), 364ps.
Kim, K.M., Im, A.R., Lee, S., Chae, S., 2017. Dual protective effects of flavonoids from petasites japonicus against UVB-induced apoptosis mediated via HSF-1 activated heat shock proteins and Nrf2-activated heme oxygenase-1 pathways. Biol. Pharm. Bull. 40 (6), 765–773.
Klein, A.M., Kowall, N.W., Ferrante, R.J., 1999. Neurotoxicity and oxidative damage of beta amyloid 1-42 versus beta amyloid 1-40 in the mouse cerebral cortex. Ann. N Y Acad. Sci. 893, 314–320.

Kumar, V., Singh, D., Singh, B.K., Singh, S., Mittra, N., Jha, R.R., Patel, D.K., Singh, C., 2018. Alpha-synuclein aggregation, Ubiquitin proteasome system impairment, and L-Dopa response in zinc-induced Parkinsonism: resemblance to sporadic Parkinson's disease. Mol. Cell. Biochem. 444 (1–2), 149–160.
Kwakowsky, A., Potapov, K., Kim, S., Peppercorn, K., Tate, W.P., Ábrahám, I.M., 2016. Treatment of beta amyloid 1-42 (Aβ(1-42))-induced basal forebrain cholinergic damage by a non-classical estrogen signaling activator in vivo. Sci. Rep. 6, 21101.
Lackie, R.E., Maciejewski, A., Ostapchenko, V.G., Marques-Lopes, J., Choy, W.Y., Duennwald, M.L., Prado, V.F., Prado, M.A.M., 2017. The Hsp70/Hsp90 chaperone machinery in neurodegenerative diseases. Front. Neurosci. 11, 254.
Landau, M., Sawaya, M.R., Faull, K.F., Laganowsky, A., Jiang, L., Sievers, S.A., Liu, J., Barrio, J.R., Eisenberg, D., 2011. Towards a pharmacophore for amyloid. PLoS Biol. 9 (6), e1001080.
Leak, R.K., 2014. Heat shock proteins in neurodegenerative disorders and aging. J. Cell Commun. Signal 8 (4), 293–310.
Livak, K.J., Schmittgen, T.D., 2001. Analysis of relative gene expression data using real-time quantitative PCR and the 2(-Delta Delta C(T)) Method. Methods 25, 402–408.
Maezawa, I., Hong, H.S., Liu, R., Wu, C.Y., Cheng, R.H., Kung, M.P., Kung, H.F., Lam, K. S., Oddo, S., Laferla, F.M., Jin, L.W., 2008. Congo red and thioflavin-T analogs detect Abeta oligomers. J. Neurochem. 104 (2), 457–468.
Maiti, P., Manna, J., Veleri, S., Frautschy, S., 2014. Molecular chaperone dysfunction in neurodegenerative diseases and effects of curcumin. BioMed Res. Int. 2014, 495091.
Mir, R.H., Sawhney, G., Pottoo, F.H., Mohi-Ud-Din, R., Madishetti, S., Jachak, S.M., Ahmed, Z., Masoodi, M.H., 2020. Role of environmental pollutants in Alzheimer's disease: a review. Environ. Sci. Pollut. Res. Int. 27 (36), 44724.
Moyano, P., García, J.M., Lobo, M., Anadón, M.J., Sola, E., Pelayo, A., García, J., Frejo, M.T., Pino, J.D., 2018. Cadmium alters heat shock protein pathways in SN56 cholinergic neurons, leading to Abeta and phosphorylated Tau protein generation and cell death. Food Chem. Toxicol. 121, 297–308.
Moyano, P., García, J.M., García, J., Anadon, M.J., Naval, M.V., Frejo, M.T., Sola, E., Pelayo, A., Pino, J.D., 2020. Manganese increases Aβ and Tau protein levels through proteasome 20S and heat shock proteins 90 and 70 alteration, leading to SN56 cholinergic cell death following single and repeated treatment. Ecotoxicol. Environ. Saf. 203, 110975.
Moyano, P., Vicente-Zurdo, D., Blázquez-Barbadillo, C., Menéndez, J.C., González, J.F., Rosales-Conrado, N., Del Pino, J., 2021. Neuroprotective action of multitarget 7-aminophenanthridin-6(5H)-one derivatives against metal-induced cell death and oxidative stress in SN56 cells. ACS Chem. Neurosci. 12 (18), 3358–3372.
Ramos, E., Romero, A., Marco-Contelles, J., López-Muñoz, F., Del Pino, J., 2018. Modulation of heat shock response proteins by ASS234, targeted for neurodegenerative diseases therapy. Chem. Res. Toxicol. 31 (9), 839–842.
Rocchi, D., Blázquez-Barbadillo, C., Agamennone, M., Laghezza, A., Tortorella, P., Vicente-Zurdo, D., Rosales-Conrado, N., Moyano, P., Pino, J.D., González, J.F., Menéndez, J.C., 2021. Discovery of 7-aminophenanthridin-6-one as a new scaffold for matrix metalloproteinase inhibitors with multitarget neuroprotective activity. Eur. J. Med. Chem. 210, 113061.
Sanders, T., Liu, Y.M., Tchounwou, P.B., 2015. Cytotoxic, genotoxic, and neurotoxic effects of Mg, Pb, and Fe on pheochromocytoma (PC-12) cells. Environ. Toxicol. 30 (12), 1445–1458.
Schmidt, M.F., Gan, Z.Y., Komander, D., Dewson, G., 2021. Ubiquitin signalling in neurodegeneration: mechanisms and therapeutic opportunities. Cell Death Differ. 28 (2), 570–590.
Strafella, C., Caputo, V., Galota, M.R., Zampatti, S., Marella, G., Mauriello, S., Cascella, R., Giardina, E., 2018. Application of precision medicine in neurodegenerative diseases. Front. Neurol. 9, 701.
Szutowicz, A., Bielarczyk, H., Gul, S., Ronowska, A., Pawełczyk, T., Jankowska-Kulawy, A., 2006. Phenotype-dependent susceptibility of cholinergic neuroblastoma cells to neurotoxic inputs. Metabol. Brain Dis. 21, 149–161.
Verma, S., Sharma, S., Ranawat, P., Nehru, B., 2020. Modulatory effects of Ginkgo biloba against amyloid aggregation through induction of heat shock proteins in Aluminium induced neurotoxicity. Neurochem. Res. 45 (2), 465–490.
Vicente-Zurdo, D., Romero-Sánchez, I., Rosales-Conrado, N., León-González, M.E., Madrid, Y., 2020. Ability of selenium species to inhibit metal-induced Aβ aggregation involved in the development of Alzheimer's disease. Anal. Bioanal. Chem. 412, 6485–6497.
White, A.R., Kanninen, K.M., Crouch, P.J., 2015. Editorial: metals and neurodegeneration: restoring the balance. Front. Aging Neurosci. 7, 127.
Wilhelmus, M.M., Otte-Höller, I., Wesseling, P., De Waal, R.M., Boelens, W.C., Verbeek, M.M., 2006. Specific association of small heat shock proteins with the pathological hallmarks of Alzheimer's disease brains. Neuropathol. Appl. Neurobiol. 32 (2), 119–130.
Wright, R.O., Baccarelli, A., 2007. Metals and neurotoxicology. J. Nutr. 137 (12), 2809–2813.
Yang, H., Lou, C., Sun, L., Li, J., Cai, Y., Wang, Z., Li, W., Liu, G., Tang, Y., 2019. AdmetSAR 2.0: web-service for prediction and optimization of chemical ADMET properties. Bioinformatics 35 (6), 1067–1069.
Yi, Chernyak, Merinova, A.P., 2017. HSP70 (HSPA1) polymorphisms in former workers with chronic mercury vapor exposure. Int. J. Occup. Med. Environ. Health 30 (1), 77–85.
Zheng, W., Monnot, A.D., 2012. Regulation of brain iron and copper homeostasis by brain barrier systems: implication in neurodegenerative diseases. Pharmacol. Ther. 133 (2), 177.
Zhu, Y.W., Lu, L., Li, W.X., Zhang, L.Y., Ji, C., Lin, X., Liu, H.C., Odle, J., Luo, X.G., 2015. Effect of dietary manganese on antioxidant status and expression levels of heat-shock proteins and factors in tissues of laying broiler breeders under normal and high environmental temperatures. Br. J. Nutr. 114 (12), 1965–1974.

Supporting Information

Neuroprotective mechanisms of multitarget 7-aminophenanthridin-6(5H)-one derivatives against metal-induced amyloid proteins generation and aggregation

Paula Moyano[a, 1], David Vicente-Zurdo[b, 1], Cristina Blázquez-Barbadillo[c], J. Carlos Menéndez[c], Juan F. González[c, *], Noelia Rosales[b, *], and Javier del Pino[a, *]

[a] Departamento de Farmacología y Toxicología, Facultad de Veterinaria, Universidad Complutense, 28040 Madrid, Spain.

[b] Departamento de Química Analítica, Facultad de Ciencias Químicas, Universidad Complutense, 28040 Madrid, Spain.

[c] Unidad de Química Orgánica y Farmacéutica, Departamento de Química en Ciencias Farmacéuticas, Facultad de Farmacia, Universidad Complutense, 28040 Madrid, Spain.

[1]Authors with equal contribution

Running Title: Neuroprotective mechanisms of multitarget 7-aminophenanthridin-6(5H)-one derivatives against metal-induced amyloid proteins generation and aggregation

***Corresponding authors**:

J. Del Pino jdelpino@pdi.ucm.es
N. Rosales-Conrado nrosales@ucm.es
J.F. González jfgonzal@ucm.es

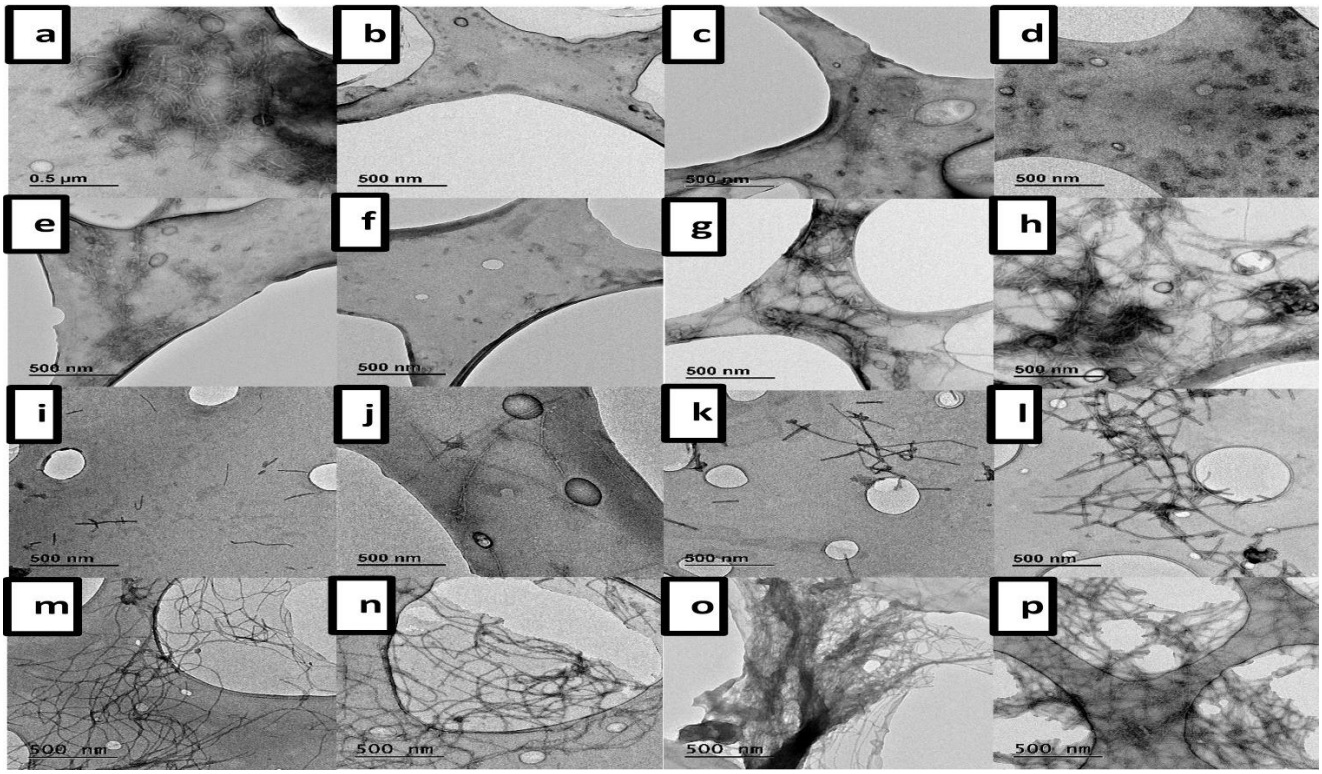


Fig. S1. TEM images of $A\beta_{1-42}$ (50 µM) aggregation assays under the presence of several metals (50 µM) and APH1-5 compounds (50 µM): a) Cu^{2+}; b) Cu^{2+} + APH1; c) Cu^{2+} + APH2; d) Cu^{2+} + APH3; e) Cu^{2+}+ APH4; f) Cu^{2+} + APH5; g) Zn^{2+}; h) Zn^{2+} + APH1; i) Zn^{2+} + APH2; j) Zn^{2+} + APH3; k) Zn^{2+} + APH4; l) Zn^{2+} + APH5; m) Fe^{2+} + APH1; n) Fe^{2+} + APH2; o) Fe^{2+} + APH4; p) Fe^{2+} + APH5.

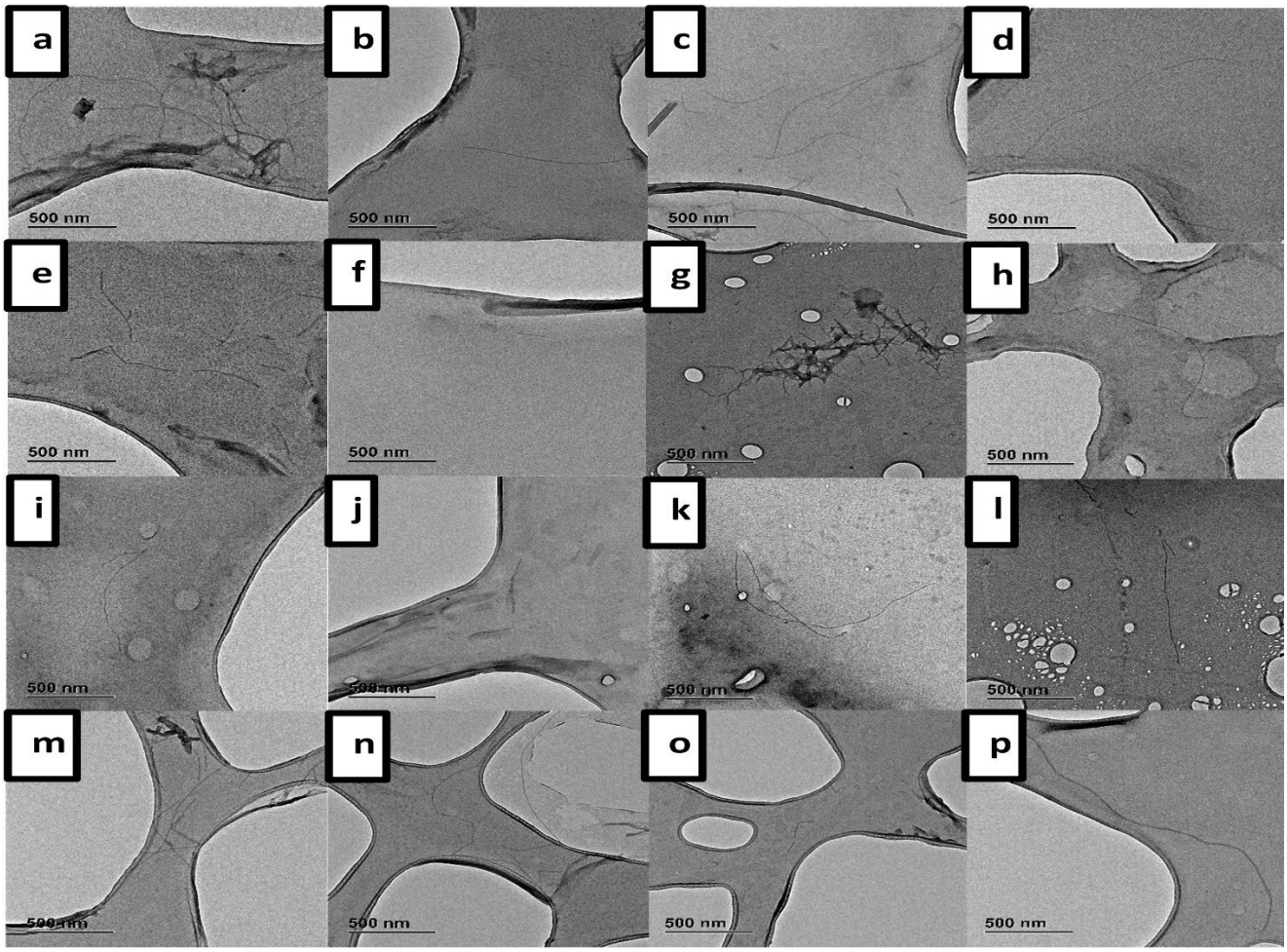


Fig. S2. TEM images of $A\beta_{1-42}$ (50 μM) aggregation assays under the presence of several metals (50 μM) and APH1-5 compounds (50 μM): a) Cd^{2+}; b) Cd^{2+} + APH1; c) Cd^{2+} + APH2; d) Cd^{2+} + APH3; e) Cd^{2+} + APH4; f) Cd^{2+} + APH5; g) Al^{3+}; h) Al^{3+} + APH1; i) Al^{3+} + APH2; j) Al^{3+} + APH3; k) Al^{3+} + APH4; l) Al^{3+} + APH5; m) Hg^{2+} + APH1; n) Hg^{2+} + APH2; o) Hg^{2+} + APH3; p) Hg^{2+} + APH4.

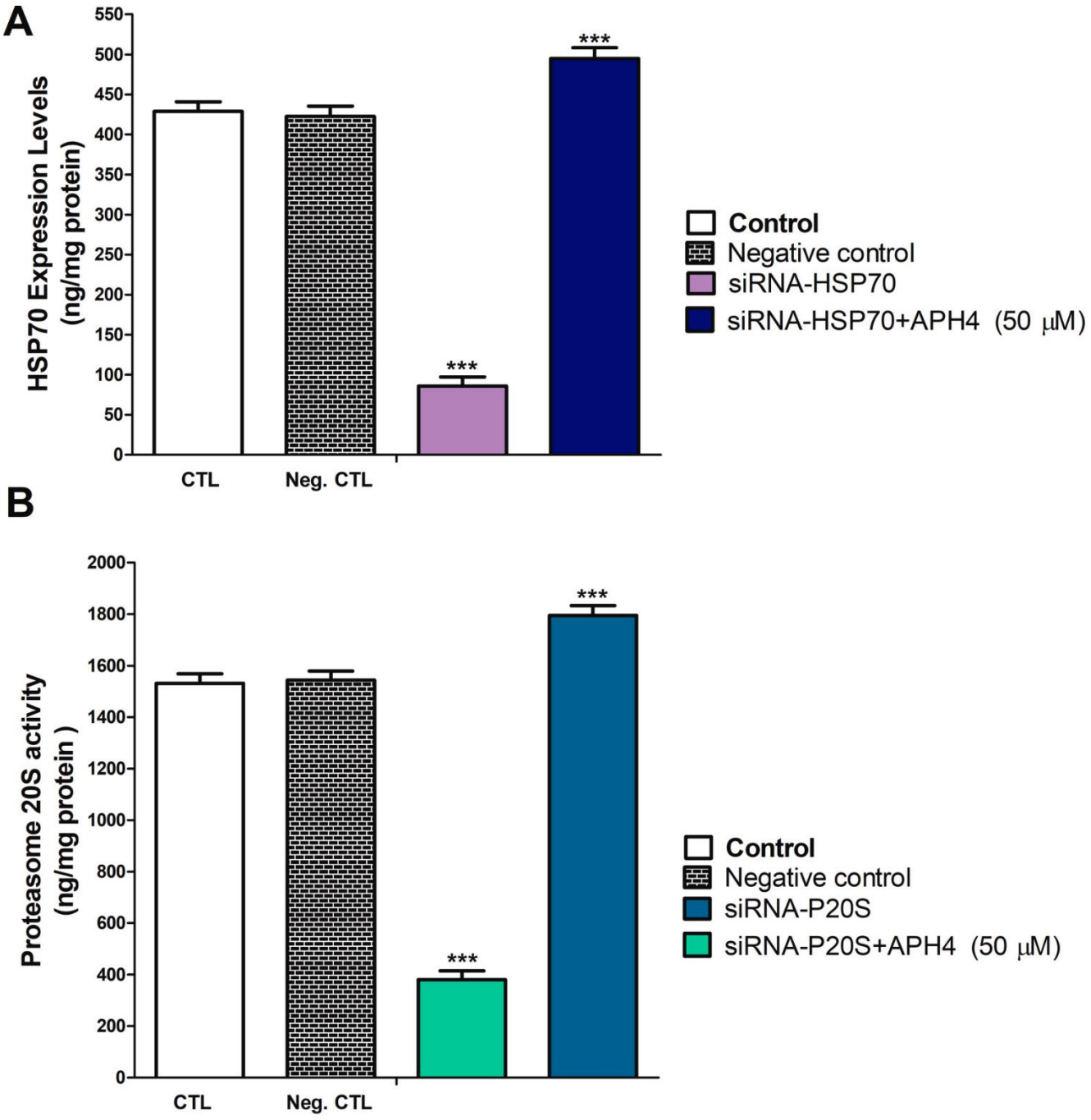


Fig. S3. Control, Negative Control (non-targeting siRNAs), HSP70 siRNA, HSP70 siRNA + APH4 (50 μM), P20S siRNA, and P20S siRNA + APH4 (50 μM) effects on HSP70 (A) and on P20S (B) proteins content in SN56 cell homogenates. Data represents the mean ± SEM of three separate experiments from cells of different cultures, each one performed in triplicate. ***$p \leq 0.001$ compared to control.

Table S1. ADMET prediction of APH compounds.

	APH1	APH2	APH3	APH4	APH5
***Physicochemical-drug-likeness:** Predicted Result	Yes	Yes	Yes	Yes	Yes
CYP3A4 substrate: Predicted Result (Probability)	Yes (0.5198)	Yes (0.5856)	Yes (0.5802)	Yes (0.6269)	Yes (0.5118)
CYP2C9 substrate: Predicted Result (Probability)	No (0.5528)	No (0.5824)	No (0.5918)	No (0.5844)	No (0.5824)
CYP2D6 substrate: Predicted Result (Probability)	No (0.8236)	No (0.8169)	No (0.8396)	No (0.8262)	No (0.8425)
****CYP inhibitory promiscuity:** Predicted Result (Probability)	Yes (0.8420)	Yes (0.8764)	Yes (0.7242)	Yes (0.8695)	Yes (0.8600)
ER binding: Predicted Result (Probability)	Yes (0.8547)	Yes (0.9035)	Yes (0.8600)	Yes (0.9031)	Yes (0.9462)
AR binding: Predicted Result (Probability)	Yes (0.8781)	Yes (0.9723)	Yes (0.9679)	Yes (0.9569)	Yes (0.9188)
THR binding: Predicted Result (Probability)	Yes (0.7416)	Yes (0.6956)	Yes (0.8107)	Yes (0.6470)	Yes (0.6375)
GR binding: Predicted Result (Probability)	Yes (0.7872)	Yes (0.8914)	Yes (0.7999)	Yes (0.9091)	Yes (0.8866)
Aromatase binding: Predicted Result (Probability)	Yes (0.8349)	Yes (0.7496)	Yes (0.7356)	Yes (0.6306)	Yes (0.8233)
PPAR gamma: Predicted Result (Probability)	Yes (0.8881)	Yes (0.9269)	Yes (0.9181)	Yes (0.9207)	Yes (0.8806)
hERG Inhibition: Predicted Result (Probability)	Yes (0.8596)	Yes (0.8107)	Yes (0.8796)	Yes (0.7901)	No (0.4682)
Hepatotoxicity: Predicted Result (Probability)	Yes (0.8250)	Yes (0.8500)	Yes (0.8750)	Yes (0.8750)	Yes (0.8500)
Acute Oral Toxicity: Predicted Result (Probability)	III (0.6502)	III (0.6572)	III (0.6999)	III (0.6479)	III (0.7477)

* Molecular weight, alogP, number of atoms, number of rings, H-bond acceptors, and H-bond donors was used to calculate this factor.

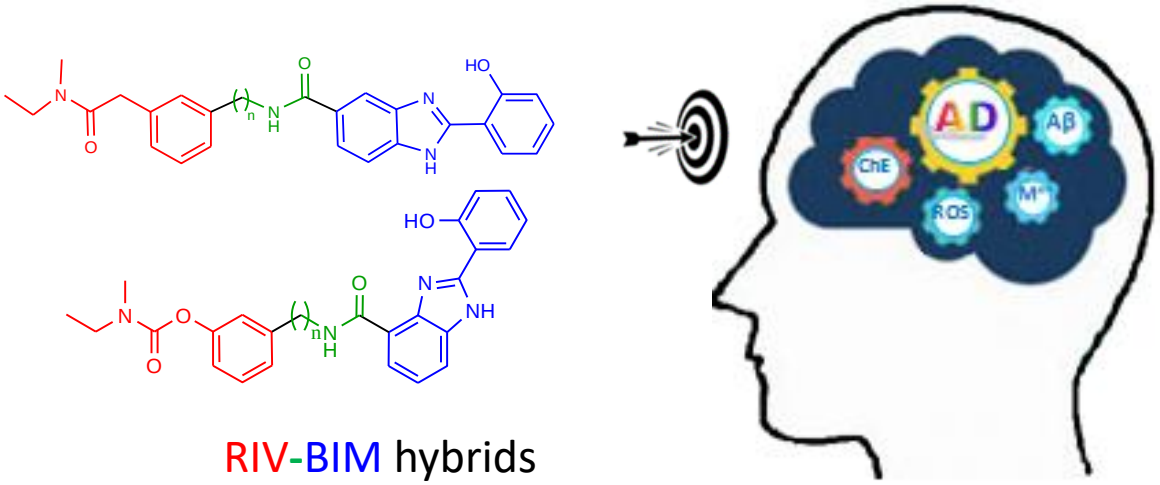
** CYP inhibitory promiscuity refers to the capacity for compounds to bind to different CYP enzymes (Substrate of CYP2C9, 2D6, 3A4 and Inhibitor of CYP1A2, 2D6, 2C9, 2C19, 3A4).

Artículo 3: **Nuevos derivados de la rivastigmina como compuestos multi-diana prometedores para el tratamiento potencial de la enfermedad de Alzheimer**

Novel rivastigmine derivatives as promising multi-target compounds for the potential treatment of Alzheimer's disease

David Vicente-Zurdo, Noelia Rosales-Conrado, M. Eugenia León-González, Leonardo Brunetti, Luca Piemontese, A. Raquel Pereira-Santos, Sandra M. Cardoso, Yolanda Madrid, Sílvia Chaves, M. Amélia Santos

Biomedicines 10 (2022) 1510 (*Impact factor: 4.757*)



Parte de los resultados de este trabajo se presentaron en:

"INTERNATIONAL SYMPOSIUM ON METAL COMPLEXES 2022 (ISMEAC 2022)". *Novel Rivastigmine-based Multi-target Hybrids for Potential Treatment of Alzheimer's Disease: Cu(II) and Fe(III) chelation studies.* Valencia, España, junio de 2022. Tipo de comunicación: póster.

"XXIII REUNIÓN DE LA SOCIEDAD ESPAÑOLA DE QUÍMICA ANALÍTICA (XXIII SEQA)". *Novel BIM-RIV hybrids as promising multi-target compounds for the potential treatment of Alzheimer's disease.* Oviedo, España, julio de 2022. Tipo de comunicación: póster.

biomedicines

MDPI

Article

Novel Rivastigmine Derivatives as Promising Multi-Target Compounds for Potential Treatment of Alzheimer's Disease

David Vicente-Zurdo [1,2], Noelia Rosales-Conrado [2], M. Eugenia León-González [2], Leonardo Brunetti [1,3], Luca Piemontese [3], A. Raquel Pereira-Santos [4], Sandra M. Cardoso [4,5], Yolanda Madrid [2], Sílvia Chaves [1,*] and M. Amélia Santos [1,*]

1 Centro de Química Estrutural, Institute of Molecular Sciences, Departamento de Engenharia Química, Instituto Superior Técnico, Universidade de Lisboa, Av. Rovisco Pais 1, 1049-001 Lisboa, Portugal; davidvic@ucm.es (D.V.-Z.); leonardo.brunetti@uniba.it (L.B.)
2 Department of Analytical Chemistry, Faculty of Chemistry, Complutense University of Madrid, Avenida Complutense s/n, 28040 Madrid, Spain; nrosales@ucm.es (N.R.-C.); leongon@ucm.es (M.E.L.-G.); ymadrid@quim.ucm.es (Y.M.)
3 Department of Pharmacy-Pharmaceutical Sciences, University of Bari Aldo Moro, Via E. Orabona 4, 70125 Bari, Italy; luca.piemontese@uniba.it
4 CNC-Center for Neuroscience and Cell Biology, University of Coimbra, 3000-370 Coimbra, Portugal; arsantos@cnc.uc.pt (A.R.P.-S.); cardoso.sandra.m@gmail.com (S.M.C.)
5 FMUC-Faculty of Medicine, University of Coimbra, 3000-370 Coimbra, Portugal
* Correspondence: silvia.chaves@tecnico.ulisboa.pt (S.C.); masantos@ist.utl.pt (M.A.S.)

Abstract: Alzheimer's disease (AD) is the most serious and prevalent neurodegenerative disorder still without cure. Since its aetiology is diverse, recent research on anti-AD drugs has been focused on multi-target compounds. In this work, seven novel hybrids (RIV–BIM) conjugating the active moiety of the drug rivastigmine (RIV) with 2 isomeric hydroxyphenylbenzimidazole (BIM) units were developed and studied. While RIV assures the inhibition of cholinesterases, BIM provides further appropriate properties, such as inhibition of amyloid β-peptide (Aβ) aggregation, antioxidation and metal chelation. The evaluated biological properties of these hybrids included antioxidant activity; inhibition of acetylcholinesterase (AChE), butyrylcholinesterase (BChE) and $A\beta_{42}$ aggregation; as well as promotion of cell viability and neuroprotection. All the compounds are better inhibitors of AChE than rivastigmine (IC_{50} = 32.1 μM), but compounds of series **5** are better inhibitors of BChE (IC_{50} = 0.9−1.7 μM) than those of series **4**. Series **5** also showed good capacity to inhibit self- (42.1−58.7%) and Cu(II)-induced (40.3−60.8%) Aβ aggregation and also to narrow (22.4−42.6%) amyloid fibrils, the relevant compounds being **5b** and **5d**. Some of these compounds can also prevent the toxicity induced in SH-SY5Y cells by $A\beta_{42}$ and oxidative stress. Therefore, RIV–BIM hybrids seem to be potential drug candidates for AD with multi-target abilities.

Keywords: Alzheimer's disease; multi-target drugs; rivastigmine; neurodegenerative; amyloid aggregation; acetylcholinesterase; butyrylcholinesterase

check for updates

Citation: Vicente-Zurdo, D.; Rosales-Conrado, N.; León-González, M.E.; Brunetti, L.; Piemontese, L.; Pereira-Santos, A.R.; Cardoso, S.M.; Madrid, Y.; Chaves, S.; Santos, M.A. Novel Rivastigmine Derivatives as Promising Multi-Target Compounds for Potential Treatment of Alzheimer's Disease. *Biomedicines* **2022**, *10*, 1510. https://doi.org/10.3390/biomedicines10071510

Academic Editors: Susana Cardoso, Cristina Carvalho and Sónia Catarina Correia

Received: 29 May 2022
Accepted: 21 June 2022
Published: 26 June 2022

Publisher's Note: MDPI stays neutral with regard to jurisdictional claims in published maps and institutional affiliations.

Copyright: © 2022 by the authors. Licensee MDPI, Basel, Switzerland. This article is an open access article distributed under the terms and conditions of the Creative Commons Attribution (CC BY) license (https://creativecommons.org/licenses/by/4.0/).

1. Introduction

Neurodegenerative diseases, such as Alzheimer's disease (AD), Parkinson's disease (PD), Huntington's disease (HD) and amyotrophic lateral sclerosis (ALS), are a group of complex disorders with multiple aetiologies and pathogeneses [1]. The most common cause of dementia is AD, representing 70% of the neurodegenerative diseases and entailing huge financial and healthcare costs [2–4]. Nowadays, AD affects around 50 million people worldwide, and this number is expected to increase in the coming years, making AD one of the top six causes of death [5]. AD is an age-related disorder, the main hallmark of which is the formation of senile plaques outside the neurons [6]. Although its origin remains unclear, the most widely accepted explanation is the "amyloid cascade hypothesis" [7–9]. In fact,

the aggregation of amyloid plaques causes irreversible damage to neurons and synapses, resulting in cognitive deficits. Senile plaques are comprised of fibrillary aggregates of amyloid-beta peptides (Aβ), which enclose elevated levels of $A\beta_{1\text{-}42}$ ($A\beta_{42}$), resulting from the proteolytic cleavage of transmembrane proteins called Amyloid Precursor Proteins (APPs) by β- and γ-secretases; $A\beta_{1\text{-}42}$ includes 42 amino acid residues from 672 (Asp) to 713 (Ala) of APP [10–12]. The process of $A\beta_{42}$ aggregation into amyloid plaques is not yet clearly understood, but several factors, such as metal ion dyshomeostasis and increased oxidative stress, have been reported to trigger their formation [13]. In fact, more than two decades ago several studies revealed the accumulation of metal ions, such as Fe(II), Cu(II) and Zn(II), in amyloid aggregates [14]. Although they have been considered one of the main reasons for the protein aggregation in AD, their role in the pathogenesis remains unresolved, with findings of copper deficiency in some regions of post-mortem brains of AD patients [15]. However, the most critical roles have been attributed to the redox active metals, such as copper and iron, which, through Fenton's reaction, can produce reactive oxygen species (ROS), induce protein misfold and favour amyloid aggregation [16,17]. Therefore, targeting metal dyshomeostasis is a strategy that has been adopted for potential AD therapy [18,19], and numerous compounds enclosing metal chelating groups have been developed with envisagement of the neutralization of several mechanisms of AD pathogenesis, namely, those associated with oxidative stress in the brain and metal binding to the aberrant amyloid peptide (Aβ) [20–24].

Some neurotransmitters also play an important role in the aetiology of AD. In particular, those of the cholinergic system, acetylcholine (ACh) and butyrylcholine (BCh), are involved in critical neuronal processes, such as memory, learning, sensory information, attention and rest [9]. However, AD also affects the cholinergic system by the interaction between Aβ and the cholinergic receptors, decreasing limbic and neocortical innervation [25,26]. For this reason, inhibitors of cholinesterases (acetylcholinesterase (AChE) and butyrylcholinesterase (BChE)) increase the availability of ACh and BCh (involved in cholinergic signalling), thus improving central nervous system (CNS) performance and leading to symptomatic relief [3,26]. Therefore, up to now, the main class of anti-AD drugs approved by the US Food and Drug Administration (FDA) has been based on inhibitors of cholinesterases. In fact, among the six drugs approved in the US to treat AD, four (tacrine, donepezil, rivastigmine and galantamine) are AChE inhibitors [27–29], memantine is a *N*-methyl-D-aspartic acid (NMDA) receptor (NMDAR) antagonist [30] and aduhelm (aducanumab) is a monoclonal antibody (amyloid targeting drug) that has been recently approved (in June 2021) [31].

Although progress has been made in understanding the mechanisms of the disease towards its treatment, all the approved anti-AD drugs have focused on only one disease target and only lead to temporary symptomatic relief. The numerous and complex pathological features of this disease are surely the main reason for the absence of disease-modifying drugs up to now. Therefore, to tackle this multi-factorial disease, the development of multi-target therapeutic agents has been increasingly recognized as a promising strategy to combat AD and many authors have pursued this drug development strategy, in many cases via drug repositioning approaches [22–24,32–34].

Following our recent multi-target approach for anti-AD drugs, based on the hybridization of tacrine and donepezil [35,36], we set up our research project to develop a novel series of molecular hybrids (RIV–BIMs) by conjugating the rivastigmine pharmacophore (RIV) with a hydroxyphenylbenzimidazole (BIM) moiety. Rivastigmine (trade name Exelon) is a well-known, second-generation carbamate ChE inhibitor drug (approved by the FDA in 2000) that alleviates the symptoms of the disease through the deceleration of its progression [37,38] and presents advantages over first-generation drugs: rapid BBB crossing and low marginal side effects [39]. Although a high number of recently developed multi-target-directed anti-AD drug candidates have included the active moiety of approved AChE inhibitor drugs (e.g., tacrine, donepezil), only a very few have enclosed the pharmacophoric moiety of the drug inhibitor of both ChEs (rivastigmine) [33,40,41]. The

selection of hydroxyphenylbenzimidazole (BIM), as the second active moiety of the (RIV–BIM) hybrids, is motivated by its analogy with thioflavin-based intercalation compounds and also by its already demonstrated good capacity to inhibit amyloid aggregation [35,42], reduce ROS and chelate metal ions involved in AD [33,42–44]. In fact, recently reported conjugates of BIM derivatives with two anti-AD approved drugs, namely, tacrine and donepezil pharmacophores, were proven to endow the corresponding molecular hybrids with improved AChE inhibitory capacity and other relevant biological activities in the context of well-recognized targets for AD therapy [35,44].

Herein, we report the design, development and study of a new set of seven RIV–BIM conjugates with some isomeric structural variations encompassing different sizes of linkers between the bioactive moieties and the positional isomerization of the BIM moiety. In particular, *para*-substituted (BIMa) and *ortho*-substituted (BIMb) resulted in two respective series (**4** and **5**) of compounds (Figure 1) with some expected differences in their biochemical properties. Molecular modelling for this series of novel potential drug candidates allows predictions of their interactions with enzymes and aids the rationalization of results as well as their pharmacokinetic properties. Specifically, docking studies of the compounds with AChE and BChE, as well as modelling of pharmacokinetic properties, were carried out by using in-house computational tools. Essential biological properties have also been evaluated, such as antioxidant activity (radical scavenging activity), inhibition of AChE and BChE, inhibition of $A\beta_{42}$ self-aggregation and Cu(II)-induced aggregation, cell viability and neuroprotection capacity. The results are discussed in terms of structure–activity relationships, with predictions for the best potential anti-AD drug candidates deserving further study.

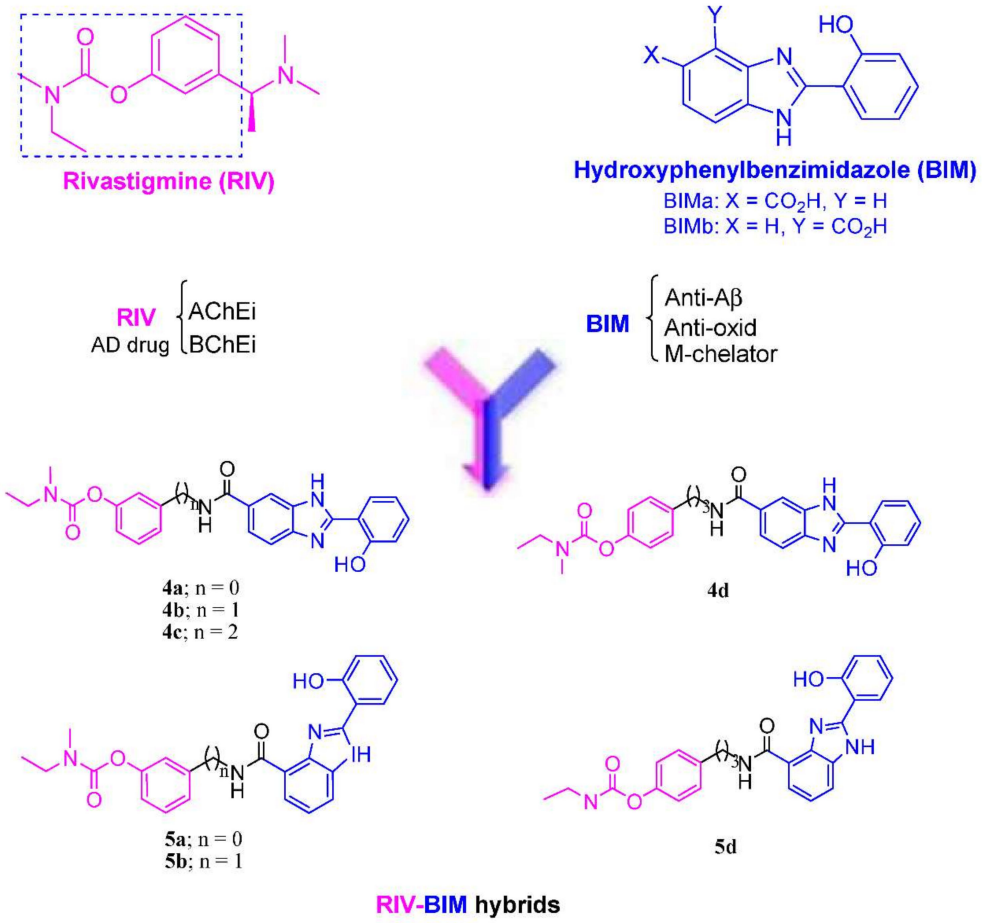


Figure 1. Design strategy for the RIV–BIM hybrids (**4a**–**4d**) and (**5a**–**5d**), from templates with rivastigmine and hydroxyphenylbenzimidazole and positional isomers.

2. Materials and Methods

2.1. Chemistry

2.1.1. General Methods and Materials

Reagents of analytical grade were acquired from Honeywell, Labchem, Sigma-Aldrich and Scharlab. Solvents were dried in consonance with standard methods [45]. TLC was performed to monitor chemical reactions using aluminium plates coated with silica gel 60 F_{254} obtained from Merck. Column chromatographic separations were performed with silica gel 60A 70–200 µ obtained from Carlo Erba Reagents. Melting points (M.P.s) were measured using a Leica Galen III hot stage microscope. NMR spectra (^{1}H and ^{13}C) were recorded on a Bruker AVANCE III-300 NMR spectrometer (at 300 and 75 MHz). Standard internal reference of tetramethylsilane (TMS) was employed to report the chemical shifts (δ). The abbreviations used are as follows: s = singlet, d = doublet, t = triplet, q = quartet, m = multiplet. Mass spectra (ESI-MS) were captured with a 500 MS LC Ion Trap mass spectrometer (Varian Inc., Palo Alto, CA, USA) equipped with an ESI ion source, operated in the positive ion mode. High-resolution mass spectra (HRMS) were obtained on a Bruker Impact II quadrupole mass spectrometer (Bruker Daltoniks, Billerica, MA, USA).

2.1.2. Preparation of Hydroxyphenylbenzimidazole Carboxylic Acids (BIMa, BIMb)

To a solution of 6 mmol of salicylaldehyde in 10 mL of DMA (*N*,*N*-dimethylacetamide) were added 6 mmol of diaminobenzoic acid (3,4-diaminobenzoic acid or 2,3-diaminobenzoic acid) and 7.2 mmol of $Na_2S_2O_5$. The mixture was heated to 100 °C for 12 h until the completion of the reaction was confirmed by TLC. The reaction mixture was then cooled at room temperature, diluted with ethyl acetate, dried with Na_2SO_4, filtered and concentrated in vacuo. The solid obtained was collected on a sintered-glass filter and washed with cold dichloromethane to provide the desired solid compound.

2-(2-Hydroxyphenyl)-1*H*-benzo[*d*]imidazole-6-carboxylic Acid (BIMa)

This was synthesized from 3,4-diaminobenzoic acid to give **BIMa** as a white-coloured solid. The completion of the reaction was controlled by TLC (CH_2Cl_2/MeOH, 15/1). Yield = 79.9%. ^{1}H NMR (300 MHz, MeOD-d_4), δ (ppm): 8.29 (s, 1H, BIMa-*Ph*), 7.92–7.97 (m, 2H, BIMa-*Ph*), 7.63 (d, 1H, *J* = 9 Hz, BIMa-*Ph*), 7.35 (t, 1H, *J* = 9 Hz, BIMa-*Ph*), 6.95–7.03 (m, 2H, BIMa-*Ph*). MS-ESI (*m*/*z*): 253.15 $(M-1)^-$, 254.12 $(M)^-$, 255.12 $(M+1)^+$, 256.14 $(M+2)^+$.

2-(2-Hydroxyphenyl)-1*H*-benzo[*d*]imidazole-7-carboxylic Acid (BIMb)

This was synthesized from 2,3-diaminobenzoic acid to give **BIMb** as a light-brown-coloured solid. The completion of the reaction was controlled by TLC (CH_2Cl_2/MeOH, 2/1). Yield = 86.6%. ^{1}H NMR (300 MHz, DMSO-d_6), δ (ppm): 8.34 (d, 1H, *J* = 9 Hz, BIMb-H-6), 7.93 (d, 1H, *J* = 6 Hz, BIMb-*Ph*), 7.84 (d, 1H, *J* = 9 Hz, BIMb-*Ph*), 7.33–7.41 (m, 2H, BIMb-*Ph*), 7.07 (d, 1H, *J* = 9 Hz, BIMb-*Ph*), 7.01 (t, 1H, *J* = 9 Hz, BIMb-*Ph*). MS-ESI (*m*/*z*): 253.17 $(M-1)^-$, 254.14 $(M)^-$, 255.04 $(M+1)^+$, 256.08 $(M+2)^+$.

2.1.2.3. General Procedure for the Synthesis of the Carbamates (**2a**–**d**)

To a solution of 1 mL of TEA (triethylamine) were added 1.65 mmol of *N*-ethylmethylcarbomyl chloride and 1.62 mmol of the nitro- or cyano-derivative (3-nitrophenol, 3-cyanophenol, (3-hydroxyphenyl)acetonitrile or 3-(4-hydroxyphenyl) propionitrile). The mixture was stirred at 95 °C for 12 h. Then, the reaction mixture was diluted with CH_2Cl_2, washed with NaOH 1M, dried over Na_2SO_4, filtrated and evaporated in vacuo to obtain the desired oiled compound.

3-Nitrophenyl Ethylmethylcarbamate (**2a**)

This was synthesized from 3-nitrophenol, affording **2a** as a pale-brown oil. The completion of the reaction was controlled by TLC (CH_2Cl_2/MeOH, 60/1). Yield = 82.9%. ^{1}H NMR (300 MHz, MeOD-d_4), δ (ppm): 8.08 (d, 1H, *J* = 9 Hz,-*Ph*), 8.00 (s, 1H, *Ph*), 7.61 (t, 1H, *J* = 9 Hz, *Ph*), 7.53 (d, 1H, *J* = 9 Hz, *Ph*), 3.51 (q, 1H, *J* = 6 Hz, N$CH_2$$CH_3$ rotamer), 3.40

(q, 1H, *J* = 6 Hz, NCH_2CH$_3$ rotamer), 3.10 (s, 1.5H, NCH_3 rotamer), 2.98 (s, 1.5H, NCH_3 rotamer), 1.26 (t, 1.5H, *J* = 6 Hz, CH$_2$CH_3 rotamer), 1.18 (t, *J* = 6 Hz, CH$_2$CH_3 rotamer). MS-ESI (*m*/*z*): 225.06 (M + 1)$^+$, 225.97 (M + 2)$^+$.

3-Cyanophenyl Ethylmethylcarbamate (**2b**)

This was synthesized from 3-cyanophenol, affording **2b** as a pale-brown oil. The completion of the reaction was controlled by TLC (CH$_2$Cl$_2$/MeOH, 60/1). Yield = 93.1%. ^{1}H NMR (300 MHz, MeOD-d_4), δ (ppm): 7.56 (s, 1H, *Ph*), 7.51–7.53 (m, 2H, *Ph*), 7.42 (d, 1H, *J* = 6 Hz, *Ph*), 3.49 (q, 1H, *J* = 9 Hz, NCH_2CH$_3$ rotamer), 3.37 (*q*, 1H, *J* = 9 Hz, NCH_2CH$_3$ rotamer), 3.08 (s, 1.5H, NCH_3 rotamer), 2.96 (s, 1.5H, NCH_3 rotamer), 1.23 (*t*, 1.5H, *J* = 9 Hz, CH$_2$CH_3 rotamer), 1.16 (t, 1.5H, *J* = 9 Hz, CH$_2$CH_3 rotamer). MS-ESI (*m*/*z*): 205.13 (M + 1)$^+$.

3-(Cyanomethyl)phenyl Ethylmethylcarbamate (**2c**)

This was synthesized from (3-hydroxyphenyl)acetonitrile, affording **2c** as a pale-brown oil. The completion of the reaction was controlled by TLC (CH$_2$Cl$_2$/MeOH, 30/1). Yield = 76.7%. ^{1}H NMR (300 MHz, MeOD-d_4), δ (ppm): 7.38 (t, 1H, *J* = 9 Hz, *Ph*), 7.21 (d, 1H, *J* = 9 Hz, *Ph*), 7.10 (s, 1H, *Ph*), 7.06 (d, 1H, *J* = 9 Hz, *Ph*), 3.90 (s, 2H, PhCH_2CN), 3.49 (q, 1H, *J* = 6 Hz, NCH_2CH$_3$ rotamer), 3.37 (q, 1H, *J* = 6 Hz, NCH_2CH$_3$ rotamer), 3.08 (s, 1.5H, NCH_3 rotamer), 2.96 (s, 1.5H, NCH_3 rotamer), 1.24 (*t*, 1.5H, *J* = 6 Hz, CH$_2$CH_3 rotamer), 1.16 (t, 1.5H, *J* = 6 Hz, CH$_2$CH_3 rotamer). MS-ESI (*m*/*z*): 219.16 (M + 1)$^+$, 220.15 (M + 2)$^+$.

4-(2-Cyanoethyl)phenyl Ethylmethylcarbamate (**2d**)

This was synthesized from 3-(4-hydroxyphenyl)propionitrile, affording **2d** as a pale-brown oil. The completion of the reaction was controlled by TLC (CH$_2$Cl$_2$/MeOH, 30/1). Yield = 99.4%. ^{1}H NMR (300 MHz, MeOD-d_4), δ (ppm): 7.30 (d, 2H, *J* = 6 Hz, *Ph*), 7.05 (d, 2H, *J* = 6 Hz, *Ph*), 3.50 (q, 1H, *J* = 6 Hz, NCH_2CH$_3$ rotamer), 3.38 (q, 1H, *J* = 6 Hz, NCH_2CH$_3$ rotamer), 3.08 (s, 1.5H, NCH_3 rotamer), 2.96 (s, 1.5H, NCH_3 rotamer), 2.92 (d, 2H, *J* = 6 Hz, PhCH_2CH$_2$), 2.72 (t, 2H, *J* = 6 Hz, CH$_2$CH_2CN), 1.25 (t, 1.5H, *J* = 6 Hz, CH$_2$CH_3 rotamer), 1.17 (t, 1.5H, *J* = 6 Hz, CH$_2$CH_3 rotamer). MS-ESI (*m*/*z*): 233.17 (M + 1)$^+$, 234.22 (M + 2)$^+$.

2.1.3. General Procedure for the Synthesis of the Amino-Carbamates (**3a**–**d**)

In this procedure, 1.45 mmol of the nitro- or cyano-carbamate derivatives (**2a–d**) (3-nitrophenyl ethylmethylcarbamate, 3-cyanophenyl ethylmethylcarbamate, 3-(cyanomethyl)phenyl ethylmethylcarbamate, 4-(2-cyanoethyl)phenylethylmethylcarbamate) was hydrogenated in 15 mL of MeOH in the presence of 2.12 mmol of 10% Pd-C for 4 h at 4 bar. Then, the catalyst was filtered off and the solution was evaporated until dryness, providing the final amine as an oil of compounds **3a** and **3b**. For the hydrogenolysis of compounds **3c** and **3d**, an identical procedure was followed, though some drops of concentrated HCl were added to the methanolic suspension. Then, the catalyst was filtered off and the solution was evaporated to dryness. The residue was diluted with CH$_2$Cl$_2$ and washed with NaOH 1 M and H$_2$O until a pH > 7 was reached. The organic layer phase was dried over Na$_2$SO$_4$ and evaporated. The crude oil compound was purified by chromatography column (with eluent MeOH/CH$_2$Cl$_2$/NH$_3$, 49/49/2).

3-Aminophenyl Ethylmethylcarbamate (**3a**)

This was synthesized from 3-nitrophenyl ethylmethylcarbamate (**2a**) to give **3a** as a pale-yellow oil. The completion of the reaction was controlled by TLC (CH$_2$Cl$_2$/MeOH, 60/1). Yield = 40.8%. ^{1}H NMR (300 MHz, MeOD-d_4), δ (ppm): 7.04 (t, 1H, *J* = 9 Hz, *Ph*), 6.53 (d, 1H, *J* = 9 Hz, *Ph*), 6.40 (s, 1H, *Ph*), 6.35 (d, 1H, *J* = 9 Hz, *Ph*), 3.42 (q, 1H, *J* = 6 Hz, NCH_2CH$_3$ rotamer), 3.35 (q, 1H, *J* = 6 Hz, NCH_2CH$_3$ rotamer), 3.03 (s, 1.5H, NCH_3 rotamer), 2.93 (s, 1.5H, NCH_3 rotamer), 1.21 (t, 1.5H, *J* = 6 Hz, CH$_2$CH_3 rotamer), 1.14 (t, 1.5H, *J* = 6 Hz, CH$_2$CH_3 rotamer). MS-ESI (*m*/*z*): 195.05 (M + 1)$^+$, 196.09 (M + 2)$^+$.

3-(Aminomethyl)phenyl Ethylmethylcarbamate (**3b**)

This was synthesized from 3-cyanophenyl ethylmethylcarbamate (**2b**) to give the crude oil of the compound. The completion of the reaction was controlled by TLC (EtOAc/NH3, 98/2). Then, the crude oil compound was purified by chromatography column (with eluent EtOAc/NH3, 98/2), affording the pure compound **3b** as a pale-yellow oil. Yield = 76.6%. ^{1}H NMR (300 MHz, MeOD-d_4), δ (ppm): 7.35 (t, 1H, *J* = 9 Hz, *Ph*), 7.21 (d, 1H, *J* = 9 Hz, *Ph*), 7.10 (s, 1H, *Ph*), 7.01 (d, 1H, *J* = 9Hz, *Ph*), 3.85 (s, 2H, PhCH_2NH$_2$), 3.49 (q, 1H, *J* = 6 Hz, NCH_2CH$_3$ rotamer), 3.37 (q, 1H, *J* = 6 Hz, NCH_2CH$_3$ rotamer), 3.08 (s, 1.5H, NCH_3 rotamer), 2.96 (s, 1.5H, NCH_3 rotamer), 1.24 (t, 1.5H, *J* = 6 Hz, CH$_2$$CH_3$ rotamer), 1.16 (t, 1.5H, *J* = 6 Hz, CH$_2$$CH_3$ rotamer). MS-ESI (*m*/*z*): 209.00 (M + 1)$^+$, 209.83 (M + 2)$^+$.

3-(2-Aminoethyl)phenyl Ethylmethylcarbamate (**3c**)

This was synthesized from 3-(cyanomethyl)phenyl ethylmethylcarbamate (**2c**), affording the pure compound **3c** as a beige oil. Yield = 22.0%. ^{1}H NMR (300 MHz, MeOD-d_4), δ (ppm): 7.30 (t, 1H, *J* = 6 Hz, *Ph*), 7.08 (d, 1H, *J* = 6 Hz, *Ph*), 6.95 (s, 1H, *Ph*), 6.94 (d, 1H, *J* = 6 Hz, *Ph*), 3.49 (q, 1H, *J* = 6 Hz, NCH_2CH$_3$ rotamer), 3.38 (q, 1H, *J* = 6 Hz, NCH_2CH$_3$ rotamer), 3.08 (s, 1.5H, NCH_3 rotamer), 2.96 (s, 1.5H, NCH_3 rotamer), 2.88 (t, 2H, *J* = 6 Hz, CH$_2$$CH_2NH_2$), 2.76 (t, 2H, *J* = 6 Hz, PheCH_2CH$_2$), 1.25 (t, 1.5H, *J* = 6 Hz, CH$_2$$CH_3$ rotamer), 1.17 (t, 1.5H, *J* = 6 Hz, CH$_2$$CH_3$ rotamer). MS-ESI (*m*/*z*): 222.49 (M)$^-$, 223.20 (M + 1)$^+$, 224.24 (M + 2)$^+$.

4-(3-Aminopropyl)phenyl Ethylmethylcarbamate (**3d**)

This was synthesized from 4-(2-cyanoethyl)phenyl ethylmethylcarbamate (**2d**), affording the pure compound **3d** as a pale-yellow oil. Yield = 30.2%. ^{1}H NMR (300 MHz, MeOD-d_4), δ (ppm): 7.23 (d, 2H, *J* = 6 Hz, *Ph*), 7.01 (d, 2H, *J* = 6 Hz, *Ph*), 3.49 (q, 1H, *J* = 6 Hz, NCH_2CH$_3$ rotamer), 3.38 (q, 1H, *J* = 6 Hz, NCH_2CH$_3$ rotamer), 3.07 (s, 1.5H, NCH_3 rotamer), 2.89–2.96 (m, 3.5H, PhCH_2CH$_2$ and NCH_3 rotamer), 2.71 (t, 2H, *J* = 6 Hz, CH$_2$$CH_2NH_2$), 1.96 (quintet, 2H, *J* = 6 Hz, CH$_2$$CH_2CH_2$), 1.24 (t, 1.5H, *J* = 6 Hz, CH$_2$$CH_3$ rotamer), 1.16 (t, 1.5H, *J* = 6 Hz, CH$_2$$CH_3$ rotamer). MS-ESI (*m*/*z*): 237.20 (M + 1)$^+$, 238.18 (M + 2)$^+$.

2.1.4. General Synthetic Procedure for the RIV–BIMa Hybrids (**4a**–**d**)

To a water-ice-cooled solution of 1 mmol of 2-(2-hydroxyphenyl)-1*H*-benzo[*d*]imidazole-6-carboxylic acid (**BIMa**) in dry DMF (5 mL), under nitrogen atmosphere, were added 2 mmol of NMM, followed by the addition of 1 mmol of TBTU, and this solution was stirred for 50 min. Then, the carboxylic acid derivative solution was added dropwise to a water-ice-cooled solution of 1 mmol of the corresponding amine derivative (3-aminophenyl ethylmethylcarbamate (**3a**), 3-(aminomethyl)phenyl ethylmethylcarbamate (**3b**), 3-(2-aminoethyl)phenyl ethylmethylcarbamate (**3c**), 4-(3-aminopropyl)phenyl ethylmethylcarbamate (**3d**)) in 5 mL of dry DMF. The reaction mixture was stirred for 20 h under nitrogen atmosphere to reaction completion. Afterwards, DMF was evaporated under high vacuum. The residue was diluted with CH_2Cl_2, and the organic solution was washed with H_2O, dried with Na_2SO_4, filtrated, roto-evaporated and dried in vacuo to obtain the crude solid.

3-(2-(2-Hydroxyphenyl)-1*H*-benzo[*d*]imidazole-6-carboxamido)phenyl Ethylmethylcarbamate, RIV–BIMa (**4a**)

This was synthesized from 3-aminophenylethylmethylcarbamate (**3a**). The completion of the reaction was controlled by TLC (AcOEt/Hexane, 5/1). The crude solid was purified by chromatography column (with eluent AcOEt/hexane, 5/1), affording the pure compound **4a** as a light-pink-coloured solid. Yield = 21.4%. M.P. = 200 °C. RF (AcOEt/hexane, 5/1) = 0.8. ^{1}H NMR (300 MHz, MeOD-d_4), δ (ppm): 8.22 (s, 1H, *Ph*), 7.95 (d, 1H, *J* = 9 Hz, *Ph*), 7.88 (d, 1H, *J* = 9 Hz, *Ph*), 7.70 (d, 1H, *J* = 9 Hz, *Ph*), 7.63 (s, 1H, *Ph*), 7.55 (d, 1H, *J* = 9 Hz, *Ph*), 7.32–7.40 (m, 2H, *Ph*), 6.97–7.04 (m, 2H, *Ph*), 6.88 (d, 1H, *J* = 9 Hz, *Ph*), 3.51 (q, 1H, *J* = 6 Hz, NCH_2CH$_3$ rotamer), 3.40 (q, 1H, *J* = 6 Hz, NCH_2CH$_3$ rotamer), 3.10

(s, 1.5H, NCH_3 rotamer), 2.98 (s, 1.5H, NCH_3 rotamer), 1.26 (t, 1.5H, J = 6 Hz, CH_2CH_3 rotamer), 1.18 (t, 1.5H, J = 6 Hz, CH_2CH_3 rotamer). ^{13}C NMR (75 MHz, MeOD-d_4), δ (ppm): 169.18, 159.69, 153.16, 141.31, 133.55, 131.02, 130.46, 127.80, 123.95, 120.70, 118.94, 118.47, 115.68, 113.94, 45.30, 34.41, 13.55. HRMS (ESI) calculated for $C_{24}H_{23}N_4O4$ [M + H] 431.1719, found 431.1732.

3-((2-(2-Hydroxyphenyl)-1*H*-benzo[*d*]imidazole-6-carboxamido)methyl) Phenyl Ethylmethylcarbamate, RIV–BIMa (**4b**)

This was synthesized from 3-(aminomethyl)phenyl ethylmethylcarbamate (**3b**). The completion of the reaction was controlled by TLC (AcOEt/hexane, 5/1). The crude solid was purified by chromatography column (with eluent AcOEt/hexane, 5/1), affording the pure compound **4b** as a white-coloured solid. Yield = 56.8%. M.P. = 230 °C. RF (AcOEt/hexane, 5/1) = 0.66. ^{1}H NMR (300 MHz, MeOD-d_4), δ (ppm): 8.15 (s, 1H, *Ph*), 7.94 (d, 1H, J = 9 Hz, *Ph*), 7.80 (d, 1H, J = 9 Hz, *Ph*), 7.66 (d, 1H, J = 9 Hz, *Ph*), 7.32–7.38 (m, 2H, *Ph*), 7.25 (d, 1H, J = 6 Hz, *Ph*), 7.12 (s, 1H, *Ph*), 6.96–7.03 (m, 3H, *Ph*), 4.61 (s, 2H, PhCH_2NH), 3.48 (q, 1H, J = 6 Hz, NCH_2CH$_3$ rotamer), 3.37 (q, 1H, J = 6 Hz, NCH_2CH$_3$ rotamer), 3.07 (s, 1.5H, NCH_3 rotamer), 2.95 (s, 1.5H, NCH_3 rotamer), 1.23 (t, 1.5H, J = 6 Hz, CH_2CH_3 rotamer), 1.15 (t, 1.5H, J = 6 Hz, CH_2CH_3 rotamer). ^{13}C NMR (75 MHz, MeOD-d_4), δ (ppm): 159.61, 133.20, 130.48, 127.53, 125.70, 120.52, 118.37, 114.11, 44.30, 42.01, 17.38. HRMS (ESI) calculated for $C_{25}H_{25}N_4O_4$ [M + H] 445.1876, found 445.1897.

3-(2-(2-(2-Hydroxyphenyl)-1*H*-benzo[*d*]imidazole-6-carboxamido)ethyl) Phenylethylmethylcarbamate, RIV–BIMa (**4c**)

This was synthesized from 3-(2-aminoethyl)phenyl ethylmethylcarbamate (**3c**). The completion of the reaction was controlled by TLC (AcOEt/hexane, 5/1). The crude solid was purified by chromatography column (with eluent AcOEt/hexane, 5/1), affording the pure compound **4c** as a white-coloured solid. Yield = 73.9%. M.P. = 212 °C. RF (AcOEt/hexane, 5/1) = 0.64. ^{1}H NMR (300 MHz, CD_3OD-d_4), δ (ppm): 8.05 (s, 1H, *Ph*), 7.94 (d, 1H, J = 9 Hz, *Ph*), 7.72 (d, 1H, J = 9 Hz, *Ph*), 7.63 (d, 1H, J = 9 Hz, *Ph*), 7.28–7.38 (m, 2H, *Ph*), 7.14 (d, 1H, J = 9 Hz, *Ph*), 6.94–7.03 (m, 4H, *Ph*), 3.64 (t, 2H, J = 9 Hz, CH_2CH_2NH), 3.47 (q, 1H, J = 6 Hz, NCH_2CH$_3$ rotamer), 3.37 (q, 1H, J = 6 Hz, NCH_2CH$_3$ rotamer), 3.06 (s, 1.5H, NCH_3 rotamer), 2.93–2.98 (m, 3.5H, PhCH_2CH$_2$ and NCH_3 rotamer), 1.20 (t, 1.5H, J = 6 Hz, CH_2CH_3 rotamer), 1.14 (t, 1.5H, J = 6 Hz, CH_2CH_3 rotamer). ^{13}C NMR (75 MHz, MeOD-d_4), δ (ppm): 170.69, 159.61, 152.93, 142.51, 133.17, 130.43, 127.50, 127.22, 123.44, 120.90, 120.51, 118.36, 114.12, 45.15, 42.53, 36.26. HRMS (ESI) calculated for $C_{26}H_{27}N_4O_4$ [M + H] 459.2032, found 459.2049.

4-(3-(2-(2-Hydroxyphenyl)-1*H*-benzo[*d*]imidazole-6-carboxamido)propyl) Phenyl Ethylmethylcarbamate, RIV–BIMa (**4d**)

This was synthesized from 4-(3-aminopropyl)phenylethylmethylcarbamate (**3d**). The completion of the reaction was controlled by TLC (CH_2Cl_2/MeOH, 15/1). The crude solid was purified by chromatography column (with eluent CH_2Cl_2/MeOH, 15/1), affording the pure compound **4d** as a light-yellow-coloured solid. Yield = 29.3%. M.P. = 231 °C. RF (AcOEt/hexane, 5/1) = 0.64. ^{1}H NMR (300 MHz, MeOD-d_4), δ (ppm): 8.08 (s, 1H, *Ph*), 7.94 (d, 1H, J = 6 Hz, *Ph*), 7.74 (d, 1H, J = 6 Hz, *Ph*), 7.64 (d, 1H, J = 9 Hz, *Ph*), 7.36 (t, 1H, J = 9 Hz, *Ph*), 7.25 (d, 2H, J = 9 Hz, *Ph*), 6.97–7.03 (m, 4H, *Ph*), 3.42–3.47 (m, 3H, CH_2CH_2NH and NCH_2CH$_3$ rotamer), 3.34 (q, 1H, J = 6 Hz, NCH_2CH$_3$ rotamer), 3.06 (s, 1.5H, NCH_3 rotamer), 2.95 (s, 1.5H, NCH_3 rotamer), 2.72 (t, 2H, J = 9 Hz, PhCH_2CH$_2$), 1.96 (quintet, 2H, J = 9 Hz, $CH_2CH_2CH_2$), 1.22 (t, 1.5H, J = 9 Hz, CH_2CH_3 rotamer), 1.18 (t, 1.5H, J = 9 Hz, CH_2CH_3 rotamer). ^{13}C NMR (75 MHz, DMSO-d_6), δ (ppm): 173.90, 166.43, 158.04, 153.75, 149.38, 138.60, 132.18, 129.04, 126.57, 121.71, 119.31, 117.30, 112.49, 48.64, 43.47, 33.91, 33.59, 32.03, 31.06, 29.34, 13.10, 12.31. HRMS (ESI) calculated for $C_{25}H_{25}N_4O_4$ [M + H] 473.2189, found 473.2203.

2.1.5. General Procedure for the RIV–BIMb Hybrids (**5a**, **5b**, **5d**)

To a water-ice-cooled solution of 1 mmol of 2-(2-hydroxyphenyl)-1*H*-benzo[*d*]imidazole-7-carboxylic acid (BIMb), under nitrogen atmosphere, was added 1 mmol of HOBT, followed by the addition of 1 mmol of EDCI, which was then stirred for 50 min. This acid solution was added dropwise to a water-ice-cooled solution of 1 mmol of the corresponding amine (3-aminophenyl ethylmethylcarbamate (3a), 3-(aminomethyl)phenyl ethylmethylcarbamate (3b), 4-(3-aminopropyl)phenyl ethylmethylcarbamate (3d)) in 5 mL of dry DMF. The reaction mixture was stirred for 20 h under nitrogen atmosphere. DMF was then evaporated under high vacuum. The residue was diluted with CH_2Cl_2, washed with H_2O, dried with Na_2SO_4, filtrated and dried to obtain the crude solid.

3-(2-(2-Hydroxyphenyl)-1*H*-benzo[*d*]imidazole-4-carboxamido)phenyl Ethylmethylcarbamate, RIV–BIMb (**5a**)

This was synthesized from 3-aminophenyl ethylmethylcarbamate (**3a**). The completion of the reaction was controlled by TLC (AcOEt/hexane, 5/1). The crude solid was purified by recrystallization in AcOEt/ethanol, affording the pure compound **5a** as a brown-coloured solid. Yield = 71.4%. M.P. = 222 °C. RF (AcOEt/hexane, 5/1) = 0.74. ^{1}H NMR (300 MHz, MeOD-d_4), δ (ppm): 8.21 (d, 1H, *J* = 9 Hz, *Ph*), 7.96 (d, 1H, *J* = 9 Hz, *Ph*), 7.79–7.83 (m, 2H, *Ph*), 7.54 (d, 1H, *J* = 9 Hz, *Ph*), 7.35–7.43 (m, 3H, *Ph*), 7.02–7.06 (m, 2H, *Ph*), 6.91 (d, 1H, *J* = 9 Hz, *Ph*), 3.54 (q, 1H, *J* = 9 Hz, NCH_2CH$_3$ rotamer), 3.42 (q, 1H, *J* = 9 Hz, NCH_2CH$_3$ rotamer), 3.13 (s, 1.5H, NCH_3 rotamer), 3.00 (s, 1.5H, NCH_3 rotamer), 1.32 (t, 1.5H, *J* = 9 Hz, CH$_2$$CH_3$ rotamer), 1.20 (t, 1.5H, *J* = 9 Hz, CH$_2$$CH_3$ rotamer). ^{13}C NMR (75 MHz, DMSO-d_6), δ (ppm): 163.66, 156.7, 153.68, 153.57, 151.76, 151.22, 139.88, 132.21, 129.61, 128.65, 122.85, 122.37, 119.82, 117.12, 117.01, 116.18, 114.17, 113.11, 43.59, 34.01, 33.67, 13.16, 12.35. HRMS (ESI) calculated for $C_{24}H_{23}N_4O_4$ [M + H] 431.1719, found 459.1731.

3-((2-(2-Hydroxyphenyl)-1*H*-benzo[*d*]imidazole-4-carboxamido)methyl) Phenyl Ethylmethylcarbamate RIV–BIMb (**5b**)

This was synthesized from 3-(aminomethyl)phenyl ethylmethylcarbamate (**3b**). The completion of the reaction was controlled by TLC (AcOEt/hexane, 5/1). The crude solid was purified by chromatography column (with eluent AcOEt/hexane, 5/1), affording the pure compound **5b** as a light-yellow-coloured solid. Yield = 38.8%. M.P. = 157 °C. RF (AcOEt/hexane, 5/1) = 0.76. ^{1}H NMR (300 MHz, MeOD-d_4), δ (ppm): 8.07 (d, 1H, *J* = 9 Hz, *Ph*), 7.84 (d, 1H, *J* = 9 Hz, *Ph*), 7.73 (d, 1H, *J* = 9 Hz, *Ph*), 7.32–7.40 (m, 2H, *Ph*), 7.20–7.29 (m, 3H, *Ph*), 7.02 (d, 1H, *J* = 6 Hz, *Ph*), 6.90 (d, 1H, *J* = 9 Hz, *Ph*), 6.76 (t, 1H, *J* = 9 Hz, *Ph*), 4.75 (s, 2H, PhCH_2NH), 3.43 (q, 1H, *J* = 6 Hz, NCH_2CH$_3$ rotamer), 3.33 (q, 1H, *J* = 6 Hz, NCH_2CH$_3$ rotamer), 3.03 (s, 1.5H, NCH_3 rotamer), 2.91 (s, 1.5H, NCH_3 rotamer), 1.18 (t, 1.5H, *J* = 6 Hz, CH$_2$$CH_3$ rotamer), 1.11 (t, 1.5H, *J* = 6 Hz, CH$_2$$CH_3$ rotamer). ^{13}C NMR (75 MHz, MeOD-d_4), δ (ppm): 168.78, 163.28, 156.33, 155.52, 153.15, 141.86, 132.84, 130.60, 129.20, 125.61, 123.12, 122.57, 121.90, 121.77, 121.10, 120.03, 118.34, 117.80, 116.04, 45.14, 44.06, 34.52, 34.29, 13.37, 12.61. HRMS (ESI) calculated for $C_{25}H_{25}N_4O_4$ [M + H] 445.1876, found 445.2189.

4-(3-(2-(2-Hydroxyphenyl)-1*H*-benzo[*d*]imidazole-4-carboxamido) Propyl) Phenyl Ethyl(methyl)carbamate, RIV–BIMb (**5d**)

This was synthesized from 4-(3-aminopropyl)phenyl ethylmethylcarbamate (**3d**). The completion of the reaction was controlled by TLC (AcOEt/hexane, 5/1). The crude solid was purified by chromatography column (with eluent AcOEt/hexane, 5/1), affording the pure compound **5d** as a pale-coloured solid. Yield = 13.1%. M.P. = 126 °C. RF (AcOEt/hexane, 5/1) = 0.69. ^{1}H NMR (300 MHz, MeOD-d$_4$), δ (ppm): 8.15 (d, 1H, *J* = 9 Hz, *Ph*), 7.81 (d, 1H, *J* = 6 Hz, *Ph*), 7.71 (d, 1H, *J* = 9 Hz, *Ph*), 7.25–7.28 (m, 4H, *Ph*), 6.97 (d, 2H, *J* = 9 Hz, *Ph*), 6.91 (d, 1H, *J* = 6 Hz, *Ph*), 6.76 (t, 1H, *J* = 9 Hz, *Ph*), 3.54 (t, 2H, *J* = 6 Hz, CH$_2$$CH_2$NH), 3.46 (q, 1H, *J* = 6 Hz, NCH_2CH$_3$ rotamer), 3.35 (q, 1H, *J* = 6 Hz, NCH_2CH$_3$ rotamer), 3.05 (s, 1.5H, NCH_3 rotamer), 2.93 (s, 1.5H, NCH_3 rotamer), 2.82 (t, 2H, *J* = 6 Hz, PhCH_2CH$_2$), 2.03 (quintet, 2H, *J* = 6 Hz, CH$_2$$CH_2CH_2$), 1.22 (t, 1.5H, *J* = 6 Hz, CH$_2$$CH_3$ rotamer), 1.14 (t, 1.5H, *J* = 6 Hz, CH$_2$$CH_3$ rotamer). ^{13}C NMR (75 MHz,

CD_3OD-d_4), δ (ppm): 168.94, 155.83, 151.10, 140.70, 140.31, 132.98, 130.51, 129.16, 123.20, 122.87, 122.61, 121.53, 120.36, 118.25, 117.50, 116.93, 116.21, 45.23, 40.23, 33.83, 32.47. HRMS (ESI) calculated for $C_{27}H_{29}N_4O_4$ [M + H] 473.2189, found 473.2211.

2.2. Molecular Modelling

Docking studies of the novel RIV–BIM hybrids with *Human* acetylcholinesterase (hAChE) and *Human* butyrylcholinesterase hBChE) were performed. For this purpose, two X-ray crystallographic structures were downloaded from RCSB Protein Data Bank (PDB entries 4EY7 for the complex of Human acetylcholinesterase (hAChE) with donepezil [46] and 4TPK for the complex of *Human* butyrylcholinesterase (hBChE) with *N*-((1-(2,3-dihydro-1*H*-inden-2-yl)piperidin-3-yl)methyl)-*N*-(2-methoxyethyl)-2-naphthamide [47]). Both crystallographic structures were chosen due to some close similarity between the ligands complexed with the enzymes, and the novel RIV–BIM hybrids. The original ligands, solvent and co-crystallization molecules of the X-ray complex structures were removed using Maestro v.9.3 [48], with the final addition of the hydrogen atoms. Then, the RIV–BIM structures were built in Maestro and, afterwards, to obtain an optimized structure with minimum energy, a random conformational search was performed using Ghemical v.2.0.0 (GPL, Burbank, CA, USA) [49]. Finally, the optimized models of the ligands were docked into the cavity of hAChE and hBChE model structures using GOLD software v.5.2. (CCDC, Cambridge, UK) [50]. Using the ASP as the best fitness function, 100 genetic algorithms steps were performed for the novel ligands to obtain the best matches between the RIV–BIM hybrids and the original ligands of hAChE (radius = 10) and hBChE (radius = 19). Figures of the hypothesized interaction between the ligands and the enzymes were obtained with Chimera software, with the residues between 0 and 5.0 Å from the original position of the ligand in the crystal structure selected as the interest zone. The docking protocol used herein was validated by re-docking the co-crystallized ligands (original ligands) into the corresponding active sites of hAChE or hBChe models [46,47].

2.3. Acetylcholinesterase and Butyrylcholinesterase Activity

The inhibition of electric eel acetylcholinesterase (eeAChE) and equine butyrylcholinesterase (eqBChE), both obtained from Sigma-Aldrich (Burlington, MA, USA), was studied using an adaptation of Elmman's method, as previously described [51]. For this, tris(hydroxymethyl)aminomethane (TRIS) 50 mM buffer at pH = 8.00, 4-(2-hydroxyethyl)-1-piperazine-ethanesulfonic acid (HEPES) 50 mM buffer at pH = 8.00 and HEPES 50 mM buffer at pH = 8.00 with NaCl 50 mM and $MgCl_2$ 20 mM were prepared. Stock solutions of 16 mM of acetylthiocholine iodide (AChI) and *S*-butyrylthiocholine iodide (BuChI) in distilled water were prepared and stored in the fridge. Working solutions of AChI and BChI were prepared daily by the proper dilution of the stock solutions in distilled water. A working solution of 5,5′-dithiobis-(2-nitrobenzoic acid) (DTNB) 3 mM in HEPES (NaCl, $MgCl_2$) was prepared daily and kept under darkness. Stock solutions of *ee*AChE and *eq*BChE were prepared by dissolving the lyophilized powder enzyme in 10 mL of TRIS buffer under ice and they were divided into aliquots of 50 and 5 UN mL^{-1} that were stored at −20 °C until needed. Stock solutions of 1 mg of each ligand in 1 mL MeOH (with 20% of DMSO) were prepared and working solutions for each ligand were obtained by the corresponding dilution from the stock solutions. A control measurement with 5 replicates (without ligand) and a calibration curve of 5 points with 3 replicates per point was derived. For each solution, fixed volumes of HEPES (374 µL) and *ee*AChE or *eq*BChE (25 µL) and different volumes of ligand (0–50 µL) and MeOH (0–50 µL) were added to quartz cells up to a total volume of 449 µL, and the solutions were left to rest for 15 min immediately after adding the eeAChE or eqBChE. A blank solution containing HEPES (399 µL) and MeOH (50 µL) was prepared at the same time. After 15 min of reaction, AChI or BChI (75 µL) and DTNB (476 µL) were added to both cuvettes and the absorption signal at 405 nm, with a slid width of 1 nm, was recorded over 5 min, with a time interval of 1 s, using a UV–Vis spectrophotometer (PerkinElmer) with the program PerkinElmer UV WinLab. The slope

for each calibration point was obtained (absorbance versus reaction time) and the inhibition for each compound was determined using the following equation:

$$\% \text{ Inhibition} = 100 - \left(\frac{v_i}{v_0} \times 100 \right)$$

where v_i is the reaction rate (slope) for each point of the calibrate (with ligand) and v_0 is the initial reaction rate (slope) for the control (without ligand). Once the inhibition values of the 5 points of the calibrate and the 3 replicates were obtained, the concentration of each point was plotted versus the percentage inhibition to obtain the inhibitor concentration corresponding to 50% inhibition of the enzyme. The experiments were performed twice.

2.4. Inhibition of Aβ$_{42}$ Aggregation

2.4.1. Fluorescence Assays

The inhibition of Aβ$_{42}$ aggregation and Cu(II)-induced Aβ$_{42}$ aggregation, carried out by the RIV–BIM hybrids, was studied using a reported method based on the fluorescence emission of thioflavin T [52,53].

Solutions of phosphate buffer 0.215 M at pH = 8.00, Na_2CO_3 300 μM in distilled water, NaOH 250 mM in distilled water, glycine-NaOH 50 mM buffer at pH = 8.50 and $CuCl_2$ 240 μM in phosphate buffer were prepared. Stock solutions of 1 mg L^{-1} of the RIV–BIM compounds were prepared in MeOH (with 20% DMSO). Working solutions of 240 μM of the RIV–BIM hybrids were prepared by the proper dilution of their stock solutions with phosphate buffer. A working solution of glycine-NaOH 50 mM buffer at pH = 8.50 containing 5 μM of thioflavin T (ThT) was prepared daily. Aβ$_{42}$ (GeneCust) was pre-treated with 1,1,1,3,3,3-hexafluoro-2-propanol (HFIP) to obtain a solution of 0.149 mM by brief sonication and vortexing, which was kept covered overnight at room temperature. From the Aβ$_{42}$ solution, aliquots of 250 μL were placed into Eppendorf tubes under ice and set to evaporate inside a hood at room temperature overnight. When the contents of the Eppendorf tubes were dried, the Aβ$_{42}$ aliquots were stored at −20 °C until needed. To obtain the Aβ$_{42}$ working solution, the Aβ$_{42}$ aliquots were dissolved with a freshly prepared mixture of 69.5 μL of CH_3CN/Na_2CO_3 (300 μM)/NaOH (250 mM) (48.3/48.3/3.4, *v*/*v*/*v*) by brief sonication and vortexing to obtain an Aβ$_{42}$ solution of 531.24 μM. To this solution, 392.5 μL of phosphate buffer was added, achieving an Aβ$_{42}$ working solution of 80 μM. To prepare the incubations, three replicates of Aβ$_{42}$ alone (30 μL Aβ$_{42}$ 80 μM + 30 μL phosphate buffer), Aβ$_{42}$ with RIV–BIM (30 μL Aβ$_{42}$ 80 μM + 10 μL RIV–BIM 240 μM + 20 μL phosphate buffer), Aβ$_{42}$ with copper (30 μL Aβ$_{42}$ 80 μM + 10 μL $CuCl_2$ 240 μM + 20 μL phosphate buffer) and Aβ$_{42}$ with copper and RIV–BIM (30 μL Aβ$_{42}$ 80 μM + 10 μL $CuCl_2$ 240 μM + 10 μL RIV–BIM 240 μM + 10 μL phosphate buffer) were placed in Eppendorfs. To obtain the blank solutions, a similar number of Eppendorfs, replacing Aβ$_{42}$ with phosphate buffer, were prepared. Incubations were performed in a water bath at 37 °C with agitation for 24 h. Afterwards, 180 μL of glycine-NaOH 50 mM buffer at pH = 8.50 containing 5 μM of ThT was added to each Eppendorf and then they were vortexed. Finally, 200 μL of solution from each Eppendorf was placed in the wells of a microplate and fluorescence measurements were monitored using a Spectramax Gemini EM (Molecular Devices) fluorimeter with an excitation wavelength of 446 nm and an emission wavelength of 485 nm. Blank signals were subtracted from the corresponding samples. The fluorescence intensity of the Aβ$_{42}$ + RIV–BIM solution was compared to that of the Aβ$_{42}$ solution to obtain the inhibition of Aβ$_{42}$ self-aggregation for each compound. The fluorescence intensity of the Aβ$_{42}$ + Cu(II) + RIV–BIM solution was compared to that of the Aβ$_{42}$ + Cu(II) solution to obtain the inhibition of the Cu(II)-induced Aβ$_{42}$ aggregation for each hybrid.

2.4.2. TEM Assays

To perform the TEM assays, commercial Aβ$_{42}$ purchased from Sigma-Aldrich was pre-treated with pure HFIP, a beta-sheet disruptor, to obtain homogeneous and monomeric

$A\beta_{42}$ [54]. Then, 222 µL of HFIP was added to 1 mg of $A\beta_{42}$, after which the mixture was vortexed and aliquoted into Eppendorfs. The Eppendorfs were placed in a Speed-Vac at 45 °C for 30 min until all HFIP was evaporated. Pre-treated $A\beta_{42}$ was stored at −20 °C until use. To start the amyloid incubations, pre-treated $A\beta_{42}$ was equilibrated at room temperature for 30 min. A solution of 5 mM was obtained by dissolution in DMSO and sonication for 5 min. Subsequently, 10 mM HCl was added to obtain a working $A\beta_{42}$ solution of 200 µM. Stock solutions of Cu(II) and RIV–BIM compounds (**4a**–**d**, **5a**,**b** and **5d**) at 200 µM were prepared on the same day and working solutions of $A\beta_{42}$, $A\beta_{42}$ + Cu(II), $A\beta_{42}$ + RIV–BIM and $A\beta_{42}$ + Cu(II) + RIV–BIM ($C_{A\beta 42} = C_{Cu} = C_L = 50$ µM) were prepared by diluting stock solutions in 10 mM HCl. Working solutions were incubated for 48 h at 37 °C before being analyzed by TEM. Samples were negatively stained with uranyl acetate 2% (*w*/*v*) and analyzed at 100 kv with a JEOL JEM 1400 Plus transmission electron microscope. Fibrils of $A\beta_{42}$ alone were compared with $A\beta_{42}$ + RIV–BIM fibrils, and fibrils of $A\beta_{42}$ + Cu(II) were compared with $A\beta_{42}$ + Cu(II) + RIV–BIM in order to evaluate the inhibition of the amyloid aggregation, and the widths and lengths of fibrils were measured for each sample. The ImageJ program was used to measure the fibrils (n = 200).

2.5. Radical Scavenging Activity

To determine the radical scavenging activity (antioxidant activity) of the novel RIV–BIM hybrids, the DPPH method was performed as previously described in the literature [49]. Working solutions of 20 mg of the ligands were prepared daily in 10 mL of MeOH (with a 10% of DMSO). A working solution of 2 mg DPPH in 100 mL MeOH was prepared daily, and its absorbance was checked to be between 0.75 and 1.00 (a.u.). A calibrate with 5 points and 3 replicates per point was measured, with a fixed volume of DPPH working solution (2.5 mL) and different volumes of ligand (0–1 mL) and MeOH (0–1 mL), up to a final volume of 3.5 mL for each point. Each one of the calibrate points was kept for 30 min under darkness to allow the ligands to exert their antioxidant effects. After 30 min, an auto-zero was performed with MeOH in both sample and reference cells, using a UV–Vis spectrophotometer. Immediately after, the calibrate points were transferred to the quartz cells and their absorbance at 517 nm was measured with a window width of 1 nm using a reference cell with MeOH. The antioxidant activity (%AA) for each point was calculated using the following equation:

$$\%AA = \frac{A_{DPPH} - A_{ligand}}{A_{DPPH}} \times 100$$

To determine the EC_{50} (i.e., the concentration of the ligand that reduces 50% the DPPH absorbance, %AA = 50%), the %AA and ligand concentration for each point were plotted.

2.6. Cell Viability and Neuroprotection of RIV–BIM Compounds in a SH-SY5Y Cell Line

SH-SY5Y human neuroblastoma cells (ATCC-CRL-2266) were kept in culture using Dulbecco's Modified Eagle Medium (DMEM) (Gibco-Invitrogen, Life Technologies Ltd., Waltham, MA, USA) containing 10% heat-inactivated fetal bovine serum (FBS), 50 U mL^{-1} penicillin and 50 µg mL^{-1} streptomycin. Incubation of the cells occurred at 37 °C in 5% CO_2. The toxicity of the compounds was tested through cell viability assays, with cells seeded with a density of 0.24×10^6 cells mL^{-1}. DMSO was used to dissolve each tested compound (**4a**–**4d**, **5a**, **5b**), affording stock solutions with concentrations of 25 mM. Aliquots of these solutions were stored at −20 °C. Concentrations from 1 µM to 10 µM were screened in order to select the highest non-toxic concentration of each compound. Consequently, compounds **4a**, **4b** and **5b** were tested at 1 µM final concentration; compounds **4c** and **5a** were tested at 2 µM final concentration; compound **4d** was tested at a final concentration of 3 µM. The DMSO concentrations in the culture media were lower than 0.05% (*v*/*v*) and the viability of the SH-SY5Y cells was not altered in a detectable manner.

Pre-incubation of the cells with each compound occurred for 1 h and was followed by incubation with $A\beta_{42}$ or with Fe/Asc for an additional 24 h. A stock solution of $A\beta_{42}$ (Bachem, Torrance, CA, USA) at a concentration of 443 μM was prepared in sterile water and was added to the culture medium at a final concentration of 1 μM. A stock solution of ferrous sulfate (Fe) (Sigma Chemical Co., St. Louis, MO, USA) was freshly prepared in sterile water at a stock concentration of 0.36 M and added to the medium at a final concentration of 2.5 mM. L-Ascorbic acid (Asc) (Sigma Chemical Co, St. Louis, MO, USA) was freshly prepared (80 mM stock solution) and added to the medium at 5 mM final concentration. In all experiments, control conditions were maintained in which $A\beta_{42}$ or Fe/Asc were not added.

The colorimetric MTT (3-(4,5-dimethylthiazol-2-yl)-2,5-diphenyltetrazolium bromide) reduction assay was used to determine cell viability [55]. In this assay, the activity of succinate dehydrogenase, which metabolizes MTT into a formazan that absorbs light at 570 nm, indicates the presence of viable cells. After cell treatments, culture medium was removed and 0.3 mL of MTT (0.5 mg mL^{-1}) was added in each well. Subsequently, the plate was incubated at 37 °C for 3 h and the formazan precipitates were solubilized with 0.3 mL of acidic isopropanol (0.04 M HCl/isopropanol). The absorbance of each well was measured at 570 nm. Cell reduction capability was normalized to untreated SH-SY5Y control cells.

All data were expressed as means ± SEMs of at least five independent experiments performed in duplicate. Statistical analyses were performed using one-way ANOVA followed by followed by Dunnett's test. A p-value < 0.05 was considered statistically significant.

2.7. Prediction of Pharmacokinetic Properties

In order to determine the drug-likeness properties of the novel RIV–BIM hybrids as anti-AD drugs, predictions of some indicators of their pharmacokinetic profiles were performed in silico. For these, the ligands were built in Maestro and their energy was minimized as described in Section 3.3. Using the program QikProp v.2.5 (Schrödinger, New York, NY, USA) [56], several parameters, such as PSA, o/w partition coefficient, interaction with human albumin, BBB permeability, CNS activity, Caco-2 and MDCK cell permeability, human oral absorption and violations of Lipinski's rule, were calculated.

2.8. Statistical Analysis

In order to simplify the data interpretation, due to the complexity of the results, a chemometric analysis was performed using Statgraphics Centurion XIX. Data were collected from Tables 1 and 2. Between the multivariant analysis, PCA was chosen to reduce the dimensionality of the data. Listwise elimination and a standardization with a minimum Eigenvalue set as 1.0 were performed.

Table 1. Biological properties of the RIV–BIM hybrids under study as well as those of the comparison compounds.

Comp	Antioxid. [a] EC_{50} (mM)	AChE Inhib [b] IC_{50} (μM)	BChE Inhib [b] IC_{50} (μM)	SI [c]	$A\beta_{42}$ Self-Aggreg. Inhib [d] (%)	$A\beta_{42}$ Cu-Ind. Aggreg. Inhib [d] (%)
4a	–	17.6 ± 0.6	5.85 ± 0.03	3.03	39.0	41.2
4b	0.9 ± 0.1	14 ± 2	6.5 ± 0.4	2.17	39.6	48.8
4c	10.6 ± 0.3	17.7 ± 0.8	4.8 ± 0.1	3.69	21.2	22
4d	–	24 ± 1	19.2 ± 0.7	1.25	20.1	21.3
5a	8 ± 1	17.6 ± 0.4	0.9 ± 0.1	19.6	44.5	45.4
5b	–	31.7 ± 0.1	0.30 ± 0.01	105.7	58.7	60.8
5d	–	21.4 ± 0.4	1.7 ± 0.2	12.6	42.1	40.3
DMHP	0.157 ± 0.008	–	–	–	–	–
Tacrine	–	0.024 ± 0.007	–	–	28.1	–
Curcumin	–	–	–	–	65.7	62.7
Donepezil	–	0.0075	1.42	0.005	–	–
Rivastigmine	–	32.1	0.39	82.3	–	–

[a] Radical scavenging activity (DPPH method). [b] The values are means of five independent experiments ± SDs. Assays with *ee*AChE and *eq*BChE. [c] Selectivity index = IC_{50} (AChE)/IC_{50} (BChE). [d] Percent of inhibition of $A\beta_{42}$ aggregation in the presence or absence of copper (40 μM) and 20 μM inhibitor (thioflavin-T fluorescence method). The values are the means of two independent measurements in duplicate (SEM < 10%).

Table 2. Predicted pharmacokinetic properties of the RIV–BIM hybrids and the parent RIV drug, obtained using the software QikProp v.2.5 [56].

Molecule	Mol. Weight [a]	PSA [b]	clog $P^{o/w}$ [c]	log *K* (HSA) Serum Protein Binding [d]	log BB [e]	Caco-2 Permeability (nm s^{-1}) [f]	MDCK Permeability (nm s^{-1}) [g]	Oral Absorption [h]
4a	430.462	114.416	3.884	0.519	−1.449	401	184	91
4b	444.489	116.724	4.045	0.563	−1.58	365	166	89
4c	458.516	117.689	4.412	0.679	−1.758	333	151	88
4d	472.543	116.719	4.695	0.743	−1.724	382	175	89
5a	430.462	113.662	4.318	0.673	−1.238	535	251	94
5b	444.489	115.249	4.737	0.803	−1.345	539	253	94
5d	472.543	115.284	5.398	0.998	−1.5	548	258	93
RIV	250.340	40.321	2.488	−0.133	0.475	1381	776	100

[a] Molecular weight (acceptable range: from 130 to 725). [b] PSA (Van der Waals surface area of polar nitrogen and oxygen atoms) (acceptable range: from 7 to 200). [c] Predicted octanol/water partition coefficient log *P* (acceptable range: from −2.0 to 6.5). [d] Interaction with human albumin (acceptable range: from −1.5 to +1.5). [e] Brain–blood barrier permeability (acceptable range: from −3.0 to +1.2). [f] Predicted Caco-2 cell permeability in nm/s (acceptable range: 25 is poor and >500 is excellent). [g] Predicted MDCK cell permeability in nm/s (acceptable range: <25 is poor and >500 is excellent). [h] Percentage of human oral absorption (acceptable range: <25% is poor and >80% is excellent).

3. Results and Discussion

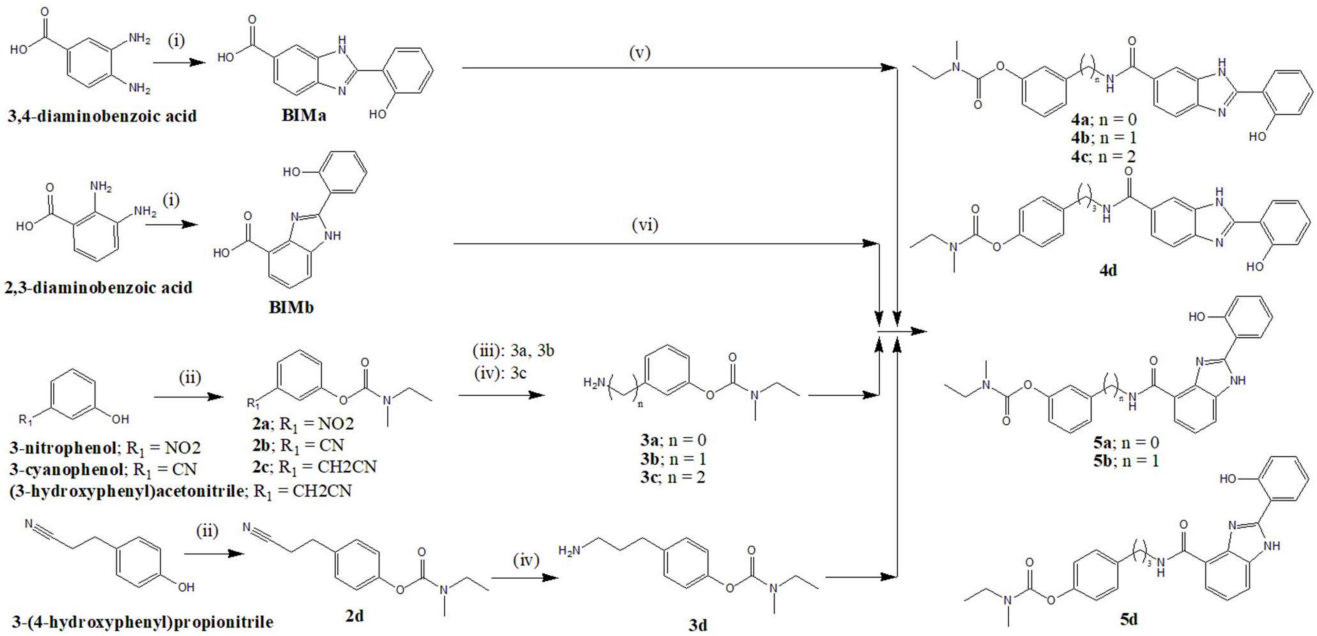
3.1. Molecular Design

The first step towards the design and development of the novel hybrids involved the selection of two different pharmacophoric moieties to endow the final compounds with multiple functionalities so as to guarantee the required multi-targeting activity to fight AD. Therefore, rivastigmine (RIV) was chosen as the first moiety to assure a good inhibition of AChE and BChE. Hydroxyphenylbenzimidazole (BIM) was selected due to its expected ability to bind metals involved in AD, inhibit self- and Cu(II)-induced $A\beta_{42}$ aggregation and reduce ROS production. In addition, variable numbers of methylene groups were included in the linkers between the RIV and BIM moieties (n = 0, 1, 2 and 3) (see Figure 1)

in order to tune the desired dual interaction with both active binding sites of the AChE (see Section 2.2). The structural variation associated with the position of the carboxylic acid substituent (BIMa, BIMb) was intended to be used to explore the potential effects of different conjugate spatial conformations (linear (4) and twisted (5) series) on interactions with the target biomolecules and metal ions.

3.2. Synthesis of the Compounds

The synthesis of the present set of seven new rivastigmine–hydroxyphenylbenzimidazole hybrids (**RIV–BIMs**; **4a**–**4d** and **5a**, **5b**, **5d**) was performed according to Scheme 1. The intermediate hydroxyphenylbenzimidazole–carboxilic acid derivatives (**BIMa** and **BIMb**) were synthesized according to a previously reported method [35] involving a Mannich reaction between the 3,4- or 3,2-diamino benzoic acid and salicylaldehyde followed by cyclization, in the presence of the reducing agent sodium metabisulfite, in *N*,*N*-dimethylacetamide (DMA) and under high temperature (100 °C), affording the expected compounds with good yields (79.9−86.6%). To obtain the amino (alkyl) rivastigmine derivatives (**3a**–**3d**), a sequential two-step reaction was used. The first step involved the reaction of *N*-ethyl-*N*-methylcarbamoyl chloride with the corresponding nitro- or cyano(alkyl)-phenols by refluxing in dry CH_3CN and basic medium, triethylamine (TEA), to obtain the corresponding phenylcarbamate intermediates (**2a–2d**) with almost quantitative yields (76.7−99.4%). The following step involved a standard hydrogenolysis of the nitro- or nitrile to the amino groups of these carbamate intermediates, which was carried out in methanol and H_2 atmosphere (4 atm), though in the case of the alkylnitrile derivatives a catalytic amount of HCl was used, with general yields in the range of 22.0−76.6%. The final step involved the condensation of the carboxylic acid derivatives (**BIMa** and **BIMb**) with the amine-rivastigmine derivatives (**3a–3d**) using standard peptide coupling reagents, namely, 2-(1*H*-benzotriazole-1-yl)-1,1,3,3-tetramethylaminium tetrafluoroborate (TBTU) or 1-ethyl-3-(3-dimethylaminopropyl)carbodiimide (EDCI), in anhydrous DMF under N_2 atmosphere, affording the corresponding final **RIV–BIM** hybrid compounds (**4a–d**, **5a**, **5b**, **5d**) with yields in the range of 23.1−73.9%.



Scheme 1. (i) Salicylaldehyde, $Na_2S_2O_5$, DMA, 100 °C, 12 h; (ii) *N*-ethyl-*N*-methylcarbamoyl chloride, TEA, 95 °C, 12 h; (iii) H_2, MeOH, 10% Pd-C, 4 h, 4 bar; (iv) H_2, MeOH/HCl, 10% Pd-C, 6 h, 4 bar; (v) 1: BIMa + NMM, TBTU, dry DMF, water-ice-cooled, N_2 atm, 50 min; 2: BIMa mixture 1 over **3a-d**, N_2 atm, 20 h; (vi) 1: BIMb + HOBT, EDCI, dry DMF, water-ice-cooled, N_2 atm, 50 min; 2: BIMb mixture 1 over **3a**, **3b**, **3d**, N_2 atm, 20 h.

3.3. Molecular Modelling

It is well recognized that the overexpression of cholinesterase enzymes results in the degeneration of cholinergic neurons, with deficiency of the neurotransmitter ACh and decline in cognitive functions. Since both AChE and BChE are involved in the blockage of this process, dual cholinesterase inhibition has been explored in the last decade as a new anti-AD drug therapy. To develop effective inhibitors, it is important to understand the structural distinctions between human AChE (hAChE) and BChE (hBChE). Both enzymes are closely related, with an amino acid sequence homology of ca 65%, as well as an active site located at the bottom of the ~20 Å deep hydrophobic gorge, while the peripheral anionic site (PAS) is positioned at the entrance of the gorge [57,58]. The active sites of both enzymes are composed of a catalytic triad, an acyl-binding pocket and a choline binding site. Their main structural differences are the dimensions of their active sites, the active site being wider in BChE due to the replacement of two phenylalanine residues in the acyl binding pocket of AChE with two flexible amino acid residues in BChE [59]. This allows a better accommodation and the binding of bulkier compounds within the active site located at the bottom of the gorge of BChE.

Our molecular modeling studies involved in silico docking-based virtual screenings of the series of RIV–BIM hybrids inside the active site cavities of hAChE and hBChE. A visualization of the docking poses of the RIV–BIM hybrids inside the hAChE cavity is shown in Figure 2 and Figure S1. A brief global analysis of these modelling results indicates that all the hybrids are well-accommodated inside the enzyme active site and in close proximity to some significant residues of the enzyme [59], such as Phe295, Trp286, Tyr124, Tyr72, Asp74, Tyr337 and Trp86. In particular, Figure 2 illustrates the docking models of hAChE and two representative examples of the series of linear (**4b**) and twisted (**5a**) compounds, showing in both cases a quite similar accommodation and spatial distribution in the hAChE active cavity as compared with the original ligand. Since all the RIV–BIM hybrids have longer structures than the original ligand (donepezil), their accommodation in the enzyme cavity results in the BIM moiety being orientated towards the PAS, while the RIV portion is inside the CAS (compounds **4a**–**4d** and **5a**; see Figure 2 and Figure S1). Moreover, in the case of compound **4b**, an established H-bond between the hydroxyl group of the BIM moiety and Tyr72 can be illustrated. For compounds **5b** and **5d** (in Figure S1), an inversion in the position of the respective moieties inside the cavity of hAChE was detected, which may signify a lower inhibitory potential for these longer compounds of the twisted series. In fact, donepezil is a more potent inhibitor due to the established π–π stacking of the aromatic groups at both ends (benzyl in CAS and indanone in PAS) [46] as well as the hydrogen bond formation between the indanone oxygen atom and Phe295.

Regarding human butyrylcholinesterase (hBChE), the docking results depicted in Figure 3 and Figure S2 show that all the RIV–BIM hybrids are well-accommodated inside the enzyme active site, with potential binding interactions with some important active residues of the enzyme [47], such as Tyr332, Trp82, His438, Ser198, Phe398, Trp231, Leu286 and Val288. Figure 3 shows the docking results for two representative examples of the series of linear (**4c**) and twisted compounds (**5b**), revealing them to be well-accommodated in the BChE active cavity, similarly to the original ligand. In the original ligand, the naphthalene moiety fully occupies the acyl binding pocket, establishing π–π stacking interaction with Trp231, while a 1*H*-indene ring is placed over residues Ile69 and Asp70 at the PAS portion. All the linear (**4a**–**4d**) RIV–BIM compounds are longer than the original ligand and those with longer chains have the BIM moiety orientated to the entrance of the gorge, while the RIV portion is accommodated inside the CAS. On the other side, the twisted series (**5a**, **5b** and **5d**) seem to bend better inside the cavity of BChE, orientating the BIM moiety to the CAS and the RIV portion to the PAS.

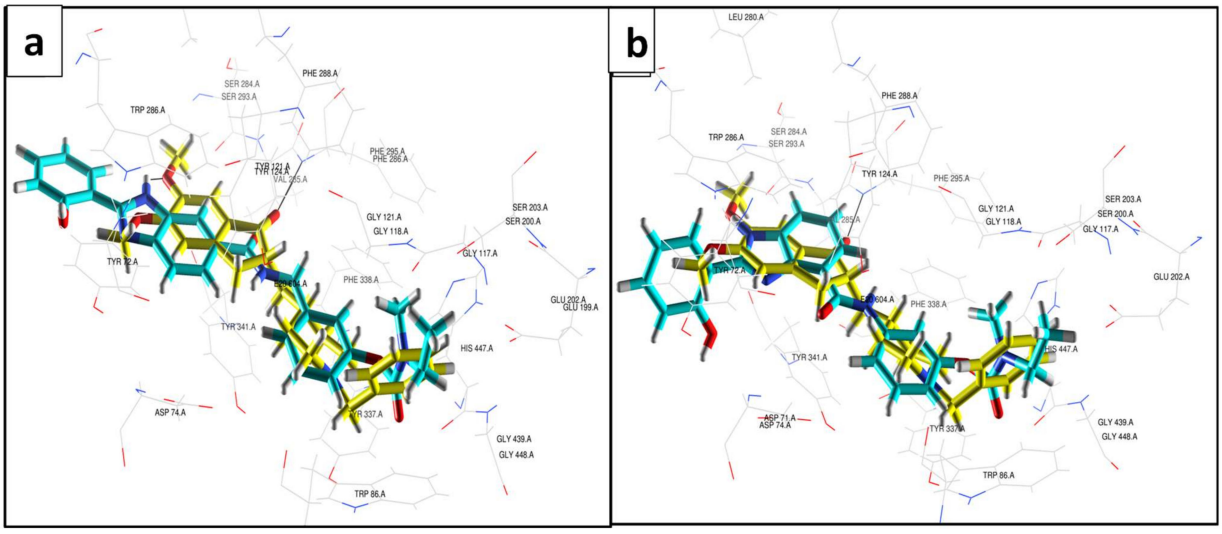


Figure 2. Docking results for RIV–BIM hybrids (blue) within hAChE and a comparison with the original ligand, donepezil (yellow; PDB code: 4EY7 [46]): (**a**) **4b**; (**b**) **5a**.

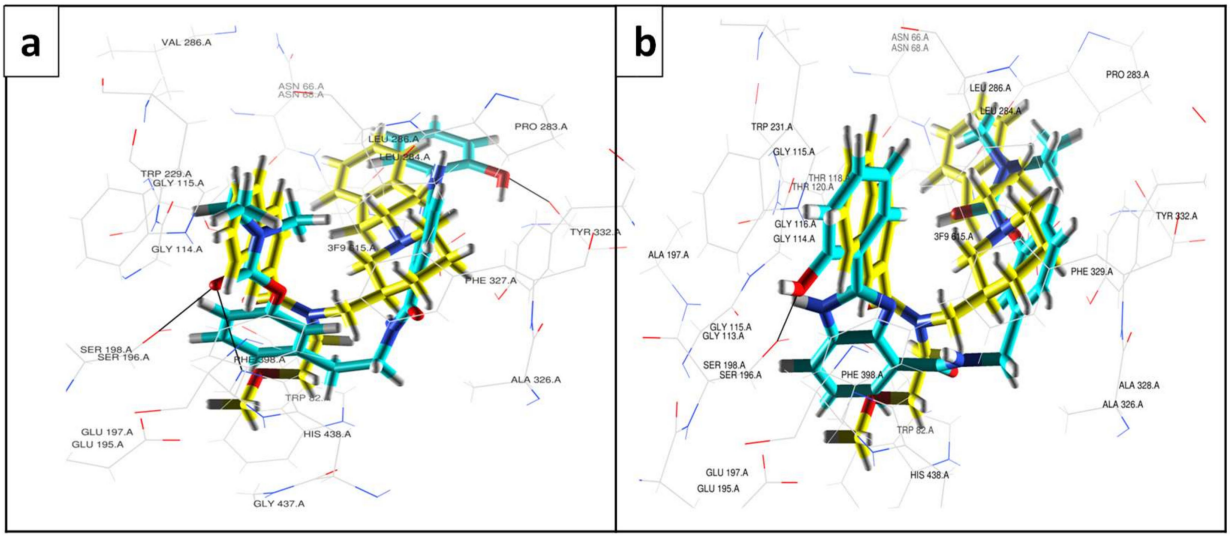


Figure 3. Docking results for RIV–BIM hybrids (blue) within hBChE and a comparison with the original ligand, *N*-((1-(2,3-dihydro-1*H*-inden-2-yl)piperidin-3-yl)methyl)-*N*-(2-methoxyethyl)-2-naphthamide (yellow; PDB code: 4TPK [46]): (**a**) **4c**; (**b**) **5b**.

Overall, the results of the molecular simulations indicate that this class of designed drugs can be good dual inhibitors of the targeted enzymes, and the twisted series eventually appears to be accommodated better in the active site of BChE, encouraging the hypothesization of eventual selective behaviour towards this enzyme.

3.4. Enzyme Inhibitory Activity of the Compounds

The inhibition of the *Electrophorus electricus* AChE (*Ee*AChE) and the equine BChE (*Eq*BChE) enzymes by the newly synthesized hybrids and some marketed anti-ChE drugs (donepezil, rivastigmine, tacrine) as reference compounds were evaluated employing a previously described method [35]. The results, expressed as IC_{50} values, are shown in Table 1. Regarding AChE inhibition, among the RIV–BIM compounds, **4b** exhibited the best inhibitory capacity value (IC_{50} = 14 μM), in accordance with the better fitting found for **4b** (see Figure 2), followed by **4a**, **5a** and **4c** with identical capacity (IC_{50} = 17.6–17.7 μM), while lower inhibitory capacities were found for compounds **5d**, **4d** and **5b** with IC_{50} values in

the range of 21.4–31.7 μM. Interestingly, the results for AChE inhibition do not show any important dependence of activity on linker size, while all the synthesized hybrids presented better AChE inhibition than rivastigmine, proving the improved activity of the RIV–BIM conjugates as compared with the RIV parent molecule. However, as expected, their activity was lower than those of the potent acetylcholinesterase inhibitors donepezil and tacrine. Concerning BChE inhibition, only compound **5b** (IC_{50} = 0.30 μM) showed improvement relative to rivastigmine (IC_{50} = 0.39 μM). Nevertheless, the twisted series (IC_{50} = 0.3–1.7 μM) showed better inhibitory power than the linear one (IC_{50} = 4.8–19.2 μM), with compounds **5a** (0.9 μM) and **5d** (1.7 μM) exhibiting similarly high BChE inhibitory activity in the same range as donepezil (IC_{50} = 1.42 μM). These results are in consonance with molecular modelling studies which revealed that twisted-like compounds (**5a**, **5b**, **5d**) are favoured when it comes to accessing the cavity of BChE, with less good results for longer linker analogues in both series (compounds **4d** and **5d**). The selectivity index (SI), a parameter that describes the different affinity for AChE and BChE, IC_{50}(AChE)/IC_{50}(BChE), was higher than 1 for all the developed hybrids, indicating a better interaction of the inhibitors with BChE than with AChE.

This can be rationalized by the inherent size and structure of the compounds. In fact, the bigger size of all the developed hybrids, when compared with those of the original ligands (see Section 2.2), seems to allow a better accommodation in the wider active site of BChE, and the twisted structure renders the compounds more flexible, allowing a better interaction with the residues of the enzyme active site.

In fact, to achieve synergistic therapeutic effects, a multi-target molecule should ideally employ balanced activities towards varied targets, with IC_{50} values in vitro within an order of magnitude of each other [60]. Indeed, the compounds developed in this study, except for **5b** (SI (**5b**) = 105.7), obey this rule in terms of cholinesterase's inhibition and therefore can be considered dual inhibitors.

3.5. Inhibition of Self- and Cu(II)-Induced Aβ$_{42}$ Aggregation

The effect of the RIV–BIM compounds on Aβ_{42} aggregation, in the presence and absence of Cu(II), was evaluated using two different techniques: molecular fluorescence spectroscopy and transmission electron microscopy (TEM). The purpose of fluorescence measurements was to quantify the aggregation of amyloid fibrils, while TEM allowed us to observe the fibrils directly and measure their widths under the effects of the compounds. Moreover, due to potential copper-induced fluorescence quenching, TEM assays were also performed as an alternative fluorescence-independent technique, therefore avoiding eventual quantitative errors.

The anti-amyloidogenic capacity of the compounds was assessed in vitro using the thioflavin T (ThT) method [35,52]. To record fluorescence emission, excitation (446 nm) and emission (485 nm) wavelengths were used. When ThT binds to amyloid fibrils, an increase in absorbance and emission of this dye occurs with concomitant red shifts of the respective spectra. The percent of inhibition of Aβ_{42} aggregation is shown in Table 1, and the assays were performed in the presence of 20 μM of inhibitor. These concentration conditions were used to overcome solubility problems of some compounds in the aqueous phosphate buffer working medium. Compounds **4c** and **4d** are very weakly effective in the inhibition of amyloid self- and Cu(II)-induced aggregation, but all the other compounds (**4a**, **4b**, **5a**, **5b** and **5d**) present average/good inhibition capacity regarding Aβ_{42} self-aggregation (39.0–58.7%) These compounds are more potent inhibitors than tacrine (28.1%), though weaker than curcumin (65.7%), a selected reference compound, as an anti-amyloidogenic agent with a 62% Aβ inhibition at 50 μM concentration reported [61]. Moreover, the inhibition of Cu(II)-induced Aβ_{42} aggregation by compounds **4a**, **4b**, **5a**, **5b** and **5d** is also moderate/good (41.2–60.8%), with values only slightly higher than those obtained for self-aggregation inhibition, suggesting that no substantial effect can be observed due to the presence of Cu(II). In fact, the role of Cu(II) in the promotion of Aβ fibril formation is not yet clear, and it can be hypothesized that either Cu(II) chelators are eventually able to

compete with the fibrils for Cu(II), therefore reducing aggregation, or that Aβ binding to Cu(II) can lead to some precipitation of amorphous deposits of the peptides rather than the formation of β sheets [62,63].

Regarding the inhibition of Aβ aggregation, the obtained results seem to indicate that, once more, the twisted series (**5**) of hybrids present better and more consistent inhibitory activity than the linear series (**4**) and that the inhibition capacity of these RIV–BIM hybrids may be ultimately related to their different abilities to intercalate between fibrils rather than to their Cu(II) chelating power.

To perform the $A\beta_{42}$ aggregation assays by TEM, fibrils were incubated using a fluorescence procedure previously described [20]. The TEM images of $A\beta_{42}$ alone and in the presence of RIV–BIM compounds are presented in Figure 4.

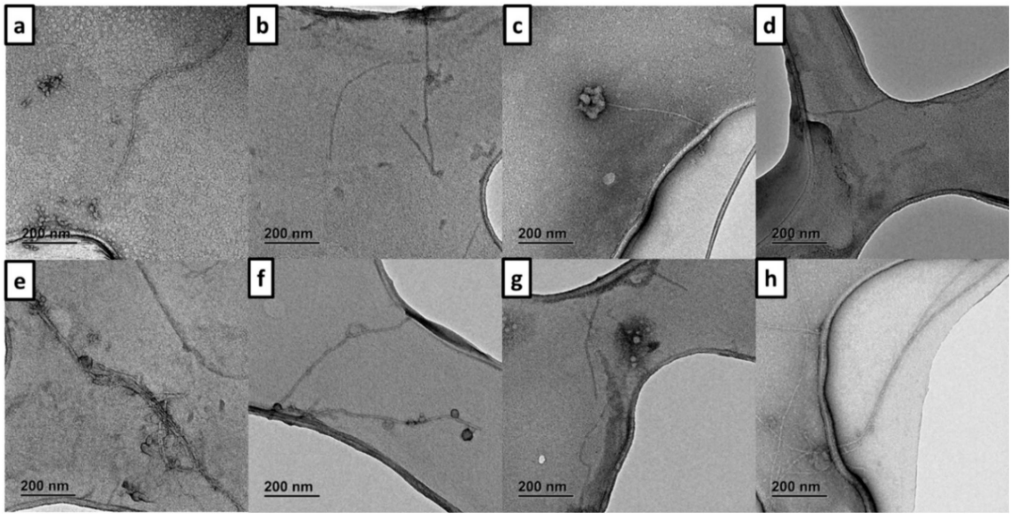


Figure 4. TEM images of $A\beta_{42}$ in the presence of RIV–BIM compounds after incubation at 37 °C for 48 h: (**a**) $A\beta_{42}$ alone; (**b**) $A\beta_{42}$ + **4a**; (**c**) $A\beta_{42}$ + **4b**; (**d**) $A\beta_{42}$ + **4c**; (**e**) $A\beta_{42}$ + **4d**; (**f**) $A\beta_{42}$ + **5a**; (**g**) $A\beta_{42}$ + **5b**; (**h**) $A\beta_{42}$ + **5d**.

Amyloid fibrils remained disaggregated under the effect of the RIV–BIM compounds after 48 h of incubation. The shortest fibrils were found in the presence of compounds **4a** (Figure 4b), **4b** (Figure 4c) and **5b** (Figure 4g), this last compound having been found to be the best inhibitor of $A\beta_{42}$ aggregation (see Table 1). On the other hand, in the presence of **4c** and **4d** (Figure 4d,e), quite elongated fibrils were present, in accordance with the low values of inhibition of Aβ aggregation previously shown in Table 1 for these compounds. For each of the performed assays, fibril width was measured, and the results are graphed in Figure 5. $A\beta_{42}$ fibril width in the absence of Cu(II) (Figure 5a) was 4.9 ± 0.2 nm, and it was modified in the presence of all RIV–BIM compounds: compound **4d** was the only one that widened amyloid fibrils (6.7 ± 0.3 nm), while the rest of the compounds narrowed them (3.3–4.5 nm). According to results discussed above in this section, compounds **5b** (3.8 ± 0.1 nm) and **5d** (3.3 ± 0.2 nm) reduced fibril width significantly (by 22.4 and 32.7%, respectively), in accordance with their already demonstrated inhibitory capacity in the absence of Cu(II).

When fibrils were incubated in the presence of Cu(II) for 48 h (Figure 6), stronger amyloid elongated aggregation was evidenced. In fact, incubation with Cu(II) in the absence of RIV–BIM compounds (Figure 5a) presented higher aggregation than that corresponding to $A\beta_{42}$ alone (Figure 5a). Based on the TEM images contained in Figure 6, compounds belonging to the linear series of hybrids (**4a**–**4d**) seem to exert minor effects on Cu(II)-induced $A\beta_{42}$ aggregation according to the previous fluorescence data. Concerning the twisted series of compounds (**5a**, **5b** and **5d**), the TEM images evidence a sparser amyloid aggregation, mainly for **5b** and **5d**, pointing towards some role of Cu(II) in the aggregation

process, although previous fluorescence results did not reveal a substantial effect of copper complexation on Cu(II)-induced Aβ aggregation.

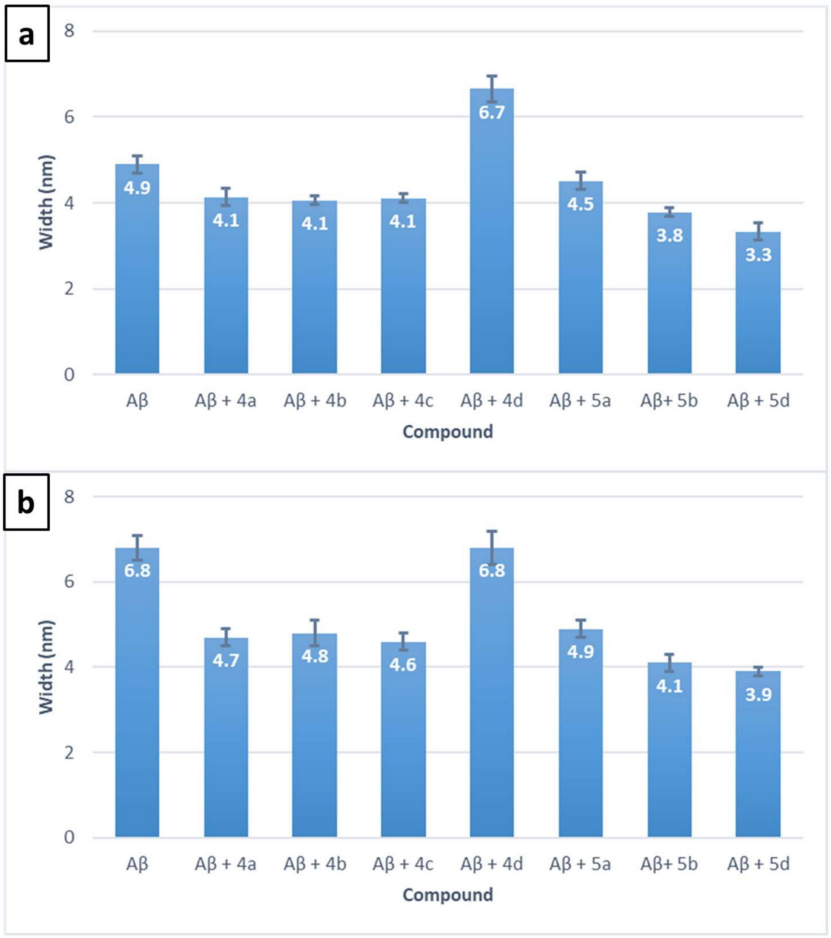


Figure 5. $A\beta_{42}$ fibril widths for TEM incubations measured with ImageJ (±SDs) (N = 200): (**a**) $A\beta_{42}$ + RIV–BIM hybrids in the absence of Cu(II); (**b**) $A\beta_{42}$ + RIV–BIM hybrids in the presence of Cu(II). Statistical analysis was performed using one-way ANOVA and Fisher's LSD test at 95% significance.

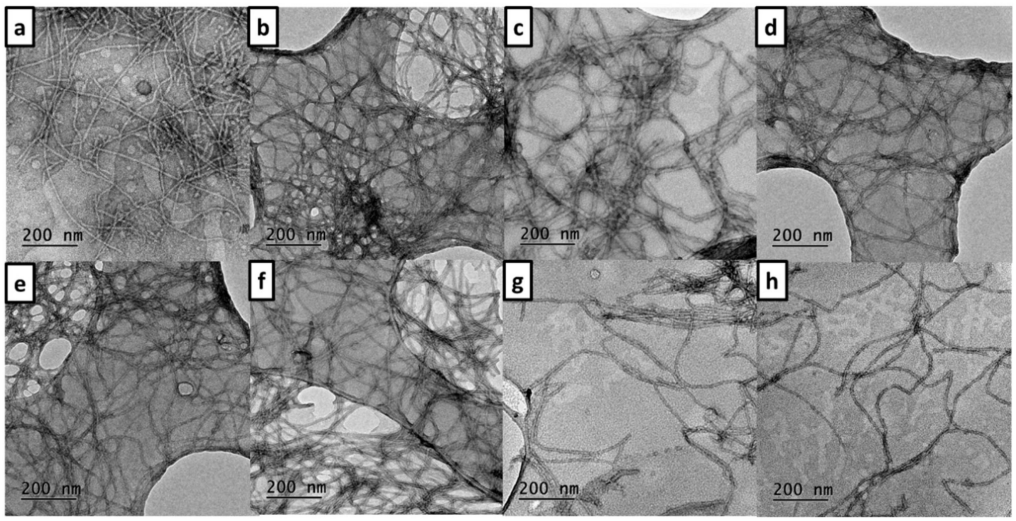


Figure 6. TEM images of $A\beta_{42}$ in the presence of Cu(II) and RIV–BIM compounds after incubation at 37 °C for 48 h (N = 3): (**a**) $A\beta_{42}$ + Cu(II); (**b**) $A\beta_{42}$ + Cu(II) + **4a**; (**c**) $A\beta_{42}$ + Cu(II) + **4b**; (**d**) $A\beta_{42}$ + Cu(II) + **4c**; (**e**) $A\beta_{42}$ + Cu(II) + **4d**; (**f**) $A\beta_{42}$ + Cu(II) + **5a**; (**g**) $A\beta_{42}$ + Cu(II) + **5b**; (**h**) $A\beta_{42}$ + Cu(II) + **5d**.

Fibril width for $A\beta_{42}$ + Cu(II) + RIV–BIM incubations was also measured (Figure 5b). When $A\beta_{42}$ was incubated with Cu(II) ((6.8 ± 0.3) nm), the amyloid fibrils suffered a width increase of 38.8%, in contrast to $A\beta_{42}$ alone (Figure 5a). On the other hand, compounds **4a**–**4c** had widths reduced to normal $A\beta_{42}$ levels (4.6–4.8 nm), as did **5a** (4.9 ± 0.2 nm), while **4d** did not undergo any width reduction. Moreover, compounds **5b** and **5d** showed a width reduction that was even greater (39.7 and 42.6%, respectively) in comparison to $A\beta_{42}$ + Cu(II) fibrils.

Therefore, based on the TEM results, combined also with the fluorescence data, compounds **5a**, **5b** and **5d** were revealed as promising candidates for the inhibition of $A\beta_{42}$ self- and Cu(II)-induced aggregation, as well as being able to effect the reduction of the widths of amyloid fibrils.

3.6. Radical Scavenging Activity

The radical scavenging activity of the RIV–BIM compounds was determined by a spectrophotometric method involving the 2,2-diphenyl-1-picrylhydrazyl (DPPH) free radical [35,64]. The results obtained, expressed as EC_{50}, are shown in Table 1, which also includes the value obtained for the reference compound 1,2-dimethyl-3-hydroxy-4-pyridinone (DMHP). Due to the demonstrated low radical scavenging activity of the RIV–BIM hybrids (mM order), only some selected compounds were evaluated. Among the compounds assayed, **4b** (0.9 mM) was the most active, followed by **5a** (8 mM) and **4c** (10 mM), all of them well below the radical scavenging ability of DMHP (0.157 mM).

3.7. Cell Viability and Neuroprotection in a SH-SY5Y Cell Line

The neuroprotective effect of RIV–BIM hybrids was tested by exposing neuroblastoma SH-SY5Y cells to $A\beta_{42}$ or ferrous sulphate and *L*-Ascorbic acid (Fe/Asc), as AD-like stressors. A concentration screening was performed to select a non-toxic concentration for each compound (Figure S3). Although several concentrations of the same compound had different non-toxic effects, some failed to prevent $A\beta_{42}$ and Fe/Asc toxicity. Therefore, concentrations were selected according to abilities to increase neuroprotection by maintaining low toxicity levels.

The increased formation of senile plaques composed of $A\beta_{42}$ peptide aggregates along with the production of reactive oxygen species (ROS) are hallmarks of the neurodegenerative process of AD [13]. Herein, it was observed that $A\beta_{42}$ leads to a 30% decrease in cell viability, and, interestingly, compound **4d** significantly prevented Aβ-induced cell toxicity (Figure 7). Although **4d** revealed moderate/low Aβ inhibition in aqueous media (see Section 2.4, Table 1), some apparent discrepancy with the good results obtained here with cell medium may be explained by the quite different experimental concentration conditions ($C_{inhibitor}$ 20 versus 3 μM), suggesting solubility limitations or intermolecular interactions for higher concentration conditions. Additionally, since ROS production is also one of the processes associated with AD [13], to study the neuroprotection of RIV–BIM compounds against oxidative stress, SH-SY5Y cells were also treated with Fe/Asc, which induced a decrease of 30% in the cell viability when compared with untreated cells (Figure 8). In this case, only compound **5a** presented a statistically significant neuroprotective effect by preventing ROS production.

This set of results suggests that compound **5a** (and **4d**) may have a potential therapeutic effect on AD, since it was shown to prevent cell toxicity induced by $A\beta_{42}$ or oxidative stress.

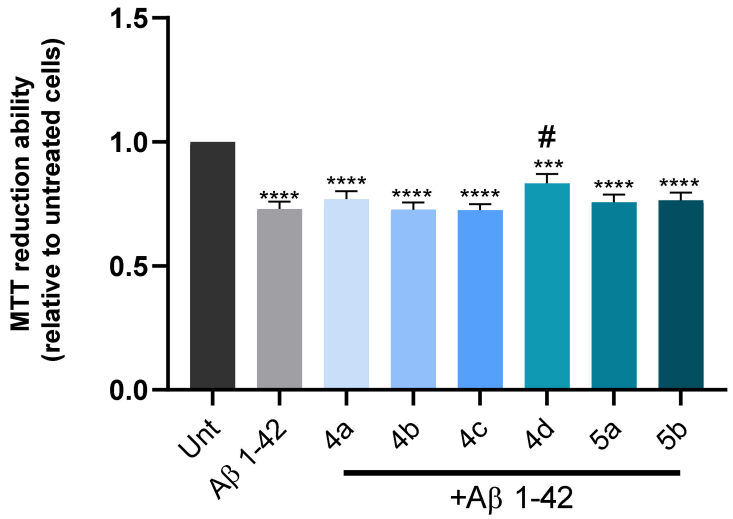


Figure 7. Neuroprotective effects of RIV–BIM compounds against $A\beta_{42}$-induced toxicity in SH-SY5Y cells. Cells were treated with the compounds for 1 h and then $A\beta_{42}$ peptide (1 μM) was added to the medium for 24 h (1 h pre-incubation + 24 h co-incubation). Cell viability evaluation was performed through MTT reduction assay, and the results are expressed relative to those for SH-SY5Y untreated cells, with the means ± SEMs derived from eight different experiments (N = 8). *** $p < 0.001$, **** $p < 0.0001$, significantly different when compared with SH-SY5Y untreated cells; # $p < 0.05$, significantly different when compared with $A\beta_{42}$-treated SH-SY5Y cells. Statistical analysis was performed using one-way ANOVA followed by Dunnett's test. The concentration used for the compounds **4a**, **4b** and **5b** was 1 μM; 2 μM was used for **4c** and **5a**; and 3 μM for **4d**.

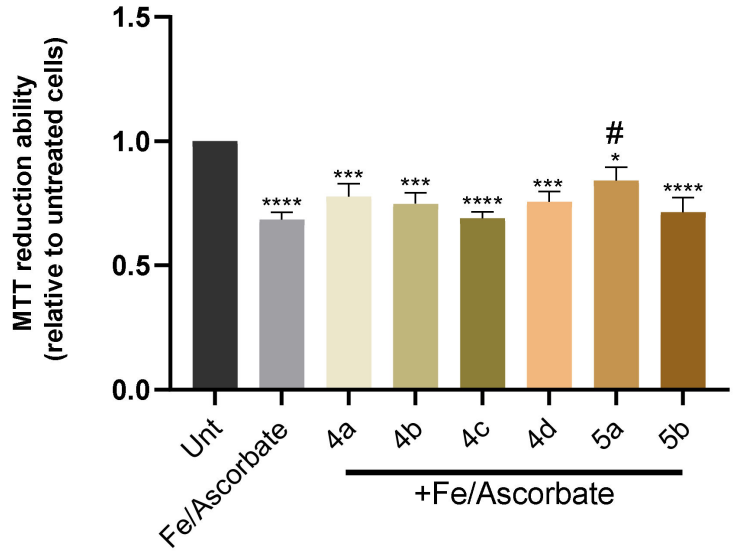


Figure 8. Neuroprotective effects of RIV–BIM compounds against *L*-Ascorbic Acid (AscH(-))/Ferrous Sulphate (Fe) toxicity in SH-SY5Y cells. Cells were treated with the compounds for 1 h and then Fe/Ascorbate (2.5 mM and 5 mM, respectively) was added to the medium for 24 h (1 h pre-incubation + 24 h co-incubation). Cell viability evaluation was performed through MTT reduction assay and results are expressed relative to SH-SY5Y untreated cells, with the means ± SEMs derived from five different experiments (N = 5). * $p < 0.05$, *** $p < 0.001$, **** $p < 0.0001$, significantly different when compared with SH-SY5Y untreated cells; # $p < 0.05$, significantly different when compared with Fe/Ascorbate-treated SH-SY5Y cells. Statistical analysis was performed using one-way ANOVA followed by Dunnett's test. The concentration used for compounds **4a**, **4b** and **5b** was 1 μM; 2 μM was used for **4c** and **5a**; and 3 μM was used for **4d**.

3.8. Predicted Pharmacokinetic Properties

To estimate the drug-like behaviour of the RIV–BIM compounds, some pharmacokinetic properties were predicted using the QikProp v.2.5. program [56] and compared with those of the parent drug rivastigmine (RIV) (Table 2). All the hybrids presented an acceptable range of values for molecular weight, PSA (Van der Waals surface area of polar nitrogen and oxygen atoms), octanol/water partition coefficient (except compound **5d**), serum protein binding and brain–blood barrier permeability. Caco-2 cell permeability was high for compounds **5a**, **5b** and **5d** (>500 nm s^{-1}) and was in the normal range for the rest of the molecules. Moreover, all hybrids presented acceptable MDCK permeability values and were demonstrated to be easily absorbed through the oral route (oral absorption >80%; see Table 2). The number of violations of Lipinski's rule of five was 0 for all the compounds, except **5d** (1 violation, clog $P_{o/w} > 5$), which indicates that all of them seem to be suitable as potential oral drug candidates. Compared with the original drug rivastigmine, the insertion of a BIM moiety in compounds of series 4 and 5 is apparently responsible for some lowering of predicted Caco-2 and MDCK cell permeabilities.

Overall, these studies predicted for the compounds generally good pharmacokinetic (PK) descriptors and drug-likeness, including potential good permeability for BBB and other important gut wall membranes as well as oral absorption capacity. However, further future studies will be necessary to complete the PK assessment of ADMET properties, as will experimental results to support the compounds' potential BBB permeability and to study their metabolism and elimination stages.

3.9. Chemometric Analysis

Due to the elevated RIV–BIM data analysed in this work, a principal component analysis (PCA) using chemometric tools was performed. This statistical analysis allowed a more precise differentiation between the RIV–BIM compounds with respect to their properties. The data contained in Table 1 (*ee*AChE and *eq*BChE inhibition (IC_{50}), SI, inhibition of $A\beta_{42}$ and Cu(II)-induced $A\beta_{42}$ aggregation) and Table 2 (PSA, clog *P*(o/w), log *K* HSA serum protein binding, log BB, Caco-2 and MDCK permeability, oral absorption and violations of Lipinkski's rule) were analysed. The PCA analysis with three components was able to explain 91.9% of the variability, demonstrating its high reliability. The 3D bigraphic diagram between the dispersion diagram and component weights (Figure 9) shows that both series of compounds (**4** and **5**) are in opposite sides of the box, indicating that they do indeed have different properties based on their structure regarding the first principal component. The first principal component is explained mainly by oral absorption, Caco-2 and MDCK permeability, clog *P*(o/w), log *K* HSA serum protein binding, inhibition of $A\beta_{42}$ and Cu(II)-induced aggregation, evidencing a relationship between each of these, this being common for compound series **5**. Therefore, these parameters represent the most important differences between series **4** and **5**. Furthermore, between compounds of the same series, there is also a pattern from **a** to **d**. This is more evident in series **4** because of the Lipinski's rule violation of compound **5d**, which had a high weight in the third principal component. The bigraphic indicates that the IC_{50} of *eq*BChE inhibition increases in the left side of the box, the compounds **4a–d** being the ones with the worst values (higher IC_{50} values). On the other hand, the higher IC_{50} of *ee*AChE inhibition generally resulted in higher SI.

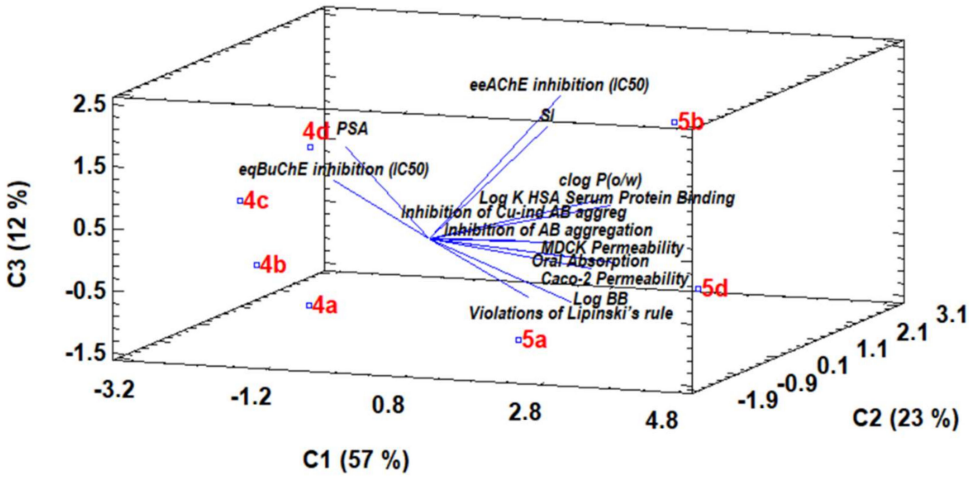


Figure 9. Three-dimensional bigraphic of a dispersion diagram and component weights obtained through a PCA analysis using chemometric tools.

4. Conclusions

Seven novel RIV–BIM hybrids based on the conjugation of the drug rivastigmine with hydroxyphenylbenzimidazole moieties were designed, prepared and evaluated for their biological properties as potential multi-target anti-Alzheimer´s disease (AD) drugs. Molecular docking modelling showed possible interactions between the RIV–BIM hybrids and the cholinesterases (AChE and BChE), indicating that all the compounds could be well accommodated inside the cholinesterase active site gorges but with dependences of inhibitory activity/selectivity on ligand structural differences. Pharmacokinetic parameters of the compounds were also evaluated *in silico*, predicting adequate drug-likeness properties and potential oral bioavailability. Regarding biological properties, all the compounds revealed higher AChE inhibitory activity than rivastigmine (IC_{50} = 32.1 μM), while compounds of series **5** displayed better inhibition of BChE than those of series **4**, **5b** (IC_{50} = 0.30 μM) and **5a** (IC_{50} = 0.9 μM) in particular. Although all the compounds showed good ChE inhibitory capacity, generally, they presented selectivity for the inhibition of BChE over AChE. Concerning the inhibition of $A\beta_{42}$ aggregation, fluorescence studies demonstrated that series **5** has higher inhibitory activity than series **4**. TEM observations of the effect of RIV–BIM hybrids in amyloid fibril aggregation, in the absence of Cu(II), showed that, generally, the compounds promote fibril narrowing (4.9 nm width in the absence of compounds), with the highest width reduction achieved by **5b** (3.8 nm) and **5d** (3.3 nm). Regarding Cu(II)-induced $A\beta_{42}$ aggregation, TEM assays indicated more intense aggregation in the presence of the metal ion than in its absence, along with a 38.8% increase in fibril width. Compounds **5b** and **5d** were responsible for the highest fibril width reduction in comparison with $A\beta_{42}$ + Cu(II) fibrils. Therefore, TEM studies seem to point towards the role of copper complexation in the inhibition of $A\beta_{42}$ aggregation, although such an effect was not much evidenced by the fluorescence studies. The effects of the compounds in terms of the reduction of toxicity induced by Aβ and ROS in neuronal cells (SH-SY5Y) were also evaluated, and **4d** and **5a,** respectively, showed the best neuroprotective capacities. A principal component analysis (PCA) of the experimental dataset allowed us to group and correlate the new compounds according to the evaluated parameters.

Overall, the novel RIV–BIM hybrids presented here show interesting properties as potential anti-AD drugs, some of them bearing diverse and important anti-AD hallmarks (inhibition of cholinesterases, inhibition of amyloid self-aggregation and Cu(II)-induced aggregation, as well as reduction of ROS and $A\beta_{42}$ toxicity in neuronal cells). Therefore, further studies on this RIV–BIM hybrid family are encouraged, with future developments of these compounds as multi-target anti-AD— and eventually also as anti-Parkinson's disease (PD)—drug candidates envisaged, since cholinergic transmission disruption and

related cognitive decline perturbations have been associated with PD pathology, besides other commonalities and correlated onsets between AD and PD.

Supplementary Materials: The following is available online: https://www.mdpi.com/article/10.3390/biomedicines10071510/s1. Figure S1. Docking results for RIV-BIM hybrids (blue) with hAChE and pose comparisons with the original ligand (yellow, PDB code 4EY7): (a) **4a**; (b) **4c**; (c) **4d**; (d) **5d**. Figure S2. Docking results for RIV-BIM hybrids (blue) with hBuChE and pose comparisons with the original ligand (yellow, PDB code 4TPK): (a) **4a**; (b) **4b**; (c) **5a**; (d) **5d**. Figure S3. Dose-response screening of RIV-BIM compounds in SH-SY5Y cell line to select a non-toxic concentration. Cells were treated with different concentrations of the mentioned compounds for 24 h. To evaluate cell viability, MTT reduction assay was performed. Results are expressed relatively to SH-SY5Y untreated cells, with the mean ± SEM derived from eight different experiments. * $p < 0.05$; ** $p < 0.01$; *** $p < 0.001$; **** $p < 0.0001$, significantly different when compared with SH-SY5Y untreated cells.

Author Contributions: Conceptualization, M.A.S. and S.C.; methodology, M.A.S., S.C., N.R.-C.; software, S.C.; validation S.C., S.M.C., N.R.-C.; formal analysis, S.C., M.A.S., S.M.C., D.V.-Z., M.E.L.-G.; investigation, D.V.-Z., L.B., A.R.P.-S.; resources, M.A.S., S.M.C., L.P.; data curation, S.C., S.M.C., M.E.L.-G.; writing—original draft preparation, D.V.-Z., M.A.S., S.C.; writing—review and editing, D.V.-Z., M.A.S., S.C., S.M.C., N.R.-C.; visualization, L.P., D.V.-Z.; supervision, M.A.S., S.C., N.R.-C., M.E.L.-G., Y.M.; project administration, M.A.S., S.C.; funding acquisition, M.A.S., S.C., S.M.C., L.P., Y.M. All authors have read and agreed to the published version of the manuscript.

Funding: This work was supported by the Portuguese Fundação para a Ciência e Tecnologia (FCT) (UIDB/00100/2020, UIDP/00100/2020, UIDB/04539/2020, UIDP/04539/2020 and LA/P/0058/2020), the Spanish Ministry of Science and Innovation (PID2020-114714RB-I00) and the Community of Madrid and European funding from FSE and FEDER programs for financial support (S2018/BAA-4393, AVANSECAL-II-CM). D.V.-Z. acknowledges the Spanish Ministry of Science, Innovation and Universities for funding through a pre-doctoral grant (FPU18/00573) and the Erasmus+ program for an international fellowship. A.R.P.S. is supported by a PD/BD/2020.06543.BD PhD fellowship.

Institutional Review Board Statement: Not applicable.

Informed Consent Statement: Not applicable.

Data Availability Statement: Data is contained within the article and supplementary files.

Acknowledgments: The authors from IST-Univ. Lisboa acknowledge the Portuguese Mass Spectrometry Networks (Node IST-CTN), the Portuguese NMR (IST-UL Center) and the Spanish National Center of Electronic Microscopy (CNME) for the use of their services. We also acknowledge the COST Action CA18202, NECTAR, supported by COST (European Cooperation in Science and Technology).

Conflicts of Interest: The authors declare no conflict of interest.

Abbreviations

ACh	Acetylthiocholine
AChI	Acetylthiocholine iodide
AD	Alzheimer's Disease
ADMET	Absorption, Distribution, Metabolism, Elimination, Toxicity
APP	Amyloid Precursor Protein
$A\beta_{42}$	Beta-amyloid protein, fragment 1-42
BBB	Blood–brain Barrier
BIM	Hydroxyphenylbenzimidazole acid
BCh	Butyrylthiocholine
BChI	S-butyrylthiocholine iodide
Caco	Human colon carcinoma cell line
CNS	Central nervous system
DMA	*N*,*N*-dimethylacetamide
DMEM	Dulbecco's Modified Eagle Medium
DMF	Dimethylformamide
DMHP	1,2-Dimethyl-3-hydroxy-4-pyridinone

DMSO	Dimethyl sulfoxide
DPPH	2,2-diphenyl-1-picrylhydrazyl free radical
DTNB	5,5′-dithiobis-(2-nitrobenzoic acid)
EC_{50}	Half maximal effective concentration
EDCI	1-ethyl-3-(3-dimethylaminopropyl)carbodiimide
*ee*AChE	Electric eel acetylcholinesterase
*eq*BChE	Equine butyrylcholinesterase
FBS	Fetal bovine serum
HD	Huntington's disease
HEPES	4-(2-hydroxyethyl)-1-piperazine-ethanesulfonic acid
HFIP	1,1,1,3,3,3-Hexafluoro-2-propanol
HSA	Human serum albumin
IC_{50}	Half maximal inhibitory concentration
LC	Liquid chromatography
MDCK	Madin–Darby canine kidney cell line
M.P	Melting points
MS-ESI	Electrospray ionization mass spectrometry
MTT	3-(4,5-dimethylthiazol-2-yl)-2,5-diphenyltetrazolium bromide
NMM	*N*-Methylmorpholine
NMR	Nuclear magnetic resonance
PCA	Principal component analysis
PD	Parkinson's disease
PSA	Polar surface area (Van der Waals surface area of polar nitrogen and oxygen atoms)
RF	Retention factor
RIV	Rivastigmine
ROS	Reactive oxygen species
SEM	Standard error of the mean
SD	Standard deviation
SI	Selectivity index (IC_{50}(AChE)/IC_{50}(BChE)
TBTU	2-(1*H*-benzotriazole-1-yl)-1,1,3,3-tetramethylaminium tetrafluoroborate
TEA	Triethylamine
TEM	Transmission electron microscopy
ThT	Thioflavin T
TLC	Thin-layer chromatography
TMS	Tetramethylsilane
TRIS	Tris(hydroxymethyl)aminomethane
UV-Vis	Ultraviolet–visible spectroscopy

References

1. Onyango, I.G.; Bennett, J.P.; Stokin, G.B. Regulation of neuronal bioenergetics as a therapeutic strategy in neurodegenerative diseases. *Neural Regen. Res.* **2021**, *16*, 1467–1482. [CrossRef] [PubMed]
2. Alzheimer's Association. 2021 Alzheimer's disease facts and figures. *Alzheimer's Dement.* **2021**, *17*, 327–406. [CrossRef] [PubMed]
3. Hung, S.-Y.; Fu, W.-M. Drug candidates in clinical trials for Alzheimer's disease. *J. Biomed. Sci.* **2017**, *24*, 47. [CrossRef] [PubMed]
4. Wimo, A.; Guerchet, M.; Ali, G.C.; Wu, Y.T.; Prina, A.M.; Winblad, B.; Jönsson, L.; Liu, Z.; Prince, M. The worldwide costs of dementia 2015 and comparisons with 2010. *Alzheimer's Dement.* **2017**, *13*, 1–7. [CrossRef]
5. Heron, M. Deaths: Leading causes for 2014. In *Natl. Vital Stat. Rep.*; 2016; 65, p. 5. Available online: https://www.cdc.gov/nchs/data/nvsr/nvsr65/nvsr65_05.pdf (accessed on 1 March 2022).
6. Nakamura, A.; Kaneko, N.; Villemagne, V.L.; Kato, T.; Doecke, J.; Doré, V.; Fowler, C.; Li, Q.-X.; Martins, R.; Rowe, C.; et al. High performance plasma amyloid-β biomarkers for Alzheimer's disease. *Nature* **2018**, *554*, 249–254. [CrossRef]
7. de Strooper, B.; Karran, E. The Cellular Phase of Alzheimer's Disease. *Cell* **2016**, *164*, 603–615. [CrossRef]
8. Karran, E.; de Strooper, B. The amyloid cascade hypothesis: Are we poised for success or failure? *J. Neurochem.* **2016**, *139*, 237–252. [CrossRef]
9. Du, X.; Wang, X.; Geng, M. Alzheimer's disease hypothesis and related therapies. *Transl. Neurodegener.* **2018**, *7*, 2. [CrossRef]
10. Gremer, L.; Schölzel, D.; Schenk, C.; Reinartz, E.; Labahn, J.; Ravelli, R.B.G.; Tusche, M.; Lopez-Iglesias, C.; Hoyer, W.; Heise, H.; et al. Fibril structure of amyloid-β(1–42) by cryo–electron microscopy. *Science* **2017**, *358*, 116–119. [CrossRef]
11. Schenk, D.; Barbour, R.; Dunn, W.; Gordon, G.; Grajeda, H.; Guido, T.; Hu, K.; Huang, J.; Johnson-Wood, K.; Khan, K.; et al. Immunization with amyloid-β attenuates Alzheimer disease-like pathology in the PDAPP mouse. *Nature* **1999**, *400*, 173–177. [CrossRef] [PubMed]

12. Sinha, S.; Anderson, J.P.; Barbour, R.; Basi, G.S.; Caccavello, R.; Davis, D.; Doan, M.; Dovey, H.F.; Frigon, N.; Hong, J.; et al. Purification and cloning of amyloid precursor protein β-secretase from human brain. *Nature* **1999**, *402*, 537–540. [CrossRef] [PubMed]
13. Cheignon, C.; Tomas, M.; Bonnefont-Rousselot, D.; Faller, P.; Hureau, C.; Collin, F. Oxidative stress and the amyloid beta peptide in Alzheimer's disease. *Redox Biol.* **2018**, *14*, 450–464. [CrossRef] [PubMed]
14. Lovell, M.A.; Robertson, J.D.; Teesdale, W.J.; Campbell, J.L.; Markesbery, W.R. Copper, iron and zinc in Alzheimer's disease senile plaques. *J. Neurol. Sci.* **1998**, *158*, 47–52. [CrossRef]
15. Xu, J.; Church, S.J.; Patassini, S.; Begley, P.; Waldvogel, H.J.; Curtis, M.A.; Faull, R.L.M.; Unwin, R.D.; Cooper, G.J.S. Evidence for widespread, severe brain copper deficiency in Alzheimer's dementia. *Metallomics* **2017**, *9*, 1106. [CrossRef]
16. Ganguly, G.; Chakrabarti, S.; Chatterjee, U.; Saso, L. Proteinopathy, oxidative stress and mitochondrial dysfunction: Cross talk in alzheimer's disease and parkinson's disease. *Drug Des. Dev. Ther.* **2017**, *11*, 797–810. [CrossRef]
17. Yarjanli, Z.; Ghaedi, K.; Esmaeili, A.; Rahgozar, S.; Zarrabi, A. Iron oxide nanoparticles may damage to the neural tissue through iron accumulation, oxidative stress and protein aggregation. *BMC Neurosci.* **2017**, *18*, 51. [CrossRef]
18. Bush, A.I.; Tanzi, R.E. Therapeutics for Alzheimer's disease based on the metal hypothesis. *Neurotherapeutics* **2008**, *5*, 421–432. [CrossRef]
19. White, A.R.; Kanninen, K.M.; Crouch, P.J. Editorial: Metals and neurodegeneration: Restoring the balance. *Front. Aging Neurosci.* **2015**, *7*, 127. [CrossRef]
20. Vicente-Zurdo, D.; Romero-Sánchez, I.; Rosales-Conrado, N.; León-González, M.E.; Madrid, Y. Ability of selenium species to inhibit metal-induced Aβ aggregation involved in the development of Alzheimer's disease. *Anal. Bioanal. Chem.* **2020**, *412*, 6485–6497. [CrossRef]
21. Li, S.Y.; Wang, X.B.; Kong, L.Y. Design, synthesis and biological evaluation of imine resveratrol derivatives as multi-targeted agents against Alzheimer's disease. *Eur. J. Med. Chem.* **2014**, *71*, 36–45. [CrossRef] [PubMed]
22. Santos, M.A.; Chand, K.; Chaves, S. Recent progress in multifunctional metal chelators as potential drugs for Alzheimer's disease. *Coord. Chem. Rev.* **2016**, *327–328*, 287–303. [CrossRef]
23. Ismaili, L.; Refouvelet, B.; Benchekroun, M.; Brogi, S.; Brindisi, M.; Gemma, S.; Campiani, G.; Filipic, S.; Agbaba, D.; Esteban, G.; et al. Multitarget compounds bearing tacrine- and donepezil-like structural and functional motifs for the potential treatment of Alzheimer's disease. *Prog. Neurobiol.* **2017**, *151*, 4–34. [CrossRef] [PubMed]
24. Chaves, S.; Várnagy, K.; Santos, M.A. Recent multi-target approaches on the development of anti-Alzheimer's agents integrating metal chelation activity. *Curr. Med. Chem.* **2021**, *28*, 7247–7277. [CrossRef]
25. Sanabria-Castro, A.; Alvarado-Echeverría, I.; Monge-Bonilla, C. Molecular pathogenesis of Alzheimer's disease: An update. *Ann. Neurosci.* **2017**, *24*, 46–54. [CrossRef]
26. Hampel, H.; Mesulam, M.M.; Cuello, A.C.; Farlow, M.R.; Giacobini, E.; Grossberg, G.T.; Khachaturian, A.S.; Vergallo, A.; Cavedo, E.; Snyder, P.J.; et al. The cholinergic system in the pathophysiology and treatment of Alzheimer's disease. *Brain* **2018**, *141*, 1917–1933. [CrossRef]
27. Terry, A.V., Jr.; Buccafusco, J.J. The cholinergic hypothesis of age and Alzheimer's disease-related cognitive deficits: Recent challenges and their implications for novel drug development. *J. Pharmacol. Exp. Ther.* **2003**, *306*, 821–827. [CrossRef]
28. Colovic, M.B.; Krstic, D.Z.; Lazarevic-Pasti, T.D.; Bondzic, A.M.; Vasic, V.M. Acetylcholinesterase inhibitors: Pharmacology and toxicology. *Curr. Neuropharmacol.* **2013**, *11*, 315–335. [CrossRef]
29. Ferreira-Vieira, T.H.; Guimaraes, I.M.; Silva, F.R.; Ribeiro, F.M. Alzheimer's disease: Targeting the cholinergic system. *Curr. Neuropharmacol.* **2016**, *14*, 101–115. [CrossRef]
30. Reisberg, B.; Doody, R.; Stoffler, A.; Schmitt, F.; Ferris, S.; Mobius, H.J. Memantine in moderateto-severe Alzheimer's disease. *N. Engl. J. Med.* **2003**, *348*, 1333–1341. [CrossRef]
31. Tolar, M.; Abushakra, S.; Hey, J.A.; Porsteinsson, A.; Sabbagh, M. Aducanumab, gantenerumab, BAN2401, and ALZ-801-the first wave of amyloid-targeting drugs for Alzheimer's disease with potential for near term approval. *Alzheimer's Res. Ther.* **2021**, *12*, 95. [CrossRef] [PubMed]
32. Sang, Z.; Wang, K.; Shi, J.; Liu, W.; Cheng, X.; Zhu, G.; Wang, Y.; Zhao, Y.; Qiao, Z.; Wu, A.; et al. The development of advanced structural framework as multi-target-directed ligands for the treatment of Alzheimer's disease. *Eur. J. Med. Chem.* **2020**, *192*, 112180. [CrossRef] [PubMed]
33. Santos, M.A.; Chand, K.; Chaves, S. Recent progress in repositioning Alzheimer´s disease drugs based on a multitarget strategy. *Fut. Med. Chem.* **2016**, *8*, 17. [CrossRef] [PubMed]
34. Jeřábek, J.; Uliassi, E.; Guidotti, L.; Korábečný, J.; Soukup, O.; Sepsova, V.; Hrabinova, M.; Kuča, K.; Bartolini, M.; Peña-Altamira, L.E.; et al. Tacrine-resveratrol fused hybrids as multi-target-directed ligands against Alzheimer's disease. *Eur. J. Med. Chem.* **2017**, *127*, 250–262. [CrossRef]
35. Hiremathad, A.; Keri, R.S.; Esteves, A.R.; Cardoso, S.M.; Chaves, S.; Santos, M.A. Novel Tacrine-hydroxyphenylbenzimidazole hybrids as potential multitarget drug candidates for Alzheimer's disease. *Eur. J. Med. Chem.* **2018**, *148*, 255–267. [CrossRef]
36. Queda, F.; Calò, S.; Gwizdala, K.; Magalhães, J.D.; Cardoso, S.M.; Chaves, S.; Piemontese, L.; Santos, M.A. Novel Donepezil-Arylsulfonamide Hybrids as Multitarget-Directed Ligands for Potential Treatment of Alzheimer's Disease. *Molecules* **2021**, *26*, 1658. [CrossRef]
37. Kumar, A.; Singh, A.; Ekavali. A review on Alzheimer's disease pathophysiology and its management: An update. *Pharmacol. Rep.* **2015**, *67*, 195–203. [CrossRef]
38. Long, J.M.; Holtzman, D.M. Alzheimer Disease: An update on pathobiology and treatment strategies. *Cell* **2019**, *179*, 312–339. [CrossRef]

39. Bar-On, P.; Millard, C.B.; Harel, M.; Dvir, H.; Enz, A.; Sussman, J.L.; Silman, I. Kinetic and structural studies on the interaction of cholinesterases with the anti-Alzheimer drug Rivastigmine. *Biochemistry* **2002**, *41*, 3555–3564. [CrossRef]
40. Chen, Z.; Digiacomo, M.; Tu, Y.; Gu, Q.; Wang, S.; Yang, X.; Chu, J.; Chen, Q.; Han, Y.; Chen, J.; et al. Discovery of novel rivastigmine-hydroxycinnamic acid hybrids as multi-targeted agents for Alzheimer's disease. *Eur. J. Med. Chem.* **2017**, *125*, 784–792. [CrossRef]
41. Sang, Z.; Wang, K.; Shi, J.; Cheng, X.; Zhu, G.; Wei, R.; Ma, Q.; Yu, L.; Zhao, Y.; Tan, Z.; et al. Apigenin-rivastigmine hybrids as multi-target-directed ligands for the treatment of Alzheimer's disease. *Eur. J. Med. Chem.* **2020**, *187*, 11958. [CrossRef] [PubMed]
42. Rodríguez-Rodríguez, C.; de Groot, N.S.; Rimola, A.; Álvarez-Larena, Á.; Lloveras, V.; Vidal-Gancedo, J.; Ventura, S.; Vendrell, J.; Sodupe, M.; González-Duarte, P. Design, selection, and characterization of thioflavin-based intercalation compounds with metal chelating properties for application in Alzheimer's disease. *J. Am. Chem. Soc.* **2009**, *131*, 1436–1451. [CrossRef] [PubMed]
43. Chaves, S.; Hiremathad, A.; Tomás, D.; Keri, R.S.; Piemontese, L.; Santos, M.A. Exploring the chelating capacity of 2-hydroxyphenyl-benzimidazole based hybrids with multi-target ability as anti-Alzheimer's agents. *New J. Chem.* **2018**, *42*, 16503–16515. [CrossRef]
44. Piemontese, L.; Tomás, D.; Hiremathad, A.; Capriati, V.; Candeias, E.; Cardoso, S.M.; Chaves, S.; Santos, M.A. Donepezil structure-based hybrids as potential multifunctional anti-Alzheimer's drug candidates. *J. Enzym. Inhib. Med. Chem.* **2018**, *33*, 1212–1224. [CrossRef]
45. Armarego, W.L.F.; Perrin, D.D. *Purification of Laboratory Chemicals*, 4th ed.; Butterworth Heinemann: Oxford, UK, 1999; pp. 1–544.
46. Cheung, J.; Rudolph, M.J.; Burshteyn, F.; Cassidy, M.S.; Gary, E.N.; Love, J.; Franklin, M.C.; Height, J.J. Structures of human acetylcholinesterase in complex with pharmacologically important ligands. *J. Med. Chem.* **2012**, *55*, 10282–10286. [CrossRef]
47. Brus, B.; Košak, U.; Turk, S.; Pišlar, A.; Coquelle, N.; Kos, J.; Stojan, J.; Colletier, J.-P.; Gobec, S. Discovery, biological evaluation, and crystal structure of a novel nanomolar selective butyrylcholinesterase inhibitor. *J. Med. Chem.* **2014**, *57*, 8167–8179. [CrossRef]
48. *Maestro, Version 9.3*; Schrödinger Inc.: Portland, OR, USA, 2012.
49. Acton, A.; Banck, M.; Bréfort, J.; Cruz, M.; Curtis, D.; Hassinen, T.; Heikkilä, V.; Hutchison, G.; Huuskonen, J.; Jensen, J.; et al. *Ghemical, Version 3.0*; GPL: Burbank, CA, USA, 2011.
50. Jones, G.; Willett, P.; Glen, R.C.; Leach, A.R.; Taylor, R. Development and validation of a genetic algorithm for flexible docking. *J. Mol. Biol.* **1997**, *267*, 727–748. [CrossRef]
51. Quintanova, C.; Keri, R.S.; Marques, S.M.; Fernandes, M.G.; Cardoso, S.M.; Serralheiro, M.L.; Santos, M.A. Design, synthesis and bioevaluation of tacrine hybrids with cinnamate and cinnamylidene acetate derivatives as potential anti-Alzheimer drugs. *MedChemComm* **2015**, *6*, 1969–1977. [CrossRef]
52. Chao, X.; He, X.; Yang, Y.; Zhou, X.; Jin, M.; Liu, S.; Cheng, Z.; Liu, P.; Wang, Y.; Yu, J.; et al. Design, synthesis and pharmacological evaluation of novel tacrine-caffeic acid hybrids as multi-targeted compounds against Alzheimer's disease. *Bioorganic Med. Chem. Lett.* **2012**, *22*, 6498–6502. [CrossRef]
53. Bartolini, M.; Bertucci, C.; Bolognesi, M.L.; Cavalli, A.; Melchiorre, C.; Andrisano, V. Insight into the kinetic of amyloid beta (1–42) peptide self-aggregation: Elucidation of inhibitors mechanism of action. *ChemBioChem* **2007**, *8*, 2152–2161. [CrossRef]
54. Lioudyno, M.I.; Broccio, M.; Sokolov, Y.; Rasool, S.; Wu, J.; Alkire, M.T.; Liu, V.; Kozak, J.A.; Dennison, P.R.; Glabe, C.G.; et al. Effect of synthetic Aβ peptide oligomers and fluorinated solvents on Kv1.3 channel properties and membrane conductance. *PLoS ONE* **2012**, *7*, e35090. [CrossRef] [PubMed]
55. Mosmann, T. Rapid colorimetric assay for cellular growth and survival: Application to proliferation and cytotoxicity assays. *J. Immunol. Meth.* **1983**, *65*, 55–63. [CrossRef]
56. *QikProp, Version 2.5*; Schrödinger, LLC.: New York, NY, USA, 2005.
57. Harel, M.; Sussman, J.L.; Krejci, E.; Bon, S.; Chanal, P.; Massoulie, J.; Silman, I. Conversion of acetylcholinesterase to butyrylcholinesterase: Modelling and mutagenesis. *Proc. Natl. Acad. Sci. USA* **1992**, *89*, 10827–10831. [CrossRef]
58. Chatonnet, A.; Lockridge, O. Comparison of butyrylcholinesterase and acetylcholinesterase. *Biochem. J.* **1989**, *260*, 625–634. [CrossRef]
59. Dighe, S.N.; Deora, G.S.; Mora, E.; Nachon, F.; Chan, S.; Parat, M.O.; Brazzolotto, X.; Ross, B.P. Discovery and structure-activity relationships of a highly selective butyrylcholinesterase inhibitor by structure-based virtual screening. *J. Med. Chem.* **2016**, *59*, 7683–7689. [CrossRef] [PubMed]
60. Benek, O.; Korabecny, J.; Soukup, O. A perspective on multi-target drugs for Alzheimer´s disease. *Trends Pharmacol. Sci.* **2020**, *41*, 434–445. [CrossRef]
61. Singh, A.; Sharma, S.; Arora, S.; Attri, S.; Kaur, P.; Gulati, H.K.; Bhagat, K.; Kumar, N.; Singh, H.; Singh, J.V.; et al. New coumarin-benzotriazole based hybrid molecules as inhibitors of acetylcholinesterase and amyloid aggregation. *Bioorganic Med. Chem. Lett.* **2020**, *30*, 127477. [CrossRef]
62. Faller, P.; Hureau, C.; Berthoumieu, O. Role of metal ions in the self-assembly of the Alzheimer's amyloid Aβ peptide. *Inorg. Chem.* **2013**, *52*, 12193–12206. [CrossRef]
63. Tahmasebinia, F.; Emadi, S. Effect of metal chelators on the aggregation of beta-amyloid peptides in the presence of copper and iron. *Biometals* **2017**, *30*, 285–293. [CrossRef]
64. Gómez-Mejía, E.; Rosales-Conrado, N.; León-González, M.E.; Madrid, Y. Citrus peels waste as a source of value-added compounds: Extraction and quantification of bioactive polyphenols. *Food Chem.* **2019**, *295*, 289–299. [CrossRef]

Supplementary Information

NOVEL RIVASTIGMINE DERIVATIVES AS PROMISING MULTI-TARGET COMPOUNDS FOR POTENTIAL TREATMENT OF ALZHEIMER'S DISEASE

David Vicente-Zurdo[a,b], Noelia Rosales-Conrado[b], M. Eugenia León-González[b], Leonardo Brunetti[a,c], Luca Piemontese[c], A. Raquel Pereira-Santos[d], Sandra M. Cardoso[d,e], Yolanda Madrid[b], Sílvia Chaves[a,*], M. Amélia Santos[a,*]

[a] Centro de Química Estrutural, Institute of Molecular Sciences, Departamento de Engenharia Química, Instituto Superior Técnico, Universidade de Lisboa, Av. Rovisco Pais 1, 1049-001, Lisboa, Portugal; [b] Department of Analytical Chemistry, Faculty of Chemistry, Complutense University of Madrid, Avenida Complutense s/n, 28040, Madrid, Spain; c) Department of Pharmacy-Pharmaceutical Sciences, University of Bari Aldo Moro, via E. Orabona 4, 70125 Bari, Italy; [d] CNC-Center for Neuroscience and Cell Biology, University of Coimbra, Coimbra, Portugal; [e] FMUC-Faculty of Medicine, University of Coimbra, Coimbra, Portugal.

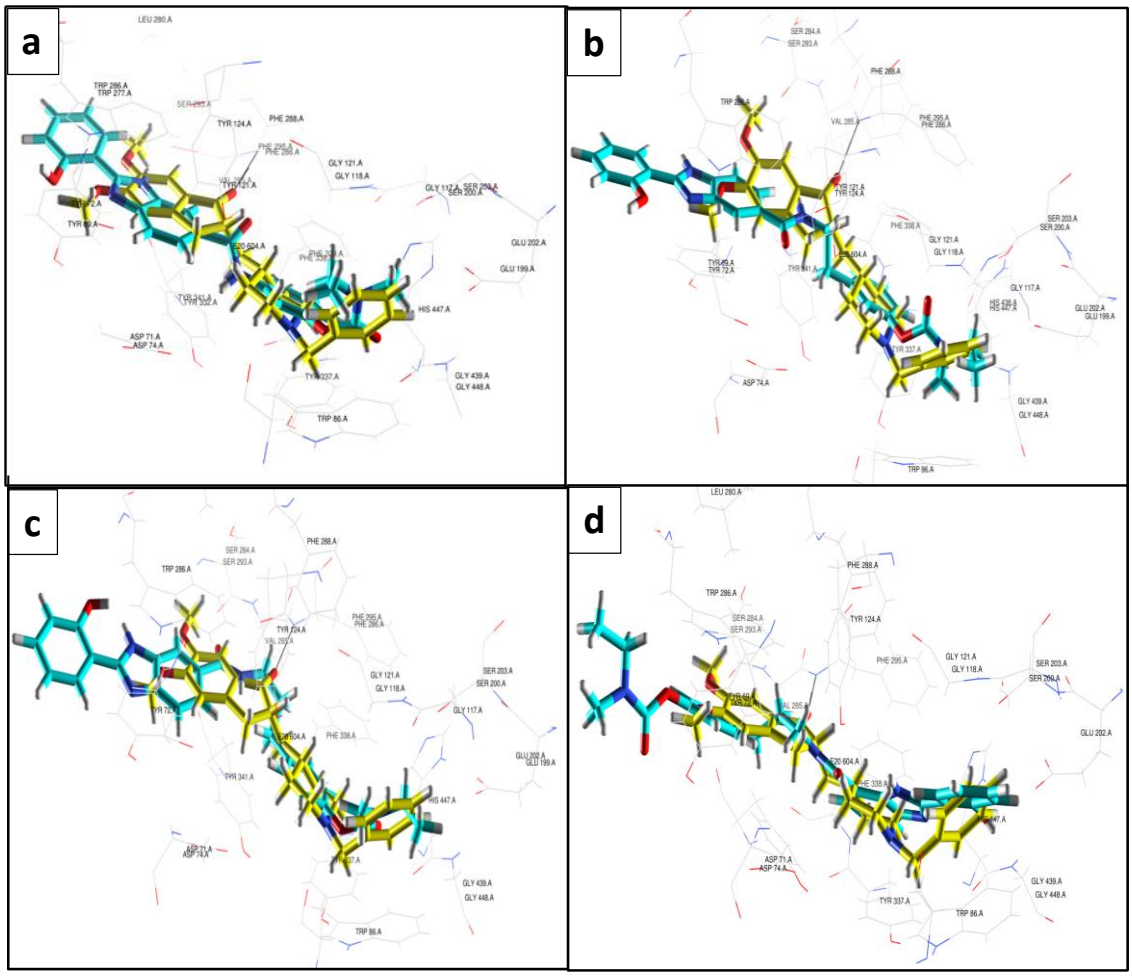


Figure S1. Docking results for RIV-BIM hybrids (blue) with hAChE and pose comparisons with the original ligand (yellow, PDB code 4EY7): (a) **4a**; (b) **4c**; (c) **4d**; (d) **5d**.

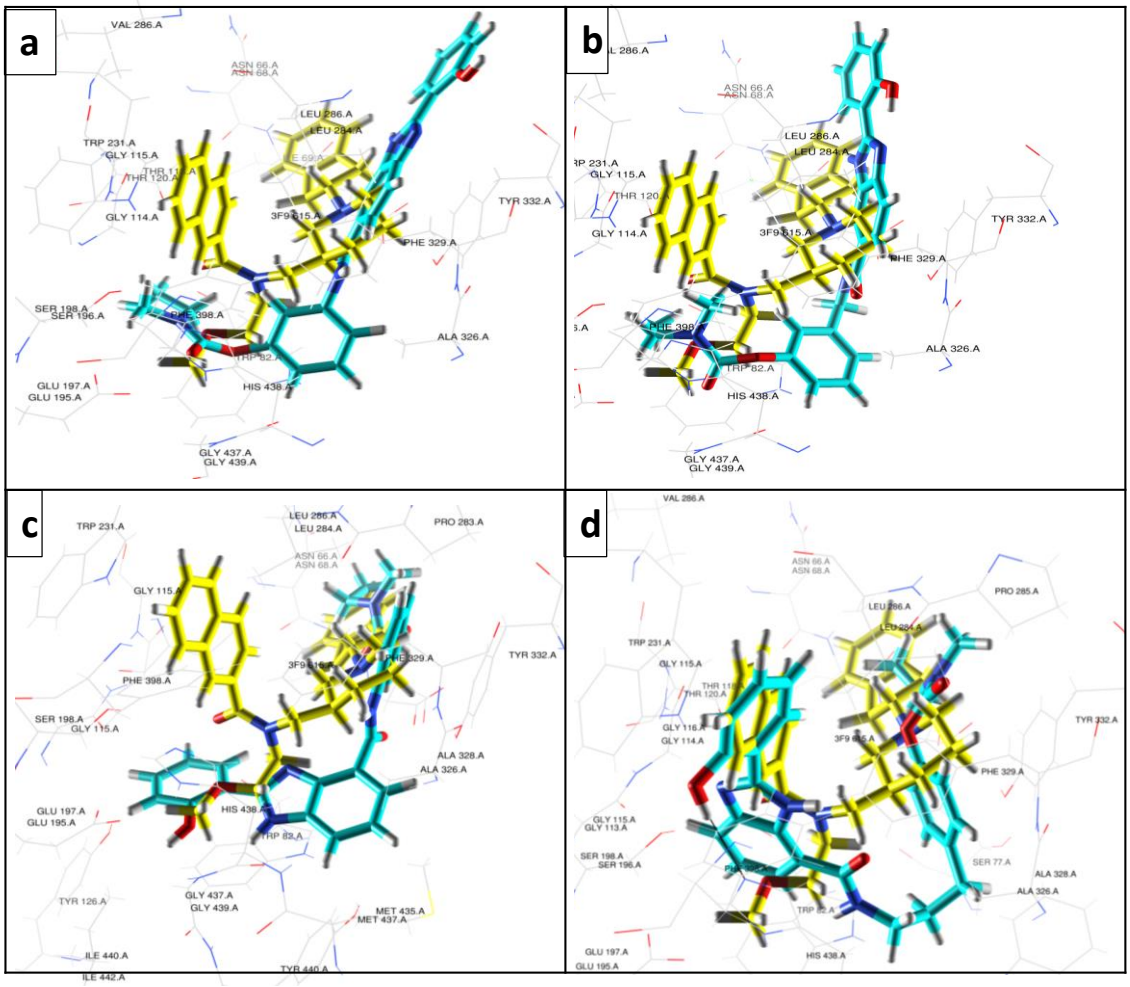


Figure S2. Docking results for RIV-BIM hybrids (blue) with hBuChE and pose comparisons with the original ligand (yellow, PDB code 4TPK): (a) **4a**; (b) **4b**; (c) **5a**; (d) **5d**.

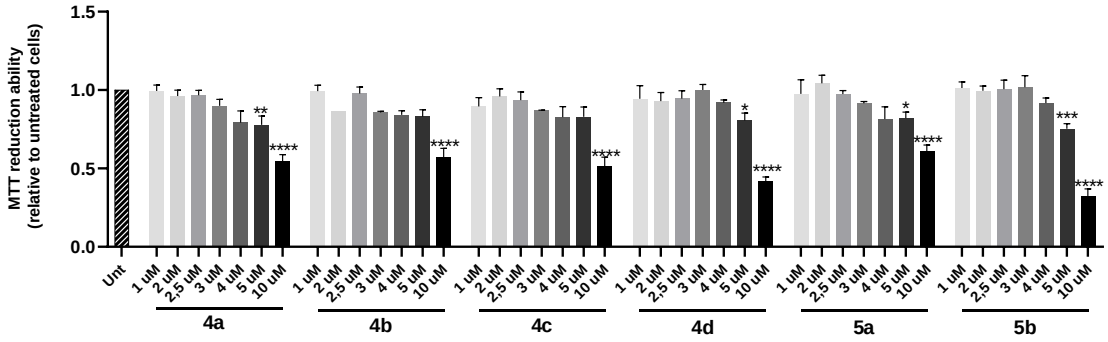


Figure S3. Dose-response screening of RIV-BIM compounds in SH-SY5Y cell line to select a non-toxic concentration. Cells were treated with different concentrations of the mentioned compounds for 24 h. To evaluate cell viability, MTT reduction assay was performed. Results are expressed relatively to SH-SY5Y untreated cells, with the mean ± SEM derived from eight different experiments. *$p < 0.05$; **$p < 0.01$; ***$p < 0.001$; ****$p < 0.0001$, significantly different when compared with SH-SY5Y untreated cells.

2. EVALUACIÓN DE LAS PROPIEDADES FISICOQUÍMICAS Y BIOLÓGICAS DE NANOPARTÍCULAS DE SELENIO EN LA ENFERMEDAD DE ALZHEIMER

El selenio es un nutriente esencial para el organismo debido a sus múltiples beneficios para la salud, que dependen a su vez de la especie química en la que se encuentre dicho elemento. Entre dichas especies cabe destacar la selenometionina (SeMet), selenometilselenocisteína (MeSeCys), selenocisteína (SeCys) y las nanopartículas de selenio.

Uno de los principales beneficios que aporta el selenio es su capacidad antioxidante, lo que puede ser de gran utilidad para combatir el efecto de los ROS provocado por el estrés oxidativo de metales como el Fe(II) y el Cu(II). Además, el selenio es capaz de interaccionar con múltiples biometales y metales tóxicos, siendo útil a la hora de inhibir el efecto neurotóxico de dichos metales. Por tanto, el selenio puede inhibir la agregación de la proteína Aβ al evitar que biometales y metales tóxicos ejerzan su papel en la "**hipótesis del ion metálico**" en sinergia con la "**hipótesis de la cascada amiloide**", principal desencadenante de la AD.

Una de las especies de selenio con más versatilidad son las nanopartículas de selenio, ya que se pueden funcionalizar con diversas moléculas que les aportan características únicas. Este es el caso de las Ch-SeNPs, que al estar estabilizadas con una sustancia quiral como el quitosano, poseen la capacidad de unirse enantioselectivamente a ciertas moléculas quirales del organismo relacionadas con la AD. De esta forma, la enantioselectividad es una característica realmente útil a la hora de interaccionar con enantiómeros potencialmente neurotóxicos, como los D-aminoácidos. Estos D-aminoácidos no se encuentran de forma natural en el organismo en condiciones normales, siendo los L-aminoácidos los predominantes. Sin embargo, los niveles de D-aminoácidos aumentan en presencia de determinadas enfermedades, como en la AD. Debido a la estrecha relación de los D-aminoácidos con la proteína Aβ, evitando su degradación y favoreciendo su agregación, una estrategia para contrarrestar su efecto puede ser el uso de compuestos quirales como las Ch-SeNPs.

Para considerar una especie de selenio, como es el caso de las Ch-SeNPs, como un potencial fármaco para prevenir o tratar la AD, es necesario realizar un estudio de toxicidad con líneas celulares para evaluar su efecto *in vitro*. Además de determinar su citotoxicidad, es importante estudiar la acumulación de selenio por parte de dichas células y observar si lo pueden internalizar.

Para investigar el efecto de diversas especies de selenio sobre los efectos neurotóxicos de metales en la AD, se llevó a cabo el siguiente trabajo (**Artículo 4**), titulado "**Ability of selenium species to inhibit metal-induced Aβ aggregation involved in the development of Alzheimer's disease**" (*Analytical and Bioanalytical Chemistry 412 (2020) 6485-6497*).

En este estudio se sintetizaron dos tipos de nanopartículas de selenio: nanopartículas estabilizadas con quitosano (Ch-SeNPs) y estabilizadas con quitosano y el polifenol ácido clorogénico (CGA@ChSeNPs). Su caracterización se realizó mediante TEM, EDXS, difracción electrónica (ED) y DLS, que permitieron obtener información sobre su composición elemental, tamaño, morfología, potencial zeta y estructura cristalina. Además, se llevó a cabo un análisis mediante cromatografía de líquidos capilar con detector UV-Vis de matriz de diodos (cLC-DAD) de las aguas resultantes tras la etapa de diálisis realizada, una vez finalizada la síntesis, para comprobar la unión del CGA a las Ch-SeNPs (CGA@ChSeNPs).

Se evaluaron las propiedades quelantes de las nanopartículas de selenio (Ch-SeNPs y CGA@ChSeNPs) y de otras especies de selenio orgánicas (SeMet, MeSeCys y $(SeCys)_2$) e inorgánicas (Se(IV) y Se(VI)), con respecto a biometales involucrados en la AD (Fe(II), Cu(II) y Zn(II)). La interacción entre las especies de selenio y los biometales se estudió mediante espectroscopía UV-Vis y d^1(UV-Vis), empleando diferentes relaciones de concentración metal:selenio, desde 1:1 hasta 1:4, con el objetivo de elucidar la posible relación de concentración óptima de la interacción.

Posteriormente, se estudiaron las propiedades anti-amiloidogénicas de las especies orgánicas de selenio y de los dos tipos de nanopartículas sintetizadas. Para los experimentos de inhibición de la agregación, se incubó el monómero $A\beta_{42}$ a 37 ºC durante 48 h en presencia o ausencia de los biometales y en presencia o ausencia de las especies de selenio. Mediante tinción negativa de las fibras con acetato de uranilo al 2% (p/v) y su posterior medida por TEM, se pudo comprobar la agregación amiloide producida por los metales y se confirmó si las especies de selenio eran capaces de inhibirla. Se midió la anchura de las fibras del fragmento de proteína $A\beta_{42}$ bajo el efecto de los diferentes metales y especies de selenio usando el programa ImageJ y se aplicó el análisis de la varianza ANOVA y, en su caso, el test LSD de Fisher al 95% de confianza a los valores de achura de fibra medidos.

Además de la inhibición de la agregación, también se estudió la desagregación que causaban las Ch-SeNPs en la acumulación de fibras producida por la presencia de Fe(II).

Para ello, se incubó el monómero $A\beta_{42}$ durante 24 h en presencia de Fe(II) y se observó la agregación mediante TEM. La misma muestra se incubó durante 24 h más en presencia de Ch-SeNPs, con el posterior análisis de las fibras mediante TEM para evaluar su desagregación.

Finalmente, debido a la importancia de la capacidad antioxidante de las especies de selenio en la AD, se midió el potencial de las especies para disminuir los ROS mediante el método del DPPH y espectroscopía UV-Vis. La capacidad antioxidante se estimó mediante el cálculo del IC_{50}, mostrando los dos tipos de nanopartículas de selenio sintetizadas la mayor capacidad antioxidante.

Con objeto de estudiar el efecto neuroprotector de las Ch-SeNPs frente a los enantiómeros de D-aminoácidos en la AD, se llevó a cabo el siguiente trabajo (**Artículo 5**) titulado "**Neuroprotective activity of selenium nanoparticles against the effect of amino acid enantiomers in Alzheimer's disease**" (*Analytical and Bioanalytical Chemistry 414 (2022) 7573-7584*).

En este estudio se seleccionaron los enantiómeros D y L de aminoácidos involucrados en la AD, como Phe, Ala, Glu, Asp, Trp, Tyr, Ser, y L- y DL-SeMet, para evaluar su efecto en la agregación del fragmento de proteína $A\beta_{42}$. Para ello, los enantiómeros de cada uno de los aminoácidos se incubaron junto con el monómero $A\beta_{42}$ a 37 ºC durante 48 h. Las fibras se tiñeron negativamente con acetato de uranilo al 2% (p/v) y se visualizaron mediante TEM. En base a estos ensayos se pudieron determinar las diferencias en el efecto que poseían los enantiómeros de aminoácidos frente a la agregación amiloide, sugiriendo que dicha agregación se veía afectada por el entorno quiral en el que se encuentra la proteína $A\beta_{42}$. Adicionalmente, se midió la anchura de las fibras amiloides para cada una de las condiciones a las que fueron sometidas mediante el programa ImageJ, y se realizó un análisis ANOVA y test LSD de Fisher al 95% de confianza para evaluar los grupos de los enantiómeros de aminoácidos que producían el mismo efecto sobre la morfología de la $A\beta_{42}$.

Los enantiómeros que mostraron propiedades amiloidogénicas se sometieron a estudios de inhibición de la agregación amiloide. Así, los enantiómeros seleccionados se co-incubaron con las Ch-SeNPs en presencia del monómero $A\beta_{42}$ a 37 ºC durante 48 h, con la posterior tinción negativa y análisis por TEM.

La interacción de las Ch-SeNPs con los diferentes enantiómeros de los aminoácidos se evaluó mediante espectroscopía UV-Vis y fluorescencia, esta última con previa derivatización de los aminoácidos con orto-ftalaldehído (OPA). Se realizó un diseño experimental factorial con dos factores (concentración de Ch-SeNPs y concentración de enantiómero de aminoácido) y tres niveles (35, 70 y 105 μM) con el objetivo de elucidar la posible relación de concentración óptima de la interacción. Las medidas mediante espectroscopía UV-Vis se realizaron a 268 nm, y para las medidas por fluorescencia se fijó una longitud de onda de excitación de 359 nm y una longitud de onda de emisión de 410 nm. Los resultados del diseño experimental realizado se analizaron a través del diagrama de Pareto de efectos estandarizados, la gráfica de efectos principales y la metodología de superficie de respuesta (RSM). De esta forma, se determinó la existencia de una interacción enantioselectiva entre las Ch-SeNPs y los enantiómeros de los aminoácidos, pudiéndose determinar, en algunos casos, la relación de concentración nanopartícula:aminoácido a la que la interacción era máxima.

Finalmente, se realizaron dos ensayos con objeto de evaluar la capacidad antioxidante de los enantiómeros de aminoácidos: los ensayos del DPPH y del TBARS, utilizando en ambos casos como sustancia antioxidante de referencia trolox. Así, se determinó el valor IC_{50} para cada uno de los enantiómeros de aminoácidos evaluados mediante espectroscopía UV-Vis, a través de las medidas de absorbancia a una longitud de onda de 515 nm en el ensayo del DPPH y de 532 nm en el ensayo del TBARS.

Para determinar el efecto *in vitro* de las Ch-SeNPs con respecto a su citotoxicidad, localización intracelular y acumulación por parte de líneas celulares de neuroblastoma, se llevó a cabo el último trabajo de esta tesis doctoral (**Artículo 6**), titulado "**Uptake and accumulation of selenium nanoparticles and other selenium species in neuroblastoma cell lines related to Alzheimer's disease by using TEM and single cell-ICP-MS**" (*European Journal of Medicinal Chemistry (enviado)*).

Debido al efecto neuroprotector mostrado anteriormente por las Ch-SeNPs, en este trabajo se procedió a determinar su citotoxicidad, junto con la de otras especies de selenio como la SeMet y la MeSeCys. Para ello, se emplearon dos líneas celulares diferentes: neuroblastoma de ratón (Neuro-2a) y neuroblastoma humano (SH-SY5Y), y dos métodos para determinar la viabilidad celular: MTT y citometría de flujo. Para ello, se estudió, en primer lugar, la estabilidad de las Ch-SeNPs a 50 μM, a 37 ºC durante 48 h, en los dos medios de cultivo pertenecientes a las células Neuro-2a y SH-SY5Y, midiendo sus

diámetros mediante TEM y comparándolas con Ch-SeNPs control (n > 100). Posteriormente, los dos tipos de células se sembraron durante 24 h en placas de cultivo y se expusieron a las concentraciones de las especies de selenio (50, 250, 500, 750 y 1000 μM) durante 48 h. Para el ensayo con el método del MTT se midió la absorbancia de los cristales de formazano a una longitud de onda de 570 nm, mientras que las medidas de citometría de flujo requirieron el uso del fluorocromo PI, fijando la longitud de onda de excitación a un valor de 535 nm y midiendo la emisión a 617 nm. Se determinó la concentración letal para el 50% de la población (LC_{50}) de cada especie de selenio, para cada uno de los métodos y de las líneas celulares empleadas. Los resultados se analizaron estadísticamente mediante ANOVA, utilizando además el test LSD de Fisher, al 95% de confianza, en caso de existir diferencias significativas, para evaluar las diferencias entre la citotoxicidad de los compuestos, las líneas celulares y los métodos bioanalíticos empleados (n = 5).

Con objeto de determinar la capacidad de las células SH-SY5Y para internalizar las Ch-SeNPs, se llevó a cabo una fijación con paraformaldehído/glutaraldehído y postfijación con tetróxido de osmio de células tratadas durante 48 h con 50 μM Ch-SeNPs. A continuación, se cortaron las células con un microtomo y se visualizaron mediante TEM, comparándolas con células control. Se observó la localización extra e intracelular de las Ch-SeNPs en diferentes compartimentos celulares, se evaluaron las células en diferentes etapas de acumulación de Ch-SeNPs, y se midió el diámetro de las membranas celulares, núcleos y nucleolos en dichas etapas utilizando el programa ImageJ. Se compararon los diámetros de los compartimentos celulares, de las células tratadas con Ch-SeNPs con células control, utilizando ANOVA, al 95% de confianza, para determinar la existencia de diferencias significativas (n = 10).

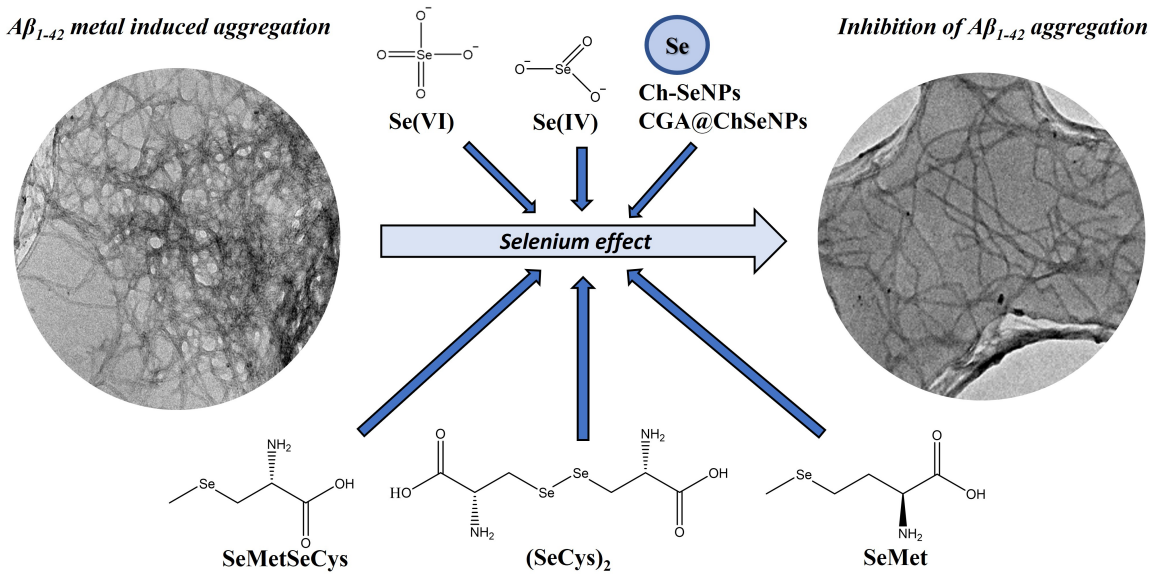
Finalmente, para evaluar la adquisición de Ch-SeNPs, SeMet y MeSeCys por parte de las líneas celulares Neuro-2a y SH-SY5Y, las células se expusieron a diferentes concentraciones de las especies de selenio (10, 50 y 250 μM) durante 48 h. Posteriormente, se desarrolló un método de análisis por SC-ICP-MS para medir el contenido celular de selenio en cada una de las dos líneas celulares evaluadas. Se representó la señal de los eventos frente al tiempo y se cuantificó, mediante un calibrado externo, la masa de selenio en cada una de las células que lo acumularon. Se compararon las tres especies de selenio y las dos líneas celulares en términos de acumulación de selenio, estableciendo un intervalo para cada condición (n > 700). Mediante los histogramas obtenidos, se pudo evaluar el perfil de adquisición de selenio que presentaba cada línea celular frente las especies de selenio que mostraron una mayor acumulación.

Artículo 4: <u>Capacidad de las especies de selenio para inhibir la agregación Aβ inducida por metales involucrados en el desarrollo de la enfermedad de Alzheimer</u>

Ability of selenium species to inhibit metal-induced Aβ aggregation involved in the development of Alzheimer's disease

<u>David Vicente-Zurdo</u>, Iván Romero-Sánchez, Noelia Rosales-Conrado, María Eugenia León-González, Yolanda Madrid

Analytical and Bioanalytical Chemistry 412 (2020) 6485-6497 (*Impact factor: 4.157*)



Parte de los resultados de este trabajo se presentaron en:

"XXII REUNIÓN DE LA SOCIEDAD ESPAÑOLA DE QUÍMICA ANALÍTICA (XXII SEQA). JORNADA DE ESPECIACIÓN. RETOS DE LA ESPECIACIÓN QUÍMICA EN EL SIGLO XXI: ESPECIACIÓN QUÍMICA Y ÓMICAS". *Role of selenium species in neurodegenerative diseases*. Valladolid, España, julio de 2019. Tipo de comunicación: póster.

"V SIMPOSIO ANUAL EN QUÍMICA AVANZADA (V SAQA)". *Evaluation of selenium species as potential multifunctional compounds for Alzheimer's disease treatment*. Madrid, España, diciembre de 2020. Tipo de comunicación: oral.

Analytical and Bioanalytical Chemistry (2020) 412:6485–6497
https://doi.org/10.1007/s00216-020-02644-2

RESEARCH PAPER

Ability of selenium species to inhibit metal-induced Aβ aggregation involved in the development of Alzheimer's disease

David Vicente-Zurdo[1] · Iván Romero-Sánchez[1] · Noelia Rosales-Conrado[1] · María Eugenia León-González[1] · Yolanda Madrid[1]

Received: 11 December 2019 / Revised: 27 March 2020 / Accepted: 3 April 2020 / Published online: 22 April 2020
© Springer-Verlag GmbH Germany, part of Springer Nature 2020

Abstract

Extracellular accumulation of amyloid beta peptide (Aβ) is believed to be one of the main factors responsible for neurodegeneration in Alzheimer's disease (AD). Metals could induce Aβ aggregation, by their redox activity or binding properties to amyloid β fibrils, leading to their accumulation and deposition outside neurons. For this reason, metal chelation may have an acknowledged part to play in AD prevention and treatment. In the current work, the role of different selenium species, including selenium nanoparticles, in Aβ aggregation, was studied by evaluating their metal-chelating properties and their ability both to inhibit metal-induced $A\beta_{1-42}$ aggregation fibrils and to disaggregate them once formed. Transition biometals such as Fe(II), Cu(II), and Zn(II) at 50 μM were selected to establish the in vitro models. The DPPH assay was used to determine the antioxidant capacity of the evaluated selenium species. Selenium nanoparticles stabilized with chitosan (Ch-SeNPs) and with both chitosan and chlorogenic acid polyphenol (CGA@ChSeNPs) showed the highest antioxidant properties with EC_{50} of 0.9 and 0.07 mM, respectively. UV–Vis and d^1(UV–Vis) spectra also revealed that selenium species, in particular selenomethionine (SeMet), were able to interact with metals. Regarding $A\beta_{1-42}$ incubation experiments, Fe(II), Cu(II), and Zn(II) induced Aβ aggregation, in a similar way to most of the evaluated selenium species. However, Ch-SeNPs produced a high inhibition of metal-induced Aβ aggregation, as well as a high disaggregation capacity of Aβ fibrils in both the presence and absence of biometals, in addition to reducing the length and width (20% of reduction in the presence of Zn(II)) of the generated Aβ fibrils.

Keywords Alzheimer's disease · Selenium species · Selenium nanoparticles · Metal-induced $A\beta_{1-42}$ aggregation · Antioxidant properties

Introduction

Nowadays, around 50 million people worldwide suffer from neurodegenerative diseases, discovering 10 million cases more every year, from which nearly 70% are affected by Alzheimer's disease (AD). This number is predicted to reach 152 million by 2050. However, at the present time, there is no treatment to cure neurodegenerative disorders [1].

Regarding AD, the amyloid cascade hypothesis assumes that neurodegeneration damage is caused by the deposition of plaques of the amyloid β peptide (Aβ) outside neurons in brain tissue [2]. Another relevant hypothesis in the AD field is the metal ion hypothesis, which is strongly intertwined with the amyloid cascade one. It suggests that some transition biometals, such as Fe(II), Cu(II), and Zn(II), can induce Aβ aggregation in the outer side of neurons, specially Aβ fragment 1–42 ($A\beta_{1-42}$). This occurs due to metal ability to bind some sites in $A\beta_{1-16}$ [3] and to produce oxidative stress that generate reactive oxygen species (ROS) [4, 5].

Due to the important and toxic role that metals have in AD, new strategies using metal chelators are being developed for the prevention and/or treatment of AD [6]. Selenium is an essential trace nutrient due to its multiple health benefits, such as its anti-inflammatory, chemopreventive, and antiviral properties [7]. Moreover, its antioxidant properties are well known, which also provide selenium a protective effect against cancer and other diseases [8–10]. Another additional property of selenium is its great ability to interact with a variety of metals,

Published in the topical collection featuring *Female Role Models in Analytical Chemistry.*

✉ Yolanda Madrid
ymadrid@quim.ucm.es

[1] Departamento de Química Analítica, Facultad de Ciencias Químicas, Universidad Complutense de Madrid, 28040 Madrid, Spain

which attributes selenium a protective effect for human health [11–13]. In fact, there are several studies that associate selenium deficiency with an alteration of brain metabolism [14]. On the other hand, selenium is also involved in some neurotransmission and dopaminergic pathways due to its antioxidant effect [14, 15], and selenoproteins may be helpful in preventing neurodegeneration [16].

However, selenium properties are different between its different species. While inorganic selenium species such as selenite and selenate are the most toxic forms, affecting even at mitochondrial level [17], organic selenium species have different beneficial properties [18, 19]. Due to its pharmacokinetics, selenomethionine (SeMet) is very effective in promoting neural stem cell proliferation and their differentiation into neurons, repairing damaged neural systems [20]. Species such as Se-methylselenocysteine (SeMetSeCys) has proved to be an anticarcinogenic compound regarding mammary tumors [21], while selenocysteine (SeCys) forms part of selenoprotein, which is involved in glutathione-dependent hydroperoxide removal, reduction of thioredoxins, thyroid hormones, and anticancer activities in the immune system among others [9].

Other selenium species, presenting different physicochemical properties than the previously mentioned ones, are selenium nanoparticles (SeNPs), with potential anticancer and antimicrobial characteristics [22] and interesting chemotherapeutic properties [23]. SeNPs can be prepared by different physicochemical methods and special features could be achieved by NP surface functionalization with various ligands, which could prevent particle aggregation and modulate cellular biological processes. Thus, SeNPs could be produced to generate tunable nanostructures with anticancer or antibacterial properties, as well as to design drug delivery systems. In fact, including active compounds in SeNPs could open new and promising applications for synergistic treatment of several diseases [24]. With this regard, SeNPs could be stabilized with chitosan, an approved, low toxicity, biodegradable, and biocompatible polymer regarded as safe for human dietary and medical uses [25], and then coated with several compounds.

Several researches have proposed nanoparticles for the treatment of AD as they are small enough to pass through the brain–blood barrier (BBB) [26]. Regarding the role of SeNPs in Alzheimer's disease studies, several compounds have been used to stabilize nanoparticles, to reduce their cytotoxicity and to reduce amyloid β aggregation. SeNPs coated with some peptides have proved to bind and to inhibit $A\beta_{40}$ fibril formation in AD, by disrupting hydrophobic and electrostatic interactions in amyloid nucleation [27]. Other SeNPs modified with chondroitin sulfate have been used in in vitro AD models to inhibit aggregation and to protect cells from Aβ-induced cytotoxicity [28]. Additionally, SeNPs can be coated with polyphenols, which are well known for their antioxidant, anticancer, antibacterial, antimicrobial, and antiviral characteristics [29–33], although there are several studies also attributing polyphenols' neurogenic properties [34–37]. For example, chlorogenic acid (CGA) stimulates the central nervous system and it presents cardioprotective, anti-inflammatory, anti-obesity, and free radical scavenger properties [38]. For these reasons, SeNP surface functionalization with polyphenols could be an interesting pathway for affecting inhibition of Aβ aggregation. In this sense, epigallocatechin-3-gallate (EGCG)-stabilized selenium nanoparticles coated with Tet-1 peptide have been employed to reduce amyloid β aggregation and cytotoxicity [39]. Lately, chiral penicillamine-modified selenium nanoparticles have been used as chiral amyloid β inhibitor. D-penicillamine@SeNPs showed an inhibitory effect of Zn^{2+} over aggregation of Aβ [40].

As it has been previously commented, there are some works related to selenium effect in inhibiting metal-induced amyloid β aggregation. However, none of them consider the comparison of selenium species of different nature. On the contrary, in most cases, only the effect of a single Se specie has been evaluated. For all mentioned above, the main aim of the present work is to evaluate the potential role of several selenium species (selenite, selenate, seleno amino acids, and SeNPs) for inhibiting the metal-induced Aβ aggregation related to Alzheimer's disease. In-house selenium nanoparticles stabilized with chitosan (Ch-SeNPs) and with both chitosan and chlorogenic acid polyphenol (CGA@ChSeNPs) were selected for this study as they combine the biocompatibility of chitosan with the antioxidative and metal-chelating properties of selenium and chlorogenic acid. To achieve this goal, different analytical techniques were applied: TEM measurements were performed for nanoparticle characterization and for investigating the metal-induced Aβ aggregation, DLS for nanoparticle characterization, UV–Vis and d^1(UV–Vis) to evaluate the interaction between metals and selenium species, and DDPH assay to determine the antioxidant activity of selenium species tested.

Materials and methods

Reagents and standards

All solvents and chemicals used were of analytical grade. Deionized water with resistance 18 MΩ cm was obtained from a Milli-Q water purification system unit (Millipore, Bedford, MA, USA), and it was used throughout the experiments. Individual selenium standards were prepared by dissolving in Milli-Q water Na_2SeO_3, Na_2SeO_4, DL-selenocystine ($(SeCys)_2$), DL-selenomethionine (SeMet), and Se-methyl-DL-selenocysteine (SeMetSeCys) reagents, which were purchased from Sigma-Aldrich (Steinheim, Germany). Working solutions were prepared daily by proper dilution of the pure standards. Both types of selenium nanoparticles (Ch-SeNPs

and CGA@ChSeNPs) were synthetized in the presence of chitosan (Sigma-Aldrich), acetic acid (Panreac, Barcelona, Spain), and ascorbic acid (Sigma-Aldrich). CGA@ChSeNPs also included the presence of chlorogenic acid (Sigma-Aldrich) in the synthesis procedure. For the cLC-DAD analysis of CGA in dialysis solution, acetonitrile (Scharlab, Barcelona, Spain) and formic acid (Fluka, Spain) were employed. For antioxidant capacity analysis, 2,2-diphenyl-1-picrylhydrazyl (DPPH) radical, from Sigma-Aldrich, was dissolved in pure methanol (Scharlab, Barcelona, Spain). For chelating studies, stock solutions of $FeSO_4 \cdot 7H_2O$ (Panreac) dissolved in 5% (v/v) of concentrated H_2SO_4 (Scharlab), $Cu(NO_3)_2 \cdot 3H_2O$ (Merck), and $ZnSO_4$ (Probus, Barcelona, Spain) were prepared daily in 100 mM phosphate (Panreac) buffer adjusted at pH 7.30. Amyloid β protein fragment 1–42 ($A\beta_{1-42}$) (A9810, CAS: 107761-42-2, MW 4514.04 g mol^{-1}) was purchased from Sigma-Aldrich for incubation assays. 1,1,1,3,3,3-Hexafluoro-2-propanol (HFIP), also from Sigma-Aldrich, was employed to pretreat $A\beta_{1-42}$. Dimethyl sulfoxide (Scharlab) was used to initially dissolve $A\beta_{1-42}$, followed by 10 mM HCl (Scharlab).

Instrumentation

The antioxidant capacity and the metal–selenium interactions were evaluated by using a diode array HP8543 UV–Vis spectrophotometer (Agilent Technologies, Madrid, Spain), equipped with a 1.0-cm quartz cuvette and the HP Chemstation software. Chromatographic analysis of CGA@ChSeNP dialysis solution by cLC was performed by an Agilent cLC instrument Mod. 1100 Series from Agilent Technologies (Madrid, Spain) equipped with a G1376A binary capillary pump, a G1379A degasser, and a G1315B diode array detector (500 nL, 10 mm pathlength). Data acquisition and processing were achieved by using the Agilent Chemstation software package for Microsoft Windows. An external stainless-steel loop with a volume of 10 μL was situated into a Rheodyne injection valve. Chromatographic separation was made on a Synergi™ Fusion 4 μm C18 (150 mm × 0.3 mm I.D.) capillary analytical column from Phenomenex (Torrance, CA, USA). A New Brunswick Scientific U410 Premium freezer (Eppendorf, Hamburg, Germany) at − 80 °C was required to preserve $A\beta_{1-42}$ commercial stock. A SpeedVac Concentrator Plus (Eppendorf) was necessary to pretreat $A\beta_{1-42}$. A WX vortex mixer from VELP Scientifica (Usmate, MB, Italy) was used to homogenize the AB_{1-42} monomeric solution, and a ThermoScientific MaxQ 4000 incubator (Fisher Scientific, Madrid, Spain) was utilized to generate $A\beta_{1-42}$ fibrils.

A TEM (JEOL JEM-2100) equipped with an energy-dispersive X-ray spectroscopy (EDXS) microanalysis composition system (Oxford Inca) and a TEM (JEOL JEM-1400 Plus) at 100 kV transmission electron microscopes were employed for SeNP characterization and evaluation of Aβ fibril formation, respectively. The hydrodynamic diameter of nanoparticles as well as the zeta potential was measured through dynamic light scattering (DLS) by using a Malvern Zetasizer Nano ZS (Malvern Instrument Ltd, Malvern UK) system, equipped with a laser of 633 nm. The scattering angle was 173° and the measuring position was 4.65 mm inside disposable plastic cuvettes.

Synthesis of selenium nanoparticles

A dispersion of 12.67 mM selenium nanoparticles (ChSeNPs) was prepared by mixing 2 mL of chitosan 0.5% (w/v), dissolved in 3% acetic acid, with 2.378 mL of ascorbic acid 0.2271 M, under continuous stirring at 250 rpm during 30 min. Then, a volume of 2.35 mL from a 53.9-mM Na_2SeO_3 aqueous solution was slowly added, and the resulting solution was stirred again at 250 rpm for 30 min. Finally, it was diluted to a final volume of 10 mL and stored in the dark at 4 °C until use.

With the aim to improve the antioxidant properties of ChSeNPs, CGA, dissolved in distilled water at 60 °C and cooled at room temperature, was added in a new synthesis. Selenium nanoparticles functionalized with chlorogenic acid (CGA@ChSeNPs) were prepared in a concentration of 12.67 mM Se and 3.40 mM CGA. For this purpose, 2 mL of chitosan 0.5% (w/v), dissolved in 3% acetic acid, was mixed with 1 mL of 33.98 mM CGA. The resulting solution was stirred at 250 rpm during 2 min. Then, 2.378 mL of ascorbic acid 0.2271 M was added to the previous solution and stirred at 250 rpm during 30 min. After this time, a volume of 2.35 mL from a 53.9-mM Na_2SeO_3 aqueous solution was slowly added, and the resulting solution was stirred again at 250 rpm for 30 min. Finally, the CGA@ChSeNP dispersion was diluted to a final volume of 10 mL and stored at 4 °C under the dark until use.

All synthetized selenium nanoparticles were subjected to dialysis before experiments, employing a dialysis sack (Sigma-Aldrich), which retains compounds with a molecular weight above 12 kDa. The sack was filled with 5 mL of the nanoparticle dispersion, and it was stirred at 300 rpm inside 1.4 L of Milli-Q water during 2 h. The purpose of the dialysis was to remove the excess of reagents that had not reacted during the nanoparticle synthesis process.

cLC-DAD analysis of chlorogenic acid in SeNP dialysis solution

Chromatographic separation was performed by a linear gradient combining solvent A (acetonitrile) and solvent B (aqueous solution 0.05% formic acid at pH 2.9). The elution program consisted of 8% A (3 min), then a linear increase to 37% A during 10 min, and finally an isocratic step at 37% A until the

end of the chromatogram. Flow rate was maintained at 10 μL min^{-1}. Chromatographic analysis was carried out using simultaneous monitoring at the following wavelengths: 220, 260, 292, 310, and 365 nm. Quantitative analyses were performed at 310 nm.

Metal–selenium interaction

Evaluation of the interaction between SeMet, $(SeCys)_2$, SeMetSeCys, Se(IV), Se(VI), Ch-SeNP, and CGA@ChSeNP species with Fe(II), Cu(II), and Zn(II) transition metals was accomplished in a 100-mM phosphate buffer at pH 7.30 media. Two different experimental conditions were established in order to study 1:1, 1:2, 1:3, and 1:4 metal–selenium species stoichiometries: (i) maintaining constant the metal concentration [$M = 50$ μM] and varying the selenium species concentration [$L = 50$, 100, 150, and 200 μM] and (ii) maintaining selenium species concentration constant [$L = 50$ μM] and varying metal concentration [$M = 50$, 25, 16.5, and 12.5 μM]. Stock aqueous solutions of Cu(II), Zn(II), and Fe(II), with 2.5 mM concentration, were freshly prepared every day by dissolving in 5% (v/v) of concentrated H_2SO_4. Stock solutions of 100 and 500 μM selenium species were daily prepared in Milli-Q water. Working solutions of metals alone, selenium species alone, and metal–selenium species at different stoichiometries (1:1, 1:2, 1:3, and 1:4) were prepared by dilution of stock solutions in phosphate buffer as required.

UV–Vis spectra of working solutions were recorded at room temperature from 190 to 600 nm. Interactions were detected as the changes in the absorption spectra at a time of 30 min, once the metal solution and the selenium solution were mixed. UV–Vis spectra were thoroughly examined in order to evaluate absorption differences and to estimate the most probable metal/ligand ratio in the hypothetical formed complexes. Derivative spectroscopy, d^1(UV–Vis), was also applied to enhance differences among spectra, to resolve overlapping bands and to reduce the effects of other absorbing compounds.

Amyloid β protein incubation assays

Incubation of $A\beta_{1–42}$ monomer was performed after the commercial $A\beta_{1–42}$ stock was pretreated with pure HFIP. HFIP was used as a beta-sheet disrupting solvent to enhance the amyloidogenicity of the purchased $A\beta_{1–42}$, generating more homogeneous and monomeric $A\beta_{1–42}$ [41]. For this purpose, an amount of 1 mg of frozen commercial $A\beta_{1–42}$ was allowed to equilibrate at room temperature during 30 min, in order to prevent condensation of the peptide. A volume of 222 μL of HFIP was added to the peptide to obtain a 1-mM solution. Then, the peptide solution was vortexed, and aliquots of 10 μL were taken. All the aliquots were introduced in a SpeedVac at 45 °C during 30 min to remove any residual amount of HFIP. Finally, pretreated solid $A\beta_{1–42}$ monomer was stored in Eppendorf vials and frozen at − 20 °C until use.

For the protein incubation experiments, pretreated $A\beta_{1–42}$ monomer was allowed to equilibrate at room temperature for 30 min. The appropriate volume of DMSO was added to the protein in order to obtain a 5-mM solution, which was sonicated during 10 min. Then, 10 mM HCl was added, and the resulting solution was sonicated again for 10 min, to obtain a final $A\beta_{1–42}$ working solution of 200 μM with 4% (v/v) of DMSO.

For the aggregation experiments, stock metal solutions of 200 μM (Fe(II), Cu(II), and Zn(II)) and selenium species (SeMet, $(SeCys)_2$, SeMetSeCys, Ch-SeNPs, and CGA@ChSeNPs) were prepared every day. Working solutions of $A\beta_{1–42}$ alone (50 μM), $A\beta_{1–42}$ + metal (50 μM + 50 μM), $A\beta_{1–42}$ + selenium species (50 μM + 50 μM), and $A\beta_{1–42}$ + metal + selenium species (50 μM + 50 μM + 50 μM) were prepared by diluting stock solutions in 10 mM HCl.

For the inhibition experiments of metal-induced Aβ aggregation, all working solutions were incubated at 37 °C during 48 h, and they were analyzed by TEM. Regarding amyloid fibril disaggregation experiments, only working solutions of $A\beta_{1–42}$ (100 μM) alone and $A\beta_{1–42}$ + Fe(II) (100 μM + 100 μM) were incubated at 37 °C during 24 h. A volume of 15 μL of these resulting solutions was mixed with 15 μL of 10 mM HCl and analyzed by TEM. Over the remaining 15 μL solutions, 7.5 μL of 200 μM Ch-SeNPs and 7.5 μL of 10 mM HCl were added to a final Ch-SeNP concentration of 50 μM. These solutions were incubated at 37 °C during 24 h more, and then, they were analyzed by TEM.

To perform the TEM analysis, 10 μL of each working solution was placed on a carbon-coated copper grid for 5 min. Each grid was stained with 10 μL uranyl acetate 2% (w/v) for 5 min, yielding $A\beta_{1–42}$ fibrils in negative staining. After draining off the excess staining solution, the prepared grids were transferred and analyzed by a JEOL JEM 1400 Plus transmission electron microscope at 100 kV. TEM Images were taken at × 12,000, × 6000 and × 1000 magnification. Comparison between the obtained images from the protein alone, in the presence of metal, in the presence of target selenium species, and in the presence of both, was performed, in order to observe the differences in the aggregation effect, as well as in the width and length of fibrils. Fibrils were measured using ImageJ program ($n = 200$).

DPPH free radical scavenging assay

Antioxidant capacity of SeMet, $(SeCys)_2$, SeMetSeCys, Se(IV), Se(VI), Ch-SeNPs, CGA@ChSeNPs, and CGA compounds was evaluated using the $DPPH^{\bullet}$ radical [42, 43]. Prior to spectrophotometric determination, a stock solution of DPPH 9.97 mM methanolic solution was prepared daily.

The 0.10-mM DPPH working solution was prepared in methanol by appropriate dilution. For establishing the stationary time (T_{EC50}), 2.5 mL of the 0.10-mM DPPH solution was mixed with 500 μL of a combination of the target compound and distilled water, whose proportion depended on the target compound. This compound:water proportion should allow a decrease of nearly 50% in the DPPH absorption band. T_{EC50} values were estimated by recording the absorbance at 515 nm in the time interval from 0 to 230 min. For calculation of the EC_{50} concentration, defined as the compound amount needed to reduce 50% of the initial $DPPH^{\bullet}$ concentration, 2.5 mL of the 0.10-mM DPPH solution was mixed with 500 μL of an aqueous solution prepared by the combination of increasing concentrations of the target compound and distilled water, to represent a calibration curve with 5 points (3 replicates each). Absorption at 515 nm was registered for each target compound at the corresponding stationary time (T_{EC50}), in order to calculate the DPPH remaining percentage ($\%DPPH^{\bullet}_{rem}$) according to the following equation:

$$\%DPPH^{\bullet}_{rem} = \frac{A_f}{A_0} \times 100 \quad (1)$$

where A_f and A_0 are the absorbance values of $DPPH^{\bullet}$ at steady state and at 0 time, respectively.

The antioxidant efficiency (AE) was also estimated as a more reliable parameter to illustrate the antioxidant properties of the target compounds (Eq. 2) [42].

$$AE = \frac{1}{EC_{50} T_{EC50}} \quad (2)$$

Statistical analysis

The width of $A\beta_{1-42}$ fibrils was measured by an ImageJ digital image processing program. The obtained width from the different assays was compared by a Fisher LSD test (95%, n = 200). The software package Statgraphics Centurion 18 (Statgraphics Technologies, Inc., Warrenton, VA, USA) was employed for the statistical data evaluation.

Results and discussion

Characterization of selenium nanoparticles

For the characterization of synthetized SeNPs, different techniques were employed such as transmission electron microscopy (TEM), EDXS, electron diffraction (ED), and DLS. These techniques allowed obtaining information regarding the elemental composition, size, shape, surface, and crystal structure of nanoparticles.

TEM micrographs in both studied media and for both types of synthetized selenium nanoparticles, Ch-SeNPs and CGA@ChSeNPs, are included in Fig. 1. TEM images evidence the presence of nanoparticles of spherical morphology. Selenium nanoparticle diameter size distribution in the synthesis medium (Fig. 1a and d) was measured through the images derived from TEM, using the ImageJ digital image processing program (n = 200, ± SD). Estimated diameters for Ch-SeNPs and CGA@ChSeNPs were (60 ± 6) nm and (80 ± 20) nm, respectively. In addition, it was demonstrated that the 10-mM HCl media, used in the amyloid β protein incubation, did not modify the original morphology of SeNPs (Fig. 1b and e). However, the particle size distribution of CGA@ChSeNPs (Fig. 1d and e) was more heterogeneous than Ch-SeNPs (Fig. 1a and b), even presenting slightly higher diameters. Additionally, electron diffraction patterns demonstrated a crystal structure, with the same interplanar distance (3.3 Å) in the first ring, for both Ch-SeNPs (Fig. 1c) and CGA@ChSeNPs (Fig. 1f). EDXS analysis confirmed the presence of Se ((Kα (1.0 keV), Lα (8.7 keV), and Lβ (9.6 keV)) in these nanoparticles in both media synthesis and 10 mM HCl solution, the latter employed to obtain the $A\beta_{1-42}$ fibrils.

In relation to the characterization of nanoparticles in solution, light scattering (DLS) analysis was also performed to determine hydrodymamic size of the synthesized SeNPs, as well as their zeta potential. As example, a diameter distribution graph for CGA@ChSeNPs dispersion as obtained for DLS is shown in Fig. 2a. The average hydrodynamic size of nanoparticles for CGA@ChSeNPs was (196 ± 1) nm and for Ch-Se NPs (91 ± 1 nm) with a polydispersity index (PDI) lower than 0.2. The low value of PDI (PDI must be smaller than 0.6–0.7 to have a reliable measurement, at least for Zetasizer) indicates that nanoparticles are mostly not aggregated suggesting a monodisperse sample with a very narrow width distribution. As it was expected, the hydrodynamic size was greater than the size estimated by TEM. The hydrodynamic diameter gives information of the inorganic core along with any coating material and the solvent layer attached to the particle as it moves under the influence of Brownian motion, while TEM only provides information about the inorganic core as this hydration layer is not present.

Zeta potential measurements provide values (n = 3, ± SD) of (− 38 ± 1) mV and (45 ± 1) mV for Ch-SeNPs and CGA@ChSeNPs, respectively. According to Kumar et al., in general, nanoparticles with zeta potential values larger ± 30 mV can be considered stable in dispersion [44]. Thus, the measured ZP values suggest the stability of both selenium particles in solution, as well as their low tendency to agglomerate due to interparticle interactions. Specifically, the zeta potential for Ch-SeNPs indicates moderate stability, while that observed for CGA@ChSeNPs reveals good stability [44]. Zeta potential value provides also an indirect

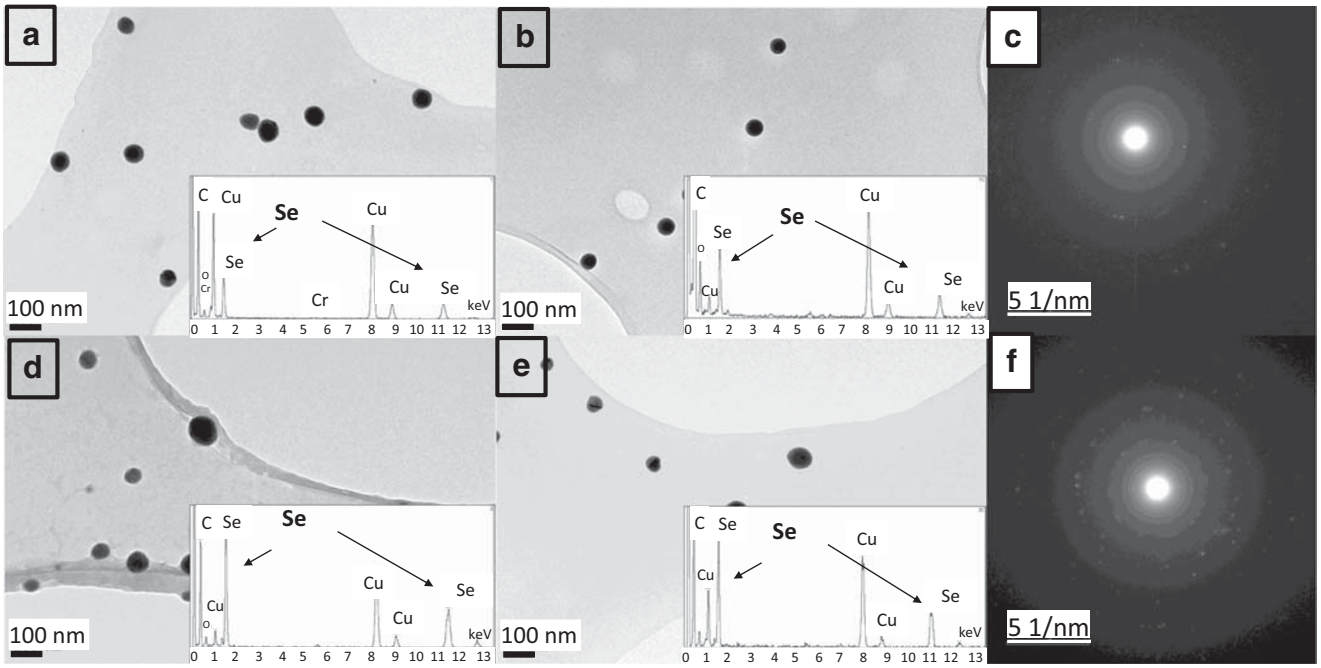


Fig. 1 TEM images and EDXS spectra of Ch-SeNPs (**a**, **b**) and CGA@ChSeNPs (**d**, **e**) in the synthesis medium (**a**, **d**) and in 10 mM HCl solution (**b**, **e**). Electron diffraction patterns of Ch-SeNPs (**c**) and CGA@ChSeNPs (**f**) were obtained by TEM

measurement of the net charge of the nanoparticle surface. This parameter greatly influences the interaction of nanoparticles with proteins and biological systems. Results from the current work evidence different charge

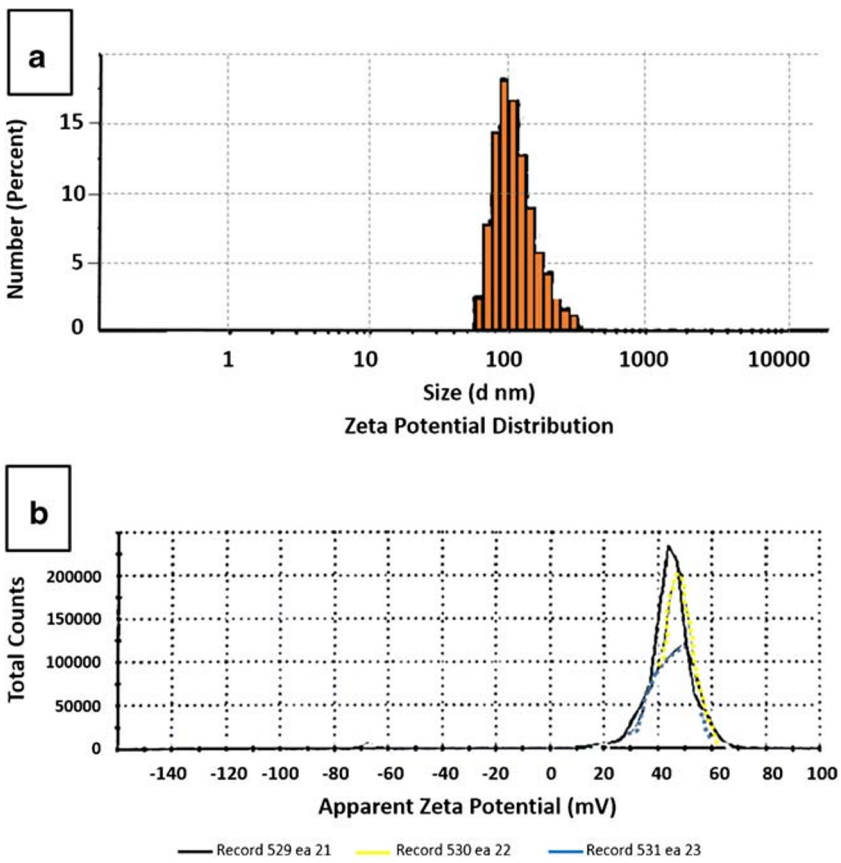


Fig. 2 DLS (**a**) and Z potential (**b**) graphs registered for CGA@ChSeNPs

of the SeNP surface with Ch-SeNPs being anionic and CGA@ChSeNPs cationic. Figure 2b includes Z potential (Fig. 2b) graph from CGA@ChSeNP measurements.

With the aim of determining whether chlorogenic molecules were bound to nanoparticles, the presence of chlorogenic acid in the dialysis solution was evaluated by direct injection of the CGA@ChSeNP dialysis solution into a cLC-DAD system. Chlorogenic acid was not detected in the dialysis solution at the method detection limit, which was estimated at 0.033 μM. This fact could suggest that chlorogenic molecules are bonded to the chitosan-CGA@ChSeNP surface, also explaining the positive value of the determined zeta potential value. Therefore, the synthesis procedure including CGA could yield added value to Ch-SeNPs, with probable antioxidant properties due to the presence of this polyphenol in the nanomaterial surface.

Ch-SeNP and CGA@ChSeNP dispersions were also characterized by TEM in different scenarios to detect potential changes in nanoparticle properties when they are exposed to different experimental conditions (interaction studies with $A\beta_{1-42}$ fibrils in the presence and absence of metals, before and after dialysis experiments, in the presence of 10 mM HCl). In all cases, both nanoparticles remained stable morphologically, without evidences of aggregation.

Evaluation of the interaction between transition metals and target selenium species

A matter of fact was to study the interaction between metals involved in AD and selenium species. The possible formation of metallic complexes and the metal-chelating properties of selenium species could reduce the negative effects of these metals. UV–Vis and d^1(UV–Vis) absorption spectra were registered for Cu(II), Fe(II), and Zn(II) solutions containing the selenium species under study: SeMet, $(SeCys)_2$, SeMetSeCys, Se(IV), Se(VI), Ch-SeNPs, and CGA@ChSeNPs. Metal–selenium interactions were deduced when new optical bands appeared or different band intensities were recorded for the metal/selenium solution, in comparison with the spectra corresponding to the metal or selenium species alone. These differences between the spectra of the selenium species alone and in the presence of bivalent metals could suggest a possible interaction and, consequently, the formation of metal complexes with metal/selenium molar ratios between 1:1 and 1:4. The first derivative of spectra was applied to explore the ability of selenium species to interact with metals.

Regarding Cu(II) studies, UV–Vis spectra proved that Cu(II) interacted with SeMet, $(SeCys)_2$, SeMetSeCys, Se(VI), Ch-SeNPs, and CGA@ChSeNPs. As example, the interaction spectra registered for different Cu(II) concentrations (12.5–50 μM) with constant Ch-SeNP concentration (50 μM) are shown in Fig. 3a. As it can be seen, the Ch-SeNP spectrum presented a maximum absorption band at 265 nm, which disappeared in the presence of any Cu(II) concentration. In fact, in the first derivative UV–Vis spectra (Fig. 3c), the only spectrum that passes through the *x*-axis (x = 265 nm) is the spectra corresponding to Ch-SeNPs alone, suggesting the simultaneous formation of metal complexes of different stoichiometries or the potential oxidation of Se(0) in Ch-SeNPs due to Cu(II) reduction to Cu(I). Concerning CGA@ChSeNPs, the UV–Vis spectrum of this compound showed absorption bands at 265 and 330 nm; however, in the presence of Cu(II), an additional band appeared at 380 nm (data not shown). The additional band at 380 nm could be due to reduction of Cu(II) in the presence of the reactive aromatic –OH groups of CGA which are oxidized to the corresponding quinone [45].

Changes in absorption bands were also appreciated for SeMet, $(SeCys)_2$, SeMetSeCys, and Se(VI) in the presence of Cu(II), also indicating the possible formation of metallic complexes of different stoichiometries or, as it was previously mentioned, to an oxidation–reduction process between selenium species and Cu(II). However, no interaction between Cu(II) and Se(IV) was observed by UV–Vis and d^1(UV–Vis) spectroscopy measurements.

Fe(II) was able to interact with SeMet, $(SeCys)_2$, SeMetSeCys, Se(IV), and Se(VI) species. Unlike with Cu(II), changes in absorption bands of both Ch-SeNPs and CGA@ChSeNPs in the presence of Fe(II) were not appreciated in any of the recorded spectra (Fig. 3b, d). As it can be observed in the interaction spectra (Fig. 3b), registered for a fixed Ch-SeNP concentration (50 μM), selenium nanoparticles presented an absorption band at a wavelength of 265 nm, which did not disappear in the presence of different Fe(II) concentrations (12.5–50 μM); neither new absorption bands appeared. In the first derivative spectra (Fig. 3d), it is clearer that spectra differences between Ch-SeNPs alone and Ch-SeNPs in the presence of Fe(II) were not observed. Similar metal interaction behavior was observed for CGA@ChSeNPs.

With respect to Zn(II) experiments, this metal only interacts with SeMet, showing the UV–Vis registered spectra a slight change in the range between 210 and 230 nm (data not shown). The rest of the selenium species ($(SeCys)_2$, SeMetSeCys, Se(IV), Se(VI), Ch-SeNPs, and CGA@ChSeNPs) did not present any absorption changes in the presence of different Zn(II) concentrations, revealing the lack of metal/selenium species interaction.

Therefore, SeMet was the most chelating among the selenium species tested, showing a clear interaction with all evaluated transition metals and being the only one that produced absorption changes in the Zn(II) UV–Vis spectra. Secondarily, SeMet, $(SeCys)_2$, SeMetSeCys, and Se(VI) presented interaction with both Fe(II) and Cu(II). The interactions with Cu(II) could be due to both complex formation and redox reaction. Finally, Se(IV) was only capable of interacting with Fe(II),

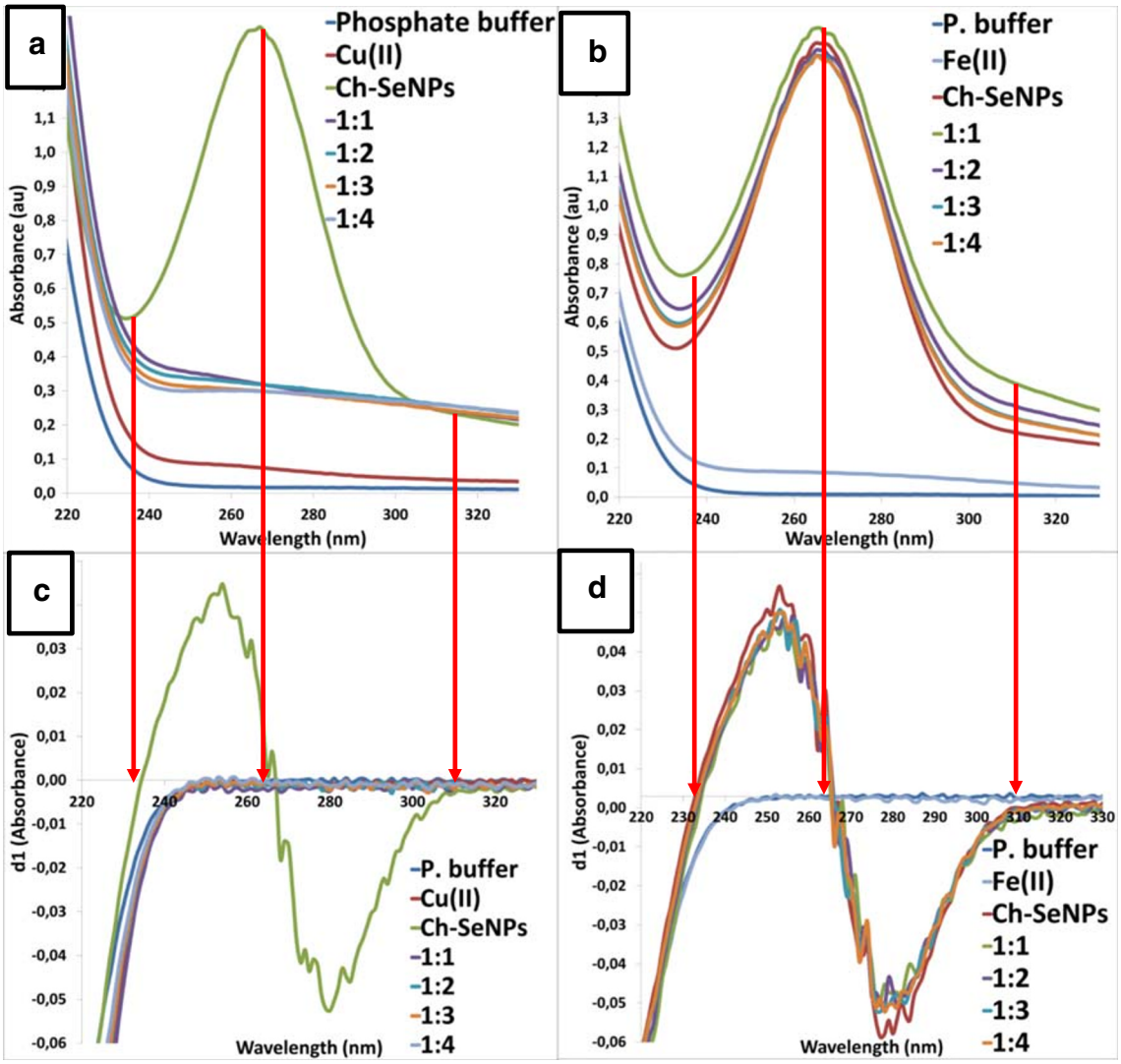


Fig. 3 Recorded UV–Vis (**a**, **b**) and d^1(UV–Vis) spectra (**c**, **d**) for Ch-SeNPs (50 μM) alone and in the presence of 50–12.5 μM Cu(II) (**a**, **c**) or 50–12.5 μM Fe(II) (**b**, **d**), registered at different metal/selenium species ratios

and both Ch-SeNPs and CGA@ChSeNPs only with Cu(II). This selenium species selectivity could be an important feature to be considered in studies in Fe(II) and/or Cu(II) involved in AD cases.

The high affinity of SeMet for all metals tested could be of relevance since this selenium species is usually present in foodstuffs and selenized supplements. Consequently, and taking into account the experimental data obtained, it could be derived that all selenium species could play an important role interacting with the metals involved in AD. These metal interactions could be general, such as SeMet, or specific, such as Ch-SeNPs and CGA@ChSeNPs with Cu(II), and Se(IV) with Fe(II). Although UV–Vis and d^1(UV–Vis) spectroscopy measurements allowed us to evaluate the interaction between selenium species and transition metals, however the use of most selective techniques such as ICPMS online coupled to field flow fractionation would be a valuable tool to corroborate the results obtained by spectroscopy measurements.

Evaluation of amyloid β protein aggregation

Previous in vitro results revealed that amyloid β aggregation is highly dependent on experimental conditions. Therefore, for $A\beta_{1–42}$ incubation assays, a previous optimization of experimental variables was required. Optimum $A\beta_{1–42}$ fibrils were generated when incubation was performed at 37 °C in 10 mM HCl medium during 48 h. Under these conditions, longer and more abundant Aβ fibrils were observed, in comparison with those obtained after incubation of amyloid β peptide in 10 mM HCl during 24 h, or in phosphate buffer 20 mM pH 7.3 for 24 h. These results are in consonance with those reported in other studies, which assessed that $A\beta_{1–42}$

assembly was dependent on ionic strength and pH, being higher in acidic pH and low ionic strength [46].

Incubation of $A\beta_{1-42}$ fragments was performed according to the procedure described in the "Amyloid β protein incubation assays" section. As it was expected, the generated amyloid fibrils (Fig. 4a, a TEM image of $A\beta_{1-42}$ fibrils alone) suffered an increase in aggregation in the presence of 50 μM Fe(II), Cu(II), and Zn(II), after 48 h of incubation in 10 mM HCl media. As example of the fibril aggregation induced by exposition to transition metals, Fig. 4b includes one of the TEM images registered for $A\beta_{1-42}$ in the presence of Fe(II). Both Cu(II) and Zn(II) induced amyloid β protein aggregation similar to Fe(II). This experimental observation corroborates the metal ion hypothesis, in which some transition metals could favor the aggregation of $A\beta_{1-42}$ fibrils.

In the presence of SeMet, $(SeCys)_2$, SeMetSeCys, Se(IV), Se(VI), and CGA@ChSeNPs, $A\beta_{1-42}$ aggregation increased when compared to the protein fibrils alone (Fig. 4a). As example, the observed $A\beta_{1-42}$ aggregation by TEM in the presence of SeMet 50 μM is shown in Fig. 4c, and in the presence of CGA@ChSeNPs 50 μM in Fig. 4f. However, only Ch-SeNPs (Fig. 4d) demonstrated an anti-aggregation effect, reducing both number and fibril length. To elucidate if CGA alone was also responsible of induced CGA@ChSeNP amyloid aggregation, CGA standard polyphenol was incubated alone with $A\beta_{1-42}$. As it could be observed by TEM images, CGA indeed showed an increase in amyloid β aggregation. Therefore, in the absence of any metal, Ch-SeNPs were the only selenium species that presented a positive effect in avoiding Aβ aggregation.

In order to evaluate the inhibition of the Aβ aggregation, selenium species and selenium nanoparticles were separately incubated with $A\beta_{1-42}$ protein in the presence of Fe(II), Cu(II), or Zn(II) individually, since all the studied metals produced an increase in amyloid β aggregation. Among those studied, Ch-SeNPs were the only selenium species able to inhibit the Fe(II) and Zn(II) metal-induced Aβ aggregation, reducing both the number and fibril length. As example, Fig. 4e shows the inhibition effect of Ch-SeNPs in the presence of Fe(II) (Fig. 4e). In contrast, both Ch-SeNPs and CGA@ChSeNPs could not inhibit the Cu(II)-induced Aβ aggregation. As demonstrated in the "Evaluation of the

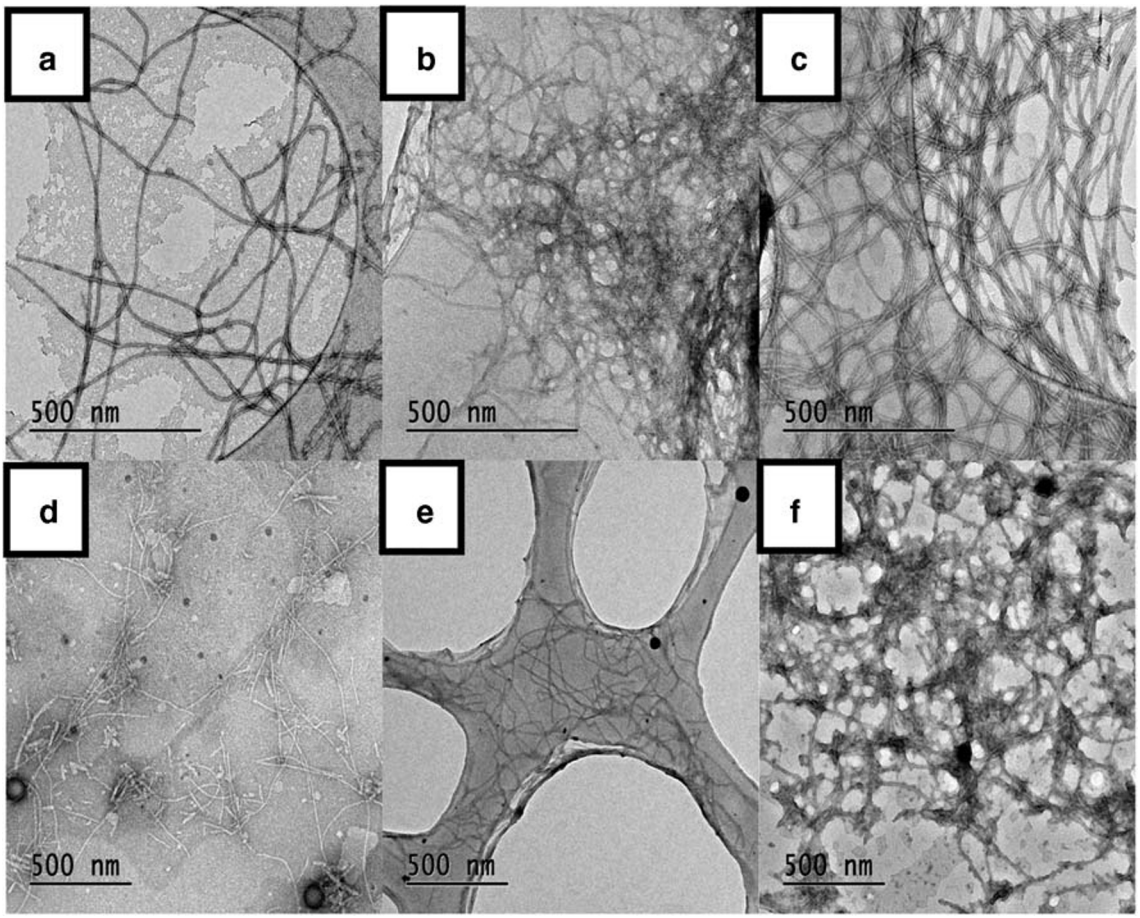


Fig. 4 TEM images of the inhibition assays of metal-induced $A\beta_{1-42}$ aggregation, after incubation at 37 °C, during 48 h in 10 mM HCl medium ($[A\beta_{1-42}] = 50$ μM, $[Fe(II)] = 50$ μM, $[Zn(II)] = 50$ μM, $[SeMet] = 50$ μM, $[Ch\text{-}SeNPs] = 50$ μM, $[CGA@ChSeNPs] = 50$ μM). **a** $A\beta_{1-42}$ alone. **b** $A\beta_{1-42}$ + Fe(II). **c** $A\beta_{1-42}$ + SeMet. **d** $A\beta_{1-42}$ + Ch-SeNPs. **e** $A\beta_{1-42}$ + Zn(II) + Ch-SeNPs. **f** $A\beta_{1-42}$ + CGA@ChSeNPs

interaction between transition metals and target selenium species" section, both were able to interact with Cu(II). But actually, Cu(II) could be probably reduced to Cu(I), oxidizing Se(0) of Ch-SeNPs. This hypothetical redox reaction could explain the loss of effectiveness of Ch-SeNPs and CGA@ChSeNPs in the presence of Cu(II) regarding inhibition of amyloid β aggregation. Interestingly, Fig. 4 d and e also evidence the presence of spherical and well-dispersed Ch-SeNPs in their interaction with $A\beta_{1-42}$ protein in the presence and absence of metals.

On the other hand, reversion of the amyloid β aggregation caused by Fe(II) was only studied with Ch-SeNPs as the most successful selenium species in aggregation inhibition experiments. Firstly, Aβ fibrils were incubated during 24 h (Fig. 5a). After an additional incubation period of 24 h in the presence of Ch-SeNPs 50 μM, an increase in Aβ aggregation was not observed (Fig. 5b). When this aggregation was induced by 50 μM Fe(II) in 24 h incubation experiments (Fig. 5c), Ch-SeNPs were able to reduce considerably amyloid aggregation and to shorten fibril length in an additional incubation period of 24 h (Fig. 5d). Amyloid β fibrils were successfully disaggregated and the scarce fibrils observed were shorter due to the effect of selenium nanoparticles.

In addition to the aggregation inhibition observed through the TEM micrographs after an incubation period of 48 h (Fig. 4), the width of Aβ fibrils was also measured using ImageJ processing program ($n = 200$), and data were statistically treated using Statgraphics Centurion 18 software. Results of the Fisher LSD test, applied for a significance level of 95%, are included in Fig. 6. While fibers of $A\beta_{1-42}$ alone had (6.3 ± 0.2) nm of width, in the presence of Fe(II), fibril width increased to (9.0 ± 0.2) nm. Similar results were obtained in the presence of SeMet, showing Aβ fibrils a width of (8.9 ± 0.2) nm. Therefore, SeMet, $(SeCys)_2$, SeMetSeCys, Se(IV), Se(VI), CGA@ChSeNPs, and CGA increased fibril width around 40% when compared to $A\beta_{1-42}$ alone, being statistically similar to the increase produced by metals. However, Ch-SeNPs shortened the measured widths both in the absence of any metal and in the presence of Zn(II), providing widths of (7.2 ± 0.2) nm and (7.1 ± 0.2), respectively, which were values similar to those measured for $A\beta_{1-42}$ fibrils alone. When comparing fibril width between amyloid β protein in the presence of metal and in the presence of both metal and Ch-SeNPs, synthetized nanoparticles reduced fibril width in a percentage of 20%.

Evaluation of antioxidant capacity

Antioxidant capacity was evaluated thorough the DPPH• free radical scavenging assay according to the procedure described in the "DPPH free radical scavenging assay" section. Estimated antioxidant parameters are shown in Table 1. The lowest EC_{50} and T_{EC50} values indicated, according to Eq. (2), that

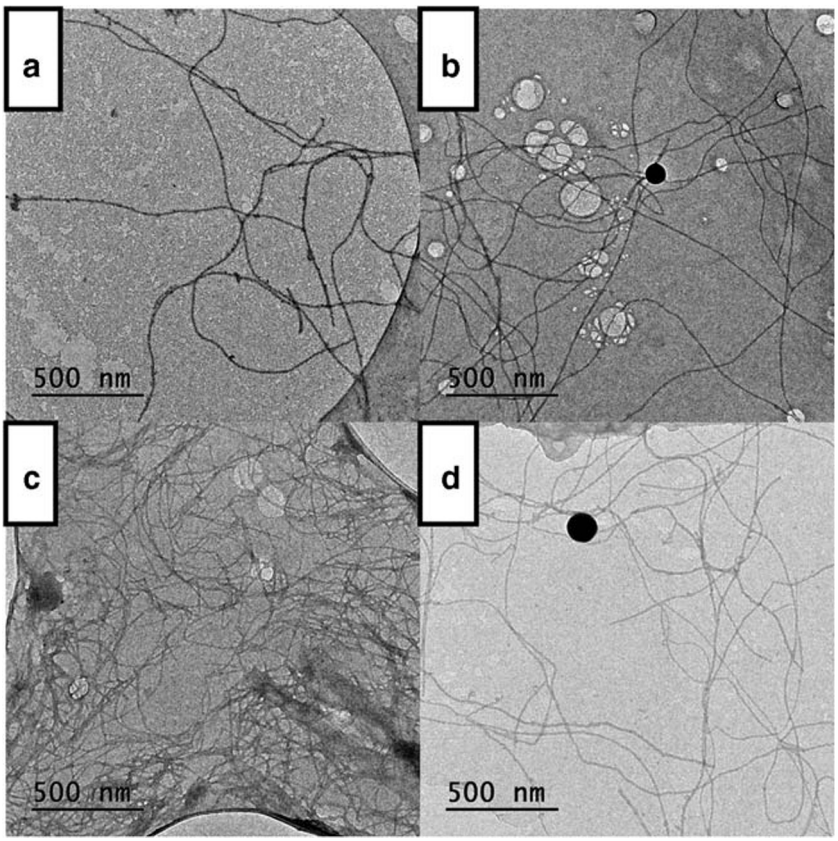


Fig. 5 TEM images of the disaggregation assays performed in 10 mM HCl medium ($[A\beta_{1-42}] = 50$ μM, [Fe(II)] = 50 μM, [Ch-SeNPs] = 50 μM). **a** $A\beta_{1-42}$, 24 h, 37 °C. **b** $A\beta_{1-42}$ incubated at 37 °C during 48 h + Ch-SeNPs added the last 24 h. **c** $A\beta_{1-42}$ + Fe(II) 24 h, 37 °C. **d** $A\beta_{1-42}$ + Fe(II) incubated at 37 °C during 48 h + Ch-SeNPs added the last 24 h

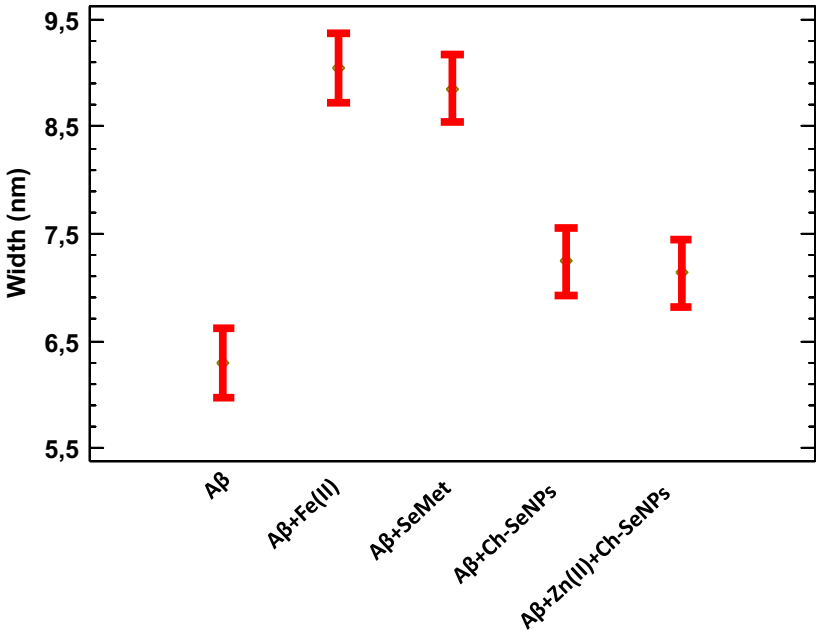


Fig. 6 Results of Fisher's LSD test (95% confidence level) applied to Aβ fibrils width (n = 200). Width measurements were performed by using ImageJ processing program

CGA@ChSeNPs presented the highest antioxidant efficiency (AE). This demonstrated that the presence of CGA improved the antioxidant properties of CGA@ChSeNPs when compared to Ch-SeNPs. The $(SeCys)_2$ was the only selenium species that did not present any antioxidant capacity. Nevertheless, the rest of the selenium species exhibited a remarkable antioxidant capacity. Therefore, the antioxidant properties of most of the selenium species could be very useful in order to mitigate the oxidative stress produced by Fe(II) and Cu(II) biometals. On the basis of the estimated antioxidant capacities, organic selenium species and synthetized selenium nanoparticles could be promising candidates to prevent and/or reverse the oxidative imbalance caused by transition metals in AD.

Conclusions

The studies performed in this work allowed us to conclude that selenium nanoparticles (Ch-SeNPs) stabilized with chitosan present interesting features regarding $A\beta_{1-42}$ fibril aggregation. Due to its antioxidant capacity, metal-chelating properties, inhibition of metal-induced $A\beta_{1-42}$ aggregation, and disaggregation of $A\beta_{1-42}$ fibrils, Ch-SeNPs could be a promising agent for further studies in the AD field.

Synthetized Ch-SeNPs showed excellent antioxidant properties, an essential aspect due to the oxidative stress caused by Fe(II) and Cu(II) biometals in AD. Moreover, they could inhibit Aβ aggregation induced by both Fe(II) and Zn(II) and disaggregate the Fe(II)-induced $A\beta_{1-42}$ aggregation fibrils, decreasing the deposition of β amyloid plaques and/or neurofibrillary tangle plaques. In addition to that, the rest of the selenium species under study showed great metal interaction abilities and excellent antioxidant properties, especially CGA@ChSeNPs, potentially functioning as a strong scavenger of reactive oxygen species, a critical aspect in AD. However, cell cultures and in vivo experiments should be required in order to confirm the potential effects of nanoparticles and selenium species in a more complex system.

Table 1 Antioxidant capacity of target compounds (expressed as mean value ± $t_{0.05}$ s, n = 3)

Compound	T_{EC50} (min)	EC_{50} (mM)	AE (mM^{-1} min^{-1})
CGA@ChSeNPs	10	0.07 ± 0.05	1.43
Ch-SeNPs	10	0.9 ± 0.1	0.111
SeMetSeCys	35	1.8 ± 0.9	0.016
SeMet	35	6.0 ± 0.8	0.005
Se(VI)	35	5.9 ± 0.2	0.005
Se(IV)	35	8.2 ± 0.4	0.004

T_{EC50}, time needed to reach stationary state at EC_{50}; EC_{50}, necessary compound concentration to reduce the DPPH amount to 50%; AE, antioxidant efficiency ($AE = \frac{1}{EC_{50} T_{EC50}}$)

Funding information This work was supported by the Community of Madrid (PB2018/BAA-4393, AVANSECAL II-CM), the Spanish Ministry of Economy and Competitiveness (CTQ2017-83569-C2-1-R), and the Complutense University of Madrid (Proyecto Investigación Santander PR26/16-16B-3). David Vicente-Zurdo acknowledges the Spanish Ministry of Science, Innovation and Universities for funding through a pre-doctoral grant (FPU18/00573).

Compliance with ethical standards

Conflict of interest The authors declare that they have no conflict of interest.

References

1. WHO. Dementia fact sheet. 2017; https://www.who.int/news-room/fact-sheets/detail/dementia. Accessed 26 Sep 2019.
2. Hardy J, Selkoe DJ. The amyloid hypothesis of Alzheimer's disease: progress and problems on the road to therapeutics. Science (80-). 2002;297:353–6. https://doi.org/10.1126/science.1072994.
3. Kepp KP. Alzheimer's disease: how metal ions define β-amyloid function. Coord Chem Rev. 2017;351:127–59. https://doi.org/10.1016/j.ccr.2017.05.007.
4. Prousek J. Fenton chemistry in biology and medicine. Pure Appl Chem. 2007;79:2325–38. https://doi.org/10.1351/pac200779122325.
5. Aruoma OI, Halliwell B, Gajewski E, Dizdaroglu M. Copper-ion-dependent damage to the bases in DNA in the presence of hydrogen peroxide. Biochem J. 1991;273:601–4. https://doi.org/10.1042/bj2730601.
6. Cherny RA, Atwood CS, Xilinas ME, Gray DN, Jones WD, McLean CA, et al. Treatment with a copper-zinc chelator markedly and rapidly inhibits β-amyloid accumulation in Alzheimer's disease transgenic mice. Neuron. 2001;30:665–76. https://doi.org/10.1016/S0896-6273(01)00317-8.
7. Duntas LH, Benvenga S. Selenium: an element for life. Endocrine. 2015;48:756–75. https://doi.org/10.1007/s12020-014-0477-6.
8. Valko M, Rhodes CJ, Moncol J, Izakovic M, Mazur M. Free radicals, metals and antioxidants in oxidative stress-induced cancer. Chem Biol Interact. 2006;160:1–40. https://doi.org/10.1016/j.cbi.2005.12.009.
9. Hatfield DL, Tsuji PA, Carlson BA, Gladyshev VN. Selenium and selenocysteine: roles in cancer, health, and development. Trends Biochem Sci. 2014;39:112–20. https://doi.org/10.1016/j.tibs.2013.12.007.
10. Trevisan R, Ferraz Mello D, Fisher AS, Schuwerack PM, Dafre AL, Moody AJ. Selenium in water enhances antioxidant defenses and protects against copper-induced DNA damage in the blue mussel Mytilus edulis. Aquat Toxicol. 2011;101:64–71. https://doi.org/10.1016/j.aquatox.2010.09.003.
11. Szlachta M, Chubar N. The application of Fe-Mn hydrous oxides based adsorbent for removing selenium species from water. Chem Eng J. 2013;217:159–68. https://doi.org/10.1016/j.cej.2012.11.100.
12. Murphy JM, Gaertner AAE, Williams T, McMillen CD, Powell BA, Brumaghim JL. Stability constant determination of sulfur and selenium amino acids with Cu(II) and Fe(II). J Inorg Biochem. 2019;195:20–30. https://doi.org/10.1016/j.jinorgbio.2019.03.001.
13. Maeda E, Murata K, Kumazawa Y, Sato W, Shirasawa H, Iwasawa T, et al. Associations of environmental exposures to methylmercury and selenium with female infertility: a case–control study. Environ Res. 2019;168:357–63. https://doi.org/10.1016/j.envres.2018.10.007.
14. Cardoso R, Roberts BR, Bush AI, Hare DJ. Selenium, selenoproteins and neurodegenerative diseases. Metallomics. 2015:1213–28. https://doi.org/10.1039/c5mt00075k.
15. Solovyev ND. Importance of selenium and selenoprotein for brain function: from antioxidant protection to neuronal signalling. J Inorg Biochem. 2015;153:1–12. https://doi.org/10.1016/j.jinorgbio.2015.09.003.
16. Pillai R, Uyehara-Lock JH, Bellinger FP. Selenium and selenoprotein function in brain disorders. IUBMB Life. 2014;66:229–39. https://doi.org/10.1002/iub.1262.
17. Romero I, de Francisco P, Gutiérrez JC, Martín-González A. Selenium cytotoxicity in Tetrahymena thermophila: new clues about its biological effects and cellular resistance mechanisms. Sci Total Environ. 2019;671:850–65. https://doi.org/10.1016/j.scitotenv.2019.03.115.
18. Letavayová L, Vlčková V, Brozmanová J. Selenium: from cancer prevention to DNA damage. Toxicology. 2006;227:1–14. https://doi.org/10.1016/j.tox.2006.07.017.
19. Tinggi U. Essentiality and toxicity of selenium and its status in Australia: a review. Toxicol Lett. 2003;137:103–10. https://doi.org/10.1016/S0378-4274(02)00384-3.
20. Zheng R, Zhang Z-H, Chen C, Chen Y, Jia S-Z, Liu Q, et al. Selenomethionine promoted hippocampal neurogenesis via the PI3K-Akt-GSK3β-Wnt pathway in a mouse model of Alzheimer's disease. Biochem Biophys Res Commun. 2017;485:6–15. https://doi.org/10.1016/j.bbrc.2017.01.069.
21. Whanger PD. Selenium and its relationship to cancer: an update. Br J Nutr. 2004;91:11–28. https://doi.org/10.1079/bjn20031015.
22. Skalickova S, Milosavljevic V, Cihalova K, Horky P, Richtera L, Adam V. Selenium nanoparticles as a nutritional supplement. Nutrition. 2017;33:83–90. https://doi.org/10.1016/j.nut.2016.05.001.
23. Wadhwani SA, Shedbalkar UU, Singh R, Chopade BA. Biogenic selenium nanoparticles: current status and future prospects. Appl Microbiol Biotechnol. 2016;100:2555–66. https://doi.org/10.1007/s00253-016-7300-7.
24. Sims CM, Hanna SK, Heller DA, Horoszko CP, Johnson ME, Montoro Bustos AR, et al. Redox-active nanomaterials for nanomedicine applications. Nanoscale. 2017;9:15226–51. https://doi.org/10.1039/c7nr05429g.
25. Mohammed MA, Syeda JTM, Wasan KM, Wasan EK. An overview of chitosan nanoparticles and its application in non-parenteral drug delivery. Pharmaceutics. 2017;9. https://doi.org/10.3390/pharmaceutics9040053.
26. Gupta J, Fatima MT, Islam Z, Khan RH, Uversky VN, Salahuddin P. Nanoparticle formulations in the diagnosis and therapy of Alzheimer's disease. Int J Biol Macromol. 2019;130:515–26. https://doi.org/10.1016/j.ijbiomac.2019.02.156.
27. Yang L, Sun J, Xie W, Liu Y, Liu J. Dual-functional selenium nanoparticles bind to and inhibit amyloid β fibers formation in Alzheimer's disease. J Mater Chem B. 2017;5:5954–67. https://doi.org/10.1039/C6TB02952C.
28. Gao F, Zhao J, Liu P, Ji D, Zhang L, Zhang M, et al. Preparation and in vitro evaluation of multi-target-directed selenium-chondroitin sulfate nanoparticles in protecting against the Alzheimer's disease. Int J Biol Macromol. 2020;142:265–76. https://doi.org/10.1016/j.ijbiomac.2019.09.098.
29. Ghosh S, Banerjee S, Sil PC. The beneficial role of curcumin on inflammation, diabetes and neurodegenerative disease: a recent update. Food Chem Toxicol. 2015;83:111–24. https://doi.org/10.1016/j.fct.2015.05.022.
30. Zhang H, Tsao R. Dietary polyphenols, oxidative stress and antioxidant and anti-inflammatory effects. Curr Opin Food Sci. 2016;8:33–42. https://doi.org/10.1016/j.cofs.2016.02.002.
31. Shahidi F, Ambigaipalan P. Phenolics and polyphenolics in foods, beverages and spices: antioxidant activity and health effects—a review. J Funct Foods. 2015;18:820–97. https://doi.org/10.1016/j.jff.2015.06.018.
32. Badhani B, Sharma N, Kakkar R. Gallic acid: a versatile antioxidant with promising therapeutic and industrial applications. RSC Adv. 2015;5:27540–57. https://doi.org/10.1039/c5ra01911g.
33. Yang L, Wang W, Chen J, Wang N, Zheng G. A comparative study of resveratrol and resveratrol-functional selenium nanoparticles: inhibiting amyloid β aggregation and reactive oxygen species formation properties. J Biomed Mater Res - Part A. 2018;106:3034–41. https://doi.org/10.1002/jbm.a.36493.
34. Dias GP, Cocks G, Cesar M, Nardi AE, Thuret S. Resveratrol: a potential hippocampal plasticity enhancer. Oxidative Med Cell Longev. 2016;2016:9651236. https://doi.org/10.1155/2016/9651236.

35. Poulose SM, Miller MG, Scott T, Shukitt-Hale B. Nutritional factors affecting adult neurogenesis and cognitive function. Adv Nutr. 2017. https://doi.org/10.3945/an.117.016261.
36. Naewla S, Sirichoat A, Pannangrong W, Chaisawang P., Wigmore P, Welbat JU. Hesperidin alleviates methotrexate-induced memory deficits via hippocampal neurogenesis in adult rats. Nutrients. 2019;11:936. doi: https://doi.org/10.3390/nu11040936.
37. Smith C, Frolinger T, Brathwaite J, Sims S, Pasinetti GM. Dietary polyphenols enhance optogenetic recall of fear memory in hippocampal dentate gyrus granule neuron subpopulations. Commun Biol. 2018;1:42. https://doi.org/10.1038/s42003-018-0043-5.
38. Naveed M, Hejazi V, Abbas M, Kamboh AA, Khan GJ, Shumzaid M, et al. Chlorogenic acid (CGA): a pharmacological review and call for further research. Biomed Pharmacother. 2018;97:67–74. https://doi.org/10.1016/j.biopha.2017.10.064.
39. Zhang J, Zhou X, Yu Q, Yang L, Sun D, Zhou Y, et al. Epigallocatechin-3-gallate (EGCG)-stabilized selenium nanoparticles coated with Tet-1 peptide to reduce amyloid-β aggregation and cytotoxicity. ACS Appl Mater Interfaces. 2014;6:8475–87. https://doi.org/10.1021/am501341u.
40. Sun D, Zhang W, Yu Q, Chen X, Xu M, Zhou Y, et al. Chiral penicillamine-modified selenium nanoparticles enantioselectively inhibit metal-induced amyloid β aggregation for treating Alzheimer's disease. J Colloid Interface Sci. 2017;505:1001–10. https://doi.org/10.1016/j.jcis.2017.06.083.
41. Lioudyno MI, Broccio M, Sokolov Y, Rasool S, Wu J, Alkire MT, et al. Effect of synthetic Aβ peptide oligomers and fluorinated solvents on Kv1.3 channel properties and membrane conductance. PLoS One. 2012;7(4):e35090. https://doi.org/10.1371/journal.pone.0035090.
42. Villaño D, Fernández-Pachón MS, Moyá ML, Troncoso AM, García-Parrilla MC. Radical scavenging ability of polyphenolic compounds towards DPPH free radical. Talanta. 2007;71:230–5. https://doi.org/10.1016/j.talanta.2006.03.050.
43. Gómez-Mejía E, Rosales-Conrado N, León-González ME, Madrid Y. Citrus peels waste as a source of value-added compounds: extraction and quantification of bioactive polyphenols. Food Chem. 2019;295:289–99. https://doi.org/10.1016/j.foodchem.2019.05.136.
44. Kumar A, Dixit CK. Methods for characterization of nanoparticles. Adv Nanomedicine Deliv Ther Nucleic Acids. 2017:44–58. https://doi.org/10.1016/B978-0-08-100557-6.00003-1.
45. Apak R, Güçlü K, Özyürek M, Çelik SE. Mechanism of antioxidant capacity assays and the CUPRAC (cupric ion reducing antioxidant capacity) assay. Microchim Acta. 2008;160:413–9. https://doi.org/10.1007/s00604-007-0777-0.
46. Stine WB, Dahlgren KN, Krafft GA, LaDu MJ. In vitro characterization of conditions for amyloid-β peptide oligomerization and fibrillogenesis. J Biol Chem. 2003;278:11612–22. https://doi.org/10.1074/jbc.M210207200.

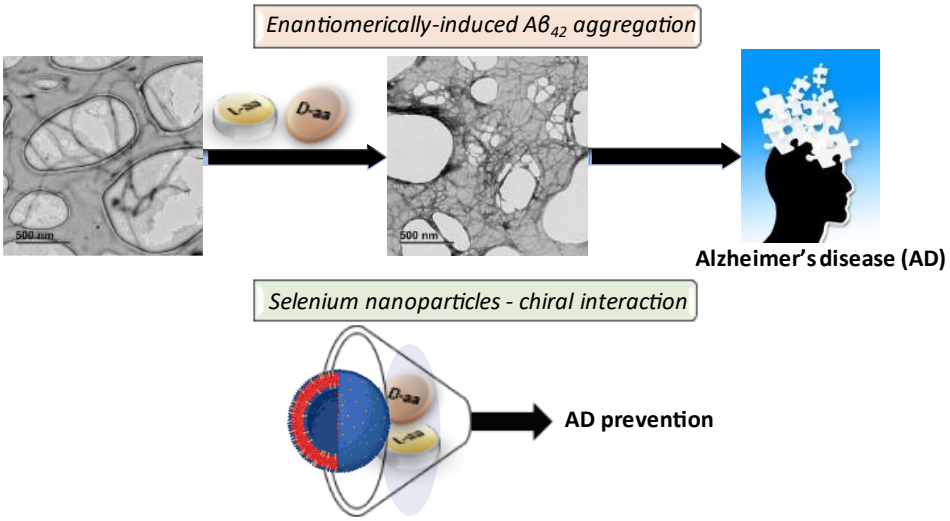
Publisher's note Springer Nature remains neutral with regard to jurisdictional claims in published maps and institutional affiliations.

Artículo 5: <u>Actividad neuroprotectora de las nanopartículas de selenio frente al efecto de enantiómeros de aminoácidos en la enfermedad de Alzheimer</u>

Neuroprotective activity of selenium nanoparticles against the effect of amino acid enantiomers in Alzheimer's disease

David Vicente-Zurdo, Sandra Rodríguez-Blázquez, Esther Gómez-Mejía, Noelia Rosales-Conrado, María Eugenia León-González, Yolanda Madrid

Analytical and Bioanalytical Chemistry 414 (2022) 7573-7584 (*Impact factor: 4.157*)



Parte de los resultados de este trabajo se presentaron en:

"V JORNADA DE PROMOCIÓN DE LA INVESTIGACIÓN BÁSICA PARA ESTUDIANTES DE CIENCIAS E INGENIERÍAS". *Selenium nanoparticles for the treatment of Alzheimer's disease: Interaction with amino acids enantiomers*. Móstoles, España, septiembre de 2021. Tipo de comunicación: oral.

"42th COLLOQUIUM SPECTROSCOPICUM INTERNATIONALE XLII (CSI XLII)". *Neuroprotective activity of selenium nanoparticles against the effect of amino acid enantiomers in Alzheimer's disease.* Gijón, España, mayo de 2022. Tipo de comunicación: póster.

"XXXVIII REUNIÓN BIENAL DE LA REAL SOCIEDAD ESPAÑOLA DE QUÍMICA (XXXVIII RSEQ)". *Cytotoxic and neuroprotective effect of selenium species in Alzheimer's disease.* Granada, España, junio de 2022. Tipo de comunicación: póster pitch. (*Premio al mejor póster en la sesión "Bioanalytical Chemistry in Health and Food Safety" otorgado por Analytical and Bioanalytical Chemistry*).

Analytical and Bioanalytical Chemistry (2022) 414:7573–7584
https://doi.org/10.1007/s00216-022-04285-z

RESEARCH PAPER

Neuroprotective activity of selenium nanoparticles against the effect of amino acid enantiomers in Alzheimer's disease

David Vicente-Zurdo[1] · Sandra Rodríguez-Blázquez[1] · Esther Gómez-Mejía[1] · Noelia Rosales-Conrado[1] · María Eugenia León-González[1] · Yolanda Madrid[1]

Received: 18 July 2022 / Revised: 9 August 2022 / Accepted: 12 August 2022 / Published online: 19 August 2022
© Springer-Verlag GmbH Germany, part of Springer Nature 2022

Abstract

Alzheimer's disease (AD), the most prevalent neurodegenerative disease, is characterized by extracellular accumulation of amyloid-beta protein (Aβ), which is believed to be the very starting event of AD neurodegeneration. In this work, D-Phe, D-Ala, and D-Glu amino acids, which are the non-occurring enantiomeric form in the human body, and also D-Asp and DL-SeMet, have proved to be amyloidogenic regarding $A\beta_{42}$ aggregation in TEM studies. These amyloidogenic amino acid enantiomers also widened $A\beta_{42}$ fibrils up to 437% regarding $A\beta_{42}$ alone, suggesting that $A\beta_{42}$ aggregation is enantiomerically dependent. To inhibit enantiomeric-induced amyloid aggregation, selenium nanoparticles stabilized with chitosan (Ch-SeNPs) were successfully synthesized and employed. Thus, Ch-SeNPs reduced and even completely inhibited $A\beta_{42}$ aggregation produced in the presence of some amino acid enantiomers. In addition, through UV–Vis spectroscopy and fluorescence studies, it was deduced that Ch-SeNPs were able to interact differently with amino acids depending on their enantiomeric form. On the other hand, antioxidant properties of amino acid enantiomers were evaluated by DPPH and TBARS assays, with Tyr enantiomers being the only ones showing antioxidant effect. All spectroscopic data were statistically analysed through experimental design and response surface analysis, showing that the interaction between the Ch-SeNPs and the amino acids studied was enantioselective and allowing, in some cases, to establish the concentration ratios in which this interaction is maximum.

Keywords Alzheimer's disease · Amino acid enantiomers · Selenium nanoparticles · $A\beta_{42}$ · Transmission electron microscopy · Experimental design

Abbreviations

$A\beta_{42}$	Amyloid-beta protein fragment 1–42
AD	Alzheimer's disease
T_{IC50}	Stationary time to reach IC_{50}
IC_{50}	Half maximal inhibitory concentration
Ch-SeNPs	Selenium nanoparticles stabilized with chitosan
ROS	Reactive oxygen species
SeMet	Selenomethionine
NMDA	*N*-Methyl-D-aspartate
TEM	Transmission electron microscopy
BBB	Blood–brain barrier
OPA	ortho-Phthalaldehyde
TBARS	Thiobarbituric acid reactive substance
DPPH	2,2-Diphenyl-1-picrylhydrazyl
HFIP	1,1,1,3,3,3-Hexafluoro-2-propanol
TBA	Thiobarbituric acid
TCA	Trichloroacetic acid
EDXS	Energy-dispersive X-ray spectroscope
UV–Vis	Ultraviolet–visible
ANOVA	Analysis of variance
LSD	Least significant difference

Parts of this work were presented at the XXXVIII Biennial Meeting of the Spanish Royal Society of Chemistry (RSEQ), Granada (Spain), in June 2022, and have been awarded with an ABC Best Poster Award.

✉ David Vicente-Zurdo
davidvic@ucm.es

✉ Noelia Rosales-Conrado
nrosales@ucm.es

[1] Analytical Chemistry Department, Faculty of Chemistry, Complutense University of Madrid, 28040 Madrid, Spain

Introduction

Alzheimer's disease (AD) is the most common form of dementia in the world, affecting more than 40% of the population over the age of 85 in Europe and North America

[1]. Since this percentage is expected to increase in the next 20 years, the need to find more effective treatments for this age-related disease is indeed crucial [2]. AD pathology involves dysregulation of the nervous system, loss of temporal and spatial perception, difficulty in performing tasks, reduced patient autonomy and long-term cognitive impairment [3].

The accumulation of extracellular deposits of amyloid-beta protein (Aβ), leading to the formation of senile plaques, is the centre of AD pathogenesis. The most amyloidogenic form of Aβ is the peptide $A\beta_{42}$, generated by the sequential cleavage of Amyloid Precursor Protein (APP) by β- and γ-secretases [4]. $A\beta_{42}$ extracellular deposition triggers apoptosis, neuronal dysfunction, or even the death of neurons and neurites [5]. Oxidative damage produced by reactive oxygen species (ROS), leading to alterations in the cell redox state, also plays a decisive role in AD [6–8].

The main known triggers of AD, in addition to an anomalous concentration of metals such as Fe(II), Cu(II) and Zn(II) [9–11], are abnormal levels of amino acid enantiomers. Aβ aggregation is stereoselective as it is composed of α-helical/β-strand structures; henceforth, any change in the chiral environment can modify the aggregation of $A\beta_{42}$ fibrils [12]. Amino acids are essential in the human body, but any alteration either in their concentration or in their isomerization can lead to the development of several diseases such as AD [13, 14].

Humans are generally composed of L-amino acids, but over time, the content of D-amino acids increases in several structures and tissues such as skin, eyes, bones and brain [15]. Racemase enzymes, such as serine racemase, are responsible for the racemization processes of L-amino acids into D-amino acids. D-Serine (D-Ser) and D-aspartate (D-Asp) are the only ones originated from intrinsic racemization, both involved in processes underlying neurotransmission and neuronal signalling [16, 17]. Additionally, food processing techniques favour the racemization process into D-enantiomers, entering human tissues via the diet [14]. When L-amino acids in a protein undergo a structural change, characteristics and functions of these proteins are altered, triggering the development of age-related diseases, such as AD [14]. The presence of D-amino acids in proteins increases their accumulation since they become resistant to enzyme degradation mechanisms [18]. Racemization of $A\beta_{42}$ residues into D-amino acids, especially D-Ser and D-Asp, leads to their deposition into amyloid plaques [19]. For this reason, the D-amino acid content in $A\beta_{42}$ is higher in the AD patient's brain [20].

Specifically, D-Asp has demonstrated to play an important role in AD, since its presence may change the higher-order structure of proteins [17]. Exposure to elevated D-Asp concentrations decreases the synaptic plasticity and cognitive functions while favouring cell death in brain regions such as the hippocampus, prefrontal cortex and substantia nigra [21]. Phenylalanine (Phe) also favours amyloid fibrillar aggregation [22]. In addition, L-Phe can be considered as a decreased biomarker candidate in AD brains [23]. Tyrosine (Tyr) phosphorylation is involved in AD development through a tau-dependent mechanism [24], and L-selenomethionine (L-SeMet) has demonstrated a protection of $A\beta_{42}$-mediated neuronal death through a reduction of $A\beta_{42}$ toxicity [25]. On the other hand, there are some studies that attribute to D-tryptophan (D-Trp) an ability to inhibit $A\beta_{42}$ aggregation [26].

Other D-amino acids, such as D-alanine (D-Ala), D-Ser, D-Asp, D-glutamate (D-Glu) and D-glycine (D-Gly), have shown to play a critical role in the development of AD, due to their high concentration in the brains of AD patients [10]. They also affect the activity of N-methyl-D-aspartate (NMDA), which is a receptor involved in memory acquisition and learning, thereby promoting the appearance of neurophysiological disorders, such as AD [16, 21, 27].

To counteract the toxic role of some amino acid enantiomers in AD development, chiral compounds are being studied [28]. Thus, in this work, selenium nanoparticles stabilized with chitosan (Ch-SeNPs) were evaluated as a useful and reliable strategy for inhibiting amino acid enantiomer–induced $A\beta_{42}$ aggregation [29, 30]. With this regard, it is worth mentioning that chitosan is the most biocompatible and biodegradable natural alkaline chiral polysaccharide widely used in drug delivery [31, 32]. Additionally, chitosan-prepared nanoparticles protect them from enzyme degradation and favour controlled release, permeability across the blood–brain barrier (BBB), and their delivery from the nasal cavity to the brain due to their absorption on the cell membrane [31–33]. Selenium species, which are mainly found in food samples such as fishes and meat [34, 35], have demonstrated a positive effect reducing AD oxidative stress due to their antioxidant properties [36–39]. Thereby, due to the chiral nature of $A\beta_{42}$, selenium nanoparticles stabilized with chitosan can be a promising candidate to inhibit amyloid aggregation [11].

The aim of this work was to evaluate the possible interactions between amino acid enantiomers related to AD (D-Phe, D-Ala, D-Glu, D-Asp and DL-SeMet) and Ch-SeNPs through UV–Vis spectroscopy and/or fluorescence combined with experimental design and RSA statistical data analysis, as well as to elucidate the protective effect of the presence of D-amino acids and/or Ch-SeNPs on amyloidogenic $A\beta_{42}$ aggregation by TEM studies. To determine chiral amino acids through fluorescence spectroscopy, previous derivatization with ortho-phthalaldehyde (OPA), a commonly used derivatization agent [40], was performed. Additionally, antioxidant properties of amino acid enantiomers were experimentally determined in brain concentration levels, by employing the 2,2-diphenyl-1-picrylhydrazyl (DPPH) free

radical scavenging and the thiobarbituric acid reactive substance (TBARS) assays.

Materials and methods

Reagents and standards

All solvents and chemicals used were of analytical grade. Deionized water with 18 MΩ•cm resistance was used throughout the experiments, obtained from a Milli-Q water purification system (Millipore, Bedford, MA, USA). Individual stock solutions of 5 mM from D- and L-enantiomers of amino acids (Ala, Asp, Glu, Phe, Ser, Trp and Tyr), L-SeMet and DL-SeMet, which were purchased from Sigma-Aldrich (St. Louis, MO, USA), were prepared by dissolving the appropriate amount in Milli-Q water. Ch-SeNPs were synthesized from 99% Na_2SeO_3 (Sigma-Aldrich) in the presence of acetic acid from Panreac (Barcelona, Spain), chitosan and ascorbic acid, both provided by Sigma-Aldrich. Dialysis sack (Sigma-Aldrich) of 12 kDa was employed to dialyze selenium nanoparticles stabilized with chitosan before their use.

Fragment 1–42 of amyloid-β protein ($A\beta_{42}$) (Sigma-Aldrich, A9810, CAS: 107761–42-2) pretreated with 1,1,1,3,3,3-hexafluoro-2-propanol (HFIP) and dissolved in DMSO and HCl (Scharlab, Barcelona, Spain) was used for amyloid incubation assays. Interaction experiments between Ch-SeNPs and amino acid enantiomers were studied at acidic and physiologic pH, using HCl and phosphate buffer (Sigma-Aldrich). Ortho-phthalaldehyde (OPA, 99%, Sigma-Aldrich) in 0.4 M borate buffer (99.8% w/w, Panreac) adjusted at pH 10.4 with sodium hydroxide (97%, Sigma-Aldrich) 2 M solution was used for amino acid derivatization.

The radical 2,2-diphenyl-1-picrylhydrazyl (DPPH) (100% w/w, Sigma-Aldrich) was dissolved in HPLC-grade methanol (99.9% v/v, Scharlab) for antioxidant analysis. For TBARS assay, Tris–HCl (99.9% w/w), $FeSO_4$ (99.0% w/w), ascorbic acid (99% w/w), trichloroacetic acid (TCA) (99.0% w/w), and thiobarbituric acid (TBA) (100% w/w), all from Sigma-Aldrich, and porcine brain acquired in a local supermarket, were employed. 6-Hydroxy-2,5,7,8-tetramethylchroman-2-carboxylic acid (Trolox) (98% w/w, Sigma-Aldrich) was used as a reference antioxidant substance.

Instrumentation

Nanoparticles were characterized by a JEOL JEM 1400 Plus transmission electron microscope coupled to an energy-dispersive X-ray spectroscope (EDXS) (Oxford Inca). $A\beta_{42}$ monomer was pretreated using a SpeedVac Concentrator Plus from Eppendorf. Then, it was placed in a Thermo Scientific MaxQ 4000 (Fisher Scientific) incubator and fibril aggregation was evaluated by a JEOL JEM 1400 Plus transmission electron microscope at 100 kV. A diode array UV–Vis (Agilent Technologies, HP 8543) equipped with a Chemstation HP software was employed in Ch-SeNP stability studies, Ch-SeNP–amino acid interaction and antioxidant assays. A Cary eclipse spectrofluorometer (Agilent Technologies, G9800A) was employed to evaluate the interaction between Ch-SeNPs and OPA-derivatized amino acids. ImageJ software was used to measure nanoparticle diameter and amyloid fibril width. Statgraphics 19 software was employed to treat statistically amyloid fibril width data and to evaluate nanoparticle–amino acid interactions.

Synthesis of selenium nanoparticles: reproducibility and storage stability study

Synthesis of selenium nanoparticles stabilized with chitosan (Ch-SeNPs) was performed following the procedure described in previous studies [11]. The synthesized nanoparticles were characterized by TEM, EDXS and UV–Vis and stored at 4 °C in the dark until use.

For reproducibility studies, Ch-SeNPs were synthesized in quadruplicate and observed with TEM and their morphology and diameter size were measured using TEM and ImageJ software. One-way analysis of variance (ANOVA) was applied to compare the differences between syntheses. For storage stability studies, Ch-SeNPs were stored at 4 °C under darkness and measured by UV–Vis at 265 nm over a 1-month period.

Evaluation of $A\beta_{42}$ aggregation induced by amino acid enantiomers

Incubation of the $A\beta_{42}$ monomer was carried out following the procedure described in previous works [11]. The $A\beta_{42}$ commercial monomer was appropriately pretreated with HFIP to disrupt any possible β-sheets previously formed and obtain a homogeneous monomeric product. Pretreated $A\beta_{42}$ was properly dissolved in DMSO and diluted with 10 mM HCl, followed by a 10-min sonication in an ultrasonic bath, to obtain a working solution of 200 μM. Working solutions of 200 μM of D- and L-amino acids were prepared every day by diluting 5-mM stock solutions using 10 mM HCl. A working solution of 200 μM Ch-SeNPs was prepared every day by the dilution of the 12.67-mM stock solution stored at 4 °C under darkness.

Samples were prepared by adding 7.5 μL of 200 μM of D- or L-amino acids, with or without 7.5 μL of 200 μM Ch-SeNPs, to 7.5 μL of $A\beta_{42}$ and being incubated during 48 h at 37 °C. Amyloid fibrils formed were placed into a copper grid and negatively stained by using uranyl acetate 2% (w/v). Finally, they were analysed by TEM at 100 kV

and aggregation of $A\beta_{42}$ fibrils under the effect of different amino acid enantiomers, as well as the inhibition due to Ch-SeNP presence, was evaluated. Fibril width in all incubation conditions evaluated was quantified by using ImageJ software.

Evaluation of interactions between selenium nanoparticles and amino acid enantiomers

Enantiomeric interaction of Ch-SeNPs with target amino acids was studied by UV–Vis and fluorescence spectroscopy. D- and L-amino acid working solutions of 1 mM were prepared daily by the dilution of the 5-mM stock solution in the appropriate buffers.

To evaluate Ch-SeNP interactions with Trp and Tyr enantiomers, the corresponding volumes of Ch-SeNPs and D- or L-amino acid stock working solutions were diluted in 100 mM phosphate buffer at pH 7.3 to achieve final concentrations of 50 µM. Samples were measured by UV–Vis spectroscopy at 268 nm absorption wavelength to find enantiomeric differences in Ch-SeNP interactions.

Ch-SeNP interactions with Phe, Asp and Ser enantiomers were studied by fluorescence spectroscopy, previous derivatization with OPA, due to the low absorption of these amino acids in UV–Vis spectroscopy. An experimental factorial design was applied to evaluate the interaction between amino acid enantiomers and Ch-SeNPs depending on the concentration ratios. Two factors (Ch-SeNP and amino acid enantiomer concentration) at three levels each (35, 70 and 105 µM) and four replicates of the centre point were planned. Thus, a total of 12 runs were accomplished for each enantiomer. D- and L-amino acid derivatizations were performed by the addition of 1 mL of 45 mM OPA in 0.4 M borate buffer at pH 10.4 to amino acid enantiomer solutions in the concentration range 35–105 µM, followed by briefly vortexing. Then, the Ch-SeNP stock solution in 100 mM phosphate buffer at pH 7.3 was diluted to achieve concentrations from 35 to 105 µM, and it was added to the OPA–amino acid enantiomer solution. Samples were measured by fluorescence spectroscopy at an excitation wavelength of 359 nm and emission wavelength of 410 nm. Statistical analysis with a Pareto chart of standardized effects, main effects plot, and surface response analysis was employed to elucidate the enantiomeric interaction of Ch-SeNPs and their possible stoichiometry.

Antioxidant assays

The antioxidant capacity of D- and L-amino acids, and trolox as a reference compound, was evaluated by two different methods: DPPH and TBARS assays. Working solutions of D- and L-amino acids were prepared daily by the proper dilution of the 5-mM stock solution in Milli-Q water.

For DPPH radical scavenging assay, a 2,2-diphenyl-1-picrylhydrazyl 10-mM stock solution in MeOH was prepared daily and stored under darkness. DPPH working solution was prepared at 100 µM by the proper dilution of stock solution in MeOH. The stationary time (T_{IC50}) for the DPPH method was determined for each compound by measuring the absorbance in a UV–Vis spectrophotometer, at 515 nm from $t = 0$ min to $t = 120$ min, of a mixture between 2.5 mL of 100 µM DPPH and 500 µL of amino acid at a concentration that decreases nearly 50% the DPPH absorption band. A calibration curve of five points, with three replicates per point, was prepared for each compound by mixing 2.5 mL of 100 µM DPPH and 500 µL of amino acid solution, to study final concentrations in the range between 20 and 800 µM of D- or L-amino acids. Calibration curve was measured at T_{IC50} at 515 nm, and the DPPH remaining percentage (%DPPH rem) was represented versus the concentration, to obtain the half maximal inhibitory concentration (IC_{50}) for each amino acid enantiomer.

For TBARS assay, following the procedure described in previous studies [41], a homozygous cell extract from porcine brain was extracted with Tris–HCl at pH 7.4, by vigorous shaking and centrifugation at 2700 g for 10 min, to obtain a solution of 3.4 g L^{-1} in 1:2 (w/v) ratio. A volume of 100 µL of the supernatant of the homozygous cell extract, 200 µL of the D- or L-amino acid (to achieve a calibration curve of five points, three replicates, with final amino acid concentrations in the range 20–800 µM), 100 µL of 0.1 mM ascorbic acid and 100 µL of 10 µM FeSO4 were mixed and incubated at 37 °C for 1 h. Then, 500 µL of TCA 28% (w/v) to stop the reaction and 380 µL of TBA 2% (w/v) were added, and samples were incubated at 80 °C for 20 min. Samples were finally centrifuged at 4200 g for 10 min, and supernatant absorbance was measured by UV–Vis spectroscopy at 532 nm to obtain the IC_{50} for each amino acid enantiomer.

Results for both antioxidant determination methods were expressed as the mean and standard deviation of three replicates at two different days.

Statistical analysis

Results were statistically treated to evaluate the great amount of data obtained. Analysis of variance (ANOVA) and Fisher least significant difference (LSD) at 95% confidence level were applied to nanoparticle synthesis reproducibility, $A\beta_{42}$ fibril width under the presence of different amino acid enantiomers and Ch-SeNPs, and to evaluate the enantiomeric interaction between Ch-SeNPs and amino acids. Factorial experimental design and response surface analysis were applied in enantiomeric interaction studies to elucidate the concentration ratios in which the interaction is maximum.

Results and discussion

Characterization of selenium nanoparticles, synthesis reproducibility and storage stability

Synthesized Ch-SeNPs were dialyzed and characterized by TEM, EDXS and UV–Vis spectroscopy. They presented a spherical shape, as observed in TEM images (Fig. 1a), a diameter of (60 ± 1) nm as derived from the measurement with ImageJ software ($n = 40$) and an absorption band at 265 nm, through analysis by UV–Vis spectroscopy (Fig. 1c). Significant differences in the diameter between four repetitions of different Ch-SeNP syntheses were not found by ANOVA test at 95% confidence level, proving the high reproducibility of this synthesis method. Variance homogeneity comparison between Ch-SeNP diameters is presented in a box plot, where the fourth synthesis presented Ch-SeNPs with a diameter of (60 ± 1) nm (Fig. 1b). Regarding storage stability, Ch-SeNPs were measured by UV–Vis spectroscopy during a period of more than 1 month (Fig. 1c). These results demonstrated their stability, at 4 °C under darkness, for at least 1 month of storage.

Inhibition of $A\beta_{42}$ aggregation

$A\beta_{42}$ aggregation into senile plaques is believed to be mainly responsible for the development of AD, as established by the "amyloid cascade hypothesis". Thereby, in this work, aggregation of $A\beta_{42}$ fibrils has been studied under the presence of different amino acid enantiomers during 48 h at 37 °C. TEM micrographs showed that several D-amino acids, such as D-Asp, related to the N-methyl-D-aspartate receptor (NMDA); D-Phe, not related to receptor NMDA; amino acids considered inactive such as D-Ala and D-Glu; and also DL-SeMet, led to a significant increase in amyloid aggregation when compared to $A\beta_{42}$ alone (Fig. 2a). As an example, the increment of the amyloid fibril aggregation produced by D-Phe is shown in Fig. 2b, where an increase in density of fibril assemblies (depicted in the TEM micrographs as black lines or fibres) is observed. However, some L-amino acids such as L-Trp, L-Tyr and L-Glu also enhanced amyloid plaque formation, as can be seen for L-Trp in Fig. 2g, with an increase in the clustered fibrils (black lines or fibres) along the diagonal of the micrograph.

On the other hand, most of the L-enantiomers, such as L-Asp, L-Phe, L-Ala, L-Ser or L-SeMet, did not produce any effect on $A\beta_{42}$ aggregation. As an example of non-aggregation effect, L-Phe co-incubation with $A\beta_{42}$ fibrils is shown in Fig. 2c, where aggregation density remained constant. Nevertheless, some D-amino acids, such as D-Trp, D-Tyr and D-Ser, also did not increase amyloid aggregation, as shown for D-Trp in Fig. 2f with almost no fibrils and supported by literature [26].

Once the first screening of amino acid enantiomers contributing to the aggregation of $A\beta_{42}$ fibrils into amyloid plaques was performed, aggregation inhibition studies were carried out. Ch-SeNPs were co-incubated with amino acid enantiomers and $A\beta_{42}$ monomer during 48 h at 37 °C, and fibril aggregation was evaluated by TEM. Ch-SeNPs showed

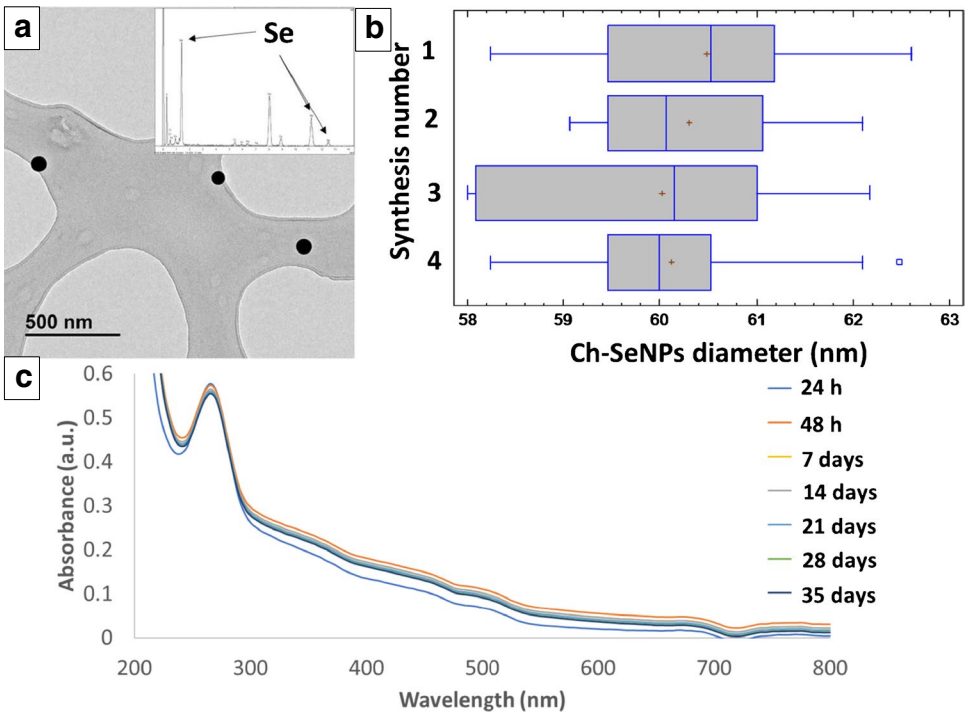


Fig. 1 Characterization of synthesized Ch-SeNPs. **a** TEM and EDXS micrographs, **b** variance homogeneity box plot of Ch-SeNP diameters belonging to four repetitions of the Ch-SeNP synthesis, **c** UV–Vis spectra of Ch-SeNPs stored from 24 h to 35 days at 4 °C under darkness

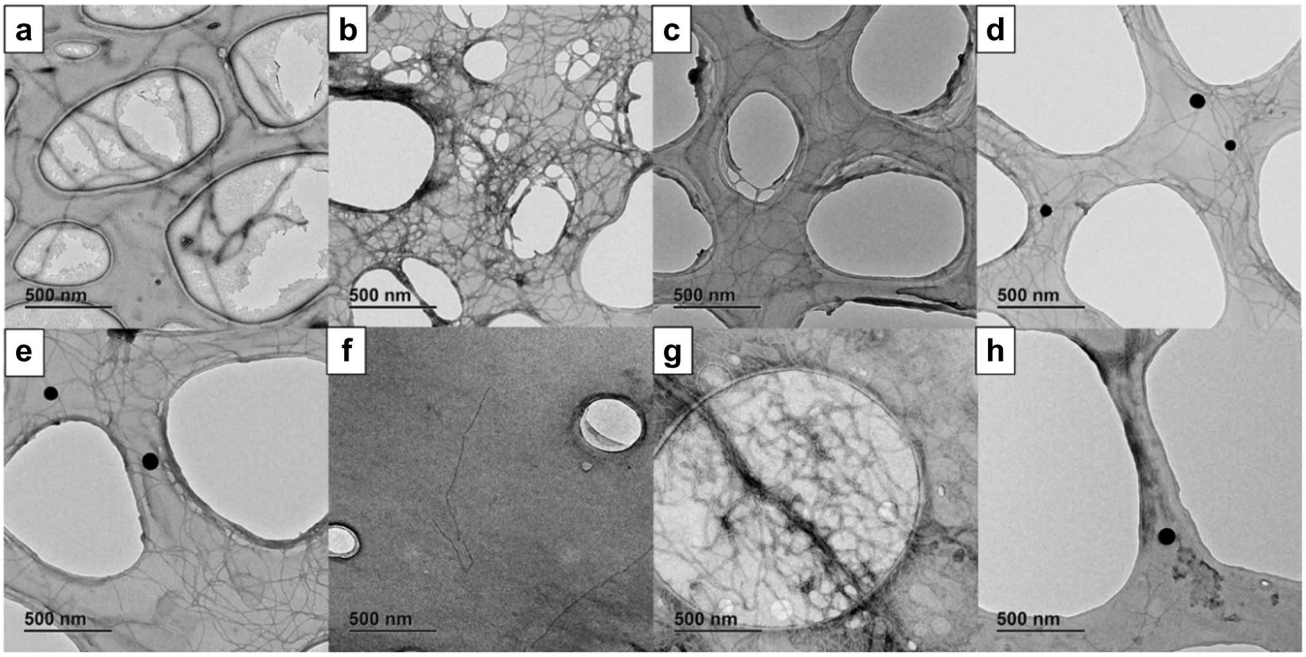


Fig. 2 $A\beta_{42}$ fibrils incubated during 48 h at 37 °C in the presence of amino acid enantiomers, and in the presence or absence of Ch-SeNPs. **a** $A\beta_{42}$ alone, **b** $A\beta_{42}$ + D-Phe, **c** $A\beta_{42}$ + L-Phe, **d** $A\beta_{42}$ + D-Phe + Ch-SeNPs, **e** $A\beta_{42}$ + L-Phe + Ch-SeNPs, **f** $A\beta_{42}$ + D-Trp, **g** $A\beta_{42}$ + L-Trp, **h** $A\beta_{42}$ + L-Trp + Ch-SeNPs. Amyloid fibrils are depicted in the TEM micrographs as black fibres or lines

an excellent amyloid aggregation inhibition since they were able to reduce drastically the enantiomer-induced aggregation of $A\beta_{42}$ fibrils. An example of Ch-SeNPs inhibition of D-amino acid-induced aggregation is shown for D-Phe in Fig. 2d, where the amyloid fibrils are more spread out with fewer amyloid fibril clusters than in the absence of Ch-SeNPs (Fig. 2b). Additionally, for L-Phe in the presence of Ch-SeNPs (Fig. 2e), fibrils remained disaggregated in a similar way as they were in the absence of selenium nanoparticles (Fig. 2c). In the case of Ch-SeNP inhibition of L-amino acid–induced aggregation, Ch-SeNPs were also able to inhibit the aggregation process, as it can be shown, for example, for L-Trp (Fig. 2h) in comparison with L-Trp alone (Fig. 2g), removing the huge black cluster of amyloid fibrils.

In addition to the evaluation of D- and L-amino acid enantiomers over amyloid aggregation, fibril width was also measured and analysed with ANOVA and Fisher LSD tests. Results are included in Table 1.

Data are expressed as mean ± standard deviation ($n = 20$). Mean values with a common letter indicate no significant differences at p values > 0.05, according to ANOVA and Fisher LSD test. *Samples correspond to L-SeMet and DL-SeMet.

As it can be observed, $A\beta_{42}$ fibrils in the absence of any amino acid enantiomer or Ch-SeNPs presented a standard width of 5.4 ± 0.7 nm. L-Amino acid enantiomers that did not show an increase in amyloid aggregation (L-Phe, L-Asp, L-SeMet, L-Ala and L-Ser) also generated the narrowest fibrils, with a reduction from 13% (L-Asp) to 31% (L-Ala) of the standard $A\beta_{42}$ fibril width. Regarding D-amino acid enantiomers that did not increase amyloid aggregation, D-Trp and D-Tyr showed a fibril width reduction of 20% and 26% respectively, whereas D-Ser, related to NMDA, widened amyloid fibrils up to 46% more than the standard $A\beta_{42}$ fibril width.

D-Amino acid enantiomers that increased $A\beta_{42}$ aggregation, such as D-Phe, D-Asp, D-Ala and D-Glu, and DL-SeMet, increased also amyloid fibril width. The slightest widened was observed for D-Asp (31%) and the largest for

Table 1 $A\beta_{42}$ fibril width of TEM incubations, under the presence of different amino acid enantiomers, measured with ImageJ software

Sample	L-Enantiomer width (nm)	D-Enantiomer with (nm)
$A\beta_{42}$	5.4 ± 0.7^{d}	
$A\beta_{42}$ + Phe	$4.3 \pm 0.5^{b,c}$	7.9 ± 0.6^{f}
$A\beta_{42}$ + Asp	4.7 ± 0.6^{c}	7.1 ± 0.6^{e}
$A\beta_{42}$ + SeMet*	$4.3 \pm 0.7^{b,c}$	9 ± 1 h
$A\beta_{42}$ + Ala	3.7 ± 0.4^{a}	7.2 ± 0.5^{e}
$A\beta_{42}$ + Glu	29 ± 1^{j}	12 ± 1^{i}
$A\beta_{42}$ + Trp	8.5 ± 0.6 g	$4.3 \pm 0.3^{b,c}$
$A\beta_{42}$ + Tyr	8.4 ± 0.7 g	$4.0 \pm 0.4^{a,b}$
$A\beta_{42}$ + Ser	4.5 ± 0.8^{c}	7.9 ± 0.9^{f}

D-Glu (122%). On the other hand, L-amino acid enantiomers that also showed an increase of $A\beta_{42}$ aggregation (L-Trp, L-Tyr and L-Glu) widened amyloid fibrils from 55% (L-Tyr) to 437% (L-Glu).

These results provide valuable information about the induction of $A\beta_{42}$ aggregation produced by amino acids. It has been demonstrated that amyloid aggregation of $A\beta_{42}$ protein is enantiomerically dependent since enantiomers of the same amino acid act differently over fibril organization. In general, D-amino acids generate greater accumulation of fibrils than L-amino acids, with some exceptions such as Tyr and Trp enantiomers. In all situations where amino acid enantiomers produced an increase in $A\beta_{42}$ aggregation, Ch-SeNPs were able to inhibit fibril accumulation, presumably due to the enantiomeric effect that chitosan, the chiral stabilizing agent, provided to selenium nanoparticles.

Fibril width also suffered the enantiomeric effect of amino acids, as shown in Table 1. In the same way as in the amyloid aggregation section, L-amino acids narrowed $A\beta_{42}$ fibrils, while D-amino acids widened them in most of the situations. However, some exceptions such as L-Trp, L-Tyr and, especially, L-Glu increased fibril width. Moreover, the latter produced the widest fibrils among all the amino acid enantiomers under study, up to 436% wider than $A\beta_{42}$ alone. On the other hand, the highest reduction was caused by the effect of L-Ala, achieving a width diminution of 31%. Leaving aside the enantiomeric effect, Glu is the only amino acid that increases, in both enantiomeric forms, the amyloid width achieving the widest fibrils among all evaluated amino acids. In addition, Asp was the amino acid that produced the slightest effect on amyloid width, either by reducing the fibril width by 13% (L-Asp) or increasing it by 31% (D-Asp).

Enantiomeric interaction of Ch-SeNPs with amino acids

Ch-SeNPs have undoubtedly demonstrated their potential to inhibit the $A\beta_{42}$ aggregation, mainly responsible for the development of AD, induced by amino acid enantiomers. To molecularly study the interaction between these nanoparticles and various enantiomers, two molecular spectroscopic techniques were employed: UV–Vis and fluorescence.

UV–Vis spectroscopy was applied to two amino acids that presented high absorption in the UV–Vis range: Trp and Tyr enantiomers. In order to observe differences as a function of the chiral environment, absorbances of individual amino acid enantiomers were compared with those of mixtures of each enantiomer with Ch-SeNPs. Regarding the interaction between Ch-SeNPs and Trp, both enantiomers individually presented the same absorption (0.12 a.u.). However, when they were measured in the presence of Ch-SeNPs, L-Trp + Ch-SeNPs showed higher absorption (0.29 a.u.) than the D-Trp + Ch-SeNPs mixture (0.23 a.u.). This increase in absorbance for L-Trp, higher than for D-Trp, indicated a different behaviour of the two enantiomers in terms of their selectivity towards Ch-SeNPs. Therefore, the interaction between Ch-SeNPs and Trp amino acid was enantioselective, with a preference for interaction with L-Trp. The UV–Vis spectra of L-Trp and D-Trp in the absence and presence of Ch-SeNPs are shown in S1 (Supplementary Information). On the other hand, differences were not found between Tyr enantiomers and Ch-SeNPs, showing the interaction identical regardless of the enantiomeric form.

While UV–Vis is a fast and versatile technique, its sensitivity and/or selectivity is limited for certain studies. Thus, to study the interaction between Phe, Asp and Ser enantiomers with Ch-SeNPs, fluorescence spectroscopy was selected. However, to endow the amino acid enantiomers with fluorescence, a derivatization process with OPA was previously required.

The spectrophotometric and spectrofluorimetric studies suggested that the interaction between Ch-SeNPs and the amino acid enantiomers strongly depends on their relative concentrations. Therefore, a factorial design of two experimental factors (Ch-SeNPs and amino acid concentrations) and three levels with four replicates at the centre point was planned and performed to evaluate the fluorescence emission and to establish the concentration ratios showing the maximum interactions.

Emission fluorescence spectra corresponding to the interaction between Ch-SeNPs and Phe enantiomers are presented, as an example, in Fig. 3.

Although different behaviours of both amino acid enantiomers with selenium nanoparticles can be observed, mainly due to the minimum intensity for D-Phe:Ch-SeNPs (3:1) and L-Phe:Ch-SeNPs (1:3) concentration ratio, the experimental design in order to enhance the differences between the interactions was highly useful.

The response variables were fitted to polynomial models according to the following equation:

$$Y = a_0 + a_1X_1 + a_2X_2 + a_3X_1^2 + a_4X_2^2 + a_5X_1X_2 \quad (1)$$

where Y is the predicted response variable (fluorescence emission at 410 nm or absorbance at 270 nm for Trp); a_0 is the intercept; a_1 and a_2 are the linear coefficients of X_1 (concentration of amino acid enantiomer) and X_2 (Ch-SeNP concentration); a_3 and a_4 are the squared coefficients of X_1 and X_2; and a_5 is the interaction coefficient of X_1 and X_2.

The coefficient of multiple determination obtained (R^2) showed that, in general, the mathematical models developed to explain the influence of these factors on the intensity signal provided an adequate explanation of the interactions (Table 2).

Coefficients a_0–a_5 represent the weight of each studied factor and their interactions in the selected response. p

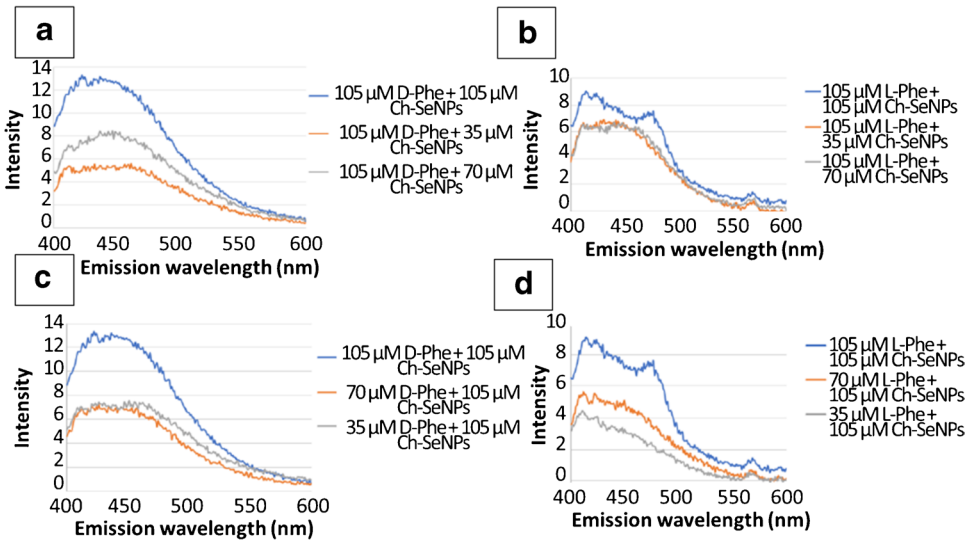


Fig. 3 Emission fluorescence spectra of the interaction between different concentrations of Ch-SeNPs and Phe enantiomers at 359 nm excitation wavelength and 410 nm emission wavelength: **a** [D-Phe] = 105 µM and [Ch-SeNPs] = 35, 70 and 105 µM; **b** [L-Phe] = 105 µM and [Ch-SeNPs] = 35, 70 and 105 µM; **c** [Ch-SeNPs] = 105 µM and [D-Phe] = 35, 70 and 105 µM; **d** [Ch-SeNPs] = 105 µM and [L-Phe] = 35, 70 and 105 µM

Table 2 Fitted parameter values obtained from the mathematical models described in Eq. (1)

Amino acid signal (Y)	a_0	a_1	a_2	a_3	a_4	a_5	R^2
L-Phe	8.907	1.045 (0.1500)	0.1833 (0.7800)	− 1.5300 (0.1581)	− 2.0060 (0.0720)	0.6800 (0.4140)	70.10
D-Phe	7.660	0.7167 (0.1748)	1.1930 (**0.0428**)	0.0837 (0.9085)	− 0.3962 (0.5912)	1.5075 (**0.0380**)	73.00
L-Asp	381.8	172.20 (0.1583)	− 118.30 (0.2048)	− 105.80 (0.5159)	263.30 (0.2339)	59.13 (0.5281)	85.47
D-Asp	392.9	− 5.620 (0.5847)	97.600 (**0.0032**)	− 25.150 (0.3092)	45.670 (0.1015)	8.369 (0.5119)	96.44
L-Ser	454.45	131.70 (0.5595)	241.21 (0.3142)	− 397.80 (0.3854)	566.10 (0.3835)	− 69.40 (0.7379)	87.80
D-Ser	421.29	80.55 (**0.0043**)	142.34 (**0.0020**)	127.97 (**0.0047**)	102.95 (**0.0083**)	− 26.55 (**0.0131**)	99.99
L-Trp	0.6508	0.2059 (0.0564)	0.04265 (0.5750)	0.0182 (0.8869)	0.0117 (0.9270)	− 0.0032 (0.9713)	76.20
D-Trp	− 1.639	0.6343 (**0.0000**)	0.3264 (**0.0001**)	− 0.0062 (0.7954)	0.00008 (0.7912)	− 0.0039 (0.8185)	99.90

Significance for 95% confidence level is <0.05

values are given in brackets (those in bold are p values ≤ 0.05 indicating the effects significantly different from 0 at the 95% confidence level).

As can be seen in Table 2, the instrumental responses predicted by the model are different for all the amino acid enantiomers evaluated, given that the interaction between the Ch-SeNPs and each enantiomer is also distinct. In the studied domain, the linear coefficient of Ch-SeNP concentration (a_2) was the most influential factor, being solely significant in the analytical responses of D-amino acids, at a confidence level of 95%. The second most frequent ones were the linear coefficient of amino acid concentration (a_1), significant for D-Ser and D-Trp, and interaction coefficient (a_5), significant for D-Phe and D-Ser. Lastly, squared coefficients of Ch-SeNPs and amino acid concentrations (a_3 and a_4) were only significant for D-Ser. This fact suggests that the interaction between the amino acid enantiomers and Ch-SeNPs, when it occurs, is enantioselective, also explaining the possible different behaviour against the aggregation of the $A\beta_{42}$ in the presence and absence of Ch-SeNPs. To establish the differences observed, and as an example, in Fig. 4, chemometric analysis graphs of the fluorescence emission between Ch-SeNPs and Phe enantiomers are shown.

As included in Fig. 5, in the Pareto charts of standardized effects and for D-Phe, there were two significant factors (Ch-SeNP concentration and Ch-SeNP:D-Phe interaction) (Fig. 4a), while for L-Phe, all factors were not significant (Fig. 4b). Secondly, in the main effects plot, D-Phe exhibited a linear response with Ch-SeNP concentration (Fig. 4c), whereas L-Phe showed a curved response (Fig. 4d). Lastly, in the surface response analysis for D-Phe, there is a minimum at D-Phe (+ 1) (105 µM) and Ch-SeNPs (− 1) (35 µM), suggesting the interaction between them at 3:1 concentration

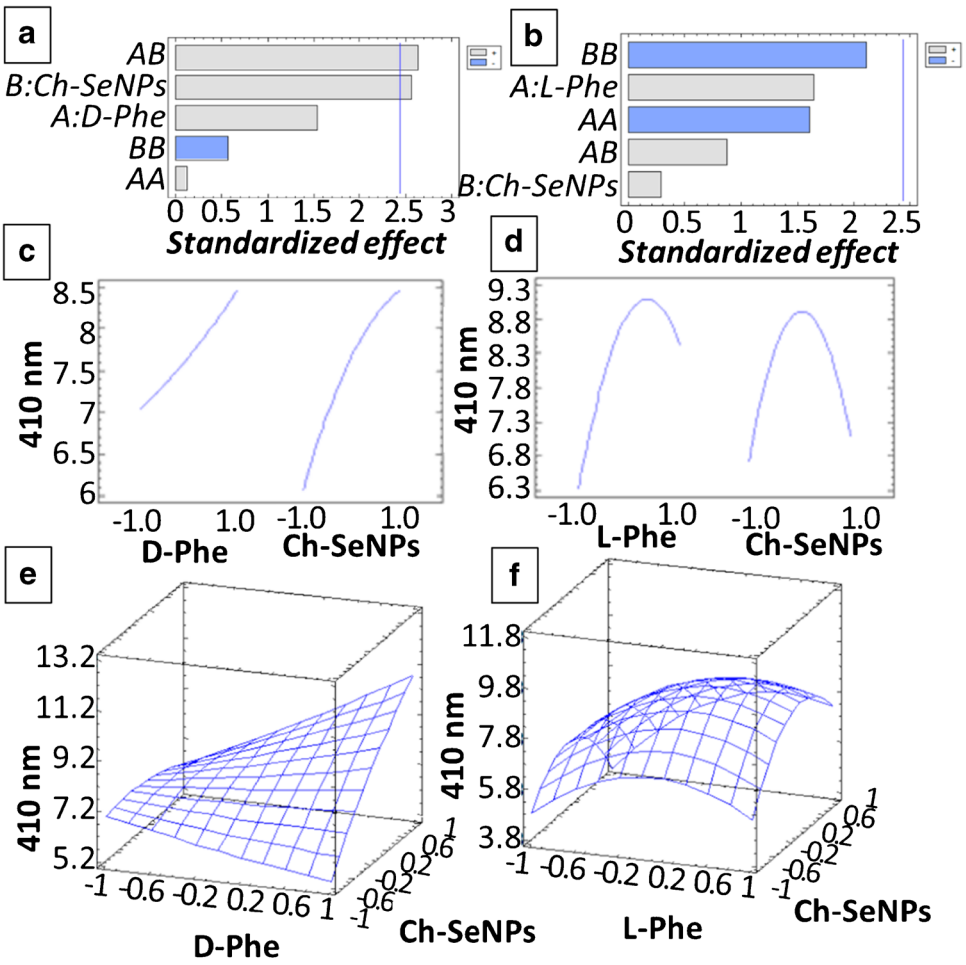


Fig. 4 Results of the experimental design performed for the evaluation of Ch-SeNP interactions with Phe enantiomers. Pareto charts of standardized effects for D-Phe (**a**) and L-Phe (**b**); main effects plot for D-Phe (**c**) and L-Phe (**d**); and surface response analysis for D-Phe (**e**) and L-Phe (**f**)

ratio (Fig. 4e). On the other hand, this behaviour is not appreciated for L-Phe interaction (Fig. 4f).

For Ch-SeNP interactions with Ser enantiomers, as shown in Fig. 5, all Pareto chart factors (Ch-SeNP and D-Ser concentrations, Ch-SeNP and D-Ser quadratic interactions, and Ch-SeNP:D-Ser interaction) were significant for D-Ser (Fig. 5a), but not for L-Ser (Fig. 5b). The D-Asp Pareto chart (Fig. 5c) presented only one significant factor (Ch-SeNP concentration), whereas the L-Asp chart (Fig. 5d) presented none. Surface response analysis also presented a different behaviour for D-Asp (Fig. 5e) than for L-Asp (Fig. 5f). Once more, Ch-SeNPs demonstrated their enantioselectivity regarding both Ser and Asp enantiomers since fluorescence response was different for each of their enantiomers.

Taking these results into account, the enantiomeric interaction of Ch-SeNPs, which also have anti-amyloidogenic properties, with some amino acids is evident. This enantiomeric interaction is orientated towards D-amino acids, which are the non-natural-occurring ones in human organisms. Lastly, chemometric tools, such as surface response analysis, can also provide information about concentration ratios of molecular interactions.

Antioxidant capacity

In addition to the induction effect of $A\beta_{42}$ aggregation and Ch-SeNP interaction, the antioxidant capacity of amino acid enantiomers was also studied. Antioxidant properties were evaluated by the IC_{50} determination for each enantiomer by two different methods: TBARS and DPPH assays ($n = 3$). Trolox antioxidant capacity was measured as a reference compound, with an IC_{50} of 170 ± 20 µM and 21.5 ± 0.4 µM for TBARS and for DPPH, respectively.

For the DPPH assay, absorbance was measured from 0 to 120 min for each amino acid enantiomer, fixing a stationary time (T_{IC50}) of 20 min for each enantiomer. Most of the amino acid enantiomers did not show antioxidant capacity by any of the methods at the brain concentration levels under study (20–800 µM). Only Tyr enantiomers presented an IC_{50} within the concentration range studied for the DPPH assay, with slight differences between the D ($IC_{50} = 314 \pm 6$ µM) and L ($IC_{50} = 370 \pm 40$ µM) forms. Results are supported by the literature, since some amino acids such as Phe, Ser and Asp are expected to show a lower antioxidant activity than Tyr [42]. However, antioxidant properties of the rest of the

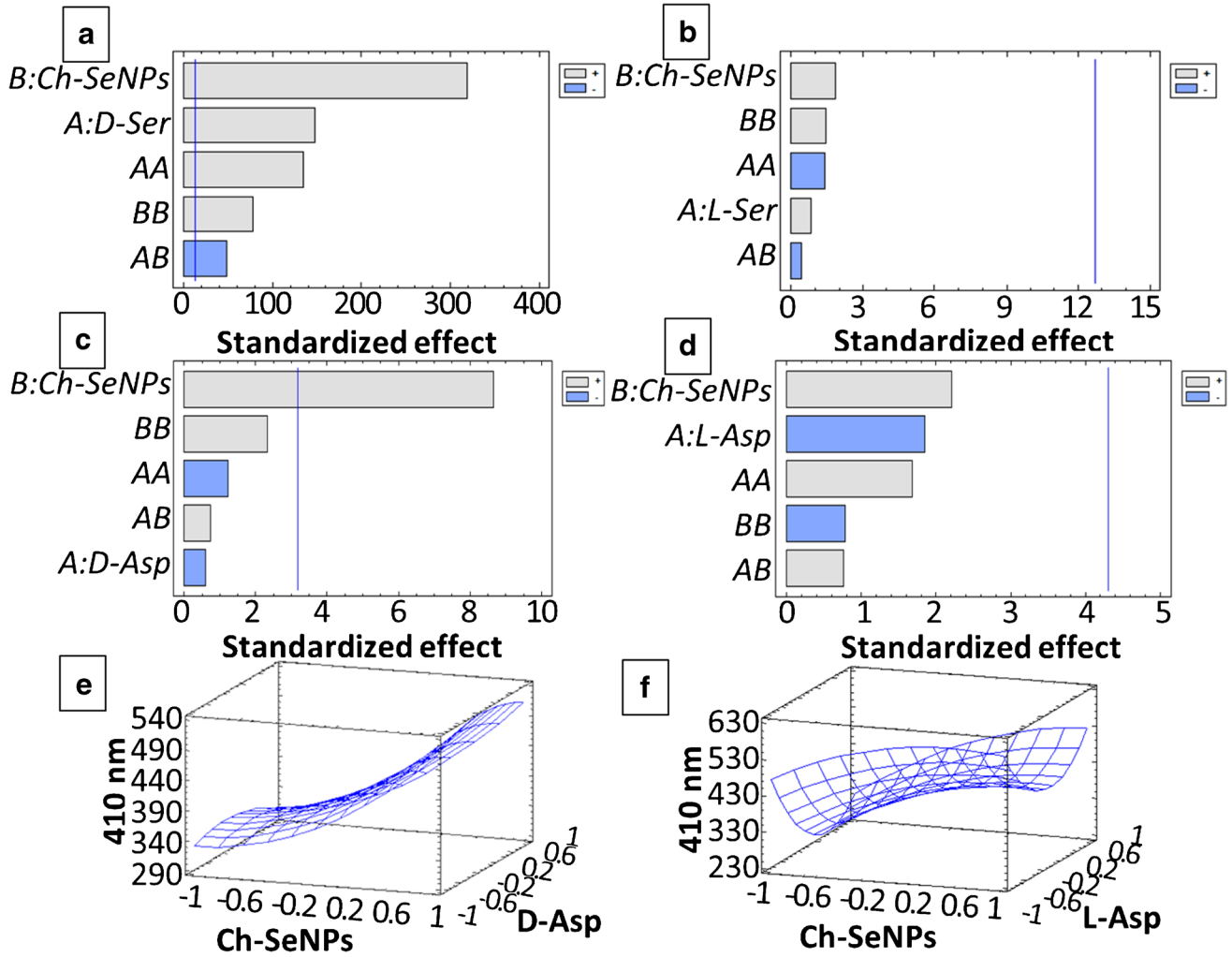


Fig. 5 Pareto charts of standardized effect for Ch-SeNP interactions with D-Ser (**a**), L-Ser (**b**), D-Asp (**c**) and L-Asp (**d**), and surface response analysis for D-Asp (**e**) and L-Asp (**f**)

amino acids are not sufficiently relevant to be considered in their neurodegenerative activity.

Conclusions

$A\beta_{42}$ extracellular aggregation into amyloid plaques is considered the trigger of neurodegeneration in AD. Herein, $A\beta_{42}$ aggregation measured by TEM has demonstrated to be influenced by the enantiomeric form of amino acids. Most of amyloidogenic amino acids were D-enantiomers, such as D-Phe, D-Asp, D-Ala, D-Glu and DL-SeMet, with some exceptions, such as D-Trp. On the other hand, most of the L-enantiomers did not affect amyloid aggregation, such as L-Phe, L-Asp, L-Ala, L-Ser and L-SeMet, with some exceptions, such as L-Trp and L-Glu. Thereby, $A\beta_{42}$ aggregation can be considered enantiomerically dependent.

In this work, it has been demonstrated that amyloid fibril width is also influenced by the chirality. $A\beta_{42}$ fibril width is strongly correlated with amyloid aggregation since all amyloidogenic amino acid enantiomers have widened fibril width.

Additionally, Ch-SeNPs, which have demonstrated anti-amyloidogenic properties regarding metal-induced $A\beta_{42}$ inhibition, are successfully being employed to inhibit enantiomeric-induced $A\beta_{42}$ aggregation. Selenium nanoparticles synthesized with chitosan, a chiral stabilizing agent, were able to prevent accumulations of amyloid fibrils, mostly produced by D-amino acid effects. Enantiomeric Ch-SeNP interaction was found in relation to some amino acids such as Trp, Phe, Ser and Asp. Therefore, the fact that Ch-SeNPs enantiomerically interact with some amino acids may be related to the inhibition of enantiomeric-induced $A\beta_{42}$ aggregation due to the presence of these nanoparticles. Thereby, Ch-SeNPs present valuable properties to be considered as a promising anti-AD compound.

On the other hand, almost none of the amino acids, except Tyr enantiomers, showed good antioxidant properties when evaluated by DPPH and TBARS assays. Thus, differences between enantiomers of the same amino acid were not significant, revealing enantiomeric–amyloid aggregation as a different process from antioxidant capacity.

Therefore, $A\beta_{42}$ fibril width and aggregation have demonstrated to be affected by the chiral environment, mainly induced by D-amino acids. Ch-SeNPs inhibited enantiomeric-induced amyloid aggregation, being also capable of interacting in a different way with enantiomers of some amino acids. Additional experiments should be performed to assess Ch-SeNPs as a beneficial compound regarding AD treatment.

Supplementary Information The online version contains supplementary material available at https://doi.org/10.1007/s00216-022-04285-z.

Acknowledgements This work was supported by the Spanish Ministry of Science and Innovation (PID2020-114714RB-I00) and the Community of Madrid and European funding from FSE and FEDER programmes (S2018/BAA-4393, PB2018/BAA-4393- AVANSECAL-II-CM). David Vicente-Zurdo acknowledges the Spanish Ministry of Science, Innovation and Universities for funding through a pre-doctoral grant (FPU18/00573). Esther Gómez-Mejía acknowledges Complutense University through a pre-doctoral grant (CT17/17-CT18/17).

Author contribution David Vicente-Zurdo: methodology, formal analysis, investigation, data curation, writing—original draft and writing—review and editing; Sandra Rodríguez-Blázquez: methodology, formal analysis, investigation, data curation and writing—review and editing; Esther Gómez-Mejía: methodology and writing—review and editing; Noelia Rosales-Conrado: conceptualization, methodology, investigation and writing—review and editing; María Eugenia León-González: conceptualization, methodology, investigation and writing—review and editing; Yolanda Madrid: conceptualization, methodology, investigation, writing—review and editing and funding acquisition

Declarations

Conflict of interest The authors declare no competing interests.

Award This work received the "Best Poster" award, sponsored by *Analytical and Bioanalytical Chemistry*, in session S9 "Bioanalytical Chemistry in Health and Food Safety" organized in the framework of the XXXVIII Biennial Meeting of the Spanish Royal Society of Chemistry (RSEQ), 27th–30th June 2022, Granada, Spain.

References

1. Lewczuk P, Mroczko B, Fagan A, Kornhuber J. Biomarkers of Alzheimer's disease and mild cognitive impairment: a current perspective. Adv Med Sci. 2015;60:76–82.
2. Reitz C, Brayne C, y Mayeux R,. Epidemiology of Alzheimer disease. Nat Rev Neurol. 2011;7:137–52.
3. de Souza LC, Sarazin M, Teixeira Júnior AL, Caramelli P, dos Santos AE, Dubois B, de Souza LC, Sarazin M, Teixeira Júnior AL, Caramelli P, dos Santos AE, Dubois B. Biological markers of Alzheimer's disease. Arq Neuropsiquiatr. 2014;72:227–31. https://doi.org/10.1590/0004-282X20130233.
4. Chow VW, Mattson MP, Wong PC, Gleichmann M. An overview of APP processing enzymes and products. Neuromolecular Med. 2010;12:1–12.
5. Crescenzi O, Tomaselli S, Guerrini R, Salvadori S, D'Ursi AM, Temussi PA, Picone D. Solution structure of the Alzheimer amyloid β-peptide (1–42) in an apolar microenvironment: similarity with a virus fusion domain. Eur J Biochem. 2002;269:5642–8. https://doi.org/10.1046/j.1432-1033.2002.03271.x.
6. Cheignon C, Tomas M, Bonnefont-Rousselot D, Faller P, Hureau C, Collin F. Oxidative stress and the amyloid beta peptide in Alzheimer's disease. Redox Biol. 2018;14:450–64. https://doi.org/10.1016/j.redox.2017.10.014.
7. Qi Y, Yi P, He T, Song X, Liu Y, Li Q, Zheng J, Song R, Liu C, Zhang Z, Peng W, Zhang Y (2020) Quercetin-loaded selenium nanoparticles inhibit amyloid-β aggregation and exhibit antioxidant activity. Colloids and Surfaces A: Physicochemical and Engineering Aspects 602:. https://doi.org/10.1016/j.colsurfa.2020.125058
8. Rocchi D, Blázquez-Barbadillo C, Agamennone M, Laghezza A, Tortorella P, Vicente-Zurdo D, Rosales-Conrado N, Moyano P, del Pino J, González JF, Menéndez JC. Discovery of 7-aminophenanthridin-6-one as a new scaffold for matrix metalloproteinase inhibitors with multitarget neuroprotective activity. Eur J Med Chem. 2021;210: 113061. https://doi.org/10.1016/j.ejmech.2020.113061.
9. Bush AI. Metals and neuroscience. Curr Opin Chem Biol. 2000;4:184–91.
10. Moyano P, Vicente-Zurdo D, Blázquez-Barbadillo C, Menéndez JC, González JF, Rosales-Conrado N, del Pino J. Neuroprotective action of multitarget 7-aminophenanthridin-6(5H)-one derivatives against metal-induced cell death and oxidative stress in SN56 cells. ACS Chem Neurosci. 2021;12:3358–72. https://doi.org/10.1021/acschemneuro.1c00333.
11. Vicente-Zurdo D, Romero-Sánchez I, Rosales-Conrado N, León-González ME, Madrid Y. Ability of selenium species to inhibit metal-induced Aβ aggregation involved in the development of Alzheimer's disease. Anal Bioanal Chem. 2020;412:6485–97. https://doi.org/10.1007/s00216-020-02644-2.
12. Gao N, Du Z, Guan Y, Dong K, Ren J, Qu X. Chirality-selected chemical modulation of amyloid aggregation. J Am Chem Soc. 2019;141:6915–21. https://doi.org/10.1021/jacs.8b12537.
13. Piubelli L, Murtas G, Rabattoni V, Pollegioni L. The role of D-amino acids in Alzheimer's disease. Journal of Alzheimer's Disease. 2021;80:475–92.
14. Bastings JJAJ, van Eijk HM, Damink SWO, Rensen SS. D-amino acids in health and disease: a focus on cancer. Nutrients. 2019;11:2205–22. https://doi.org/10.3390/nu11092205.
15. Sun D, Zhang W, Yu Q, Chen X, Xu M, Zhou Y, Liu J. Chiral penicillamine-modified selenium nanoparticles enantioselectively inhibit metal-induced amyloid β aggregation for treating Alzheimer's disease. J Colloid Interface Sci. 2017;505:1001–10. https://doi.org/10.1016/j.jcis.2017.06.083.
16. Genchi G. An overview on d-amino acids. Amino Acids. 2017;49:1521–33. https://doi.org/10.1007/s00726-017-2459-5.
17. Fujii N, Takata T, Fujii N, Aki K, Sakaue H. D-Amino acids in protein: the mirror of life as a molecular index of aging. Biochimica et Biophysica Acta - Proteins and Proteomics. 2018;1866:840–7.
18. Ha S, Kim I, Takata T, Kinouchi T, Isoyama M, Suzuki M, Fujii N. Identification of D-amino acid-containing peptides in human serum. PLoS ONE. 2017;12: e0189972. https://doi.org/10.1371/journal.pone.0189972.
19. Readel ER, Wey M, Armstrong DW. Rapid and selective separation of amyloid beta from its stereoisomeric point mutations implicated in neurodegenerative Alzheimer's disease. Anal Chim Acta. 2021;1163: 338506. https://doi.org/10.1016/j.aca.2021.338506.

20. Seckler JM, Lewis SJ. Advances in D-amino acids in neurological research. Int J Mol Sci. 2020;21:1–20. https://doi.org/10.3390/ijms21197325.
21. Nuzzo T, Feligioni M, Cristino L, Pagano I, Marcelli S, Iannuzzi F, Imperatore R, D'Angelo L, Petrella C, Carella M, Pollegioni L, Sacchi S, Punzo D, de Girolamo P, Errico F, Canu N, Usiello A. Free D-aspartate triggers NMDA receptor-dependent cell death in primary cortical neurons and perturbs JNK activation, Tau phosphorylation, and protein SUMOylation in the cerebral cortex of mice lacking D-aspartate oxidase activity. Exp Neurol. 2019;317:51–65. https://doi.org/10.1016/j.expneurol.2019.02.014.
22. Azriel R, Gazit E. Analysis of the minimal amyloid-forming fragment of the islet amyloid polypeptide. An experimental support for the key role of the phenylalanine residue in amyloid formation. J Biol Chem. 2001;276:34156–61. https://doi.org/10.1074/jbc.M102883200.
23. Takayama T, Mochizuki T, Todoroki K, Min JZ, Mizuno H, Inoue K, Akatsu H, Noge I, Toyo'oka T,. A novel approach for LC-MS/MS-based chiral metabolomics fingerprinting and chiral metabolomics extraction using a pair of enantiomers of chiral derivatization reagents. Anal Chim Acta. 2015;898:73–84. https://doi.org/10.1016/j.aca.2015.10.010.
24. Derkinderen P, Scales TME, Hanger DP, Leung KY, Byers HL, Ward MA, Lenz C, Price C, Bird IN, Perera T, Kellie S, Williamson R, Noble W, van Etten RA, Leroy K, Brion JP, Reynolds CH, Anderton BH. Tyrosine 394 is phosphorylated in Alzheimer's paired helical filament tau and in fetal tau with c-Abl as the candidate tyrosine kinase. J Neurosci. 2005;25:6584–93. https://doi.org/10.1523/JNEUROSCI.1487-05.2005.
25. Xiong S, Markesbery WR, Shao C, Lovell MA. Seleno-L-methionine protects against β-amyloid and iron/hydrogen peroxide-mediated neuron death. Antioxid Redox Signal. 2007;9:457–67. https://doi.org/10.1089/ars.2006.1363.
26. Rammes G, Parsons CG. The Aβ aggregation modulator MRZ-99030 prevents and even reverses synaptotoxic effects of Aβ1-42 on LTP even following serial dilution to a 500:1 stoichiometric excess of Aβ1-42, suggesting a beneficial prion-like seeding mechanism. Neuropharmacology. 2020;179: 108267. https://doi.org/10.1016/j.neuropharm.2020.108267.
27. Wu S-Z, Bodles AM, Porter MM, Griffin ST, Basile AS, Barger SW. Induction of serine racemase expression and D-serine release from microglia by amyloid β-peptide. J Neuroinflammation. 2004;1:1–11. https://doi.org/10.1186/1742-2094-1-2.
28. Abbas M. Potential role of nanoparticles in treating the accumulation of amyloid-beta peptide in Alzheimer's patients. Polymers (Basel). 2021;13:1051. https://doi.org/10.3390/polym13071051.
29. Yang L, Wang W, Chen J, Wang N, Zheng G. A comparative study of resveratrol and resveratrol-functional selenium nanoparticles: inhibiting amyloid β aggregation and reactive oxygen species formation properties. Journal of Biomedical Materials Research - Part A. 2018;106:3034–41. https://doi.org/10.1002/jbm.a.36493.
30. Schweizer U, Bräuer AU, Köhrle J, Nitsch R, Savaskan NE. Selenium and brain function: a poorly recognized liaison. Brain Res Rev. 2004;45:164–78. https://doi.org/10.1016/j.brainresrev.2004.03.004.
31. Mohammed MA, Syeda JTM, Wasan KM, Wasan EK. An overview of chitosan nanoparticles and its application in non-parenteral drug delivery. Pharmaceutics. 2017;9:53. https://doi.org/10.3390/pharmaceutics9040053.
32. Yu S, Xu X, Feng J, Liu M, Hu K. Chitosan and chitosan coating nanoparticles for the treatment of brain disease. Int J Pharm. 2019;560:282–93. https://doi.org/10.1016/j.ijpharm.2019.02.012.
33. Gupta J, Fatima MT, Islam Z, Khan RH, Uversky VN, Salahuddin P. Nanoparticle formulations in the diagnosis and therapy of Alzheimer's disease. Int J Biol Macromol. 2019;130:515–26. https://doi.org/10.1016/j.ijbiomac.2019.02.156.
34. Vicente-Zurdo D, Gómez-Gómez B, Pérez-Corona MT, Madrid Y. Impact of fish growing conditions and cooking methods on selenium species in swordfish and salmon fillets. J Food Compos Anal. 2019;83: 103275. https://doi.org/10.1016/j.jfca.2019.103275.
35. dos Santos M, da Silva Júnior FMR, Vicente-Zurdo D, Baisch PRM, Muccillo-Baisch AL, Madrid Y. Selenium and mercury concentration in drinking water and food samples from a coal mining area in Brazil. Environ Sci Pollut Res. 2019;26:15510–7. https://doi.org/10.1007/s11356-019-04942-4.
36. Wojsiat J, Zoltowska KM, Laskowska-Kaszub K, Wojda U. Oxidant/antioxidant imbalance in Alzheimer's disease: therapeutic and diagnostic prospects. Oxid Med Cell Longev. 2018;2018:6435861. https://doi.org/10.1155/2018/6435861.
37. Nirmala C, Bisht MS, Bajwa HK, Santosh O. Bamboo: a rich source of natural antioxidants and its applications in the food and pharmaceutical industry. Trends Food Sci Technol. 2018;77:91–9. https://doi.org/10.1016/j.tifs.2018.05.003.
38. Tamtaji OR, Heidari-soureshjani R, Mirhosseini N, Kouchaki E, Bahmani F, Aghadavod E, Tajabadi-Ebrahimi M, Asemi Z. Probiotic and selenium co-supplementation, and the effects on clinical, metabolic and genetic status in Alzheimer's disease: a randomized, double-blind, controlled trial. Clin Nutr. 2019;38:2569–75. https://doi.org/10.1016/j.clnu.2018.11.034.
39. Zhang ZH, Wu QY, Zheng R, Chen C, Chen Y, Liu Q, Hoffmann PR, Ni JZ, Song GL. Selenomethionine mitigates cognitive decline by targeting both tau hyperphosphorylation and autophagic clearance in an Alzheimer's disease mouse model. J Neurosci. 2017;37:2449–62. https://doi.org/10.1523/JNEUROSCI.3229-16.2017.
40. Liu F, Lai S, Tong H, Lakey PSJ, Shiraiwa M, Weller MG, Pöschl U, Kampf CJ. Release of free amino acids upon oxidation of peptides and proteins by hydroxyl radicals. Anal Bioanal Chem. 2017;409:2411–20. https://doi.org/10.1007/s00216-017-0188-y.
41. Gómez-Mejía E, Mikkelsen LH, Rosales-Conrado N, León-González ME, Madrid Y. A combined approach based on matrix solid-phase dispersion extraction assisted by titanium dioxide nanoparticles and liquid chromatography to determine polyphenols from grape residues. J Chromatogr A. 2021;1644: 462128. https://doi.org/10.1016/j.chroma.2021.462128.
42. Xu N, Chen G, Liu H. Antioxidative categorization of twenty amino acids based on experimental evaluation. Molecules. 2017;22:2066. https://doi.org/10.3390/molecules22122066.

Publisher's note Springer Nature remains neutral with regard to jurisdictional claims in published maps and institutional affiliations.

Springer Nature or its licensor holds exclusive rights to this article under a publishing agreement with the author(s) or other rightsholder(s); author self-archiving of the accepted manuscript version of this article is solely governed by the terms of such publishing agreement and applicable law.

Supporting Information

Neuroprotective Activity of Selenium Nanoparticles Against the Effect of Amino Acid Enantiomers in Alzheimer's Disease

David Vicente-Zurdo*, Sandra Rodríguez-Blázquez, Esther Gómez-Mejía, Noelia Rosales-Conrado*, María Eugenia León-González, Yolanda Madrid

Analytical Chemistry Department, Faculty of Chemistry, Complutense University of Madrid, E-28040, Madrid, Spain

Running Title: Neuroprotective Activity of Selenium Nanoparticles Against the Effect of Amino Acid Enantiomers in Alzheimer's Disease

Journal: Analytical and Bioanalytical Chemistry

***Corresponding authors**:

D. Vicente-Zurdo davidvic@ucm.es
N. Rosales-Conrado nrosales@ucm.es

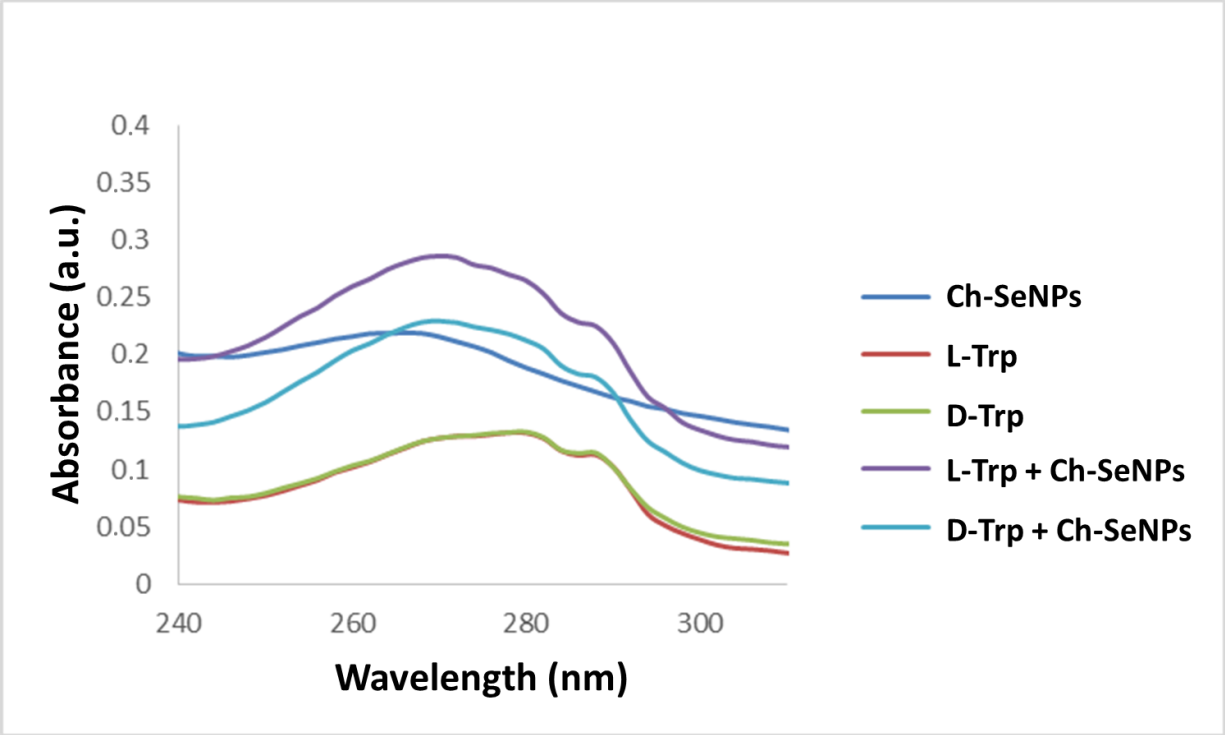


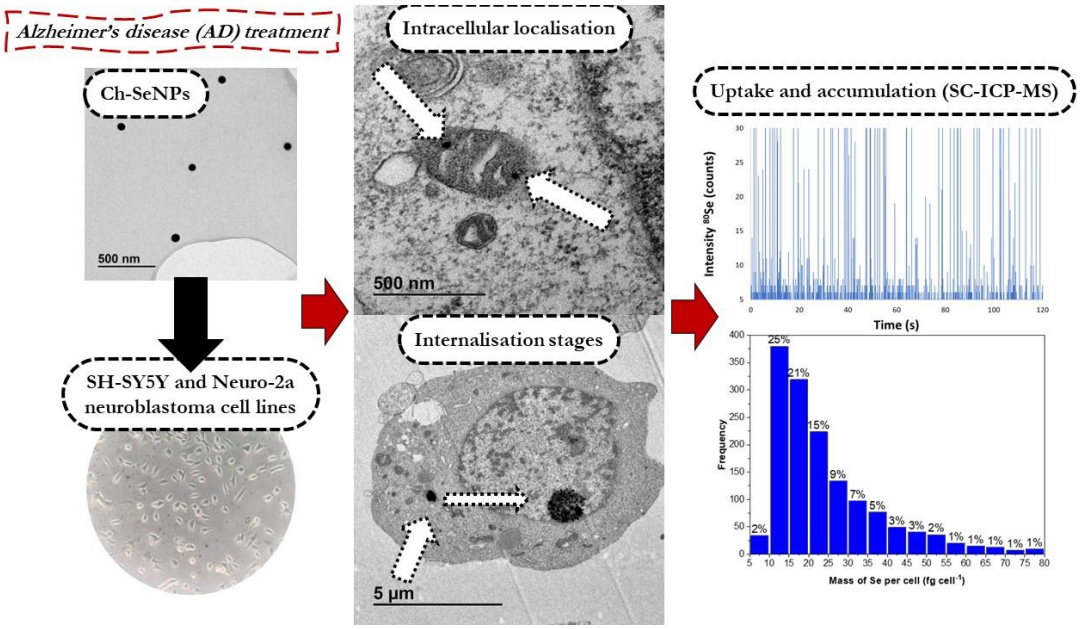
Fig. S1. UV-Vis spectra of L-Trp and D-Trp in absence and presence of Ch-SeNPs.

Artículo 6: <u>Acumulación de nanopartículas de selenio y otras especies de selenio en líneas celulares de neuroblastoma relacionadas con la enfermedad de Alzheimer mediante TEM y single cell-ICP-MS</u>

Uptake and accumulation of selenium nanoparticles and other selenium species in neuroblastoma cell lines related to Alzheimer's disease by using TEM and single cell-ICP-MS

<u>David Vicente-Zurdo</u>, Beatriz Gómez-Gómez, Iván Romero-Sánchez, Noelia Rosales-Conrado, María Eugenia León-González, Yolanda Madrid

European Journal of Medicinal Chemistry (enviado)



European Journal of Medicinal Chemistry

Uptake and accumulation of selenium nanoparticles and other selenium species in neuroblastoma cell lines related to Alzheimer's disease by using TEM and single cell-ICP-MS

--Manuscript Draft--

Manuscript Number:	EJMECH-D-22-02842
Article Type:	Full Paper
Keywords:	Alzheimer's disease; selenium nanoparticles; Cytotoxicity; intracellular localisation; single cell-ICP-MS
Corresponding Author:	David Vicente-Zurdo Complutense University of Madrid Faculty of Chemical Sciences Madrid, SPAIN
First Author:	David Vicente-Zurdo
Order of Authors:	David Vicente-Zurdo
	Beatriz Gómez-Gómez
	Iván Romero-Sánchez
	Noelia Rosales-Conrado
	María Eugenia de León-González
	Yolanda Madrid
Abstract:	Alzheimer's disease (AD) is the most prevalent neurodegenerative disease, representing 80% of the total dementia cases. The "amyloid cascade hypothesis" stablishes that the aggregation of the beta-amyloid protein (Aβ42) is the first event that subsequently triggers AD development. Selenium nanoparticles stabilised with chitosan (Ch-SeNPs) have demonstrated excellent anti-amyloidogenic properties in previous works, leading to an improvement of AD aetiology. Here, the in vitro effect of selenium species has been study to obtain a better assessment of their effects in AD treatment. Two different AD model cell lines have been used to this purpose: mouse neuroblastoma (Neuro-2a) and human neuroblastoma (SH-SY5Y). Cytotoxicity of selenium species, such as selenomethionine (SeMet), Se-methylselenocysteine (MeSeCys) and Ch-SeNPs, has been determined by MTT and flow cytometry methods. Intracellular localisation of Ch-SeNPs, and their pathway through SH-SY5Y cell line, have been evaluated by transmission electron microscopy (TEM). The uptake and accumulation of selenium species by both neuroblastoma cell lines have been quantified at single cell level by single cell- Inductively Coupled Plasma with Mass Spectrometry detection (SC-ICP-MS), being 1.2-89.5 fg Se cell-1 for Neuro-2a and 3.1-129.8 fg Se cell-1 for SH-SY5Y exposed to 250 μM Ch-SeNPs. Data obtained were statistically treated using chemometric tools. These results provide an important insight into the interaction of Ch-SeNPs with neuronal cells, which could support their potential use in AD treatment.
Suggested Reviewers:	Micaela Pescuma National Scientific and Technical Research Council mpescuma@ciefap.org.ar She is an expert in selenium nanoparticles
	M. Amélia Santos University of Lisbon Higher Technical Institute masantos@ist.utl.pt She is an expert in the finding of new drugs for neurodegenerative diseases

Powered by Editorial Manager® and ProduXion Manager® from Aries Systems Corporation

European Journal of Medicinal Chemistry

Dear Editor,

Please find enclosed the manuscript we wish to publish in European Journal of Medicinal Chemistry if considered appropriate. The present manuscript is entitled "Uptake and accumulation of selenium nanoparticles and other selenium species in neuroblastoma cell lines related to Alzheimer's disease by using TEM and single cell-ICP-MS". This paper includes original research, which has not been published, and is not being considered for publication elsewhere.

Significance of the work

Alzheimer's disease (AD) is the most prevalent neurodegenerative disease, with no treatment or cure at present. The pathogenesis of AD is characterized by the extracellular accumulation of amyloid-beta protein, with the 42 amino acid fragment ($A\beta_{42}$) being the most amyloidogenic. The aggregation of $A\beta_{42}$ is the main responsible for the neurodegeneration explained in the "amyloid cascade hypothesis". In previous works, selenium nanoparticles stabilized with chitosan (Ch-SeNPs) have demonstrated excellent anti-amyloidogenic properties, inhibiting $A\beta_{42}$ aggregation induced by metals and even disaggregating fibrils once formed, and also inhibiting the $A\beta_{42}$ aggregation enantiomerically induced by amyloidogenic amino acids. However, *in vitro* effects of Ch-SeNPs on AD model cell lines have not been studied so far. In order to consider Ch-SeNPs as a potential drug against AD, is therefore essential to evaluate their *in vitro* effect over neuronal cell lines, considering cytotoxicity, uptake and accumulation of selenium as basic parameters to take into account. Effects of Ch-SeNPs compared with other selenium species such as selenomethionine (SeMet) and Se-methylselenocysteine (MeSeCys), both naturally occurring in living organisms, is also a key fact to investigate.

Novelty statement.

In this work, several techniques and methodologies such as transmission electron microscopy (TEM), MTT and flow cytometry assays, as well as single cell-ICP-MS (SC-ICP-MS) were applied to study the effect of selenium species, especially Ch-SeNPs, over

two different cell lines: human (SH-SY5Y) and mouse (Neuro-2a) neuroblastoma cells. Ch-SeNPs were synthetized in presence of chitosan, a natural biocompatible and biodegradable alkaline chiral polysaccharide that provides additional characteristics to selenium nanoparticles. Cytotoxicity of SeMet, MeSeCys and Ch-SeNPs over a 48 h exposure to SH-SY5Y and Neuro-2a cell lines was evaluated by MTT and flow cytometry methods. Cytotoxicity results were studied in terms of bioanalytical method, neuroblastoma cell line, selenium species and exposure concentration. Internalisation of Ch-SeNPs by SH-SY5Y cells, and uptake pathway were evaluated by TEM. Ch-SeNPs were observed on the outside of the cell membrane, in the mitochondria, nucleus and nucleolus of neuroblastoma cells. SC-ICP-MS allowed the quantification at single cell level of the uptake and accumulation of SeMet, MeSeCys and Ch-SeNPs by both neuroblastoma cell lines, presenting significant variabilities between selenium species, exposure concentration and cell line. The use of chemometric tools also allowed to properly evaluate the obtained results.

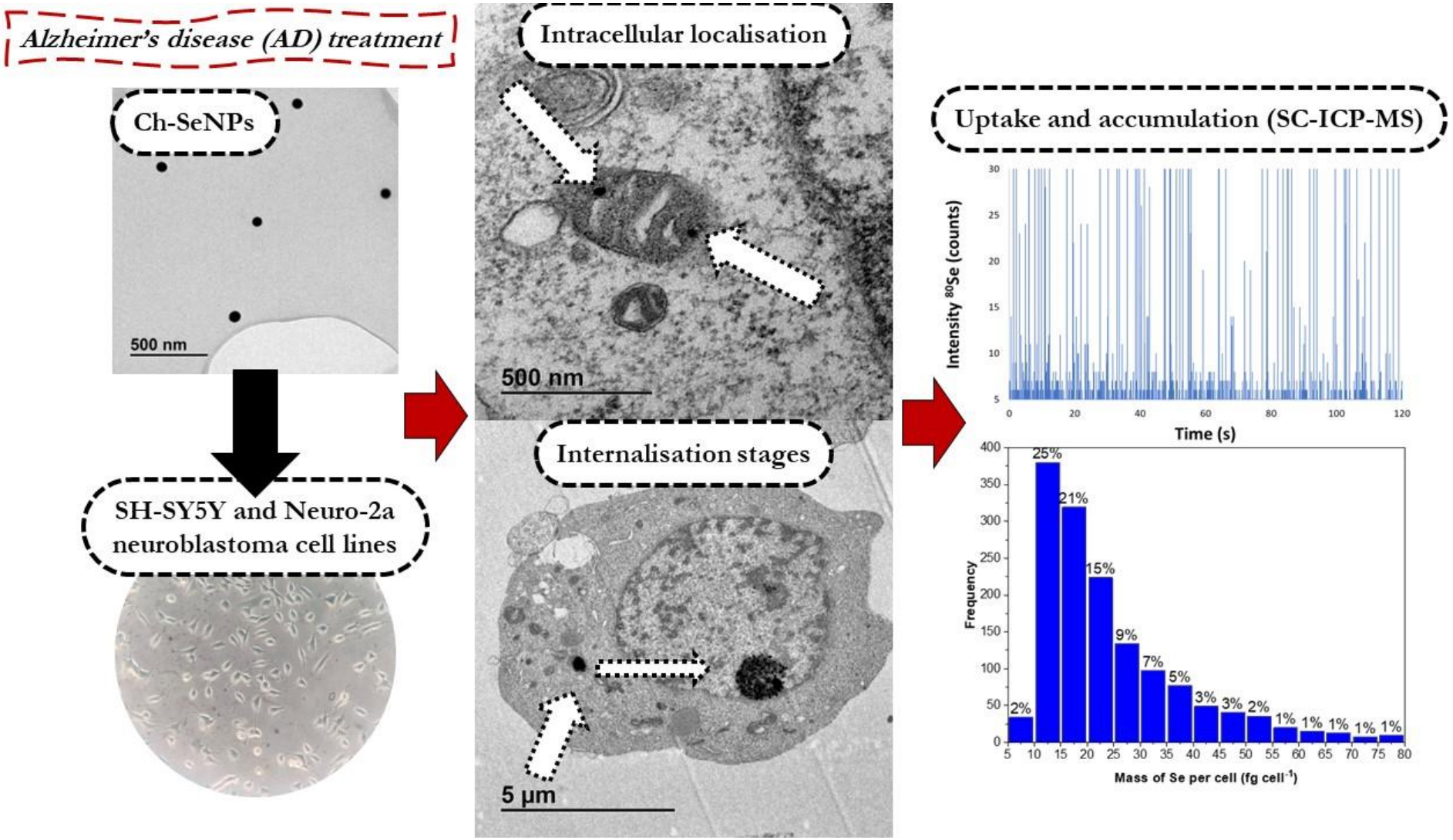
Contribution to the field

The present work evidences, for the first time, the *in vitro* effect of Ch-SeNPs on neuronal cells. The obtained results provide valuable data of the use of Ch-SeNPs as a potential drug against AD, since they are accumulated in relevant parts of the neuronal cells, such as the outside of the cell membrane, in the mitochondria, nucleus and nucleoli, were $A\beta_{42}$ and tau protein exert their neurodegeneration in the AD. Thereby, this work provides a deep insight in the use of Ch-SeNPs as a promising neuroprotective compound.

Thank you very much in advance.

Sincerely yours,

David Vicente Zurdo
Department of Analytical Chemistry, Faculty of Chemistry Sciences
Avda. Complutense s/n 28040 Madrid
e-mail: **davidvic@ucm.es**
Phone: +34 91 394 4318


Alzheimer's disease (AD) treatment
Ch-SeNPs
500 nm
SH-SY5Y and Neuro-2a neuroblastoma cell lines
Intracellular localisation
500 nm
Internalisation stages
5 µm
Uptake and accumulation (SC-ICP-MS)
Intensity ^{80}Se (counts)
Time (s)
Frequency
Mass of Se per cell (fg cell^{-1})
25%
21%
15%
9%
7%
5%
3%
3%
2%
2%
1%
1%
1%
1%

- Selenium nanoparticles (Ch-SeNPs) are promising compounds against AD
- SH-SY5Y and Neuro-2a neuroblastoma cell lines were employed as *in vitro* AD model
- Cytotoxicity of selenium species was evaluated by MTT and flow cytometry assays
- Ch-SeNPs intracellular localisation in mitochondria and nucleus was observed by TEM
- SC-ICP-MS provided quantification at single cell level of selenium accumulation

Uptake and accumulation of selenium nanoparticles and other selenium species in neuroblastoma cell lines related to Alzheimer's disease by using TEM and single cell-ICP-MS

David Vicente-Zurdo*, Beatriz Gómez-Gómez*, Iván Romero-Sánchez, Noelia Rosales-Conrado, María Eugenia León-González, Yolanda Madrid

Analytical Chemistry Department, Faculty of Chemistry Sciences, Complutense University of Madrid, E-28040, Madrid, Spain

(*) To whom correspondence must be addressed: davidvic@ucm.es, beatrgom@ucm.es, phone number: +34 91 394 5145

Abstract

Alzheimer's disease (AD) is the most prevalent neurodegenerative disease, representing 80% of the total dementia cases. The "amyloid cascade hypothesis" stablishes that the aggregation of the beta-amyloid protein ($A\beta_{42}$) is the first event that subsequently triggers AD development. Selenium nanoparticles stabilised with chitosan (Ch-SeNPs) have demonstrated excellent anti-amyloidogenic properties in previous works, leading to an improvement of AD aetiology. Here, the *in vitro* effect of selenium species has been study to obtain a better assessment of their effects in AD treatment. Two different AD model cell lines have been used to this purpose: mouse neuroblastoma (Neuro-2a) and human neuroblastoma (SH-SY5Y). Cytotoxicity of selenium species, such as selenomethionine (SeMet), Se-methylselenocysteine (MeSeCys) and Ch-SeNPs, has been determined by MTT and flow cytometry methods. Intracellular localisation of Ch-SeNPs, and their pathway through SH-SY5Y cell line, have been evaluated by transmission electron microscopy (TEM). The uptake and accumulation of selenium species by both neuroblastoma cell lines have been quantified at single cell level by single cell- Inductively Coupled Plasma with Mass Spectrometry detection (SC-ICP-MS), being 1.2-89.5 fg Se $cell^{-1}$ for Neuro-2a and 3.1-129.8 fg Se $cell^{-1}$ for SH-SY5Y exposed to 250 µM Ch-SeNPs. Data obtained were statistically treated using chemometric tools. These results provide an important insight into the interaction of Ch-SeNPs with neuronal cells, which could support their potential use in AD treatment.

Keywords

Alzheimer's disease; selenium nanoparticles; cytotoxicity; intracellular localisation; single cell-ICP-MS

1. Introduction

Neurodegenerative diseases are the leading cause of disability and the second leading cause of death globally [1]. They are characterised by progressive deterioration in various cognitive aspects, such as memory, language, executive capacity, spatial vision, personality, and behaviour [2]. Alzheimer's disease (AD) represents more than 80% of all dementia cases, often coexisting with other neurodegenerative diseases [3].

The "amyloid cascade hypothesis" is the most widely accepted explanation of the triggering of AD. Considering this hypothesis, the aggregation of beta-amyloid protein ($A\beta_{42}$) is the main responsible for neuronal damage and death, which leads to the development of AD [4]. This hypothesis is in close symbiosis with the "metal ion hypothesis", where some biometals such as Cu(II), Fe(II) and Zn(II) increase $A\beta_{42}$ extracellular aggregation [5].

Therefore, recent approaches to halt the progression of AD focus on the search for compounds capable of chelating biometals, to interfere with the "metal ion hypothesis" and, subsequently, with the "amyloid cascade hypothesis" [6]. Selenium is an essential micronutrient that can improve spatial memory and learning, increases neuronal activity, and supports synaptic preservation, being therefore useful against AD [7]. Specifically, selenium nanoparticles stabilised with chitosan (Ch-SeNPs) have demonstrated great ability to chelate biometals involved in AD, inhibit $A\beta_{42}$ fibrils aggregation induced by biometals, and even disaggregate amyloid fibrils once formed [8]. Furthermore, the same Ch-SeNPs were able to interact enantioselectively with amino acid enantiomers, thus affecting the chiral environment of $A\beta_{42}$ plaques, and inhibiting the enantioselectively-induced amyloid aggregation [9]. For these reasons, Ch-SeNPs could be a promising anti-AD agent, since they interfere in the "metal ion hypothesis", interact with amyloidogenic amino acid enantiomers, and may halt the "amyloid cascade hypothesis".

However, it becomes essential to evaluate the biological behaviour of potential neuroprotective compounds in order to consider them for future research in the field of AD. With this aim, two cell lines are widely used for *in vitro* assays: mouse (Neuro-2a) and human (SH-SY5Y) neuroblastoma cell lines [10,11]. One of most important parameters to consider is the assessment of the cytotoxicity of these neuroprotective compounds over cell lines related to AD [12]. To this purpose, two main bioanalytical methods are widely employed: 3-(4,5-dimethylthiazol-2-yl)-2,5-diphenyltetrazolium bromide (MTT) and flow cytometry assays [13,14]. Cytotoxicity is often indicated as

lethal concentration for 50% of cell population (LC_{50}) values [15]. The lower LC_{50} value, the higher cytotoxicity of the compound.

Cellular uptake and accumulation of nanoparticles are important parameters to determine their effect in living organisms [16]. These parameters depend on nanoparticles characteristics, such as the chemical composition, the surface functionalisation and diameter size as well as the cellular line under study [17]. Chitosan is a natural polymer, which can be used to stabilize nanoparticles, and enhances cellular uptake efficiency [18]. Chitosan also favours the interaction with phospholipids, which constitute the membrane of liposomes, thus favouring their endocytosis by neuronal cell lines [19].

Transmission electron microscopy (TEM) is a powerful technique which allows the visualisation of single nanoparticles in cellular compartments and organelles [20]. Mitochondria of mammalian cells are well known producers of reactive oxygen species (ROS), which contribute to many pathologies [21]. DNA oxidation in the nucleus, and especially in mitochondria, are frequently observed in neurons affected by AD [22]. For this reason, TEM may be useful to provide information on the pathway of these nanoparticles in their internalisation by cells.

However, TEM does not provide quantitative information about the concentration of nanoparticles inside a single cell [23]. With this purpose, Inductively Coupled Plasma with Mass Spectrometry detection (ICP-MS) can provide quantitative results of bioaccumulation at trace level due to its sensitivity, selectivity and accuracy [24]. While ICP-MS offers a mean value of nanoparticles uptake in a cell population, it fails to provide information about the real variability in the distribution of nanoparticles in single cells [25]. Consequently, single cell-ICP-MS (SC-ICP-MS) can be applied to obtain more in-dept information about nanoparticles and other selenium species behaviour in a cell population [26].

In the present work, Ch-SeNPs, which were considered promising anti-AD agents in previous studies [8,9], were evaluated *in vitro* using mouse (Neuro-2a) and human (SH-SY5Y) neuroblastoma cell lines. Additionally, other selenium species were evaluated for comparative purposes. Cytotoxicity of selenium species (selenomethionine (SeMet), Se-methylselenocysteine (MeSeCys) and selenium nanoparticles stabilized with chitosan (Ch-SeNPs) was evaluated by using MTT and flow cytometry methods. Internalisation of Ch-SeNPs in SH-SY5Y cells was studied by TEM, and details of the different stages

of Ch-SeNPs route are provided. Cellular uptake and accumulation of selenium species by both neuroblastoma cell lines were quantified by SC-ICP-MS. These results provide biologically valuable information about the behaviour of Ch-SeNPs and other selenium species as potential and promising compounds for the treatment of AD.

2. Materials and methods

2.1. Reagents and standards

All solvents and reagents used were of analytical grade. Milli-Q water, from a Milli-Q water purification system (Millipore, Bedford, MA, USA), with 18 MΩ cm^{-1} was used throughout all the experiments. Selenomethionine (SeMet) and Se-methylselenocysteine (MeSeCys) from Sigma-Aldrich (St. Louis, MO, USA) were employed in cytotoxicity and Single cell-Inductively Coupled Plasma with Mass Spectrometry detection (SC-ICP-MS) analysis.

2.2. Culture of Neuro-2a and SH-SY5Y cells

Two different neuroblastoma cell lines, mouse neuroblastoma (Neuro-2a, CCL-131) and human neuroblastoma (SH-SY5Y, CRL-2266), which are related to AD [10,11], were acquired from the ATCC. Cells were stored in 90% FBS (ThermoFisher Scientific) and 10% DMSO (Sigma-Aldrich) at -130 ºC in liquid nitrogen vapor until use. Neuro-2a cells (*Figures 1.c* and *1.d*) were kept at 37 ºC and 5% CO_2 in a Dulbecco's Modified Eagle Medium (DMEM) supplemented with 1% penicillin/streptomycin and 10% fetal bovine serum (FBS), acquired from ThermoFisher Scientific (Madrid, Spain). SH-SY5Y cells (*Figures 1.a* and *1.b*) were kept at 37 ºC and 5% CO_2 in a Dulbecco's Modified Eagle Medium/Nutrient Mixture F-12 (DMEM/F12) supplemented with 1% penicillin/streptomycin and 10% fetal bovine serum (FBS), acquired from ThermoFisher Scientific (Madrid, Spain). For the subculture procedure, phosphate-buffered saline (PBS) at pH 7.4 and trypsin-EDTA (0.05%) from ThermoFisher Scientific were employed. Cells were checked for absence of mycoplasma infection with the Look Out Mycoplasma PCR Detection Kit acquired from Sigma-Aldrich (Madrid, Spain).

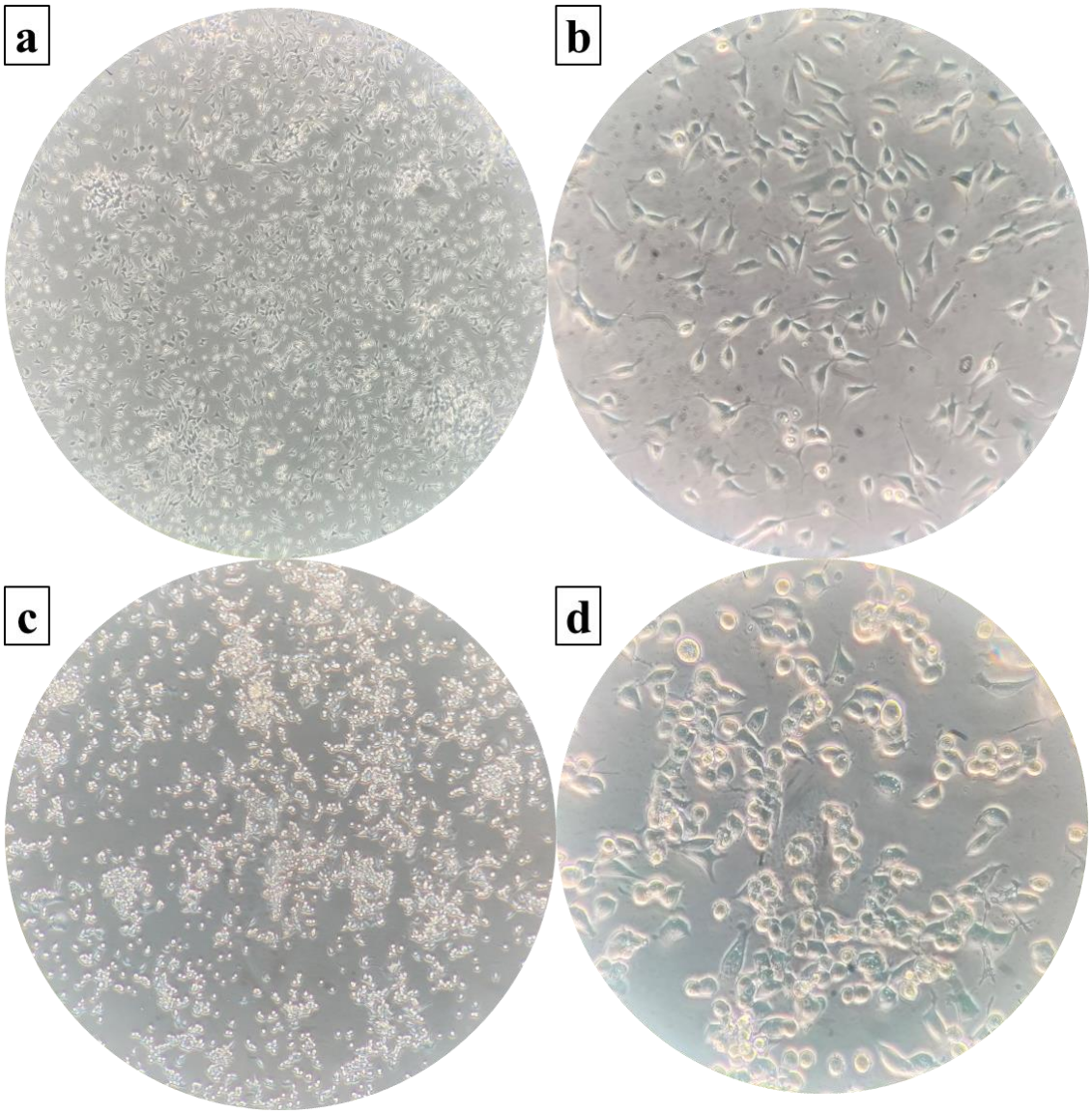


Figure 1. Optical microscope images of confluent neuroblastoma cell lines: a) SH-SY5Y at 10X magnification power; b) SH-SY5Y at 40X magnification power; c) Neuro-2a at 10X magnification power; d) Neuro-2a at 40X magnification power.

2.3. Synthesis of selenium nanoparticles

Selenium nanoparticles stabilised with chitosan (Ch-SeNPs) were synthetized from Na_2SeO_4 (99%, Sigma-Aldrich), L-ascorbic acid (Sigma-Aldrich) and chitosan (Sigma-Aldrich) dissolved in 3% of acetic acid (Panreac, Barcelona, Spain) as described in previous studies [8]. Ch-SeNPs were dialysed by using dialysis sacks of 12 kDa (Sigma-Aldrich) and were stored at 4 ºC under darkness until use. Characterisation was performed by using a JEOL JEM 1400 Plus transmission electron microscope (TEM) at 100 kV and

energy-dispersive X-Ray spectroscopy (EDXS). ImageJ software was employed to measure Ch-SeNPs diameter through TEM micrographs (n > 100).

Ch-SeNPs stability was studied in both culture mediums with 10% FBS: DMEM (Neuro-2a) and DMEM/F12 (SH-SY5Y). In 60 mm diameter dishes from ThermoFisher Scientific, 3mL of 50 µM Ch-SeNPs were incubated in triplicate in the corresponding culture medium at 37 ºC with 5% CO_2 during 48 h. Afterwards, culture medium was observed by TEM using a JEOL JEM 1400 Plus microscope at 100 kV and EDXS. ImageJ software was employed to compare Ch-SeNPs diameter before and after the incubation in DMEM and DMEM/F12 medium (n > 100).

2.4. MTT and flow cytometry assays

To assess the cytotoxicity of selenium species over Neuro-2a and SH-SY5Y cell lines, 3-(4,5-Dimethylthiazol-2-yl)-2,5-diphenyltetrazolium bromide (MTT) and flow cytometry methods were employed.

For MTT assay, cells were seeded in 96-well plates at a density of $8 \cdot 10^3$ cells well^{-1}. After 24 h, culture medium was removed and cells were exposed to SeMet, MeSeCys and Ch-SeNPs at various compound concentrations (50-1000 µM) during 48 h. Afterwards, 20 µL of 5 mg mL^{-1} MTT solution in PBS was added to each well followed by an incubation at 37 ºC during 4 h. Then, culture medium was removed and 100 µL of dimethyl sulfoxide (DMSO) from Scharlab (Barcelona, Spain) were added to dissolve formazan crystals. Absorbance was recorded at 570 nm, after 15 min of incubation at room temperature, using a microplate reader (Sunrise, Tecan). Cell viability was calculated using the equation 1.

$$\%Cell\ viability = \frac{A_S - A_{C-}}{A_{C+} - A_{C-}} \times 100 \quad (1)$$

Being A_S, A_{C-} and A_{C+} the absorbances of the sample, the negative control, and the positive control, respectively. At least 5 concentration points and 5 replicate wells concentration^{-1} were used. Positive and negative control groups were employed in parallel for each experiment.

For the flow cytometry assay, cells were seeded in 60 mm diameter dishes, from ThermoFisher Scientific, at a density of $4 \cdot 10^5$ cells dish^{-1}. After 24 h, culture medium was removed, and cells were exposed separately to SeMet, MeSeCys and Ch-SeNPs at

various compound concentrations (50-1000 µM) during 48 h. Afterwards, culture medium was removed, cells were washed with PBS and trypsinized. Cells were neutralized with culture medium and centrifuged. Supernatant was removed and cells were resuspended in 1 mL of PBS in a FACScalibur tube (BD Biosciences). For negative controls, 200 µL of MeOH from Scharlab (Barcelona, Spain) were added to the FACScalibur tubes. For positive controls and samples, propidium iodide (IP), from ThermoFisher Scientific, in PBS was added to each tube to a final concentration of 2 µg mL^{-1}. Blank solutions had no fluorochrome. Samples were measured with a Becton Dickinson FACScalibur (BD Biosciences) flow cytometer equipped with CellQuest Pro 4.0.2 software (BD Biosciences). IP fluorescence was measured at an emission wavelength of 617 nm after excitation at 535 nm. Cell viability was obtained based on the intensity of IP fluorescence through damaged cell membranes, indicating the percentage of dead cells. At least 5 concentration points and 5 replicate dish $concentration^{-1}$ were used. Positive and negative control groups were employed in parallel for each experiment.

Cytotoxicity data of SeMet, MeSeCys and Ch-SeNPs over Neuro-2a and SH-SY5Y neuroblastoma cell lines, using MTT and flow cytometry assays, was evaluated to determine the lethal concentration for 50% of cell population (LC_{50}) for every compound, cell line and bioanalytical method. Data were adjusted to a logarithmic regression curve, by using the equation 2.

$$y = a\ln(x) + b \quad (2)$$

Being a the slope, b the intercept, y the percentage of viable cells and x the concentration of the compound. Calculated LC_{50} were compared using ANOVA.

2.5. Transmission electron microscopy analysis

To visualize the internalisation of Ch-SeNPs inside SH-SY5Y cell line, cells were seeded at a density of $2 \cdot 10^6$ $cells\ dish^{-1}$ in 100 mm diameter dishes. After 24 h, culture medium (DMEM/F12 with 10% FBS) was removed, and cells were exposed to 50 µM Ch-SeNPs during 48 h. Afterwards, culture medium was recovered to study the SH-SY5Y cell death induced by Ch-SeNPs in non-adherent cells. Adherent, viable, SH-SY5Y cells were washed with PBS and trypsinized. Cells were neutralized with 8 mL of culture medium and centrifuged. Supernatant was removed, cells were washed twice with 10 mL

of PBS and centrifuged. Supernatant was removed, and a volume of 1 mL of paraformaldehyde/glutaraldehyde/PBS (4/2.5/93.5) from Electron Microscopy Sciences was added to each sample. Cells were stored at 4 ºC during 4 h until fixation process was achieved. Afterwards, cells were washed twice with 1 mL of PBS and stored at 4 ºC overnight.

To perform post fixation procedure, cells were centrifuged, supernatant was removed and 1 mL of osmium tetroxide 1% (w/w) in distilled water (Electron Microscopy Sciences) was added. Cells were kept at room temperature under darkness during 1 h. Cells were washed twice with 1 mL of distilled water during 10 min. Cells were dehydrated during 15 min in increasing percentages of acetone (30/50/70/80/90/95/100) from Panreac. Acetone was progressively removed by adding growing percentages of Spurr resin (25% during 1 h/50% during 1 h/75% during 2 h/100% overnight) from Electron Microscopy Sciences. Cells were incubated at 70 ºC during 48 h, cut with a microtome and visualized with a JEOL JEM 1400 Plus transmission electron microscope. At least 3 replicate dish treatment were used. A positive control group was employed in parallel.

ImageJ software was used to measure SH-SY5Y cells and nucleus diameter, as well as liposomes and mitochondria sizes in TEM micrographs (n = 10). OriginPro 2021 software was employed to graphically represents data obtained.

2.6. SC-ICP-MS analysis

To evaluate the uptake and accumulation of the selenium species (SeMet, MeSeCys and Ch-SeNPs) at single cell level, an analytical methodology based on the use of single cell-ICP-MS (SC-ICP-MS) was employed. Neuro-2a and SH-SY5Y cells were seeded in 60 mm diameter dishes at a density of $4 \cdot 10^5$ cells $dish^{-1}$. After 24 h, culture medium was removed and cells were exposed to selenium species at 10, 50 and 250 µM concentration levels during 48 h. After the exposition, culture medium was removed, cells were washed with PBS and trypsinized. Then, cells were centrifuged and washed three times with 3 mL of PBS until a concentration of $6 \cdot 10^4$ cells mL^{-1} before their measurement by SC-ICP-MS. Three replicates for every tested condition and positive controls were performed.

SC-ICP-MS analysis was carried out by using an Agilent 7700x collision/reaction cell ICP–MS (using H_2 reaction gas) from Agilent Technologies (Santa Clara, CA, USA), equipped with a micromist nebulizer combined with a total consumption spray chamber (High Sensitivity Single-Cell Sample Introduction System for ICP-MS, Glass Expansion, Port Melbourne, Australia). Samples and standards were introduced into the plasma at a flow rate of 10 µL min^{-1}, using an Infusion Syringe Pump from FisherScientific. Measurements were carried out with time resolved analysis (TRA) mode during 2 min for each sample, stablishing a dwell time of 3 ms and monitoring the isotope ^{80}Se. Transport efficiency was calculated daily through the particle frequency method using citrate-gold nanoparticles (citrate-AuNPs) reference material LGC5050, nominal diameter (32.7 ± 2) nm, from LGC (Teddington, UK), diluted until a concentration of 40 ng L^{-1} and EQ Four Element Calibration Beads containing natural abundance europium ($^{151}Eu/^{153}Eu$), at a concentration of 33000 particles mL^{-1} (Fluidigm Corporation, San Francisco, CA, USA). Quantification curve of ionic selenium was prepared daily from concentrations between 0.25 to 25 µg L^{-1} from a selenium standard for ICP of 1000 mg L^{-1} obtained from Merck (MA, USA) in Milli-Q water. Raw signal from SC-ICP-MS analysis was processed by applying an iterative procedure [27,28].

OriginPro 2021 software was employed to plot the selenium accumulation from SeMet, MeSeCys and Ch-SeNPs exposure to Neuro-2a and SH-SY5Y individual cells. Data were compared in terms of neuroblastoma cell line, selenium species under study and their concentration.

2.7. Statistical analysis

To evaluate the obtained results chemometric tools, such as analysis of variance (ANOVA) and Fisher least significant difference (LSD) at 95% confidence level, were employed. Ch-SeNPs sizes under incubation in different culture mediums ($n > 100$), cytotoxicity results ($n = 5$), and cell structures diameters during the stages of Ch-SeNPs internalisation ($n = 10$) were evaluated. Statistical analysis of data was carried out using Statgraphics Centurion XIX (Statgraphics Technologies, Inc., Warrenton, VA, USA).

3. Results and discussion

3.1. Characterisation of selenium nanoparticles

Ch-SeNPs were dialysed and characterised using TEM and EDXS (*Figure 2*). Ch-SeNPs sizes in dialysis medium and under the effect of the incubation parameters of neuroblastoma cell cultures were measured by using ImageJ software. Ch-SeNPs diameters were compared by ANOVA at 95% confidence level (n > 100).

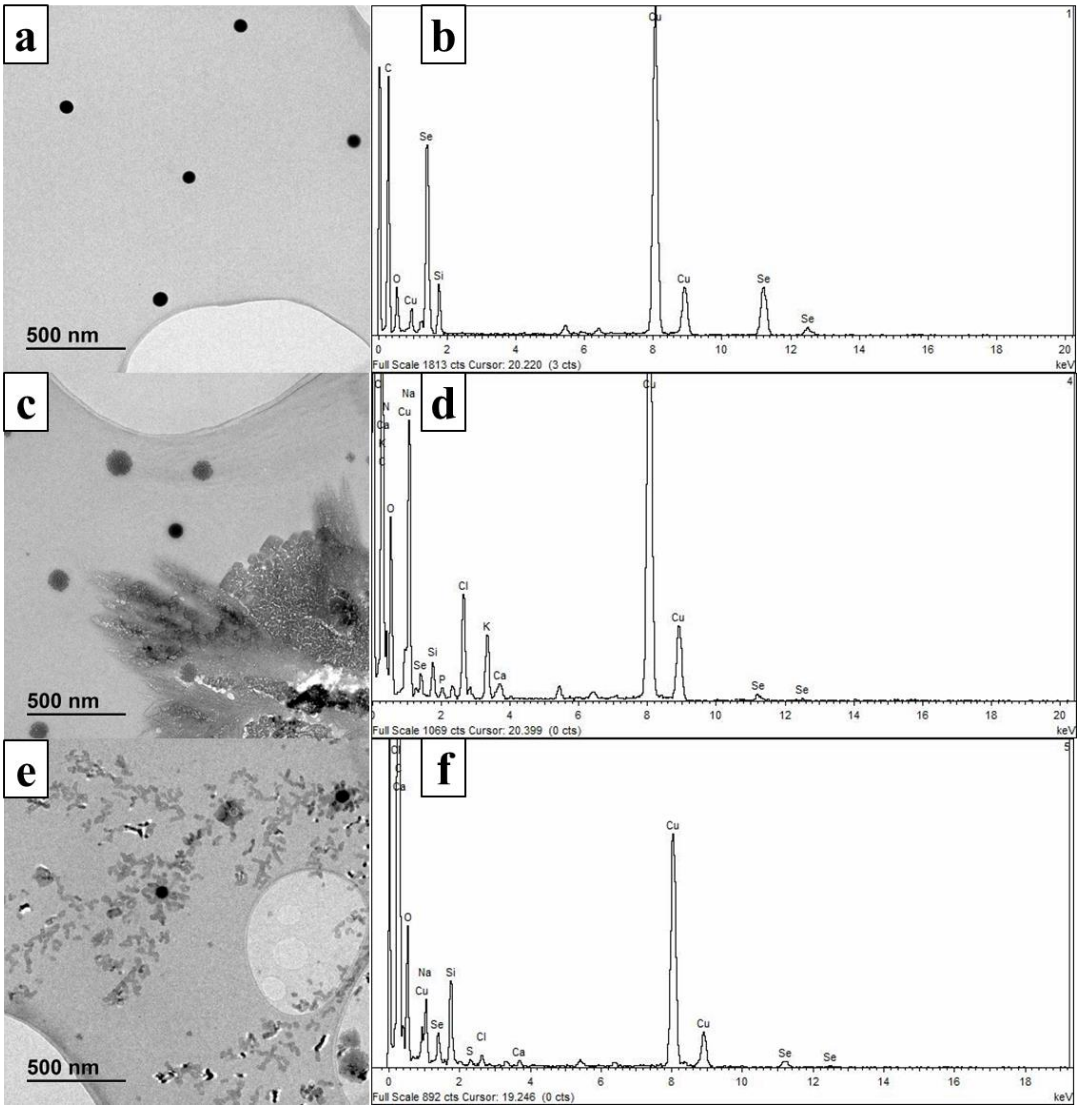


Figure 2. TEM micrographs (a, c, e) and EDXS (b, d, f) of 50 µM Ch-SeNPs in different mediums: a) and b) Ch-SeNPs in synthesis medium; c) and d) Ch-SeNPs incubated at 37 ºC during 48 h in Neuro-2a culture medium; e) and f) Ch-SeNPs incubated at 37 ºC during 48 h in SH-SY5Y culture medium.

Ch-SeNPs after dialysis presented a mean diameter of (60 ± 1) nm (*Figure 2.a*), in Neuro-2a culture medium (61 ± 1) nm (*Figure 2.c*) and (60 ± 2) nm in SH-SY5Y culture medium (*Figure 2.e*). Selenium presence was confirmed by EDXS analysis under all conditions studied, among other elements intrinsic to the TEM procedure (Cu, C and Si) (*Figures 2.b, d, f*). For Ch-SeNPs incubation in Neuro-2a (*Figure 2.d*) and SH-SY5Y (*Figure 2.f*) mediums, EDXS also showed the presence of elements belonging to culture medium composition (Na, K, Ca and Cl; from NaCl, KCl, $CaCl_2$ and $NaHCO_3$). Additionally, Ch-SeNPs interaction with some SH-SY5Y culture medium components was observed (*Figure 2.e*), when compared to Neuro-2a culture medium (*Figure 2.c*). No statistical differences in Ch-SeNPs diameters were found between incubations in different culture mediums by using ANOVA at 95% confidence level. Thus, Ch-SeNPs remained stable during incubation conditions (37 ºC, 48 h) in both Neuro-2a and SH-SY5Y neuroblastoma cell lines.

3.2. Cytotoxicity of selenium species

To assess the toxic effects of SeMet, MeSeCys and Ch-SeNPs over Neuro-2a and SH-SY5Y neuroblastoma cell lines, MTT and flow cytometry methods were employed. Results of cell viability for every cell line and selenium species are represented in *Figure 3*. As it can be appreciated, cytotoxicity at 48 h was higher as the concentration of selenium species increased, while both determination methods showed a similar pattern.

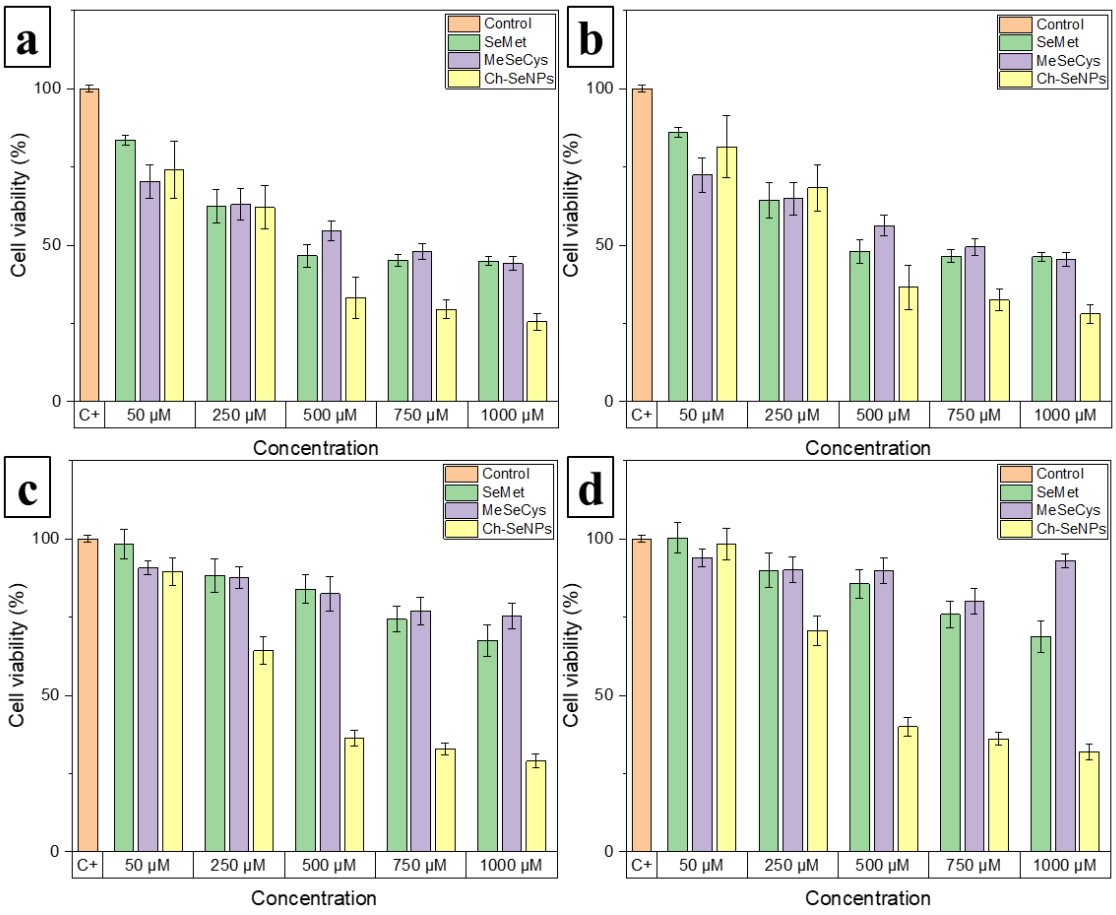


Figure 3. Cytotoxicity of selenium species at 48 h, represented as percentage of viable cells, calculated by MTT and flow cytometry bioanalytical methods. a) MTT method on Neuro-2a cell line; b) Flow cytometry method on Neuro-2a cell line; c) MTT method on SH-SY5Y cell line; d) Flow cytometry method on SH-SY5Y cell line. Results are expressed as mean ± SD (n = 5).

Viable cells for every selenium species and concentration under exposure were adjusted to a logarithmic regression curve, as explained in "*2.4. MTT and flow cytometry assays*" section. LC_{50} values were calculated for every selenium species, both neuroblastoma cell lines and both bioanalytical methods, and compared using chemometric tools. Obtained results are presented in *Table 1*.

Table 1. Cytotoxicity of selenium species expressed as LC_{50} (μM) regarding Neuro-2a and SH-SY5Y neuroblastoma cell lines, by using MTT and flow cytometry assays. Data are expressed as mean ± standard deviation (n = 5). Mean values with a common letter indicate no significant differences at p-values > 0.05, according to ANOVA and Fisher LSD tests.

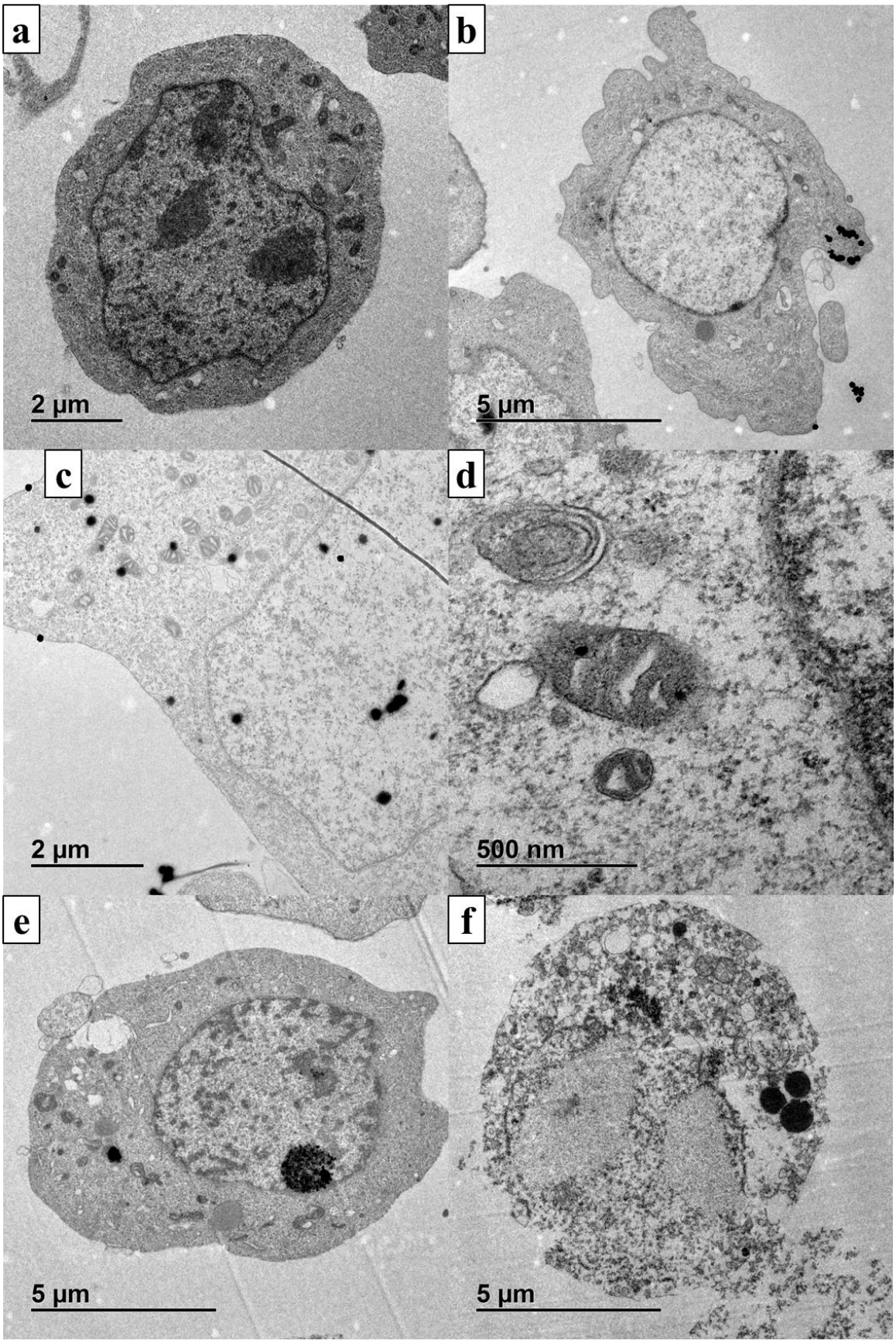
Species	LC_{50} (μM); MTT		LC_{50} (μM); Flow cytometry	
	Neuro-2a	SH-SY5Y	Neuro-2a	SH-SY5Y
SeMet	550 ± 20^{d}	$> 1000^{h}$	610 ± 20^{e}	$> 1000^{h}$
MeSeCys	690 ± 40^{f}	$> 1000^{h}$	830 ± 70^{g}	$> 1000^{h}$
Ch-SeNPs	250 ± 30^{a}	350 ± 10^{b}	330 ± 20^{b}	430 ± 10^{c}

Firstly, cytotoxicity results revealed that flow cytometry method offered statistically higher LC_{50} values for Neuro-2a cell line than those obtained by MTT method. In contrast, LC_{50} values for SH-SY5Y cell line obtained by flow cytometry methods were, in general, statistically similar. Secondly, mouse neuroblastoma cell line (Neuro-2a) was more sensitive to selenium species, with lower LC_{50} values than human neuroblastoma cell line (SH-SY5Y). As expected, Ch-SeNPs were the most toxic species, probably due to the non-natural occurrence in living organism. On the other hand, organic selenium-containing amino acids (SeMet and MeSeCys) were the less cytotoxic species, possibly due to their essential role in cell metabolism.

These results provided valuable information about the concentration of Ch-SeNPs, SeMet and MeSeCys, which is relatively safe to perform *in vitro* studies in AD field. For this reason, Ch-SeNPs at 50 μM, which have demonstrated interesting anti-amyloidogenic properties in previous studies carried out by Vicente-Zurdo et al., could be considered a standard concentration for *in vitro* studies with SH-SY5Y cell line, being seven times lower than LC_{50} [8,9].

3.3. Intracellular localisation of selenium nanoparticles in neuroblastoma cell lines

The interest in the use of Ch-SeNPs as a potential drug against AD is increasing, mainly supported by previous studies in which selenium nanoparticles stabilized with chitosan could inhibit $A\beta_{42}$ aggregation induced either by metal ions or amino acid enantiomers at 50 μM [8,9]. With this aim, effect of Ch-SeNPs exposition over SH-SY5Y and Neuro-2a cell lines was studied by TEM. Thereby, SH-SY5Y and Neuro-2a cells were incubated during 48 h with and without 50 μM of Ch-SeNPs, a concentration seven times lower than the LC_{50} for human cell line. TEM micrographs of human neuroblastoma cell line under the effect of selenium nanoparticles are shown in *Figure 4*, since Ch-SeNPs internalisation in mouse neuroblastoma cell line could not be evaluated due to their lower LC_{50} and the low sensitivity of TEM.



1

Figure 4. Micrographs of Ch-SeNPs internalisation in SH-SY5Y cells observed by TEM. a) Control SH-SY5Y cell; b) SH-SY5Y cell at early stage of Ch-SeNPs internalisation; c) SH-SY5Y cell at intermediate stage of Ch-SeNPs internalisation; d) Ch-SeNPs location inside mitochondria; e) SH-SY5Y cell at advanced stage of Ch-SeNPs internalisation; f) Dead SH-SY5Y cell due to Ch-SeNPs effect.

Control SH-SY5Y cells, incubated in absence of Ch-SeNPs, are shown in *Figure 4.a*. Typically, they presented a cell diameter, limited by the cell membrane, of (7.7 ± 0.4) µm (*Figure 5*). Cell membrane morphology of control cells was mainly circular, with the double nuclear membrane separating the cytoplasm from the nucleus. Nuclei of control cells had a diameter of (5.5 ± 0.3) µm, containing within them between 1 and 3 nucleoli with diameters of (1.16 ± 0.06) µm (*Figure 5*). These results are in consonance with the number of nucleoli per nucleus and their diameter in SH-SY5Y cell line, depending on the cell-cycle progression and proliferation, and their stress response [29].

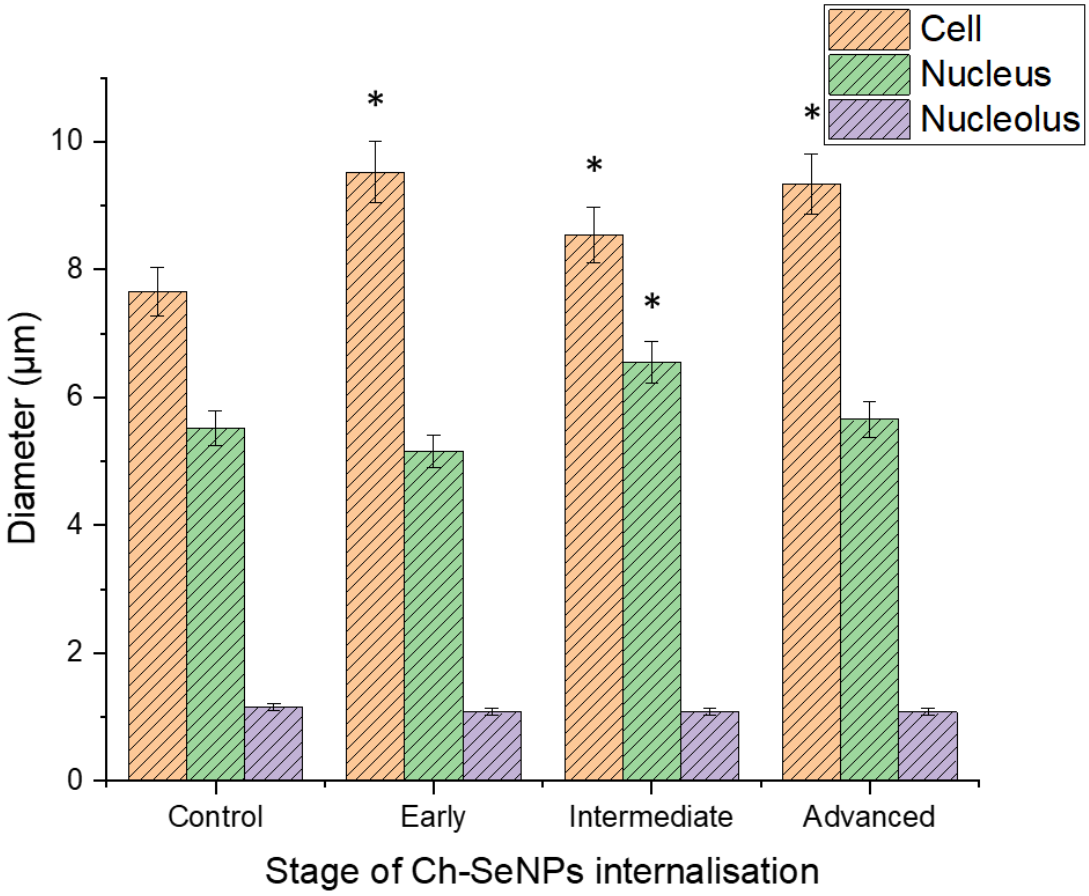


Figure 5. SH-SY5Y cell structures diameters (µm) during the stages of Ch-SeNPs internalisation (n = 10), measured by ImageJ in TEM micrographs. * $p < 0.05$ compared to control.

However, when SH-SY5Y cells were exposed to Ch-SeNPs, internalisation of the latter was observed. SH-SY5Y cells treated with Ch-SeNPs could be classified in three categories, depending on the stage of internalisation of these nanoparticles. All of them had between 1 and 3 nucleoli per nucleus, with diameters of (1.08 ± 0.05) µm, similarly to control cells (*Figure 5*). It could be observed that in early stages of Ch-SeNPs internalisation, the cell membrane underwent an expansion, with a diameter of (9.5 ± 0.5) µm (*Figure 5*), and lost its circular morphology for an irregular one (*Figure 4.b*). Liposomes, with diameters ranging from 0.22 to 1.67 µm, were released by the cell membrane and endocytosis of Ch-SeNPs was achieved by SH-SY5Y cells, locating selenium nanoparticles inside the cytosol. It is important to notice that chitosan, which stabilises selenium nanoparticles, is reported to interact with phospholipids present in the liposome membrane, and thus enhancing cellular uptake [18,19]. While this process occurs, Ch-SeNPs are able to adhere to the outside of the cell membrane, likely due to the interaction of chitosan with the phospholipids in the membrane, as can be seen in *Figure 4.b*, where they can probably inhibit $A\beta_{42}$ extracellular aggregation, mainly responsible of the development of AD, or even disaggregate amyloid fibrils [8]. This early stage of the internalisation is characterized by the presence of Ch-SeNPs in the outside of the cell membrane and in the outermost parts of the cytosol, with none of the selenium nanoparticles inside the cell nucleus, maintaining the latter a diameter of (5.2 ± 0.3) µm (*Figure 5*).

In intermediate stages of Ch-SeNPs internalisation, cell membrane recovered its circular morphology (*Figure 4.c*), with a diameter of (8.5 ± 0.4) µm, higher than control cells (*Figure 5*). In this point, Ch-SeNPs are spread between the cytosol and the nucleus, demonstrating their ability to cross the double nuclear membrane, with diameters of (6.5 ± 0.3) µm, slightly higher than control (*Figure 5*). Regarding Ch-SeNPs location in the cytosol, selenium nanoparticles showed a high affinity for internalisation in mitochondria (*Figure 4.d*). These mitochondria were 221 to 282 nm wide and 404 to 706 nm long, while the presence of Ch-SeNPs within them could provide antioxidant properties due to the possible interaction with the electron transport chain that occurs inside. This intermediate stage of the Ch-SeNPs internalisation is characterized by the presence of most of the selenium nanoparticles inside the cell, distributed between the mitochondria and inside the nucleus in a disperse way, while some of them remained attached to the outside of the cell membrane (*Figure 4.c*).

Finally, in advanced stages of Ch-SeNPs internalisation, cell membrane diameter presented a slight increase, with a diameter of (9.3 ± 0.5) µm (*Figure 5*), while maintaining its circular morphology (*Figure 4.e*). At this point, most of Ch-SeNPs have entered inside the nuclei, with diameters of (5.7 ± 0.3) µm and similar to control ones (*Figure 5*), building up vast structures of selenium nanoparticles with diameters between 1.28 and 1.42 µm. However, it can be noticed the presence of few Ch-SeNPs inside the nucleolus of the nucleus (*Figure 4.e*). This advanced stage of Ch-SeNPs internalisation is characterized by some small clusters of selenium nanoparticles in the cytosol, with diameters ranging from 0.32 to 0.37 µm, while most of Ch-SeNPs are forming large structures inside nuclei, and even entering inside nucleoli. AD pathology also is characterized by the hyperphosphorylation of tau protein (p-tau), forming neurofibrillary tangles (NFTs) inside neurons. The presence of p-tau has been detected in the cytosol, nucleus and nucleolus of SH-SY5Y, and cellular stress promotes phosphorylation of p-tau through Thr_{231} residue inside nucleoli [30]. Due to the presence of Ch-SeNPs, in advanced stages of SH-SY5Y internalisation, in the same places that p-tau aggregates in NFTs, it could be possible that Ch-SeNPs also had a role against this secondary hallmark of AD progression, regarding the antioxidant capacity of selenium nanoparticles, and should be further investigated.

In order to observe the SH-SY5Y cell death caused by Ch-SeNPs, non-adherent cells, which represents between 2 and 10% of the total, were visualized by TEM after 48 h of incubation with 50 µM selenium nanoparticles (*Figure 4.f*). It can be seen the partial loss of the cell membrane integrity, with diameters ranging from 7.17 to 10.67 µm, as well as the destruction of the nucleus structure. In this final stage, the number of vacuoles reached its maximum and can be also appreciated Ch-SeNPs clusters, with diameters from 0.66 to 0.92 µm, inside the cells.

These results confirmed the Ch-SeNPs internalisation inside SH-SY5Y neuroblastoma cell line. Moreover, it could be observed the three stages of the internalisation (early, intermediate and advanced), providing valuable insight into the effect of Ch-SeNPs on SH-SY5Y cells. Thus, it could be concluded that Ch-SeNPs attach to the external surface of the cell membrane at early and intermediate stages, which could be of interest in AD treatment, as $A\beta_{42}$ is accumulated and aggregated there, and Ch-SeNPs are well known for their anti-amyloidogenic properties [8,9]. Additionally, in intermediate stages, Ch-SeNPs are also located in mitochondria. Given that mammalian

mitochondria are a major producer of ROS, which contributes to many pathologies, and that mitochondrial DNA oxidation is frequently observed in AD, Ch-SeNPs could probably exert their antioxidant properties and counteract oxidative stress in mitochondria [21,22]. In advanced stages, Ch-SeNPs are mostly located inside the nuclei, and in a lesser extent inside the nucleoli, of SH-SY5Y cells. Since p-tau can be also found in the nucleus and nucleolus of neuronal cells, it should be interesting to explore the role of Ch-SeNPs in the NFTs formation during AD development [30].

3.4. Selenium uptake and accumulation by Neuro-2a and SH-SY5Y neuroblastoma cell lines

As it has been stated in the previous section, "*3.3. Intracellular localisation of selenium nanoparticles in neuroblastoma cell lines*", accumulation of selenium species by neuroblastoma cell lines presents high variability. For this reason, conventional methods such as ICP-MS are no longer representative for the quantification of uptake and accumulation of selenium species in cell populations. With this aim, SC-ICP-MS has been chosen as a powerful tool to provide quantitative information about the real distribution of selenium per individual cell.

To quantify accumulation of non-nanoparticulated selenium species (SeMet and MeSeCys) and Ch-SeNPs, three concentration levels, all below LC_{50} criteria previously stated in "*3.2. Cytotoxicity of selenium species*" section, were chosen (10, 50 and 250 µM). SH-SY5Y and Neuro-2a neuroblastoma cell lines were incubated during 48 h in presence of these selenium species. Due to the elevated sensitivity of SC-ICP-MS technique and the reduced number of steps for its analysis, Ch-SeNPs were detected in both neuroblastoma cell lines, in contrast to TEM analysis.

Figure 6.a displays a representative example of a time scan obtained after SC-ICP-MS analysis of SH-SY5Y cells exposed to 250 µM MeSeCys, in which several events above the signal background can be observed. Time-resolved transient signals provided information about the number of cells which accumulate selenium (frequency) and the amount of selenium inside every single cell (intensity). Unfortunately, a significant number of events were only detected when SH-SY5Y cells were incubated with 50 µM and 250 µM SeMet, and 250 µM MeSeCys. Likewise, no single Neuro-2a cells were found in the temporal profile except for those treated with 250 µM SeMet. However, as

opposed to the rest of selenium species, signal spikes for cells incubated with Ch-SeNPs were detected for both neuroblastoma cell lines at all concentrations studied, which may indicate that Ch-SeNPs would be more readily accumulated by both neuroblastoma cell lines than organic selenium species. This fact may be due to the chitosan, which stabilizes the selenium nanoparticles, and it has properties that enhance cellular uptake and accumulation [18,19].

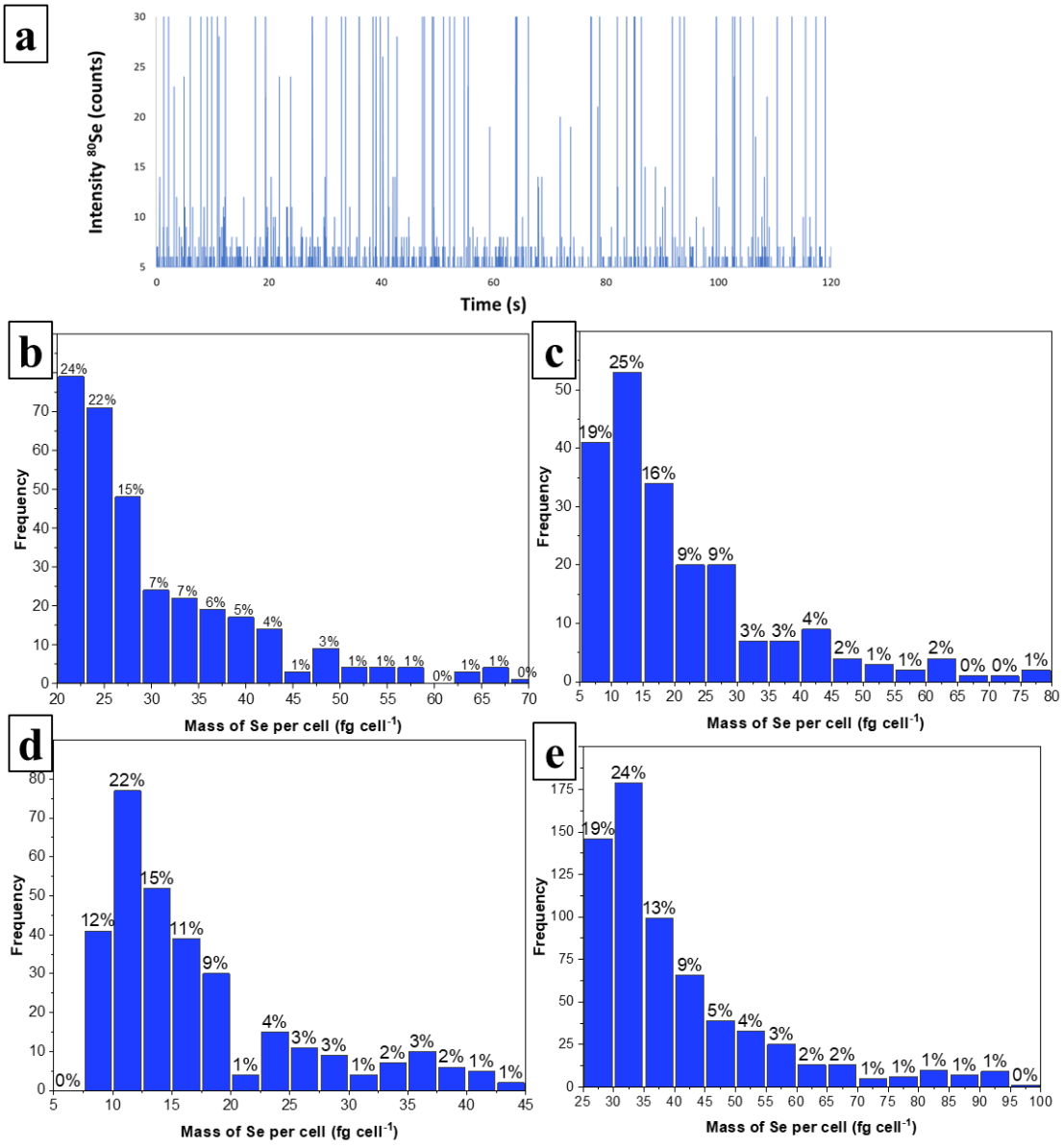


Figure 6. Time-resolved scan of ^{80}Se obtained for SH-SY5Y cells exposed to 250 µM MeSeCys (a) and frequency histograms (b-e) for SH-SY5Y and Neuro-2a cell lines incubated with non-nanoparticulated selenium species at different concentrations: b) Neuro-2a + 250 µM SeMet; c) SH-SY5Y + 250 µM MeSeCys; d) SH-SY5Y + 50 µM SeMet; e) SH-SY5Y + 250 µM SeMet.

The amount of selenium species (expressed as Se) at single-cell levels was calculated from time-resolved transient signals by using an external calibration curve, followed by data processing as described in the experimental section. Most of the cells (up to 83%) belonging to the populations under study accumulated between 5 and 35 fg of Se per cell, independently of the selenium species exposed, non-particulated (*Figure 6*) or Ch-SeNPs (*Figure 7*), and neuroblastoma cell line.

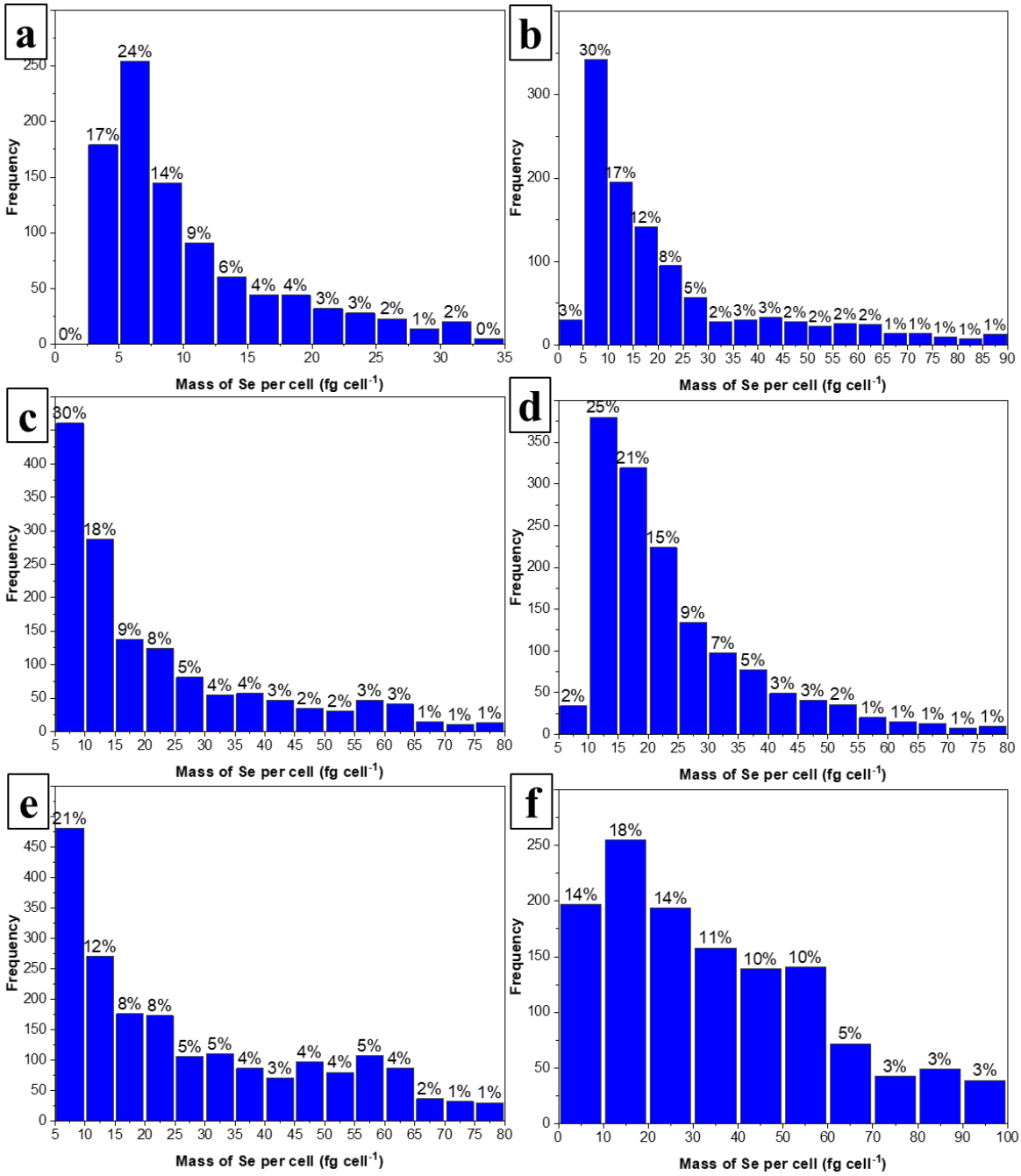


Figure 7. Frequency histograms of ^{80}Se from SC-ICP-MS analyses for Neuro-2a and SH-SY5Y cell lines incubated with Ch-SeNPs at different concentrations: a) Neuro-2a + 10 µM Ch-SeNPs; b) SH-SY5Y + 10 µM Ch-SeNPs; c) Neuro-2a + 50 µM Ch-SeNPs; d) SH-SY5Y + 50 µM Ch-SeNPs; e) Neuro-2a + 250 µM Ch-SeNPs; f) SH-SY5Y + 250 µM Ch-SeNPs.

Nevertheless, differences in Se uptake were noticeable when maximums of Se mass accumulated in every condition were compared. As previously stated, for non-nanoparticulated selenium species, Neuro-2a cells were only able to accumulate selenium from 250 µM SeMet (< 41.4 fg cell^{-1}), while SH-SY5Y cells could accumulate from 50 µM SeMet (< 47.1 fg cell^{-1}), 250 µM SeMet (< 167.5 fg cell^{-1}) and even 250 µM MeSeCys (< 64.6 fg cell^{-1}). On the other side, both neuroblastoma cell lines were able to accumulate selenium from every concentration of Ch-SeNPs exposed. Once again, Neuro-2a cells exposed to 10 µM (< 37.4 fg cell^{-1}), 50 µM (< 63.9 fg cell^{-1}) and 250 µM Ch-SeNPs (< 89.5 fg cell^{-1}), accumulated less amount than SH-SY5Y cells exposed to the same Ch-SeNPs concentrations (< 54.1, < 76.8 and < 129.8 fg cell^{-1}). *Table 2* gathers Se mass (fg) per single cell ranges accumulated by SH-SY5Y and Neuro-2a cell lines after exposure of different concentration of selenium species.

Table 2. Accumulation of selenium species by individual neuroblastoma cells expressed as fg of Se per cells (n > 700). Limit of detection (LOD) = 1.2 fg cell^{-1}.

Selenium species	Exposure concentration (µM)	Neuro-2a	SH-SY5Y
		fg (Se) cell^{-1}	fg (Se) cell^{-1}
SeMet	10	< *LOD*	< *LOD*
	50	< *LOD*	1.2 – 47.1
	250	19.9 – 41.4	1.2 – 167.5
MeSeCys	10	< *LOD*	< *LOD*
	50	< *LOD*	< *LOD*
	250	< *LOD*	1.2 – 64.6
Ch-SeNPs	10	1.2 – 37.4	1.2 - 54.1
	50	1.2 – 63.9	7.0 – 76.8
	250	1.2 – 89.5	3.1 – 129.8

It could be determined that upon increasing the dose of Se cells were exposed to, independently of the species it came from, also the mass of Se accumulated by both cell lines raised. Moreover, between both cell lines, SH-SY5Y accumulated more selenium than Neuro-2a regardless of the selenium species to which they were exposed. MeSeCys was the selenium species with lesser uptake among all studied, in contrast to Ch-SeNPs, which were accumulated at all exposure concentrations. Additionally, human neuroblastoma cell line demonstrated higher accumulation of Ch-SeNPs than mouse neuroblastoma cells, being double at 10 µM, slightly higher at 50 µM and far higher at 250 µM. It is also important to highlight that SC-ICP-MS analysis revealed the existence of a great cell to cell variability in terms of selenium species accumulation, which is reflected in the frequency histograms displays in *Figures 6* and *7*. These results confirmed the high variability of selenium accumulation by neuroblastoma cell lines, thus requiring the use of advanced techniques such as SC-ICP-MS to provide reliable information of selenium distribution at single cell level.

4. Conclusions

Effect of selenium species, especially selenium nanoparticles stabilized with chitosan (Ch-SeNPs), have been evaluated in two different cell lines: human (SH-SY5Y) and mouse (Neuro-2a) neuroblastoma ones. Cytotoxicity of selenium species at 48 h of incubation was studied by two bioanalytical methods: MTT and flow cytometry assays. Both methods provided similar results, with flow cytometry offering slightly higher LC_{50} values. Regarding cell lines, Neuro-2a showed less resistance than SH-SY5Y cells to selenium species cytotoxicity. Between selenium species under study, organic selenium-containing amino acids (SeMet and MeSeCys) presented less cytotoxicity than Ch-SeNPs, likely caused by the natural presence of the formers in living organisms.

Ch-SeNPs internalisation in SH-SY5Y neuroblastoma cell line was confirmed by TEM and different stages of the uptake pathway were characterized. Ch-SeNPs were observed on the outside of the cell membrane, in the mitochondria, nucleus and nucleolus of neuroblastoma cells. Since $A\beta_{42}$ accumulation is produced extracellularly on the outside of the cell membrane, and Ch-SeNPs have demonstrated in previous studies their anti-amyloidogenic properties, these results are of great interest in the AD field. Considering selenium antioxidant properties, their presence in the mitochondria also

could face ROS generation which produce mitochondrial DNA oxidation in AD development. Since p-tau, the second hallmark of AD, aggregates and hyperphosphorylates intracellularly in the cytosol, nucleus and nucleoli, the presence of Ch-SeNPs in these cellular compartments should be further investigated.

Furthermore, selenium species uptake and accumulation by Neuro-2a and SH-SY5Y cell lines at single cell level were studied by SC-ICP-MS. SH-SY5Y cells demonstrated a higher accumulation of selenium than Neuro-2a ones, regardless of the species they were exposed. Among all selenium species, Ch-SeNPs were the most accumulated, followed by SeMet and, lastly, MeSeCys, demonstrating the potential of selenium nanoparticles stabilized with chitosan to adhere and cross the cell membrane of neuroblastoma cells. In conclusion, the present work revealed *in vitro* interesting properties of Ch-SeNPs which could be useful for further studies in AD field.

Credit authorship contribution statement

David Vicente-Zurdo: Methodology, Formal analysis, Investigation, Data curation, Writing –original draft, Writing –review & editing. **Beatriz Gómez-Gómez**: Methodology, Formal analysis, Investigation, Data curation, Writing –review & editing. **Iván Romero-Sánchez**: Methodology, Formal analysis, Investigation, Data curation, Writing –review & editing. **Noelia Rosales-Conrado**: Conceptualization, Methodology, Investigation, Writing –review & editing. **María Eugenia León-González**: Conceptualization, Methodology, Investigation, Writing –review & editing. **Yolanda Madrid**: Conceptualization, Methodology, Investigation, Writing –review & editing, Funding acquisition.

Acknowledgements

This work was supported by the Spanish Ministry of Science and Innovation (PID2020-114714RB-I00) and the Community of Madrid and European funding from FSE and FEDER programs (S2018/BAA-4393, PB2018/BAA-4393- AVANSECAL-II-CM). David Vicente-Zurdo acknowledges the Spanish Ministry of Science, Innovation and Universities for funding through a pre-doctoral grant (FPU18/00573). Iván Romero-

Sánchez acknowledges the Complutense University through a pre-doctoral grant [CT63/19-CT64/19].

Conflict of interest

The authors declare no conflict of interest.

Abbreviations

AD, Alzheimer's disease; ANOVA, Analysis of variance; AuNPs, gold nanoparticles; $A\beta_{42}$, beta-amyloid protein; Ch-SeNPs, selenium nanoparticles stabilized with chitosan; EDXS, Energy-dispersive X-Ray Spectroscopy; ICP-MS, Inductively Coupled Plasma with Mass Spectrometry detection; IP, propidium iodide; LC_{50}, lethal concentration for 50% of cell population; LOD, Limit of detection; LSD, least significant difference; MeSeCys, Se-methylselenocysteine; MTT, 3-(4,5-Dimethylthiazol-2-yl)-2,5-diphenyltetrazolium bromide; NFTs, neurofibrillary tangles; p-tau, tau protein; ROS, reactive oxygen species; SC-ICP-MS, Single cell-Inductively Coupled Plasma with Mass Spectrometry detection; SD, standard deviation; SeMet, selenomethionine; TEM, Transmission Electron Microscopy.

References

[1] GBD 2015 Neurological Disorders Collaborator Group, Global, regional, and national burden of neurological disorders during 1990–2015: a systematic analysis for the Global Burden of Disease Study 2015, Lancet Neurol. 16 (2017) 877–897. https://doi.org/10.1016/S1474-4422(17)30299-5.

[2] J. Weller, A. Budson, Current understanding of Alzheimer's disease diagnosis and treatment, F1000Res. 7 (2018) 1–9. https://doi.org/10.12688/f1000research.14506.1.

[3] M. Crous-Bou, C. Minguillón, N. Gramunt, J.L. Molinuevo, Alzheimer's disease prevention: From risk factors to early intervention, Alzheimers Res Ther. 9 (2017) 71. https://doi.org/10.1186/s13195-017-0297-z.

[4] P.P. Liu, Y. Xie, X.Y. Meng, J.S. Kang, History and progress of hypotheses and clinical trials for Alzheimer's disease, Signal Transduct Target Ther. 4 (2019) 29. https://doi.org/10.1038/s41392-019-0063-8.

[5] S.A. James, Q.I. Churches, M.D. de Jonge, I.E. Birchall, V. Streltsov, G. McColl, P.A. Adlard, D.J. Hare, Iron, Copper, and Zinc Concentration in Aβ Plaques in the APP/PS1 Mouse Model of Alzheimer's Disease Correlates with Metal Levels in the Surrounding Neuropil, ACS Chem Neurosci. 8 (2017) 629–637. https://doi.org/10.1021/acschemneuro.6b00362.

[6] S. Chaves, A. Hiremathad, D. Tomás, R.S. Keri, L. Piemontese, M. Amélia Santos, Exploring the chelating capacity of 2-hydroxyphenyl-benzimidazole based hybrids with multi-target ability as anti-Alzheimer's agents, New Journal of Chemistry. 42 (2018) 16503–16515. https://doi.org/10.1039/c8nj00117k.

[7] Z.H. Zhang, L. Wen, Q.Y. Wu, C. Chen, R. Zheng, Q. Liu, J.Z. Ni, G.L. Song, Long-Term Dietary Supplementation with Selenium-Enriched Yeast Improves Cognitive Impairment, Reverses Synaptic Deficits, and Mitigates Tau Pathology in a Triple Transgenic Mouse Model of Alzheimer's Disease, J Agric Food Chem. 65 (2017) 4970–4979. https://doi.org/10.1021/acs.jafc.7b01465.

[8] D. Vicente-Zurdo, I. Romero-Sánchez, N. Rosales-Conrado, M.E. León-González, Y. Madrid, Ability of selenium species to inhibit metal-induced Aβ aggregation involved in the development of Alzheimer's disease, Anal Bioanal Chem. 412 (2020) 6485–6497. https://doi.org/10.1007/s00216-020-02644-2.

[9] D. Vicente-Zurdo, S. Rodríguez-Blázquez, E. Gómez-Mejía, N. Rosales-Conrado, M.E. León-González, Y. Madrid, Neuroprotective activity of selenium nanoparticles against the effect of amino acid enantiomers in Alzheimer's disease, Anal Bioanal Chem. 414 (2022) 7573–7584. https://doi.org/10.1007/s00216-022-04285-z.

[10] K. Laulagnier, C. Javalet, F.J. Hemming, M. Chivet, G. Lachenal, B. Blot, C. Chatellard, R. Sadoul, Amyloid precursor protein products concentrate in a subset of exosomes specifically endocytosed by neurons, Cellular and Molecular Life Sciences. 75 (2018) 757–773. https://doi.org/10.1007/s00018-017-2664-0.

[11] D. Knez, N. Coquelle, A. Pišlar, S. Žakelj, M. Jukič, M. Sova, J. Mravljak, F. Nachon, X. Brazzolotto, J. Kos, J.P. Colletier, S. Gobec, Multi-target-directed ligands for treating Alzheimer's disease: Butyrylcholinesterase inhibitors displaying antioxidant and neuroprotective activities, Eur J Med Chem. 156 (2018) 598–617. https://doi.org/10.1016/j.ejmech.2018.07.033.

[12] D. Vicente- Zurdo, N. Rosales- Conrado, M.E. León- González, L. Brunetti, L. Piemontese, A. Raquel Pereira- Santos, S.M. Cardoso, Y. Madrid, S. Chaves, M.A. Santos, Novel Rivastigmine Derivatives as Promising Multi- Target Compounds for Potential Treatment of Alzheimer's Disease, Biomedicines. 10 (2022) 1510. https://doi.org/10.3390/biomedicines10071510.

[13] D. Ezhilarasan, V.S. Apoorva, N. Ashok Vardhan, Syzygium cumini extract induced reactive oxygen species-mediated apoptosis in human oral squamous carcinoma cells, Journal of Oral Pathology and Medicine. 48 (2019) 115–121. https://doi.org/10.1111/jop.12806.

[14] T. Sathiya Kamatchi, M.K. Mohamed Subarkhan, R. Ramesh, H. Wang, J.G. Małecki, Investigation into antiproliferative activity and apoptosis mechanism of new arene Ru(ii) carbazole-based hydrazone complexes, Dalton Transactions. 49 (2020) 11385–11395. https://doi.org/10.1039/d0dt01476a.

[15] P. Kumari, P.K. Panda, E. Jha, K. Kumari, K. Nisha, M.A. Mallick, S.K. Verma, Mechanistic insight to ROS and Apoptosis regulated cytotoxicity inferred by Green synthesized CuO nanoparticles from Calotropis gigantea to Embryonic Zebrafish, Sci Rep. 7 (2017) 16284. https://doi.org/10.1038/s41598-017-16581-1.

[16] R. Zhang, X. Qin, F. Kong, P. Chen, G. Pan, Improving cellular uptake of therapeutic entities through interaction with components of cell membrane, Drug Deliv. 26 (2019) 328–342. https://doi.org/10.1080/10717544.2019.1582730.

[17] N.S. Aminabad, M. Farshbaf, A. Akbarzadeh, Recent Advances of Gold Nanoparticles in Biomedical Applications: State of the Art, Cell Biochem Biophys. 77 (2019) 123–137. https://doi.org/10.1007/s12013-018-0863-4.

[18] P. Dash, A.M. Piras, M. Dash, Cell membrane coated nanocarriers - an efficient biomimetic platform for targeted therapy, Journal of Controlled Release. 327 (2020) 546–570. https://doi.org/10.1016/j.jconrel.2020.09.012.

[19] W.H. de Jong, P.J. Borm, Drug delivery and nanoparticles: Applications and hazards, Int J Nanomedicine. 3 (2008) 133–149.

[20] A. Roy, B. Das, M. Sengupta, B. Mohanta, Cellular uptake of spherical and triangular shaped gold nanoparticles synthesised using Eupatorium odoratum leaf extract, Advances in Natural Sciences: Nanoscience and Nanotechnology. 12 (2021) 1–7. https://doi.org/10.1088/2043-6262/ac00a4.

[21] M.P. Murphy, How mitochondria produce reactive oxygen species, Biochemical Journal. 417 (2009) 1–13. https://doi.org/10.1042/BJ20081386.

[22] R.X. Santos, S.C. Correia, X. Zhu, H.G. Lee, R.B. Petersen, A. Nunomura, M.A. Smith, G. Perry, P.I. Moreira, Nuclear and mitochondrial DNA oxidation in Alzheimer's disease, Free Radic Res. 46 (2012) 565–576. https://doi.org/10.3109/10715762.2011.648188.

[23] M. Wu, H. Guo, L. Liu, Y. Liu, L. Xie, Size-dependent cellular uptake and localization profiles of silver nanoparticles, Int J Nanomedicine. 14 (2019) 4247–4259. https://doi.org/10.2147/IJN.S201107.

[24] S. Squadrone, P. Brizio, C. Stella, M. Mantia, S. Pederiva, G. Giordanengo, G. Pistone, M.C. Abete, Distribution and bioaccumulation of trace elements and lanthanides in apples from Northwestern Italy, Journal of Trace Elements in Medicine and Biology. 62 (2020) 126646. https://doi.org/10.1016/j.jtemb.2020.126646.

[25] L. Yin, Z. Zhang, Y. Liu, Y. Gao, J. Gu, Recent advances in single-cell analysis by mass spectrometry, Analyst. 144 (2019) 824–845. https://doi.org/10.1039/c8an01190g.

[26] B. Gomez-Gomez, M. Corte-Rodríguez, M.T. Perez-Corona, J. Bettmer, M. Montes-Bayón, Y. Madrid, Combined single cell and single particle ICP-TQ-MS analysis to quantitatively evaluate the uptake and biotransformation of tellurium nanoparticles in bacteria, Anal Chim Acta. 1128 (2020) 116–128. https://doi.org/10.1016/j.aca.2020.06.058.

[27] M. Corte Rodríguez, R. Álvarez-Fernández García, E. Blanco, J. Bettmer, M. Montes-Bayón, Quantitative Evaluation of Cisplatin Uptake in Sensitive and

Resistant Individual Cells by Single-Cell ICP-MS (SC-ICP-MS), Anal Chem. 89 (2017) 11491–11497. https://doi.org/10.1021/acs.analchem.7b02746.

[28] G. Moreno-Martín, B. Gómez-Gómez, M.E. León-González, Y. Madrid, Characterization of AgNPs and AuNPs in sewage sludge by single particle inductively coupled plasma-mass spectrometry, Talanta. 238 (2022) 123033. https://doi.org/10.1016/j.talanta.2021.123033.

[29] M.K. Singleton, M.L. Gonzales, K.N. Leung, D.H. Yasui, D.I. Schroeder, K. Dunaway, J.M. LaSalle, MeCP2 is required for global heterochromatic and nucleolar changes during activity-dependent neuronal maturation, Neurobiol Dis. 43 (2011) 190–200. https://doi.org/10.1016/j.nbd.2011.03.011.

[30] M.B. Maina, L.J. Bailey, S. Wagih, L. Biasetti, S.J. Pollack, J.P. Quinn, J.R. Thorpe, A.J. Doherty, L.C. Serpell, The involvement of tau in nucleolar transcription and the stress response, Acta Neuropathol Commun. 6 (2018) 70. https://doi.org/10.1186/s40478-018-0565-6.

Figure legends

Figure 1. Optical microscope images of confluent neuroblastoma cell lines: a) SH-SY5Y at 10X magnification power; b) SH-SY5Y at 40X magnification power; c) Neuro-2a at 10X magnification power; d) Neuro-2a at 40X magnification power.

Figure 2. TEM micrographs (a, c, e) and EDXS (b, d, f) of 50 µM Ch-SeNPs in different mediums: a) and b) Ch-SeNPs in synthesis medium; c) and d) Ch-SeNPs incubated at 37 ºC during 48 h in Neuro-2a culture medium; e) and f) Ch-SeNPs incubated at 37 ºC during 48 h in SH-SY5Y culture medium.

Figure 3. Cytotoxicity of selenium species at 48 h, represented as percentage of viable cells, calculated by MTT and flow cytometry bioanalytical methods. a) MTT method on Neuro-2a cell line; b) Flow cytometry method on Neuro-2a cell line; c) MTT method on SH-SY5Y cell line; d) Flow cytometry method on SH-SY5Y cell line. Results are expressed as mean ± SD (n = 5).

Figure 4. Micrographs of Ch-SeNPs internalisation in SH-SY5Y cells observed by TEM. a) Control SH-SY5Y cell; b) SH-SY5Y cell at early stage of Ch-SeNPs internalisation;

c) SH-SY5Y cell at intermediate stage of Ch-SeNPs internalisation; d) Ch-SeNPs location inside mitochondria; e) SH-SY5Y cell at advanced stage of Ch-SeNPs internalisation; f) Dead SH-SY5Y cell due to Ch-SeNPs effect.

Figure 5. SH-SY5Y cell structures diameters (µm) during the stages of Ch-SeNPs internalisation (n = 10), measured by ImageJ in TEM micrographs. * $p < 0.05$ compared to control.

Figure 6. Time-resolved scan of ^{80}Se obtained for SH-SY5Y cells exposed to 250 µM MeSeCys (a) and frequency histograms (b-e) for SH-SY5Y and Neuro-2a cell lines incubated with non-nanoparticulated selenium species at different concentrations: b) Neuro-2a + 250 µM SeMet; c) SH-SY5Y + 250 µM MeSeCys; d) SH-SY5Y + 50 µM SeMet; e) SH-SY5Y + 250 µM SeMet.

Figure 7. Frequency histograms of ^{80}Se from SC-ICP-MS analyses for Neuro-2a and SH-SY5Y cell lines incubated with Ch-SeNPs at different concentrations: a) Neuro-2a + 10 µM Ch-SeNPs; b) SH-SY5Y + 10 µM Ch-SeNPs; c) Neuro-2a + 50 µM Ch-SeNPs; d) SH-SY5Y + 50 µM Ch-SeNPs; e) Neuro-2a + 250 µM Ch-SeNPs; f) SH-SY5Y + 250 µM Ch-SeNPs.

Table legends

Table 1. Cytotoxicity of selenium species expressed as LC_{50} (µM) regarding Neuro-2a and SH-SY5Y neuroblastoma cell lines, by using MTT and flow cytometry assays. Data are expressed as mean ± standard deviation (n = 5). Mean values with a common letter indicate no significant differences at p-values > 0.05, according to ANOVA and Fisher LSD tests.

Table 2. Accumulation of selenium species by individual neuroblastoma cells expressed as fg of Se per cells (n > 700). Limit of detection (LOD) = 1.2 fg $cell^{-1}$.

Declaration of interests

☒The authors declare that they have no known competing financial interests or personal relationships that could have appeared to influence the work reported in this paper.

☐The authors declare the following financial interests/personal relationships which may be considered as potential competing interests:

IX.DISCUSIÓN INTEGRADORA

IX. DISCUSIÓN INTEGRADORA

En este apartado se realizará una discusión global de los resultados correspondientes a los trabajos expuestos en la sección experimental de la presente Tesis Doctoral, cuyo objetivo ha sido la evaluación de las propiedades neuroprotectoras de **moléculas orgánicas** y de **nanopartículas de selenio** sobre el efecto de **metales** y **aminoácidos** en la AD. Los resultados obtenidos, tanto en la subsección de moléculas orgánicas como en la de nanopartículas de selenio, han permitido profundizar en el uso de estos compuestos como potenciales agentes anti-AD, debido a sus diferentes propiedades neuroprotectoras.

En primer lugar, se estudió el efecto neuroprotector de moléculas orgánicas derivadas de la 7-aminofenantridin-6-ona, denominadas **APH1, APH2, APH3, APH4** y **APH5**. Para ello, en el **Artículo 1**, se exploró su uso como moléculas capaces de reducir la citotoxicidad y el estrés oxidativo provocado por metales como el Fe(II), Cu(II), Zn(II), Hg(II), Cd(II) y Al(III) en la línea celular SN56.

Estas moléculas se diseñaron como ligandos bidentados, los cuales emplean el oxígeno del grupo lactama y el nitrógeno exocíclico para interaccionar con los cationes metálicos. Los diferentes sustituyentes incorporados al esqueleto **APH** modularían, por tanto, la afinidad del nitrógeno por dichos metales. Inicialmente, y para determinar la capacidad de las moléculas **APH1-5** de **quelar** los **biometales** y **metales tóxicos** involucrados en la AD, se estudió su interacción mediante espectroscopía de absorción UV-Vis, técnica muy empleada para evaluar la formación y posible relación de concentración óptima de los complejos metálicos formados.

Con este fin, se compararon los espectros de absorción UV-Vis de las moléculas **APH** y de los metales estudiados por separado con los espectros de las mezclas APH y metal, a diferentes relaciones de concentración metal:APH. Con respecto a los ensayos del Fe(II) y Cu(II) con las moléculas **APH1-5**, y del Hg(II) con las moléculas **APH3**, **APH4** y **APH5**, no se observaron nuevas bandas de absorción en los espectros registrados, por lo que los máximos de absorción mantuvieron la misma longitud de onda en los espectros de APH/metal con respecto a los espectros de ambos por separado. Sin embargo, sí se observaron diferencias de intensidad en las bandas de absorción de las moléculas APH cuando se evaluaron en presencia de los metales indicados a diferentes relaciones de concentración metal:APH, sugiriendo una interacción y la formación de complejos de hierro y cobre con las moléculas **APH1-5** y de mercurio con las moléculas **APH3**, **APH4**

y **APH5**. Este efecto hipercrómico observado en los espectros UV-Vis se podría deber a una mayor conjugación de los electrones, pertenecientes a las moléculas orgánicas, en presencia de los metales mencionados, aumentando, por tanto, la intensidad en las bandas de absorción.

Con respecto a la evaluación del Hg(II) con las moléculas **APH1** y **APH2** y al resto de metales como el Zn(II), Cd(II) y Al(III) con las moléculas **APH1-5**, no se observaron diferencias en el espectro de absorción cuando se mezclan con diferentes relaciones de concentración metal:APH. La ausencia de variaciones en el espectro podría ser indicativa de la nula interacción entre estos metales y las moléculas mencionadas.

Posteriormente, se procedió a derivar los espectros anteriores, ya que la **espectroscopía derivada** permite una mejor visualización de las diferencias entre espectros, además de resolver solapamientos de bandas y/o eliminar o reducir el fondo. Para ello, una vez registrado el espectro de absorción, se aplicaron tratamientos matemáticos para generar el correspondiente espectro d^1(UV-Vis). Los máximos de absorción pertenecientes al espectro UV-Vis se correlacionaron con la intersección en el eje X en el espectro d^1(UV-Vis), mientras que los máximos y mínimos en el espectro d^1(UV-Vis) se correspondieron con los puntos en los que la pendiente es mayor (puntos de inflexión), bien sea creciente o decreciente, en el espectro UV-Vis. De esta forma se pudo determinar, con mayor precisión, el máximo de absorción de las correspondientes moléculas y diferenciarlo de otras bandas cercanas de absorción. Así, en primer lugar, la utilización de la primera derivada permitió confirmar los resultados obtenidos con respecto a la formación de los respectivos complejos metálicos. En segundo lugar, manteniendo la concentración del metal constante y variando la concentración de la molécula APH y viceversa, se pudo estimar la relación de concentración más probable para los complejos formados mediante la comparación de los espectros d^1(UV-Vis) a diferentes relaciones de concentración metal:APH.

En el caso de la interacción del Fe(II) con la molécula **APH4** se observó en el espectro una banda de absorción a 280 nm, independientemente de la relación de concentración metal:APH4 estudiada. La intensidad de dicha banda se incrementaba a medida que aumentaba la concentración de Fe(II), lo que permitió relacionarla con el complejo Fe(II)-APH4 y con un máximo en la relación de concentraciones 1:1. Adicionalmente, se detectó otra banda de absorción a 300 nm en el espectro de la molécula APH4 en ausencia de metal, correspondiéndose con un máximo en el espectro UV-Vis y con un corte con el eje

X en el espectro d^1(UV-Vis). Esta banda se atribuyó a la molécula **APH4,** por su corte con el eje X en el espectro d^1(UV-Vis) solo en ausencia de Fe(II), puesto que dicha banda se solapaba con la del complejo formado con el hierro en todas relaciones de concentración estudiadas. De esta forma, se dedujo que la relación de concentración más probable para el complejo **Fe(II)-APH4** formado era la 1:1, si bien no se puede descartar la formación de otros complejos con diferentes estequiometrías.

Con respecto al resto de complejos del hierro, todos ellos mostraron el mismo comportamiento, siendo predominante la relación de concentración 1:1 y las longitudes de onda correspondientes a los máximos de absorción de las bandas de los complejos metálicos las siguientes: **Fe(II)-APH1** = 280 nm, **Fe(II)-APH2** = 270 y 305 nm, **Fe(II)-APH3** = 280 nm y **Fe(II)-APH5** = 270 nm. En el caso de los complejos formados con el cobre, también presentaron mayoritariamente la relación de concentración 1:1, con las siguientes longitudes de onda para las bandas de absorción: **Cu(II)-APH1** = 275 y 300 nm, **Cu(II)-APH2** = 265 nm, **Cu(II)-APH3** = 260 nm, **Cu(II)-APH4** = 265 nm y **Cu(II)-APH5** = 270 nm. En el caso de los complejos de mercurio se observó, como relación de concentración principal, la 1:1 para los complejos **Hg(II)-APH4** (con máximos de absorción a 295 y 300 nm) y los complejos **Hg(II)-APH5** (con máximos de absorción a 300 y 305 nm), mientras que para el complejo **Hg(II)-APH3** no se pudo elucidar su relación de concentración óptima y se observó una banda de absorción a la longitud de onda de 305 nm. Todas las bandas de absorción presentes en los espectros UV-Vis fueron confirmadas como cortes con el eje X en los espectros d^1(UV-Vis).

Adicionalmente, la espectroscopia derivada d^1(UV-Vis) permitió confirmar la ausencia de interacción, por la inexistencia de cortes con el eje X en los espectros de absorción UV-Vis para el Hg(II), con las moléculas **APH1** y **APH2**, y en el del Zn(II), Cd(II) y Al(III) con las moléculas **APH1-5**. Así, gracias al espectro de la primera derivada se pudo determinar con una mayor precisión, la nula interacción de estas moléculas con dichos metales.

Para corroborar de forma teórica las observaciones experimentales de la quelación metálica por parte de las moléculas **APH1-5**, se realizó un análisis de la diferencia energética entre los orbitales **HOMO** y **LUMO** para cada molécula, en ausencia y presencia de Fe(II). Un incremento en la diferencia de energía entre los orbitales HOMO y LUMO implica una mayor reactividad, mientras que una disminución se traduce en una mayor estabilidad. Por tanto, se calculó la diferencia energética para las moléculas en ausencia y en presencia de

Fe(II) obteniendo: 7.049 eV para **APH1** y 0.917 eV para **Fe(II)-APH1**, 7.799 eV para **APH2** y 0.712 eV para **Fe(II)-APH2**, 4.494 eV para **APH3** y 3.922 para **Fe(II)-APH3**, 5.982 eV para **APH4** y 0.145 eV para **Fe(II)-APH4**, y 6.643 eV para **APH5** y 0.299 eV para **Fe(II)-APH5**. Esta disminución en el intervalo de energía entre los orbitales HOMO y LUMO sugiere una mayor estabilidad de los complejos **Fe(II)-APH** con respecto a las moléculas **APH** en solitario, por lo que la formación de los complejos metal:APH1-5 estaría favorecida, corroborándose, por tanto, la formación de estos complejos metálicos.

Además, los resultados teóricos obtenidos sugirieron que las moléculas **APH** podrían quelar cationes poco voluminosos como el Fe(II) y Cu(II) a través de la sección bidentada formada por el oxígeno del grupo lactama y el nitrógeno exocíclico, mientras que no podrían unirse a cationes de mayor tamaño como el Cd(II), Hg(II) y Al(III). La interacción del Hg(II) observada experimentalmente con la molécula **APH3** se podría dar, por tanto, con el nitrógeno del grupo dimetilamina, mientras que la interacción con **APH4** y **APH5** podría ocurrir a través del azufre del grupo tiofeno.

Para evaluar el uso potencial de las moléculas **APH** como fármacos en la AD se realizó la predicción de sus **propiedades farmacocinéticas** mediante un análisis computacional *in silico* de las propiedades de absorción, distribución, metabolismo, excreción y toxicidad (ADMET) utilizando los programas ADMETsar y SwissADME. Estos sistemas permiten evaluar la absorción de las moléculas por el sistema nervioso central (CNS) y su idoneidad como posibles fármacos a través de la regla de Lipinski. Con respecto a esta regla, todas las moléculas cumplieron todos los parámetros excepto el correspondiente a la solubilidad acuosa, para el cual presentaron valores cercanos al límite establecido por Lipinski. Con respecto a las propiedades ADMET, se predijo una elevada absorción y permeabilidad gastrointestinal. En relación con la penetración de la barrera hematoencefálica (BBB), el método ADMETsar proporcionó valores óptimos para las moléculas APH, mientras que el método SwissADME predijo la permeabilidad de la molécula **APH1**, dejando al resto de moléculas al límite de los valores óptimos. En general, se predijeron propiedades farmacocinéticas favorables para todas las moléculas **APH**, cumpliendo los requisitos establecidos por la regla de Lipinski, por lo que todas ellas se podrían considerar candidatos potenciales a fármacos.

Para determinar el **efecto citotóxico** de las moléculas **APH**, se realizaron ensayos *in vitro* con la línea celular SN56 utilizando el método del MTT. Se expusieron dichas células a concentraciones crecientes de las moléculas (1-200 μM) durante 24 h, observando

ausencia de citotoxicidad a concentraciones iguales o inferiores a 150 μM de las moléculas APH. Por tanto, se seleccionaron concentraciones comprendidas entre 10 y 100 μM para los posteriores ensayos. Adicionalmente, se seleccionó una concentración para cada metal a la cual mostrase un efecto citotóxico relevante. En el caso de los biometales Fe(II), Cu(II) y Zn(II), se emplearon las concentraciones 200, 20 y 250 μM respectivamente, y para los metales tóxicos Hg(II), Cd(II) y Al(III) se utilizaron las concentraciones 30, 100 y 300 μM respectivamente.

Con objeto de evaluar la **actividad neuroprotectora** de las moléculas **APH** frente a la citotoxicidad inducida por los biometales y metales tóxicos, se pretrataron las células con concentraciones comprendidas entre 10 y 100 μM de las moléculas APH durante 2 h. Posteriormente, se co-incubaron con los biometales y metales tóxicos a las concentraciones previamente seleccionadas y se midió la viabilidad celular con el método del MTT. Todas las moléculas mostraron un efecto neuroprotector parcial o total, dependiendo del metal y de la molécula, aumentando la neuroprotección a medida que aumentaba la concentración de la molécula APH. Con respecto a la reducción de la citotoxicidad inducida por los biometales, la actividad neuroprotectora de las moléculas APH se detectó a partir de 10 μM para APH2, APH3, APH4 y APH5, y de 50 μM para APH1, mientras que para los metales tóxicos la disminución de la citotoxicidad se produjo a partir de 10 μM para todas las moléculas APH1-5 evaluados.

La molécula **APH1** redujo parcialmente la toxicidad de Hg(II) a partir de 10 μM, y de Fe(II), Cu(II), Zn(II), Cd(II) y Al(III) a partir de 50 μM, mientras que no logró reducir totalmente la toxicidad inducida por estos metales a ninguna de las concentraciones estudiadas. La molécula **APH2** redujo parcialmente la toxicidad de Cu(II), Zn(II), Hg(II) y Al(III) a partir de 10 μM, y de Fe(II) y Cd(II) a partir de 50 μM, pero no fue capaz de reducir en su totalidad la toxicidad inducida por los metales. Las moléculas **APH3** y **APH4** redujeron de forma parcial la toxicidad de Fe(II), Cu(II), Zn(II), Cd(II), Hg(II), y Al(III) a partir de 10 μM, reduciendo además en su totalidad la toxicidad del Cu(II), Zn(II), Cd(II), Hg(II) y Al(III) a 100 μM. Finalmente, la molécula **APH5** redujo parcialmente la toxicidad de Cd(II), Hg(II) y Al(III) a partir de 10 μM, y de Fe(II), Cu(II) y Zn(II) a partir de 50 μM, mientras que redujo totalmente la toxicidad de Zn(II), Cd(II) y Hg(II) a 100 μM. Como se ha demostrado en el apartado de interacción de las moléculas APH con los biometales y metales tóxicos, ninguna de las moléculas mostró capacidad de quelación de Zn(II), Cd(II) ni Al(III), y en el caso de las moléculas APH1 y APH2, tampoco se observó quelación con Hg(II). Por otra parte, todas las moléculas APH mostraron protección frente a la

citotoxicidad inducida por metales, por lo que los efectos neuroprotectores de las moléculas anteriormente mencionadas, frente al Zn(II), Cd(II), Al(III) y en algunos casos Hg(II), no son debidos a la capacidad quelante de dichas moléculas. Sin embargo, el efecto neuroprotector frente a la citotoxicidad inducida por el resto de los metales se puede explicar, al menos de forma parcial, por la quelación por parte de las moléculas APH1-5, siendo la molécula **APH4**, seguida por la molécula **APH3**, la que demostró mayor neuroprotección.

La aplicación posterior de la técnica PCR en tiempo real y de kits ELISA para determinar la expresión proteica de Keap1, Nrf2, GPx y la catalasa evidenció que todas las moléculas APH presentaban un **efecto antioxidante** a través de la inducción de la vía Nrf2. Este efecto fue más significativo al aumentar la concentración de las moléculas APH. La inducción de la vía Nrf2 se produjo a través de dos mecanismos: dependiente e independiente de la proteína Keap1. En el caso del mecanismo independiente de la proteína Keap1, se observó la sobreexpresión génica de Nrf2, provocando por tanto un aumento de la expresión de dicha proteína con el consecuente efecto antioxidante. En relación al segundo mecanismo, mediante la reducción en la expresión génica de Keap1 se redujo la expresión de la proteína Keap1, aumentando por tanto la expresión proteica de la Nrf2. Este aumento de la proteína Nrf2 provocó un aumento de las enzimas antioxidantes GPx y catalasa, ya que están reguladas por dicha proteína. De este modo, la molécula **APH4** mostró una mayor capacidad antioxidante, seguida por la molécula **APH3**.

Por otra parte, la cuantificación intracelular mediante espectroscopía UV-Vis del contenido de malondialdehido (MDA) en ensayos *in vitro* con la línea celular SN56 puso de manifiesto la capacidad de las moléculas APH de reducir la **peroxidación lipídica** inducida por biometales como el Fe(II) y por metales tóxicos como el Cd(II). El MDA es el marcador más utilizado de la peroxidación lipídica ya que es un producto procedente de la degradación del ácido araquidónico por parte de los ROS. Los resultados mostraron que las moléculas APH no aumentaron los niveles de MDA. Posteriormente, se seleccionaron concentraciones de Fe(II) y Cd(II) que produjesen peroxidación lipídica y aumentasen, por tanto, los niveles de MDA. Finalmente, se pretrataron las células con las moléculas APH y se expusieron a los metales durante 24 h, cuantificando el contenido intracelular de MDA. Todas las moléculas demostraron una reducción de la peroxidación lipídica a partir de una concentración de la molécula APH de 10 μM para ambos metales, siendo mayor la reducción de la peroxidación lipídica a medida que aumentaba la concentración de la molécula APH. La molécula **APH1** fue la que menor actividad antioxidante demostró,

debido a su incapacidad de revertir totalmente la peroxidación lipídica a ninguna de las concentraciones estudiadas. Por otra parte, las moléculas **APH2**, **APH3** y **APH5** a 100 μM inhibieron totalmente la producción de MDA con respecto al control, siendo más antioxidantes que el trolox utilizado como sustancia antioxidante de referencia. Así, la molécula **APH4** resultó ser la más eficaz, ya que a una concentración de 50 μM redujo totalmente la peroxidación lipídica.

Por tanto, evaluando en conjunto los resultados de citotoxicidad y de peroxidación lipídica, la molécula **APH4** a una concentración de 50 μM no protegió totalmente de la citotoxicidad de los metales, mientras que a esa misma concentración sí fue capaz de inhibir totalmente la peroxidación lipídica del Fe(II) y del Cd(II). Además, las moléculas **APH2**, **APH3** y **APH5** a concentraciones de 100 μM tampoco protegieron totalmente de la toxicidad del Fe(II), mientras que a esa concentración disminuyeron los niveles de MDA y, por tanto, la peroxidación lipídica. Así, se puede concluir que el efecto citotóxico de los biometales y metales tóxicos, relacionados con la progresión de la AD, involucra más mecanismos, además de la simple generación del estrés oxidativo. De la misma forma, la neuroprotección ofrecida por las moléculas APH, además de atribuirse a su capacidad quelante y antioxidante, estaría relacionada con otros mecanismos, tal y como se discutirá posteriormente.

La continuación del estudio de los mecanismos neuroprotectores de las moléculas **APH** se recoge en el **Artículo 2**, en el que se evaluó el efecto de estas moléculas orgánicas sobre la **generación y agregación de proteínas amiloides** inducidas por metales neurotóxicos en la AD. Los efectos que producen estos metales en el cerebro alteran el plegamiento, la desagregación y los mecanismos de degradación de proteínas tóxicas como la **Aβ$_{42}$**, mediados por las **proteínas de choque térmico** y los **proteosomas**.

Debido a la elevada importancia de la agregación de la proteína Aβ$_{42}$ en la AD, a través de la "**hipótesis de la cascada amiloide**", y el efecto de los biometales y metales tóxicos mediante la "**hipótesis del ion metálico**", se estudió la **inhibición de la agregación de la proteína Aβ$_{42}$** inducida por los metales mediante la co-incubación de las moléculas **APH1-5** y su posterior visualización mediante TEM.

En primer lugar, se evaluó el efecto que producían las moléculas APH sobre la **agregación de la proteína Aβ$_{42}$**, co-incubándolos durante 48 h. Ninguna de las moléculas APH1-5 aumentó la agregación natural de las fibras amiloides, en comparación a la proteína Aβ$_{42}$ incubada en solitario. Posteriormente, se evaluó el efecto de los biometales y metales

tóxicos sobre la agregación amiloide, obteniendo en todos los casos un aumento de la agregación de las fibras de $A\beta_{42}$, conforme con lo establecido por la "**hipótesis del ion metálico**". Finalmente, para determinar el efecto neuroprotector ejercido por las moléculas APH en relación con la agregación amiloide, se procedió a co-incubar la proteína $A\beta_{42}$ en presencia de metales y de dichas moléculas orgánicas. La molécula **APH1** fue capaz de inhibir la agregación amiloide inducida por el Fe(II), Cu(II), Hg(II), Cd(II) y Al(III), pero no la agregación inducida por el Zn(II). La molécula **APH4** inhibió la agregación amiloide inducida por todos los metales, excepto la producida por el Fe(II). Finalmente, las moléculas **APH2**, **APH3** y **APH5** inhibieron la agregación amiloide inducida por todos los biometales y metales tóxicos siendo, por ello, las más eficaces en relación a esta propiedad.

Además de evaluar la agregación amiloide, también se estudió la **morfología de las fibras de la proteína $A\beta_{42}$** a través de su anchura en presencia de metales y moléculas APH. La anchura de las fibras amiloides en condiciones normales presentó un valor de (5.4 ± 0.7) nm, reduciéndose en presencia de las moléculas APH1-5: APH1 = (5 ± 1) nm, APH2 = (4.6 ± 0.8) nm, APH3 = (4.3 ± 0.7) nm, APH4 = (4.2 ± 0.7) nm y APH5 = (4.5 ± 0.9) nm. Esta anchura aumentó en presencia de los biometales y metales tóxicos, siendo el Hg(II) el que indujo una mayor anchura de las fibras, hasta (16 ± 2) nm, seguido por el Zn(II), con (13 ± 1) nm. Con respecto a la reducción de la anchura de las fibras inducida por el **Fe(II)** ((6.6 ± 0.9) nm), la molécula APH3 ((3.4 ± 0.4) nm) presentó la mayor efectividad, seguida por APH1 ((4.2 ± 0.3) nm), APH5 ((4.2 ± 0.8) nm) y APH2 ((4.5 ± 0.8) nm), siendo el efecto de esta última similar al de APH4 ((4.9 ± 0.6) nm). Por lo que respecta a la anchura inducida por el **Cu(II)** ((7 ± 1) nm), las moléculas APH1 ((3.7 ± 0.4) nm) y APH4 ((3.9 ± 0.4) nm) fueron las que presentaron una mayor reducción, siendo el efecto de la última estadísticamente similar al de APH5 ((4.3 ± 0.8) nm), que a su vez fue comparable al de APH2 ((4.6 ± 0.6) nm) y APH3 ((4.5 ± 0.5) nm). El aumento en anchura debido al **Zn(II)** fue reducido en gran medida por las moléculas APH2 ((4.7 ± 0.5) nm), APH3 ((4.8 ± 0.4) nm) y APH4 ((4.7 ± 0.9) nm), seguido por APH1 ((6 ± 1) nm) y APH5 ((6 ± 1) nm). En el caso de la anchura inducida por el **Hg(II)**, las moléculas APH1 ((3.8 ± 0.5) nm), APH2 ((3.6 ± 0.5) nm) y APH3 ((4.1 ± 0.6) nm) fueron las que presentaron una mayor reducción, siendo el efecto de la última estadísticamente similar al de APH5 ((4.7 ± 0.8) nm), que a su vez fue igual al de APH4 ((5 ± 1) nm). Con respecto a la reducción de la anchura de las fibras amiloides provocada por el **Cd(II)** ((6.7 ± 0.7) nm), las moléculas APH3 ((3.7 ± 0.6) nm) y APH4 ((4.1 ± 0.6) nm) presentaron el efecto más significativo,

siendo la última similar a la APH5 ((4.2 ± 0.5) nm), seguida por APH2 ((4.6 ± 0.6) nm) y APH1 ((5.3 ± 0.5) nm). La anchura inducida por el **Al(III)** ((8.9 ± 0.8) nm) se redujo en mayor medida por la acción de APH2 ((4 ± 1) nm) y APH5 ((3.5 ± 0.5) nm), en segundo lugar por APH1 ((4.7 ± 0.7) nm) y APH4 ((4.6 ± 0.7) nm), y en menor medida por APH3 ((7 ± 0.8) nm). Así, en función de los efectos observados se puede deducir que todas las moléculas **APH** fueron capaces de **reducir la anchura de las fibras de la proteína Aβ$_{42}$** cuando este aumento se debía a la incubación de biometales y metales tóxicos. Este efecto se observó en mayor o menor medida en función de la molécula APH y del metal utilizado en la co-incubación.

Las interacciones π-π entre residuos aromáticos de la Aβ$_{42}$, como Phe$_4$, Phe$_{19}$, Phe$_{20}$ y Tyr$_{10}$ son probablemente los puntos de anclaje entre los diferentes estados de agregación de los monómeros Aβ$_{42}$ en su proceso de formación de fibras amiloides. Estos enlaces no covalentes se pueden romper mediante la intercalación de moléculas planas que interfieren con dichas interacciones π-π. De esta forma, las moléculas APH1-5, que poseen un porcentaje elevado de planaridad, podrían interferir en el proceso de fibrilación amiloide, reduciendo la anchura de las fibras y su consecuente agregación. Puesto que ninguna de las moléculas APH demostró capacidad para quelar el Zn(II), Cd(II), Al(III), ni en algunos casos el Hg(II), la inhibición de la agregación amiloide inducida por dichos metales debería estar mediada, en estos casos concretos, por un proceso diferente de la interacción APH-metal. Este proceso podría ser la interacción directa con las fibras Aβ$_{42}$ mediante la intercalación entre las interacciones π-π, inhibiendo la formación de agregados de Aβ$_{42}$ por la planaridad de las moléculas. Con respecto a los metales Fe(II), Cu(II) y en algunos casos Hg(II), con los cuales sí se observó una interacción APH-metal, las moléculas APH podrían actuar por estas dos vías, dependiente e independiente de la quelación metálica, en el proceso de reducción de la agregación amiloide.

Posteriormente, el efecto que producían metales, como el Fe(II) y Cd(II), y las moléculas APH1-5 sobre la expresión de las proteínas **HPS70** y **P20S**, encargadas de la degradación de proteínas tóxicas como la Aβ$_{42}$, se estudió *in vitro* utilizando la línea celular SN56. La expresión de dichas proteínas aumentó al tratar las células con las moléculas APH a partir de una concentración de 50 μM, en comparación al control. Sin embargo, la expresión se redujo al incubar las células con Fe(II) o con Cd(II) durante 24 h. No obstante, al pretratar las células durante 2 h con las moléculas APH y co-incubarlas con los diferentes metales, se revirtió esta disminución en su expresión, y en mayor medida según aumentaba la concentración de la molécula APH. Con respecto a la reducción de la expresión de la

proteína HSP70 inducida por el Fe(II) o el Cd(II), esta fue revertida parcialmente por las moléculas APH3, APH4 y APH5 a partir de una concentración de 10 μM, y por las moléculas APH1 y APH2 a partir de una concentración de 50 μM, siendo totalmente inhibida por las moléculas APH3, APH4 y APH5 a una concentración de 100 μM en el caso del Cd(II), y APH3 y APH4 a 100 μM en el caso del Fe(II). En el caso de la reducción de la expresión de la P20S por parte de los metales, esta se revirtió parcialmente por parte de las moléculas APH1-5 a partir de concentraciones de 50 μM, y totalmente por la acción de las moléculas APH3 y APH4 en concentraciones de 100 μM. Este aumento de la expresión de las proteínas HSP70 y P20S por parte de las moléculas APH se podría atribuir a la inducción de la vía Nrf2 demostrada en el trabajo anterior. Debido a que la inducción de la vía Nrf2 se produjo a concentraciones inferiores a las que generalmente se observó el efecto en el aumento de la expresión de las proteínas HSP70 y P20S, se llega a la conclusión de que existen otros mecanismos adicionales a la vía Nrf2 que contribuyen al aumento en la expresión de dichas proteínas por parte de las moléculas APH.

Siguiendo los experimentos *in vitro*, se demostró que los metales Fe(II) y Cd(II) aumentaron el contenido de $A\beta_{42}$ en las células cuando estas se incubaron en su presencia durante 24 h. Sin embargo, mediante el pretratamiento con las moléculas APH durante 2 h y la posterior incubación con Fe(II) y Cd(II) durante 24 h adicionales, se logró reducir el contenido de la proteína $A\beta_{42}$ parcial o totalmente en las células, en función de la molécula y su concentración, con respecto a las células tratadas con los metales. En el caso del aumento de la proteína debido al Fe(II), se produjo una reducción parcial por parte de las moléculas APH3 y APH4 a partir de una concentración de 10 μM, y para las moléculas APH1, APH2 y APH5 a partir de una concentración de 50 μM, alcanzando niveles similares al control para las moléculas APH3, APH4 y APH5 a concentraciones de 100 μM. Por lo que respecta a la inducción de la expresión de la $A\beta_{42}$ por parte del Cd(II), se produjo una reducción parcial del contenido de dicha proteína por las moléculas APH3, APH4 y APH5 a partir de una concentración de 10 μM, y de las moléculas APH1 y APH2 a partir de una concentración de 50 μM, siendo esta reducción total para las moléculas APH3, APH4 y APH5 a una concentración de 100 μM. Ni la pre-incubación de las células con las moléculas APH, ni la co-incubación con las proteínas recombinantes HSP70 y P20S alteró el contenido de proteína $A\beta_{42}$ en las células. Sin embargo, en presencia de niveles elevados de expresión de la proteína $A\beta_{42}$ inducidos por los metales, el co-tratamiento con HSP70, P20S o HSP70 + P20S revirtió de forma parcial el aumento de dicha proteína. Por tanto, es probable que ambos mecanismos, HSP70 y P20S, inducidos por las moléculas APH1-5

sean los responsables mayoritarios de la eliminación de las proteínas tóxicas, como la $A\beta_{42}$. Sin embargo, otros mecanismos no dependientes de la inducción en la expresión de las proteínas HSP70 y P20S, como por ejemplo su carácter antioxidante a través de la vía Nrf2 o la quelación metálica, pueden contribuir al efecto neuroprotector de las moléculas APH con respecto al aumento de la proteína $A\beta_{42}$ inducido por los metales.

Finalmente, el efecto producido por la proteína $A\beta_{42}$ en la viabilidad celular y en la inducción apoptótica, y cómo dicho efecto tóxico era reducido por las moléculas APH se estudió mediante experimentos *in vitro*. Para ello, se pretrataron las células SN56 durante 2 h con las moléculas APH1-5. A continuación, se co-incubaron con la proteína $A\beta_{42}$ y se midió la viabilidad celular por el método del MTT y la actividad apoptótica por luminiscencia. Así, se observó la reducción parcial de la citotoxicidad de la $A\beta_{42}$ con el pretratamiento con las moléculas APH2, APH3, APH4 y APH5 a partir de una concentración de 10 μM, y APH1 a partir de una concentración de 50 μM, siendo total dicha reducción de la toxicidad para las moléculas APH3 y APH4 a una concentración de 100 μM. Utilizando las caspasas 3 y 7 como marcadores de la actividad apoptótica celular, se detectó un incremento de dicha actividad con el tratamiento con la proteína $A\beta_{42}$. Sin embargo, la apoptosis se vio disminuida con el pretratamiento de las moléculas APH2, APH3, APH4 y APH5 a partir de 10 μM, y APH1 a partir de 50 μM, siendo totalmente inhibida la actividad apoptótica con el pretratamiento de las moléculas APH3 y APH4 a 100 μM. Por tanto, existe una correlación entre la actividad apoptótica inducida por la proteína $A\beta_{42}$ y su correspondiente citotoxicidad.

A modo de resumen de estos dos primeros trabajos, se puede concluir que las moléculas APH1-5 presentaron propiedades farmacocinéticas acordes a la regla de Lipinski y propiedades ADMET aceptables, lo que permite su consideración como fármacos potenciales en la AD. Por lo que respecta a su interacción con los metales involucrados en la AD, los resultados obtenidos mediante espectroscopía UV-Vis y d^1(UV-Vis) demostraron que las moléculas APH1-5 eran capaces de quelar el Fe(II) y el Cu(II) y las moléculas APH3, APH4 y APH5 el Hg(II). La mayoría de estas interacciones se produjeron a relaciones de concentración metal:APH 1:1, sin que se pudiese descartar la presencia, en menor medida, de complejos metálicos de diferente estequiometría. Estos resultados experimentales fueron corroborados por el análisis *in silico* de los orbitales HOMO y LUMO. Mediante ensayos *in vitro* con la línea celular SN56 se observó que todas las moléculas APH reducían de forma, parcial o total, el efecto citotóxico inducido por los biometales y metales tóxicos, siendo el **APH4** la molécula más prometedora. Además,

todos ellos indujeron la vía Nrf2, directa e indirectamente, aumentando la expresión de enzimas antioxidantes. Esta capacidad antioxidante fue capaz de disminuir la peroxidación lipídica inducida por biometales y metales tóxicos en la AD.

Por otro lado, las moléculas APH han mostrado capacidad para reducir tanto la agregación de la proteína $A\beta_{42}$, como el aumento de la anchura de las fibras amiloides y la acumulación de $A\beta_{42}$ inducida por biometales y metales tóxicos. Esto se ha relacionado con el aumento que estas moléculas producen en la expresión de las proteínas HSP70 y P20S, encargadas de la degradación de proteínas tóxicas. Además, las moléculas APH reducen la citotoxicidad y la actividad apoptótica generadas por la proteína $A\beta_{42}$. Las propiedades neuroprotectoras mostradas por las moléculas **APH1-5** evidencian, por tanto, su capacidad para inhibir o retrasar los eventos acontecidos en la "**hipótesis del ion metálico**" en sinergia con la "**hipótesis de la cascada amiloide**", principal responsable del desarrollo de la AD, favoreciendo la eliminación de la proteína $A\beta_{42}$ a través de diversos mecanismos.

Con el objetivo de profundizar en el desarrollo de moléculas orgánicas con propiedades neuroprotectoras, potencialmente eficaces en el tratamiento de la AD, en el **Artículo 3** se llevó a cabo la síntesis de siete híbridos (**4a**, **4b**, **4c**, **4d**, **5a**, **5b** y **5d**) entre la rivastigmina (RIV) y el hidroxifenilbenzimidazol (BIM). Para ello, las moléculas se sintetizaron, purificaron, caracterizaron y, posteriormente, se estudiaron en términos de capacidad antioxidante, inhibición enzimática, inhibición de la agregación de la proteína $A\beta_{42}$, viabilidad celular y neuroprotección *in vitro*.

En primer lugar, se seleccionaron las moléculas RIV y BIM, como precursores para la síntesis de moléculas híbridas con el fin de asegurar la obtención de moléculas finales con propiedades multi-diana en la AD. La propiedad más relevante de la RIV es la elevada inhibición que presenta con respecto a las enzimas acetilcolinesterasa (AChE) y butirilcolinesterasa (BChE), encargadas de la degradación de los neurotransmisores acetilcolina (ACh) y butirilcolina (BCh), respectivamente. Por otra parte, el BIM posee la capacidad de quelar metales involucrados en la AD, inhibir la agregación de la proteína $A\beta_{42}$ y reducir la producción de ROS. Para modificar la conformación espacial de los híbridos, se utilizaron dos tipos de BIM en las síntesis realizadas: BIMa (serie **4**) y BIMb (serie **5**). Además, con objeto de modular la interacción con la zona activa de la AChE, se introdujeron un número variable de grupos metileno entre ambas moléculas: n = 0 (a), n = 1 (b), n = 2 (c) y n = 3 (d). Para la síntesis de los siete híbridos, se utilizaron diversos métodos, como la reacción de Mannich, ciclaciones, carbametilaciones, hidrogenaciones y

condensaciones, aportando todos ellos buenas recuperaciones en la obtención del producto de síntesis.

En segundo lugar, se realizó una **modelización molecular** para predecir la inhibición, por parte de los híbridos RIV-BIM sintetizados, de las enzimas AChE y BChE. Ambas enzimas tienen una elevada similitud, con un porcentaje de homología en su secuencia de aminoácidos del 65% y un sitio activo con una triada catalítica y el sitio periférico de unión aniónico (PAS) orientado hacia la entrada. Sin embargo, sus diferencias radican en el tamaño del sitio activo de la BChE, superior al de la AChE, permitiendo la unión de la primera con moléculas de mayor tamaño. Los resultados obtenidos *in silico* mostraron que todos los híbridos RIV-BIM eran capaces de penetrar en el sitio activo de la AChE, interaccionando con residuos clave como Phe_{295}, Trp_{286}, Tyr_{124}, Tyr_{72}, Asp_{74}, Tyr_{337} y Trp_{86}. La mayoría de los híbridos (**4a-d** y **5a**) orientaron el extremo BIM hacia el PAS, mientras que el extremo RIV lo hizo hacia el sitio catalítico aniónico (CAS). Además, en el caso de la molécula **4b** se pudo observar un enlace de hidrógeno entre el grupo hidroxilo del extremo BIM con el residuo Tyr_{72}. Sin embargo, las moléculas **5b** y **5d** mostraron una posición invertida de los extremos RIV y BIM, lo que se podría traducir en una peor inhibición de las moléculas más voluminosas (serie **5**) con respecto a la AChE. Con respecto a la BChE, todos los híbridos mostraron una buena interacción con su sitio activo, interaccionando con residuos clave como Tyr_{332}, Trp_{82}, His_{438}, Ser_{198}, Phe_{398}, Trp_{231}, Leu_{286} y Val_{288}. Los híbridos de la serie **4** (**4a-d**) orientaron su extremo BIM hacia el PAS, mientras que el RIV se orientó hacia el CAS. Por otra parte, las moléculas de la serie **5** (**5a**, **5b** y **5d**) entraron de forma preferente en la cavidad, orientando el extremo BIM hacia el CAS y el extremo RIV hacia el PAS. Estos resultados ponen de manifiesto la habilidad potencial de los híbridos RIV-BIM en la inhibición de las enzimas AChE y BChE. Además, las moléculas de la serie **5**, mostraron una mayor afinidad por la BChE comparada con la AChE.

Posteriormente, se procedió a determinar experimentalmente la **capacidad inhibitoria de los híbridos con respecto a las enzimas AChE y BChE**. Además, y con fines de comparación, se evaluaron otras moléculas de referencia que han demostrado buena capacidad de inhibición frente a la AChE, como el donepezilo (DNP) (IC_{50} = 0.0075 μM), RIV (IC_{50} = 32.1 μM) y la tacrina (TAC) (IC_{50} = (0.024 ± 0.007) μM). Las moléculas que presentaron una mayor inhibición de la AChE fueron **4b** (IC_{50} = (14 ± 2) μM), siendo además el híbrido que mejor se acopló al sitio activo en la modelización molecular, seguido por **4a** (IC_{50} = (17.6 ± 0.6) μM), **5a** (IC_{50} = (17.6 ± 0.4) μM) y **4c** (IC_{50} = (17.7 ± 0.8) μM),

mientras que las moléculas **5d** (IC_{50} = (21.4 ± 0.4) μM), **4d** (IC_{50} = (24 ± 1) μM) y **5b** (IC_{50} = (31.7 ± 0.1) μM) mostraron la peor inhibición. Sin embargo, no se apreció ninguna relación entre el número de metilos en la unión entre la RIV y el BIM con la actividad inhibitoria de la AChE, mientras que todos los híbridos fueron más eficaces que la RIV, mejorando, por tanto, las propiedades de esta molécula de referencia. No obstante, su actividad inhibidora resultó ser menor que la de las moléculas de referencia DNP y TAC, como se ha indicado anteriormente, por su elevada efectividad en la inhibición de dicha enzima.

En la inhibición de la BChE, la única molécula que aumentó la inhibición con respecto a la anterior enzima fue **5b** (IC_{50} = (0.30 ± 0.01) μM), siendo a su vez la mejor BChEi, incluso por encima de la RIV (IC_{50} = 0.39 μM). Los híbridos de la serie **5**, **5a** (IC_{50} = (0.9 ± 0.1) μM), **5b** y **5d** (IC_{50} = (1.7 ± 0.2) μM), exhibieron mejores resultados, comparables al DNP (IC_{50} = 1.42 μM). Las moléculas de la serie **4**, **4a** (IC_{50} = (5.85 ± 0.03) μM), **4b** (IC_{50} = (6.5 ± 0.4) μM), **4c** (IC_{50} = (4.8 ± 0.1) μM) y **4d** (IC_{50} = (19.2 ± 0.7) μM), por el contrario, fueron peores BChEi. Estos resultados también están en consonancia con la predicción realizada mediante modelización molecular, en la que las moléculas de la serie **5** mostraron una mayor accesibilidad a la cavidad de la BChE. El índice de selectividad (SI), un parámetro que indica la afinidad en la inhibición de la BChE con respecto a la inhibición de la AChE, para los híbridos indica una mayor actividad frente a la BChE, probablemente debido al elevado tamaño de las moléculas RIV-BIM. Sin embargo, la mayoría de los híbridos puede actuar como inhibidor dual de la AChE y BChE, ya que los SI se encontraron, generalmente, dentro del mismo orden de magnitud, mostrando un efecto dual. Sin embargo, cabe resaltar el SI de la molécula **5b** (SI = 105.7), lo cual indica su elevada afinidad por la BChE frente a la AChE.

Con respecto a la **inhibición de la agregación de la proteína $A\beta_{42}$**, natural e inducida por el Cu(II), se procedió a incubar la proteína con las moléculas híbridas RIV-BIM en ausencia y presencia de dicho metal. Posteriormente, se cuantificó la inhibición de la agregación mediante ThT y espectroscopía de fluorescencia y se visualizó la morfología de las fibras mediante TEM. Las moléculas **4c** y **4d** fueron las que menor inhibición de la agregación mostraron: 21.2% y 20.1% para la natural, y 22.0% y 21.3% para la inducida por el Cu(II), respectivamente. El resto de las moléculas híbridas mostraron una inhibición natural más alta que la TAC (28.1%), aunque menor que la curcumina (65.7%), siendo dichos valores 39.0% para **4a**, 39.6% para **4b**, 42.1% para **5d**, 44.5% para **5a** y 58.7% para **5b**. Con respecto a la inhibición de la agregación inducida por el Cu(II), las moléculas

híbridas mostraron, en general, un porcentaje ligeramente mayor que en ausencia de cobre, siendo tales resultados 40.3% para **5d**, 41.2% para **4a**, 45.4% para **5a**, 48.8% para **4b** y 60.8% para **5b**, siendo también inferiores al de la curcumina (62.7%). De la misma forma que ocurría en la inhibición enzimática, las moléculas de la serie **5** demostraron, en general, una mayor habilidad para inhibir la agregación de la proteína $A\beta_{42}$.

Para estudiar la **morfología de las fibras amiloides**, se analizaron las incubaciones mediante TEM. Así, se pudo observar que las moléculas RIV-BIM no aumentaron la agregación de las fibras de la proteína $A\beta_{42}$ en comparación con el control, ambas en ausencia de Cu(II). Con respecto a la longitud de las mismas, las moléculas **4a**, **4b** y **5b**, fueron las que presentaron las fibras más cortas, siendo la última de ellas la que más inhibió la agregación (58.7%). Por otra parte, las moléculas **4c** y **4d**, además de ser las que presentaron peores resultados de inhibición (21.2% y 20.1%, respectivamente), mostraron las fibras más largas. La muestra control en ausencia de Cu(II), presentó un valor de anchura de las fibras amiloides de (4.9 ± 0.2) nm, siendo la molécula **4d**, en concordancia con los resultados previos, la única que aumentó la anchura de las fibras ((6.7 ± 0.3) nm), mientras que el resto de las moléculas la disminuyó (3.3-4.5 nm). Así, las moléculas más prometedoras en este aspecto fueron, una vez más, **5b** ((3.8 ± 0.1) nm) y **5d** ((3.3 ± 0.2) nm), reduciendo la anchura de las fibras un 22.4% y un 32.7% respectivamente.

En presencia de Cu(II), la agregación de las fibras amiloides aumentó sustancialmente, con fibras más largas y aglomeradas que para las incubaciones en ausencia del metal. Las moléculas de la serie **5** mostraron una mayor efectividad reduciendo la agregación inducida por el Cu(II) de las fibras amiloides, especialmente **5b** y **5d**, en consonancia con los resultados previos. La anchura del control de fibras incubadas en presencia de Cu(II) presentó un valor de (6.8 ± 0.3) nm, un 38.8% superior al control en ausencia de Cu(II). Las moléculas **4a**, **4b**, **4c** y **5a** redujeron la anchura de las fibras hasta alcanzar valores similares a los obtenidos por la proteína $A\beta_{42}$ en ausencia de Cu(II) (4.6-4.9 nm), mientras que la molécula **4d** no la disminuyó con respecto al control en presencia de Cu(II). Con respecto a las moléculas más prometedoras en este apartado, **5b** y **5d**, de la misma forma que demostraron una buena inhibición de la agregación amiloide en ausencia y presencia de Cu(II), y un acortamiento y estrechamiento de las fibras en ausencia de Cu(II), también redujeron la anchura inducida por el Cu(II) de las fibras amiloides hasta un 39.7% y 42.6% respectivamente.

Por otro lado, la **actividad antioxidante** mostrada por los híbridos RIV-BIM se determinó mediante el método de captación de radicales libres DPPH, utilizando la molécula 1,2-dimetil-3-hidroxi-4-piridona (DMHP) como referencia. En general, ninguno de ellos demostró una capacidad antioxidante considerable, estando por debajo del DMHP (IC_{50} = 0.157 mM), siendo **4b** el que presentó el mejor valor de IC_{50} (IC_{50} = (0.9 ± 0.1) mM).

Posteriormente, se determinó la **viabilidad celular y la neuroprotección *in vitro*** con la línea celular SH-SY5Y. En primer lugar, se determinó la citotoxicidad de los híbridos RIV-BIM para seleccionar una concentración no tóxica para cada uno de ellos que a su vez demostrase neuroprotección en los siguientes ensayos, siendo esta 1 μM para **4a**, **4b** y **5b**, 2 μM para **4c** y **5a** y 3 μM para **4d**. En segundo lugar, se procedió a estudiar la reducción, por parte de los híbridos, de la citotoxicidad provocada por la incubación con el monómero $A\beta_{42}$ (30%). En este sentido, la molécula **4d** fue el que mostró mayor neuroprotección, aumentando la viabilidad celular con respecto a las células tratadas con $A\beta_{42}$. Por último, se determinó la reducción de la producción de ROS provocada por el hierro por parte de las moléculas, siendo la molécula **5a** la única que demostró un efecto neuroprotector significativo con respecto a la reducción del estrés oxidativo.

Finalmente, se realizó un análisis *in silico* con el objetivo de predecir las **propiedades farmacocinéticas** de los híbridos RIV-BIM, comparándolas con aquellas predichas para la RIV como molécula inicial en las síntesis de los mismos. Todos los híbridos presentaron valores adecuados de peso molecular (430.462 - 472.543 g mol^{-1}), PSA (113.662 – 117.689), lipofilicidad (clog P(o/w) = 3.884 – 5.398), interacción con la albúmina de suero humano (HSA) (log K = 0.519 – 0.998), y permeabilidad de la barrera hematoencefálica (BBB) (log = (-1.758) – (-1.238)). La permeabilidad predicha frente a las Caco-2 fue normal para todas las moléculas, siendo las de la serie **5** las que mejores resultados aportaron (> 500 nm s^{-1}). Además, todos ellos demostraron una buena permeabilidad frente a las células de riñón canino de Madin-Darby (MDCK) (151 - 258 nm s^{-1}) y elevada absorción oral (88% – 94%). Estos híbridos RIV-BIM demostraron propiedades farmacocinéticas aceptables para ser considerados fármacos orales, debido a que no presentaron ninguna violación de la regla de Lipinski, excepto la molécula **5d** que tuvo alta lipofilicidad y, por tanto, tuvo una violación en dicha regla. Sin embargo, todos fueron menos permeables frente a las Caco-2 y a las MDCK que la propia RIV, ya que presentó unos valores de 1381 nm s^{-1} y 776 nm s^{-1} respectivamente.

Para evaluar la gran cantidad de datos sobre propiedades neuroprotectoras obtenida en este trabajo y resaltar las diferencias de las moléculas en cuanto a las propiedades evaluadas, se realizó un análisis de componentes principales (PCA). Este método quimiométrico permitió explicar un 91.9% de la variabilidad de los datos con tres componentes principales, lo que demostró la fiabilidad del modelo. La bigráfica 3D obtenida en este análisis permitió visualizar un agrupamiento de las moléculas de la serie **4** en el lado izquierdo de la gráfica, mientras que las moléculas de la serie **5** se encontraron en el lado opuesto, por lo que ambas series poseen diferentes propiedades basadas en su estructura con respecto al primer componente principal. Este primer componente se explica, principalmente, por la absorción oral, la permeabilidad frente a las Caco-2 y las MDCK, la lipofilicidad, la interacción con la HSA, y la inhibición de la agregación de la proteína $A\beta_{42}$. Además de existir diferencias entre los híbridos de la serie **4** y de la serie **5**, también se encontró un patrón de comportamiento con respecto al número de metilos entre los extremos RIV y BIM de los híbridos, mostrando una secuencia ordenada de las moléculas desde la **a** hasta la **d**. Esta linealidad se observa mejor para las moléculas de la serie **4**, ya que ninguna presentó violaciones de la regla de Lipinski, propiedad con alto peso en el tercer componente principal, mientras que la molécula **5d** tuvo una violación que rompió con el patrón **a**-**d**. Los valores más altos de IC_{50} y, por tanto, menos eficaces en la inhibición de la BChE aumentan en el lado izquierdo del gráfico, donde efectivamente se encuentran las moléculas de la serie **4**.

A modo de resumen de este trabajo, donde se evalúan las propiedades neuroprotectoras de siete híbridos entre la RIV y el BIM como potenciales fármacos multi-diana contra la AD, se pueden concluir los elevados beneficios de la hibridación en la síntesis de nuevas moléculas. La modelización molecular permitió predecir *in silico* la posible interacción entre las moléculas y las enzimas AChE y BChE, obteniendo resultados satisfactorios y anticipando la inhibición de las moléculas de las series **4** y **5**. Las herramientas computacionales también permitieron predecir las propiedades farmacocinéticas, evidenciando la idoneidad de los híbridos como potenciales fármacos y su posible administración por vía oral. Con respecto a la inhibición de la AChE, la molécula **4b** ((IC_{50} = (14 ± 2) μM) fue la que más destacó, aunque todas ellas mejoraron las propiedades de la RIV (IC_{50} = 32.1 μM). Con relación a la inhibición de la BChE, generalmente todas las moléculas mejoraron sus resultados con respecto a la anterior enzima, y la serie **5** demostró mucha más eficacia que la serie **4**, especialmente las moléculas **5b** ((IC_{50} = (0.30 ± 0.01) μM) y **5a** ((IC_{50} = (0.9 ± 0.1) μM). Los SI obtenidos permiten concluir el uso de los híbridos

como inhibidores duales de AChE y BChE. La cuantificación de la agregación de la proteína $A\beta_{42}$ mostró la eficacia de las moléculas de la serie **5**, superior a los de la serie **4**, con respecto a la inhibición amiloide natural e inducida por el Cu(II). Además, la morfología de las fibras observada con el TEM también demostró diferencias entre los híbridos, siendo las moléculas **5b** y **5d** las que más redujeron la anchura de dichas fibras en ausencia de metal, mientras que **4d** no afectó a este parámetro. También se observó un aumento de la agregación debida al Cu(II) en comparación al control de la proteína, cuya anchura disminuyó notablemente en presencia de las moléculas **5b** y **5d**. Los experimentos *in vitro* demostraron que las moléculas **4d** y **5a** fueron las mejores en términos de reducción de la toxicidad de la proteína $A\beta_{42}$ y reducción del estrés oxidativo, respectivamente. Por otro lado, las herramientas quimiométricas, como el PCA, ayudaron a la interpretación de un elevado número de datos variados y complejos, permitiendo agrupar a los híbridos sintetizados en función de su serie (**4** o **5**) y del número de grupos metilo entre los extremos RIV y BIM (**a**-**d**). Como conclusión, los híbridos desarrollados y evaluados en este trabajo presentan propiedades muy interesantes como fármacos potenciales en la AD, destacando en diversas propiedades neuroprotectoras.

Por todo ello, en esta primera parte de la Tesis Doctoral, se ha evaluado el potencial neuroprotector de determinadas moléculas orgánicas, como las denominadas **APH1-5** derivadas de la 7-aminofenantridin-6-ona, y los híbridos **4a-d**, **5a**, **5b** y **5d** de la RIV y el BIM, siendo ambas familias candidatos potenciales a fármacos en la AD.

A continuación, con objeto de estudiar el efecto de las especies de selenio en la AD, en el **Artículo 4** se evaluaron las propiedades neuroprotectoras de algunas especies de selenio y, en concreto, de las **nanopartículas de selenio** (Ch-SeNPs).

En este trabajo, se lograron sintetizar con éxito dos tipos de nanopartículas: nanopartículas de selenio estabilizadas con quitosano (**Ch-SeNPs**) y nanopartículas de selenio estabilizadas con quitosano y ácido clorogénico (**CGA@ChSeNPs**). Para confirmar la presencia de ácido clorogénico (CGA) en las CGA@ChSeNPs y la consecuente aportación de las propiedades antioxidantes de este polifenol, se realizó un análisis mediante cLC-DAD en el dializado, no detectándose CGA ($CGA < 0.033\ \mu M$) y confirmando, por tanto, su unión a las nanopartículas. La caracterización mediante TEM y EDXS de ambos tipos de nanopartículas de selenio evidenció una morfología esférica para todas ellas, con un diámetro de (60 ± 6) nm para Ch-SeNPs y de (80 ± 20) nm para CGA@ChSeNPs, mostrando estas últimas una distribución más heterogénea. Mediante

difracción electrónica (ED) se observó una estructura cristalina, con una distancia interplanar de 3.3 Å en el primer anillo, para ambos tipos de nanopartículas. El diámetro hidrodinámico obtenido mediante DLS fue de (91 ± 2) nm para Ch-SeNPs y de (196 ± 1) nm para CGA@ChSeNPs, con un bajo índice de polidispersidad indicativo de la monodispersidad y homogeneidad de las nanopartículas. El diámetro hidrodinámico es superior al obtenido mediante TEM, ya que el primero incluye el efecto de agentes estabilizantes y capas del solvente adheridas a la superficie de las nanopartículas, mientras que el segundo solo tiene en cuenta el tamaño del núcleo inorgánico. Los ZP fueron (-38 ± 1) mV y (45 ± 1) mV, para Ch-SeNPs y CGA@ChSeNPs respectivamente, indicativos de la alta estabilidad de las nanopartículas y su baja tendencia a aglomerarse, especialmente en el caso de las segundas. Además, se demostró que la presencia de CGA en las nanopartículas de selenio afecta a la carga neta superficial de las mismas, positiva para Ch-SeNPs y negativa para CGA@ChSeNPs, por lo que pueden demostrar diferencias con respecto a su interacción con sistemas biológicos y proteínas.

Para determinar los efectos del selenio sobre los biometales involucrados en la AD se estudió su **interacción** mediante espectroscopía UV-Vis y d^1(UV-Vis), a través de la aparición de nuevas bandas de absorción o de la modificación de las existentes en los espectros registrados. Los análisis de la interacción entre las especies de selenio orgánicas (selenometionina (SeMet), selenometilselenocisteína (MeSeCys) y selenocistina $(SeCys)_2$), inorgánicas (Se(IV) y Se(VI)) y nanoparticuladas (Ch-SeNPs y CGA@ChSeNPs) con los biometales Fe(II), Cu(II) y Zn(II), mostraron las diferencias en función de la especie en la que el selenio se encontrase presente. Con respecto al **Fe(II)**, se observó su interacción con SeMet, $(SeCys)_2$, MeSeCys, Se(IV) y Se(VI), mientras que no se produjo ningún cambio en el espectro de absorción con ningún tipo de nanopartículas. En relación al **Cu(II)**, se observó su interacción con SeMet, $(SeCys)_2$, MeSeCys, Se(VI), Ch-SeNPs y CGA@ChSeNPs, pero no con Se(IV). En el caso concreto de las Ch-SeNPs, presentaron una banda de absorción a 265 nm en ausencia de Cu(II) en el espectro UV-Vis y un corte en el eje X en d^1(UV-Vis), mientras que dicha banda desapareció en presencia del cobre. Finalmente, el **Zn(II)** solo mostró interacción con SeMet, no observándose cambios con las demás especies.

Estos resultados sugieren la elevada capacidad de interacción de la **SeMet**, una especie de gran relevancia debido a su presencia en alimentos y suplementos alimenticios, siendo la única que mostró efecto sobre los tres biometales estudiados. Además, las especies $(SeCys)_2$, MeSeCys y Se(VI) mostraron interacción tanto con Fe(II) como con Cu(II).

Finalmente, el Se(IV) solo interaccionó con Fe(II), y Ch-SeNPs y CGA@ChSeNPs solo con Cu(II). Por tanto, existe una gran diversidad entre las interacciones de las especies de selenio con los biometales, siendo las mismas generales como la **SeMet**, o específicas como las **Ch-SeNPs** y **CGA@ChSeNPs**.

Posteriormente se estudió la inhibición, por parte de las especies de selenio, de la **agregación inducida por los biometales de la proteína Aβ_{42}**. Las fibras de la muestra control, incubadas en ausencia de especies de selenio y biometales, mostraron una distribución no agregada. La disposición de las fibras amiloides cambió drásticamente al ser incubadas en presencia de los biometales, sufriendo una agregación similar para el Fe(II), Cu(II) y Zn(II), corroborando de nuevo la "**hipótesis del ion metálico**". Esta agregación también aumentó en presencia de la totalidad de especies orgánicas de selenio (SeMet, $(SeCys)_2$ y MeSeCys), inorgánicas (Se(IV) y Se(VI)) y de un tipo de nanopartículas (CGA@ChSeNPs) en ausencia de metal. Sin embargo, las **Ch-SeNPs** fueron la única especie de selenio que consiguió inhibir la agregación natural de las fibras amiloides, reduciendo su número y su longitud. Para determinar si las diferencias observadas entre los dos tipos de nanopartículas se debían a la presencia del CGA, se incubó la proteína Aβ_{42} en presencia de dicho polifenol, obteniendo también una distribución agregada y confirmando su papel amiloidogénico en el recubrimiento de las nanopartículas.

El siguiente paso fue determinar si las especies de selenio eran capaces de **inhibir la agregación amiloide** inducida por los metales. En este aspecto, una vez más, las **Ch-SeNPs** fueron las únicas capaces de inhibir la agregación inducida por el Fe(II) y el Zn(II), reduciendo tanto el número de fibras como su longitud. La morfología de las nanopartículas permaneció intacta al ser incubadas con la proteína Aβ_{42}, tanto en ausencia como en presencia de los metales. Sin embargo, no lograron inhibir la agregación amiloide inducida por el Cu(II), siendo el único metal cuyo efecto no se pudo neutralizar en presencia de ninguna especie de selenio. Por ello, los cambios espectrofotométricos observados en la interacción de Ch-SeNPs y CGA@ChSeNPs con el Cu(II) se podrían deber a una reacción redox entre el Se(0) y el Cu(II) más que a una posible quelación.

Con ánimo de profundizar en los mecanismos anti-amiloidogénicos de las Ch-SeNPs, y habiendo demostrado potencial inhibitorio, se estudió su capacidad de **revertir la agregación amiloide** provocada por el Fe(II). Los resultados mostraron que este tipo de nanopartículas de selenio era capaz de desagregar las fibras amiloides previamente agregadas por la acción del Fe(II), reduciendo también la longitud de las mismas.

Adicionalmente, se estudió el efecto de las especies de selenio y los biometales en la **anchura de las fibras de la proteína Aβ$_{42}$**. En condiciones control, las fibras mostraron una anchura de (6.3 ± 0.2) nm, y sufrieron un incremento en presencia de los metales, por ejemplo el Fe(II) ((9.0 ± 0.2) nm), y de la mayoría de especies de selenio (40%): SeMet, (SeCys)$_2$, MeSeCys, Se(IV), Se(VI) y CGA@ChSeNPs. Sin embargo, en presencia de Ch-SeNPs la anchura se redujo hasta un 20% en ausencia y en presencia de metales, alcanzando niveles similares a los de la proteína Aβ$_{42}$ control.

Finalmente, debido a la importancia del estrés oxidativo en la progresión de la AD, se estudió la **capacidad antioxidante** de todas las especies de selenio. Los resultados mostraron que ambos tipos de nanopartículas ejercían su efecto antioxidante en 10 min, en comparación al resto de especies (35 min). Tal y como era de esperar, las nanopartículas recubiertas con el polifenol, **CGA@ChSeNPs**, mostraron el mejor resultado en términos de capacidad antioxidante (IC_{50} = (0.07 ± 0.05) mM), otorgando el CGA propiedades antioxidantes adicionales en comparación a las Ch-SeNPs (IC_{50} = (0.9 ± 0.1) mM). El resto de las especies de selenio, excepto la (SeCys)$_2$, presentaron una capacidad antioxidante considerable, aunque inferior a la mostrada por las nanopartículas.

Como conclusión, en este trabajo se ha puesto de manifiesto el potencial de las **Ch-SeNPs** para combatir la AD, debido a las propiedades neuroprotectoras mostradas. Entre ellas, cabe destacar sus excelentes propiedades antioxidantes, superiores al resto de especies no nanoparticuladas de selenio, útiles a la hora de mitigar el estrés oxidativo provocado por los biometales Fe(II) y Cu(II) en la AD. Además, las nanopartículas fueron capaces de inhibir la agregación de la proteína Aβ$_{42}$ inducida por los biometales Fe(II) y Zn(II) y de desagregar las fibras amiloides previamente agregadas por el Fe(II), disminuyendo, por tanto, la formación de placas amiloides extracelulares, lo que podría inhibir el desarrollo de la "**hipótesis de la cascada amiloide**" y evitar la formación de ovillos neurofibrilares de la proteína tau. Así, las Ch-SeNPs constituyen una especie de selenio prometedora para futuros ensayos en la AD. Sin embargo, el resto de las especies de selenio también mostraron propiedades neuroprotectoras interesantes, como la amplia y variada interacción con los biometales, especialmente la **SeMet**, y sus elevadas propiedades antioxidantes, como en el caso de las **CGA@ChSeNPs**, ya que pueden actuar como desactivador de ROS, claves en el desarrollo de la AD.

Debido a la importancia que poseen determinados aminoácidos en la AD, y cómo su comportamiento quiral puede influir en el desarrollo de dicha enfermedad, se procedió a

estudiar en el **Artículo 5** el efecto neuroprotector ejercido por las Ch-SeNPs frente a determinados enantiómeros de aminoácidos.

Para ello, en primer lugar, se realizó la caracterización, reproducibilidad de la síntesis y estabilidad de almacenamiento de las Ch-SeNPs. Mediante las micrografías de TEM se observó la morfología de las nanopartículas, siendo esféricas y con un diámetro de (60 ± 1) nm. Se aplicó el test ANOVA al 95% de confianza a cuatro repeticiones de esta síntesis y no se observaron diferencias significativas en el diámetro de las Ch-SeNPs, poniéndose de manifiesto la reproducibilidad del método de síntesis. Mediante UV-Vis se observó la presencia de una banda de absorción a 265 nm, característica de estas nanopartículas, y la invariabilidad de esta banda durante el periodo de almacenamiento de las Ch-SeNPs, a 4 ºC en oscuridad a lo largo de un mes, evidenciándose su estabilidad durante el almacenamiento.

En segundo lugar, se estudió la **agregación de la proteína $A\beta_{42}$** bajo el efecto de diferentes enantiómeros de aminoácidos. Se observó un aumento de la agregación amiloide, en comparación al control, cuando el monómero $A\beta_{42}$ fue incubado junto con determinados **D-aminoácidos**. Este es el caso de enantiómeros como el D-Asp relacionado con el receptor N-metil-D-aspartato (NMDA) involucrado en la adquisición de memoria y el aprendizaje, no relacionados con el NMDA como la D-Phe, y enantiómeros inactivos como la D-Ala, el D-Glu y la DL-SeMet. Sin embargo, algunos L-aminoácidos como el L-Trp, L-Tyr y L-Glu también aumentaron la agregación de la proteína $A\beta_{42}$. No obstante, la mayoría de **L-aminoácidos**, considerados la forma enantiomérica natural del cuerpo humano, no afectaron a la agregación amiloide, como es el caso del L-Asp, L-Phe, L-Ala, L-Ser y L-SeMet. Por otra parte, algunos D-aminoácidos como D-Trp, D-Tyr y D-Ser tampoco aumentaron la agregación de la proteína $A\beta_{42}$. Estos resultados demuestran el efecto del entorno quiral en la agregación amiloide siendo, por tanto, un factor a considerar en la AD.

Posteriormente, se estudió el efecto de **inhibición de la agregación amiloide** por parte de las **Ch-SeNPs**, una especie de selenio prometedora en anteriores ensayos. Estas nanopartículas fueron capaces de inhibir la agregación inducida enantioméricamente por los aminoácidos en todos los casos, con fibras de la proteína $A\beta_{42}$ dispersas, demostrando la inhibición del proceso de agregación inducido por el entorno quiral producido por los aminoácidos.

Los resultados del estudio de la **morfología de las fibras de la proteína $A\beta_{42}$** mostraron una anchura de (5.4 ± 0.7) nm en ausencia de enantiómeros de aminoácidos y Ch-SeNPs. En presencia de los **L-aminoácidos no amiloidogénicos**, L-Phe ((4.3 ± 0.5) nm), L-Asp ((4.7 ± 0.6) nm), L-SeMet ((4.3 ± 0.7) nm), L-Ala ((3.7 ± 0.4) nm) y L-Ser ((4.5 ± 0.8) nm), se observaron las fibras más estrechas, con reducciones entre 13% y 31% con respecto a las fibras control. En presencia de los **D-aminoácidos no amiloidogénicos**, se redujo la anchura de las fibras un 20% en el caso de D-Trp ((4.3 ± 0.3) nm) y un 26% para el D-Tyr ((4.0 ± 0.4) nm), mientras que la anchura aumentó un 46% en el caso del D-Ser ((7.9 ± 0.9) nm), estando este último aminoácido relacionado con el receptor NMDA. En presencia de los **D-aminoácidos amiloidogénicos**, D-Phe ((7.9 ± 0.6) nm), D-Asp ((7.1 ± 0.6) nm), D-Ala ((7.2 ± 0.5) nm), D-Glu ((12 ± 1) nm) y DL-SeMet ((9 ± 1) nm) las anchuras de las fibras sufrieron un incremento significativo, desde un 31% hasta un 122%. En presencia de los **L-aminoácidos amiloidogénicos**, L-Trp ((8.5 ± 0.6) nm), L-Tyr ((8.4 ± 0.7) nm) y L-Glu ((29 ± 1) nm), las fibras aumentaron drásticamente su anchura en algunos casos, desde un 55% hasta un 437%.

Los resultados obtenidos en la evaluación de la agregación de la proteína $A\beta_{42}$ por parte de estos aminoácidos, proporcionan información valiosa acerca del carácter enantioméricamente dependiente de la agregación amiloide. Como norma general, los D-aminoácidos, la forma no natural presente en el organismo, producen una mayor acumulación de fibras amiloides que los L-aminoácidos, con algunas excepciones como la Tyr y el Trp. Las Ch-SeNPs son capaces de inhibir la agregación amiloide producida por los enantiómeros de los aminoácidos, presumiblemente debido a la naturaleza quiral del quitosano utilizado como agente estabilizante en la síntesis de las nanopartículas. La anchura de las fibras de la proteína $A\beta_{42}$ también se vio afectada por el entorno quiral, siendo generalmente disminuida en presencia de L-aminoácidos, con algunas excepciones como Trp, Tyr y especialmente Glu, cuyos enantiómeros produjeron las fibras más anchas de entre todas las estudiadas. El aminoácido Asp produjo el efecto más leve sobre la anchura de las fibras, reduciéndola un 13% para el L-Asp o aumentándola un 31% para el D-Asp.

Para profundizar en la **interacción entre las Ch-SeNPs y los enantiómeros de los aminoácidos**, se emplearon técnicas espectroscópicas. Mediante espectroscopía de absorción UV-Vis se determinó la interacción enantioselectiva entre las Ch-SeNPs y el Trp, mostrando una mayor absorbancia la banda conjunta de Ch-SeNPs + D-Trp que la correspondiente a Ch-SeNPs + L-Trp, mientras que ambos enantiómeros presentaron la

misma absorbancia en ausencia de las nanopartículas. Sin embargo, no se apreciaron diferencias para los enantiómeros de la Tyr. Con el fin de estudiar la posible interacción entre aminoácidos que presentan una baja o nula absorción en la zona del UV, fue necesario realizar una derivatización con orto-ftalaldehído (OPA) de los diferentes enantiómeros de los aminoácidos evaluados. Para establecer la existencia de diferencias espectrales en presencia de los diferentes enantiómeros, a diversos niveles de concentración con cantidades diferentes de Ch-SeNPs, se planteó un diseño experimental factorial y se aplicaron modelos de regresión para la correcta apreciación de las diferencias en la interacción enantiomérica de los aminoácidos con las Ch-SeNPs. Los modelos matemáticos de regresión aplicados, con unos coeficientes de determinación múltiple (R^2) superiores al 70%, lograron explicar las diferencias observadas en las interacciones de las Ch-SeNPs con los enantiómeros de la Phe, Asp, Ser y Trp. El ANOVA en el que se basa el diseño experimental factorial permite descomponer el modelo en diferentes factores y evaluar cada uno de ellos por separado (*ecuación 1*).

$$Y = a_0 + a_1X_1 + a_2X_2 + a_3X_1^2 + a_4X_2^2 + a_5X_1X_1 \qquad (ecuación\ 1)$$

Donde Y es la variable de respuesta predicha (intensidad de la señal), a_0 es la intercepción, a_1 y a_2 son los coeficientes lineales de X_1 (concentración del enantiómero de aminoácido) y X_2 (concentración de las Ch-SeNPs), a_3 y a_4 con los coeficientes cuadráticos de X_1 y X_2, y a_5 es el coeficiente de interacción de X_1 y X_2.

De esta forma, el factor correspondiente a la concentración lineal de Ch-SeNPs fue el que presentó una mayor influencia, siendo solo significativo en el caso de los D-aminoácidos. En segundo lugar, se encontraron el coeficiente lineal de la concentración de aminoácido, significativo solo para D-Ser y D-Trp, y el de la interacción entre nanopartículas y aminoácidos, significativo para D-Phe y D-Ser. En último lugar, los coeficientes cuadráticos de concentración de Ch-SeNPs y aminoácidos fueron solo significativos para la D-Ser. Estos resultados evidenciaron la interacción enantioselectiva de las Ch-SeNPs, explicando en parte la diferencia en la agregación amiloide inducida por los aminoácidos en presencia y ausencia de Ch-SeNPs.

El diagrama de Pareto de efectos estandarizados mostró diferencias entre la interacción de las Ch-SeNPs con la D-Phe y la L-Phe. Como ya se vio en el modelo de regresión aplicado, mientras que en el caso de la D-Phe la concentración de Ch-SeNPs y la interacción con los aminoácidos fueron factores significativos, ningún factor fue significativo en el caso de la L-Phe. En la gráfica de efectos principales, la D-Phe presentó

una respuesta lineal mientras que la L-Phe tuvo una respuesta curva. Finalmente, en la metodología de superficie de respuesta (SRM) se obtuvo un mínimo para la concentración 105 μM de D-Phe y 35 μM de Ch-SeNPs, sugiriendo una relación de concentraciones 3:1 para la máxima interacción, mientras que este efecto no se apreció en la L-Phe. En el caso de las interacciones entre las Ch-SeNPs y los enantiómeros de la Ser, todos los factores lineales y cuadráticos, de concentraciones de Ch-SeNPs y aminoácidos, y de la interacción entre ambos, fueron significativos en el caso de la D-Ser, mientras que ninguno fue significativo en el caso de la L-Ser. Con respecto al aminoácido Asp, la emisión del enantiómero D-Asp mostró únicamente un factor significativo, correspondiente a la concentración lineal de las Ch-SeNPs, mientras que para la emisión del L-Asp ningún factor fue significativo.

Los resultados correspondientes a la interacción de las Ch-SeNPs con los enantiómeros de aminoácidos ponen de manifiesto la **naturaleza enantioselectiva** de dicha interacción, estando orientada hacia los D-aminoácidos, generalmente más amiloidogénicos y constituyendo la forma no natural en el organismo.

Finalmente, debido a la importancia comentada con anterioridad del estrés oxidativo en la AD, se determinó la **capacidad antioxidante** de los enantiómeros de los diferentes aminoácidos evaluados. Sin embargo, la mayoría de los aminoácidos no mostraron capacidad antioxidante significativa, a las concentraciones estudiadas y habitualmente presentes en el cerebro humano, en ninguno de los dos métodos experimentales (DPPH y TBARS) utilizados. Únicamente los enantiómeros de la Tyr mostraron un efecto antioxidante, con ligeras diferencias entre el enantiómero L-Tyr (IC_{50} = (370 ± 40) μM) y el enantiómero D-Tyr (IC_{50} = (314 ± 6) μM). Así, por lo general, la capacidad antioxidante de los aminoácidos estudiados no tuvo un efecto significativo con respecto a estos estudios.

Por todo ello, y a modo de conclusión en este trabajo, se ha podido determinar la influencia del entorno quiral en la agregación de la proteína $A\beta_{42}$, principal responsable en la "**hipótesis de la cascada amiloide**". La mayoría de los enantiómeros amiloidogénicos fueron los D-aminoácidos, con algunas excepciones, mientras que los L-aminoácidos, la forma natural en el organismo, no afectaron, generalmente, al aumento de la agregación amiloide. De la misma forma, la anchura de las fibras de la proteína $A\beta_{42}$ también fue afectada por el entorno quiral. Las Ch-SeNPs, que en trabajos anteriores inhibieron la agregación amiloide inducida por metales, demostraron además ser capaces de inhibir la agregación amiloide inducida enantioméricamente por aminoácidos amiloidogénicos. Estas

nanopartículas también demostraron una interacción enantioselectiva con Trp, Phe, Ser y Asp, por lo que el mecanismo de inhibición de la agregación amiloide mostrado por las nanopartículas podría estar relacionado con la naturaleza quiral de las Ch-SeNPs.

Dado el potencial neuroprotector de las Ch-SeNPs, se profundizó acerca de su comportamiento *in vitro* en el **Artículo 6**, ofreciendo resultados de las diferentes especies de selenio en términos de **citotoxicidad** y **acumulación en células individuales**, además de permitir evaluar la **localización intra** y **extracelular** de las Ch-SeNPs.

Las líneas celulares estudiadas fueron las células de neuroblastoma humano (**SH-SY5Y**) y de neuroblastoma de ratón (**Neuro-2a**), debido a que se consideran modelos *in vitro* para estudios en la enfermedad de Alzheimer. En primer lugar, se evaluó la **estabilidad de las Ch-SeNPs** al nivel de concentración 50 μM en ambos medios de cultivo: DMEM con 10% FBS (Neuro-2a) y DMEM/F12 con 10% FBS (SH-SY5Y), incubando las Ch-SeNPs a 37 ºC durante 48 h. Los espectros EDXS mostraron la presencia de selenio en todas las muestras estudiadas, además de elementos pertenecientes al medio de cultivo como Na, K, Ca y Cl (NaCl, KCl, $CaCl_2$ y $NaHCO_3$). En las micrografías registradas mediante TEM, se observó la presencia de nanopartículas esféricas tanto en las muestras control como en las Ch-SeNPs incubadas en los diferentes medios de cultivo celulares. No obstante, las Ch-SeNPs en el medio de cultivo de las células SH-SY5Y mostraron una ligera interacción con los componentes del medio, al contrario de lo que ocurrió con el medio de las células Neuro-2a. Los diámetros se midieron con el programa ImageJ, siendo para las Ch-SeNPs control de (60 ± 1) nm, Ch-SeNPs en medio de cultivo de las células Neuro-2a de (61 ± 1) nm, y en medio de cultivo de las células SH-SY5Y de (60 ± 2) nm. Estos diámetros se compararon mediante ANOVA al 95% de confianza, no encontrando diferencias significativas entre los diferentes tratamientos ($n > 100$). Por tanto, se pudo concluir que las **Ch-SeNPs presentaban estabilidad en las condiciones estudiadas** para realizar los siguientes ensayos *in vitro*.

En segundo lugar, se estudió el **efecto citotóxico** de las **Ch-SeNPs**, además de otras especies de selenio presentes en el organismo como **SeMet** y **MeSeCys**, sobre ambas líneas celulares, empleando el método del **MTT** y la **citometría de flujo** con el fluorocromo yoduro de propidio (PI). Las concentraciones estudiadas fueron 50, 250, 500, 750 y 1000 μM para todas las especies de selenio. Los resultados obtenidos mostraron que estos dos métodos bioanalíticos utilizados para determinar la citotoxicidad presentaban, en general, resultados similares, siendo la citometría de flujo la que ofrecía valores de LC_{50} ligeramente

superiores, en comparación al método del MTT, para las células Neuro-2a. Comparando los resultados de ambas líneas, las células de neuroblastoma de ratón (Neuro-2a) fueron menos resistentes al efecto de todas las especies de selenio, con valores de LC_{50} inferiores, que las células de neuroblastoma humano (SH-SY5Y). En relación con las especies de selenio, las menos citotóxicas fueron aquellas que se encuentran de forma natural en el organismo, la SeMet y la MeSeCys, formando parte de los aminoácidos que contienen selenio y que desempeñan un papel biológico esencial dentro del organismo. Con respecto a las Ch-SeNPs, los LC_{50} que determinaron su citotoxicidad fueron (250 ± 30) μM (MTT) y (330 ± 20) μM (citometría de flujo) para las células Neuro-2a, y (350 ± 10) μM (MTT) y (430 ± 10) μM (citometría de flujo) para las células SH-SY5Y. Por tanto, se confirmó que las **Ch-SeNPs a una concentración de 50 μM no producían un efecto citotóxico relevante**, siendo la misma siete veces inferior al mínimo LC_{50} obtenido para las células SH-SY5Y y, confirmando, por tanto, su potencial como compuesto anti-AD.

Una vez obtenido un valor de concentración de Ch-SeNPs relativamente seguro para las células de neuroblastoma, por debajo del LC_{50}, se procedió a estudiar su **localización intra y extracelular mediante TEM**. Para ello, se sembraron las células durante 24 h. Posteriormente se expusieron a 50 μM de Ch-SeNPs durante 48 h adicionales, y mediante una fijación con paraformaldehído/glutaraldehído y postfijación con tetróxido de osmio, seguido por cortes de microtomo, se visualizaron por TEM. Debido al elevado número de pasos que requiere la metodología de TEM, y al mayor valor de LC_{50} para la línea SH-SY5Y, solo se pudo observar el efecto de las Ch-SeNPs sobre esta línea celular de neuroblastoma humano. Las células SH-SY5Y control, en ausencia de Ch-SeNPs, mostraron una morfología circular con un diámetro medio de la membrana celular de (7.7 ± 0.4) μm, y un tamaño del núcleo de (5.5 ± 0.3) μm. En el interior del núcleo se pudieron observar entre 1 y 3 nucleolos, con un tamaño medio de (1.16 ± 0.06) μm, variando el número de estos en función de la progresión del ciclo celular en la que se encontraba cada célula.

En las células SH-SY5Y tratadas con Ch-SeNPs se encontraron diferencias entre las **distintas etapas de internalización** de las nanopartículas. En todas ellas se observó el mismo número de nucleolos que en las células control dentro de cada núcleo, entre 1 y 3, con un tamaño medio de (1.08 ± 0.05) μm. En **etapas tempranas** de la internalización de Ch-SeNPs, la membrana celular sufrió una expansión hasta (9.5 ± 0.5) μm, perdiendo la morfología circular y adoptando una forma irregular. Es en esta etapa cuando la célula comienza a liberar liposomas, con diámetros comprendidos entre 0.22 y 1.67 μm, y además

se realiza la endocitosis de las Ch-SeNPs, atrapándolas en el interior del citosol. En esta etapa temprana, parte de las Ch-SeNPs se encuentran **adheridas al exterior de la membrana celular** debido, probablemente, a la interacción entre el quitosano que estabiliza las nanopartículas y los fosfolípidos de la membrana celular. Esta zona es de especial importancia, puesto que la agregación extracelular de la proteína $A\beta_{42}$ se produce alrededor de las neuronas. Por ese motivo, la presencia de Ch-SeNPs adheridas a la membrana celular, teniendo en cuenta los anteriores estudios que demuestran su capacidad para inhibir la agregación de las fibras amiloides e incluso desagregarlas una vez formadas, sería un factor clave para detener la "hipótesis de la cascada amiloide". Adicionalmente, las Ch-SeNPs también se encontraban en las **partes más externas del citosol**, sin llegar a acercarse al núcleo de la célula, cuyo diámetro fue de (5.2 ± 0.3) μm.

En **etapas intermedias de la internalización de las Ch-SeNPs** en las células SH-SY5Y, se observó una recuperación de la morfología circular de la membrana celular, que presentaba un diámetro de (8.5 ± 0.4) μm, siendo aún superior al control. Parte de las Ch-SeNPs permanecieron **adheridas al exterior de la membrana celular**, mientras que las Ch-SeNPs del citosol se encontraron en las **mitocondrias**, cuyas dimensiones oscilaban de 221 a 282 nm de ancho y de 404 a 706 nm de largo. Las mitocondrias de los mamíferos son grandes productoras de ROS, que a su vez oxidan el ADN mitocondrial y esto contribuye al desarrollo de la AD. Debido al excelente efecto antioxidante que poseen las Ch-SeNPs, su localización en las mitocondrias puede ayudar a disminuir la generación de ROS y ralentizar la progresión de la AD. Además, en esta fase intermedia se observó la **presencia de Ch-SeNPs dentro del núcleo**, cuyo diámetro fue de (6.5 ± 0.3) μm, superior a las células control, confirmando la habilidad de estas nanopartículas para atravesar la doble membrana nuclear.

Finalmente, en **etapas avanzadas de internalización de las Ch-SeNPs** en las células SH-SY5Y, la membrana celular adquirió un diámetro de (9.3 ± 0.5) μm, significativamente mayor que en las células control, manteniendo la morfología circular. La mayoría de las Ch-SeNPs se localizaron en el **interior del núcleo**, cuyo diámetro fue de (5.7 ± 0.3) μm, similar al control. Estas agrupaciones de Ch-SeNPs dentro del núcleo mostraron diámetros comprendidos entre 1.28 y 1.42 μm, mientras que algunas nanopartículas se ubicaron **dentro de los nucleolos**. Debido a la presencia e hiperfosforilación de la p-tau en zonas del citosol, del núcleo y del nucleolo, la localización de las Ch-SeNPs en esos mismos compartimentos podría dar lugar a su interacción con dicha proteína, también involucrada en la AD.

Adicionalmente, se estudió la morfología de la fracción flotante de las células SH-SY5Y bajo el efecto citotóxico de las Ch-SeNPs, correspondientes a un 2-10% del total. Se confirmó la pérdida de la integridad estructural de la membrana celular, con diámetros comprendidos entre 7.17 y 10.67 μm, y de su núcleo. En este estado, se apreció un mayor incremento del número de vacuolas y pequeñas agrupaciones de Ch-SeNPs con diámetros en el intervalo de 0.66 a 0.92 μm.

Debido a la **alta variabilidad en la acumulación de Ch-SeNPs** por parte de las líneas celulares de neuroblastoma, se empleó la técnica single cell-ICP-MS (**SC-ICP-MS**) para evaluar la **acumulación de selenio de células individuales** expuestas a Ch-SeNPs, y otras especies de selenio como SeMet y MeSeCys. Se estudió el efecto de la exposición de especies de selenio a concentraciones por debajo del LC_{50} (10, 50 y 250 μM) durante 48 h sobre las líneas celulares Neuro-2a y SH-SY5Y. Gracias a la elevada sensibilidad de esta técnica, y al reducido número de etapas en la preparación de muestras en comparación a la TEM, se pudo evaluar el efecto de las Ch-SeNPs en ambas líneas celulares.

Con este objetivo, se registró la señal del isótopo ^{80}Se frente al tiempo, obteniendo un número específico de eventos para cada una de las condiciones. En función de la frecuencia de los eventos y de la intensidad de los mismos, se obtuvo información del número de células que acumulaban selenio y la masa de dicho elemento que contenía cada una de ellas. Con respecto a la acumulación de selenio proveniente de las especies no nanoparticuladas, para las células **SH-SY5Y** solo se obtuvo un número significativo de eventos con la exposición a concentraciones superiores de **SeMet** (50 y 250 μM) y de **MeSeCys** (250 μM), y para las **Neuro-2a** expuestas a la máxima concentración de **SeMet** (250 μM). Sin embargo, ambas líneas celulares mostraron un número significativo de eventos correspondientes a la acumulación de **Ch-SeNPs a todas las concentraciones estudiadas** (10, 50 y 250 μM). La cuantificación de la masa de selenio por célula se realizó mediante un calibrado externo empleando selenio iónico y los resultados se representaron en histogramas de acumulación de selenio por célula, siendo el límite de detección (LOD) 1.2 fg Se célula^{-1}. La mayoría de las células (hasta el 83%) acumularon entre 5 y 35 fg de Se, independientemente de la línea celular, la especie de selenio expuesta y su concentración. Sin embargo, las diferencias fueron más apreciables al comparar el máximo de acumulación en los intervalos de cada condición.

Con respecto a las especies no nanoparticuladas (SeMet y MeSeCys), las células Neuro-2a solo demostraron la habilidad por internalizar selenio al ser expuestas a 250 μM SeMet

(< 41.4 fg célula^{-1}), mientras que las células SH-SY5Y lo internalizaron a partir de 50 μM (< 47.1 fg célula^{-1}) y 250 μM SeMet (< 167.5 fg célula^{-1}), además de 250 μM MeSeCys (< 64.6 fg célula^{-1}). Por otra parte, tanto las células Neuro-2a (< 37.4, < 63.9 y < 89.5 fg célula^{-1}) como las SH-SY5Y (< 54.1, < 76.8 y < 129.8 fg célula^{-1}) demostraron su habilidad para internalizar el selenio cuando fueron expuestas a 10, 50 y 250 μM Ch-SeNPs respectivamente.

Por tanto, se demostró que, al aumentar la concentración expuesta de la especie de selenio, las células de neuroblastoma lograban acumular más masa de dicho elemento, independientemente de la especie y de la línea celular. Con relación a las líneas de neuroblastoma, las células **SH-SY5Y** demostraron una mayor facilidad para asimilar y acumular el selenio que las células **Neuro-2a**, independientemente de la especie expuesta y su concentración. La especie de selenio que menos se acumuló por ambas líneas fue la **MeSeCys**, siendo solo observada en las células SH-SY5Y expuestas a la mayor concentración (250 μM). En cambio, las **Ch-SeNPs** fueron la especie de selenio más acumulada por ambas líneas celulares, siendo asimiladas en todas las concentraciones estudiadas (10, 50 y 250 μM). Finalmente, el análisis por SC-ICP-MS reveló la existencia de una **alta variabilidad en la población celular con respecto a la acumulación de selenio** proveniente de las especies estudiadas, haciendo indispensable el uso de técnicas que permitan cuantificar la masa de selenio en células individuales.

Como conclusión de este último trabajo, se ha evaluado el efecto *in vitro* de las Ch-SeNPs y otras especies no nanoparticuladas de selenio, sobre dos líneas celulares de neuroblastoma (Neuro-2a y SH-SY5Y). Se estudió la **citotoxicidad** a las 48 h de incubación mediante los métodos MTT y citometría de flujo, ofreciendo en general ambos métodos resultados similares, y siendo las células Neuro-2a menos resistentes frente a las especies de selenio. Se observó la acumulación de las Ch-SeNPs en las células SH-SY5Y a concentraciones siete veces inferiores al LC_{50}, **estableciéndose la ruta de internalización de las nanopartículas** desde el exterior de la membrana hasta el núcleo de la célula, mediante TEM. La presencia de las Ch-SeNPs en determinadas secciones de las células de neuroblastoma podría ser de utilidad en la AD, mediante la inhibición de la agregación extracelular de la proteína $A\beta_{42}$ o la disminución de los ROS responsables de la oxidación del ADN mitocondrial, frenando el avance de esta enfermedad. Se llevó a cabo la **cuantificación de la acumulación de selenio**, proveniente de Ch-SeNPs, SeMet y MeSeCys, a nivel de células individuales en las líneas Neuro-2a y SH-SY5Y mediante la técnica **SC-ICP-MS**. Se observó una mayor acumulación cuando las células se expusieron

a concentraciones más elevadas de las especies de selenio, presentando las células SH-SY5Y mayores valores de acumulación de selenio que las células Neuro-2a, y siendo las **Ch-SeNPs** las **más fácilmente asimiladas** por ambas líneas celulares.

X.CONCLUSIONES

X. CONCLUSIONES

A partir de los resultados obtenidos en la presente Tesis Doctoral se pueden inferir dos conclusiones generales:

I. Para una correcta **evaluación de las propiedades neuroprotectoras** de los candidatos potenciales a fármacos en la **enfermedad de Alzheimer (AD)** se hace necesario el uso de múltiples métodos y técnicas multidisciplinares. Entre ellas se encuentran la **espectroscopía UV-Vis** y su primera derivada (**d^1(UV-Vis)**), la **espectroscopía de fluorescencia**, la **microscopía electrónica de transmisión** (**TEM**), ensayos *in vitro* con **líneas celulares de fenotipo neuronal** (Neuro-2a, SH-SY5Y y SN56), el empleo de **single cell-ICP-MS** (**SC-ICP-MS**), la **modelización computacional** y **herramientas de predicción** *in silico*. Además, debido a la elevada complejidad de los datos obtenidos, es indispensable el uso de **herramientas quimiométricas** que faciliten su correcto análisis, interpretación y comparación.

II. Las moléculas orgánicas **derivadas de la 7-aminofenantridin-6-ona** (**APH1-5**), las moléculas **híbridas** entre la **rivastigmina** y el **hidroxifenilbenzimidazol** (**4a-d, 5a-b y 5d**) y las **nanopartículas de selenio estabilizadas con quitosano** (**Ch-SeNPs**) presentan una amplia gama de propiedades neuroprotectoras frente al **efecto tóxico de biometales, metales tóxicos y enantiómeros de aminoácidos**, con potencial aplicación para el **tratamiento y/o prevención de la AD**. Las propiedades neuroprotectoras mostradas por estos compuestos son particularmente relevantes para detener los eventos de la "**hipótesis de la cascada amiloide**", en sinergia con la "**hipótesis del ion metálico**", y principal responsable del **desarrollo de la AD**.

Una vez establecidas las conclusiones generales derivadas de esta Tesis Doctoral, se exponen a continuación las siguientes conclusiones específicas extraídas de las mismas:

Métodos y técnicas para la evaluación de propiedades neuroprotectoras

1. El empleo de la **espectroscopía UV-Vis y d^1(UV-Vis)** ha permitido evaluar la **quelación** de **moléculas orgánicas** y **especies de selenio** frente a diversos **biometales** (Fe(II), Cu(II) y Zn(II)) y **metales tóxicos** (Hg(II), Cd(II) y Al(III)) involucrados en el desarrollo de la AD. Además, gracias al uso de la **espectroscopía derivada**, ha sido posible establecer, en algunos casos, la relación de concentración óptima de los complejos metálicos formados. Mediante el análisis *in silico* de los orbitales HOMO y LUMO, empleando **herramientas de modelización**

computacional, se ha podido predecir y justificar la interacción de las moléculas orgánicas con los metales objeto de estudio. La **quelación metálica** es la principal estrategia a seguir para detener la "**hipótesis del ion metálico**", por lo que la evaluación de la capacidad de quelación resulta imprescindible.

2. El método de captación de radicales libres **DPPH** y el método de las sustancias reactivas del ácido tiobarbitúrico (**TBARS**) han posibilitado, mediante **espectroscopía UV-Vis**, evaluar la capacidad antioxidante de especies de selenio, moléculas orgánicas y enantiómeros de aminoácidos. La **capacidad antioxidante** es de especial relevancia debido a la importancia que posee el **estrés oxidativo**, desencadenado por los ROS generados por los metales, en el desarrollo de la AD.

3. La combinación de la **espectroscopía de fluorescencia**, empleando tioflavina T (ThT), y de la **TEM**, empleando la tinción negativa con acetato de uranilo, ha permitido evaluar uno de los factores fundamentales involucrados en la AD: **la agregación de la proteína beta-amiloide** (**Aβ**). Mediante las micrografías obtenidas en el análisis mediante TEM se ha podido evaluar la **agregación y anchura de las fibras amiloides**, el efecto **neurotóxico** presentado por los **metales** y los **enantiómeros de aminoácidos** mediante el aumento en la agregación, y el efecto **neuroprotector** mostrado por las **moléculas orgánicas** y las **Ch-SeNPs** inhibiendo la misma. Por otra parte, la cuantificación del efecto de las moléculas orgánicas sobre la inhibición de la agregación amiloide se ha realizado mediante medidas de **espectroscopía de fluorescencia**. La inhibición y/o desagregación de las fibras amiloides, constituyentes principales de las placas amiloides, representa una vía directa para detener la "**hipótesis de la cascada amiloide**".

4. La **espectroscopía de fluorescencia** ha permitido, además, estudiar la **interacción enantioselectiva** de las **Ch-SeNPs** con los principales **aminoácidos** involucrados en la AD, previa derivatización de estos últimos con orto-ftalaldehído (OPA), debido a la importancia que posee el **entorno quiral** en la **agregación de la proteína Aβ**, principal responsable del desarrollo de la AD.

5. Mediante **herramientas de modelización computacional** *in silico* se ha podido predecir la **interacción** de las **moléculas orgánicas** en las cavidades enzimáticas de la **acetilcolinesterasa** (**AChE**) y **butirilcolinesterasa** (**BChE**), degradadoras de importantes neurotransmisores como la **acetilcolina** (**ACh**) y **butirilcolina** (**BCh**), respectivamente. La capacidad de las moléculas orgánicas para inhibir las enzimas

AChE y BChE se ha determinado de forma experimental mediante la aplicación del método de Ellman empleando espectroscopía UV-Vis. La **inhibición enzimática** por parte de moléculas con potencial efecto neuroprotector es un factor a tener en cuenta, dado que intervienen en la "**hipótesis colinérgica**", aumentando los niveles de neurotransmisores como la **ACh** y **BCh** en las sinapsis interneuronales, y **retrasando por tanto el desarrollo de la AD**.

6. Los ensayos *in vitro* utilizando **líneas celulares de fenotipo neuronal**, como las **células de neuroblastoma humano** (**SH-SY5Y**), de **neuroblastoma de ratón** (**Neuro-2a**) y de **prosencéfalo basal murino** (**SN56**), han permitido estudiar los efectos de las moléculas orgánicas y las especies de selenio en medios bioquímicos más complejos. Mediante el ensayo colorimétrico del bromuro de 3-(4,5- dimetiltiazol-2-ilo)-2,5-difeniltetrazol (**MTT**), empleando **espectroscopía UV-Vis**, y **citometría de flujo**, utilizando el fluorocromo yoduro de propidio (PI), se ha podido determinar la **citotoxicidad** de los compuestos objeto de estudio. Adicionalmente, se ha evaluado la **reducción** que producen los compuestos neuroprotectores en la **citotoxicidad inducida por la proteína Aβ, los biometales y los metales tóxicos**, además de la reducción en el **estrés oxidativo** producido por estos metales. Estos ensayos son de vital importancia para un potencial candidato a fármaco, puesto que debe poseer una **baja citotoxicidad** a las concentraciones a las que ejerce su efecto neuroprotector.

7. Mediante el uso de **TEM**, y la previa fijación de las células expuestas a las **Ch-SeNPs**, se ha podido observar la presencia de estas nanopartículas en partes de especial relevancia en las **células SH-SY5Y**, pudiendo establecer la **ruta de internalización** a través de esta línea de neuroblastoma humano.

8. La aplicación de la técnica **SC-ICP-MS** ha permitido la cuantificación de la **acumulación de selenio**, a nivel de células individuales, proveniente de diversas especies como la selenometionina (**SeMet**), selenometilselenocisteína (**MeSeCys**) y las **Ch-SeNPs**, por parte de dos poblaciones celulares diferentes: **SH-SY5Y** y **Neuro-2a**. Estos resultados aportaron información relevante acerca de la acumulación de las especies de selenio sobre **líneas celulares de fenotipo neuronal**.

9. La utilización de **herramientas de predicción** *in silico*, como ADMETsar, Swiss ADME y QikProp, ha permitido predecir las propiedades de **absorción, distribución, metabolismo, excreción y toxicidad** (**ADMET**) y las **propiedades farmacocinéticas** de las moléculas orgánicas neuroprotectoras. La predicción de

dichas propiedades tiene un papel clave en el desarrollo de medicamentos, otorgando información sobre la **idoneidad** de las moléculas neuroprotectoras como **potenciales candidatos a fármacos** en función del cumplimiento de la regla de Lipinski.

10. El uso de **herramientas quimiométricas** facilita la **simplificación** e **interpretación de** la gran multitud de datos obtenidos sobre la capacidad neuroprotectora de las moléculas orgánicas evaluadas y las Ch-SeNPs. Entre las herramientas utilizadas, cabe destacar el **análisis de la varianza** (**ANOVA**), el **diseño de experimentos** (**DOE**), la **metodología de superficie de respuesta** (**RSM**) y el **análisis de componentes principales** (**PCA**).

Principales compuestos con potencial neuroprotector frente a la AD

11. Las moléculas orgánicas **derivadas de la 7-aminofenantridin-6-ona** (**APH1**, **APH2**, **APH3**, **APH4** y **APH5**) han demostrado, *in silico*, **propiedades farmacocinéticas** y **ADMET** aceptables, pudiéndose considerar **fármacos potenciales**. Además, poseen propiedades neuroprotectoras excelentes en términos de **quelación metálica** con respecto al Fe(II), Cu(II) y Hg(II), predominando la interacción a relación de concentración 1:1 (metal:APH), **reducción de la citotoxicidad** inducida por biometales y metales tóxicos, **reducción del estrés oxidativo y la peroxidación lipídica** *in vitro*. También son eficaces deteniendo los eventos de la cascada amiloide mediante dos vías: directa, **reduciendo de la anchura y agregación de las fibras de la proteína $A\beta_{42}$** inducidas por biometales y metales tóxicos; e indirecta, **aumentando la expresión de proteínas de choque térmico** (**HSP70**) y **proteosomas** (**P20S**), encargadas de la degradación de proteínas tóxicas y mal plegadas, como la proteína $A\beta_{42}$. Además, han demostrado capacidad para **reducir la citotoxicidad** y **la actividad apoptótica inducidas por la proteína $A\beta_{42}$** *in vitro*. Entre las cinco moléculas orgánicas derivadas de la 7-aminofenantridin-6-ona evaluadas, la molécula **APH4** ha resultado ser la más prometedora, sobresaliendo en la mayoría de las propiedades neuroprotectoras consideradas.

12. Las moléculas orgánicas **híbridas** entre la **rivastigmina** (**RIV**) y el **hidroxifenilbenzimidazol** (**BIM**) (**4a**, **4b**, **4c**, **4d**, **5a**, **5b** y **5d**) han demostrado, con éxito, las ventajas de la hibridación en la síntesis química. La predicción *in silico* de sus **propiedades farmacocinéticas** ha evidenciado la idoneidad de los híbridos RIV-BIM como **potenciales fármacos** y su posible administración por vía oral. Todas ellas demostraron ser buenas **inhibidoras** de la **AChE** y, especialmente la serie 5, de la

BChE. Otra propiedad neuroprotectora fundamental fue **la inhibición de la anchura y agregación**, propia e inducida por el Cu(II), de las **fibras de la proteína Aβ$_{42}$**, más acusada en el caso de las moléculas de la serie 5. Algunos de estos híbridos fueron capaces de **reducir**, *in vitro*, la **citotoxicidad de la proteína Aβ$_{42}$** y el **estrés oxidativo** generado por los metales. Entre las siete moléculas híbridas **RIV-BIM** evaluadas, las más prometedoras fueron las pertenecientes a la serie 5 (**5a**, **5b** y **5d**), destacando excepcionalmente en la **inhibición de la agregación de la proteína Aβ$_{42}$** y en la **reducción** *in vitro* del **estrés oxidativo**.

13. Las nanopartículas de selenio estabilizadas con quitosano (**Ch-SeNPs**) demostraron ser la especie de selenio, entre todas las estudiadas, con mayor **capacidad antioxidante**, presentando además **propiedades quelantes** con respecto a los **biometales** involucrados en la AD. En concreto, las **Ch-SeNPs** demostraron propiedades **anti-amiloidogénicas** mediante la **inhibición de la agregación de la proteína Aβ$_{42}$**, inducida por Fe(II) y Zn(II) y la **desagregación** de las fibras previamente formadas mediante la acción del Fe(II). Además, mediante el quitosano actuando como estabilizante quiral, las Ch-SeNPs lograron **inhibir la agregación de la proteína Aβ$_{42}$**, **enantioméricamente inducida** por los **aminoácidos** amiloidogénicos, predominantemente D-enantiómeros, y **reducir la anchura de las fibras amiloides** inducida por los mismos. Se ha demostrado la interacción **enantioselectiva** de las Ch-SeNPs con ambas formas quirales de los aminoácidos involucrados en el desarrollo de la AD. Adicionalmente, el **efecto neuroprotector** mostrado por las Ch-SeNPs fue **efectivo** a **concentraciones siete veces menores** a la concentración letal para el 50% de la población (**LC$_{50}$**)**.** Mediante la **adherencia a la membrana extracelular**, se ha confirmado su potencial para inhibir y/o reducir la agregación extracelular de la proteína Aβ$_{42}$, y su presencia en las **mitocondrias** podría dar lugar a la reducción de los ROS generados por las mismas y evitar, posiblemente, la oxidación del ADN mitocondrial que agrava la AD. Además, se observó la presencia de las Ch-SeNPs en el interior del **núcleo**, indicativo de su habilidad para atravesar la doble membrana nuclear. Mediante SC-ICP-MS se **cuantificó** su **acumulación en células individuales** de neuroblastoma (SH-SY5Y y Neuro-2a), siendo la especie de selenio más fácilmente asimilada por ambas líneas celulares, y presentando una elevada variabilidad en la población estudiada a las tres concentraciones de exposición (Neuro-2a: **1.2 – 89.5 fg Se célula^{-1}**; SH-SY5Y: **1.2 – 129.8 fg Se célula^{-1}**).

XI.CONCLUSIONS

XI. CONCLUSIONS

Two general conclusions can be derived from the results obtained in this Doctoral Thesis:

I. The correct **evaluation of the neuroprotective properties** of potential drug candidates against **Alzheimer's disease (AD)** requires the use of multiple multidisciplinary methods and techniques. Some of them include **UV-Vis spectroscopy** and its first derivative (**d^1(UV-Vis)**), **fluorescence spectroscopy**, **transmission electron microscopy** (**TEM**), *in vitro* assays with **neuronal phenotype cell lines** (Neuro-2a, SH-SY5Y and SN56), **single cell-ICP-MS** (**SC-ICP-MS**), **computational modelling** and *in silico* **prediction tools**. In addition, due to the high complexity of the data obtained, the use of **chemometric tools** that enable their correct analysis, interpretation and comparison is required.

II. Organic molecules **derived from 7-aminophenanthrenanthridin-6-one** (**APH1-5**), **hybrid** molecules between **rivastigmine** and **hydroxyphenylbenzimidazole** (**4a-d**, **5a-b** and **5d**) and **selenium nanoparticles stabilized with chitosan** (**Ch-SeNPs**) exhibit a wide range of neuroprotective properties, against the **toxic effect of biometals, toxic metals and amino acid enantiomers**, with potential application for the **treatment and/or prevention of AD**. The neuroprotective properties exhibited by these compounds are particularly relevant when it comes to stopping the events of the "**amyloid cascade hypothesis**", in synergy with the "**metal ion hypothesis**", and mainly responsible for the **development of AD**.

Once established the general conclusions derived from this Doctoral Thesis, the following specific conclusions drawn from them are set out below:

Methods and techniques for the evaluation of neuroprotective properties

1. The use of **UV-Vis** and **d^1(UV-Vis) spectroscopy** has allowed the evaluation upon **chelation** of **organic molecules** and **selenium species** against various **biometals** (Fe(II), Cu(II) and Zn(II)) and **toxic metals** (Hg(II), Cd(II) and Al(III)) involved in the development of AD. Furthermore, using **derivative spectroscopy**, it has been possible to stablish, in some cases, the optimum relationship of the metallic complexes formed. By means of *in silico* analysis of the HOMO and LUMO orbitals, using **computational modelling tools**, it has been possible to predict and justify the interaction of the organic molecules with the metals under study. **Metal chelation** is

the main strategy to overcome the "**metal ion hypothesis**", so the evaluation of chelation ability is essential.

2. The **DPPH** free radical scavenging method and the thiobarbituric acid reactive substances (**TBARS**) method have allowed, using **UV-Vis spectroscopy**, the evaluation of the antioxidant capacity of selenium species, organic molecules and amino acid enantiomers. **Antioxidant capacity** is particularly relevant due to the importance of **oxidative stress**, triggered by ROS generated by metals, in the development of AD.

3. By the combination of **fluorescence spectroscopy**, employing thioflavin T (ThT), and **TEM** employing a negative staining with uranyl acetate, it has been possible to evaluate one of the fundamental factors involved in AD: **the aggregation of the beta-amyloid protein** (**Aβ**). Through analysis of micrographs obtained by TEM, it has been possible to evaluate the **aggregation and width of the amyloid fibrils**, the **neurotoxic** effect **of metals** and **amino acid enantiomers** through the increase in the aggregation, and the **neuroprotective** effect of **organic molecules** and **Ch-SeNPs** through their inhibition thereof. On the other hand, the quantification of the effect of organic molecules on the inhibition of amyloid aggregation has been carried out by **fluorescence spectroscopy**. Inhibition and/or disaggregation of amyloid fibrils, the main constituents of amyloid plaques, represents a direct way to halt the "**amyloid cascade hypothesis**".

4. Additionally, **fluorescence spectroscopy** has made it possible to study the **enantioselective interaction** of **Ch-SeNPs** with the main **amino acids** involved in AD, after derivatization of the latter with ortho-phthalaldehyde (OPA), since the **chiral environment** is relevant in the **aggregation of the Aβ protein**, which is the main factor responsible for the development of AD.

5. Using *in silico* **computational modelling tools**, the **interaction** of **organic molecules** in the enzymatic cavities of **acetylcholinesterase** (**AChE**) and **butyrylcholinesterase** (**BChE**), which degrade important neurotransmitters such as **acetylcholine** (**ACh**) and **butyrylcholine** (**BCh**) respectively, has been predicted. The ability of organic molecules to inhibit AChE and BChE enzymes has been experimentally determined by the application of the Ellman method. **Enzyme inhibition** by molecules with potential neuroprotective effect is a factor to be taken into account, as they participate in the

"cholinergic hypothesis", increasing the levels of neurotransmitters such as **ACh** and **BCh** in interneuronal synapses, and thus **delaying the development of AD**.

6. *In vitro* assays using **neuronal phenotype cell lines**, such as **human neuroblastoma** (**SH-SY5Y**), **mouse neuroblastoma** (**Neuro-2a**) and **murine basal forebrain** (**SN56**) **cells**, have allowed to study the effects of organic molecules and selenium species in more complex biochemical medium. By means of the 3-(4,5-dimethylthiazol-2-yl)-2,5-diphenyltetrazole bromide (**MTT**) colorimetric assay, using **UV-Vis spectroscopy**, and **flow cytometry**, employing the fluorochrome propidium iodide (PI), it has been possible to determine the **cytotoxicity** of the compounds under study. In addition, the effect of neuroprotective compounds in the **reduction** of the **cytotoxicity induced by protein Aβ**, **biometals** and **toxic metals**, as well as the reduction in the **oxidative stress** produced by these metals, has been evaluated. These assays are of vital importance for a potential drug candidate, as it must possess **low cytotoxicity** at the concentrations at which it exerts its neuroprotective effect.

7. By means of **TEM**, and prior fixation of the cells exposed to the **Ch-SeNPs**, it has been possible to detect the presence of these nanoparticles in particularly relevant regions of **SH-SY5Y cells**, and to establish the **internalisation pathway** through this human neuroblastoma line.

8. The application of the **SC-ICP-MS** technique has allowed the quantification, at single cell level, of the **accumulation of selenium**, from different selenium species such as selenomethionine (**SeMet**), selenomethylselenocysteine (**MeSeCys**) and **Ch-SeNPs**, by two different cell populations: **SH-SY5Y** and **Neuro-2a**. These results provided relevant information about the accumulation of selenium species on **neuronal phenotype cell lines**.

9. Using *in silico* **prediction tools**, such as ADMETsar, Swiss ADME and QikProp, the **absorption, distribution, metabolism, excretion and toxicity** (**ADMET**) and **pharmacokinetic properties** of neuroprotective organic molecules have been predicted. Prediction of these properties has a key role in drug development, providing information on the **suitability** of neuroprotective molecules as **potential drug candidates** based on compliance with Lipinski's rule.

10. The application of **chemometric tools** facilitates the **simplification** and **interpretation** of the large amount of data obtained related to the neuroprotective

capacity of organic molecules and Ch-SeNPs under study. Among these tools used, the **analysis of variance** (**ANOVA**), **design of experiments** (**DOE**), **response surface methodology** (**RSM**) and **principal component analysis** (**PCA**) are worth mentioning.

Main compounds with neuroprotective potential against AD

11. Organic molecules **derived from 7-aminophenanthrenanthridin-6-one** (**APH1**, **APH2**, **APH3**, **APH4** and **APH5**) have demonstrated, *in silico*, acceptable **pharmacokinetic** and **ADMET properties** and can be considered as **potential drugs**. Furthermore, they possess excellent neuroprotective properties, in terms of **metal chelation** with respect to Fe(II), Cu(II) and Hg(II), predominantly at 1:1 concentration ratio (metal:APH), **reduction of cytotoxicity** induced by biometals and toxic metals, **reduction of oxidative stress and lipid peroxidation** *in vitro*. They are also effective in disrupting amyloid cascade events via two pathways: directly, by **reducing the width and aggregation of $A\beta_{42}$ protein fibrils** induced by biometals and toxic metals; and indirectly, by **increasing the expression of heat shock proteins** (**HSP70**) and **proteosomes** (**P20S**), which are responsible for the degradation of toxic and misfolded proteins, such as $A\beta_{42}$ protein. Additionally, they have shown ability to **reduce $A\beta_{42}$-induced cytotoxicity** and **apoptotic activity** *in vitro*. Among the five organic molecules derived from 7-aminophenanthrenanthridin-6-one evaluated, the **APH4** molecule has proved to be the most promising, excelling in most of the neuroprotective properties assessed.

12. **Hybrid** organic molecules between **rivastigmine** (**RIV**) and **hydroxyphenylbenzimidazole** (**BIM**) (**4a**, **4b**, **4c**, **4d**, **5a**, **5b** and **5d**) have successfully demonstrated the advantages of hybridisation in chemical synthesis. *In silico* prediction of their **pharmacokinetic properties** has shown the suitability of RIV-BIM hybrids as **potential drugs** and their potential for oral administration. All of them proved to be good **inhibitors** of **AChE** and, especially series 5, of **BChE**. Another key neuroprotective property was the **inhibition** of self- and Cu(II)-induced **aggregation and broadening of $A\beta_{42}$ protein fibrils**, which was more pronounced in the case of the molecules of series 5. Some of these hybrids were able to reduce, *in vitro*, **$A\beta_{42}$ protein cytotoxicity** and metal-mediated **oxidative stress**. Among the seven **RIV-BIM** hybrid molecules under evaluation, the most promising were those belonging to

the series 5 (**5a**, **5b** and **5d**), excelling exceptionally in **inhibiting $A\beta_{42}$ protein aggregation** and **reducing oxidative stress** *in vitro*.

13. Selenium nanoparticles stabilized with chitosan (**Ch-SeNPs**) proved to be the selenium species, among those studied, with the highest **antioxidant capacity**, also presenting **chelating properties** with respect to **biometals** involved in AD. Specifically, **Ch-SeNPs demonstrated anti-amyloidogenic** properties by **inhibiting the aggregation of the $A\beta_{42}$ protein**, induced by Fe(II) and Zn(II), and the **disaggregation** of the fibrils previously formed by the action of Fe(II). Furthermore, through chitosan acting as a chiral stabiliser, Ch-SeNPs were able to **inhibit the enantiomerically induced aggregation of $A\beta_{42}$ protein** by amyloidogenic **amino acids**, predominantly D-enantiomers, and to **reduce the width of amyloid fibrils** induced by them. The interaction of Ch-SeNPs with both chiral forms of amino acids involved in the development of AD has been demonstrated to be **enantioselective**. Additionally, the **neuroprotective effect** shown by Ch-SeNPs was **effective at concentrations seven times lower** than the lethal concentration for 50% of the population (**LC_{50}**). By **attaching to the extracellular membrane**, it is confirmed their potential to inhibit and/or reduce extracellular aggregation of $A\beta_{42}$ protein. Their presence in **mitochondria** could lead to the reduction of ROS generated by them, and possibly prevent the oxidation of mitochondrial DNA that aggravates AD. In addition, the presence of Ch-SeNPs was observed inside the **nucleus**, indicative of their ability to cross the nuclear double membrane. By SC-ICP-MS, their **accumulation** was **quantified in individual** neuroblastoma **cells** (SH-SY5Y and Neuro-2a), being the selenium species most easily assimilated by both cell lines, and presenting a high variability in the studied population at the three exposure concentrations (Neuro-2a: **1.2 - 89.5 fg Se cell^{-1}**; SH-SY5Y: **1.2 - 129.8 fg Se cell^{-1}**).

XII.ANEXO

XII. ANEXO-Producción científica

A.1. Artículos científicos incluidos en la Tesis Doctoral

- **Vicente-Zurdo, D.**; Romero-Sánchez, I.; Rosales-Conrado, N.; León-González, M. E.; Madrid, Y. *Ability of selenium species to inhibit metal-induced Aβ aggregation involved in the development of Alzheimer's disease*. Analytical and Bioanalytical Chemistry 412 (2020) 6485–6497.
- Moyano, P.[1]; **Vicente-Zurdo, D.[1]**; Blázquez-Barbadillo, C.; Menéndez, J. C.; González, J. F.; Rosales-Conrado, N.; Del Pino, J. *Neuroprotective action of multitarget 7-aminophenanthridin-6(5H)-one derivatives against metal-induced cell death and oxidative stress in SN56 cells*. ACS Chemical Neuroscience 12 (2021) 3358-3372.
- **Vicente-Zurdo, D.**; Rosales-Conrado, N.; León-González, M. E.; Brunetti, L.; Piemontese, L.; Pereira-Santos, A. R.; Cardoso, S. M.; Madrid, Y.; Chaves, S.; Santos, M. A. *Novel Rivastigmine Derivatives as Promising Multi-Target Compounds for Potential Treatment of Alzheimer's Disease*. Biomedicines 10 (2022) 1510.
- Moyano, P.[1]; **Vicente-Zurdo, D.[1]**; Blázquez-Barbadillo, C.; Menéndez, J. C.; González, J. F.; Rosales-Conrado, N.; del Pino, J. *Neuroprotective mechanisms of multitarget 7-aminophenanthridin-6(5H)-one derivatives against metal-induced amyloid proteins generation and aggregation*. Food and Chemical Toxicology 167 (2022) 113264.
- **Vicente-Zurdo, D.**; Rodríguez-Blázquez, S.; Gómez-Mejía, E.; Rosales-Conrado, N.; León-González, M. E.; Madrid, Y. *Neuroprotective activity of selenium nanoparticles against the effect of amino acids enantiomers in Alzheimer's disease.* Analytical and Bioanalytical Chemistry 414 (2022) 7573-7584.
- **Vicente-Zurdo, D.**; Gómez-Gómez, B.; Romero-Sánchez, I.; Rosales-Conrado, N.; León-González, M. E.; Madrid, Y. *Uptake and accumulation of selenium nanoparticles and other selenium species in neuroblastoma cell lines related to Alzheimer's disease by using TEM and single cell-ICP-MS*. European Journal of Medicinal Chemistry (*enviado*).

A.2. Otros artículos científicos

- **Vicente-Zurdo, D.**; dos Santos, M.; Madrid, Y. *Selenium and mercury in fish. Protective effect of Se in methylmercury toxicity*. Nutrición Clínica y dietética hospitalaria 38(1) (2018) 88.

- **Vicente-Zurdo, D.**; Gómez-Gómez, B.; Pérez-Corona, M. T.; Madrid, Y. *Especiación de selenio en muestras de pez espada mediante HPLC-ICP-MS. Influencia del proceso de cocinado.* Actualidad Analítica 61 (2018) 16-19.
- Dos Santos, M.; da Silva Júnior, F. M. R.; **Vicente Zurdo, D.**; Martins Baisch, P. R.; Muccillo-Baisch, A. L.; Madrid, Y. *Selenium and mercury concentration in drinking water and food samples from a coal mining area in Brazil.* Environmental Science and Pollution Research 26 (2019) 15510-15517.
- **Vicente-Zurdo, D.**; Gómez-Gómez, B.; Pérez-Corona, M. T.; Madrid, Y. *Impact of fish growing conditions and cooking methods on selenium species in swordfish and salmon fillets.* Journal of Food Composition and Analysis 83 (2019) 103275.
- Rocchi, D.; Blázquez-Barbadillo, C.; Agamennone, M.; Laghezza, A.; Tortorella, P.; **Vicente-Zurdo, D.**; Rosales-Conrado, N.; Moyano, P.; del Pino, J.; González, J. F.; Menéndez, J. C. *Discovery of 7-aminophenanthridin-6-one as a new scaffold for matrix metalloproteinase inhibitors with multitarget neuroprotective activity.* European Journal of Medicinal Chemistry 210 (2021) 113061.
- Gomez-Mejía, E.; **Vicente-Zurdo, D.**; Rosales-Conrado, N.; León-González, M. E.; Madrid, Y. *Optimising the extraction process of phenolic compounds from pressed grape seed residue: towards an integrated and sustainable management of viticultural waste.* LWT - Food Science and Technology 169 (2022) 113988.

A.3. Comunicaciones a congresos

- **Vicente-Zurdo, D.**; Gómez-Gómez, B.; Pérez-Corona, M. T.; Madrid, Y. *Especiación de selenio en muestras de pez espada y salmón, mediante HPLC-ICP-MS. Influencia del proceso de cocinado.* **XXI Reunión de la Sociedad Española de Química Analítica (XXI SEQA). Jornada de Especiación**. Valencia, septiembre de 2017. Tipo de comunicación: oral.
- **Vicente-Zurdo, D.**; Gómez-Gómez, B.; Pérez-Corona, M. T.; Madrid, Y. *Selenio: Elemento tóxico y esencial.* **I Jornada: CyTA con la Seguridad Alimentaria en la URJC, Investigando en seguridad alimentaria: El programa AVANSECAL-CM.** Móstoles, noviembre de 2017. Tipo de comunicación: oral.
- **Vicente-Zurdo, D.**; dos Santos, M.; Madrid, Y. *Selenium and mercury in fish. Protective effect of Se in methylmercury toxicity*. **XII Congreso Internacional Nutrición, Alimentación**

y Dietética. XXII Jornadas de Nutrición Práctica. Madrid, abril de 2018. Tipo de comunicación: póster.

- **Vicente-Zurdo, D.**; dos Santos, M.; Madrid, Y. *Selenium and mercury in fish. Protective effect of Se against methylmercury toxicity*. **40th International Conference on Environmental & Food Monitoring (ISEAC-40)**. Santiago de Compostela, junio de 2018. Tipo de comunicación: oral.
- **Vicente-Zurdo D.**; Rosales-Conrado N.; León-González M. E.; Madrid, Y. *Role of selenium species in neurodegenerative diseases*. X**XII Reunión de la Sociedad Española de Química Analítica (XXII SEQA). Jornada de Especiación. Retos de la Especiación Química en el siglo XXI: Especiación Química y Ómicas**. Valladolid, julio de 2019. Tipo de comunicación: póster.
- **Vicente-Zurdo, D**. *Evaluation of selenium species as potential multifunctional compounds for Alzheimer's disease treatment*. **V Simposio Anual en Química Avanzada (VSAQA)**. Madrid, diciembre de 2020. Tipo de comunicación: oral.
- **Vicente Zurdo, D**. *Selenium nanoparticles for the treatment of Alzheimer's disease: Interaction with amino acids enantiomers*. **V Jornada de Promoción de la Investigación Básica para Estudiantes de Ciencias e Ingenierías**. Móstoles, septiembre de 2021. Tipo de comunicación: oral.
- **Vicente-Zurdo, D.**; Rodríguez-Blázquez, S.; Gómez-Mejía, E.; Rosales-Conrado, N.; León-González, M. E.; Madrid, Y. *Neuroprotective activity of selenium nanoparticles against the effect of amino acid enantiomers in Alzheimer's disease*. **42th Colloquium Spectroscopicum Internationale 2022 (CSI XLII)**. Gijón, mayo de 2022. Tipo de comunicación: póster.
- **Vicente-Zurdo, D.**; Brunetti, L.; Piemontese, L.; Madrid, Y.; Chaves, S.; Santos, M. A. *Novel Rivastigmine-Based Multitarget Hybrids For Potential Treatment of Alzheimer's Disease: Cu(II) And Fe(III) Chelation Studies*. **International Symposium on Metal Complexes 2022 (ISMEC 2022)**. Valencia, junio de 2022. Tipo de comunicación: póster.
- **Vicente-Zurdo, D.**; Romero-Sánchez, I.; Rosales-Conrado, N.; León-González, M. E.; Madrid, Y. *Cytotoxic and Neuroprotective Effect of Selenium Species in Alzheimer's Disease*. **XXXVIII Reunión Bienal de la Sociedad Española de Química (XXXVIII RSEQ)**. Granada, junio de 2022. Tipo de comunicación: póster pitch. Premio al mejor póster en la sesión "Bioanalytical Chemistry in Health and Food Safety" otorgado por Analytical and Bioanalytical Chemistry.
- Gómez-Mejía, E.; **Vicente-Zurdo, D.**; Rosales-Conrado, N.; León-González, M. E.; Madrid, Y. *Valorisation of Grape Seeds for the Development of Potential Antioxidant and*

Neuroprotective Food Additive. **XXXVIII Reunión Bienal de la Sociedad Española de Química (XXXVIII RSEQ)**. Granada, junio de 2022. Tipo de comunicación: póster pitch.

- **Vicente-Zurdo, D.**; Rosales-Conrado, N.; León-González, M. E.; Chaves, S.; Santos, M. A.; Madrid, Y. *Novel BIM-RIV Hybrids as Promising Multitarget Compounds for the Potential Treatment of Alzheimer's Disease*. **XXIII Reunión de la Sociedad Española de Química Analítica (XXIII SEQA)**. Oviedo, julio de 2022. Tipo de comunicación: póster.

A.4. Estancias de investigación y colaboraciones

Estancia predoctoral internacional en el grupo "**Bioinorganic Chemistry and Drug Development**" del Centro de Química Estrutural (**CQE**), en el Complexo Interdisciplinar del Instituto Superior Técnico (**IST**) perteneciente a la Universidad de Lisboa (**ULisboa**), Portugal, entre el **11 de enero de 2021 y el 12 de julio de 2021** (6 meses), bajo la supervisión de la profesora Sílvia de Vasconcelos Chaves. En dicha estancia se sintetizaron y purificaron siete moléculas híbridas entre la rivastigmina y el hidroxifenilbenzimidazol (RIV-BIM), siendo caracterizadas mediante ^{1}H y ^{13}C RMN, ESI(-) y ESI(+), punto de fusión y RF. Se realizaron estudios de modelización computacional de los híbridos RIV-BIM con hAChE y hBChE, se predijeron sus propiedades farmacocinéticas *in silico* y se evaluó su capacidad neuroprotectora (actividad antioxidante, inhibición de eeAChE y eqBChE, e inhibición de la agregación propia de la Aβ y de la agregación inducida por el Cu(II).

Colaboración con el grupo de investigación de Heterociclos de Interés Biológico y Terapéutico del Departamento de Química en Ciencias Farmacéuticas de la Facultad de Farmacia y con el grupo de investigación de Evaluación, Control y Bioseguridad de la Toxicidad de Agentes Terapéuticos, Ambientales y Alimentarios del Departamento de Farmacología y Toxicología de la Facultad de Veterinaria de la Universidad Complutense de Madrid en la evaluación de las propiedades neuroprotectoras de moléculas orgánicas derivadas de la 7-aminofenantridin-6-ona contra la enfermedad de Alzheimer.

A.5. Otros méritos

- **Censor de revistas científicas internacionales** indexadas en el JCR en el área de conocimiento de Química Analítica, Farmacología y Farmacia, Bioquímica y Biología Molecular, Química Multidisciplinar, Medicina General e Interna, Genética y Herencia, Ingeniería Química y Energía y Combustibles: Analytica Chimica Acta (IF: 6.911, Q1), Pharmaceutics (IF: 6.525, Q1), Journal of Analytical and Applied Pyrolysis (IF: 6.437, Q1), International Journal of Molecular Sciences (IF: 6.208, Q1), Journal of Clinical Medicine (IF: 4.964, Q1), Molecules (IF: 4.927, Q2), Genes (IF: 4.141, Q2) y Chinese Journal of Analytical Chemistry (IF: 1.193, Q4).

- Miembro del **comité organizador** del **V Simposio Anual en Química Avanzada (VSAQA)**. Madrid, diciembre de 2020.
- Miembro del equipo investigador del Artículo 83 titulado "Determinación de elementos traza en muestras de líquenes/Determination of trace elements in lichen samples" con la financiación del Dr. Rolf Herzig, director del AGB (Arbeitsgemeinschaft für Biondication), Berna, Suiza, con el objetivo de medir metales tóxicos en muestras de líquenes cercanos a una autopista.

A.6. Competencias lingüísticas

- First Certificate in English (FCE). B2 level. Cambridge Assesment English. Marzo de 2019.
- English C1.1. Idiomas Complutense- Centro Superior de Idiomas Modernos (CSIM), Universidad Complutense de Madrid (UCM). Junio de 2019.